

Dissertation zur Erlangung des Doktorgrades
der Fakultät für Chemie und Pharmazie
der Ludwig-Maximilians-Universität München

**Hybrid Peptide-Helical
Aromatic Foldamer Macrocycles**

Sebastian Georg Dengler

aus

Bad Aibling, Deutschland

2022

Erklärung

Diese Dissertation wurde im Sinne von § 7 der Promotionsordnung vom 28. November 2011 von Herrn Prof. Dr. Ivan Huc betreut.

Eidesstattliche Versicherung

Diese Dissertation wurde eigenständig und ohne unerlaubte Hilfe erarbeitet.

München, den 19.08.2022

Unterschrift:

Sebastian, Dengler

Dissertation eingereicht am 24.08.2022

1. Gutachter: Prof. Dr. Ivan Huc

2. Gutachter: Prof. Dr. Franz Bracher

Mündliche Prüfung am 27.10.2022

Danksagung

Als Erstes möchte ich mich bei Prof. Dr. Ivan Huc bedanken. Dafür das er mich als einer seiner ersten Doktoranden in München aufgenommen hat und mir die Möglichkeit gegeben hat bei ihm in seiner Gruppe zu arbeiten und zu promovieren. Dank seiner hervorragenden Betreuung konnte diese Arbeit entstehen.

Des Weiteren möchte ich mich bei der Prüfungskommission bedanken. Mein Dank gilt Prof. Dr. Franz Bracher für die Übernahme des 2. Gutachtens.

Mein Dank gilt ferner der Arbeitsgruppe Huc und allen Kollegen, die mir eine angenehme Arbeitsatmosphäre in den vergangenen Jahren ermöglicht haben. Der tägliche wissenschaftliche Austausch haben einen wichtigen Beitrag zu dieser Arbeit geleistet. Besonders möchte ich hier Dr. Céline Douat danken, für ihre Unterstützung im Labor sowie Korrektur und Unterstützung bei der Erstellung der Veröffentlichungen. Vieles konnte ich von Ihr lernen. Des Weiteren möchte ich mich insbesondere bei Dr. Sunbum Kwon und Dr. Pradeep Kumar Mandal bedanken, die mich insbesondere zu Beginn meiner Arbeit gut gefördert haben.

Für die Gesellschaft in den Kaffeepausen möchte ich Christoph, Sonja, Lorenz, Maxi und Eva danken. Ihr habt immer für eine tolle Abwechslung gesorgt. Für die gemeinsame Zeit vor allem während des Studiums möchte ich meinem langjährigen Freund Jürgen danken.

Ein besonderer Dank gilt Dr. Lars Allmendinger. Vor allem für seinen Rat vor und während der Promotion – Wissenschaftlicher und nicht-Wissenschaftlicher Natur, als Oberassistent im Praktikum, Sportpartner und für die Ausführung aller NMR Experimente.

Des Weiteren möchte ich mich bei Manuel, Daniel und Niklas bedanken. Für die gemeinsame Zeit als direkte Laborpartner, für unzählige gemeinsame Mittagessen und das hervorragende Miteinander auch außerhalb der Arbeit.

Ein großer Dank gilt meiner Familie: Meinen Eltern, Magdalena, Sophia, Andreas und Manuela. Eure langjährige Unterstützung hat diese Doktorarbeit ermöglicht. Ich danke euch von ganzem Herzen.

Meinen Eltern gewidmet

Table of Content

1. Abstract.....	8
2. Introduction	10
2.1. Peptides in Pharmaceutical Sciences	10
2.2. Foldamers	26
2.3. Cyclic Peptide - Foldamer Hybrids	35
3. Objectives	37
4. Bibliography	39
5. List of Publications	45
6. Main Text: Conformational Interplay in Hybrid Peptide–Helical Aromatic Foldamer Macrocyces	46
7. Supplementary Information: Conformational Interplay in Hybrid Peptide–Helical Aromatic Foldamer Macrocyces	57
7.1. Materials and methods for chemical synthesis	58
7.2. Experimental procedures for chemical synthesis.....	62
7.3. Materials and Methods for HPLC, MS, UV, NMR and CD.....	77
7.4. 2D TOCSY and variable temperature NMR spectra.....	80
7.5. Crystallization and X-ray diffraction measurements	83
7.6. Biodegradation assay of foldamer-peptide hybrids in the presents of Pronase E, Trypsin or alpha-Chymotrypsin	97
7.7. ¹ H NMR spectra and HPLC profiles	105
8. Main Text: Display Selection of a Hybrid Foldamer-Peptide Macrocycle	123
9. Supporting Information: Display Selection of a Hybrid Foldamer-Peptide Macrocycle.....	131
9.1. Supporting figures.....	132
9.2. Biochemistry and Structural Biology	162
9.3. Chemical synthesis.....	171
9.4. General methods for solid-phase synthesis.....	172
9.5. Solid-phase peptide synthesis (SPPS)	172
9.6. Solid-phase foldamer synthesis (SPFS) for compounds 1–9, 11–12.....	172
9.7. Solid-phase foldamer synthesis (SPFS) of F10	172
9.8. Fragment condensation.....	172
9.9. N-terminal acetylation.....	173
9.10. N-terminal chloroacetylation	173
9.11. Cleavage of resin-bound oligomers.....	173
9.12. Cyanomethyl ester (CME) installation	173

9.13.	Boc/ <i>tert</i> -Bu deprotection of CME containing foldamer-peptide hybrids.....	173
9.14.	General methods for NMR, HRMS, HPLC analysis and purification	173
9.15.	Experimental procedures for chemical synthesis	175
9.16.	¹ H NMR spectra and HPLC profiles.....	188
9.17.	Supporting references.....	211
10.	Main Text: Differential Peptide Multi-Macrocyclizations at the Surface of a Helical Foldamer Template	213
11.	Supporting Information: Differential Peptide Multi-Macrocyclizations at the Surface of a Helical Foldamer Template	224
11.1.	Supporting Figures and Tables.....	225
11.2.	Material and Methods	270
11.3.	NMR spectra of new monomers and isolated macrocycles.....	314
12.	Summary and Perspective	325

1. Abstract

Macrocyclic peptides are an emerging class of important drug candidates as they combine advantages from small molecules and antibodies - the two dominant families of pharmaceuticals. This class of cyclic macromolecules shows great resistance to proteolytic degradation, the potential to cross the cell membrane, high binding affinity upon target engagement, and structural pre-organization. Due to their size and structural complexity, cyclic peptides are particularly attractive scaffolds for the study of difficult biomolecular interactions, *e.g.*, protein-protein interactions. One strategy for the development of new pharmaceutically relevant macrocyclic peptides involves the incorporation of non-canonical amino acid residues. These residues can stabilize the macrocycle's secondary structures, modify its intramolecular hydrogen-bonding network or optimize its passive membrane permeability. Inserting an aromatic foldamer segment exhibiting a strong propensity to fold into helical objects within a cyclic peptide will impact the remaining peptide conformation. A foldamer can impose the peptide fragment to rearrange and adjust its conformation thus driving its folding. For example, if the peptide length is short, the foldamer will constrain the peptide to an extended conformation. This structural restriction can hamper proteolytic degradation and increase binding affinity towards a biomolecule.

In this work, we show that by incorporating foldamers into cyclic peptides, we generate a class of compounds with unique conformational behavior. We could demonstrate that the foldamer and the peptide segments in peptide-foldamer hybrid macrocyclic structures reciprocally influence each other. The foldamer stretches the peptide while maintaining its conformation. Conversely, the peptide stabilizes the helical folding and biases the handedness of the foldamer. We also confirmed that cyclic peptide-foldamer hybrids are less susceptible to proteolytic degradation than their linear variants. Further, we could demonstrate that peptide-foldamer hybrid macrocycles are compatible with mRNA display selection experiments. This allowed us to generate and screen a library of hybrid macrocycles within the RaPID (random nonstandard peptides integrated discovery) platform against the c-lobe of E6AP HECT domain, a ubiquitin E3 ligase. After selection, several hybrid macrocycles were identified as binders, one of which provided a high-resolution binder-target co-crystal X-ray structure. The combination of solid state data with MD simulations led to structural insights into the macrocyclic binder itself and its interactions with the target protein. In similar peptide-foldamer macrocyclic systems, we showed that rigid, helical foldamers template multiple macrocyclization steps on their outer surface. We could demonstrate, that peptide loops can be stitched on the outer edge of the foldamer helix in some sort of selective reaction trail. The trail was predictable and allowed up to four cyclization steps through the same chemically identical irreversible macrocyclization reaction between a cysteine thiol and a chloroacetamide.

Overall, these results give hope that the unique conformational properties of cyclic peptide-foldamer hybrids will allow preserving the secondary structure of cyclic peptides which might result in unique 3-dimensional arrangements. Their compatibility with screening assays could eventually enable the discovery of specific high affinity ligands for therapeutically relevant targets. It is also hoped that the foldamer segment in cyclic peptide-foldamer hybrids may have a positive effect on cell penetration to reach a cytoplasmic target. Furthermore, the resistance toward proteolytic digestion could pave the way for further *in vivo* experiments. In addition,

multicyclic peptide-foldamer hybrid macrocycles resemble small-protein structures and can therefore be considered as potential multivalent protein binders.

2. Introduction

2.1. Peptides in Pharmaceutical Sciences

General Introduction

One century ago, in 1921, the first peptide-based drug, insulin, was discovered, and its first medical use – the treatment of a 14-year-old boy – began in 1922. During that time, the peptide hormone was extracted from the pancreas of dogs, and injection of the pancreatic extract was the first treatment for type 1 diabetes.^[1] Besides being the first peptide-based drug, insulin remains the most commercially successful in its class^[2], and for its discovery, Banting and Macleod were awarded the Nobel Prize in 1923. Since then, the progression of the development of peptides as drugs has continued: in 1944, gramicidin S was discovered by Gause and Brazhinkova and was the first cyclic peptide used as an antibiotic active drug which was particularly useful during the Second World War to treat gunshot wounds.^[3] In 1954, oxytocin was the first polypeptide produced by chemical synthesis. The synthesis of this cyclic peptide hormone, which can be used medically to induce labor for pregnant women, rewarded Vincent du Vigneauds one year later with the Nobel Prize in Chemistry.^[4] Large-scale peptide manufacturing *in vivo* by recombinant technologies with genetically engineered *E.Coli* overall was discovered in the 1980s.^[5] This was particularly important for the production of synthetic insulin which allowed the manufacturing of bigger quantities and with the advantage of greater immunocompatibility compared to animal-derived insulin.^[6] Other important natural peptide-deriving drugs such as eptifibatid (1998), ziconotide (2004), and linaclotide (2012) were approved and the pharmaceutical market of peptides as drugs is currently growing.

The increasing interest in peptide drug development can be explained by the fact that peptides can be applied to a wide range of targets. Known targets are antimicrobial targets, ion channels, inhibition of protein-protein interactions (PPIs), kinases, integrins (cell-adhesion receptors), and G-protein coupled receptors.^[7] Many of these targets, especially those incorporating large protein binding interfaces, are considered particularly challenging to address since small molecules, on which the pharmaceutical industry has relied for many years, are usually not able to bind such large surface areas with high affinity. These interface areas range between 1000 and 2000 Å² in contrast to defined small molecule pockets which are around 300-500 Å².^[8] Antibodies do accommodate these huge binding sites with high specificity and high binding affinity – which made them an extremely successful class of compounds^[9] – yet they cannot cross the cell membrane to reach intracellular targets. As peptides are in a molecular range where they can be located between small molecules (<500 Da) and proteins/antibodies (>5000 Da), sometimes called “middle space” (**Figure 1**), they can be considered ideal drug candidates as their surface area is large enough to bind to such large binding sites with antibody-like affinity but are also potentially able to penetrate cell membranes. Further, with respect to proteins, they have higher metabolic stability, are less immunologically reactive and have a lower cost of production.^[10] In

addition, non-natural modifications can be added to synthetic peptides during and after synthesis to compensate for their disadvantages.

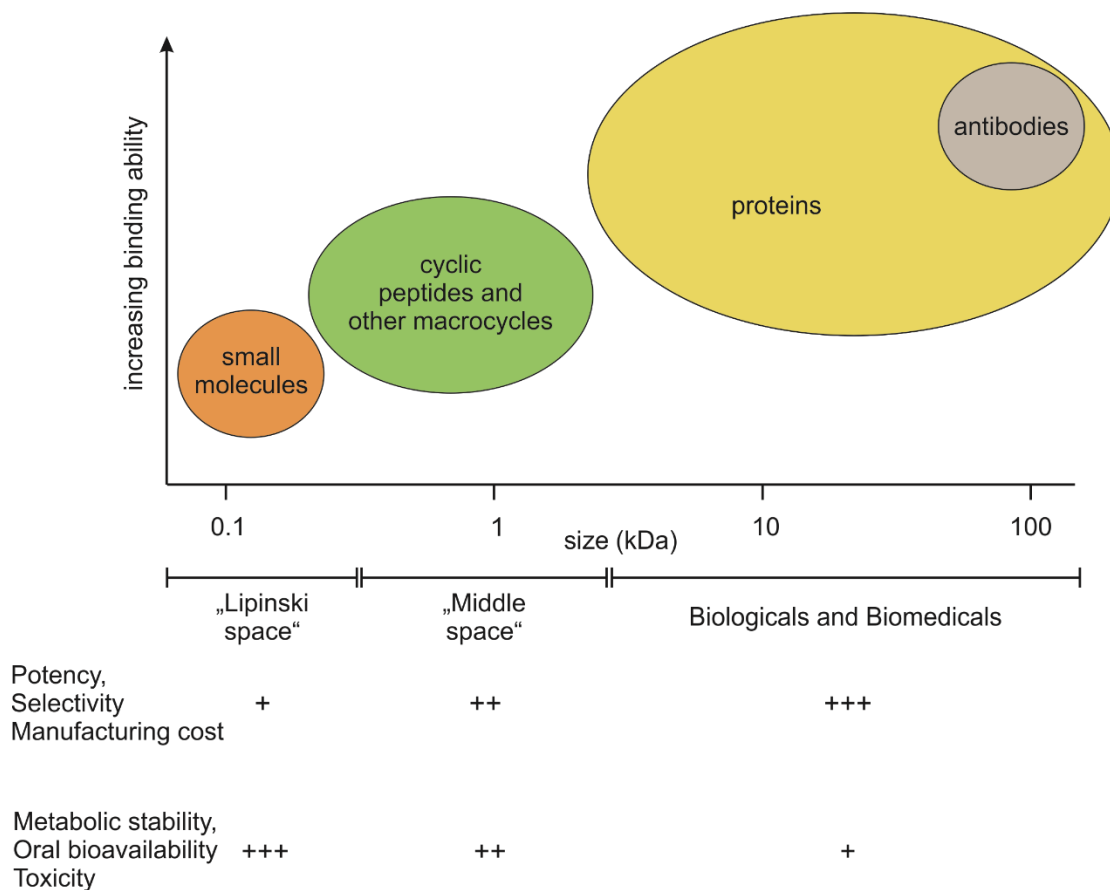


Figure 1 - Comparison of different drug modalities. Cyclic peptides are in the “middle space” between small molecules and biologicals by size and properties.^[10c]

Despite the success of some key examples, the global pharmaceutical market share in peptide-based drugs remains low (5% in 2019).^[2] The low appearance of peptides as drugs so far can be explained by the fact that interest in this field got momentum quite recently (the late 90s), and, overcoming the overall poor pharmacokinetic profile associated with the use of peptides as drugs, remains challenging in the field of peptide drug design and optimization. Peptides, except for short peptides (<10 amino acids), generally violate Lipinski’s rule of five^[11]: a simple model to determine the likelihood of oral bioavailability of a potential drug molecule. The rule describes that a majority of established drugs are not bigger than 500 g/mol, do not have more than five hydrogen bond donors, not more than 10 hydrogen bond acceptors, and the calculated cLogP value is not greater than 5. A different model, more specific for peptides described by Veber *et al.*^[12] predicts good oral bioavailability if the peptide’s polar surface area is below 140 Å² and has 10 or fewer rotatable bonds. Both models can guide the design of peptides as drug candidates but it remains that oral administration of peptides is generally problematic. One reason for this is that amide bonds within a peptide are prone to proteolytic degradation by intestinal enzymes such as pepsin or cathepsin which digest peptides rapidly before they can be absorbed by the body. That mainly limits the administration of peptides to intravenous, subcutaneous, or intramuscular routes.^[13] The formulation of peptide drugs is therefore often more laborious, expensive, and the usage of needles to penetrate the patient’s skin can lead to reduced compliance in comparison to

small molecules, which can be often swallowed in tablets or similar formulations.^[14] If peptides do reach the bloodstream, renal clearance is very rapid – within minutes. Due to their relatively small size and high hydrophilicity, peptide drugs are filtered through the glomeruli of the kidney which results in a low system circulation time and a low *in-vivo* half-life.^[15]

This list of obstacles might suggest that peptides are overall poor candidates for drug development. Nevertheless, the interest in peptides as drug candidates, as well as academic research in peptide-based technologies, has continued to grow over the past 30 years.^[16] Today, more than 80 FDA/EMA-approved peptides are on the market, of which around two-thirds are cyclic.^[2, 7a, 13, 17] Peptide macrocyclization overall helps to overcome many of the disadvantages which come from using linear peptides (*vide infra*) and enables the production of a potentially highly valuable class of drugs that are easy to screen^[18], to produce^[19], highly versatile and specific^[20], bind with high affinity and overall have low metabolic toxicity.^[21] Some of these points will be discussed in detail in subsequent sections.

Peptide Macrocycles

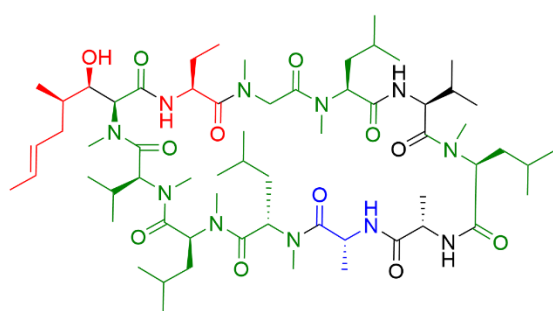
Linear, unconstrained peptides usually are less pre-organized and thus generally more disordered in aqueous environment. Reducing the degrees of conformational freedom available to peptides can result in tighter and more selective binding towards a target. A linear peptide can adopt more different non-active conformations than a rigidified peptide which can result in a greater entropic penalty for the linear peptide upon specific binding to a target. To rigidify peptides, and as a result, reduce conformational freedom, macrocyclization is an important and often-used chemical tool. In a work of Duncan *et al.*^[22], a small library of heptapeptides identified by phage display was modified with two Cys residues introduced at both termini to allow disulfide bridge cyclization. The researchers compared the binding of the cyclic and linear versions at various concentrations (against a target involved in cancer) and found that the best cyclic analog had an 85-fold higher receptor binding affinity in comparison to its linear version.

Peptide macrocycles are much more resistant to proteolytic degradation than their linear counterparts. Enzymatic hydrolysis by endopeptidases often requires a certain peptide backbone conformation that a peptide macrocycle cannot readily adopt, slowing down their hydrolysis by this class of peptidases.^[23] Furthermore, when cyclized from head-to-tail, N- or C-termini which are prone to enzymatic hydrolysis from exopeptidases are masked, preventing such degradation mechanisms.^[24] In the work of Byk *et al.*^[25], the enzymatic stability of a macrocyclic hexapeptide against its linear versions was examined. In the assay, they performed (incubation on liver tissue), they could show that the macrocyclic version had a half-life of about 30 minutes compared to 4 min of its linear version. In another study, performed by Pakkala *et al.*^[26], a linear nonapeptide was cleaved by trypsin within 30 min whereas 43% of a disulfide bridged macrocyclic version was still present in solution after 4 h of incubation. A similar result is presented by Aloaofi *et al.*^[27] The researchers produced cyclic hexapeptides and studied the influence of macrocyclization on plasma stability. The macrocycle had a plasma half-life (13h) more than five times longer than its linear version (2.4h).

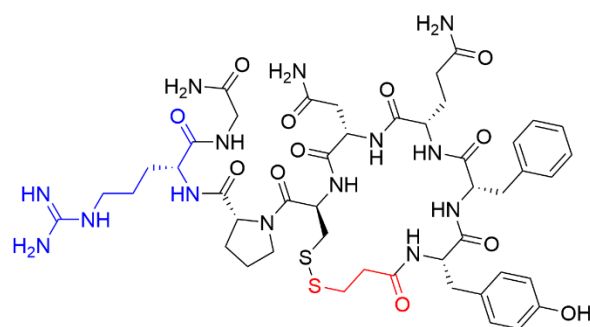
If the intended target is located in the cytosol, the molecule candidate has to pass the cell membrane. Cyclization of peptides can be used as a tool to help peptides penetrate cells, yet, the

effect of cyclization on cell penetration remains to be quantified.^[10a, 28] There are only a few examples of peptides^[29] that can enter the cytosol from which only two cyclic peptides (romidepsin and voclosporin) target intracellular proteins got approval by the FDA within the last two decades.^[30] Peptides and small molecules which are intended to be cell-permeable require well-defined physicochemical properties according to their molecular weight, lipophilicity, hydrogen bonding potential, charge state, and conformation.^[31] Fine-tuning properties during drug development is difficult, as the mechanisms associated with cell penetration are not fully understood.^[30] The cyclic geometry of the peptide macrocycle can be beneficial. It is believed that cyclic peptides vary their 3D arrangement depending on their surrounding environment. They can dynamically modulate the exposure of atoms depending on the environment they are exposed to. In aqueous environment, the macrocycle's polar side chains are exposed to the outside. That hydrophilic conformation changes upon entering a hydrophobic environment *e.g.* when entering the membrane bilayer. The conformation of the macrocycle changes so much so that the polar side chains are masked from the hydrophobic environment making the macrocycle more hydrophobic. This dynamic conformational flexibility, “chameleon” behavior is believed to be associated with cell penetration.^[32]

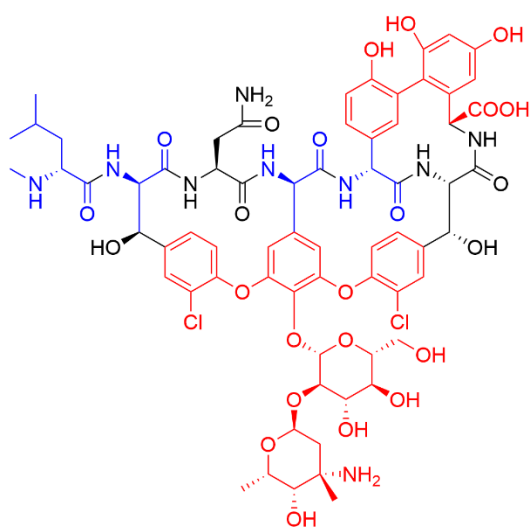
Besides cyclization, other non-canonical modifications have been developed to increase the cell permeability of cyclic peptides. Introducing unnatural amino acids *e.g.* D-amino acids, as well as chemical modifications such as N-methylation, C α -methylation, or amide bond isosteres, are established strategies.^[33] One example where a fine-tuning of the physicochemical properties was achieved by a combination of different chemical modifications is cilengitide (**Figure 2**). This cyclic pentapeptide was modified with D-amino acid residues and N-methylation to increase its metabolic stability. Due to these structural modifications, it is excreted without any metabolically introduced structural changes and has a half-life *in-vivo* of four hours.^[34] Many of these chemical modifications are also found in natural products.



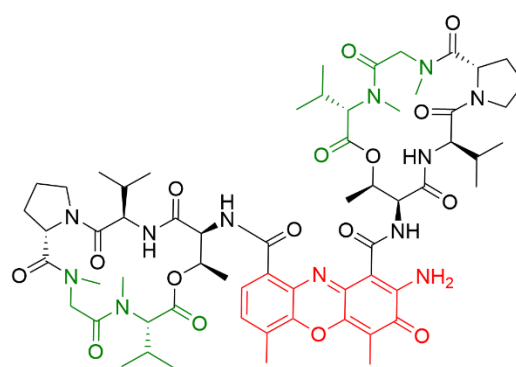
Cyclosporin A



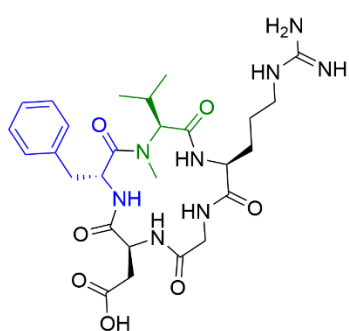
Desmopressin



Vancomycin



Actinomycin D



Cilengitide

D-amino acid
 N-methylated amide
 non-canonical-amino acid
 building blocks

Figure 2 - Bioavailable peptide macrocycles and their common structural features. Non-canonical amino acids are highlighted in red, D-amino acids in blue, and N-methylated amino acids in green. Cyclosporin A, desmopressin, and actinomycin D are orally bioavailable. Cyclosporin A, actinomycin D, and vancomycin are natural products. Apart from cilengitide, all are approved for pharmaceutical use.

High-affinity cyclic peptide binders can be found in nature, and have been isolated from plants, bacteria, fungi, sponges, algae, and mammals.^[35] Their structures have been an inspiration for scientists in drug development and some of these natural products *e.g.* cyclosporin A,

vancomycin, and caspofungin, have been isolated and directly used as commercially available drugs.^[30, 36] Besides ribosomally synthesized cyclic peptides, some bacteria and fungi produce peptide macrocycles using non-ribosomal peptide synthetases or via post-translational modifications.^[37] As a result of natural selection, they convert their role as defensive agents to protect their producing organism by having an antimicrobial activity or acting as a pesticide. More than 1000 cyclic peptides of varying lengths (12 to 80 amino acids) have been discovered in nature from which some are orally bioavailable.^[10a] Oral bioavailability of less than 1% is not unusual for peptides, yet there are some which can reach more than 10%.^[29] The influence of structural modifications of peptides on their oral uptake overall is difficult to predict, however poor oral bioavailability can be tolerated due to their strong and specific biological target engagement.^[33c] One FDA-approved example is cyclosporin A (**Figure 2**): A cyclic, naturally occurring undecapeptide and orally administered immunosuppressant drug. Even though it deviates from Lipinski's rule of five, it can enter mammalian cells via passive diffusion and is largely resistant to proteolytic degradation.^[38] This is thought to be due to its unnatural modifications including seven N-methylated backbone amides, one D-amino acid residue, two non-canonical amino acid residues, and overall high lipophilicity. Desmopressin, an antidiuretic peptide for the treatment of *diabetes insipidus*, has an oral bioavailability of only 1%, however, its non-natural modifications, namely Cys deamination and D-Arg incorporation, improve the biological half-life such that a clinically effective concentration is achieved.^[39] Another example of an orally available peptide macrocycle is actinomycin D. This cytotoxic antibiotic suppresses transcription and is used effectively in cancer therapy. Two pentapeptide macrocycles each bearing two N-methyl amino acids are connected with a phenoxazinone linker that promotes intercalation into DNA. The two rings are preorganized by intramolecular hydrogen bonds between two Val residues of each ring keeping the macrocycles in close spatial proximity.^[40] These examples underpin that structural variations with non-canonical amino acid residues can be beneficial for the overall pharmacokinetic profile of peptide macrocycles as drug candidates.

Peptide Macrocycles with Non-Canonical and Artificial Components

As discussed, drug discovery of peptide macrocycles as therapeutics need to circumvent obstacles such as low metabolic resistance, poor cell permeability, and overall low oral bioavailability. The introduction of non-natural entities into peptide macrocycles increases the repertoire of building blocks for constructing macrocyclic architectures, allowing fine-tuning of peptide macrocycle properties and providing additional versatility compared to what nature can provide. Taking inspiration from nature which transforms cognate amino acids to indoles, imidazoles, oxazoles, thiazoles, pyridines, or other diverse functionalities, chemists have studied the introduction of aromatic building blocks into peptides and their macrocycles. Non-natural synthetic aromatic moieties such as triazoles, pyrimidines, furans, and many others have been successfully incorporated into peptide macrocycles.^[41] Replacement of amino acids on dedicated positions in the peptide sequence by these flat, robust aromatic residues, can restrict the overall macrocycle conformation. This allows the peptides to adopt stable secondary structures which are usually not accessible to a short linear polypeptide.^[42] These stabilized secondary structures^[42] can mimic binding motifs *e.g.* to inhibit protein-protein interactions (PPIs).^[43] Predefining the peptide conformation by such aromatic modifications has been shown to generate peptides with extraordinary binding affinities and target specificities with respect to their biological target,

higher resistance to enzymatic degradation, and lipophilicity, which generally improves cell permeability.^[44]

Some mushroom species in the *Amanita* genus produce amatoxins and phallotoxins, two families of highly potent bicyclic peptide macrocycles which are crosslinked by a central indole residue. The most potent macrocycle in this class of compounds is α -amanitin and it is responsible for the high toxicity of the death-cap mushroom, *Amanita phalloides*.^[45] After exposure to α -amanitin, eukaryotic cells become apoptotic as the toxin inhibits the RNA polymerase Pol-II allosterically, an enzyme that produces mRNA in eukaryotes by transcribing protein-encoding genes. The chemical structure is shown in **Figure 3a**. The aromatic core is based on both tryptophan and cysteine residues which is unique among natural products and has been, until recently, not accessible via total chemical synthesis.^[46] The orally available, highly water-soluble peptide bicycle binds with extremely high affinity to its target ($K_d = 10^{-9}$ M) and has thus received increasing interest in the field of medicinal chemistry and cancer research *e.g.* as cytotoxic chemotherapy.^[47] The unique architecture of the peptide-macrocycle α -amanitin and its derivatives are responsible for their extraordinary properties and the overall structure was determined by X-ray crystallography.^[48] Additionally, Liu *et al.*^[49] recently provided a high resolution cryogenic electron microscopy (cryo-EM) structure of α -amanitin bound to the mammalian Pol-II elongation complex (**Figure 3a**).

One particular strategy of modifying peptides to modulate/stabilize secondary structures with aromatic residues is the stapling approach. In stapled peptides, peptide chains are forced into α -helices by an external clamp which is located at the side chain of two amino acids at the right distance (i+4, i+7, i+11) and on the same side of the helix. To introduce the staple, mild reaction conditions which are chemically orthogonal to not interfere with amino acid functional groups are used, with some examples being click reactions, lactamizations, olefine metathesis, and others.^[50] These intramolecular crosslinks reduce the peptide's rotational freedom and, if well-optimized, stabilize α -helical conformation. This is of particular relevance when stapled peptides are produced for mimicking binding motifs of protein domains.^[51] Additionally, stapled peptides are often more resistant to proteolytic degradation and some even show cell permeability.^[52] In a work of Yu Heng Lau *et al.*^[53], the α -helical peptide segment of a peptide chain was stabilized by an azide-alkyne cycloaddition reaction towards an eight-membered ring with two adjacent triazole and two benzene moieties. The fully biocompatible *in cell* reaction (stapling reaction in cell culture) led to the rapid production of a stapled peptide with nanomolar affinity against the oncogene MDM2 protein (regulator of tumor suppressor p53). A high-resolution co-crystal structure of the complex (**Figure 3c**) was obtained and the authors could also validate that the stapled peptide degrades slower in a biodegradation assay than its unstapled counterpart.

In different objectives, peptides can also be constrained by small organic cores towards bicyclic structures. Trivalent thiol-reactive organic scaffolds react readily with Cys-containing peptides. As a result, two macrocyclic rings are generated, greatly reducing the conformational flexibility of the peptide. This new structural motif can *i)* improve the binding properties of the resulting bicyclic peptide, *ii)* allows the incorporation of unnatural amino acid residues in the sequence, and *iii)* show good compatibility with screening assay methods such as phage-display technology.^[54] Before the affinity selection of these compounds against a biological target, phage-encoded, randomized peptide libraries, whose sequences contains three Cys residues (N- and C-termini plus one in the middle of the sequence), can be tethered to C3 symmetrical organic

scaffolds such as TBMB (tris(bromomethyl) benzene).^[55] The three Cys thiol groups react via a nucleophilic substitution reaction on the TBMB, thus producing bicyclic peptides with the benzene moiety as a core. Other reactive organic linkers such as TATA (1,3,5-triacryloyl-1,3,5-triazinane) and TBAB (benzene-1,3,5-triyl)-tris(2-bromoacetamide) have been developed and were also successfully implemented into phage display.^[56] In contrast to TBMB, these cores are more hydrophilic and promote intramolecular hydrogen bonding to the peptide chain. These interactions stabilize the 3-dimensional structure which results in higher target binding affinity of such bicyclic peptides. In a study performed by Chen *et al.*^[56], a three Cys-containing peptide library was developed (10^8 members) and bicyclic peptides were formed with either TBMB, TATA, or TBAB against uPA, a human protease involved in tumor proliferation and invasion. In all three cases, high affinity bicyclic peptide binders could be identified and their peptide sequences were different if the bicycle contained TBMB, TATA, or TBAB as an organic core. These results suggested that the overall peptide architecture is distinct among the three cores, reflecting different non-covalent interactions between the core unit and the surrounding peptide. This finding was reinforced as it was demonstrated that high affinity binders with one given core lost their binding affinity against uPA when the scaffold was swapped for another. Structural investigations in the presence of the protease provided an atomic resolution X-ray crystal structure allowing the identification of the non-covalent interactions between the TBAB scaffold and the peptide sequence. (**Figure 3b**)

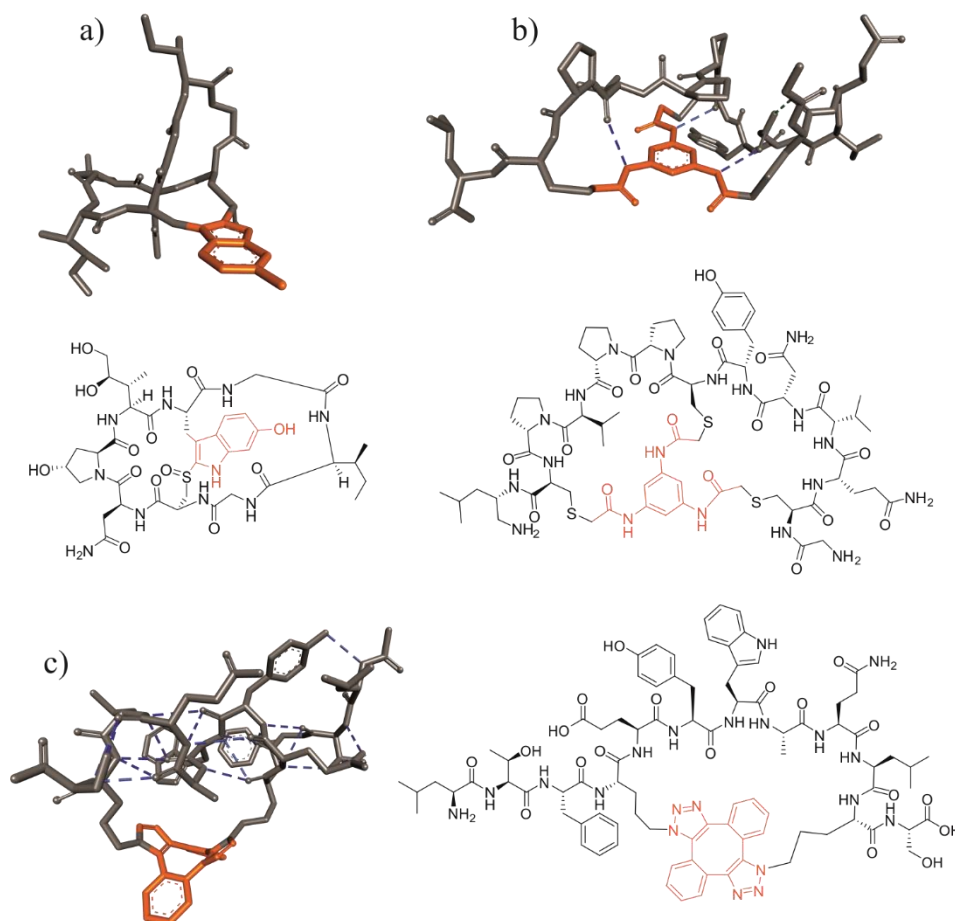


Figure 3 - High-affinity peptide macrocycles with aromatic, central core unit. a) Cryo-EM structure of α -amanitin^[49] (PDBID: 6EXV) b) X-ray crystal structure of a bicyclic peptide cyclized with three primary

amines and central benzene scaffold^[56] (PDBID: 4MNY) and c) a stapled peptide^[53] (PDBID: 5AFG). Target protein structure omitted for clarity. Central aromatic unit colored in orange, peptide in grey, and intramolecular short distance contacts in blue dashed lines.

Chemical Synthesis

Chemical synthesis of linear and macrocyclic peptides can be achieved with the use of solid-phase peptide synthesis (SPPS). In 1963, the concept of SPPS was developed by Robert B. Merrifield – a milestone in peptide synthesis – for which he was awarded the Nobel Prize in 1984.^[57] The breakthrough is built upon the solution-phase concept of elongating amino acids via amide bond formation from the C- to the N-terminus. In SPPS the initial C-terminal amino acid of the sequence is covalently bound to μm sized beads (resin) and the sequence is constructed on-resin before being cleaved into solution. This immobilization onto μm scale beads enables the physical separation of the growing polypeptide chain from the liquid reaction medium by simple filtration through porous material. This makes previously laborious intermediate peptide or final product purifications much simpler as undesired reactants or reaction byproducts that are not covalently bound to the resin are simply washed away. This process speeds up and enables easy purification of each synthetic step, and as a result, overall peptide synthesis becomes quicker. The covalent attachment to the resin via a so-called “linker” facilitates temporary anchoring during the peptide elongation procedure. The covalent bond between linker and resin is orthogonal to the conditions which are applied during peptide synthesis and depending on the linker used, it can be cleaved selectively, at any point during the synthesis.

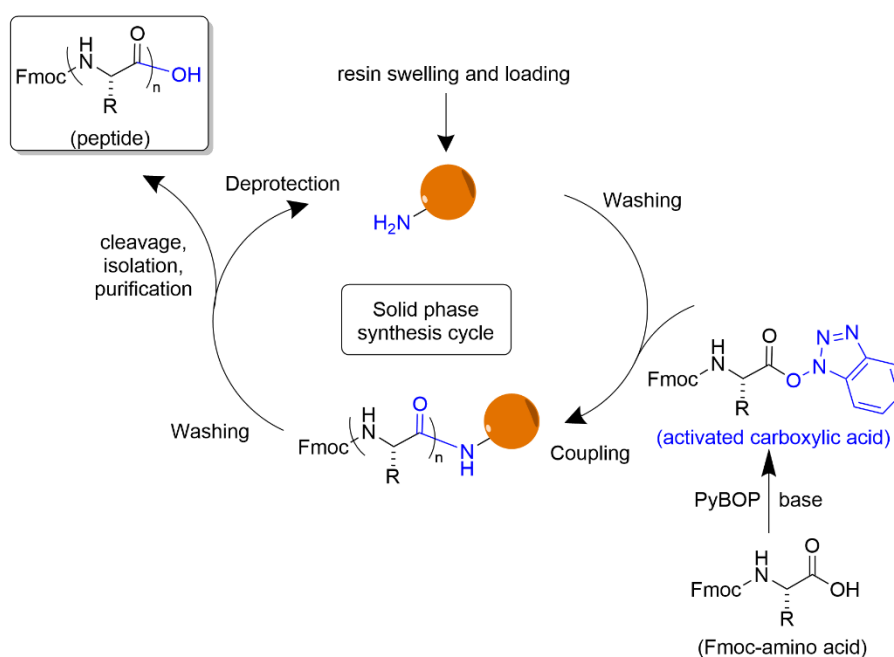


Figure 4 - Solid-phase peptide synthesis cycle. The carboxylic acid of Fmoc-protected amino acids (proteinogenic amino acids) is activated *in situ* (in the presence of the resin) or before addition to the resin. The N-terminal, resin-bound amine reacts with the activated carboxylic acid to form an amide bond (coupling) resulting in chain elongation. The Fmoc group is removed (deprotection) and the sequence can be elongated. Full removal of all side chain protecting groups and resin linker cleavage is usually achieved

simultaneously (cleavage). Resin beads are shown as orange spheres. PyBOP = benzotriazol-1-yloxytripyrrolidinophosphonium hexafluorophosphate

During the last decades, the development of SPPS has progressed by keeping the overall concept invented by Merrifield. In 1970, Carpino introduced the fluorenylmethoxycarbonyl- (Fmoc-) protecting group into SPPS.^[58] The secondary amine-based deprotection conditions enabled the use of acid labile protecting groups on amino acid side-chains, which made the benzyl-protected side-chains and their cleavage with HF (used by Merrifield) obsolete. Additionally, the Fmoc-based strategy is orthogonal to many other protecting groups and has therefore become the most commonly used strategy for SPPS today. Amide coupling conditions, the essential reaction for making peptide oligomers, have been constantly refined. Microwave systems for fine-tuning heat regulation, or novel, more efficient, and less toxic coupling reagents are just two of the parameters changed to improve SPPS procedures.^[59]

As well as the evolution of the synthetic strategies within SPPS, the solid supports on which the peptides are synthesized have also been improved. These now include the most common crosslinked polystyrene (PS)-divinylbenzene beads, as well as polyethylene glycol (PEG) graft resins, PEG-PS, or polyamide supports have been developed.^[60] Since SPPS reactions take place inside the swollen resin network and reaction kinetics are diffusion-controlled, the swelling behavior of a resin is crucial for an efficient solid-phase synthesis. PEG graft resins (such as ChemMatrix) are among the highest-swelling resins and are thus often needed to facilitate long, sterically hindered, and thus difficult syntheses.^[61]

Furthermore, the development of new linkers to connect the growing polypeptide chain to these resins has progressed, enabling varying synthetic strategies on solid support. Specifically, the linker type used for SPPS dictates the conditions needed for cleavage from the resin and determines the C-terminal functional group of the final peptide. Modern linkers which are adapted to the Fmoc-based SPPS strategy can be cleaved by trifluoroacetic acid (TFA), which also cleaves most of the amino acid's side-chain protections simultaneously. The most common linker for obtaining a free carboxyl group on the C-terminus is the Wang-linker.^[62] Primary amides at the C-termini can be achieved by the usage of Rink amide linkers^[63], and also fully side-chain protected peptides can be liberated from the resin by the usage of chlorotriyl or SASRIN (super acid sensitive resin) linkers.^[64] The latter two can be cleaved under very mild acidic conditions. These peptides, which can be used as segments, can be purified, characterized, and reattached to the solid support. This enables the synthesis of longer peptide chains with fragment condensation approaches.^[65] Even if peptide synthesis nowadays became routine, extending peptide chains greater than 50 amino acids, even further to reach protein domain size, is still challenging and often requires either a well-optimized SPPS protocol or adapted synthetic protocols to couple peptide fragments together. In a recent study performed in the Pentelute group^[66], Fmoc-N-protected amino acid monomers were coupled to produce peptide chains up to 164 amino acids long, a length in the range of single-domain proteins. After the synthetic procedure which allowed for relatively high sequence complexity, high purity, and good yields (1–5%), these peptides were able to fold into active proteins that demonstrated similar behavior in activity essays to their recombinantly expressed equivalents. Besides synthesizing proteins or protein-sized peptides in a consecutive, linear manner, even bigger proteins are synthetically accessible via convergent approaches. In a work of Nishiuchi *et al.* ^[67], the

researchers published the chemical synthesis of a 238 amino acid long, green fluorescent protein. To achieve this, they synthesized 26 full side-chain protected peptide segments independently, if necessary purified them, and coupled them together in solution by straightforward amide coupling/condensation reactions. Another approach to synthesizing proteins is native chemical ligation (NCL). Side-chain unprotected peptides are ligated with *e.g.* other peptides at the ligation site by the formation of, for example, thioester, thioethers, oximes, or others but can also be formed with a natural peptide bond.^[68] NCL as a strategy enabled the synthesis of many proteins^[69], one being a 304 amino acid long tetraubiquitin protein.^[70] These examples illustrate the versatility and efficiency with which peptides can be made with SPPS, that with different strategies chemically synthesized peptides can be combined towards functional proteins and that the limitations of SPPS after six decades of research are not yet reached.

Besides linear peptides, cyclic peptides are also fully or partially synthetically accessible via SPPS. A macrocycle, defined by the IUPAC needs a least 12 atoms and can be chemically synthesized by several different routes. Different types can be simply described as head-to-tail, side-chain to side-chain, or side-chain to terminus cyclizations (**Figure 5a**).^[71] The success of cyclizing peptides, especially head-to-tail, is often ring size-dependent. Smaller peptides (<7 amino acids) are often problematic whereas peptides with a greater amount of α -amino acid residues are considered easier to cyclize.^[72] To successfully establish cyclization, the linear peptide precursors must be arranged in a way so that the reactive ends, which take place in the cyclization reaction, are in close spatial environment. The extended conformation of a peptide, which is often not the conformation that promotes cyclization, is the energetically favored conformation. Strategies for conformational preorganization, which often include the energetically disfavoured *cis* amide bond configuration, are thus sometimes needed to facilitate macrocyclization. They can be achieved by internal- and external conformational elements. Internal conformational elements such as N-alkylation, L- to D-amino acid exchange, and use of prolines or pseudoprolines (threonine or serin derivatization) are chemical modifications of the peptide main chain. The addition of metal ions such as Na, Li, Cs, or Ag are examples of external conformational elements and are usually added to the cyclization reaction without chemical modification of the peptide main chain. Metals such as Na can coordinate to amide oxygens atoms along the peptide chain, which bends the peptide and brings its C- and N-terminus into proximity. Those can then cyclize in a head-to-tail fashion readily.^[73] Both strategies promote difficult macrocyclizations for certain examples.^[71] Macrocyclization reaction conditions overall sometimes need to be fine-tuned because the reaction is prone to oligo- or polymerization. Highly diluted conditions reduce undesired intermolecular reactions. Another possibility is to perform macrocyclization on solid support. Bound to the beads, the linear peptides can not diffuse in the solvent which reduces the risk of intermolecular processes provided that the resin loading is low (below 0.5 mmol/g).^[74]

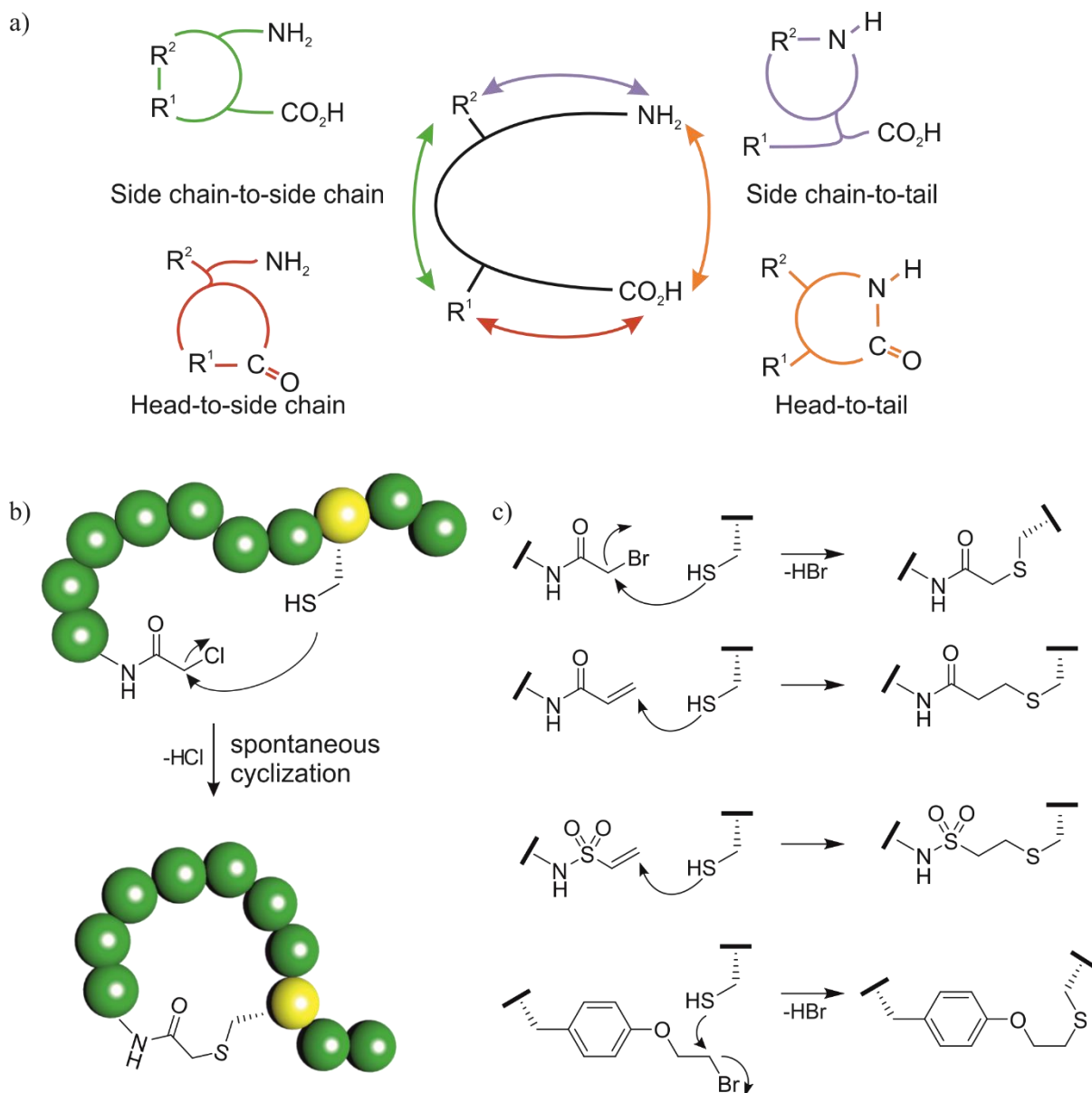


Figure 5 – Peptide macrocyclization. a) Possibilities a peptide can be cyclized. b) Spontaneous peptide cyclization by the formation of a thioether between a cysteine thiol and an N-terminal chloroacetamide. Amino acids are represented as green balls; cysteine as yellow balls. c) Other bioassays compatible macrocyclization reactions that form thioether bonds.^[71, 75]

The most suitable amino acid side chains for reactions towards peptide macrocycles resulting in different bond types are lysine (amides), cysteine (disulfides, thioethers), and tyrosine (ethers) or glutamic acid (esters).^[76] The thioether can be formed by the cysteine thiol, which is a nucleophile that can react with electrophiles such as bromo-, chloroacetamide moieties, vinyl acetamido groups (second scheme in **Figure 5c**), or Michael acceptors (*e.g.* vinyl sulfonamides, see **Figure 5c**).^[75] The reaction can be triggered by the deprotonation of the thiol group on Cys residue by pH raising from acidic to basic (pH 8). The S_N2 reaction with chloro- or bromoacetamide which provides peptide macrocycles *i*) does not need additives for the reaction to progress, *ii*) is regioselective and *iii*) the formed thioether bond is stable under physiological conditions.^[77] The reactive moiety can be tethered to side chains *e.g.* ornithine^[78] or the N-

terminus of the peptide, the latter being particularly relevant for mRNA display technologies (see Chapter: “Screening Methods”). As an alternative, the phenol group of Tyr residues can be derivatized to *O*-[2-bromoethyl-]tyrosine^[79] which reacts with Cys side chains similarly and is also compatible with peptide screening technologies such as phage display. In a work of Owens *et al.*^[80], the researchers developed a strategy to generate combinatorial libraries of peptide macrocycles linked via the side-chains of Cys and modified Tyr with a thioether linkage. The post-translationally occurring cyclization was integrated into bacteriophage display, enabling the generation of an up to 10⁸-membered library of peptide macrocycles. Screening this library against three different protein targets resulted in three high affinity ligands each having nanomolar affinity. As peptide macrocycles gain increasing interest as potential therapeutics, methods for generating combinatorial libraries and screening these libraries against biological targets have been developed.

Screening Methods

Phage display

Natural peptide macrocycles are used in the pharmaceutical field and some of their structural motifs have been a source of inspiration for scientists to develop new peptide-based drug candidates. High throughput screening methodologies provide access to new peptide macrocycle architectures and can be exploited for pharmaceutical applications and relevant targets. There are various technologies to identify new peptide molecules as potential binders for a variety of biological targets. In 1985, phage display technology was published for the first time and awarded the Nobel Prize in 2018.^[81] Libraries (up to 10¹⁰ individuals) of peptide sequences (or full-length proteins *e.g.* antibody fragments) are expressed by bacteriophages in a way that each virion carries the genetic material for a semi-randomized but unique peptide to be expressed as a fusion construct with the virus coat protein. These bacteriophage-peptide fusion libraries can then be screened against an immobilized target of interest (**Figure 6**). Peptide binders with their fused phage bind to the target and non-binders are removed in the subsequent washing steps. Binders can then be isolated and clonally amplified in bacterial hosts. Iterative rounds of this selection process can lead to high-affinity peptides. Identification of the top-binding peptides is performed by sequencing the viral strains that remain after these rounds of selection.^[82] This technique has provided high-affinity antibody fragments one being adalimumab, the first clinically approved humanized antibody.^[83] Using phage display to screen for high affinity proteins has been also successful and led to FDA-approved drugs namely *i*) ecallantide, a small protein kallikrein inhibitor for the treatment of hereditary angioedema, *ii*) romiplostim a protein analog of thrombopoietin to treat an autoimmune disease called immune thrombocytopenic purpura and *iii*) the withdrawn glucagon-like peptide 1 receptor agonist albiglutide for the treatment of type 2 diabetes.^[84]

Combining the phage display technology with peptide macrocyclization strategies has been successful yet this is often limited to the formation of disulfides, which are rather unstable in biological environments^[85], or posttranslational chemical cross-linking reactions.^[86] Another drawback of this technology, with some specific exceptions, is its restriction to the repertoire of 20 canonical amino acids.

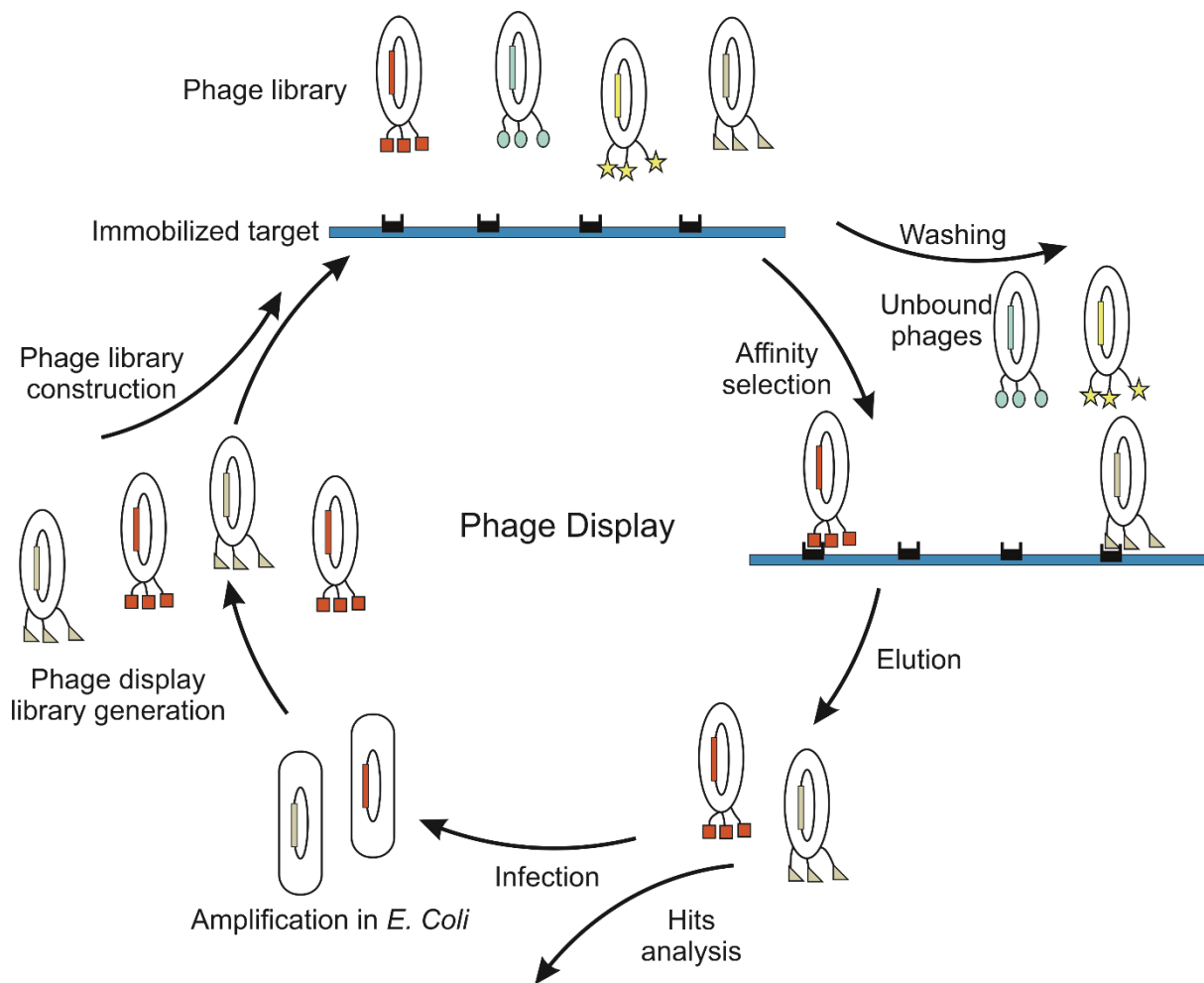


Figure 6 – Phage display cycle. The immobilized target is presented to the phage-displayed library. After incubation, unbound or nonspecific phages are washed away. Phages that carry on their surface a peptide with specific affinity to the target bind and can be recovered by an elution step. The eluted phages can reinfect *E. Coli* and be amplified. These phages can be added to the next round of selection.

mRNA display

A cell-free, alternative peptide screening technology is mRNA display and was originally studied by Roberts and Szostak.^[87] The first high-affinity binding peptide selected using mRNA display was published in 2001.^[88] A linear randomized polypeptide library (10^{12}) each individual 80 amino acids long, was screened against ATP and led to four ATP binding proteins. Similar to phage display, mRNA display applies a linkage between genotype (mRNA) and phenotype (expressed peptide). The linkage of mRNA to its cognate translated peptide is facilitated by puromycin – an antibiotic that mimics tRNA – which connects the 3'-end of the mRNA with the C-terminus of the translated peptide via an amide bond. Similar to phage display, these hybrid structures can be screened against an immobilized target of interest. Ligands with low affinity are removed by washing steps whereas those with high affinity remain bound to the target. The genotype of these high affinity binders can be recovered and amplified by polymerase chain reaction (PCR). This pool of DNA now contains the genetic information of peptides with an

increased binding affinity to the target compared to the starting library. This DNA can be transcribed to mRNA and iteratively screened against the target to enrich the library with exquisitely high affinity ligands. Hits can be identified by DNA sequencing. A major advantage of mRNA display over phage display is that the technology operates without relying on a living translation system. Libraries from 10^{12} to 10^{14} peptide-mRNA hybrids are thus possible.^[82b, 89] Another advantage of this technology is that it allows for post-translational chemical modification such as macrocyclization, as long as they are compatible with the translation machinery. For example, Millward *et al.*^[90] introduced an activated diester (disuccinimidyl glutarate) to cross-link N-terminal amines with downstream ϵ -amino lysine side chains via amide bond formation to produce a library of peptide-macrocycles fused to their encoding mRNA. In a later study, the same researchers identified peptide macrocycles as inhibitors of the signaling protein G α i1 which exhibited nanomolar affinities for their target.^[91] Another key advantage of mRNA display over phage display is that it allows expansion of the repertoire of the 20 cognate amino acids by, for example, genetic code reprogramming approaches, as described below.

FIT and RaPID technologies

Non-standard amino acids can be incorporated into peptides by using a flexible *in vitro* translation (FIT) system. In this FIT system, the genetic code which encodes for a peptide sequence can be reprogrammed with the use of special RNA-based enzymes (flexizymes). Flexizymes are artificially evolved, highly flexible ribozymes which can charge tRNA with canonical or, crucially, non-canonical (amino) acids.^[92] In a cell-free system such as mRNA display, the tRNA acylated with the desired acid substrate can be supplemented into the *in vitro* mixture of the translation machinery. The anticodon of the charged tRNA hybridizes with its complementary mRNA codon and the cargo acid is incorporated during translation by the ribosome in the peptide sequence. This allows the reassignment of mRNA codons from their cognate amino acids to other, chosen (amino) acids. A polypeptide can thus be modified at one or multiple desired positions. The flexizyme as well as the ribosome have shown remarkable tolerance for non-canonical amino acids or even more sophisticated building blocks. Among these, N-alkylated amino acids^[93], D-amino acids^[94], β -amino acids, γ -amino acids^[94a], as well as α -hydroxyacids^[95], fluorophores^[96], terpenes^[97], different kinds of aromatic and non-aromatic foldamers^[98] and many other (amino) acid variations.^[99] Furthermore, the insertion of a reactive moiety that can mediate intramolecular cyclization reactions has been successful. The chloroacetamide functionality, a reactive electrophile, can be incorporated at the N-terminus of translated peptide sequences allowing spontaneous intramolecular cyclization with the first downstream cysteine moiety (with some exceptions).^[100]

When FIT is integrated into mRNA display it is referred to as RaPID (Random non-standard Peptide Integrated Discovery). RaPID can serve as a tool to screen libraries of peptide macrocycles (up to 10^{14} individuals) with “nature-like” structures and properties against targets. The incorporation of non-canonical amino acids into this system can reduce biodegradation, and increase membrane permeability or binding affinity of the peptide macrocycle.^[77] With this technology, high-affinity peptide-macrocyclic binders against various targets have been screened and identified. In a work of Kawamura *et al.*^[101], a 14-residue peptide macrocycle, with nanomolar affinity against a histone lysine demethylase subfamily 4 (KDM4 isoforms A–C)

involved in tumor cell proliferation, was identified via RaPID. An X-ray crystal structure of the histone-peptide macrocycle complex was obtained and guided further derivatization of the first hit resulting in a more proteolytically resistant macrocycle peptide. In another work performed by Jongkees *et al.*^[102], the authors screened a library consisting of 10^{12} peptide macrocycles with the RaPID system against HPA, a pancreatic amylase that is a clinical target to treat obesity and diabetes. They implemented a non-canonical amino acid with a structural motif of L-DOPA into their library. A nonapeptide macrocycle ligand exhibiting a 7 nM K_i for the protein was identified and successfully co-crystallized with HPA. Additionally, the ligand showed selective inhibition of the target protein over related enzymes. Both examples highlight that RaPID system provides peptide macrocycles with nanomolar affinity and high selectivity against pharmaceutically relevant protein targets. Commercial screening companies such as PeptiDream use this technology to provide high-affinity binders to their customers.^[103]

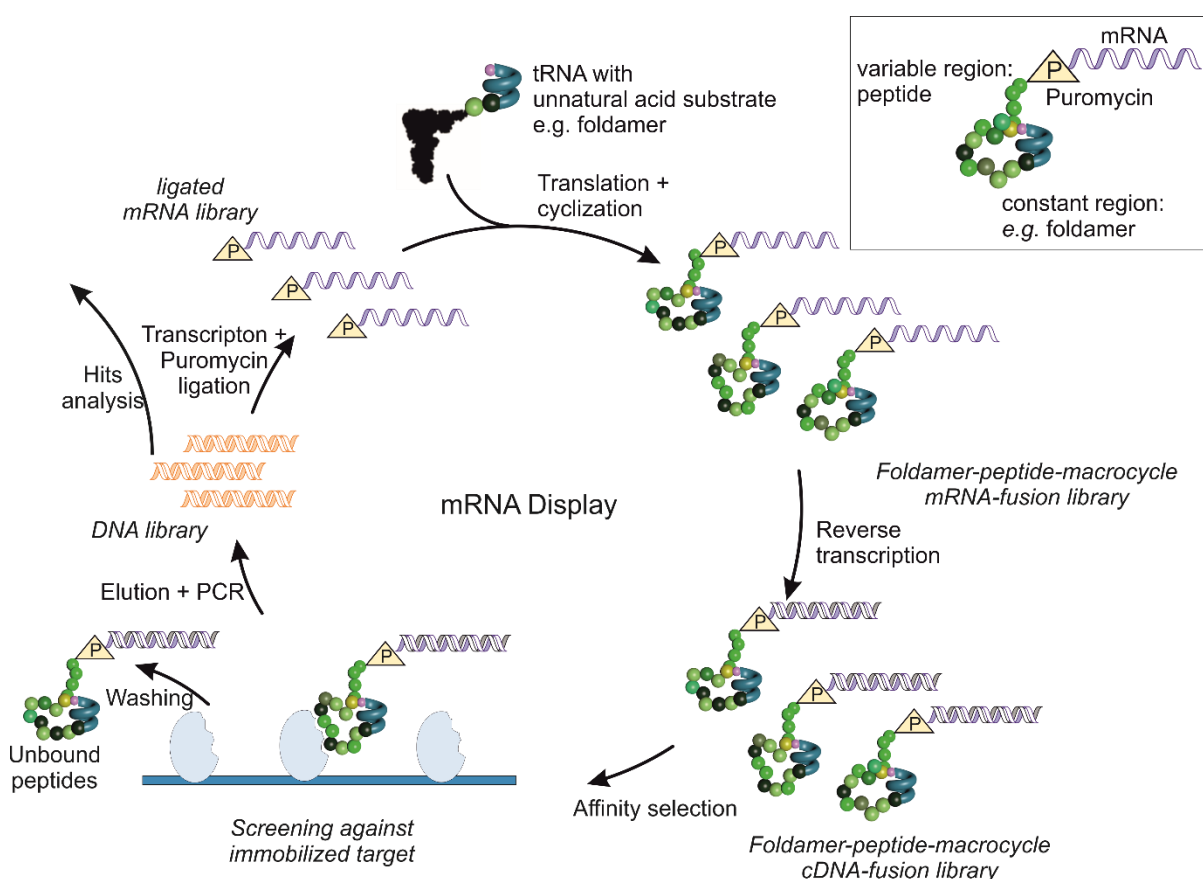


Figure 7 - RaPID selection of macrocyclic foldamer-peptide hybrids against an immobilized target.

The RaPID selection cycle starts with a semi-randomized DNA library which is transcribed to a 3'-puromycin mRNA library. Puromycin, a protein synthesis inhibitor, forms a covalent linkage between the peptide and its encoding mRNA. Translation of this library in a FIT reaction leads to a library of peptide macrocycles with its covalently linked cognate mRNA. This fusion library is then reverse transcribed which generates the cDNA of each mRNA and the library is screened against an immobilized biomolecule (e.g. protein target). Peptides with high affinity are retained initially and then eluted afterward. The cognate DNA, which encoded the peptide binder, can be recovered by PCR which results in an enriched library. This process can be repeated iteratively until the library converts to consensus sequences. Next-generation sequencing of the enriched DNA library leads to clone identification.

Recent studies showed that the ribosome translation machinery can accommodate short helically folded aromatic oligoamides (foldamers) into the peptide sequence. Cyclic and non-cyclic foldamer-peptide hybrids could thus be produced.^[98b, 104] Studies, on if these hybrids are compatible with mRNA display selection experiments (**Figure 7**) are part of this thesis and are described in paragraph 8. There is hope that inserting foldamer moieties into peptide macrocycles may lead to functional improvements such as increasing cell-penetration properties.

2.2. Foldamers

General Introduction

In nature, proteins are large folded objects that are responsible for catalytic processes, signal transduction, and biomolecule recognition, among other processes. Proteins are composed of peptide chains that often preorganize into well-defined, specific, and compact conformations. These complex three-dimensional architectures, the result of millions of years of evolution, arise from a folding pattern regulated and dictated by the primary amino acid sequence. Protein folding is a spontaneous occurring process mediated mainly by hydrogen bonding, but also by van der Waals interactions, backbone angle preferences, electrostatic interactions, chain entropy, disulfide bridging, and hydrophobic interactions. General folding motifs include sheets and helices which are connected by turns and loops.^[105] These are examples of protein secondary structures and they are largely defined by site proximal hydrogen bonding between amides in the peptide backbone. Also, the specific primary sequence of side-chain appendages determines the permitted angular rotation around the peptide bonds, leading to these different secondary structures. Yet, peptide fragments composing proteins do not have a stable conformation when they exist alone. Long-range interactions which are present between non-adjacent amino acids in the protein are essential for conformational stability.^[106] As a result, amino acid functional groups dictate the three-dimensional protein structure and this form of preorganization is crucial for most of the activity of the protein.

Many chemists have used these protein folding patterns as inspiration to generate artificially folded molecules. Many have sought to mimic architectures similar to what nature provides but are more remote, distinct, versatile, and predictable. These so-called “foldamers” *i.e.* polymers with a strong propensity to fold into a specific compact conformation^[107], can be built up from a repertoire of unnatural building blocks distinct from what nature can provide. Proteins are encoded by a repertoire of only 20 canonical amino acids, whereas foldamers are not dependent on such a restriction. Building blocks, so-called monomers, can be elongated stepwise or by iterative chemical reactions towards foldamers with the only limitation being synthetic accessibility and availability of building blocks. In contrast to what is found in nature, foldamers are not restricted to a single class of building blocks for a particular polymer and can be combined to form heterogeneous oligomers as a broad variety of different monomer classes are accessible. There are several different approaches to mimic folding, which differ mainly by the choice of monomers and their chemical linkages. The foldamer field, a part of supramolecular chemistry, is constantly expanding, and some notable examples are discussed below.

The most common secondary structure motif found in an average globular protein is the α -helical structure (*i.e.* 30%).^[108] Hydrogen bond interactions between backbone amide hydrogens and

amide carbonyl groups are fundamental to induce the α -helix conformation, a stable, right-handed peptide spiral with a pitch of 5.4 Å and 3.6 residues per turn. The amino acids pack densely with almost no space in between the helix. The amide backbone is located in the centre, while the amino acid side chains point outward (**Figure 8a**). Helix formation is mainly driven by the peptide sequence, the amino acid side chains, and is dependent on the surrounding environment to which the peptide is exposed.^[109]

Foldamers developed to reproduce the secondary structure of peptides can be referred to as peptidomimetics or biotic foldamers. Monomers used to build peptidomimetic foldamers can be modified so that the side chain composition is more versatile (compared to amino acids). The core structure of the monomer can also act as a constraint to stabilize a desired secondary structure.^[110] Further, the peptide backbone can itself be systematically modified. For example, poly-N-substituted glycines, also called peptoids, are a class of foldamers where the amide protons are substituted with alkyl groups to tertiary amides. The lack of stereochemistry on the α -carbon makes the monomers achiral and the absence of the amide hydrogen prevents the formation of intramolecular C=O:H–N hydrogen bonds found in natural amino acid backbones. Folding of this class of molecules is thus characterized by steric and electronic interactions which show stability in a wide range of solvents.^[111] Already short, pentameric peptoid sequences fold into stable helices similar to peptidic α -helices.^[112]

Notable examples are β -amino acid oligomers, so-called β -peptides. A polymer composed of β -amino acids that each carry one additional α -methylene group might be expected to be more flexible, however, this family of polyamide oligomers adopts remarkably well-defined, stable secondary structures such as turns, β -sheet-like arrangements, and helices.^[113] Gellman studied β -peptides in which the backbone carbons were cyclized towards short 3-, 4-, 5- or 6-membered carbocycles which substantially increased rigidification. This class of oligoamides folds into stable helices which are dictated by intramolecular C=O:H–N hydrogen bonds.^[114] Besides folding, β -peptide oligomers show greater tolerance to enzymatic degradation compared to their α -counterparts.^[115]

Another prominent peptidomimetic scaffold is the oligoureia-based foldamer consisting of *N,N'*-linked urea bridging units. These γ -peptide-like foldamers originated by the Guichard group, have a strong propensity to fold into helical secondary structures in the solid state and in solution, in a similar manner to α -helices in respect to both helix macrodipole and pitch (**Figure 8b**). The stabilization is promoted by conformational backbone restrictions and a remote hydrogen bonding network. The hydrogen bonds are three centered between the carbonyl C=O, the urea N–H (*i*-3), and N–H'(*i*-2) to form 12- and 14-membered pseudorings.^[116] Folding is largely independent of the side chains which stand in contrast to naturally occurring peptidic α -helices. When combining oligoureias with short peptide sequences to form hybrid sequences, the folding propensity of the urea part propagates and induces folding on the peptidic segment towards a continuous helix.^[117] Further, oligoureias can be considered for possible biological applications as they show strong resistance toward proteolytic degradation^[118], modulate PPIs^[119], penetrate cells^[120], and can mimic bioactive peptides.^[121]

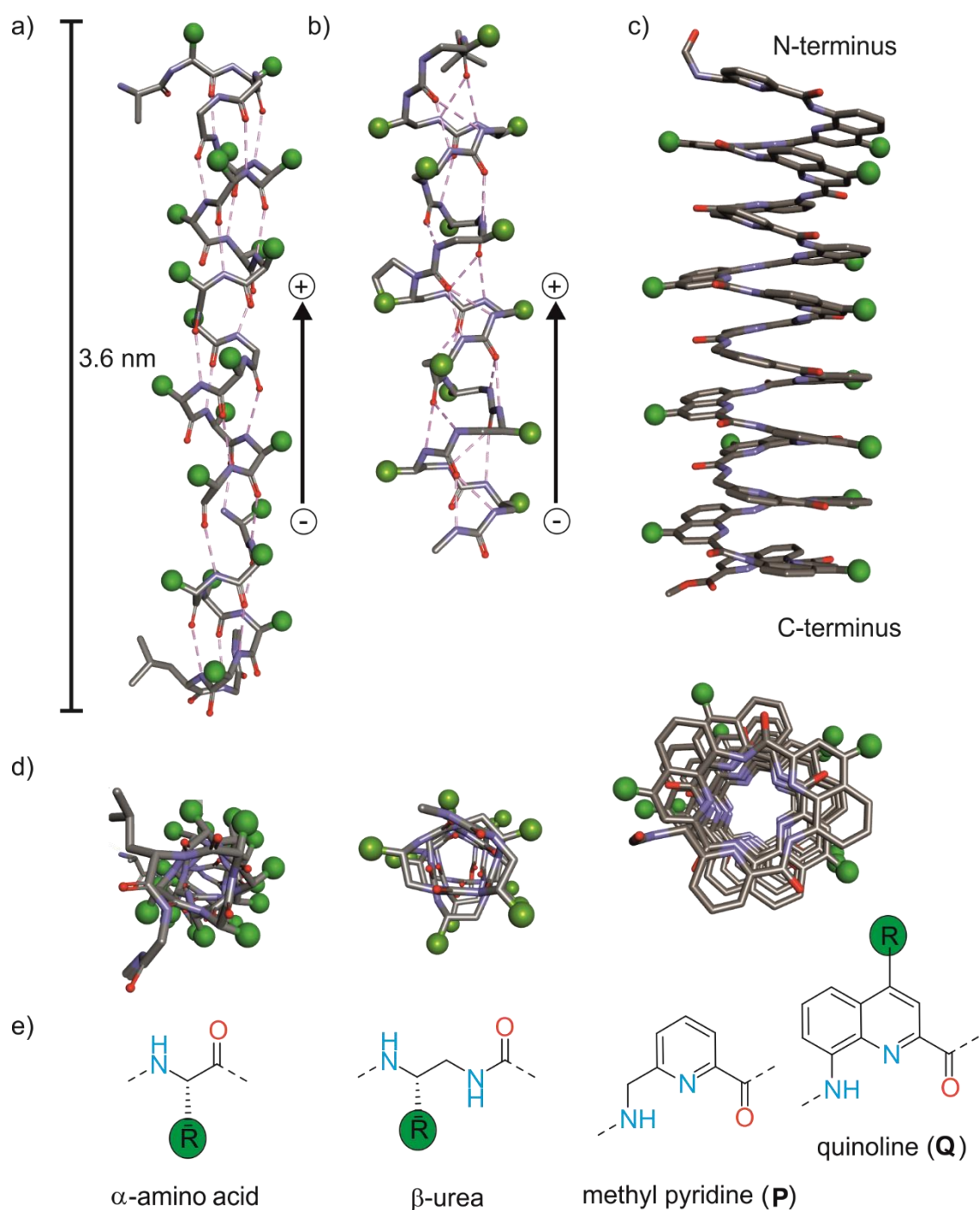


Figure 8 - Helical folding. Side view X-ray crystal structure of a) natural peptide α -helix in a protein (blackfin tuna myoglobin, PDBID: 2NRL)^[122] one helix shown in stick and ball representation the rest of the protein omitted for clarity. b) a biomimetic oligourea helix (CCDC: 836811)^[123] c) and an abiotic aromatic oligoamide foldamer helix (CCDC: 745001)^[124] (Boc-(PQ₄)₄-OMe) and d) their top views all shown on the same scale in stick-and-ball representation. e) Chemical structure of monomers. Green balls represent placeholders for side-chains. Arrow indicates macrodipole. Hydrogen bonds are shown in pink dashed lines.

Peptoids, β -amino acid-based foldamers, and urea-based foldamers can be classified as biotic foldamers as they share a folding principle that is similar to what can be found in nature. Moreover, they consist of an aliphatic backbone and the monomers of which they are composed

are derived from α -amino acids. In contrast, abiotic foldamers rely on folding principles that are distinct from what is found in nature. Abiotic foldamers are often aromatic. Among these, aromatic amide-based oligomers have emerged as a successful class of foldamers. This success stems from remarkable properties such as highly predictable folding, high stability, and ease of synthesis. Quinoline-^[125], pyridine-^[126], pyrazine-^[127], benzene-^[128], and anthracene-based^[129] are, a few among other, aromatic building blocks which form abiotic foldamers.

One of the most successful examples of aromatic oligoamide foldamers is based on fully or partially repetitive sequences of 8-amino-2-quinolinecarboxylic acid (**Q**) monomers. They are a remarkable class of abiotic foldamers and have been successfully utilized in a variety of different scientific applications for example B-DNA mimicking foldamers^[130], host-guest complexation^[131], charge transport^[132], and as molecular shuttles^[133]. Homo-2,8-substituted **Q** oligomers form stable helices where helix pitch is governed by the overall configuration of the aromatic ring (**Figure 9**). In all oligomers, the **Q** building blocks are connected via amide bonds and the positioning of the NH aniline group on the **Q** induces helix curvature. For example, foldamers synthesized with 2,8-substituted **Q** monomers are oriented at a 60° angle, with respect to each other, which results in 2.5 units per turn. Other substitution patterns such as *e.g.* 2,7-quinoline (**H**) result in a 120° angle^[134] which have been introduced in foldamer sequences in which different aromatic building blocks were combined (**Figure 9c**). In addition, 2,6-quinoline oligomers^[135] can adapt, when there are additional sterically demanding side chains, and linear rods as their substitution pattern results in a 180° angle. (**Figure 9d**)

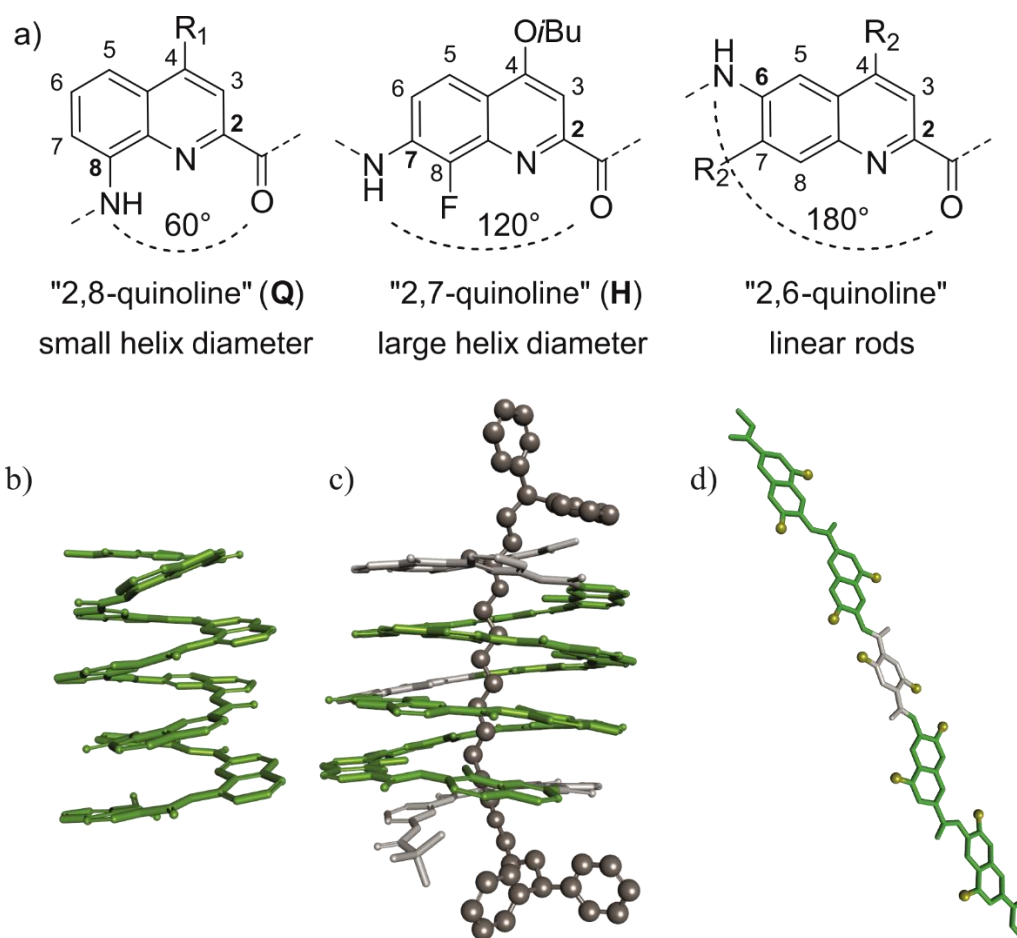


Figure 9 – Monomer design and folding shape. a) Different quinoline monomer substitution patterns that configure the resulting foldamer helix diameter, which enables narrow or wider helix diameter or linear foldamer rods. R_2 : $\text{OCH}_2\text{CH}(\text{CH}_2\text{CH}_3)_2$ b) X-ray structures of a foldamer helix consisting of 10 consecutive 2,8-**Q** units^[136] (CCDC: 630236) c) X-ray structures of a foldamer-amido carbamate host-guest complex^[137] (CCDC: 1868144). d) X-ray structure of a pentamer rod^[135]. Quinoline units are colored in green, other monomers are dyed in light grey. Guest dyed in dark grey and ball and stick representation. All side chains are omitted for clarity.

In 2,8-**Q** oligomers, the helix cavity is extremely narrow, usually allowing the occupation of only one proton, whereas in other substitution patterns *e.g.* 2,7-oligomers, usually combined with other monomers such as pyridines or anthracenes, a cavity within the foldamer with a much larger volume is generated (**Figure 9**). This cavity can be filled with guests such as ions, organic acids, or carbohydrates.^[131] Besides this, **Q** monomer functionalization with a variety of side chains has been developed over the past two decades (**Figure 10**). Polar or non-polar groups allow for the fine-tuning of solubility in almost all solvents^[134a] but do not alter helix shape. The hydrophobic nature of aromatic **Q** foldamers can be thus compensated by the usage of anionic, cationic, or hydrophilic side chains to achieve fully water-soluble foldamers.^[138] Besides that, **Q** side-chain modification allows altering the overall foldamer side surface which enables functionalization^[139], interactions towards other surfaces (*e.g.* proteins)^[140], or foldamer-foldamer side chain communication.^[141] 2-(2-aminophenoxy)acetic acid (**B**) and 6-(aminomethyl)pyridine-2-carboxylic acid (**P**) monomers are two additional classes of aromatic units which have been developed to enlarge the monomer repertoire while maintaining the same 60° angle curvature of the helical folding when they are incorporated in a **Q**-rich foldamer sequence.^[142] In comparison

to the quinoline ring, both monomers have a reduced surface for aromatic stacking, which reduces hydrophobicity. The presence of a rotatable bond in these two monomers affords additional flexibility which allows helical folding disruption and thus a quicker helix handedness interconversion rate in comparison to pure **Q** foldamers.^[142]

One major advantage of using oligoamide foldamers is their full synthetic accessibility on solid support. Repetitive monomer couplings can be performed which builds up the quinoline oligoamide foldamer sequentially on the resin. However, compared to solid phase peptide synthesis, where the amide bond is formed between an aliphatic amine and a carboxylic acid, the quinoline amine is less nucleophilic reactive due to the adjacent electron-poor ring, and, folding after one helix turn which occurs on resin hampers the reactivity further.^[134a] Thus, to enable high conversion yields which are inevitable during solid phase foldamer synthesis, the carboxylic acid which is involved in the amide bond formation has to be activated via an acid chloride before coupling. Activating the Fmoc-protected quinoline carboxylate via tetramethyl- α -chloroamine (Ghosez's reagent) or an modified Appel reaction (trichloroacetonitrile, triphenylphosphine and collidine) have been proven to be the most successful and practical methods (**Figure 10**).^[143] The acid chloride formation with Ghosez's reagent has the disadvantage of being performed in a separate reaction step, due to the side reaction with the solid-phase bound free amine terminus (the chloroamine acts as an electrophile and terminates the resin bound amine upon nucleophilic amine attack). This makes the activation step more time-consuming and laborious. The activation via the Appel reaction can be performed *in situ*, which means in the presence of an unprotected free amine, without the risk of terminating the amine. As no separate activation step is required, and carboxylic acid activation and amide bond formation can be performed in one vessel, the process (activation + coupling) is thus quicker. Synthesizing quinoline-based oligoamide foldamers via an Appel reaction has recently led to an automatized foldamer synthesis process.

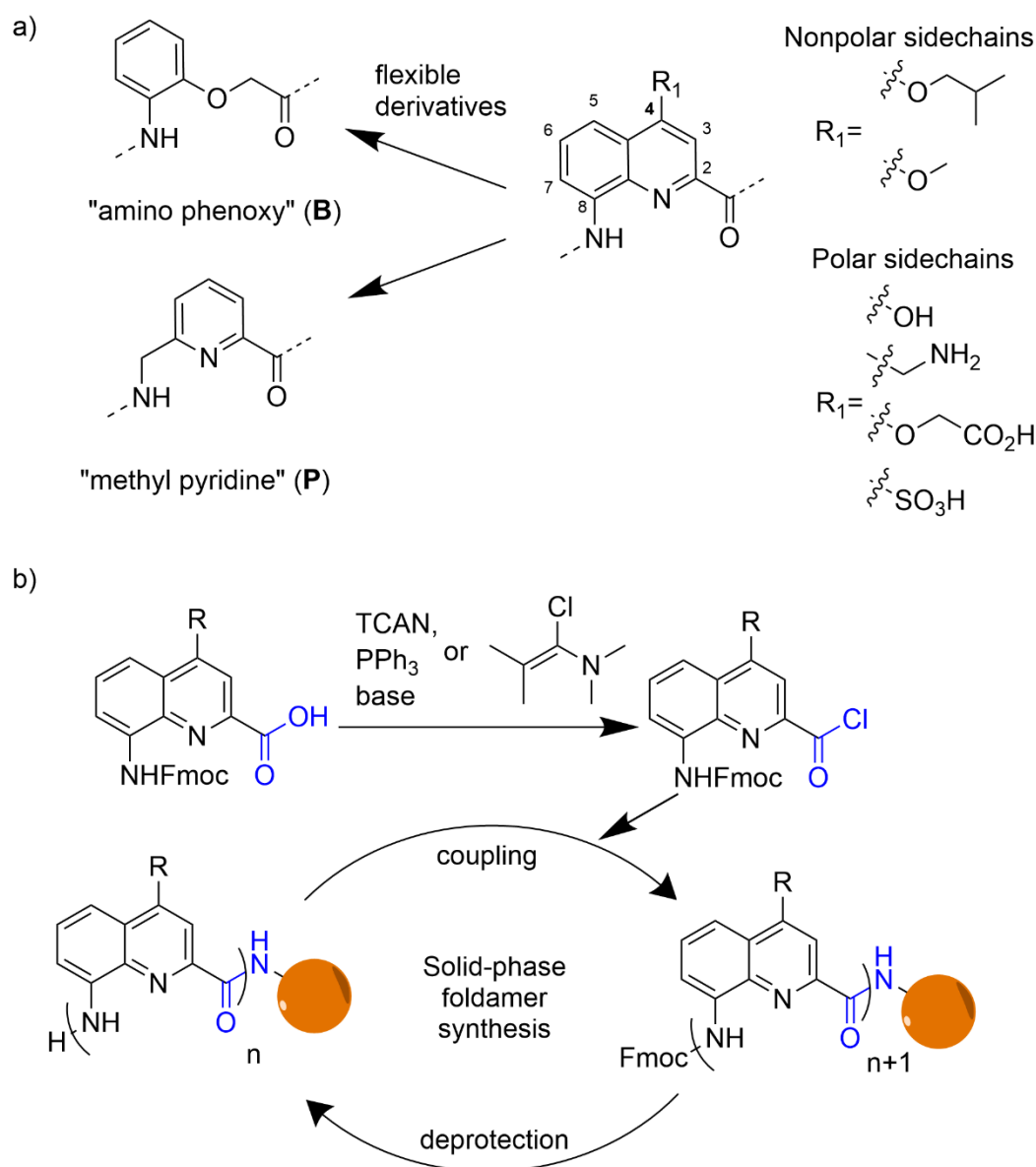


Figure 10 – Monomers and their design. a) **Q**, **B** and **P** monomer backbone. **B** and **P** are less rigid **Q** derivatives with the same resulting foldamer helix diameter. Some nonpolar and polar **Q**-side chains in position four on the quinoline ring are shown exemplarily. They allow solubility of the resulting helical foldamer in different solvents. b) **Q**-monomer carboxylic acid activation via the formation of an acid chloride to enable solid-phase foldamer synthesis. TCAN: Trichloroacetonitrile

Folding

The folding reaction is driven by multiple non-covalent interactions between non-adjacent monomer units and transforms conformationally disordered molecule chains into folded architectures. The folding reaction for foldamers is by definition dynamic, *i.e.* a foldamer can unfold and refold depending on different factors *e.g.* temperature, pH, salt concentration, or solvent. This order-disorder transition stands in contrast to „locked“ conformational preorganized molecules such as helicenes which are not considered foldamers.^[144] The equilibrium between the folded and unfolded states of a foldamer is thermodynamically driven and favors the folded state

when its energy minimum is much lower than the unfolded state. To reach this energy minimum, favorable energetic interactions have to be maximized and unfavorable interactions minimized. Gain in entropy of the environment by *e.g.* release of water due to hydrophobic interactions or the increase of enthalpic interactions *e.g.* hydrogen bonds have to be strong enough to compensate for the unfavorable entropy loss which is present when flexible molecules fold. The folding of oligomers is dictated by internal and external parameters. Internal parameters are mainly guided by the building blocks which are embedded in the sequence and which later define the overall conformation. Size, shape, linkage orientation, and rotational restrictions of the chosen monomers are the most important parameters which govern if, and to what form, the final foldamers can establish intramolecular non-covalent interactions. External factors which guide folding are solvent effects, host-guest complexation, aggregation, and surface interactions.^[144-145]

Oligoamide foldamers, based on the 2,8-quinoline (**Q**) building blocks require 2.5 units per turn so three consecutive **Q** units have already a helical shape. In comparison, a **Q** dimer results in a bent, flat conformation.^[134a] Stable folding of **Q** oligomers towards helices is based on synergistically occurring effects. Due to steric clashes of the extremities, a torsion into either a right- (*P*) or left- (*M*) handed helix is forced with three or more consecutive **Q** units (**Figure 11**). Folding is mediated by bifurcated hydrogen bonds between amide N–H and endocyclic, adjacent **Q** nitrogen atoms. This results in an eight-membered hydrogen-bond network between the two neighboring monomers which results in a strong force towards folding. Furthermore, electrostatic repulsion between amide carbonyls and endocyclic **Q** nitrogen atoms drives **Q** units into a bent conformation. Aromatic **Q** rings, which are embedded in multiturn helix curvatures stack over each other, giving rise to strong π - π interactions.

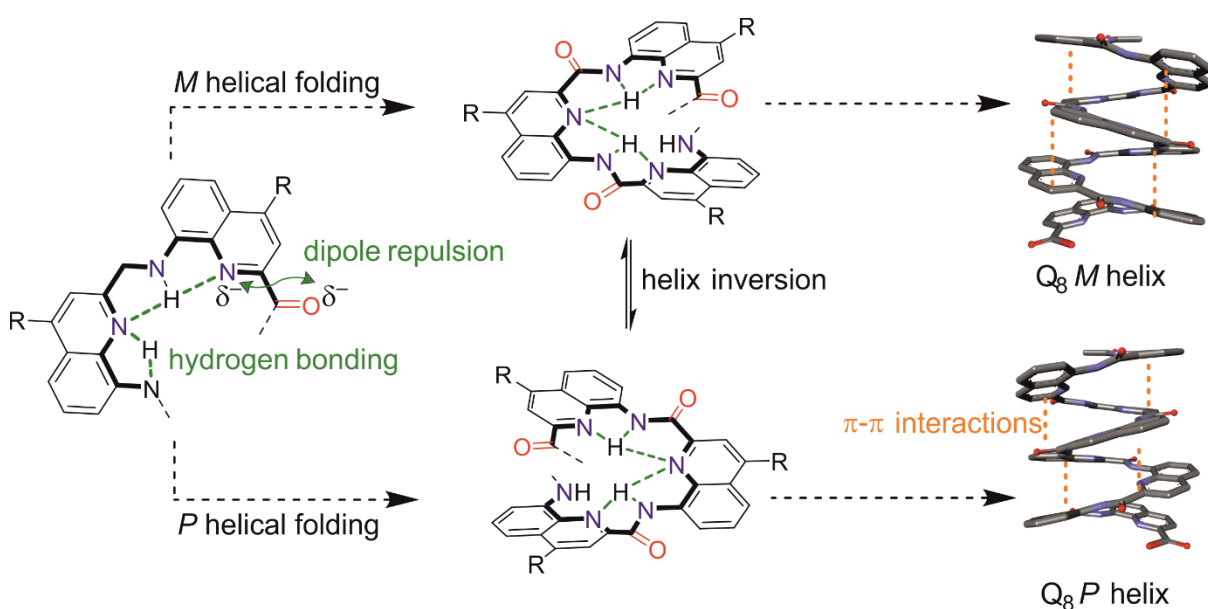


Figure 11 – Quinoline helix folding. Non-covalent interactions (dipole repulsion and hydrogen bonds) which mediate folding are indicated by green lines. π - π interactions are indicated in orange. Without a chiral group, **Q** helical structures fold into 50% left (*M*) and 50% right-handed (*P*) helices.

The overall dynamics of helix interconversion between *M* and *P* enantiomers through partially unfolded intermediates are dependent on helix length, temperature, and solvent. Longer helices undergo interconversion slower than shorter helices if the solvent and temperature are the same. Increasing temperature also increases the helicity interconversion rate. For example, the helix-handedness inversion half-life of a **Q** heptamer helix is 30 minutes in comparison to an octamer which is two hours in the same solvent mixture (hexane/chloroform) and same temperature (at 30 °C).^[146] In polar solvents, overall helix-handedness (h-h) inversion is much slower; a **Q** pentamer needs several hours to invert its helicity.^[147] A **Q** octamer helix, for example, does not show any sign of h-h inversion even at 120 °C in pure DMSO^[134a] whereas in pure chloroform a **Q**8mer, has a half-life of h-h inversion of 6 min at room temperature.^[148] Thus, the helicity of water-soluble **Q** octamers can be considered locked on a laboratory time scale. Overall, **Q** monomer-based folded helices are extremely stable. Furthermore, the mechanical stability has been experimentally investigated by atomic force microscopy (AFM)-based single-molecule force spectroscopy. In this study, different **Q** foldamer helices were covalently immobilized on a gold surface. The helices were slowly stretched by moving an AFM-tip in a controlled manner upwards until intramolecular foldamer interactions broke and the helix unwound. The forces which were necessary to unwind the helix were by one order of magnitude greater than in comparable biological systems for example peptide α -helices of similar length. After helix unwinding, the **Q** foldamer applied strong forces against the pulling force to rewind quickly back into the folded, helical state.^[149]

When not equipped with a chiral group, **Q** helices present *P*- and *M*- helices in equal proportions in solution and the solid state. Helix handedness can be controlled by placing chiral monomers on the C-^[150] or N-terminus^[151] or, as described in a recent study, within the foldamer sequence. In this study performed in our group by Bindl *et al.*^[152], a chiral benzene-based monomer (**B**^{RMe}) was developed as a δ -peptidic analog of **Q**. This **B** monomer carries a stereogenic methyl group with an *R* configuration. Upon introduction into a **Q** oligomer, the CH₃ group is embedded in between the aromatic backbone units of the helix which results in an energy imbalance between the compact *M* or *P* foldamer conformations. As a result, the foldamer helix is biased towards *M* helicity and – if the *S* version of the **B** monomer is used – *P* helicity. This enables the synthesis of (almost) quantitatively chiral **Q** sequences with leaving both ends of the helix available for further modification such as functionalization with a chromophore, protein ligand, or introducing the foldamer sequence in a head-to-tail macrocycle.

2.3. Cyclic Peptide - Foldamer Hybrids

The folding properties of single-stranded helices, sheets, and turns rely primarily on small-range interactions between monomer residues which are adjacent, or very close in the oligomeric chain, to each other. Long-range interactions, so, interactions that are further apart in the oligomeric chain, can be observed in folded biomolecules such as proteins or nucleic acids and are often responsible for higher-ordered structures. These are more difficult to access in abiotic foldamers. Cyclization of foldamers or implementing foldamers into macrocyclic molecules enables to bring otherwise remote groups in closer spatial proximity. This might answer *i)* how foldamer moieties interact with themselves in cycles, *ii)* how foldamer moieties interact with non-foldamer units in the cycle within a larger ring system or *iii)* how folding and macrocyclization affect each other.

Combinations of peptides and foldamers to cyclic hybrid structures are rare in the literature. In one work, non-natural building blocks were combined with peptides to peptide macrocycle-foldamer hybrid systems to mimic β -sheet assemblies. Khakshoor *et al.*^[153] synthesized a 52-membered ring macrocycle with an extended heptapeptide β -strand combined with unnatural, benzene core-based amino acid that mimics β -sheet-like dimers. The peptidic part of the macrocycle self-associates through β -sheet dimerization towards a tetramer (dimer of β -sheet dimers). The macrocycle is thus a partially folded object with edge-to-edge interactions and hydrophobic face-to-face interactions. (**Figure 12a**)

Another example of a cyclic foldamer hybrid was published in a study by Katoh *et al.*^[98d] The researcher demonstrated the incorporation of multiple cyclic β -2,3 amino acids (c β AAs), which are known to fold into stable helices or sheets, into peptide chains by ribosomal expression. One is 2-aminocyclohexanecarboxylic acid, which due to its restricted conformation is a strong helix/turn inducer. The incorporation of these artificial building blocks into peptides was achieved by genetic code reprogramming and combining it with mRNA display technology achieved to generate randomized libraries of macrocyclic – c β AAs-peptide hybrids. Ligands with nanomolar affinity against an interferon- γ receptor which also shows inhibitory effects were selected from those generated libraries (10^{12} individual hybrids) and co-crystallization with the target protein led to a high-resolution co-crystal structure (**Figure 12b**). The crystal structure of the nanomolar hybrid macrocycle revealed that it folds into an anti-parallel β -sheet which is governed by the two successive γ -turns – a result of the folding propensity of the β -amino acids. Additionally, intramolecular interactions between the amino acids of the peptide chain were observed.

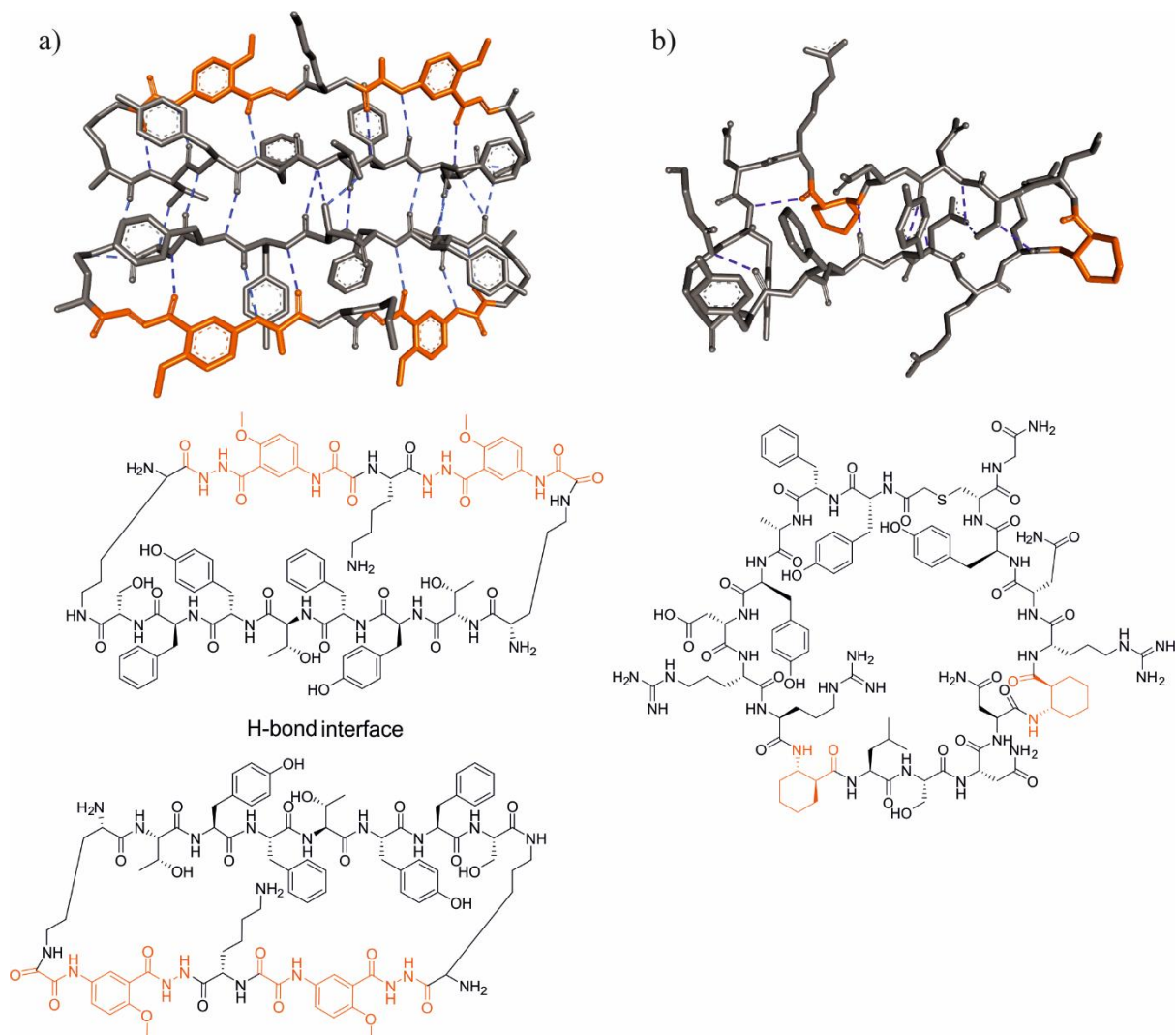


Figure 12 – Structures of foldamer-peptide hybrid macrocycles. X-ray crystal structure of a) β -sheet mimic dimer^[153b] (CCDC: 782650) and b) bioactive β -amino acid-containing macrocycle^[98d] (PDBID: 6L63). Peptide residues are represented in grey, foldamer residues are presented in orange. Hydrogen bonds are represented in blue dashed lines. Bound protein in b) is not shown for better visualization.

3. Objectives

This thesis describes the synthesis and structural characterization of peptide-aromatic oligoamide foldamer hybrid macrocycles. Various aromatic oligoamide-foldamer segments that are helically folded were combined with peptides of various lengths and side chain compositions to form head-to-side chain monocycles or side chain-to-side chain mono-, di-, tri- and tetracyclic structures.

Paragraph 6 outlines the conformational interplay between the peptide and the foldamer parts within a given designed hybrid macrocycle. Based on a previous report, we hoped that both parts (*i.e.* the foldamer and the peptide) had a reciprocal influence on structural conformation and protease stability. This means that the foldamer folding toward a right-handed or left-handed helix is influenced by the chirality of the peptide and, conversely, the foldamer serves as a kind of staple that restricts the conformation of the peptide chain. We also hoped that this reciprocal influence, which was initially studied for short, relatively flexible foldamer tetramers^[98b], can be transferred to longer foldamer-peptide hybrid systems. We knew that quinoline (**Q**)-based octamers (or longer) adopt a stable 2.5 units per turn helix conformation in water that does not interconvert. Inserting such long helices into peptide-foldamer macrocycles would then result in diastereomers (*i.e.* *M*-helix-L-peptide and *P*-helix-L-peptide macrocycles) exhibiting different physico-chemical properties which allow their potential characterization by RP-HPLC analysis. Furthermore, we believed that by introducing some flexible methylpyridine (**P**) units in quinoline-based foldamer nonamers, the *M/P*-helicity interconversion would be (*i*) rendered faster in aqueous environment and (*ii*) biased through the peptide chain, similar to what has been observed for shorter macrocycles. Since it is well documented that peptide macrocycles are more stable in a proteolytic environment than their linear versions, we wanted to expose short foldamer-peptide hybrid macrocycles to different proteases and hoped that these structures would be more resistant compared to their noncyclic versions.

Short foldamers are remarkably compatible with ribosomal expression.^[98b, 104, 154] Foldamer segments can be indeed charged on tRNA thanks to the use of flexible ribozymes (flexizymes) which next allow genetic code reprogramming of the initiator codon. With this, foldamers consisting of **Q**- and **P**- based monomers can be incorporated into polypeptide chains by the ribosome during translation. As long as the foldamer part is short and remains flexible, it can traverse the ribosome exit tunnel and foldamer-peptide hybrid sequence can be expressed *in vitro*. Reactive functionalities, such as chloroacetamides, can additionally be incorporated to the N-terminus of the foldamer, allowing spontaneous cyclization with the first downstream cysteine thiol of the nascent peptide chain. This enables the generation of peptide-foldamer hybrid macrocycles by the ribosome machinery. In this subsequent study which is the content of paragraph 8, we aimed to use this technology to generate a trillion-membered library of different foldamer-peptide macrocycle hybrids within the RaPID platform (see Screening Methods chapter). The generated macrocyclic hybrids library should be screened against a protein target to identify a high affinity peptide-foldamer macrocyclic binder to provide proof of concept. The first sequences we aimed at in this study, were prepared to identify short foldamers with a variety of side-chain appendages that are well-tolerated by the ribosome but cannot cyclize. Here, we wanted to vary the foldamer length and foldamer side-chain appendages so high flexizyme mediated tRNA acylation yields and high ribosomal peptide initiation can be achieved. Once the best performers from this series were identified, we wanted to prepare analogs in which the chloroacetamide electrophile was installed at the N-terminus of the foldamer. This

chloroacetamide containing short foldamer initiators can then be submitted in generating the hybrid macrocycle library. As a model protein, the catalytic C-lobe of the E6AP HECT domain was first selected. Besides providing proof-of-concept in this project, this ubiquitin ligase (E3) is an interesting target in a pharmaceutical context as it is associated with neurodevelopmental disorders and human papillomavirus-induced cervical tumorigenesis.^[155] To gain further structural insight into the binding site and the association between the target and the selected foldamer peptide macrocycle, the identified macrocyclic binders could then be chemically synthesized in mg quantities and further co-crystallized with the protein target. Binding studies in solution could be performed by surface plasmon resonance, isothermal titration calorimetry, or by fluorescence polarization. If measured binding is high, cell permeability or activity assays can be considered. Additionally, as the foldamer part of each macrocycle in the library remains identical (invariable part during the selection), we believe that only the peptide part, as such, provides the binding affinity to C-lobe and the foldamer furnishes conformational restrictions. This could eventually allow modulations of the foldamer appendages to improve the overall pharmacological profile (*e.g.* cell permeability) while maintaining overall good binding affinity.

As mentioned, quinoline oligoamide foldamers are stable, folded helices in aqueous environment. Different side chains can be attached to the surface of the helix at precise positions by synthetically changing the foldamer sequence at the monomer level. In the three-dimensional space, the position of the side chains is well-defined and can be simulated with molecular modeling software (*e.g.* Maestro). The foldamer side chains allow derivatization with, for example, synthetically orthogonal protecting groups. In paragraph 10, we describe our objective to install electrophiles (*i.e.* chloroacetamide function) that allow cyclization on the outer rim of the helix. When combining this foldamer with cysteine-rich peptide chains on the foldamer C-terminus, spontaneous cyclization with the Cys-thiol towards the foldamer side chain can occur. In comparison to the foldamer, the peptide chain is more flexible and can adjust its conformation in aqueous environment. Thus, cyclization between the thiol and the chloroacetamide can only happen when the peptide is long enough to reach the electrophile. As a consequence, if *e.g.* one cysteine is placed in the peptide and two chloroacetamides are introduced on the foldamer surface, macrocyclization would be selective towards the electrophile the thiol can reach. We hoped that this applied when the peptide chain was long enough so that the Cys-thiol could potentially reach several electrophiles but the closest electrophile in terms of 3D arrangement would be selectively involved in the macrocyclization reaction, at the condition that the distance differences between the competing electrophiles were large enough. The farther away located electrophile would not be attacked and stayed orphan. In addition, we hoped that this system also applied when multiple electrophiles and multiple cysteines were present in the hybrid sequence. If during the competition, highly selective cyclization conversions were achieved, multiple irreversible macrocyclization steps occurred one after the other, and multi-cyclic structures could be generated via some sort of reaction trail. This would allow, that peptide-foldamer macrocycles could be designed on which a peptide was stitched to the outside of a foldamer helix. Aromatic helical folded objects that were decorated on the outside with a peptide would then be synthetically accessible.

4. Bibliography

- [1] C. C. Quianzon, I. Cheikh, *J. Community Hosp. Internal Med. Perspect.* **2012**, *2*, 18701.
- [2] M. Muttenthaler, G. F. King, D. J. Adams, P. F. Alewood, *Nat. Rev. Drug. Discov.* **2021**, *20*, 309-325.
- [3] G. F. Gause, M. G. Brazhnikova, *Nature* **1944**, *154*, 703-703.
- [4] V. Du Vigneaud, C. Ressler, J. M. Swan, C. W. Roberts, P. G. Katsoyannis, *J. Am. Chem. Soc.* **1954**, *76*, 3115-3121.
- [5] V. Gupta, M. Sengupta, J. Prakash, B. C. Tripathy, *Basic and Appl. Aspects of Biotechnology*, Springer Singapore, **2017**, pp. 77-101.
- [6] I. Vecchio, C. Tornali, N. L. Bragazzi, M. Martini, *Front. Endocrinol. (Lausanne)* **2018**, *9*, 613.
- [7] a) J. L. Lau, M. K. Dunn, *Bioorg. Med. Chem.* **2018**, *26*, 2700-2707; b) R. Santos, O. Ursu, A. Gaulton, A. P. Bento, R. S. Donadi, C. G. Bologa, A. Karlsson, B. Al-Lazikani, A. Hersey, T. I. Oprea, J. P. Overington, *Nat. Rev. Drug. Discov.* **2017**, *16*, 19-34.
- [8] X. Wang, D. Ni, Y. Liu, S. Lu, *Front. Chem.* **2021**, *9*, 682675.
- [9] P. J. Carter, G. A. Lazar, *Nat. Rev. Drug. Discov.* **2018**, *17*, 197-223.
- [10] a) P. G. Dougherty, A. Sahni, D. Pei, *Chem. Rev.* **2019**, *119*, 10241-10287; b) E. A. Villar, D. Beglov, S. Chennamadhavuni, J. A. Porco, D. Kozakov, S. Vajda, A. Whitty, *Nat. Chem. Biol.* **2014**, *10*, 723-731; c) L. Wang, N. Wang, W. Zhang, X. Cheng, Z. Yan, G. Shao, X. Wang, R. Wang, C. Fu, *Signal Transduct. Target Ther.* **2022**, *7*.
- [11] C. A. Lipinski, F. Lombardo, B. W. Dominy, P. J. Feeney, *Adv. Drug Deliv.* **2001**, *46*.
- [12] D. F. Veber, S. R. Johnson, H.-Y. Cheng, B. R. Smith, K. W. Ward, K. D. Kopple, *J. Med. Chem.* **2002**, *45*, 2615-2623.
- [13] S. S. Usmani, G. Bedi, J. S. Samuel, S. Singh, S. Kalra, P. Kumar, A. A. Ahuja, M. Sharma, A. Gautam, G. P. S. Raghava, *PLOS ONE* **2017**, *12*, e0181748.
- [14] S. Mitragotri, P. A. Burke, R. Langer, *Nat. Rev. Drug. Discov.* **2014**, *13*, 655-672.
- [15] L. Pollaro, C. Heinis, *MedChemComm* **2010**, *1*, 319-324.
- [16] A. A. Vinogradov, Y. Yin, H. Suga, *J. Am. Chem. Soc.* **2019**, *141*, 4167-4181.
- [17] A. Zorzi, K. Deyle, C. Heinis, *Curr. Opin. Chem. Biol.* **2017**, *38*, 24-29.
- [18] a) K. Patel, L. J. Walport, J. L. Walshe, P. D. Solomon, J. K. K. Low, D. H. Tran, K. S. Mouradian, A. P. G. Silva, L. Wilkinson-White, A. Norman, C. Franck, J. M. Matthews, J. M. Guss, R. J. Payne, T. Passioura, H. Suga, J. P. Mackay, *Proc. Natl. Acad. Sci.* **2020**, *117*, 26728-26738; b) C. Sohrabi, A. Foster, A. Tavassoli, *Nat. Rev. Chem.* **2020**, *4*, 90-101.
- [19] K. Shinbara, W. Liu, R. H. P. van Neer, T. Katoh, H. Suga, *Front. Chem.* **2020**, *8*, 447.
- [20] a) J.-S. Choi, S. H. Joo, *Biomol. Ther.* **2020**, *28*, 18-24; b) A. D. Cunningham, N. Qvit, D. Mochly-Rosen, *Curr. Opin. Struct.* **2017**, *44*, 59-66.
- [21] a) K. Fosgerau, T. Hoffmann, *Drug Discov. Today* **2015**, *20*, 122-128; b) P. Vlieghe, V. Lisowski, J. Martinez, M. Khrestchatsky, *Drug Discov. Today* **2010**, *15*, 40-56.
- [22] K. E. Duncan, B. R. Dempsey, L. E. Killip, J. Adams, M. L. Bailey, G. A. Lajoie, D. W. Litchfield, C. J. Brandl, G. S. Shaw, B. H. Shilton, *J. Med. Chem.* **2011**, *54*, 3854-3865.
- [23] A. T. Bockus, C. M. McEwan, R. S. Lokey, *Curr. Top. Med. Chem.* **2013**, *13*, 821-836.
- [24] M. Werle, A. Bernkop-Schnürch, *Amino Acids*, **2006**, *30*, 351-367.
- [25] G. Byk, D. Halle, I. Zeltser, G. Bitan, Z. Selinger, C. Gilon, *J. Med. Chem.* **1996**, *39*, 3174-3178.
- [26] M. Pakkala, C. Hekim, P. Soininen, J. Leinonen, H. Koistinen, J. Weisell, U. H. Stenman, J. Vepsäläinen, A. Narvanen, *J. Pept. Sci.* **2007**, *13*, 348-353.
- [27] A. Alaofi, N. On, P. Kiptoo, T. D. Williams, D. W. Miller, T. J. Siahaan, *J. Pharm. Sci.* **2016**, *105*, 797-807.
- [28] D. J. Drucker, *Nat. Rev. Drug. Discov.* **2020**, *19*, 277-289.
- [29] D. S. Nielsen, N. E. Shepherd, W. Xu, A. J. Lucke, M. J. Stoermer, D. P. Fairlie, *Chem. Rev.* **2017**, *117*, 8094-8128.

- [30] H. Zhang, S. Chen, *RSC Chem. Biol.* **2022**, *3*, 18-31.
- [31] N. J. Yang, M. J. Hinner, in *Site-Specific Protein Labeling*, Springer New York, **2015**, pp. 29-53.
- [32] L. K. Buckton, M. N. Rahimi, S. R. McAlpine, *Chem.* **2021**, *27*, 1487-1513.
- [33] a) J. Samanen, F. Ali, T. Romoff, R. Calvo, E. Sorenson, J. Vasko, B. Storer, D. Berry, D. Bennett, M. Strohsacker, D. Powers, J. Stadel, A. Nichols, *J. Med. Chem.* **1991**, *34*, 3114-3125; b) W. Bauer, U. Briner, W. Doepfner, R. Haller, R. Huguenin, P. Marbach, T. Petcher, J., J. Pless, *Life Sci.* **1982**, *31*, 1133-1140; c) A. F. B. Rader, M. Weinmuller, F. Reichart, A. Schumacher-Klinger, S. Merzbach, C. Gilon, A. Hoffman, H. Kessler, *Angew. Chem. Int. Ed.* **2018**, *57*, 14414-14438; d) G. Pauletti, M., S. Gangwar, T. Siahhaan, J., J. Aubé, R. Borchardt, T., *Adv. Drug Deliv. Rev.* **1997**, *27*, 235-256.
- [34] a) C. Mas-Moruno, F. Rechenmacher, H. Kessler, *Anti-Cancer Agents Med. Chem.*, **2010**, *10*, 753-768; b) A. Becker, O. von Richter, A. Kovar, H. Scheible, J. J. van Lier, A. Johnne, *J. Clin. Pharmacol.* **2015**, *55*, 815-824.
- [35] M. Abdalla, L. MCGAW, *Molecules* **2018**, *23*, 2080.
- [36] L. Thorstholm, D. J. Craik, *Drug Discov. Today Technol.* **2012**, *9*, e1-e70.
- [37] a) R. D. Sussmuth, A. Mainz, *Angew. Chem. Int. Ed.* **2017**, *56*, 3770-3821; b) B. J. Burkhart, C. J. Schwalen, G. Mann, J. H. Naismith, D. A. Mitchell, *Chem. Rev.* **2017**, *117*, 5389-5456.
- [38] D. Faulds, K. L. Goa, P. Benfield, *Drugs* **1993**, *45*, 953-1040.
- [39] A. Rembratt, C. Graugaard-Jensen, T. Senderovitz, J. Norgaard, J. Djurhuus, *Eur. J. Clin. Pharmacol.*, **2004**, *60*.
- [40] S. C. Jain, H. M. Sobell, *J. Mol. Bio* **1972**, *68*, 1-20.
- [41] I. V. Smolyar, A. K. Yudin, V. G. Nenajdenko, *Chem. Rev.*, **2019**, *119*, 10032-10240.
- [42] J. E. Bock, J. Gavenonis, J. A. Kritzer, *ACS Chem. Biol.*, **2013**, *8*, 488-499.
- [43] J. Gavenonis, B. A. Sheneman, T. R. Siegert, M. R. Eshelman, J. A. Kritzer, *Nat. Chem. Biol.*, **2014**, *10*, 716-722.
- [44] a) H. S. Soor, S. D. Appavoo, A. K. Yudin, *Bioorg. Med. Chem.* **2018**, *26*, 2774-2779; b) S. D. Appavoo, T. Kaji, J. R. Frost, C. C. G. Scully, A. K. Yudin, *J. Am. Chem. Soc.* **2018**, *140*, 8763-8770.
- [45] J. D. Walton, H. E. Hallen-Adams, H. Luo, *Biopolymers*, **2010**, *94*, 659-664.
- [46] K. Matinkhoo, A. Pryyma, M. Todorovic, B. O. Patrick, D. M. Perrin, *J. Am. Chem. Soc.* **2018**, *140*, 6513-6517.
- [47] a) A. Pahl, C. Lutz, T. Hechler, *Drug Discov. Today Technol.* **2018**, *30*, 85-89; b) M. A. J. Siegert, C. H. Knittel, R. D. Süssmuth, *Angew. Chem. Int. Ed.* **2020**, *59*, 5500-5504; c) G. Yao, C. H. Knittel, S. Kosol, M. T. Wenz, B. G. Keller, H. Gruss, A. C. Braun, C. Lutz, T. Hechler, A. Pahl, R. D. Sussmuth, *J. Am. Chem. Soc.* **2021**, *143*, 14322-14331.
- [48] a) E. C. Kostansek, W. N. Lipscomb, R. R. Yocum, W. E. Thiessen, *J. Am. Chem. Soc.* **1977**, *99*, 1273-1274; b) D. A. Bushnell, P. Cramer, R. D. Kornberg, *Proc. Natl. Acad. Sci.* **2002**, *99*, 1218-1222.
- [49] X. Liu, L. Farnung, C. Wigge, P. Cramer, *J. Biol. Chem.* **2018**, *293*, 7189-7194.
- [50] M. Moiola, M. G. Memeo, P. Quadrelli, *Molecules* **2019**, *24*, 3654.
- [51] Y. H. Lau, P. de Andrade, Y. Wu, D. R. Spring, *Chem. Soc. Rev.* **2015**, *44*, 91-102.
- [52] L. D. Walensky, G. H. Bird, *J. Med. Chem.* **2014**, *57*, 6275-6288.
- [53] Y. H. Lau, Y. Wu, M. Rossmann, B. X. Tan, P. De Andrade, Y. S. Tan, C. Verma, G. J. Mckenzie, A. R. Venkitaraman, M. Hyvönen, D. R. Spring, *Angew. Chem. Int. Ed.* **2015**, *54*, 15410-15413.
- [54] I. Rentero Rebollo, C. Heinis, *Methods* **2013**, *60*, 46-54.
- [55] C. Heinis, T. Rutherford, S. Freund, G. Winter, *Nat. Chem. Biol.* **2009**, *5*, 502-507.
- [56] S. Chen, D. Bertoldo, A. Angelini, F. Pojer, C. Heinis, *Angew. Chem. Int. Ed.* **2014**, *53*, 1602-1606.
- [57] R. B. Merrifield, *J. Am. Chem. Soc.* **1963**, *85*, 2149-2154.
- [58] L. A. Carpino, G. Y. Han, *J. Am. Chem. Soc.* **1970**, *92*, 5748-5749.
- [59] S. L. Pedersen, A. P. Tofteng, L. Malik, K. J. Jensen, *Chem. Soc. Rev.* **2012**, *41*, 1826-1844.

- [60] a) S. Kates, A., B. McGuinness, F., C. Blackburn, G. Griffin, William, N. Solé, A., G. Barany, F. Albericio, *Biopolymers* **1998**, *47*, 365-380; b) E. Atherton, D. L. J. Clive, R. C. Sheppard, *J. Am. Chem. Soc.* **1975**, *97*, 6584-6585.
- [61] F. García-Martín, M. Quintanar-Audelo, Y. García-Ramos, L. J. Cruz, C. Gravel, R. Furic, S. Côté, J. Tulla-Puche, F. Albericio, *J. Comb. Chem.* **2006**, *8*, 213-220.
- [62] S.-S. Wang, *J. Am. Chem. Soc.* **1973**, *95*, 1328-1333.
- [63] R. Hans, *Tetrahedron Lett.* **1987**, *28*, 3787-3790.
- [64] M. Mergler, R. Tanner, J. Gosteli, P. Grogg, *Tetrahedron Lett.* **1988**, *29*, 4005-4008.
- [65] a) F. Albericio, P. Lloyd-Williams, E. Giralt, *Methods Enzymol.* **1997**, *289*, 313-336; b) B. Bray, L., *Nat. Rev. Drug Disco.* **2003**, *2*, 587-593.
- [66] N. Hartrampf, A. Saebi, M. Poskus, Z. P. Gates, A. J. Callahan, A. E. Cowfer, S. Hanna, S. Antilla, C. K. Schissel, A. J. Quartararo, X. Ye, A. J. Mijalis, M. D. Simon, A. Loas, S. Liu, C. Jessen, T. E. Nielsen, B. L. Pentelute, *Science* **2020**, *368*, 980-987.
- [67] Y. Nishiuchi, T. Inui, H. Nishio, J. Bódi, T. Kimura, F. I. Tsuji, S. Sakahibara, *Proc. Natl. Acad. Sci.* **1998**, *95*, 13549-13554.
- [68] L. Raibaut, N. Ollivier, O. Melnyk, *Chem. Soc. Rev.* **2012**, *41*, 7001.
- [69] S. S. Kulkarni, J. Sayers, B. Premdjee, R. J. Payne, *Nat. Rev. Chem.* **2018**, *2*, 0122.
- [70] K. S. Kumar, S. N. Bavikar, L. Spasser, T. Moyal, S. Ohayon, A. Brik, *Angew. Chem. Int. Ed.* **2011**, *50*, 6137-6141.
- [71] C. J. White, A. K. Yudin, *Nat. Chem.* **2011**, *3*, 509-524.
- [72] a) U. Schmidt, J. Langner, *J. Pept. Res.* **1997**, *49*, 67-73, b) A. K. Yudin, *Chem. Sci.* **2015**, *6*, 30.
- [73] Y.-H. Yep, X.-M. Gao, M. Liu, Y.-C. Tang, G.-L. Tian, *Int. J. Pept. Res. Ther.* **2003**, *10*, 571-579.
- [74] M. Malesevic, U. Strijowski, D. Bachle, N. Sewald, *J. Biotechnol.* **2004**, *112*, 73-77.
- [75] J. A. Iannuzzelli, R. Fasan, *Chem. Sci.* **2020**, *11*, 6202-6208.
- [76] a) Lundquist, J. C. Pelletier, *Org. Lett.* **2002**, *4*, 3219-3221; b) S. Punna, J. Kuzelka, Q. Wang, M. G. Finn, *Angew. Chem. Int. Ed.* **2005**, *44*, 2215-2220.
- [77] C. Tsiamantas, M. E. Otero-Ramirez, H. Suga, *Methods Mol. Biol.* **2019**, *2001*, 299-315.
- [78] F. M. Brunel, P. E. Dawson, *Chem. Commun.* **2005**, 2552.
- [79] N. Bionda, A. L. Cryan, R. Fasan, *ACS Chem. Biol.* **2014**, *9*, 2008-2013.
- [80] A. E. Owens, J. A. Iannuzzelli, Y. Gu, R. Fasan, *ACS Central Sci.* **2020**, *6*, 368-381.
- [81] G. Smith, P., *Science* **1985**, *228*, 1315-1317.
- [82] a) G. P. Smith, V. A. Petrenko, *Chem. Rev.* **1997**, *97*, 391-410; b) T. Passioura, T. Katoh, Y. Goto, H. Suga, *Annu. Rev. Biochem* **2014**, *83*, 727-752; c) S. Sidhu, S., H. Lowman, B., B. Cunningham, C., J. Wells, A., *Methods Enzymol.* **2000**, *328*, 333-363.
- [83] a) G. Winter, A. D. Griffiths, R. E. Hawkins, H. R. Hoogenboom, *Annu. Rev. Immunol.* **1994**, *12*, 433-455; b) A. Frenzel, T. Schirrmann, M. Hust, *mAbs.* **2016**, *8*, 1177-1194.
- [84] S. Mimmi, D. Maisano, I. Quinto, E. Iaccino, *Trends Pharmacol. Sci.* **2019**, *40*, 87-91.
- [85] H. Gilbert, F., *Methods Enzymol.* **1995**, *251*, 8-28.
- [86] C. Heinis, T. Rutherford, S. Freund, G. Winter, *Nat. Chem. Biol.* **2009**, *5*, 502-507.
- [87] R. W. Roberts, J. W. Szostak, *Proc. Natl. Acad. Sci.* **1997**, *94*, 12297-12302.
- [88] A. D. Keefe, J. W. Szostak, *Nature* **2001**, *410*, 715-718.
- [89] M. S. Newton, Y. Cabezas-Perusse, C. L. Tong, B. Seelig, *ACS Synth. Biol.* **2020**, *9*, 181-190.
- [90] S. W. Millward, T. T. Takahashi, R. W. Roberts, *J. Am. Chem. Soc.* **2005**, *127*, 14142-14143.
- [91] S. W. Millward, S. Fiacco, R. Austin, J., R. W. Roberts, *ACS Chem. Biol.* **2007**, *2*, 625-634.
- [92] Y. Goto, T. Katoh, H. Suga, *Nat. Prot.* **2011**, *6*, 779-790.
- [93] T. Kawakami, H. Murakami, H. Suga, *J. Am. Chem. Soc.* **2008**, *130*, 16861-16863.
- [94] a) Y. Goto, H. Suga, *J. Am. Chem. Soc.* **2009**, *131*, 5040-5041; b) Y. Goto, H. Murakami, H. Suga, *RNA* **2008**, *14*, 1390-1398.
- [95] A. Ohta, H. Murakami, H. Suga, *Chembiochem* **2008**, *9*, 2773-2778.
- [96] Y. Yamagishi, H. Ashigai, Y. Goto, H. Murakami, H. Suga, *Chembiochem* **2009**, *10*, 1469-1472.
- [97] K. Torikai, H. Suga, *J. Am. Chem. Soc.* **2014**, *136*, 17359-17361.

- [98] a) T. Katoh, H. Suga, *J. Am. Chem. Soc.* **2022**; b) J. M. Rogers, S. Kwon, S. J. Dawson, P. K. Mandal, H. Suga, I. Huc, *Nat. Chem.* **2018**, *10*, 795; c) T. Katoh, H. Suga, *J. Am. Chem. Soc.* **2021**, *143*, 18844-18848; d) T. Katoh, T. Sengoku, K. Hirata, K. Ogata, H. Suga, *Nat. Chem.* **2020**, *12*, 1081-1088.
- [99] C. Tsiamantas, J. M. Rogers, H. Suga, *Chem. Commun.* **2020**, *56*, 4265-4272.
- [100] a) Y. Goto, A. Ohta, Y. Sako, Y. Yamagishi, H. Murakami, H. Suga, *ACS Chem. Biol.* **2008**, *3*, 120-129; b) K. Iwasaki, Y. Goto, T. Katoh, H. Suga, *Org. Biomol. Chem.* **2012**, *10*, 5783.
- [101] A. Kawamura, M. Münzel, T. Kojima, C. Yapp, B. Bhushan, Y. Goto, A. Tumber, T. Katoh, O. N. F. King, T. Passioura, L. J. Walport, S. B. Hatch, S. Madden, S. Müller, P. E. Brennan, R. Chowdhury, R. J. Hopkinson, H. Suga, C. J. Schofield, *Nat. Commun.* **2017**, *8*, 14773.
- [102] S. A. K. Jongkees, S. Caner, C. Tysoe, G. D. Brayer, S. G. Withers, H. Suga, *Cell Chem. Biol.* **2017**, *24*, 381-390.
- [103] a) D. R. Cary, M. Ohuchi, P. C. Reid, K. Masuya, *J. Synth. Org. Chem Jpn.* **2017**, *75*, 1171-1178; b) Y. Huang, M. M. Wiedmann, H. Suga, *Chem. Rev.* **2019**, *119*, 10360-10391.
- [104] C. Tsiamantas, S. Kwon, C. Douat, I. Huc, H. Suga, *Chem. Commun.* **2019**, *55*, 7366-7369.
- [105] a) K. A. Dill, J. L. MacCallum, *Science* **2012**, *338*, 1042-1046; b) G. D. Rose, P. J. Fleming, J. R. Banavar, A. Maritan, *Proc. Natl. Acad. Sci.* **2006**, *103*, 16623-16633.
- [106] A. Cao, *The Protein Journal* **2020**, *39*, 422-433.
- [107] S. H. Gellman, *Acc. Chem. Res.* **1997**, *31*, 173-180.
- [108] C. Nick Pace, J. Martin Scholtz, *Biophys. J.* **1998**, *75*, 422-427.
- [109] a) P. Y. Chou, G. D. Fasman, *Annu. Rev. Biochem.* **1978**, *47*, 251-276; b) W. Kabsch, C. Sander, *Biopolymers* **1983**, *22*, 2577-2637.
- [110] J. S. Nowick, E. M. Smith, M. Pairish, *Chem. Soc. Rev.* **1996**, *25*, 401-415.
- [111] A. S. Culf, R. J. Ouellette, *Molecules* **2010**, *15*, 5282-5335.
- [112] K. Kirshenbaum, A. E. Barron, R. A. Goldsmith, P. Armand, E. K. Bradley, K. T. V. Truong, K. A. Dill, F. E. Cohen, R. N. Zuckermann, *Proc. Natl. Acad. Sci.* **1998**, *95*, 4303-4308.
- [113] D. Seebach, J. L. Matthews, *Chem. Commun.* **1997**, 2015-2022.
- [114] a) D. H. Appella, L. A. Christianson, D. A. Klein, D. R. Powell, X. Huang, J. J. Barchi Jr, S. H. Gellman, *Nature* **1997**, *387*, 381-384; b) D. H. Appella, L. A. Christianson, I. L. Karle, D. R. Powell, S. H. Gellman, *J. Am. Chem. Soc.* **1996**, *118*, 13071-13072.
- [115] D. Seebach, M. Overhand, F. N. M. Kühnle, B. Martinoni, *Helv. Chim. Acta.* **1996**, *79*, 913-941.
- [116] a) L. Fischer, P. Claudon, N. Pendem, E. Miclet, C. Didierjean, E. Ennifar, G. Guichard, *Angew. Chem. Int. Ed.* **2010**, *49*, 1067-1070; b) N. Pendem, C. Douat, P. Claudon, M. Laguerre, S. Castano, B. Desbat, D. Cavagnat, E. Ennifar, B. Kauffmann, G. Guichard, *J. Am. Chem. Soc.* **2013**, *135*, 4884-4892.
- [117] J. Fremaux, L. Mauran, K. Pulka-Ziach, B. Kauffmann, B. Odaert, G. Guichard, *Angew. Chem. Int. Ed.* **2015**, *54*, 9816-9820.
- [118] E. Teyssieres, J. P. Corre, S. Antunes, C. Rougeot, C. Dugave, G. Jouvion, P. Claudon, G. Mikaty, C. Douat, P. L. Goossens, G. Guichard, *J. Med. Chem.* **2016**, *59*, 8221-8232.
- [119] L. Cussol, L. Mauran-Ambrosino, J. Buratto, A. Y. Belorusova, M. Neuville, J. Osz, S. Fribourg, J. Fremaux, C. Dolain, S. R. Goudreau, N. Rochel, G. Guichard, *Angew. Chem. Int. Ed.* **2021**, *60*, 2296-2303.
- [120] C. Douat, M. Bornerie, S. Antunes, G. Guichard, A. Kichler, *Bioconjugate Chem.* **2019**, *30*, 1133-1139.
- [121] J. Fremaux, C. Venin, L. Mauran, R. Zimmer, F. Koensgen, D. Rognan, S. Bitsi, M. A. Lucey, B. Jones, A. Tomas, G. Guichard, S. R. Goudreau, *Chem. Sci.* **2019**, *10*, 9872-9879.
- [122] E. R. Schreiter, M. M. Rodríguez, A. Weichsel, W. R. Montfort, J. Bonaventura, *J. Biol. Chem.* **2007**, *282*, 19773-19780.
- [123] J. Fremaux, L. Fischer, T. Arbogast, B. Kauffmann, G. Guichard, *Angew. Chem. Int. Ed.* **2011**, *50*, 11382-11385.

- [124] D. Sánchez-García, B. Kauffmann, T. Kawanami, H. Ihara, M. Takafuji, M.-H. Delville, I. Huc, *J. Am. Chem. Soc.* **2009**, *131*, 8642-8648.
- [125] I. Huc, *Eur. J. Org. Chem.* **2004**, 17-29.
- [126] a) I. Huc, V. Maurizot, H. Gornitzka, J. M. Leger, *Chem. Commun.* **2002**, 578-579; b) Y. Hamuro, S. J. Geib, A. D. Hamilton, *J. Am. Chem. Soc.* **1996**, *118*, 7529-7541.
- [127] D. A. P. Delnoye, R. P. Sijbesma, J. A. J. M. Vekemans, E. W. Meijer, *J. Am. Chem. Soc.* **1996**, *118*, 8717-8718.
- [128] B. Gong, *Chem. Eur. J.* **2001**, *7*, 4336-4342.
- [129] E. Berni, C. Dolain, B. Kauffmann, J.-M. Léger, C. Zhan, I. Huc, *J. Org. Chem.* **2008**, *73*, 2687-2694.
- [130] K. Ziach, C. Chollet, V. Parissi, P. Prabhakaran, M. Marchivie, V. Corvaglia, P. P. Bose, K. Laxmi-Reddy, F. Godde, J. M. Schmitter, S. Chaignepain, P. Pourquier, I. Huc, *Nat. Chem.* **2018**, *10*, 511-518.
- [131] Y. Ferrand, I. Huc, *Acc. Chem. Res.* **2018**, *51*, 970-977.
- [132] A. Mendez-Ardoy, N. Markandeya, X. Li, Y. T. Tsai, G. Pecastaings, T. Buffeteau, V. Maurizot, L. Muccioli, F. Castet, I. Huc, D. M. Bassani, *Chem. Sci.* **2017**, *8*, 7251-7257.
- [133] Q. Gan, Y. Ferrand, C. Bao, B. Kauffmann, A. Grélard, H. Jiang, I. Huc, *Science* **2011**, *331*, 1172-1175.
- [134] a) H. Jiang, J.-M. Léger, C. Dolain, P. Guionneau, I. Huc, *Tetrahedron* **2003**, *59*, 8365-8374; b) Q. Gan, C. Bao, B. Kauffmann, A. Grelard, J. Xiang, S. Liu, I. Huc, H. Jiang, *Angew. Chem. Int. Ed.* **2008**, *47*, 1715-1718.
- [135] 2,6-quinoline monomers will be reported in due course. Manuscript in preparation.
- [136] E. R. Gillies, C. Dolain, J. M. Leger, I. Huc, *J. Org. Chem.* **2006**, *71*, 7931-7939.
- [137] X. Wang, Q. Gan, B. Wicher, Y. Ferrand, I. Huc, *Angew. Chem. Int. Ed.* **2019**, *58*, 4205-4209.
- [138] X. Hu, S. J. Dawson, P. K. Mandal, X. de Hatten, B. Baptiste, I. Huc, *Chem. Sci.* **2017**, *8*, 3741-3749.
- [139] C. Tsiamantas, X. de Hatten, C. Douat, B. Kauffmann, V. Maurizot, H. Ihara, M. Takafuji, N. Metzler-Nolte, I. Huc, *Angew. Chem. Int. Ed.* **2016**, *55*, 6848-6852.
- [140] J. Buratto, C. Colombo, M. Stupfel, S. J. Dawson, C. Dolain, B. Langlois d'Estaintot, L. Fischer, T. Granier, M. Laguerre, B. Gallois, I. Huc, *Angew. Chem. Int. Ed.* **2014**, *53*, 883-887.
- [141] S. De, B. Chi, T. Granier, T. Qi, V. Maurizot, I. Huc, *Nat. Chem.* **2018**, *10*, 51-57.
- [142] D. Bindl, P. K. Mandal, I. Huc, *Chem. Eur. J.* **2022**.
- [143] a) X. Hu, S. J. Dawson, Y. Nagaoka, A. Tanatani, I. Huc, *J. Org. Chem.* **2016**, *81*, 1137-1150; b) B. Baptiste, C. Douat-Casassus, K. Laxmi-Reddy, F. Godde, I. Huc, *J. Org. Chem.* **2010**, *75*, 7175-7185.
- [144] D. Hill, J., M. Mio, J., B. Prince, R., T. Hughes, S., J. Moore, S., *Chem. Rev.* **2001**, *101*, 3893-4011.
- [145] a) G. Guichard, I. Huc, *Chem. Commun.* **2011**, *47*, 5933; b) S. Hecht, I. Huc, *Foldamers: Structure, Properties, and Applications*, Wiley-VCH, Weinheim, **2007**.
- [146] N. Delsuc, T. Kawanami, J. Lefeuvre, A. Shundo, H. Ihara, M. Takafuji, I. Huc, *Chemphyschem* **2008**, *9*, 1882-1890.
- [147] M. Jewginski, L. Fischer, C. Colombo, I. Huc, C. D. Mackereth, *Chembiochem* **2016**, *17*, 727-736.
- [148] T. Qi, V. Maurizot, H. Noguchi, T. Charoenraks, B. Kauffmann, M. Takafuji, H. Ihara, I. Huc, *Chem. Commun.* **2012**, *48*, 6337.
- [149] F. Devaux, X. Li, D. Sluysmans, V. Maurizot, E. Bakalis, F. Zerbetto, I. Huc, A.-S. Duwez, *Chem.* **2021**, *7*, 1333-1346.
- [150] L. Yang, C. Ma, B. Kauffmann, D. Li, Q. Gan, *Org. Biomol. Chem.* **2020**, *18*, 6643-6650.
- [151] A. M. Kendhale, L. Poniman, Z. Dong, K. Laxmi-Reddy, B. Kauffmann, Y. Ferrand, I. Huc, *J. Org. Chem.* **2011**, *76*, 195-200.
- [152] D. Bindl, E. Heinemann, P. K. Mandal, I. Huc, *Chem. Commun.* **2021**, *57*, 5662-5665.

- [153] a) O. Khakshoor, B. Demeler, J. S. Nowick, *J. Am. Chem. Soc.* **2007**, *129*, 5558-5569; b) O. Khakshoor, A. J. Lin, T. P. Korman, M. R. Sawaya, S.-C. Tsai, D. Eisenberg, J. S. Nowick, *J. Am. Chem. Soc.* **2010**, *132*, 11622-11628.
- [154] C. Tsiamantas, S. Kwon, J. M. Rogers, C. Douat, I. Huc, H. Suga, *Angew. Chem.* **2020**, *132*, 4890-4894.
- [155] J. Weber, S. Polo, E. Maspero, *Front. Physiol.* **2019**, *10*, 370.

5. List of Publications

This thesis is based on the following original publications and manuscripts.

“Conformational interplay in hybrid peptide–helical aromatic foldamer macrocycles”

Sebastian Dengler, Pradeep K. Mandal, Lars Allmendinger, Céline Douat and Ivan Huc

Published in: *Chem. Sci.*, 2021, **12**, 11004

“Display Selection of a Hybrid Foldamer-Peptide Macrocycle”

Sebastian Dengler, Ryan T. Howard, Vasily Morozov, Christos Tsiamantas, Zhiwei Liu, Christopher Dobrzanski, Vojislava Pophristic, Wei-En Huang, Sophie Brameyer, Céline Douat, Hiroaki Suga and Ivan Huc

An earlier version of the manuscript was posted preprint on *ChemRxiv* on 03.02.2022

“Differential Multi-Macrocyclizations at the Surface of a Helical Template”

Sebastian Dengler, Céline Douat and Ivan Huc

Published in: *Angew. Chem. Int. Ed.* 2022, **61**, e202211138

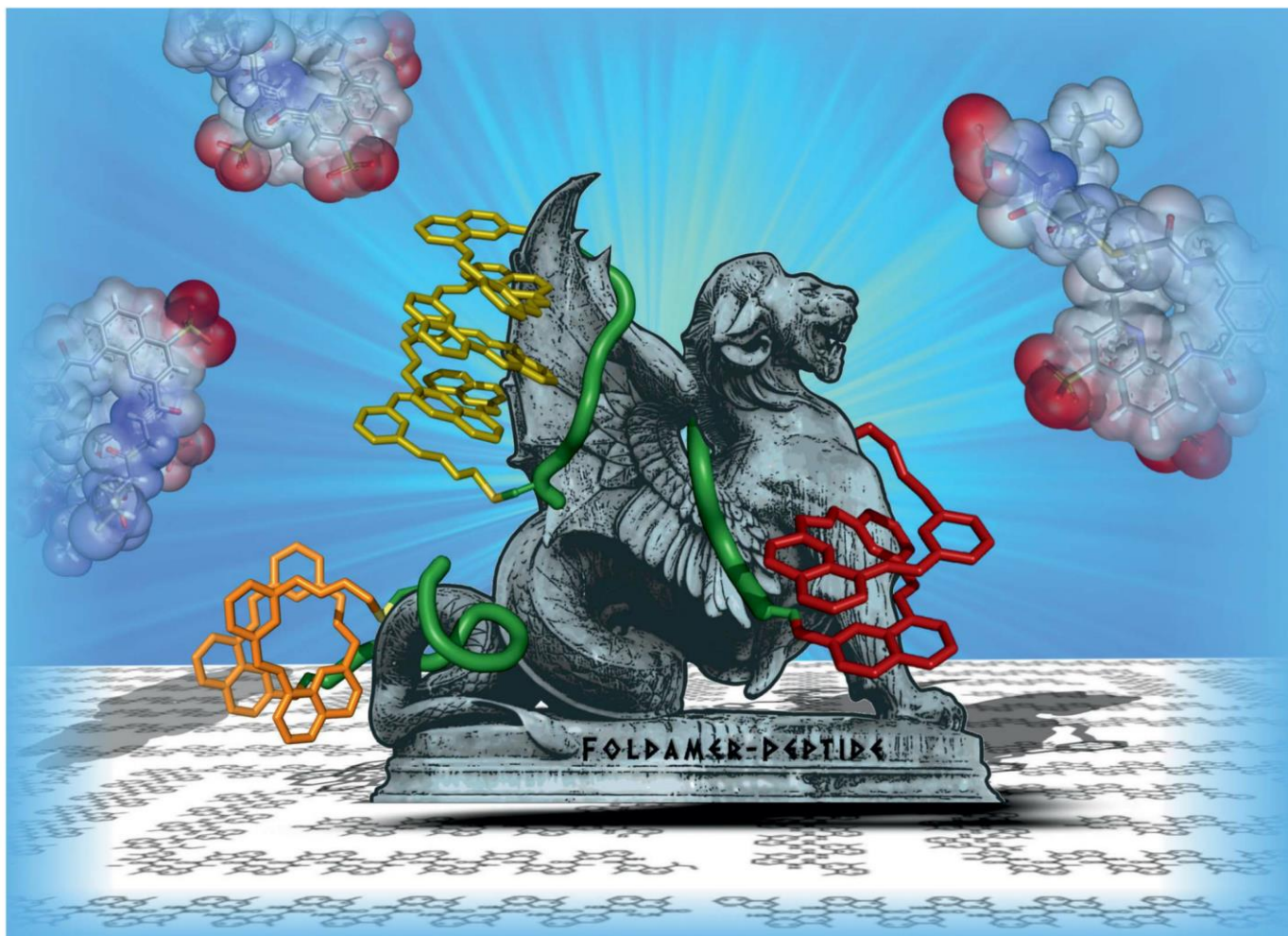
6. Main Text: Conformational Interplay in Hybrid Peptide–Helical Aromatic Foldamer Macrocycles

Authors: Sebastian Dengler, Pradeep K. Mandal, Lars Allmendinger, Céline Douat and Ivan Huc

Published: *Chem. Sci.*, 2021, **12**, 11004

DOI: <https://doi.org/10.1039/D1SC03640H>

Author contribution: The project was conceptualized and supervised by I. Huc. C. Douat co-supervised the work and contributed to synthesis and CD studies. P.K. Mandal performed X-ray data collection, crystal structure elucidation, assisted with crystal growth and data refinement. L. Allmendinger planned and executed NMR measurements. The manuscript was written by C. Douat, I. Huc and me. Most of the experimental work was performed by me.



Showcasing research from Professor Huc's laboratory,
Faculty of Chemistry and Pharmacy, Ludwig Maximilians
University, Munich, Germany.

Conformational interplay in hybrid peptide-helical aromatic
foldamer macrocycles

As some mythological creatures, chimeric molecules composed of disparate parts may express unusual interactions between their subunits. Peptides and aromatic foldamers display different folding propensities. When peptides and aromatic foldamers are combined in the same macrocycle, a strong interplay of their properties is observed, including helix handedness bias, helix stabilization, peptide stretching and peptide resistance to proteolytic degradation.

Copyright: Lars Allmendinger.

As featured in:



See Ivan Huc *et al.*, *Chem. Sci.*,
2021, 12, 11004.



Cite this: *Chem. Sci.*, 2021, 12, 11004

All publication charges for this article have been paid for by the Royal Society of Chemistry

Received 2nd July 2021
Accepted 26th July 2021

DOI: 10.1039/d1sc03640h

rsc.li/chemical-science

Conformational interplay in hybrid peptide–helical aromatic foldamer macrocycles†

Sebastian Dengler,^{ID} Pradeep K. Mandal,^{ID} Lars Allmendinger, Céline Douat^{ID} and Ivan Huc^{ID}*

Macrocytic peptides are an important class of bioactive substances. When inserting an aromatic foldamer segment in a macrocyclic peptide, the strong folding propensity of the former may influence the conformation and alter the properties of the latter. Such an insertion is relevant because some foldamer–peptide hybrids have recently been shown to be tolerated by the ribosome, prior to forming macrocycles, and can thus be produced using an *in vitro* translation system. We have investigated the interplay of peptide and foldamer conformations in such hybrid macrocycles. We show that foldamer helical folding always prevails and stands as a viable means to stretch, *i.e.* unfold, peptides in a solvent dependent manner. Conversely, the peptide systematically has a reciprocal influence and gives rise to strong foldamer helix handedness bias as well as foldamer helix stabilisation. The hybrid macrocycles also show resistance towards proteolytic degradation.

Introduction

Ribosomal translation of mRNA into peptidic sequences has been shown to be tolerant to a great variety of peptide chain modifications and non-peptidic appendages.¹ In turn, this tolerance has enabled the development of nucleic-acid-encoded display selection methods of non-natural peptides.² Non-native peptide modifications may indeed bring advantages, *e.g.* with respect to bioavailability, resistance to proteolytic degradation, or achieving high binding affinity for a given biological target. For example, a beneficial modification is to introduce an electrophilic chloroacetamide at the peptide N-terminus in combination with the encoding of one mandatory cysteine in the peptide sequence.² Spontaneous substitution of the chlorine by the thiol of the cysteine then gives access to libraries of ribosomally expressed thioether macrocycles, which have been shown to be better candidates than linear peptides as high affinity protein ligands. For the same purpose, libraries of peptide sequences derived from natural amino acids may also be macrocyclised through post-translational modifications.³

Recently, it was shown that ribosomal translation tolerates peptide appendages consisting of aromatic amide foldamer sequences of quinoline-based monomer Q^{Xxx} and pyridine-based monomer P (Fig. 1a).^{4–6} These appendages are far larger

and more remote from peptides than what had been previously envisaged. They can be placed either at the N-terminus, *i.e.* on the peptide chain initiator,^{4,5} or within the sequence on an α -amino acid side chain.⁶ They can also be included within thioether peptide macrocycles such as previously described compound 3 (Fig. 1b). Interest for such peptide modifications stems from the high propensity of Q^{Xxx}/P sequences to adopt

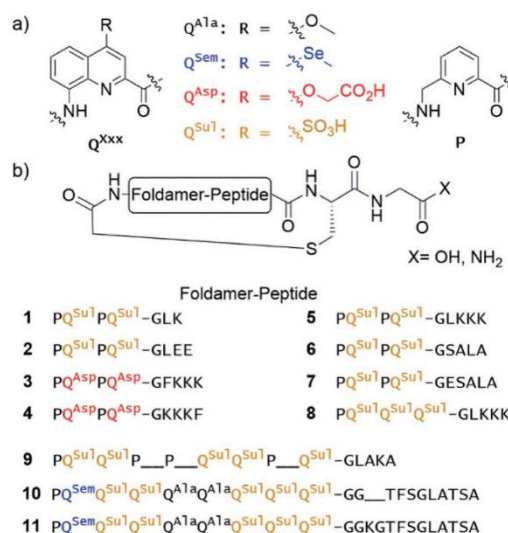


Fig. 1 (a) Foldamer aromatic building blocks colour coded according to their side chain composition. (b) Sequence of macrocyclic foldamer–peptide hybrids synthesised on solid-phase. Most of the macrocycles possess a C-terminal carboxylic acid at the exception of 5 and 8 which possess a primary amide.

Department of Pharmacy and Center for Integrated Protein Science, Ludwig-Maximilians-Universität, Butenandtstraße 5-13, D-81377 Munich, Germany. E-mail: ivan.huc@cup.lmu.de

† Electronic supplementary information (ESI) available: Synthetic protocols, details of crystallographic studies, characterisation of new compounds. CCDC 2002474, 2010131 and 2010173. For ESI and crystallographic data in CIF or other electronic format see DOI: 10.1039/d1sc03640h



stable helically folded conformations, particularly in water.^{7,8} The folding propensity of Q units is so high that they promote folding in otherwise flexible units, including α -amino acids,^{9,10} when these flexible units are inserted within Q_n oligomers. The folding propensity of P units is weaker. For example, the rate of interconversion between right-handed (*P*) and left-handed (*M*) helical conformers increases when the proportion of P units within a Q_n sequence increases,¹¹ and P units promote less ordered conformations in organic solvents.¹² P units were required for ribosomal expression, presumably because sequences must transiently unfold to transit through the ribosome exit tunnel.⁴ In macrocyclic aromatic foldamer-peptide hybrids, the first role of the foldamer is thus to bring prevalent folding information that may influence the peptide conformation. This approach can therefore be related to other synthetic appendages used to induce peptide conformations, *e.g.* molecular rotors,¹³ or α -helix staples.¹⁴ It also relates to the observation that natural macrocyclic peptides are the object of multiple biosynthetic modifications that expand their functions beyond what can be achieved with proteinogenic α -amino acids only.

Herein, we present an investigation of the interplay of foldamer and peptide conformations within such hybrid macrocycles upon varying parameters such as foldamer and peptide segment length and side-chain composition as well as the proportion of P and Q units within the foldamer. We find that, within macrocycles, foldamer helices may have a strong impact on peptide conformation. For example, we introduce the concept of peptide stretching *via* helical foldamer folding. We show that, concomitantly to conformational effects, the foldamers confer enhanced resistance of the peptides to proteolytic degradation. Furthermore, we observe a systematic reciprocal effect of the peptide whose chirality controls the foldamer helix handedness. The peptide loop also stabilises the foldamer helix conformation, thus acting as a sort of staple. Altogether, our results highlight the singular nature of these macrocyclic hybrids and the interest in involving them in future nucleic acid-encoded display selection experiments.

Results and discussion

Design and synthesis

Eleven hybrid macrocycles were considered that can be divided into two groups (Fig. 1). As a first group, compounds 1–7 and 8 consist of a PQPQ or PQQQ tetraamide foldamer segment, respectively, and peptide chains of variable length and composition. With three consecutive Q units, the foldamer helix of 8 was expected to be conformationally more stable, yet able to undergo handedness reversal in water.¹⁵ The Q^{Sul} monomer was considered instead of the Q^{Asp} of previously described compound 3,⁴ because it confers very good water solubility as well as crystal growth ability.¹⁶ The intracyclic peptide segments ranged from three to six amino acids. Depending on the amino acid sequence and on the OH or NH₂ C-terminal functionality, these eight compounds encompassed a variety of charge states at neutral pH, between –5 for 2 and +1 for 5.

In a second group, we considered longer sequences with a foldamer segment encompassing nine P or Q units, and

intracyclic peptide segments ranging from five to thirteen amino acids. Compounds 9–11 thus comprise exactly five more aromatic units than 1–8, which amounts to exactly two helix turns.¹⁷ Thus, the aromatic helices differ in length across the two series but the anchor points of the peptides on the helices are positioned similarly so as to form a loop on one face of the helix. In 10 and 11, the eight consecutive Q units will confer the aromatic helix with such a high stability that handedness reversal is expected to remain kinetically inert in water.¹⁸ In contrast, hybrid macrocycle 9 has a mix of P and Q units, including two consecutive Ps, which was predicted to allow for helix handedness reversal in water at room temperature.¹¹ Compound 9 also has a much shorter peptide segment than 10 and 11, whose peptides differ only by two additional amino acids in 11. The Q^{Sem} unit was introduced to facilitate X-ray crystal structure elucidation using the anomalous scattering of Se, but this was not implemented as X-ray quality crystals of 10 and 11 were not obtained.

Of note, compounds 1–7 may in principle be expressed by the ribosome using a PQQQ-GF initiator, whereas 8–11 are more rigid (8) or longer (9–11) than what the ribosome has been shown to tolerate until now.^{4,5} One may nevertheless consider introducing large and rigid foldamer helices, such as those of 8–11 into hybrid macrocycles through a post-translational modification, *i.e.* after ribosomal translation of the peptide.³ For the purpose of the present study, all compounds were produced by chemical synthesis. The microwave-assisted solid phase synthesis (SPS) of the non-cyclic *N*-chloroacetamido-terminated foldamer peptide hybrid precursors was performed using established protocols.^{4,8} The precursors of 5 and 8 were synthesised by iterative coupling on low-loading (LL) Rink amide resin with the use of HBTU for peptide couplings and couplings on the aliphatic amine of P units, and acid chloride activation for couplings on the aromatic amines of Q units (see ESI and Fig. S1† for details).⁸ The C-terminal primary amide of both 5 and 8 was found to hydrolyse under the conditions used for structural investigations. Consequently, most other oligomers were prepared on LL Fmoc-Gly-Wang resin to yield acid-terminated sequences. We also investigated the benefits of the ProTide™ resin, which contains a PEG and polystyrene core and possesses excellent swelling properties. We found that using the commercially available LL Cl-MPA ProTide™ resin resulted in significant improvements in SPS recovered crude yield and product purity (see ESI†). The precursors of the longest hybrid molecules 9–11 were thus synthesised on this resin.

The non-cyclic precursors of 1, 3, 4 and 9 were prepared using identical SPS protocols to those used for the precursors of 5 and 8. For the precursors of 2, 6, and 7, which share the same foldamer segment, as well as for the precursors of 10 and 11, a fragment condensation approach was developed and implemented. This consisted in the SPS and purification of an Fmoc-foldamer-G-OH segment and then of the coupling of this entire segment to the N-terminal amine of the resin-bound peptide using a phosphonium-based coupling reagent (Fig. S1†). This strategy allows for faster diversification of either the peptide or the foldamer parts, which could be independently constructed



and assembled in a second stage. After chloroacetylation and final resin cleavage, the non-cyclic precursors produced by fragment condensation were recovered in high purity and good yield (see ESI†).

Macrocyclisations were performed *via* substitution of the chlorine by the Cys thiol side chain at low concentration (100 μM) with triethylamine as base (see ESI†). The PQQ-containing sequences 1–5 macrocyclised within 30 min in aqueous medium. Reverse phase HPLC (RP-HPLC) monitoring showed that, under the same conditions, it took 3 h to observe full conversion to sequences 6–8, and one day for 10 and 11. RP-HPLC analysis of crude 11 showed two peaks with the same integration. The corresponding products were separated by semi-preparative RP-HPLC. ESI-MS, NMR and circular dichroism (CD) spectroscopies allowed us to identify these compounds as the right-handed *P*-11 and the left-handed *M*-11 diastereomers. As planned in the initial design, interconversion between these compounds is kinetically hampered in water at room temperature. The separation of *P*-10 and *M*-10 could not be achieved.

Sequence 9, which possesses a short peptide chain with respect to its foldamer segment, did not cyclise in water, but slowly cyclised in DMF. RP-HPLC analysis showed reaction completion after 36 hours. This result unveils that compound 9 may cyclise only when its foldamer helix is partly unfolded, a situation that required both multiple P units and a solvent like DMF that is less favourable to aromatic helix folding. This peculiar behaviour has been further investigated as reported below.

Helix folding and handedness bias in solution

Circular dichroism (CD) spectra of hybrid macrocycles 1–9 all showed bands in the 260–460 nm region (Fig. 2), where the peptides do not absorb light, providing qualitative evidence of helical folding of the foldamer segments, and of helix handedness bias. Thus, we can infer that in macrocycles 1–8 that contain a tetraamide foldamer, and in macrocycle 9 that contains a nonaamide foldamer with multiple P units, helix handedness is dynamic in solution and is biased by the *L*-chirality of the peptide despite the fact that the helices themselves bear no stereogenic centre. This type of remote communication of stereogenic information requires a transmission mechanism along the macrocycle, a phenomenon that has been observed in other systems.^{19–23} The positive sign of the CD bands at 331 or 408 nm indicate that *P*-helicity is favoured regardless of peptide length and sequence.²⁴ In contrast, the diastereomeric conformers *P*-11 and *M*-11 obtained by chromatographic separation showed opposite CD spectra that did not evolve with time. In this case, helix handedness is kinetically inert. The same kinetic inertness may be expected for the related macrocycle 10. Thus, the flat CD spectrum of 10 reflects the fact that *P*-10 and *M*-10 were recovered as 1 : 1 mixture after SPS and that their CD spectra cancel each other. The chiral centres on the peptide may in principle stabilise one or the other helical sense, but this influence does not operate because helix handedness inversion is kinetically locked on the laboratory time scale.

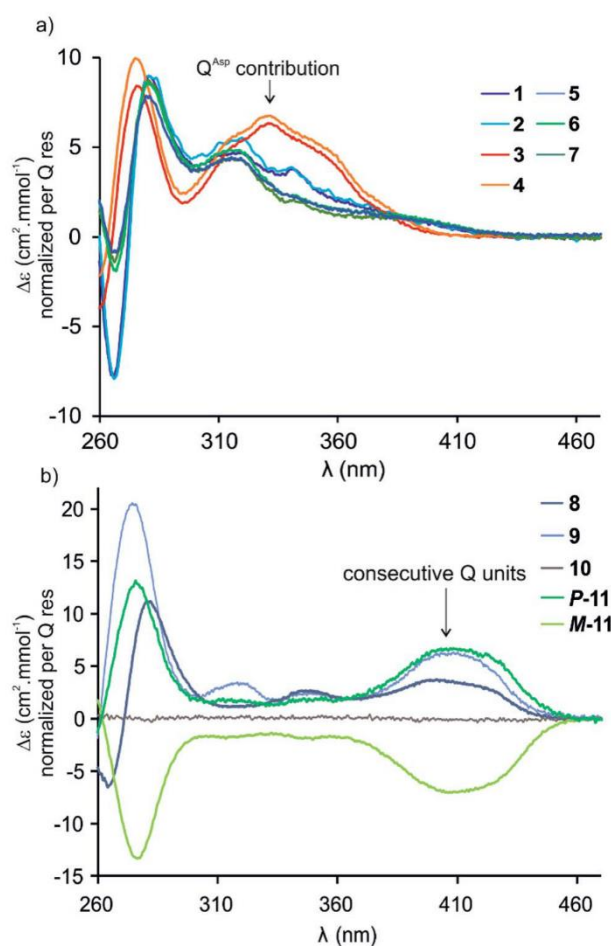


Fig. 2 CD spectra of 1–11 in water/acetonitrile (75 : 25, v/v) at 20 °C. (a) Sequences 1–7 composed of a PQQ segment. (b) Sequences 8–11 containing consecutive Q units. The *P* and *M* helical conformers of 11 are stable and were separated by RP-HPLC. The flat CD spectrum of 10 indicates a 50 : 50 mixture of *P*- and *M*-helical conformers.

By comparison with other chiral Q_n oligomers^{18,24} the intensity of CD spectra of 1–9 ($\Delta\epsilon$ values normalised by Q residue in Fig. 2) suggest that helix handedness bias is strong. Nevertheless, it is difficult to precisely quantify diastereomeric excess on the sole basis of CD intensity because the CD bands vary according to the foldamer sequence. For instance, the band at 408 nm is observed only when consecutive Q units are present (Fig. 2b). Bands at 331 or 320 nm are observed depending on whether Q units are Q^{ASP} (3–4), or Q^{Sul} (1–2) and (5–7), respectively (Fig. 2a).

NMR spectroscopy provided additional evidences of foldamer helical folding and helix handedness bias (Fig. 3). Two typical indicators are the spreading of resonances over a large range of chemical shift values and significant upfield shifts of the signals of protons shielded by ring current effects associated with aromatic stacking within the helix. Typically, the signal of one quinoline H3 proton of PQQ foldamers 1–2 and 5–7 is found near 8.7 ppm, and the other near 7.9–7.6 ppm (Fig. S3†). In foldamers 3 and 4 which bear different side chains on their Q units, H3 signals are shifted to 7.6–7.4 ppm for one and 6.7–



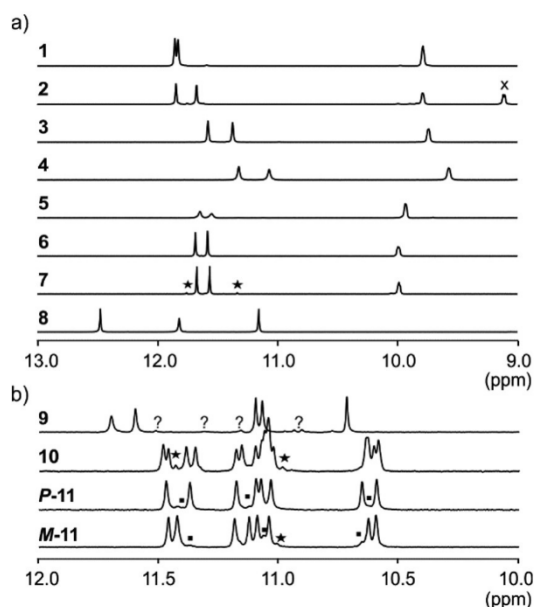


Fig. 3 Excerpts from the 500 MHz ^1H NMR spectra of (a) compounds 1–8 recorded at 25 °C in $\text{H}_2\text{O}/\text{CD}_3\text{CN}$ 75 : 25 (v/v) and (b) compounds 9 and 10, 11 recorded at 25 °C in $\text{H}_2\text{O}/\text{D}_2\text{O}$ 9 : 1 (v/v), and $\text{H}_2\text{O}/\text{CD}_3\text{CN}$ 1 : 1 (v/v), respectively. The spectra show amide resonances *i.e.* typically all NHs belonging to Q and some NHs belong to P units. Other NHs belonging to P units are found at lower field and overlap with aromatic resonances. X indicates the signal of an aromatic proton. Resonances marked with stars have been interpreted as impurities. Squares in the spectra of *P*-11 and *M*-11 correspond to the other diastereoisomer resulting from incomplete separation. Resonances marked with (?) in 9 could be an impurity or the other diastereomeric conformer.

6.5 ppm for the other, but the chemical shift difference nevertheless remains. This difference shows that only one quinoline H3 proton is exposed to ring current effects mediated by aromatic stacking, in agreement with solid state structures of the helices (see below).

The ^1H NMR aromatic amide signals of *P*-11 and *M*-11 were found to differ (Fig. 3b). Their purity confirmed the good separation of these two compounds by RP-HPLC. The chemical shift differences between aromatic NH resonances of these two compounds is remarkable considering that the corresponding protons lie within the helix and not in close proximity of the peptide stereogenic centre. This highlights the fact that diastereomeric conformers should be distinguishable by NMR when they exchange slowly on the NMR timescale. The foldamer helices of 8 and 9 are both expected to undergo slow handedness inversion on the NMR time scale, as do previously described sequences as short as Ac-Q₃-G-OH and Ac-QPQPQ-G-OH.⁴ The presence of a single set of signals in the ^1H NMR spectra of 8 and 9 (Fig. 3) thus reflects that handedness bias is quantitative, as far as NMR can detect, in these two cases.

The NMR spectra of 1–7 also show a single set of signals. This may reflect either quantitative helix handedness bias, *i.e.* exchange is slow but the other diastereomer is not abundant enough to be detected, or that exchange remains fast even at low temperatures. Indeed, fast *P/M*-helix equilibrium on the NMR

timescale might be expected for these compounds on the basis that Ac-PQ^{ASP}PQ^{ASP}-G-OH undergoes fast exchange at room temperature.⁴ We probed the anisochronicity of the main chain NH-CH₂-aryl methylene protons in the centre of the PQ^{Sul}PQ^{Sul} foldamer segment of 1, 2, 5 and 7 (Fig. S5†). Total correlation spectroscopy (TOCSY) spectra recorded at different temperatures showed distinct signals for the two protons and variable $\Delta\delta$ values. However, this information alone remains inconclusive: Clayden *et al.* have thoroughly illustrated how a chemical shift difference $\Delta\delta$ between diastereotopic protons is compatible with fast exchange combined with helix handedness bias.²⁵ Thus the observed anisochronous CH₂ signals do not directly inform about helix handedness dynamics and the extent of handedness bias. We therefore decided to synthesise achiral compounds to assess whether exchange is slow or fast on the NMR timescale and whether the peptide loop may stabilise the helix.

Stabilisation of the foldamer helix by the peptide loop

Macrocycle 13 (Fig. 4a) is achiral: it contains five glycines and a cysteamine instead of the cysteine of other macrocycles. It was

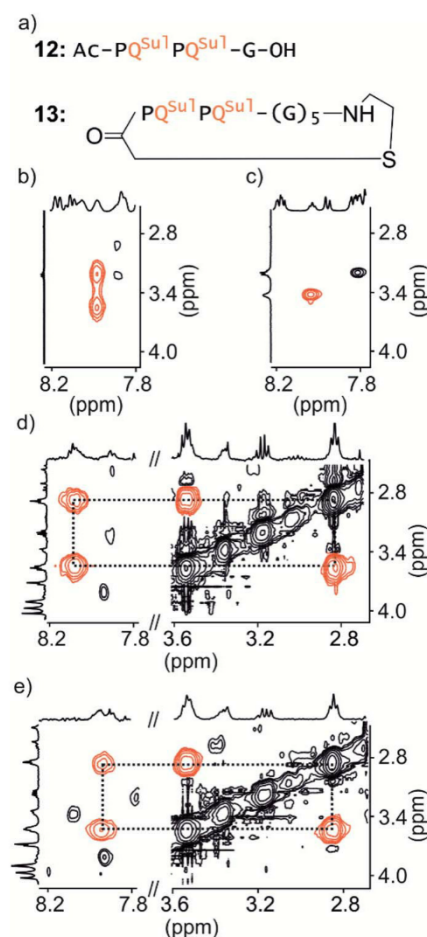


Fig. 4 Parts of TOCSY spectra showing NH-CH₂ J-couplings of 12 (a) in 50 mM NaHCO₃ in $\text{H}_2\text{O}/\text{D}_2\text{O}$ (9 : 1 v/v) at -5 °C (b) and 25 °C (c) respectively and of 13 (a) in 12.5 mM NH₄OAc in $\text{H}_2\text{O}/\text{CD}_3\text{CN}$ (75 : 25 v/v) at 0 °C (d) and 25 °C (e) respectively.



prepared by SPS using commercially available cysteamine 2-chlorotriyl resin. Compound **12** was prepared as a non-cyclic control.

We have shown before that the benzylic diastereotopic CH₂ protons of P units have different chemical shift values in the context of aromatic helices: they are anisochronous.⁸ However, if the *P* and *M* conformers equilibrate rapidly on the NMR time-scale, only average signals are observed. In basic medium (50 mM NaHCO₃), the TOCSY spectrum of **12** show no anisochronicity of these CH₂ protons at room temperature indicating fast helix handedness inversion (Fig. 4c and S6†), as was previously observed for Ac-PQ^{Asp}PQ^{Asp}-G-OH.⁴ Upon cooling to -5 °C, diastereotopic CH₂ signals coupled to amide NH groups split (Fig. 4b), indicating that slow exchange is reached. Unfortunately, cyclic compound **13** is not well soluble in this medium and showed only broad peaks. Measurements were instead performed in H₂O/CD₃CN 75 : 25 (v/v). In the presence of acetonitrile, the signals of diastereotopic protons of **12** no longer split, even at -10 °C, indicating that helix handedness inversion is faster in the presence of acetonitrile. In contrast, the spectrum of **13** shows anisochronous signals for its diastereotopic protons even at 25 °C (Fig. 4d, e and S7†) with $\Delta\delta$ values up to 0.68 ppm. We thus conclude that the peptide loop slows down helix handedness inversion, *i.e.* that it stabilises the foldamer helix. This result also indicates that the single set of NMR signals of **1-7** reflect slow exchange combined with quantitative handedness control of the foldamer helix by the chiral peptide.

Solid state structure elucidation

The solid state structures of foldamer peptide macrocycles **1**, **7** and **9** were elucidated by single crystal X-ray crystallography, in

addition to the previously described structure of **3**.⁴ Racemic crystallography²⁶ had proven essential in the case of **3** as well as for other chiral foldamers and peptides.^{9,27} In anticipation, *D*-**1** and *D*-**9** were synthesised and mixed with the *L*-enantiomer to produce racemic mixtures. Eventually, this proved unnecessary in the case of **1** since single crystals of *D*-**1** diffracting at atomic resolution (0.8 Å) were obtained (Fig. S9†). The structure was solved in space group *P6*₅. The image shown in Fig. 5a is actually the mirror-image conformation of *D*-**1** to allow for comparison with the *L*-enantiomers of the other structures. We also obtained crystals of **7** that diffracted at 1.06 Å, and the structure could be solved in space group *P1* with eight independent molecules in the asymmetric unit (Fig. 5c, d and S10†). In the structures of **1** and **3**, and in the eight independent molecules of **7**, the aromatic foldamer PQQP segment was found to invariably adopt the same compact helical conformation whose ends are connected by a peptide loop. Changing loop size and sequence has no visible effect on foldamer conformation. The helices are right-handed in agreement with the sign of the CD bands in solution (Fig. 2a).

An inter-segment hydrogen bond between the NH of the third amino acid of the peptide segment and an amide CO of the foldamer segment had been previously seen in the structure of **3**.⁴ This interaction was invoked as a possible mechanism for the transmission of stereochemical information from the peptide to the foldamer handedness. The same hydrogen bond can be observed in the structure of **3** and in six out of the eight structures of **7**, and also in the structure of **9** (see below). However, no such interactions are observed within the shorter peptide loop of **1**. How stereochemical information is conveyed

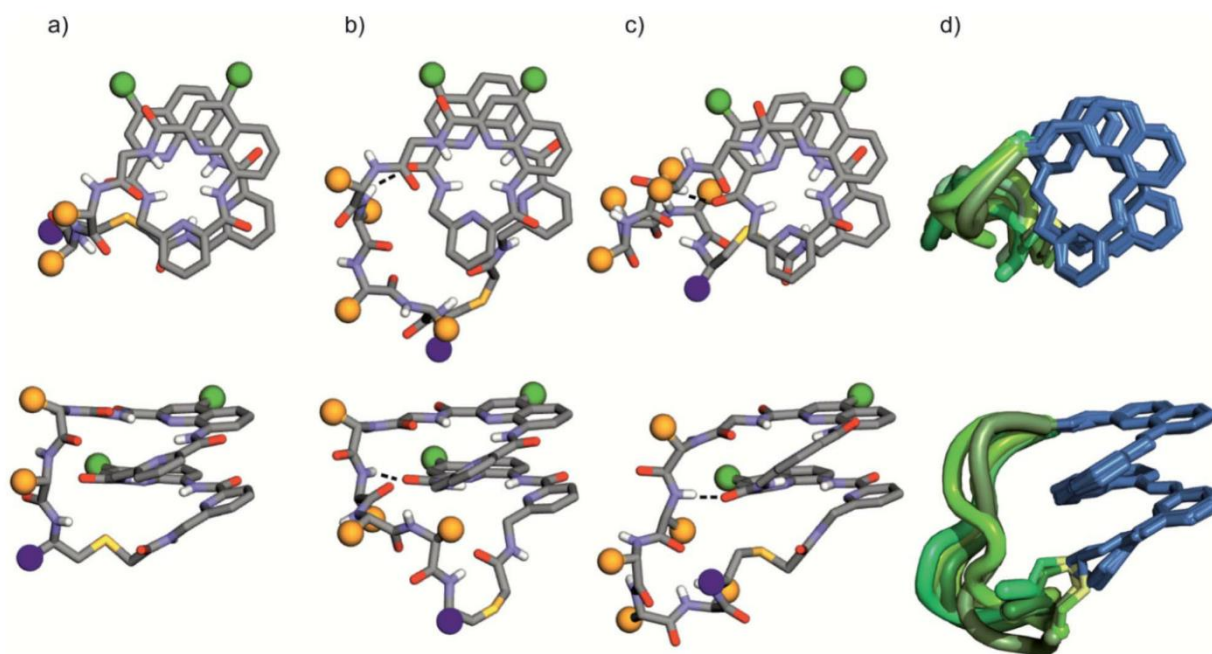


Fig. 5 Solid-state structures of **1** (a), **3** (b), and **7** (c) in ball and stick representation shown in top views (above) and side views (below). Amino acid side chains in the peptide loop are represented as orange spheres. Foldamer side chains are shown as green spheres, and peptide C-termini are shown as purple spheres. Peptide-foldamer hydrogen bonding is shown as dashed lines. (d) Overlay of eight different conformers obtained from the crystal structure of **7**. The foldamer is represented in blue, the thioether linker in yellow, and the peptide loops in different green tones.



from the peptide to the foldamer is thus not always apparent. The mechanism may not necessarily entail the stabilisation of the observed favoured diastereomeric conformer but may instead rest on the destabilisation of the less favoured conformer. Furthermore, stereochemical information may also be conveyed directly through the main chain.^{20,21} The crystal structures also reveal that all peptide side chains point away from the foldamer. This hints at the possibility that handedness bias is independent from the peptide sequence, as seems to be the case for all macrocycles in this study, despite their sequence and charge state variability.

The eight molecules of **7** highlight some differences in the long peptide loop conformation (Fig. 5d and S10†) which may contain intrapeptide hydrogen bonds. When the peptide loop is short with respect to helix length as in **1**, its conformational freedom is reduced because the helical folding of the foldamer amounts to stretching the peptide segment. Peptide stretching was also obvious in the crystal structure of **9** which was obtained concurrently (Fig. 6). In this case, crystals of the pure enantiomer only diffracted at a resolution of 2.4 Å whereas the racemate produced crystals that diffracted at 1.2 Å. The X-ray structure of the racemate could be solved and refined in the *P1* space group. The asymmetric unit contains three molecules of each enantiomer where *L*-**9** adopted a canonical right-handed helix conformation and its *D*-counterpart the opposite handedness (Fig. 6a and S11†). Thus, the foldamer helix folds despite the relatively short peptide which is stretched as a result. The six conformers were overlaid after inverting the three *D*-enantiomers (Fig. 6b), showing high conservation of the helix shape and minimal variations of the peptide loop. A certain analogy may be drawn between the effect of the foldamer and the effect of the multiple staples that have been shown to stabilise α -helical peptide conformations.¹⁴ Inserting a rigid component in a peptide macrocycle may favour an extended or a helical peptide conformation, depending on the rigid component's length.

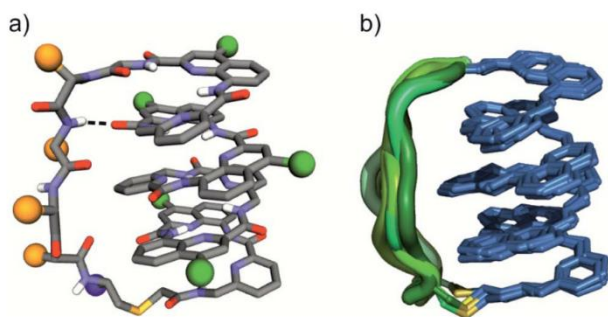


Fig. 6 (a) Solid state structure of **9** in ball and stick representation; amino acid side chains in the peptide loop are represented as orange spheres; foldamer side chains are shown as green spheres; the C-terminus is shown as a purple sphere; and a peptide–foldamer hydrogen bond is shown as a dashed line. (b) Overlay of six different conformers obtained from the crystal structure of **9**; the foldamer represented in blue, the thioether linker is represented in yellow and the peptide loops are represented in different green tones.

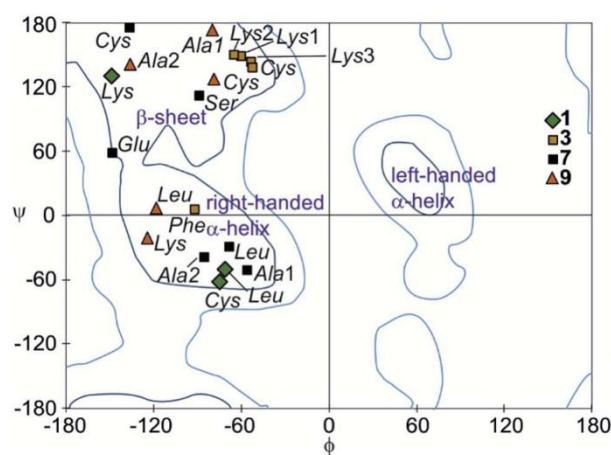


Fig. 7 Peptide chain dihedral angles (ϕ and ψ) obtained from X-ray crystal structures of compounds **1**, **3**, **7**, and **9** shown in a Ramachandran plot. Dark blue lines represent favoured regions; light blue lines represent allowed regions.

The peptide ϕ and ψ angles of the solid state structure of **1**, **3**, **7** and **9** were measured and reported in a Ramachandran plot²⁸ (Table S1,† Fig. 7). The plot showed that a wide range of values, typical of α -helices and β -sheets, are covered. All of these values are within the classical favoured regions. No values were found within the left-handed α -helix area, unlike when individual amino acids are inserted within Q_n sequences.¹⁰ Thus, the influence of the foldamer helices on the peptides do not extend to the induction of disfavoured conformations.

Foldamer folding induces peptide extension

The stretched peptide in the solid state conformation of **9** likely explains why the macrocyclisation step that produces **9** did not work in water, unlike the other macrocyclisation reactions reported here, and why macrocyclisation of **9** proceeded smoothly in DMF. The foldamer segment of **9** contains four flexible P units out of nine monomers. The P units were introduced to accelerate helix handedness inversion and allow for helix sense bias to take place in water. The helix destabilising effect of P units is enhanced in organic solvents to the point that $(PQ)_n$ oligomers do not adopt a canonical helix conformation in chloroform but instead include 90° kinks between PQ dimers.¹² Conversely, water stabilises canonical helix conformations⁷ and $(PQ)_n$ oligomers are normally folded in water.⁸ Compound **9** may not have cyclised in water precisely because of its well-folded structure, so the peptide would have had to stretch for cyclisation to take place. In contrast, the foldamer may not be fully folded or not always folded in DMF, thus allowing for cyclisation without stretching the peptide (Fig. 8a). To test this hypothesis, we measured the CD spectrum of *D*-**9** in DMF and monitored its change as water is progressively added (Fig. 8b). Note that *D*-**9** has opposite chirality to **9** and thus an opposite CD spectrum (compound *D*-**9** was available, and a resynthesis of *L*-**9** for this experiment was thus unneeded). We found that



a weaker CD signal is observed in pure DMF than in water, and that its sign suggests *P*-handedness, thus confirming a different folding behaviour in this solvent. Upon adding water, the CD signal progressively evolves to that of the one handed *M*-helix characterised by NMR and X-ray crystallography. In contrast, no such solvent-induced variation is observed when performing the same experiment with shorter macrocycle **8** (Fig. S4†), whose PQ₃ segment folds regardless of solvent. These results thus allow to formulate the original concept of peptide extension directed by solvent-induced aromatic foldamer folding.

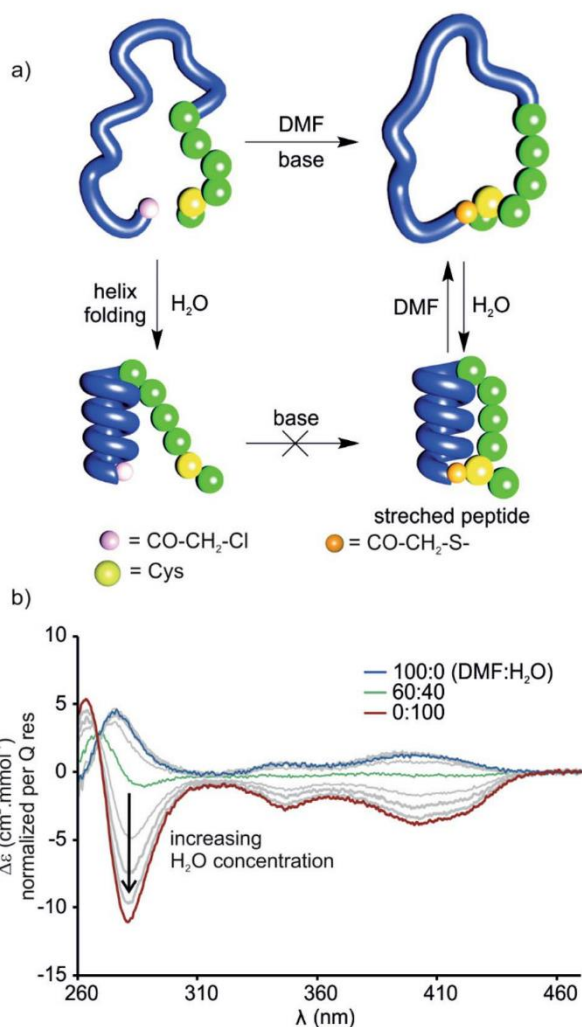


Fig. 8 (a) Cartoon representation of the folding of a macrocyclic foldamer-peptide hybrid (compound **9**, foldamer segment depicted as a blue strand, α -amino acid residues represented as green spheres) in DMF and water before and after cyclisation. Thioether formation (the cysteine thiol reacts with chloroacetamide under basic conditions) progressed rapidly in DMF whereas in water no cyclisation was observed. Folding of the helix could be induced in an aqueous environment which resulted in stretching of the peptide segment in the macrocycle. (b) CD-spectra of **9** in various DMF/H₂O mixtures at 25 °C. *M*-helical handedness of the foldamer is promoted by increasing water concentration (grey lines represent increasing water concentration in 10% steps).

The foldamer confers resistance to proteolytic degradation

We further evaluated the proteolytic stability of the macrocyclic foldamer-peptide hybrids. Improved stability in biological media would be of interest for their potential future translatability as therapeutic molecules as demonstrated for other peptidic macrocycles, for example in the field of protein-protein interaction modulation. We focused on sequences **1**, **3** and **4**, the latter two being sequence isomers, and assessed their degradation by three proteases, namely α -chymotrypsin, trypsin and pronase E (Fig. 9 and S12†). Chymotrypsin cleaves amide bonds on the C-terminal side of hydrophobic and/or aromatic

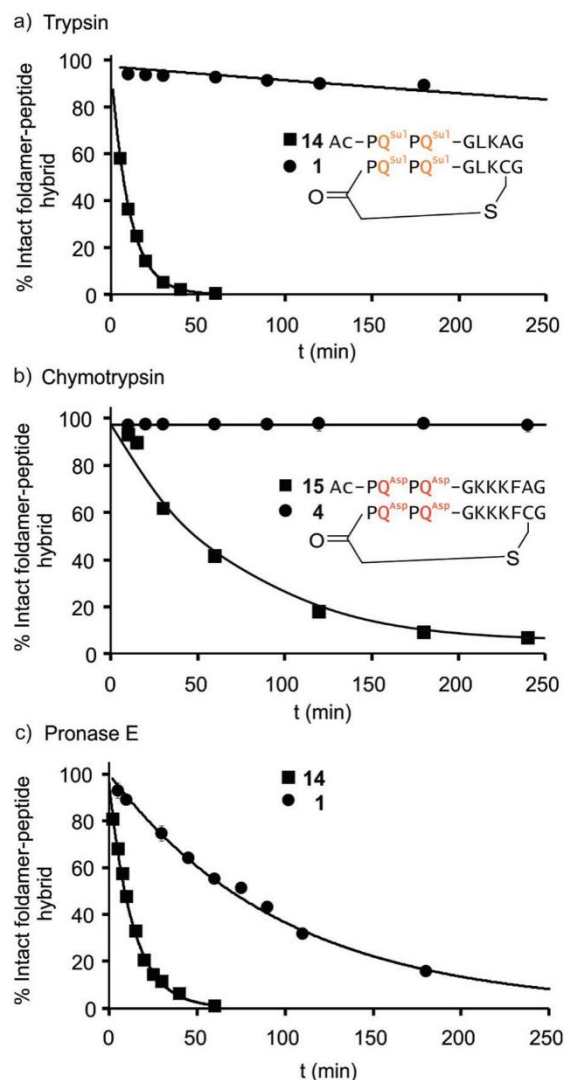


Fig. 9 Representative enzymatic degradation of foldamer-peptide hybrids in the presence of (a) trypsin E; (b) α -chymotrypsin; and (c) pronase E. The decreasing abundance of intact macrocyclic compound **1** [(a) and (c)] and compound **4** [(b)] (circles) are shown along with their respective non-cyclic analogues **14** and **15** (squares). The percentage of intact foldamer-peptide hybrid was calculated as the area under the HPLC chromatogram corresponding to the foldamer-peptide hybrid at each time point relative to $t = 0$. Lines are for guiding the eye only, they do not represent a fit.



residues (Leu or Phe). Trypsin cleaves on the C-terminal side of positively charged residues (Lys). Pronase E acts at many different sites of α -peptides. In order to assess the importance of macrocyclisation in resistance towards proteolytic degradation, non-cyclic analogues **14**, **15** (Fig. 9) and **16** (see ESI†) were synthesised as reference compounds for **1**, **4** and **3**, respectively. To avoid problems with oxidation, Cys was replaced by Ala in the acyclic molecules.

The kinetics of proteolysis was monitored by RP-LC-MS.^{29,30} Representative degradation curves are depicted in Fig. 8 and S13.† In all cases, acyclic analogues containing cognate cleavage sites were degraded rapidly and had disappeared within one to four hours under the conditions used. In contrast, macrocycle **4** was completely resistant to degradation by chymotrypsin (Fig. 9b) and above 90% of **1** was still present in trypsin-containing medium after 250 min (Fig. 9a). Compound **1** was more prone to degradation by pronase E, with a half-life of $t_{1/2} = 69$ min (Fig. 9c). But this degradation was still considerably slower than that of its acyclic analogue **14** ($t_{1/2} = 9$ min). Compound **3** was more sensitive than **1** to the action of trypsin – due to the fact that it possesses three Lys residues instead of one – and pronase E, but its degradation was nevertheless slower ($t_{1/2} = 41$ min) than that of its acyclic analogue **16** ($t_{1/2} = 3.6$ min, Fig. S12†).

LC-MS analyses also allowed us to characterise the degradation products (Fig. S13–S17†). The action of pronase E on macrocycle **1** induced the loss of central Leu–Lys dipeptide, which entails hydrolysis after Gly and before Cys, but it is unclear which of these two cleavages occurs first since the second cleavage is faster and intermediates do not accumulate (Fig. S13†). The non-cyclic analogue **14** evolved into the Ac-PQ^{Sul}PQ^{Sul}-G fragment and intermediates show that cleavage occur at multiple sites. As anticipated, the action of trypsin on **14** induced the loss of the Ala–Gly dipeptide (Fig. S14†). The same dipeptide was released during the incubation of **15** with chymotrypsin (Fig. S15†). As mentioned above, macrocycles **1** and **4** are much less prone to these cleavages. For sequences **3** and **16** LC-MS analysis confirmed that trypsin cleaves at different lysine residues whereas pronase has a different degradation pattern (Fig. S16 and S17†). Overall, these experiments highlight that proteolytic degradation is dependent on which protease and which peptide sequence are involved, but that in all cases, significant resistance is conferred by insertion of the peptide in a hybrid macrocycle containing a foldamer helix. These results bode well for the possible use of such macrocycles *in vivo*.

Conclusions

Our results demonstrate extensive conformational interplay between peptides and helical aromatic foldamers within hybrid macrocycles. The peptide loop stabilises the foldamer helix conformations and quantitatively biases its handedness. Conversely, aromatic helix folding restricts the peptide conformation to an extended structure when the length of the two segments (peptide *vs.* folded helix) match. We also showed that proteolytic degradation of the peptide is slowed down considerably within these hybrid macrocycles. Altogether these results

suggest that hybrid foldamer–peptide macrocycles extend the range of properties beyond what can be achieved with peptide macrocycles alone. Further investigation may concern the contribution of the foldamer segment to enhance the cell penetration of the peptide,³¹ or to enhance the peptide's ability to bind to a protein target. Progress along these lines is being made and will be reported in due course.

Data availability

Crystallographic data for **1**, **7**, and **9** has been deposited at the CCDC under accession numbers 2002474, 2010173 and 201013, respectively, and can be obtained from <https://www.ccdc.cam.ac.uk>.

Author contributions

S. D. carried out most of the experimental work. P. K. M. assisted with crystal growth, X-ray data collection, crystal structure elucidation and refinement. L. A. carried out NMR data collection. C. D. contributed to synthesis and CD studies, and co-supervised the work. I. H. conceptualised and supervised the study. S. D., C. D. and I. H. wrote the manuscript. All authors commented the data and reviewed the manuscript.

Conflicts of interest

There are no conflicts to declare.

Acknowledgements

We thank Dr J. Basquin and Dr G. Pompidor for assistance in synchrotron measurement at the PXII beamline at Swiss Light Source (SLS, Villigen, Switzerland) and the P13 beamline operated by EMBL Hamburg at PETRA III storage ring (DESY, Hamburg, Germany) respectively.

Notes and references

- C. J. Noren, S. J. Anthony-Cahill, M. C. Griffith and P. G. Schultz, *Science*, 1989, **244**, 182; K. Josephson, M. C. T. Hartman and J. W. Szostak, *J. Am. Chem. Soc.*, 2005, **127**, 11727; Y. V. Schlippe, M. C. Hartman, K. Josephson and J. W. Szostak, *J. Am. Chem. Soc.*, 2012, **134**, 10469; Y. Sako, J. Morimoto, H. Murakami and H. Suga, *J. Am. Chem. Soc.*, 2008, **130**, 7232; H. Neumann, K. Wang, L. Davis, M. Garcia-Alai and J. W. Chin, *Nature*, 2010, **464**, 441; T. Kawakami, K. Ogawa, T. Hatta, N. Goshima and T. Natsume, *ACS Chem. Biol.*, 2016, **11**, 1569.
- Y. Goto, A. Ohta, Y. Sako, Y. Yamagishi, H. Murakami and H. Suga, *ACS Chem. Biol.*, 2008, **3**, 120; Y. Yamagishi, I. Shoji, S. Miyagawa, T. Kawakami, T. Katoh, Y. Goto and H. Suga, *Chem. Biol.*, 2011, **18**, 1562; S. A. K. Jongkees, S. Caner, C. Tysoe, G. D. Brayer, S. G. Withers and H. Suga, *Cell Chem. Biol.*, 2017, **24**, 381; T. Passioura, W. Liu, D. Dunkelmann, T. Higuchi and H. Suga, *J. Am. Chem. Soc.*, 2018, **140**, 11551.



- 3 P. Timmerman, J. Beld, W. C. Puijk and R. H. Meloen, *ChemBioChem*, 2005, **6**, 821; C. Heinis, T. Rutherford, S. Freund and G. Winter, *Nat. Chem. Biol.*, 2009, **5**, 502; S. S. Kale, C. Villequey, X. D. Kong, A. Zorzi, K. Deyle and C. Heinis, *Nat. Chem.*, 2018, **10**, 715; D. E. Streefkerk, M. Schmidt, J. H. Ippel, T. M. Hackeng, T. Nuijens, P. Timmerman and J. H. van Maarseveen, *Org. Lett.*, 2019, **21**, 2095; G. K. Mothukuri, S. S. Kale, C. L. Stenbratt, A. Zorzi, J. Vesin, J. Bortoli Chapalay, K. Deyle, G. Turcatti, L. Cendron, A. Angelini and C. Heinis, *Chem. Sci.*, 2020, **11**, 7858.
- 4 J. M. Rogers, S. Kwon, S. J. Dawson, P. K. Mandal, H. Suga and I. Huc, *Nat. Chem.*, 2018, **10**, 405.
- 5 C. Tsiamantas, S. Kwon, C. Douat, I. Huc and H. Suga, *Chem. Commun.*, 2019, **55**, 7366.
- 6 C. Tsiamantas, S. Kwon, J. M. Rogers, C. Douat, I. Huc and H. Suga, *Angew. Chem., Int. Ed.*, 2020, **59**, 4860.
- 7 T. Qi, V. Maurizot, H. Noguchi, T. Charoenraks, B. Kauffmann, M. Takafuji, H. Ihara and I. Huc, *Chem. Commun.*, 2012, **48**, 6337.
- 8 B. Baptiste, C. Douat-Casassus, K. Laxmi-Reddy, F. Godde and I. Huc, *J. Org. Chem.*, 2010, **75**, 7175.
- 9 M. Kudo, V. Maurizot, B. Kauffmann, A. Tanatani and I. Huc, *J. Am. Chem. Soc.*, 2013, **135**, 9628.
- 10 X. Hu, P. K. Mandal, B. Kauffmann and I. Huc, *ChemPlusChem*, 2020, **85**, 1580–1586.
- 11 M. Vallade, P. Sai Reddy, L. Fischer and I. Huc, *Eur. J. Org. Chem.*, 2018, 5489.
- 12 N. Delsuc, F. Godde, B. Kauffmann, J.-M. Léger and I. Huc, *J. Am. Chem. Soc.*, 2007, **129**, 11348.
- 13 D. B. Diaz, S. D. Appavoo, A. F. Bogdanchikova, Y. Lebedev, T. J. McTiernan, G. dos Passos Gomes and A. K. Yudin, *Nat. Chem.*, 2021, **13**, 218.
- 14 Y. H. Lau, P. De Andrade, Y. Wu and D. R. Spring, *Chem. Soc. Rev.*, 2014, **44**, 91; G. L. Verdine and G. J. Hilinski, *Methods Enzymol.*, 2012, **503**, 3; C. E. Schafmeister, J. Po and G. L. Verdine, *J. Am. Chem. Soc.*, 2000, **122**, 5891.
- 15 J. Buratto, C. Colombo, M. Stupfel, S. J. Dawson, C. Dolain, B. Langlois d'Estaintot, L. Fischer, T. Granier, M. Laguerre, B. Gallois and I. Huc, *Angew. Chem., Int. Ed.*, 2014, **53**, 883.
- 16 X. Hu, S. J. Dawson, P. K. Mandal, X. de Hatten, B. Baptiste and I. Huc, *Chem. Sci.*, 2017, **8**, 3741.
- 17 H. Jiang, J.-M. Léger and I. Huc, *J. Am. Chem. Soc.*, 2003, **125**, 3448.
- 18 S. J. Dawson, Á. Mészáros, L. Pethő, C. Colombo, M. Csékei, A. Kotschy and I. Huc, *Eur. J. Org. Chem.*, 2014, 4265.
- 19 J. Clayden, A. Lund, L. Vallverdú and M. Helliwel, *Nature*, 2004, **431**, 966; R. A. Brown, V. Diemer, S. J. Webb and J. Clayden, *Nat. Chem.*, 2013, **5**, 853; F. Lister, B. Le Bailly, S. J. Webb and J. Clayden, *Nat. Chem.*, 2017, **9**, 420.
- 20 C. Tsiamantas, X. de Hatten, C. Douat, B. Kauffmann, V. Maurizot, H. Ihara, M. Takafuji, N. Metzler-Nolte and I. Huc, *Angew. Chem., Int. Ed.*, 2016, **55**, 6848.
- 21 Z. J. Kinney, V. C. Kirind and C. Scott Hartley, *Chem. Sci.*, 2019, **10**, 9057.
- 22 R. Ishidate, A. J. Markvoort, K. Maeda and E. Yashima, *J. Am. Chem. Soc.*, 2019, **141**, 7605; T. Ikai, S. Kawabata, F. Mamiya, D. Taura, N. Ousaka and E. Yashima, *J. Am. Chem. Soc.*, 2020, **142**, 21913.
- 23 E. Suarez-Picado, E. Quinoa, R. Riguera and F. Freire, *Angew. Chem., Int. Ed.*, 2020, **59**, 4537; F. Freire, J. M. Seco, E. Quinoa and R. Riguera, *Angew. Chem., Int. Ed.*, 2011, **50**, 11692.
- 24 A. M. Kendhale, L. Poniman, Z. Dong, K. Laxmi-Reddy, B. Kauffmann, Y. Ferrand and I. Huc, *J. Org. Chem.*, 2011, **76**, 195.
- 25 J. Clayden, A. Castellanos, J. Solà and G. A. Morris, *Angew. Chem., Int. Ed.*, 2009, **48**, 5962.
- 26 For a review, see: J. Jacques, A. Collet and S. H. Wilen in *Enantiomers, racemates and resolutions*, Krieger, Malabar, 3rd edn, 1994.
- 27 D. F. Kreitler, Z. Yao, J. D. Steinkruger, D. E. Mortenson, L. Huang, R. Mittal, B. R. Travis, K. T. Forest and S. H. Gellman, *J. Am. Chem. Soc.*, 2019, **141**, 1583; D. E. Mortenson, J. D. Steinkruger, D. F. Kreitler, D. V. Perroni, G. P. Sorenson, L. Huang, R. Mittal, H. G. Yun, B. R. Travis, M. K. Mahanthappa, K. T. Forest and S. H. Gellman, *Proc. Natl. Acad. Sci. U. S. A.*, 2015, **112**, 13144; C. Toniolo, C. Peggion, M. Crisma, F. Formaggio, X. Shui and D. S. Eggleston, *Nat. Struct. Biol.*, 1994, **1**, 908; K. Mandal, B. L. Pentelute, D. Bang, Z. P. Gates, V. Y. Torbeev and S. B. H. Kent, *Angew. Chem., Int. Ed.*, 2012, **51**, 1481; P. Mateus, N. Chandramouli, C. D. Mackereth, B. Kauffmann, Y. Ferrand and I. Huc, *Angew. Chem., Int. Ed.*, 2020, **59**, 5797; G. Lautrette, B. Wicher, B. Kauffmann, Y. Ferrand and I. Huc, *J. Am. Chem. Soc.*, 2016, **138**, 10314; M. Lee, J. Shim, P. Kang, M.-G. Choia and S. H. Choi, *Chem. Commun.*, 2016, **52**, 5950.
- 28 G. N. Ramachandran, C. Ramakrishnan and V. Sasisekharan, *J. Mol. Biol.*, 1963, **7**, 95.
- 29 J. D. Sadowsky, J. K. Murray, Y. Tomita and S. H. Gellman, *ChemBioChem*, 2007, **8**, 903.
- 30 E. Teyssières, J.-P. Corre, S. Antunes, C. Rougeot, C. Dugave, G. Jouvion, P. Claudon, G. Mikaty, C. Douat, P. L. Goossens and G. Guichard, *J. Med. Chem.*, 2016, **59**, 8221.
- 31 J. Iriondo-Alberdi, K. Laxmi-Reddy, B. Bouguerne, C. Staedel and I. Huc, *ChemBioChem*, 2010, **11**, 1679; M. Oba, *ChemBioChem*, 2019, **20**, 2041.



7. Supplementary Information: Conformational Interplay in Hybrid Peptide–Helical Aromatic Foldamer Macrocycles

7.1. Materials and methods for chemical synthesis

General

Fmoc-Q^{Sul}-OH, Fmoc-Q^{Ala}-OH, Fmoc-Q^{Asp(tBu)}-OH, and P monomer were prepared by following the reported synthetic protocols.^{1,2,3,4} The synthetic procedure for Fmoc-Q^{Sem}-OH will be reported in due course. If not otherwise mentioned, chemical reagents were purchased from Sigma-Aldrich, and solvents from Fisher Scientific and used without further purification. Anhydrous tetrahydrofuran (THF) and anhydrous dichloromethane (DCM) were obtained from MBRAUN SPS-800 solvent purification system. Anhydrous chloroform (CHCl₃) and *N,N*-diisopropylethylamine (DIPEA) were distilled over CaH₂ prior to use. Exclusively ultrapure water was used. DMF and NMP (peptide grade) were purchased from Carlo Erba. Rink amide MBHA, Cl-MPA ProTide[®], and low-loading preloaded Fmoc-Gly-Wang resins were purchased from CEM. Low-loading Wang and cysteamine 2-chlorotriyl resins were purchased from Sigma. Fmoc-*N*-protected amino acids, benzotriazol-1-yl-oxytripyrrolidinophosphonium hexafluorophosphate (PyBOP), benzotriazol-1-yl-oxytris(dimethylamino)phosphonium hexafluorophosphate (BOP) and 2-(1H-Benzotriazol-1-yl)-1,1,3,3-tetramethyl-uronium-hexafluorophosphate (HBTU) were purchased from IRIS. α -Chymotrypsin and Trypsin were obtained from bovine pancreas; Pronase E from *Streptomyces Griseus* and were all purchased from Sigma-Aldrich.

Methods for Solid-Phase Synthesis

Solid Phase Peptide Synthesis

The peptide segment was assembled by using a Liberty Blue CEM[®] synthesizer at a minimum scale of 50 μ mol. Microwave couplings were performed twice at 75 °C for 10 min with *N*-Fmoc- α -amino acid (10 equiv. relative to the resin loading), HBTU (9 equiv.), and DIPEA (12 equiv.) in DMF. Fmoc deprotection was performed twice with 20% piperidine in DMF at 75 °C (1 \times 30 sec. and 1 \times 180 sec.). Wang and Rink amide resins were washed with DMF (2 \times 2 mL) after each deprotection step and one time 3 mL after each coupling step. When ProTide[®] resin was used, after the Fmoc deprotection the resin was extensively washed with DMF (4 \times 4 mL) and one time with 4 mL DMF after the coupling step.

¹ B. Baptiste, C. Douat-Casassus, K. Laxmi-Reddy, F. Godde and I. Huc, *J Org Chem*, 2010, **75**, 7175-7185.

² J. Buratto, C. Colombo, M. Stupfel, S. J. Dawson, C. Dolain, B. Langlois d'Estaintot, L. Fischer, T. Granier, M. Laguerre, B. Gallois and I. Huc, *Angew Chem Int Ed Engl*, 2014, **53**, 883-887.

³ M. Vallade, P. Sai Reddy, L. Fischer and I. Huc, *European Journal of Organic Chemistry*, 2018, **2018**, 5489-5498.

⁴ X. Hu, S. J. Dawson, P. K. Mandal, X. de Hatten, B. Baptiste and I. Huc, *Chem Sci*, 2017, **8**, 3741-3749.

Solid Phase Foldamer Synthesis

The microwave-assisted solid-phase synthesis (SPS) of foldamer-peptide hybrids was carried out on a Discover-Bio CEM® microwave oven in an open vessel mode. The temperature of the reaction mixture within the reactor vessel was monitored with an optical fiber probe.

Two different solid-phase synthesis approaches of foldamer-peptide hybrids have been implemented. Linear oligomers **1a**, **3a-5a**, **8a**, **9a**, **13a**, **14a**, **15a** were synthesized by iterative couplings of Fmoc-P-OH and Fmoc-Q-OH on corresponding resin-bound peptides. Linear oligomers **2a**, **6a**, **7a**, **10a**, and **11a** were built by relying on a fragment condensation approach of Fmoc-foldamer-OH segments on resin-bound H-Gly-peptides by using BOP/DIPEA as coupling reagents.

Sequences **9a-11a** were assembled on ProTide® resin because the PEG-polystyrene resin matrix appeared to give much better yield and crude purity of the resulting foldamer-peptide hybrids.

✓ **Fmoc Deprotection.** The resin was suspended at room temperature in a solution of 20% piperidine in DMF for 1 × 3 min and 1 × 7 min with one DMF washing in between the two cycles. To note, in the case of Q^{Sul}-rich sequences, after the Fmoc deprotection of the first installed Q^{Sul} residue, the resin was incubated for 3 × 10 minutes with a solution of 20% DIPEA in NMP to substitute the piperidine salt formed on the sulfonic acid side chain.⁴ This process was next performed until the end of the SPFS. The resin was finally washed with dry THF (3 × 3 mL) prior to perform the in situ coupling.

✓ **In situ Coupling of Fmoc-Q-OH or Fmoc-P-OH on resin-bound H-Q-oligomers.** To the pre-swollen resin in dry THF (1.25 mL) was added 2,4,6-Collidine (9.0 equiv. relative to the resin loading). Concurrently, the Fmoc-aromatic monomer (*i.e.* Fmoc-Q-OH or Fmoc-P-OH, 3 equiv.) was suspended in 1.25 mL anhydrous CHCl₃ together with triphenylphosphine (8 equiv). Trichloroacetonitrile (TCAN) was quickly added and the reaction mixture was vigorously mixed before to be added to the suspended resin within 30-60 sec. The reaction vessel was then placed under microwave irradiation (25 W, ramp to 50 °C over 5 min, then hold at 50 °C for 15 min). The resin was filtered off and washed with anhydrous THF (2 × 3 mL). The coupling step was repeated once. The resin was then filtered off and washed with THF (3 × 3 mL) and DMF (2 × 3 mL).⁵

✓ **HBTU coupling to resin-bound NH₂-P-oligomer or resin-bound H-Gly-peptide.** To the pre-swollen resin in DMF (2.5 mL), Fmoc-Q-OH (3 equiv.), HBTU (2.9 equiv.), and DIEA (6 equiv.) were successively added. The reaction vessel was next placed in the microwave oven and heating was applied (25 W, ramp to 50 °C over 5 min, then hold at 50 °C for 10 min). The resin was filtered off,

⁵ X. Hu, S. J. Dawson, Y. Nagaoka, A. Tanatani and I. Huc, *J Org Chem*, 2016, **81**, 1137-1150.

rinsed twice with DMF (3 mL) and the coupling step was repeated once. The resin was then filtered off and washed with and DMF (3 x 3 mL).

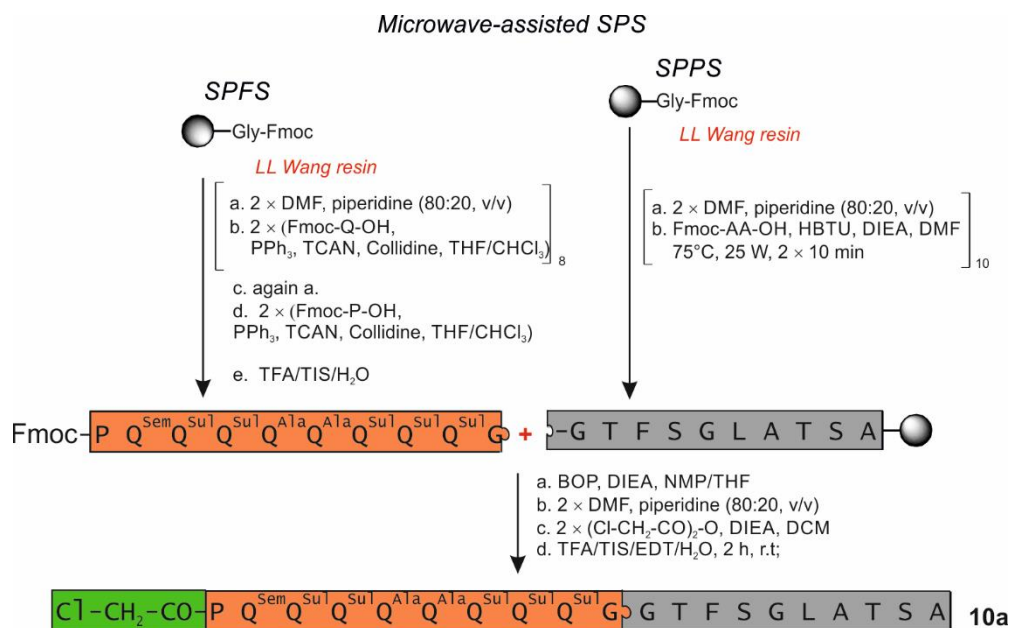


Figure S1: Schematic representation of the fragment condensation approach between a pre-build Fmoc-foldamer-OH segment and a resin-bound peptide.

✓ **Fragment condensation.** Prior to use, the crude Fmoc-foldamer-OH (1 equiv. relative to resin-bound H-Gly-peptide) was lyophilized to remove any remaining moisture. The freeze-dried solid was dissolved in a mixture of anhydrous NMP and anhydrous THF (50:50, v/v, 250 μL) directly followed by the addition of anhydrous DIPEA (4.5 equiv.) and BOP (1.5 equiv.). After 3 minutes of pre-activation, the mixture was added to resin-bound H-Gly-peptide under nitrogen atmosphere. The mixture was stirred for four days at r.t. To note after one day, 1.5 equiv. of BOP and 4.5 equiv of DIPEA were added immediately followed by one additional equiv. of resin-bound H-Gly-peptide to drive the reaction to completion. The progress of the reaction was monitored by analyzing the reaction mixture via RP-HPLC. The disappearance of the Foldamer from the supernatant indicated the progress of the reaction. Afterward, the resin was filtered off, washed with DMF (3 x 3 mL) and any remaining resin-bound free amine peptide was acetylated by using an acetic anhydride mixture in DCM (see conditions below).

✓ **N-capping of truncated sequences**

Any remaining free amine (aromatic or aliphatic) resulting from an incomplete coupling step was acetylated by incubating the resin with a solution of acetic anhydride in DCM (50:50, v/v) for 10 minutes at r.t. The resin was then filtered off and washed with DCM (3 × 3 mL) and DMF (3 × 3 mL).

✓ **General procedure for N-terminal chloroacetylation**

Before performing the chloroacetylation step on the resin-bound NH₂-oligomer, the resin was transferred to a 5 mL syringe equipped with a filter and washed with DCM (3 × 3 mL). Chloroacetic anhydride (10 equiv. in respect to N-terminal amine) was dissolved together with DIPEA (20 equiv.) in DCM. The reaction mixture was directly added to the resin and shaken for 15 minutes at r.t. This coupling step was repeated once without any washing in between. The resin was then filtered off, washed with DCM (3 × 3 mL) and dried briefly under a nitrogen stream.

✓ **Cleavage of resin-bound oligomers**

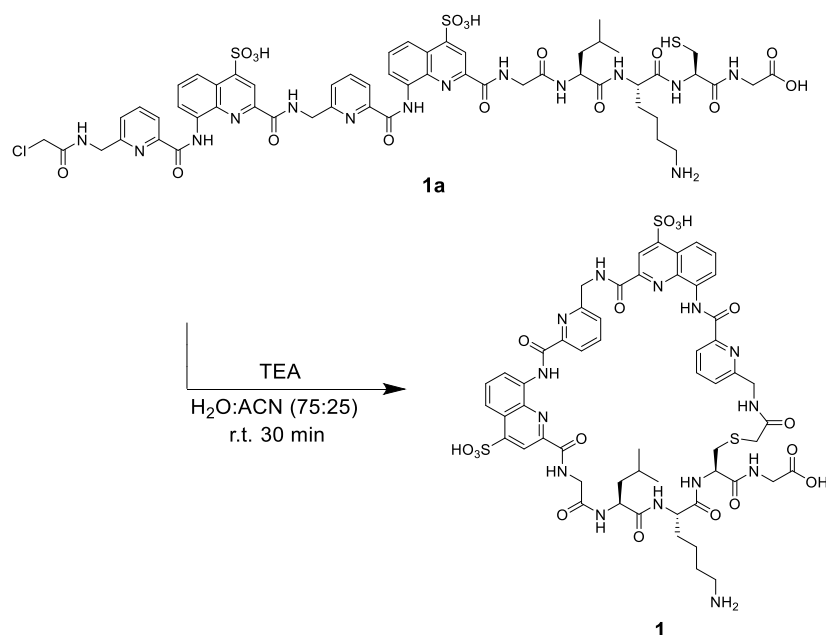
Sidechain deprotection and cleavage were performed simultaneously by treatment of the resin with a cleavage cocktail (10-15 mL per gram of resin) consisting of TFA/TIS/EDT/H₂O (92.5:2.5:2.5:2.5, v/v/v/v) for 120 min at r.t for Cys-containing foldamer-peptides and TFA/TIS/H₂O (95:2.5:2.5, v/v/v) for Fmoc-foldamer-Gly-OH segments. Foldamer-peptide hybrids (or Fmoc-foldamer-Gly-OH) were precipitated by adding cold Et₂O and centrifugation. The precipitate was dried under a nitrogen stream, suspended in an acetonitrile/water mixture containing 0.1 % TFA, filtered, and lyophilized to obtain the crude linear oligomers as a yellowish powder.

In the case of Q^{Sul}-rich oligomers, incubating the LL-Wang resin with 1 mL of DMF after TFA cleavage for several hours could increase the yield.

Foldamer-peptide hybrid macrocyclization

A diluted solution of Cl-CH₂-CO-foldamer-peptide-OH oligomer was incubated either in a 0.5 M Et₃N/DMF or a 0.5 M Et₃N/water/CH₃CN solution at room temperature. Completion of the macrocyclization was monitored by RP-HPLC and the crude mixture was then lyophilized before to be purified by semi-preparative RP-HPLC to give the expected macrocycle in high purity and good yield.

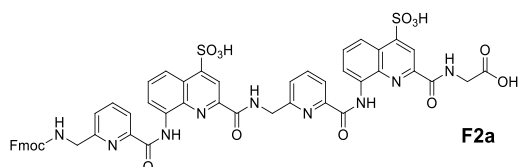
7.2. Experimental procedures for chemical synthesis



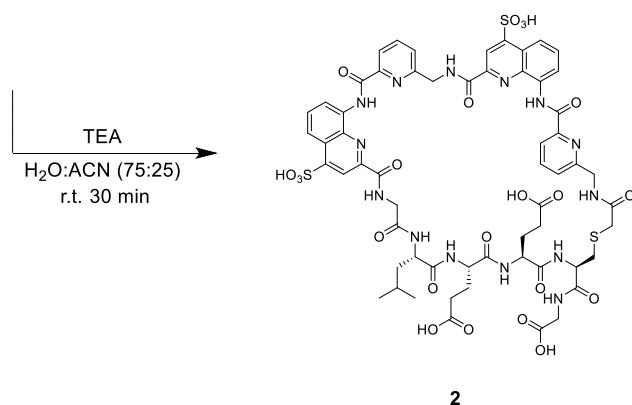
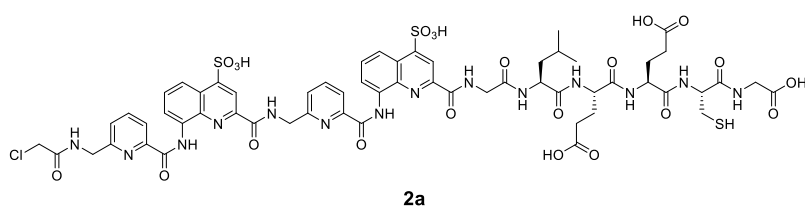
Compound 1a: Foldamer-peptide **1a** was built by relying on the CEM Liberty Blue microwave automated peptide synthesizer for the peptide segment and on the Liberty Bio for the stepwise assembly of the foldamer part on a 50 μmol scale. After chloroacetylation, the resin was cleaved with TFA/TIS/H₂O and the crude product (57 mg, 86%) was directly used in the macrocyclization reaction. HRMS (ESI⁺) m/z calcd for C₅₅H₆₂ClN₁₄O₁₇S₃ [M+H]⁺ 1321.3268 found 1321.3064.

Compound 1: Compound **1a** was dissolved in 5 mL of a water/CH₃CN 75:25 (v/v) solvent mixture to a 7.5 mM dilution and TEA (352 μL , 0.5 M) was added. After 30 min at r.t. without agitation, the solvents were evaporated by freeze drying and the crude macrocycle was purified by using semi-preparative RP-HPLC (gradient: from 10% to 40% solvent D over 15 minutes at 50 °C) to give **1** as a light yellow solid (35.0 mg, 61%). ¹H NMR (500 MHz, acetonitrile-*d*₃) δ 11.85 (s, 1H), 11.82 (s, 1H), 9.79 (s, 1H), 8.70 (s, 1H), 8.61 – 8.55 (m, 1H), 8.52 (d, J = 8.5 Hz, 1H), 8.45 (d, J = 9.6 Hz, 1H), 8.35 (m, 3H), 8.21 (dd, J = 26.7, 8.0 Hz, 3H), 8.05 – 7.80 (m, 8H), 7.71 (t, J = 9.0 Hz, 1H), 7.35 (d, J = 8.0 Hz, 1H), 4.80-4.40 (water suppression region), 4.07 – 3.86 (m, 1H), 3.73 (q, J = 11.8, 9.7 Hz, 2H), 3.17 (q, J = 7.9 Hz, 4H), 3.07 (m, 7H), 1.80 – 1.70 (m, 2H), 1.54 (m, 6H), 1.27 (t, J = 7.9 Hz, 5H), 0.81 (d, J = 7.0 Hz, 3H), 0.67 (d, J = 6.8 Hz, 3H). HRMS (ESI⁻) m/z calcd for C₅₅H₅₉N₁₄O₁₇S₃ [M-H]⁻ 1284.3423 found 1283.3613

Compound D-1: For compound **D-1** the synthesis, purification and analyses was repeated as described for **1** respectively **1a** by using D-amino acids instead of L-amino acids in the peptide segment. Similar yields and purities were obtained.



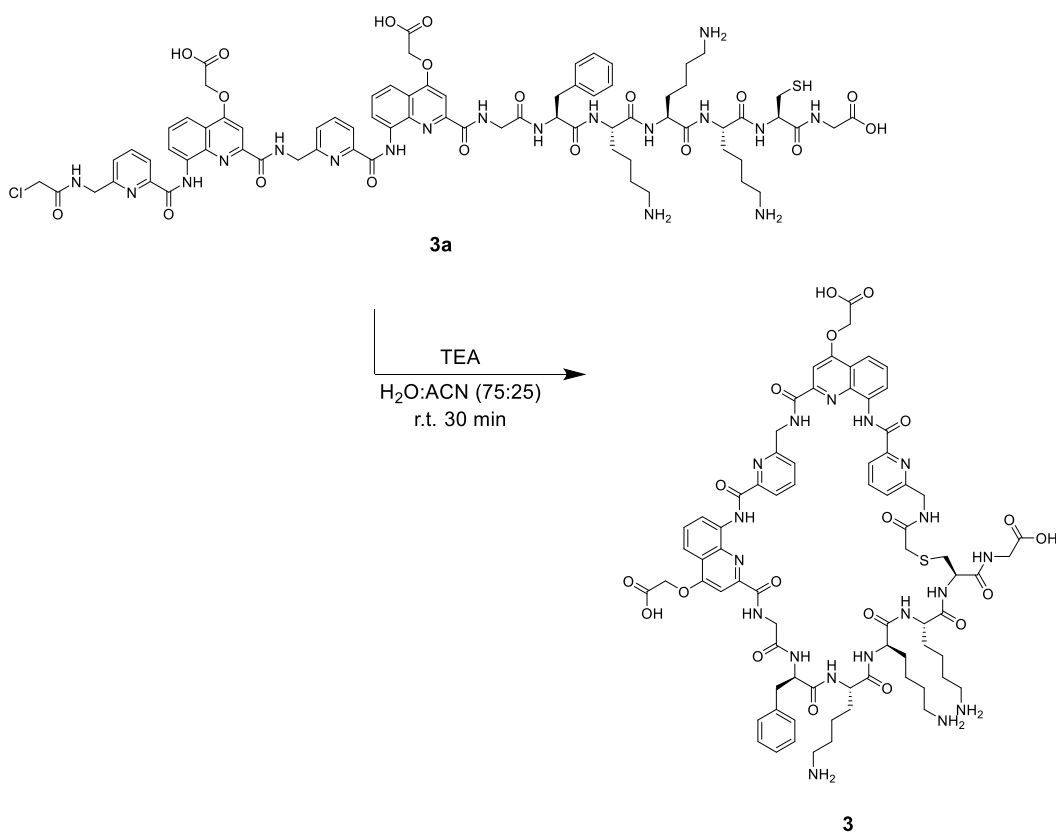
Foldamer fragment F2a: **F2a** was synthesized on a preloaded Fmoc-Gly-Wang resin (loading: 0.31 mmol/g) using general SPFS procedure on a 100 μ mol scale. **F1a** was recovered in 65% yield (70 mg) after cleavage using 4 mL of TFA/water 95:5 (v/v) mixture for 2h at r.t and was used without any further purification. HRMS (ESI⁻) m/z calcd for C₅₁H₃₈N₉O₁₄S₂ [M-H]⁻¹ 1064.1985 found 1064.2127.



Compound 2a: Peptide Fmoc-Gly-Leu-Glu(*t*Bu)-Glu(*t*Bu)-Cys(*Trt*)-Gly was loaded on a Fmoc-Gly-Wang resin (0.32 mmol/g) using CEM Liberty Blue microwave automated peptide synthesizer on a 50 μ mol scale. After Fmoc deprotection, **F2a** was coupled by fragment condensation on an 8 μ mol scale. After final chloroacetylation and TFA cleavage, crude **2a** (8 mg, 61%) was directly used in the macrocyclization reaction without further purification.

Compound 2: Compound **2a** was dissolved in 1.1 mL water/CH₃CN 70:30 (v/v) to a 7.5 mM dilution and TEA (480 μ L, 0.5 M) was added. After 30 min at r.t. without agitation and monitoring the reaction by HPLC, the reaction mixture was acidified using TFA. The solvents were evaporated by freeze drying and the crude macrocycle was purified by using semi-preparative RP-HPLC with a gradient from 5% to 35% solvent D over 10 minutes to give **2** as a light yellow solid (2.4 mg, 30%). ¹H NMR was performed in 12.5 mM ammonium acetate buffer at pH 8.5 with 25% acetonitrile-*d*₃. ¹H NMR (500 MHz, acetonitrile-*d*₃) δ 11.83 (s, 1H), 11.66 (s, 1H), 9.78 (s, 1H), 9.10 (d, J = 7.6 Hz, 1H), 8.77 (d, J = 7.9 Hz, 2H), 8.50 (d, J = 9.4 Hz, 2H), 8.39 (dd, J = 27.5, 9.4 Hz, 2H), 8.31 (d, J = 10.0 Hz, 1H), 8.25 (t, J = 8.7 Hz, 1H), 8.10 – 7.92 (m, 8H), 7.87 (t, J = 9.2 Hz, 1H), 7.81 (d, J = 9.3 Hz, 1H), 7.74 (s,

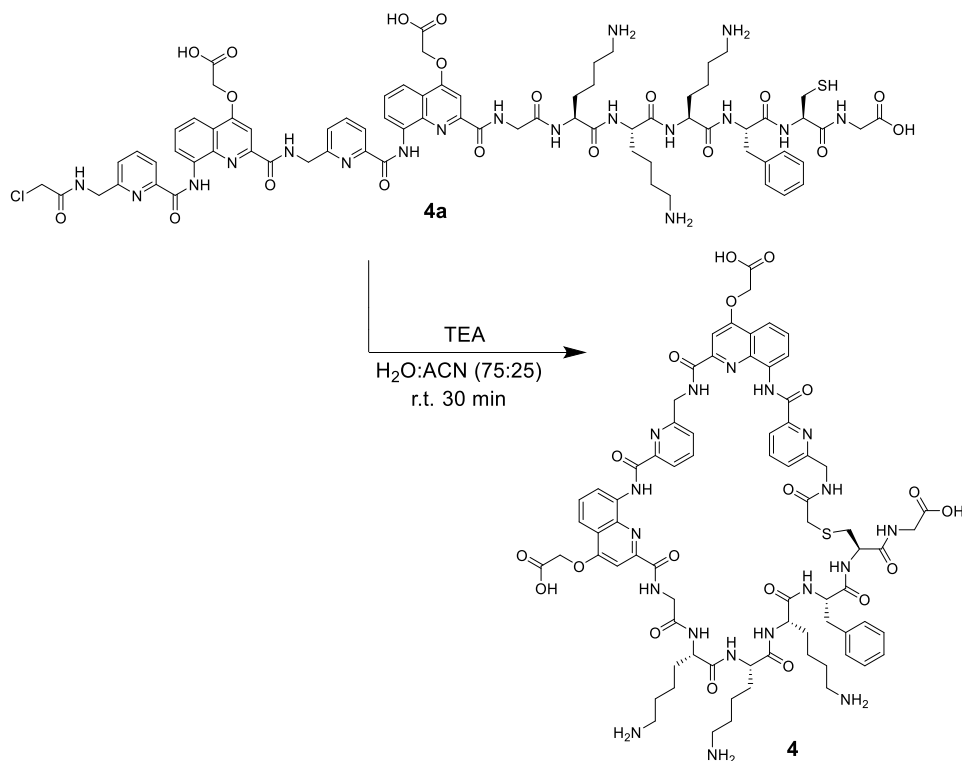
1H), 7.63 (t, $J = 9.3$ Hz, 1H), 7.40 (d, $J = 9.2$ Hz, 1H), 4.80-4.40 (water suppression region), 3.94 (d, $J = 15.9$ Hz, 1H), 3.89 – 3.76 (m, 1H), 3.73 (dd, $J = 14.8, 8.6$ Hz, 3H), 3.53 – 3.43 (m, 1H), 3.26 (d, $J = 16.3$ Hz, 1H), 3.21 – 2.93 (m, 4H), 2.48 (dq, $J = 24.2, 9.1, 8.2$ Hz, 4H), 2.33 – 2.09 (m, 5H), 1.85 – 1.72 (m, 1H), 1.60 – 1.47 (m, 2H), 1.47 – 1.34 (m, 1H), 1.26 (dd, $J = 16.6, 7.9$ Hz, 2H), 1.21 – 1.08 (m, 1H), 0.89 (s, 1H), 0.83 (d, $J = 7.7$ Hz, 3H), 0.68 (d, $J = 7.4$ Hz, 3H). HRMS (ESI) m/z calcd for $C_{59}H_{61}N_{14}O_{22}S_3$ [M-H]⁻ 1413.3325 found 1413.3066.



Compound 3a: Foldamer-peptide **3a** was synthesized by relying on the CEM Liberty Blue microwave automated peptide synthesizer for the peptide segment and on the Liberty Bio for the stepwise assembly of the foldamer part on a 50 μmol scale. The crude product (74 mg, 93%) was directly engaged in the macrocyclization step without further purification. HRMS (ESI⁺) m/z calcd for $C_{74}H_{88}ClN_{18}O_{19}S$ [M+H]⁺ 1599.5877 found 1599.5671.

Compound 3: Compound **3a** was dissolved in 6.2 mL of water/acetonitrile mixture 75:25 (v/v) to reach a 7.5 mM concentration and TEA (433 μL , 0.5 M) was added. After 30 min at r.t. without agitation, the reaction mixture was lyophilized and the crude macrocycle was purified by using semi-preparative RP-HPLC with a gradient from 10% to 40% solvent D over 15 minutes at 50 °C to give **3** as a colorless solid (31 mg, 42%). ¹H NMR spectrum was performed in a water/acetonitrile-*d*₃ 1:1 (v/v). ¹H NMR (500 MHz, acetonitrile-*d*₃) δ 11.40 (s, 1H), 11.15 (s, 1H), 9.65 (d, $J = 6.5$ Hz, 1H), 9.05 (d, $J = 7.8$ Hz, 1H), 8.63 (d, $J = 7.0$ Hz, 1H), 8.38 (d, $J = 10.1$ Hz, 1H), 8.28 (p, $J = 6.7, 5.3$ Hz, 3H), 8.10 – 7.81

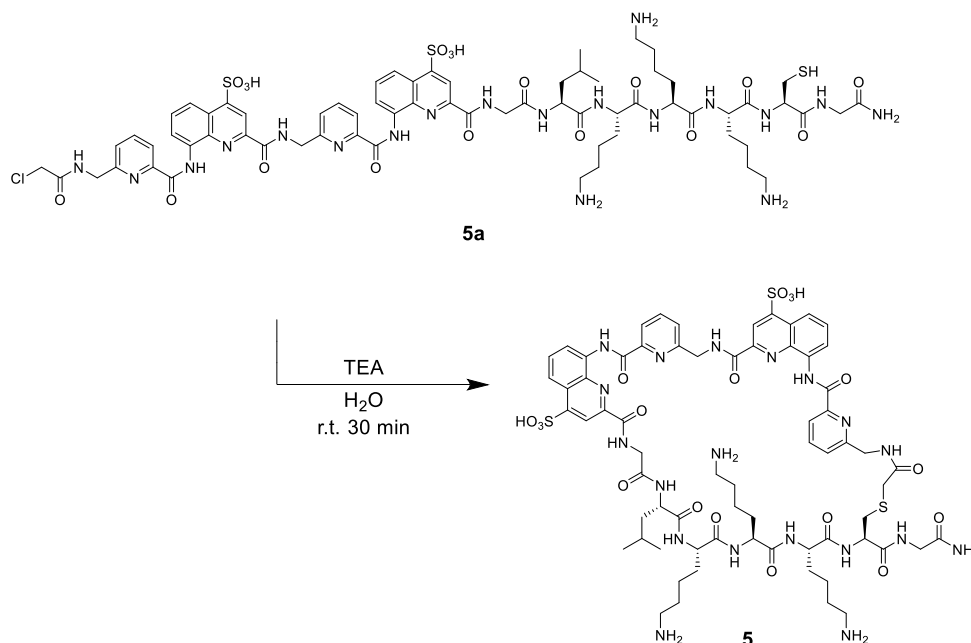
(m, 10H), 7.57 (t, $J = 8.8$ Hz, 2H), 7.46 (s, 1H), 7.34 (d, $J = 8.7$ Hz, 2H), 7.27 – 7.11 (m, 5H), 6.59 (s, 1H), 5.22 (dd, $J = 18.1, 6.9$ Hz, 1H), 4.89 (m, 1H), 3.75 (dd, $J = 16.9, 6.3$ Hz, 1H), 3.53 (d, $J = 17.9$ Hz, 1H), 3.48 – 3.32 (m, 4H), 3.25 (q, $J = 8.2$ Hz, 3H), 3.08 (q, $J = 6.8, 6.2$ Hz, 6H), 3.02 – 2.91 (m, 1H), 2.81 (m, 1H), 2.25 (dd, $J = 23.2, 10.7$ Hz, 2H), 2.07 (s, 2H), 1.95 (m, 8H), 1.79 (m, 6H), 1.60 (m, 4H), 1.42 – 1.33 (m, 2H). HRMS (ESI⁻) m/z calcd for C₇₄H₈₅N₁₈O₁₉S [M-H]⁻ 1561.5959 found 1561.6431.



Compound 4a: Foldamer-peptide **4a** was synthesized by relying on the CEM Liberty Blue microwave automated peptide synthesizer for the peptide segment and on the Liberty Bio for the stepwise assembly of the foldamer part on a 50 μ mol scale. After final chloroacetylation and TFA cleavage, the crude product (95 mg, 98%) was directly used in the macrocyclization reaction without further purification. HRMS (ESI⁺) m/z calcd for C₇₄H₈₈ClN₁₈O₁₉S [M+H]⁺ 1599.5882 found 1599.5824.

Compound 4: Compound **4a** was dissolved in 6.0 mL of a water/acetonitrile solvent mixture 75:25 (v/v) to reach a concentration of 7.5 mM. TEA (433 μ L, 0.5 M) was then added. After 30 min at r.t. without agitation, the reaction mixture was freeze dried and the obtained crude macrocycle was purified by using semi-preparative RP-HPLC with a gradient from 20% to 45% solvent B over 15 minutes at 50 °C to give **4** as a colorless solid (25 mg, 26%). ¹H NMR was performed in a water/acetonitrile-*d*₃ 1:1 (v:v). ¹H NMR (500 MHz, acetonitrile-*d*₃) δ 11.57 (s, 1H), 11.37 (s, 1H), 9.74 (d, $J = 6.4$ Hz, 1H), 8.73 (d, $J = 7.9$ Hz, 1H), 8.65 (d, $J = 6.7$ Hz, 1H), 8.40 (d, $J = 9.2$ Hz, 1H), 8.26 – 7.73 (m, 15H), 7.71 – 7.55 (m, 4H), 7.55 – 7.21 (m, 13H), 6.68 (s, 1H), 5.16 (dd, $J = 18.2, 6.8$ Hz, 1H), 5.01 (q, $J = 15.9$ Hz, 1H), 4.90 – 4.70 (m, 1H), 3.93 – 3.79 (m, 1H), 3.62 (d, $J = 19.1$ Hz, 1H), 3.46 (t, $J = 7.9$

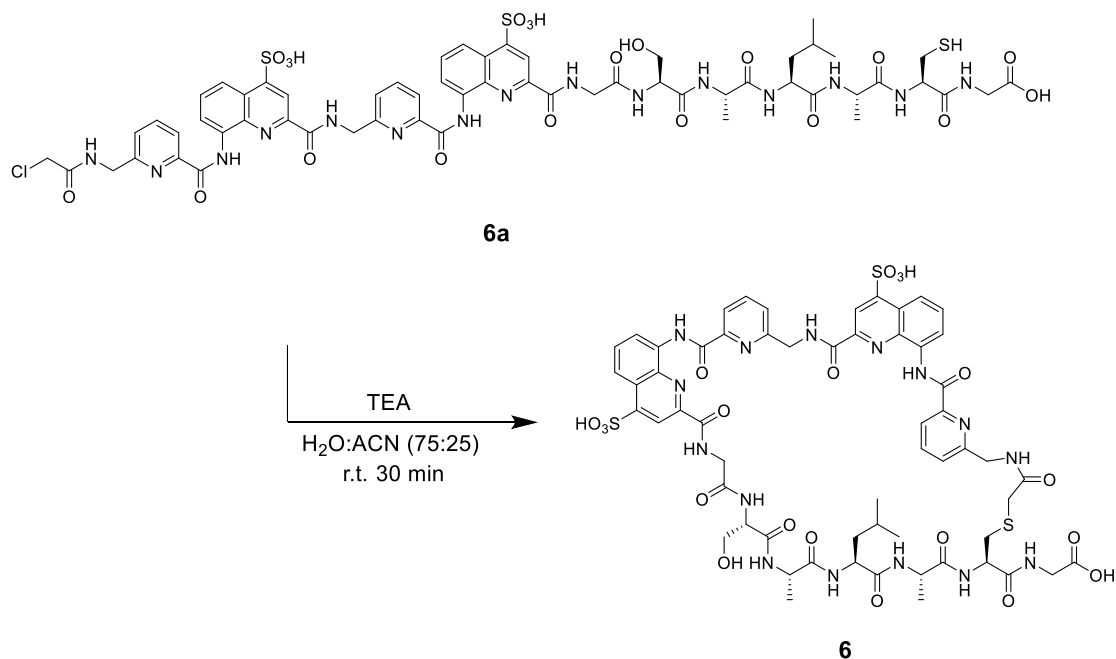
Hz, 1H), 3.28 – 3.02 (m, 9H), 2.84 (m, 9H), 2.39 (t, $J = 8.9$ Hz, 1H), 1.98 (t, $J = 10.5$ Hz, 2H), 1.89 – 1.48 (m, 14H), 1.49 – 1.13 (m, 6H). HRMS (ESI⁺) m/z calcd for C₇₄H₈₈N₁₈O₁₉S [M+2H]²⁺ 782.3091 found 782.3081.



Compound 5a: Foldamer-peptide **5a** was built on Rink Amide MBHA resin (0.33 mmol/g) by relying on the CEM Liberty Blue peptide synthesizer for the peptide segment and on the Liberty Bio for the stepwise assembly of the foldamer part on a 50 μ mol scale. After chloroacetylation the resin was cleaved with TFA/TIS/H₂O and the crude product (39 mg, 52%) was directly used in the macrocyclization reaction without further purification. MALDI-TOF m/z calcd for C₆₇H₈₅ClN₁₉O₁₈S₃ [M-H]⁻ 1574.5 found 1572.9

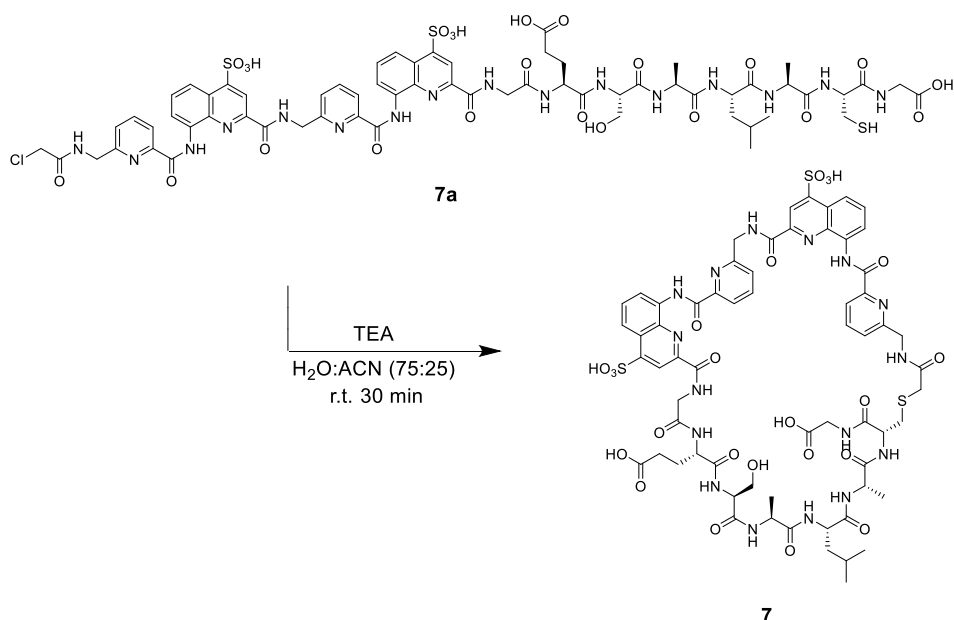
Compound 5: Compound **5a** was dissolved in 3.5 mL water to a 7.5 mM dilution and TEA (230 μ L, 0.5 M) was added. After 30 min at r.t. without agitation, the solvents were evaporated by freeze drying and the obtained crude macrocycle was purified by using semi-preparative RP-HPLC (general procedure 3) with a gradient from 0% to 40% solvent D over 25 minutes to give **5** as a light yellow solid (5 mg, 12%). ¹H NMR was performed in 12.5 mM ammoniumacetate buffer at pH 8.5 with 25% acetonitrile-*d*₃. ¹H NMR (500 MHz, acetonitrile-*d*₃) δ 11.56 (s, 1H), 11.49 (s, 1H), 9.85 (s, 1H), 8.68 (s, 1H), 8.42 (d, $J = 9.5$ Hz, 1H), 8.29 (d, $J = 9.4$ Hz, 2H), 8.18 (t, $J = 8.5$ Hz, 2H), 8.03 (t, $J = 9.9$ Hz, 3H), 7.95 (t, $J = 8.2$ Hz, 1H), 7.91 – 7.70 (m, 4H), 7.59 (t, $J = 8.9$ Hz, 1H), 7.36 (d, $J = 8.5$ Hz, 1H), 4.80-4.40 (water suppression region), 3.86 (t, $J = 14.5$ Hz, 2H), 3.74 (d, $J = 18.5$ Hz, 1H), 3.53 (d, $J = 16.0$ Hz, 1H), 3.40 (d, $J = 16.2$ Hz, 1H), 3.24 (q, $J = 15.0$ Hz, 2H), 3.12 (q, $J = 11.7, 8.5$ Hz, 2H), 2.97 (m, 4H), 2.84 (m, 4H), 1.84 – 1.27 (m, 25H), 0.78 (d, $J = 7.2$ Hz, 3H), 0.66 (d, $J = 6.9$ Hz, 3H). Amino acid amide

resonances between 8.4 ppm and 7.7 ppm partially suppressed. HRMS (ESI⁻) m/z calcd for C₆₇H₈₄N₁₉O₁₈S₃ [M-H]⁻ 1538.5482 found 1538.5360.



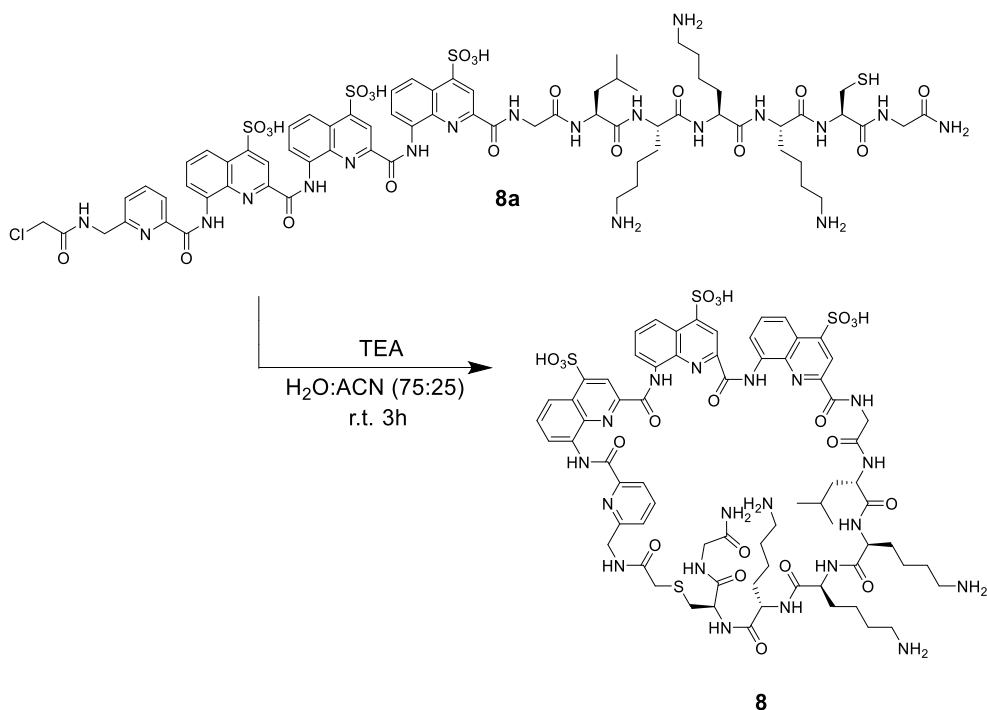
Compound 6a: Peptide Fmoc-Ser(*t*Bu)-Ala-Leu-Ala-Cys(Trt)-Gly was loaded on Fmoc-Gly-Wang resin (0.31 mmol/g) using CEM Liberty Blue peptide synthesizer. Fragment **F2a** was next condensed on the resin-bound amine-free peptide on a 10 μmol scale. After final chloroacetylation followed by TFA cleavage the crude product (12 mg, 86%) was directly used in the cyclization reaction. HRMS (ESI⁺) m/z calcd for C₅₈H₆₅ClN₁₅O₂₀S₃ [M+H]⁺ 1422.3380 found 1422.3610

Compound 6: Compound **6a** was dissolved in 34 mL of water/acetonitrile 75:25 (v/v) solution mixture and TEA (1.7 mL, 0.5 M) was added. After 3h at r.t. without agitation, the solvents were evaporated by freeze drying and the crude macrocycle was purified by using semi-preparative RP-HPLC with a gradient from 10% to 30% solvent D over 20 minutes to give **6** as a light yellow solid (2.3 mg, 20%). ¹H NMR was performed in 12.5 mM ammonium acetate buffer at pH 8.5 with 25% acetonitrile-*d*₃. ¹H NMR (400 MHz, acetonitrile-*d*₃) δ 11.68 (s, 1H), 11.58 (s, 1H), 9.99 (d, *J* = 5.2 Hz, 1H), 8.77 (s, 1H), 8.72 (s, 1H), 8.55 – 8.47 (m, 2H), 8.37 – 8.32 (m, 1H), 8.32 – 8.19 (m, 4H), 8.06 (td, *J* = 7.6, 5.6 Hz, 4H), 7.95 – 7.82 (m, 7H), 7.66 (t, *J* = 8.5 Hz, 1H), 7.43 (d, *J* = 8.3 Hz, 1H), 4.80-4 – 4.0 (water suppression region), 3.96 (td, *J* = 13.6, 12.6, 4.3 Hz, 1H), 3.85 (dd, *J* = 25.4, 4.1 Hz, 1H), 3.78 – 3.69 (m, 4H), 3.68 – 3.61 (m, 1H), 3.27 (d, *J* = 23.3 Hz, 3H), 3.01 (dd, *J* = 14.1, 5.6 Hz, 1H), 2.90 (dd, *J* = 14.0, 8.0 Hz, 1H), 1.67 (d, *J* = 7.3 Hz, 3H), 1.45 (d, *J* = 7.1 Hz, 4H), 1.38 (d, *J* = 6.9 Hz, 1H), 1.27 (t, *J* = 7.6 Hz, 6H), 0.96 – 0.84 (m, 2H), 0.78 (d, *J* = 6.9 Hz, 3H), 0.62 (d, *J* = 6.9 Hz, 3H). HRMS (ESI⁻) m/z calcd for C₅₈H₆₂N₁₅O₂₀S₃ [M-H]⁻ 1384.3457 found 1384.3375.



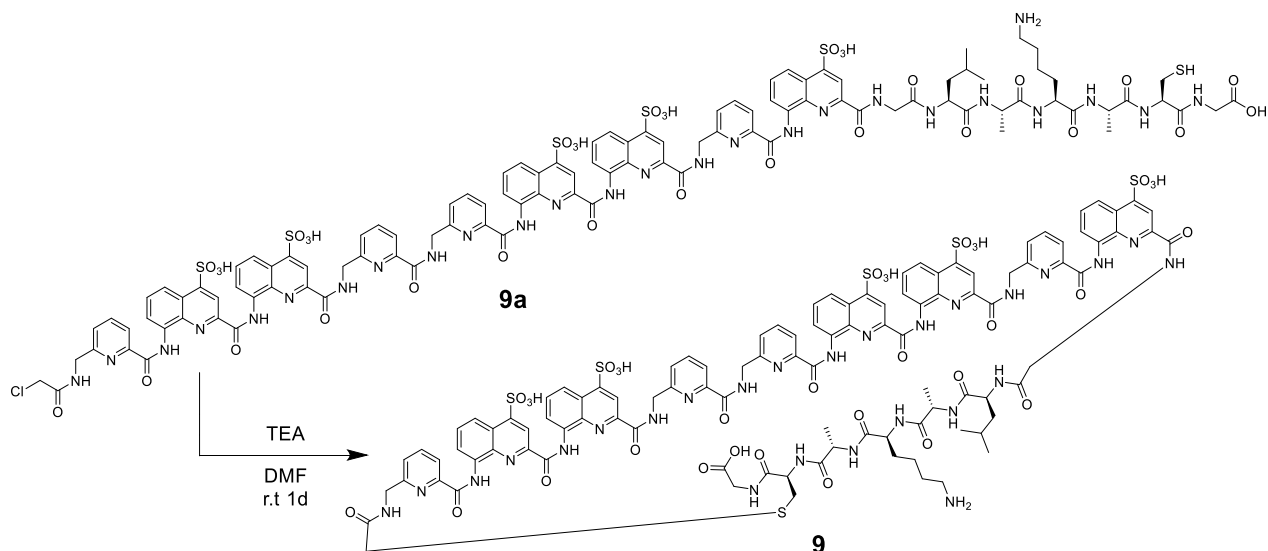
Compound 7a: The peptide fragment was synthesized on a preloaded Fmoc-Gly-Wang resin (loading: 0.31 mmol/g) using CEM Liberty Blue peptide synthesizer. Fragment **F2a** was next condensed on the resin-bound amine-free peptide by relying on the fragment condensation approach on a 10 μ mol scale. After final chloroacetylation followed by TFA cleavage the crude product (13 mg, 87%) was directly engaged in the macrocyclization reaction. HRMS (ESI⁺) m/z calcd for C₆₃H₇₂ClN₁₆O₂₃S₃ [M+H]⁺ 1551.3801 found 1551.4003.

Compound 7: Compound **7a** (0.25 mM) was dissolved in 36 mL of water/acetonitrile 75:25 (v/v) solution mixture and TEA (1.7 mL, 0.5 M) was added. After 3h at r.t. without agitation, the solvents were evaporated by freeze drying. The crude macrocycle was next purified by using semi-preparative RP-HPLC with a gradient from 5% to 28% solvent D over 20 minutes to give **7** as a light yellow solid (2.6 mg, 20%). ¹H NMR was performed in 12.5 mM ammonium acetate buffer at pH 8.5 with 25% acetonitrile-*d*₃. ¹H NMR (400 MHz, acetonitrile-*d*₃) δ 11.67 (s, 1H), 11.56 (s, 1H), 9.99 (s, 1H), 8.73 (s, 1H), 8.58 – 8.47 (m, 3H), 8.42 (d, J = 8.3 Hz, 1H), 8.38 – 8.28 (m, 3H), 8.25 (t, J = 7.9 Hz, 1H), 8.12 – 7.85 (m, 11H), 7.83 (d, J = 8.3 Hz, 1H), 7.75 (t, J = 5.8 Hz, 1H), 7.66 (t, J = 8.5 Hz, 1H), 7.42 (d, J = 8.3 Hz, 1H), 4.80-4.40 (water suppression region), 4.10 – 3.94 (m, 1H), 3.85 (td, J = 17.1, 16.4, 4.9 Hz, 1H), 3.77 – 3.68 (m, 3H), 3.63 (dd, J = 17.3, 5.4 Hz, 1H), 3.24 (d, J = 5.2 Hz, 2H), 3.17 (q, J = 7.5 Hz, 4H), 3.04 (d, J = 5.2 Hz, 1H), 2.86 (dd, J = 14.2, 8.3 Hz, 1H), 2.17 (d, J = 7.6 Hz, 2H), 1.60 (d, J = 6.1 Hz, 3H), 1.43 (d, J = 7.2 Hz, 3H), 1.38 (d, J = 7.1 Hz, 3H), 1.26 (t, J = 7.5 Hz, 6H), 0.86 (dd, J = 6.2, 4.5 Hz, 6H). HRMS (ESI⁻) m/z calcd for C₆₃H₆₉N₁₆O₂₃S₃ [M-H]⁻ 1513.3883 found 1515.3924.



Compound 8a: Foldamer-peptide **8a** was built on Rink Amide MBHA resin (loading: 0.33 mmol/g) by relying on the CEM Liberty Blue peptide synthesizer for the peptide segment and on the Liberty Bio for the stepwise assembly of the foldamer part on a 50 μ mol scale. After final chloroacetylation and TFA cleavage the crude product (80 mg, 97%) was directly used in the macrocyclization reaction without further purification. HRMS (ESI⁻) m/z calcd for C₇₀H₈₅ClN₁₉O₂₁S₄ [M-H]⁻¹ 1690.4738 found 1690.4170.

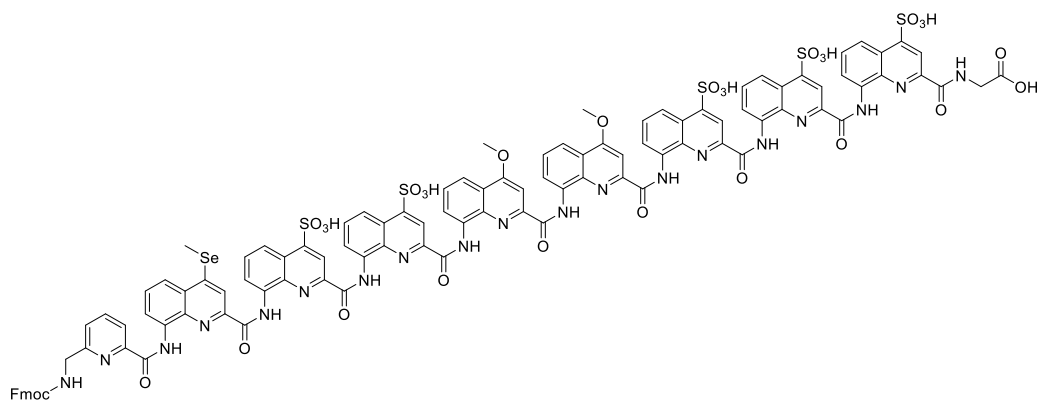
Compound 8: Compound **8a** was dissolved in 6.3 mL of a water/acetonitrile solvent mixture 75:25 (v:v) to reach a 7.5 mM dilution and TEA (0.4 mL, 0.5 M) was added. After 3h at r.t. without agitation, the solvents were evaporated by freeze drying and the obtained crude macrocycle was purified by using semi-preparative RP-HPLC with a gradient from 0% to 40% solvent D over 25 minutes to give compound **8** as a light yellow solid (8.2 mg, 10%). ¹H NMR was performed in 12.5 mM ammonium acetate buffer at pH 8.5 with 25% acetonitrile-*d*₃ performing water suppression experiment. ¹H NMR (500 MHz, acetonitrile-*d*₃) δ 12.47 (s, 1H), 11.81 (s, 1H), 11.15 (s, 1H), 8.88 (d, J = 8.1 Hz, 1H), 8.76 (s, 1H), 8.60 (d, J = 9.4 Hz, 2H), 8.50 (m, 2H), 8.39 (s, 1H), 8.33 (d, J = 8.4 Hz, 1H), 8.26 (d, J = 9.1 Hz, 1H), 8.11 (d, J = 10.0 Hz, 1H), 8.01 (q, J = 8.9, 8.4 Hz, 3H), 7.90 – 7.83 (m, 4H), 7.77 (t, J = 4.0 Hz, 1H), 7.70 (d, J = 8.2 Hz, 1H), 7.45 (t, J = 8.6 Hz, 1H), 7.35 (d, J = 9.2 Hz, 2H), 6.96 (s, 1H), 4.80-4.40 (water suppression region) 3.86 (t, J = 15.7 Hz, 2H), 3.69 (d, J = 20.1 Hz, 1H), 3.64 – 3.53 (m, 2H), 3.30 (d, J = 14.8 Hz, 1H), 3.18 – 3.04 (m, 7H), 2.96 (m, 2H), 2.87 (d, J = 3.9 Hz, 1H), 2.70 (dd, J = 14.9, 10.0 Hz, 1H), 2.41 (d, J = 20.2 Hz, 1H), 2.22 (d, J = 4.6 Hz, 2H), 1.88 – 1.73 (m, 10H), 1.64 – 1.39 (m, 11H), 1.23 – 1.13 (m, 1H), 0.99 (s, 1H), 0.55 (d, J = 7.0 Hz, 3H), 0.14 (d, J = 7.1 Hz, 3H). HRMS (ESI⁻) m/z calcd for C₇₀H₈₃N₁₉O₂₁S₄ [M-2H]⁻² 826.7452 found 826.7511



Compound 9a: Foldamer-peptide **9a** was synthesized on the CEM Liberty Blue peptide synthesizer for the peptide segment and on the Liberty Bio for the stepwise assembly of the foldamer part. Half of the resin was cleaved in the presence of TFA/TIS/H₂O/EDT and the crude product (30 mg, 47%) was directly engaged in the macrocyclization reaction without further purification. HRMS (ESI⁻) *m/z* calcd for C₁₀₅H₉₉ClN₂₆O₃₃S₆ [M-2H]⁻² 1239.7473 found 1239.7576

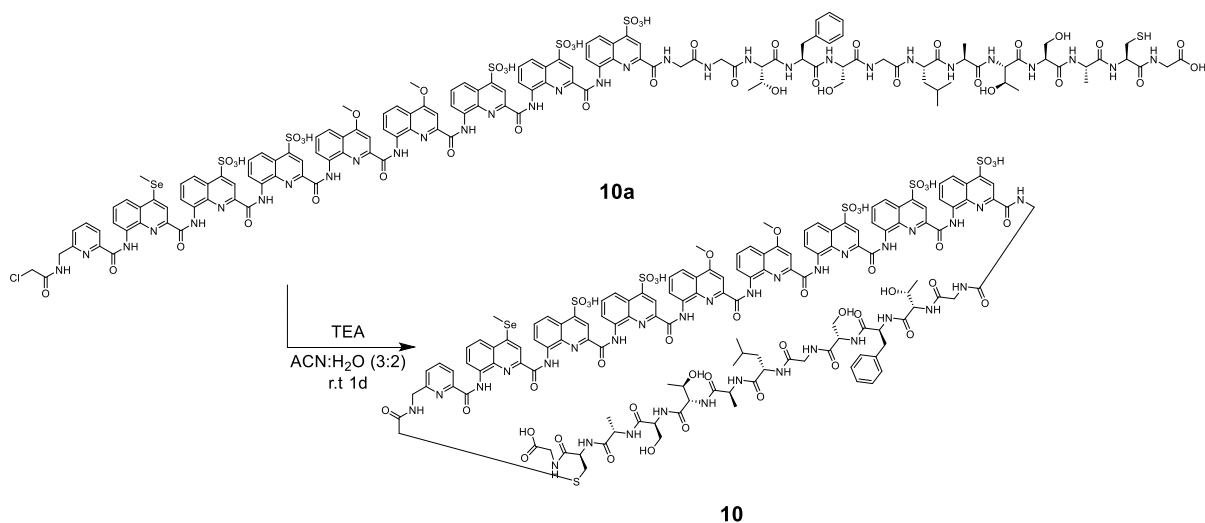
Compound 9: Compound **9a** was dissolved in 48 mL DMF containing triphenylphosphine (3.1 mg, 12 μmol) at a concentration of 0.25 mM. TEA (3.3 mL, 0.5 M) was added under nitrogen atmosphere and the reaction mixture was kept for 36 h at r.t. without any stirring. The solvents were next evaporated under reduced pressure, remaining traces of DMF were removed by lyophilizing the sample. The obtained crude macrocycle was purified by using semi-preparative RP-HPLC with a gradient from 8% to 32% solvent D over 20 minutes to give compound **9** as a light yellow solid (3.4 mg, 11%). ¹H NMR was performed in 12.5 mM ammonium acetate buffer at pH 8.5 with 10% D₂O. ¹H NMR (500 MHz, TPS) δ 11.70 (s, 1H), 11.60 (s, 1H), 11.10 (s, 1H), 11.07 (s, 1H), 10.72 (s, 1H), 8.72 (d, *J* = 9.3 Hz, 2H), 8.54 (dd, *J* = 16.4, 8.7 Hz, 2H), 8.46 – 8.23 (m, 8H), 8.17 – 8.08 (m, 3H), 8.04 – 7.27 (m, 27H), 7.12 (d, *J* = 8.1 Hz, 1H), 7.06 (d, *J* = 8.0 Hz, 1H), 6.99 (t, *J* = 9.1 Hz, 1H), 4.80-4.40 (water suppression region), 3.94 – 3.75 (m, 4H), 3.71 – 3.50 (m, 4H), 3.26 – 3.14 (m, 5H), 2.93 (m, 2H), 2.85 – 2.64 (m, 4H), 2.12 (d, *J* = 8.3 Hz, 1H), 1.86 – 1.78 (m, 3H), 1.71 (m, 5H), 1.30 (m, 10H), 0.88 (dd, *J* = 21.0, 6.6 Hz, 2H), 0.78 (d, *J* = 6.9 Hz, 3H), 0.65 (d, *J* = 6.8 Hz, 3H). HRMS (ESI⁻) *m/z* calcd for C₁₀₅H₉₈N₂₆O₃₃S₆ [M-2H]⁻² 1221.7590 found 1221.7500.

Compound D-9: For compound **D-9** the synthesis, purification, and analyses were repeated as described for **9** respectively **9a** by using *D*-amino acids instead of *L*-amino acids in the peptide segment. Similar yields and purities were obtained.



F10a

Compound F10a: Foldamer segment **F10a** was synthesized on a preloaded Fmoc-Gly Wang resin (0.31 mmol/g) on a 100 μmol scale. After TFA cleavage **F10a** (200 mg, 85%) was used in subsequent reactions without any further purification. HRMS (ESI⁻) m/z calcd for $\text{C}_{107}\text{H}_{73}\text{N}_{19}\text{O}_{30}\text{S}_5\text{Se}$ $[\text{M}-2\text{H}]^{-2}$ 1172.1303 found 1172.1785.

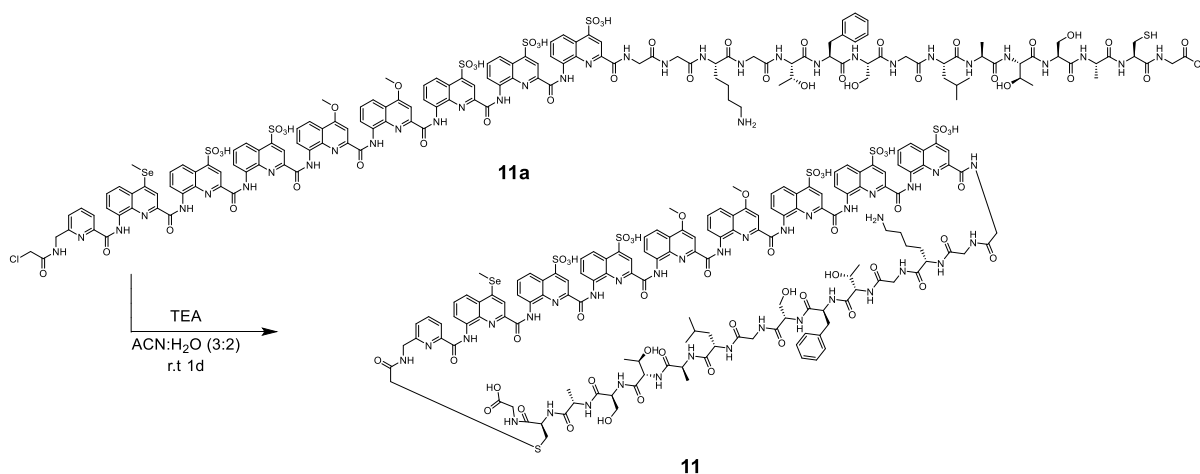


10

Compound 10a: The peptide fragment was synthesized on Cl-MPA ProTide® (LL) resin (0.23 mmol/g) on a 50 μmol scale. For the initial loading step, Fmoc-Gly-OH (149 mg, 0.5 mM, 10 equiv.) was dissolved in 2.5 mL DMF and added to the resin together with a solution containing CsI (32 mg, 0.125 mM, 2.5 equiv.) and DIPEA (174 μL , 1mM, 20 equiv.) in 1 mL DMF. The suspension was heated to 50 $^{\circ}\text{C}$ by microwave irradiation for 15 min at 25W. The peptide was elongated by using CEM Liberty Blue peptide synthesizer. **F10a** was next engaged to the fragment condensation on the resin-bound free amine peptide in a 10 μmol scale. After final chloroacetylation and TFA cleavage, the obtained crude product was directly engaged in the macrocyclization reaction without further purification (22 mg, 75%). HRMS (ESI⁻) m/z calcd for $\text{C}_{138}\text{H}_{132}\text{ClN}_{31}\text{O}_{45}\text{S}_6\text{Se}$ $[\text{M}-2\text{H}]^{-2}$ 1625.3119 found 1625.3047

Compound 10: With the increase of size and sequence complexity, we decided to perform all the subsequent macrocyclizations in an oxygen-free media. Compound **10a** was dissolved in a 67 mL of a

degassed water/acetonitrile mixture 40:60 (v/v) to reach a final 0.1 mM concentration and TEA (4.5 mL, 0.5 M) was added under positive nitrogen pressure. After 24h under nitrogen atmosphere at r.t. without stirring, the solvents were removed by rotary evaporation and remaining water was removed by lyophilization. The obtained crude macrocycle was purified by using semi-preparative RP-HPLC on C8 column at 50 °C with a gradient from 10% to 25% solvent D over 15 minutes to afford compound **10** (2.0 mg, 10%) as a diastereomeric mixture. ^1H NMR was performed in 12.5 mM ammonium acetate buffer at pH 8.5 with 50% acetonitrile- d_3 . ^1H NMR (500 MHz, Acetonitrile- d_3) δ 11.39 (s, 1H), 11.37 (s, 1H), 11.30 (s, 1H), 11.26 (s, 1H), 11.09 (s, 1H), 11.06 (s, 1H), 11.00 (s, 1H), 10.96 (m, 5H), 10.52 (m, 4H), 8.42 (m, 7H), 8.34 – 8.14 (m, 12H), 8.14 – 7.90 (m, 12H), 7.90 – 7.59 (m, 22H), 7.59 – 7.39 (m, 23H), 7.39 – 6.91 (m, 27H), 6.79 (d, $J = 38.9$ Hz, 2H), 6.53 (d, $J = 5.8$ Hz, 2H), 6.31 (d, $J = 9.8$ Hz, 2H), 4.80-4.40 (water suppression region), 3.75 – 2.28 (m, 51H), 1.78 – 1.61 (m, 13H), 1.46 – 1.15 (m, 51H), 1.09 – 0.75 (m, 29H). HRMS (ESI $^-$) m/z calcd for $\text{C}_{138}\text{H}_{130}\text{N}_{31}\text{O}_{45}\text{S}_6\text{Se}$ [$\text{M}-3\text{H}$] $^{-3}$ 1071.3410 found 1071.2499.



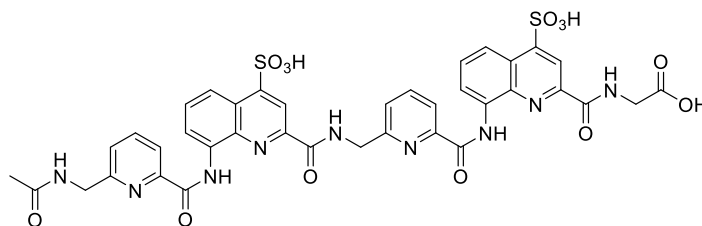
Compound 11a: The peptide fragment was synthesized on Cl-MPA ProTide® (LL) resin (0.23 mmol/g) on a 50 μmol scale by using CEM Liberty Blue peptide synthesizer. Foldamer segment **F10** was next engaged in the fragment condensation on the resin-bound free amine peptide on a 17 μmol scale. After final chloroacetylation and TFA cleavage, the crude product (18 mg, 29%) was directly used in the macrocyclization step without further purification. HRMS (ESI $^+$) m/z calcd for $\text{C}_{146}\text{H}_{147}\text{ClN}_{34}\text{O}_{47}\text{S}_6\text{Se}$ [$\text{M}-2\text{H}$] $^{-2}$ 1717.8690 found 1718.4410.

Compound 11: Compound **11a** was dissolved in 45 mL of an oxygen-free water/acetonitrile mixture 40:60 (v/v) to reach a 0.1 mM concentration and TEA (3.5 mL, 0.5 M) was added under nitrogen atmosphere. The reaction mixture was kept one day under nitrogen atmosphere at r.t. without agitation. Solvents were then removed by rotary evaporation and the remaining water was removed by freeze-drying. The obtained crude macrocycle was purified by using semi-preparative RP-HPLC on

C8 column at 50 °C with a gradient from 10% to 25% solvent D over 15 minutes to furnish **(P)-11** (0.6 mg, 4%) and **(M)-11** (0.6 mg, 4%) as solids. ¹H NMR spectra were recorded in 12.5 mM ammonium acetate buffer at pH 8.5 with 50% acetonitrile-*d*₃ performing water suppression experiment.

Compound (M)-11: ¹H NMR(500 MHz, acetonitrile-*d*₃) δ 11.40 (s, 1H), 11.30 (s, 1H), 11.11 (s, 1H), 11.02 (s, 1H), 11.00 (s, 1H), 10.96 (s, 1H), 10.58 (s, 1H), 10.52 (s, 1H), 8.48 (d, *J* = 10.8 Hz, 2H), 8.41 (d, *J* = 10.2 Hz, 1H), 8.34 – 7.90 (m, 13H), 7.90 – 7.62 (m, 11H), 7.62 – 7.26 (m, 22H), 7.22 (d, *J* = 9.2 Hz, 1H), 7.14 (d, *J* = 9.3 Hz, 2H), 7.02 (d, *J* = 9.3 Hz, 1H), 6.57 (s, 1H), 6.35 (s, 1H), 4.50-4.20 (water suppression range), 4.01 – 3.34 (m, 9H), 3.33 – 2.86 (m, 7H), 2.60 (m, 5H), 2.43 – 2.27 (m, 2H), 2.16 (m, 2H), 1.81 – 1.52 (m, 12H), 1.51 – 1.15 (m, 25H), 1.15 – 0.89 (m, 16H). HRMS (ESI⁻) *m/z* calcd for C₁₄₆H₁₄₅N₃₄O₄₇S₆Se [M-3H]⁻³ 1133.0818 found 1132.9717.

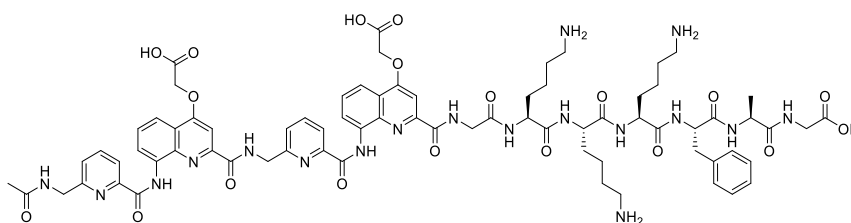
Compound (P)-11: ¹H NMR(500 MHz, acetonitrile-*d*₃) δ 11.39 (s, 1H), 11.35 (s, 1H), 11.11 (s, 1H), 11.05 (s, 1H), 11.02 (s, 1H), 10.97 (s, 1H), 10.55 (s, 1H), 10.52 (s, 1H), 8.52 – 8.33 (m, 4H), 8.33 – 7.96 (m, 12H), 7.87 – 7.65 (m, 12H), 7.59 – 7.26 (m, 22H), 7.22 (d, *J* = 9.1 Hz, 1H), 7.13 (d, *J* = 9.1 Hz, 1H), 7.09 – 7.00 (m, 2H), 6.60 (s, 1H), 6.33 (s, 1H), 4.50 – 4.20 (water suppression range), 4.00 – 3.31 (m, 8H), 3.31 – 2.83 (m, 8H), 2.60 (d, *J* = 15.8 Hz, 1H), 2.54 (m, 4H), 2.50 – 2.16 (m, 3H), 1.82 – 1.50 (m, 14H), 1.47 – 1.15 (m, 26H), 1.15 – 0.87 (m, 20H). HRMS (ESI⁻) *m/z* calcd for C₁₄₆H₁₄₅N₃₄O₄₇S₆Se [M-3H]⁻³ 1133.0818 found 1132.9702.



12

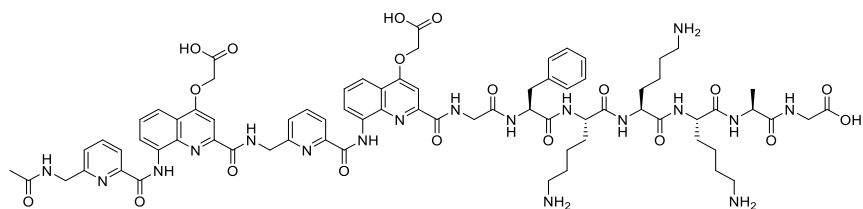
Compound 12: **12** was synthesized on a preloaded Fmoc-Gly-Wang resin (loading: 0.31 mmol/g) using general SPFS procedure on a 25 μmol scale. After final acetylation, **12** was recovered in 73% yield (16 mg) after cleavage using 2 mL of TFA/water (95:5, v/v) mixture for 2h at r.t. This crude product was further purified on semi-preparative RP-HPLC with a gradient from 5% to 15% solvent D over 15 min at 50 °C. **12** was obtained as a light yellow powder (4 mg, 25%) after lyophilization. ¹H NMR (400 MHz, Deuterium Oxide) δ 11.64 (s, 1H), 11.38 (s, 1H), 9.93 (d, *J* = 4.0 Hz, 1H), 8.65 (s, 1H), 8.35 (d, *J* = 9.4 Hz, 1H), 8.25 (d, *J* = 9.3 Hz, 1H), 8.17 (dt, *J* = 8.1, 4.0 Hz, 2H), 8.02 (t, *J* = 5.1 Hz, 1H), 7.95 (d, *J* = 8.0 Hz, 1H), 7.87 – 7.74 (m, 5H), 7.66 (s, 1H), 7.64 – 7.52 (m, 2H), 7.19 (d, *J* = 8.6 Hz, 1H), 3.42 (s, 1H), 3.20 (q, *J* = 6.4, 4.8 Hz, 1H). HRMS (ESI⁻) *m/z* calcd for C₃₈H₃₀N₉O₁₃S₂ [M-H]⁻¹ 884.1409 found 884.2050.

Compound 14: Foldamer-peptide **14** was synthesized on a preloaded Fmoc-Gly-Wang resin (0.31 mmol/g) using the CEM Liberty Blue peptide synthesizer for the peptide segment and on the Liberty Bio for the stepwise assembly of the foldamer part on a 50 μ mol scale. After final acetylation and TFA cleavage the crude product was recovered as light white powder (61 mg, 45 μ mol, 97%) was purified on semi-preparative RP-HPLC (with a gradient from 10% to 40% solvent D at 50 $^{\circ}$ C. **14** was obtained as light orange powder (32.0 mg, 52%) after freeze drying. 1 H NMR (500 MHz, DMSO- d_6) δ 12.26 (s, 2H), 9.59 (t, J = 6.4 Hz, 1H), 9.12 (t, J = 6.1 Hz, 1H), 8.94 (ddd, J = 18.0, 7.7, 1.3 Hz, 2H), 8.63 – 8.56 (m, 3H), 8.50 (s, 1H), 8.28 (t, J = 6.1 Hz, 1H), 8.21 (d, J = 8.0 Hz, 1H), 8.14 (dd, J = 7.7, 1.1 Hz, 1H), 8.10 – 8.05 (m, 2H), 8.01 (t, J = 7.7, 7.2 Hz, 2H), 7.88 (d, J = 8.0 Hz, 1H), 7.84 – 7.76 (m, 3H), 7.72 – 7.69 (d, 1H), 7.38 (dd, J = 7.8, 1.1 Hz, 1H), 5.02 (d, J = 6.5 Hz, 2H), 4.39 – 3.99 (m, 8H), 3.79 – 3.62 (m, 2H), 2.72 (t, J = 7.1 Hz, 2H), 1.57 (s, 3H), 1.53 – 1.46 (m, 4H), 1.41 – 1.21 (m, 5H), 1.17 – 1.15 (m, 3H), 0.67 (dd, J = 12.5, 6.5 Hz, 6H). HRMS (ESI $^-$) m/z calcd for C₅₅H₆₁N₁₄O₁₇S₂ [M-H] $^-$ 1253.3786 found 1253.4049.



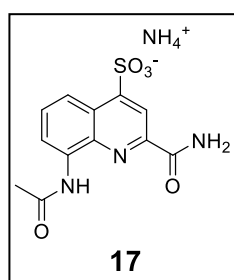
15

Compound 15: Foldamer-peptide **15** was synthesized on a preloaded Fmoc-Gly-Wang resin (0.31 mmol/g) using the CEM Liberty Blue peptide synthesizer for the peptide segment and on the Liberty Bio for the stepwise assembly of the foldamer part on a 50 μ mol scale. After final acetylation and TFA cleavage the crude product was recovered as a light white powder (29 mg, 19 μ mol, 76%). After purification on semi-preparative RP-HPLC with a gradient from 25% to 35% solvent B at 50 $^{\circ}$ C within 20 minutes, **15** was obtained as a colorless powder (6.2 mg, 21%). 1 H NMR (500 MHz, DMSO- d_6) δ 11.77 (s, 1H), 11.65 (s, 1H), 9.60 (s, 1H), 8.44 (s, 2H), 8.38 (s, 1H), 8.20 (d, J = 7.8 Hz, 1H), 8.16 (t, J = 7.7 Hz, 1H), 8.13 – 8.05 (m, 4H), 8.02 – 7.96 (m, 2H), 7.92 – 7.84 (m, 5H), 7.80 (d, J = 7.9 Hz, 1H), 7.76 – 7.59 (m, 11H), 7.57 (t, J = 8.1 Hz, 1H), 7.36 (dd, J = 7.8, 1.1 Hz, 1H), 7.21 (m, 5H), 7.18 – 7.12 (m, 1H), 6.94 (s, 1H), 5.14 (s, 2H), 4.95 (m, 4H), 4.51 (td, J = 8.8, 4.6 Hz, 1H), 4.34 – 4.21 (m, 2H), 4.13 (d, J = 6.4 Hz, 2H), 3.86 – 3.67 (m, 4H), 3.08 – 3.01 (m, 1H), 2.80 – 2.61 (m, 9H), 1.66 (s, 3H), 1.57 – 1.36 (m, 11H), 1.32 – 1.10 (m, 13H). HRMS (ESI $^+$) m/z calcd for C₇₄H₉₀N₁₈O₁₉ [M+2H] $^{+2}$ 767.3309 found 767.3392.



16

Compound 16: Foldamer-peptide **16** was synthesized on a preloaded Fmoc-Gly-Wang resin (0.31 mmol/g) using CEM Liberty Blue peptide synthesizer and the Liberty Bio for the stepwise assembly of the foldamer part on a 50 μmol scale. After final acetylation and TFA cleavage, a crude light white powder was recovered in 91% yield (70 mg). This crude product was further purified on semi-preparative RP-HPLC with a gradient from 20% to 50% solvent D at 50 $^{\circ}\text{C}$. **16** was obtained as a colorless powder (40.0 mg, 57%) after lyophilization. ^1H NMR (500 MHz, $\text{DMSO-}d_6$) δ 11.84 (s, 1H), 11.81 (s, 1H), 9.40 (s, 1H), 8.69 (m, 2H), 8.60 (dd, $J = 16.1, 7.5$ Hz, 2H), 8.23 (d, $J = 6.2$ Hz, 2H), 8.09 (m, 3H), 8.03 (s, 1H), 7.97 (t, $J = 7.7$ Hz, 1H), 7.94 – 7.87 (m, 4H), 7.74 (dd, $J = 7.0, 1.7$ Hz, 1H), 7.58 (m, 3H), 7.43 (s, 1H), 7.38 (d, $J = 7.6$ Hz, 1H), 7.16 – 7.08 (m, 3H), 7.01 (t, $J = 7.5$ Hz, 2H), 6.90 (t, $J = 7.3$ Hz, 1H), 5.05 – 4.85 (m, 2H), 4.73 – 4.54 (m, 4H), 4.35 (d, $J = 7.2$ Hz, 1H), 4.24 – 4.09 (m, 4H), 4.01 (dd, $J = 26.1, 13.2$ Hz, 1H), 3.85 (dd, $J = 15.1, 5.9$ Hz, 1H), 3.76 – 3.57 (m, 2H), 2.97 (d, $J = 12.4$ Hz, 1H), 2.76 (dd, $J = 36.8, 10.4$ Hz, 5H), 1.89 (s, 3H), 1.68 (s, 6H), 1.64 – 1.21 (m, 18H), 1.18 (t, $J = 9.0$ Hz, 6H). HRMS (ESI $^-$) m/z calcd for $\text{C}_{74}\text{H}_{87}\text{N}_{18}\text{O}_{19}$ $[\text{M-H}]^-$ 1531.6394 found 1531.6647.



17

Compound 17: Compound **17** was synthesized on solid support using Rink amide MBHA resin on a 33 μmol scale. Fmoc- Q^{Sul} -OH (47 mg, 96 μmol , 3 equiv) was attached on solid support using PyBOP (48 mg, 96 μmol , 3 equiv), DIPEA (33 μL , 192 μmol , 6 equiv) in 1 mL DMF for 1h at r.t. After Fmoc removal, the amine was acetylated using acetic anhydride in DCM 50:50 (v:v) for 30 min at rt. The crude compound was obtained after cleavage from the resin (general procedure 2.6) and TFA was removed under reduced pressure. **17** was obtained after purification on semi-preparative HPLC (general procedure 3) using a gradient from 0% to 40% solvent D over 25 minutes as a yellow solid (7 mg, 69%). ^1H NMR (500 MHz, $\text{DMSO-}d_6$) δ 10.33 (s, 1H), 9.14 (s, 1H), 8.72 (dd, $J = 7.8, 1.3$ Hz, 1H), 8.51 (s, 1H), 8.48 (dd, $J = 8.6, 1.3$ Hz, 1H), 7.81 (s, 1H), 7.62 (dd, $J = 8.6, 7.8$ Hz, 1H), 7.05 (s, 4H), 2.33 (s, 3H). HRMS (ESI $^-$) m/z calcd for $\text{C}_{12}\text{H}_{10}\text{N}_3\text{O}_5\text{S}$ $[\text{M-H}]^-$ 308.0347 found 308.0349.

7.3. Materials and Methods for HPLC, MS, UV, NMR and CD

HPLC

RP-HPLC analyses as well as semi-preparative purification were performed on an Ultimate 3000 HPLC System (ThermoFisher Scientific). For analytical analysis, a Nucleodur C18 Gravity column (4 x 100 mm, 5 μ m, Macherey-Nagel) was used, and semi-preparative purifications were performed on a Nucleodur C18 Gravity column (10 x 250 mm, 5 μ m, Macherey-Nagel). A Nucleodur C8 Gravity column (4 x 50 mm, 5 μ m, Macherey-Nagel) was also used in analytic mode and for semi-preparative purification, the Nucleodur C8 Gravity column (10 x 100 mm, 5 μ m, Macherey-Nagel) was employed. Semi-preparative purification was performed with an automated fraction collector system from ThermoFisher Scientific. When using acidic conditions 0.1% TFA was added to aqueous mobile phase (referred to as mobile phase A) and to acetonitrile (referred to as mobile phase B). When using basic conditions, a $\text{NH}_4\text{OAc-NH}_4\text{OH}$ buffer (12.5 mM, pH 8.5) was used as the aqueous mobile phase (referred to as mobile phase C) in combination with pure acetonitrile (referred to as mobile phase D). For analytical RP-HPLC analysis, a flow rate of 1.0 mL/min was applied; semi-preparative purification on RP-HPLC was performed at a flow rate of 5.0 mL/min. The column eluent was monitored by UV detection at 214, 254, and 300 nm with a diode array detector.

High-resolution electrospray mass (HR-MS)

HR-MS spectra were recorded on a Bruker microTOF II by direct infusion from aqueous media in either positive or negative ionization mode. The instrument was calibrated in positive and negative mode by direct infusion of a calibration solution (Agilent Technologies ESI-L Low Concentration Tuning Mix).

UV calibration curve to determine the molar extension coefficient of Q^{Sul} residue.

Compound **15** (7.0 mg) was dissolved in $\text{NH}_4\text{OAc-NH}_4\text{OH}$ buffer (12.5 mM pH 8.5) to reach a 0.3 mM concentration. This reference solution was next used to prepare seven diluted solution at concentrations 0.3 mM, 0.15 mM, 0.1 mM, 0.075 mM, 0.050 mM, 0.025 mM, and 0.0125 mM. The UV absorbance at 375 nm was recorded on a Nanodrop One instrument (Thermo Fisher Scientific) by using a 1 cm quartz cuvette. The absorbance values were plotted against the concentration to generate a calibration curve. The molar extinction coefficient was calculated from the slope and a value for $\epsilon = 2678 \text{ L}\cdot\text{mol}^{-1}\cdot\text{cm}^{-1}$ at 375 nm was found. This ϵ value was used for determining the concentration of Q^{Sul} -rich foldamer-peptide hybrid solutions. To note, this ϵ is in good agreement with the previously $\epsilon_{370 \text{ nm}}$ value of a $(\text{Q}^{\text{Sul}})_8$ octamer of $20959 \text{ L}\cdot\text{mol}^{-1}\cdot\text{cm}^{-1}$.⁴

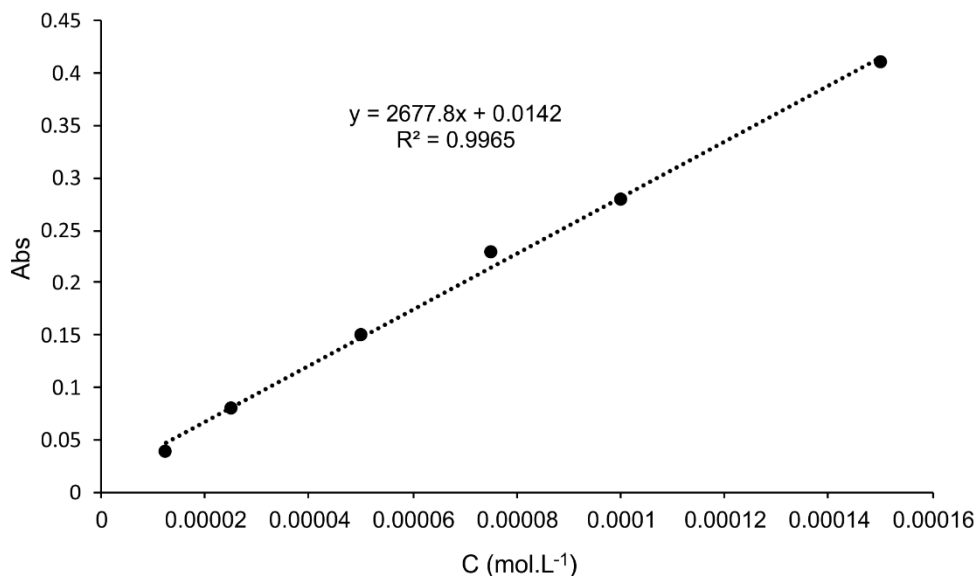


Figure S2: UV calibration curve at 375 nm of the Ac-Q^{sul}-NH₂ residue (**15**) to get access of the $\epsilon_{375\text{nm}}$ value.

Nuclear Magnetic Resonance (NMR)

¹H NMR spectra were recorded on Avance III HD 400 MHz Bruker BioSpin and Avance III HD 500 MHz Bruker BioSpin spectrometers. All chemical shifts are reported in ppm and calibrated against residual solvent signals of DMSO-*d*₆ (δ 2.50 ppm) and CD₃CN (δ 2.05) (δ value in an NH₄OAc/CD₃CN 3:1 (v/v)). In the case of ¹H NMR spectra recorded in H₂O/D₂O 90:10 (v/v), 3-(trimethylsilyl)propionic-2,2,3,3-*d*₄ acid sodium salt (TPS) was added (δ 0.00 ppm) to the medium. Coupling constants (*J*) are reported in Hz. Signal multiplicities were abbreviated as *s*, singlet; *d*, doublet; *t*, triplet; *q*, quartet, and *m*, multiplet.

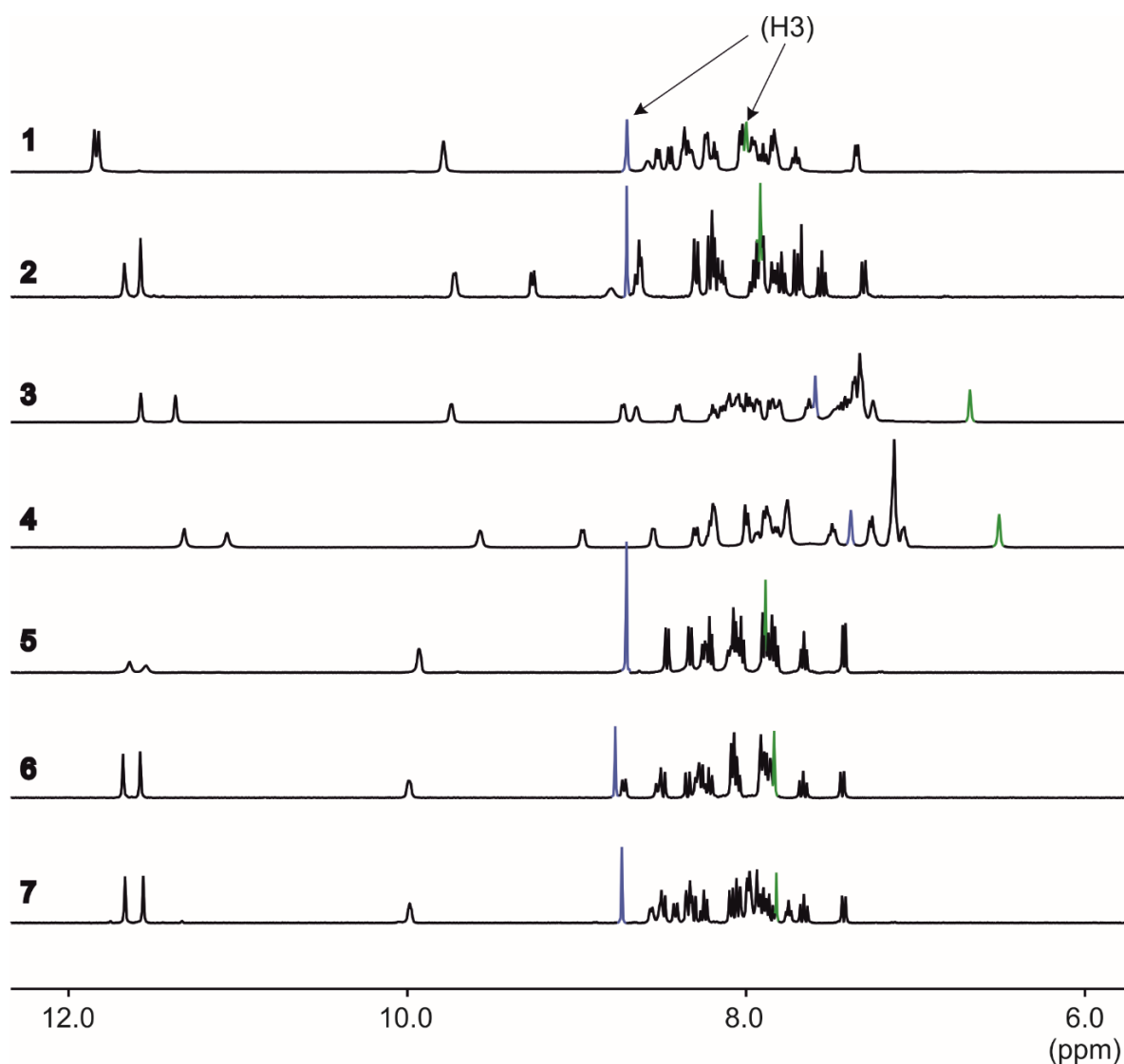


Figure S3: ^1H NMR Spectrum overlay of **1-7**. (500 MHz, in water:acetonitrile- d_3 75:25 (v:v), water suppression at 25 °C. Quinoline H3 protons marked in blue and green.

Circular dichroism (CD)

All CD curves were recorded on a Jasco J-810 spectrometer with 2 mm quartz cuvette. Following parameters were used: Wavelength range from 500 to 250 nm (for PQQ containing sequences) and 650 to 250 nm (consecutive Q containing oligomers), scan speed: 50 nm/min, accumulation: 2, response time: 1.0 s, bandwidth: 2, temperature: 20 °C, sensitivity: standard, data pitch: 0.1 nm, nitrogen gas flow rate: 500L/h. If not otherwise mentioned, the sample solution was prepared in degassed ultrapure water/acetonitrile solvent mixture 75:25 (v/v). $\Delta\epsilon$ values were obtained by using the formula: $\Delta\epsilon = m^\circ / (C \cdot l \cdot 32980)$; $\Delta\epsilon = \text{cm}^2 \cdot \text{mmol}^{-1}$, $m^\circ = \text{CD value in milli degrees}$, $l = \text{cuvette pathlength in cm}$, $C = \text{sample concentration in mol/L}$.

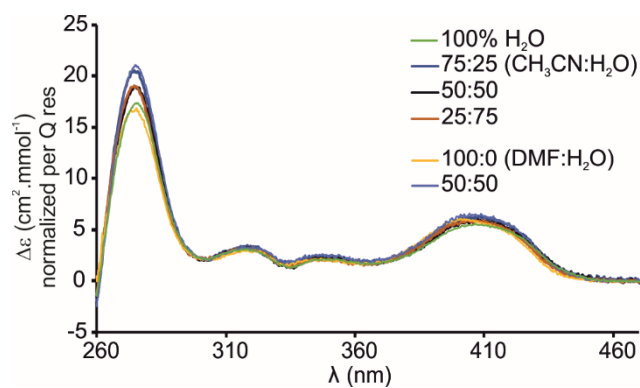


Figure S4: CD spectra of **8** in different acetonitrile:water mixtures. The composition of the solvent did not induce a change of handedness control of the Foldamer.

7.4. 2D TOCSY and variable temperature NMR spectra

The two-dimensional TOCSY experiments were recorded at different temperatures (50 °C, 25 °C, 0 °C and -5 °C) at Avance III NMR spectrometers (Bruker BioSpin GmbH) operating at a spectrometer frequency of 400 MHz equipped with 5-mm direct PABBO/BB/19F-1H/D probes with single axis Z gradient capabilities. Processing was performed with MestReNova (v.12.0.0) NMR processing software from Mestrelab Research.

2D TOCSY spectra were recorded with a phase-sensitive pulse sequence using composite pulse scheme MLEV with water suppression employing an excitation sculpting element (mlevsgpph) from the Bruker pulse program library. Data acquisition was performed with 2048 (F2) x 256 (F1) data points in States-TPPI mode. The recycling delay was 2.0 s and 8 transients per increment were applied at a sweep width of 8 kHz in both dimensions resulting in an acquisition time of 0.1283 s. The TOCSY mixing time was set to 80 ms. Special acquisition parameters regarding the water suppression element of the pulse sequence were adopted from the optimized parameter set of the respective one-dimensional experiment. A 90° shifted sine-square multiplication and an exponential window of 1.0 Hz in both dimensions prior to FT was applied. Zero filling and forward LP with MIST algorithm in F1 has been used to yield a final matrix of 1K x 1K real points. Automatic phase correction as well as baseline correction was applied in both dimensions. 1D Traces of the 2D plot showing the TOCSY correlation from the respective NH resonance to the methylene Hs were made by extracting slices from the respective cross peaks in F1.

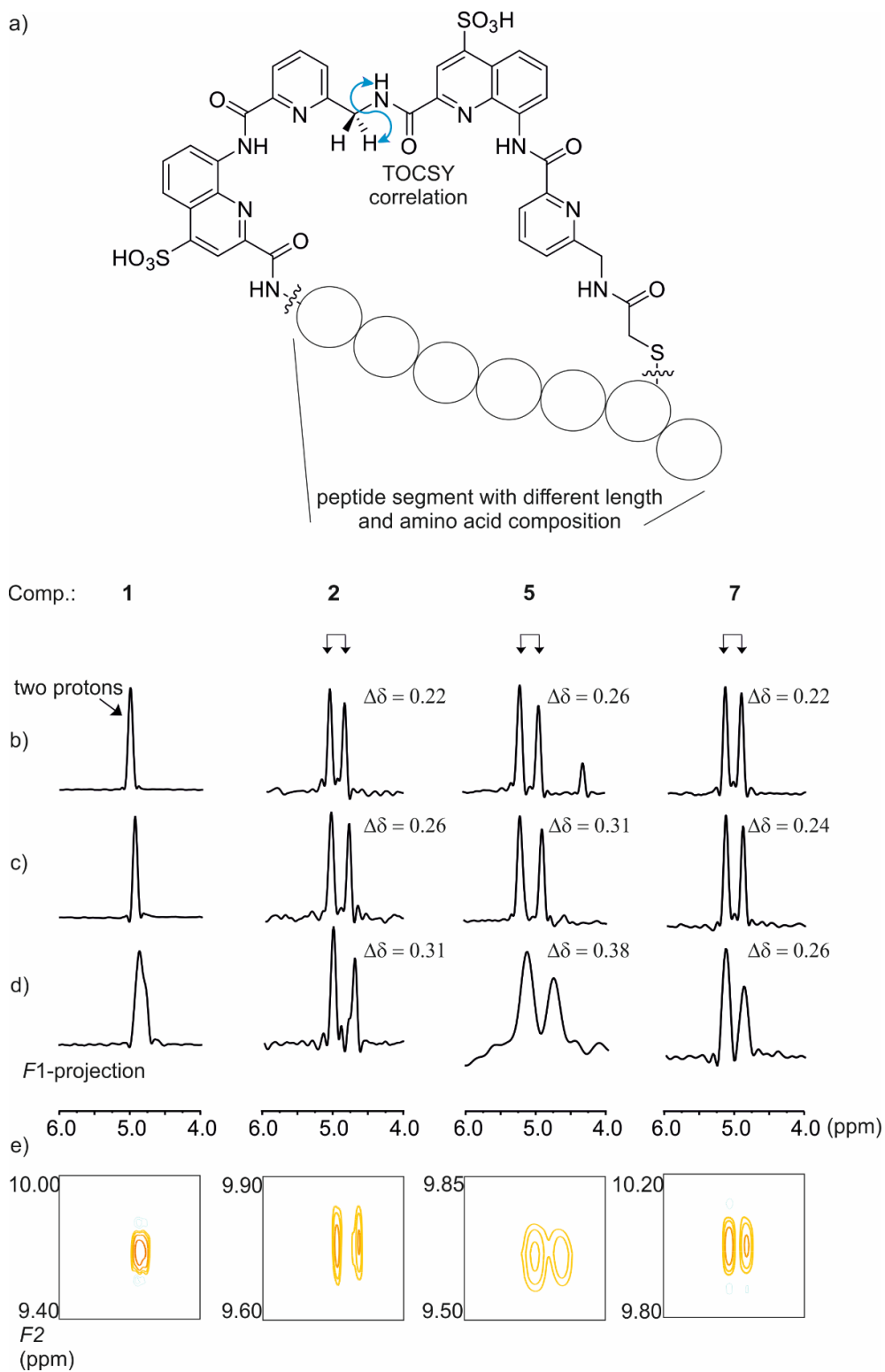


Figure S5: Schematic chemical representation of PQQ-Foldamer-peptide macrocycle (a). F1 projection of traces derived from TOCSY correlations between the amide adjacent to the methylene group protons of **1**, **2**, **5** and **7** at 50 °C (b), 25 °C (c) and 0 °C (d). Excerpts of 2D TOCSY at 0 °C (e).

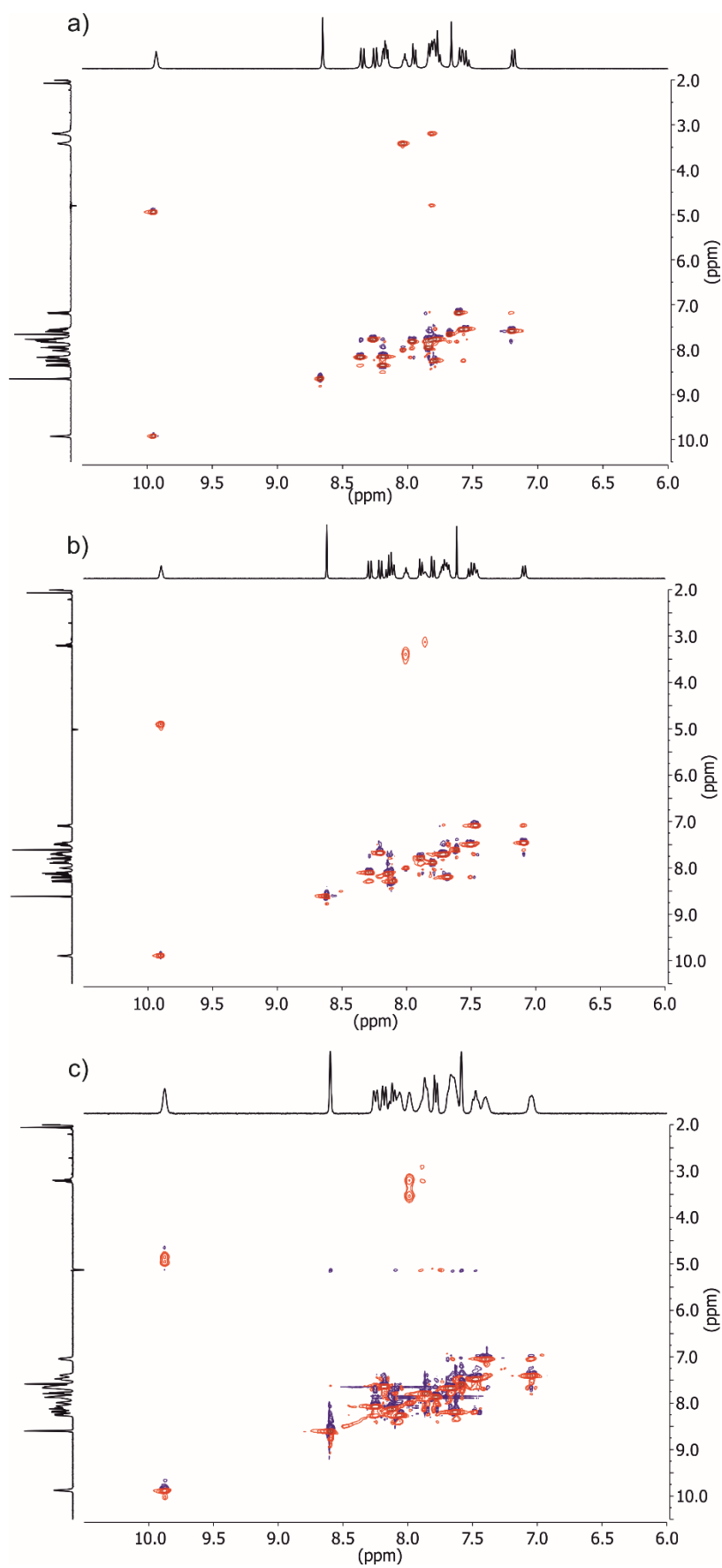


Figure S6: Zoom of TOCSY spectra (400 MHz, 50 mM NaHCO₃ in H₂O/10% D₂O, water suppression) of **12** at 25 °C (a), 0 °C (b) and -5 °C (c).

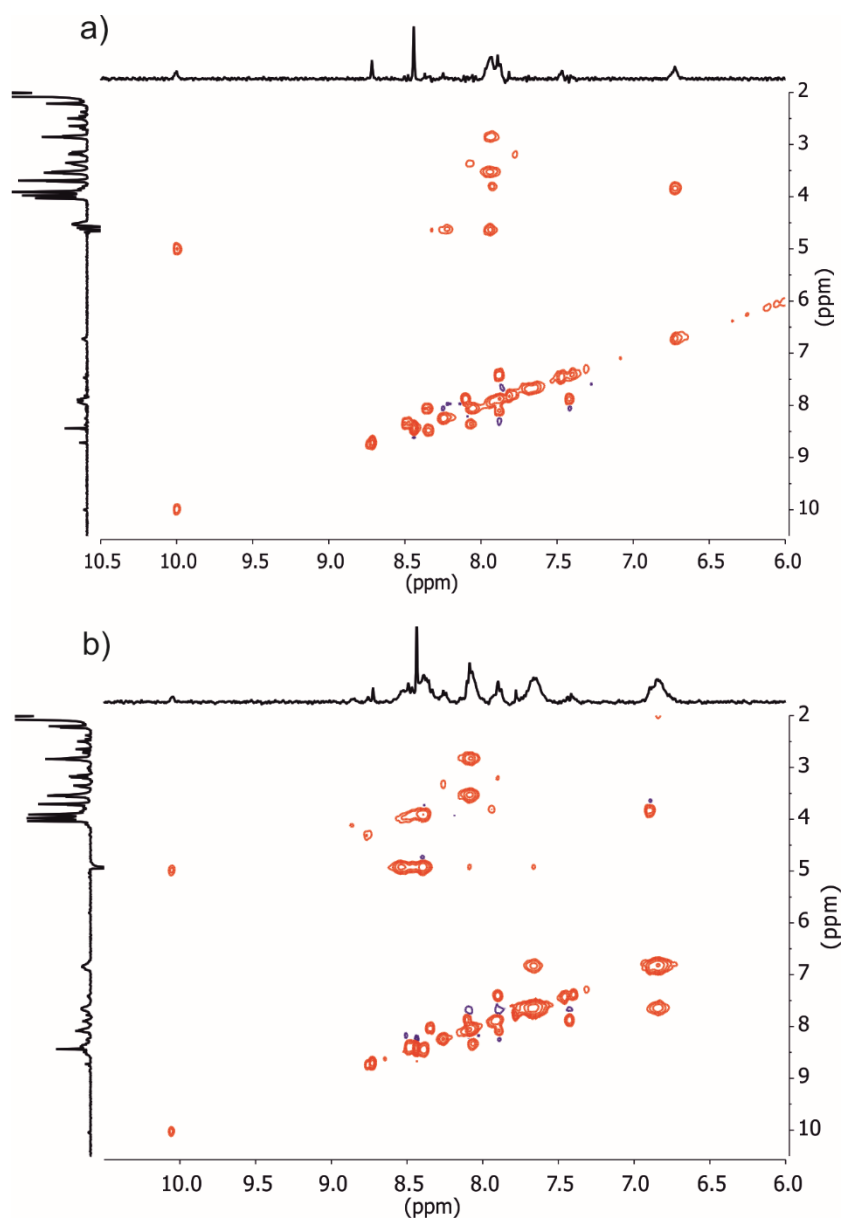


Figure S7: Zoom of TOCSY spectra (400 MHz, 12.5 mM NH_4OAc in $\text{H}_2\text{O}/25\% \text{CD}_3\text{CN}$, water suppression) of **13** at 25 °C (a) and 0 °C (b).

7.5. Crystallization and X-ray diffraction measurements

In the following section (bio)crystallization using vapor diffusion method, X-ray diffraction measurement at Synchrotron Radiation facility, structure determination and refinement of compounds **1**, **7**, and **9** are described. All three crystal structures were determined using the dual space method in structure solution software *ShelxD*⁶ and refined by performing full-matrix least-squares method on F^2 with *Shelxl-2014*⁷ within the *Olex2*⁸ suite.

⁶ G. M. Sheldrick, *Acta Crystallogr A Found Adv*, 2015, **71**, 3-8.

⁷ G. M. Sheldrick, *Acta Crystallogr C Struct Chem*, 2015, **71**, 3-8.

⁸ O. V. Dolomanov, L. J. Bourhis, R. J. Gildea, J. A. K. Howard and H. Puschmann, *Journal of Applied Crystallography*, 2009, **42**, 339-341.

Crystallization and X-ray diffraction of compounds **1**, **7** and **9**

For crystallization, the lyophilized powder of hybrid macrocycles was dissolved in ultrapure water. Screening trials were performed using sparse matrix screen JBScreen Basic 1 - 3, Wizard 1 - 4, PACT ++4, and NucPro1 from Jena Bioscience on 96-well plate by sitting drop vapor diffusion at 25 °C. For each screening condition, 0.8 µL of the compound solution was mixed with 0.8 µL of crystallization reagent. The crystallization screening hit was optimized by means of increasing drop size and hanging drop vapor diffusion method in a 24-well Linbro-style plate.

Crystallization of compound **9** as an enantiopure solution lead to crystals that diffracted poorly. Consequently, the *D*-enantiomer of **9** was synthesized and the lyophilized powder was dissolved in ultrapure water. A racemic mixture of *L*- and *D*-enantiomers was prepared by mixing in a 1:1 ratio the solutions of enantiopure *L*- and *D*-compound **9**. The mixture was again lyophilized and redissolved in ultrapure water to a final concentration of 10 mM.

For mounting, a single crystal was fished from the drop with a micro-loop, quickly soaked in cryo-protectant solution, and flash-frozen in liquid nitrogen.

For compound *D*-**1**, diffraction measurements at atomic resolution were obtained in the X10SA (PXII) beamline, Swiss Light Source, with a Pilatus 6M detector.⁹ Diffraction data were measured at T = -173 °C and $\lambda = 0.8000 \text{ \AA}$. The crystal was exposed for 0.5 s and 0.5° oscillation per frame. Diffraction data were processed with *CrysAlis^{Pro}* suite version 39.46.¹⁰

For compounds **7** and **9**, diffraction measurements at atomic resolution were obtained in the P13 beamline operated by EMBL Hamburg at the Petra III storage ring (DESY, Hamburg), with a Pilatus 6M detector.¹¹ Diffraction data were measured at T = -173 °C and $\lambda = 0.97625 \text{ \AA}$. The crystal was exposed for 0.04 s and 0.1° oscillation per frame. Diffraction data were processed with *CrysAlis^{Pro}* suite version 39.46.¹⁰

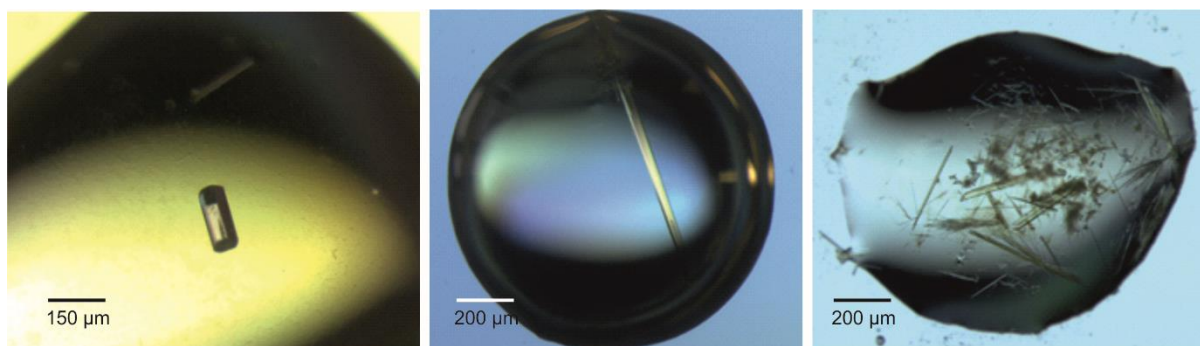
⁹ M. R. Fuchs, C. Pradervand, V. Thominet, R. Schneider, E. Panepucci, M. Grunder, J. Gabadinho, F. S. Dworkowski, T. Tomizaki, J. Schneider, A. Mayer, A. Curtin, V. Olieric, U. Frommherz, G. Kotrle, J. Welte, X. Wang, S. Maag, C. Schulze-Briese and M. Wang, *J Synchrotron Radiat*, 2014, **21**, 340-351.

¹⁰ Rigaku Oxford Diffraction, 2015, CrysAlisPro Software System, (Version 1.171, Rigaku Corporation, Oxford, UK)

¹¹ M. Cianci, G. Bourenkov, G. Pompidor, I. Karpics, J. Kallio, I. Bento, M. Roessle, F. Cipriani, S. Fiedler and T. R. Schneider, *J Synchrotron Radiat*, 2017, **24**, 323-332.

Table 1: Crystallization conditions of compound **1**, **7** and **9**

Compound	Conc. (in H ₂ O)	Crystallization reagent (reservoir solution)	Crystallogenesis Duration	Cryo-protectand
<i>D-1</i>	7 mM	28% polyethylene glycol 400, 100 mM HEPES, pH 7.5, 200 mM CaCl ₂	7 days	50% v/v PEG 400 solution
<i>L-7</i>	5mM	1.6 M NaH ₂ PO ₄ , 0.4M K ₂ HPO ₄ , 0.1 M Sodium phosphate citrate, pH 4.2	7 days	Glycerol + reservoir solution (1:1)
9	10mM	15% PEG 400, 0.1 TRIS, 0.08 M CaCl ₂ , and 15 mM NaCl at pH 8.5	4 days	Glycerol + reservoir solution (1:1)

**Figure S8:** Crystals of **1**, **3** and **7** from left to right in the crystallization medium under the microscope. Drop size 1.5 µL to 2.0 µL.

Structure determination and refinement:

The crystal of *D-1* belonged to space group P6₅ with one molecule in the asymmetric unit. The structure was solved by dual space solution method using *ShelxD*⁶ and refined by full-matrix least-squares method on F² with *Shelxl-2014*⁷ within *Olex2*.⁸ After each refinement step, visual inspection of the model and electron density was carried out in *Coot*.¹² Except for the C-terminal Gly residue, all non-hydrogen atoms were refined with anisotropic displacement parameters. Hydrogen atoms were inserted by using HFIX into idealized positions with a riding model. After several failed attempts to model disordered water molecules, the PLATON/SQUEEZE protocol was performed.¹³ DFIX, SADI, and FLAT instructions were used to improve the geometry of the molecules and their displacement

¹² P. Emsley, B. Lohkamp, W. G. Scott and K. Cowtan, *Acta Crystallogr D Biol Crystallogr*, 2010, **66**, 486-501

¹³ A. L. Spek, *Acta Crystallogr D Biol Crystallogr*, 2009, **65**, 148-155.

parameters. One calcium ion from the crystallization solution could be identified together with five coordination oxygens which were anisotropically refined.

The structure of 7 was resolved in the triclinic space group P1 with eight molecules in the asymmetric unit. The structure was solved by dual space solution method using *ShelxD*⁶ and refined by full-matrix least-squares method on F₂ with *Shelxl-2014*⁷ within *Olex2*.⁸ After each refinement step, visual inspection of the model and electron density was carried out in *Coot*.¹² All non-hydrogen atoms of the Foldamer backbone as well as peptide main chain could be refined with anisotropic displacement parameters. Peptide side-chain atoms were left isotropic. Medium resolution diffraction patterns as well as incompleteness of data led to imprecisions in the electron density map. Thus, the peptide side chains for glutamic acid and leucine could only be refined partially. Hydrogen atoms were inserted by using HFIX into idealized positions and refined with a riding model. The PLATON/SQUEEZE¹³ procedure was implemented after several attempts to model disordered water molecules. Shelx compatible restraints and constraints (FLAT, DFIX, RIGU, AFIX, EADP) instructions were performed to improve the 3D geometry of the model and temperature parameters.

The crystal of 9 belonged to space group P1 with six molecules in the asymmetric unit. The structure was solved by dual space solution method using *ShelxD*⁶ and refined by full-matrix least-squares method on F² with *Shelxl-2014*⁷ within *Olex2*.⁸ After each refinement step, visual inspection of the model and electron density was carried out in *Coot*.¹² The majority of all non-hydrogen atoms of the Foldamer backbone as well as peptide main chain could be refined with anisotropic displacement parameters. Atoms with a high degree of disorder were refined with isotropic displacement parameters. Medium resolution diffraction patterns as well as incompleteness of data led to imprecisions in the electron density map. Thus, the peptide side chains lysine and C-terminal glycine could only be refined partially. Four calcium atoms from the crystallization drop with their hydration shell could be identified and modeled with full occupancy. Hydrogen atoms were inserted by using HFIX into idealized positions and refined with a riding model. The PLATON/SQUEEZE¹³ procedure was implemented after several attempts to model disordered water molecules. Shelx compatible restraints and constraints FLAT, DFIX, SIMU, RIGU, SADI, AFIX, and EADP instructions were performed to improve the geometry of the molecule and thermal parameters.

The obtained cif file for compound **1** was examined using IUCr's *checkcif* algorithm. After several failed attempts to upload the CIF files of compounds **7** and **9** into IUCr's *checkcif* algorithm, the PLATON „Validation Mode“ tool was performed to examine the structures. All level A and B alerts are listed.

Table 2: Group 1 alerts in crystal structures of **1**, **7** and **9**

Compound	Alert
<i>D-1</i>	
	PLAT234 ALERT 4 A Large Hirshfeld Difference N76 --C75 . 0.40 Ang.

This alert concerns the side-chain lysine residue and is inherent to the quality of the data. It does not reflect wrong assignment.

Compound	Alert
7	
	023_ALERT_3_A Resolution (too) Low [sin(theta)/Lambda < 0.6].. 27.42 Degree
	029_ALERT_3_A _diffrn_measured_fraction_theta_full value Low . 0.877 Why?
	201_ALERT_2_A Isotropic non-H Atoms in Main Residue(s) 18 Report O593 N594 C563 C564 C580 C581 etc.

Amino acid side chain atoms have been left isotropic due to their disorder. These alerts are inherent to the quality of the data.

	375_ALERT_2_A Strange C-O-H Geometry (C-O > 1.45 Ang) O570 Check
	375_ALERT_2_A Strange C-O-H Geometry (C-O > 1.45 Ang) O169 Check

Compound	Alert
9	
	023_ALERT_3_A Resolution (too) Low [sin(theta)/Lambda < 0.6].. 24.66 Degree
	029_ALERT_3_A _diffrn_measured_fraction_theta_full value Low . 0.910 Why?
	201_ALERT_2_A Isotropic non-H Atoms in Main Residue(s) 18 Report O363 O964 N350 N364 N951 N965 etc.

Peptide side chains have been left isotropic due to their disorder. Mentioned alerts are inherent to the quality of the data.

	412_ALERT_2_A Short Intra XH3 .. XHn H73F ..H733 . 1.65 Ang. x,y,z = 1_555 Check
	413_ALERT_2_A Short Inter XH3 .. XHn H33C ..H52 . 1.88 Ang. x,y,z = 1_555 Check

414_ALERT_2_A Short Intra D-H..H-X H34E ..H35E 1.77 Ang.
x,y,z = 1_555 Check

414_ALERT_2_A Short Intra D-H..H-X H960 ..H965 1.76 Ang.
x,y,z = 1_555 Check

430_ALERT_2_A Short Inter D...A Contact O3X ..O30 . 2.50 Ang.
-1+x,y,1+z = 1_456 Check

Short oxygen-oxygen inter distance contact represents two symmetry-related atoms and does not reflect wrong assignment.

Table 3: Group 2 alerts in crystal structures of 1, 7 and 9

Compound	Alert
<i>D-1</i>	
	<u>PLAT084_ALERT_3_B</u> High wR2 Value (i.e. > 0.25) 0.36 Report This alert is inherent to the quality of the data.
	<u>PLAT201_ALERT_2_B</u> Isotropic non-H Atoms in Main Residue(s) 3 Report O86 O87 C85 This alert concerning a side chain COOH group. ANIS displacement parameters could not be performed for mentioned atoms due to their disorder.
	<u>PLAT234_ALERT_4_B</u> Large Hirshfeld Difference O88 --C82 . 0.30 Ang. <u>PLAT234_ALERT_4_B</u> Large Hirshfeld Difference C79 --C82 . 0.26 Ang. These alerts concerning disordered cys-gly side-chain atoms and are inherent to the quality of the data.
	<u>PLAT241_ALERT_2_B</u> High 'MainMol' Ueq as Compared to Neighbors of C84 Check
	<u>PLAT242_ALERT_2_B</u> Low 'MainMol' Ueq as Compared to Neighbors of Ca89 Check
	<u>PLAT341_ALERT_3_B</u> Low Bond Precision on C-C Bonds 0.02051 Ang.
	<u>PLAT430_ALERT_2_B</u> Short Inter D...A Contact O54 ..O95 . 2.55 Ang. 1+x-y,x,-1/6+z = 2_454 Check
	<u>PLAT430_ALERT_2_B</u> Short Inter D...A Contact O86 ..O93 . 2.66 Ang. 1+y,-x+y,1/6+z = 6_655 Check
	Alerts 2B concerns side-chain atoms and calcium hydration shell atoms. However, they do not indicate an incorrect atom-type assignment.
	<u>PLAT934_ALERT_3_B</u> Number of (lobs-lcalc)/Sigma(W) > 10 Outliers .. 4 Check

Compound	Alert
7	

241_ALERT_2_B	High	'MainMol'	Ueq as Compared to Neighbors of C18 Check
241_ALERT_2_B	High	'MainMol'	Ueq as Compared to Neighbors of C104 Check
241_ALERT_2_B	High	'MainMol'	Ueq as Compared to Neighbors of C159 Check
241_ALERT_2_B	High	'MainMol'	Ueq as Compared to Neighbors of C278 Check
241_ALERT_2_B	High	'MainMol'	Ueq as Compared to Neighbors of C392 Check
241_ALERT_2_B	High	'MainMol'	Ueq as Compared to Neighbors of C417 Check
241_ALERT_2_B	High	'MainMol'	Ueq as Compared to Neighbors of S694 Check
241_ALERT_2_B	High	'MainMol'	Ueq as Compared to Neighbors of C689 Check
242_ALERT_2_B	Low	'MainMol'	Ueq as Compared to Neighbors of N103 Check
242_ALERT_2_B	Low	'MainMol'	Ueq as Compared to Neighbors of N277 Check
242_ALERT_2_B	Low	'MainMol'	Ueq as Compared to Neighbors of C279 Check
242_ALERT_2_B	Low	'MainMol'	Ueq as Compared to Neighbors of S451 Check
242_ALERT_2_B	Low	'MainMol'	Ueq as Compared to Neighbors of N691 Check
242_ALERT_2_B	Low	'MainMol'	Ueq as Compared to Neighbors of C600 Check
315_ALERT_2_B	Singly Bonded	Carbon Detected	(H-atoms Missing). C564 Check
315_ALERT_2_B	Singly Bonded	Carbon Detected	(H-atoms Missing). C595 Check
315_ALERT_2_B	Singly Bonded	Carbon Detected	(H-atoms Missing). C766 Check
315_ALERT_2_B	Singly Bonded	Carbon Detected	(H-atoms Missing). C65 Check
315_ALERT_2_B	Singly Bonded	Carbon Detected	(H-atoms Missing). C81 Check
315_ALERT_2_B	Singly Bonded	Carbon Detected	(H-atoms Missing). C163 Check
315_ALERT_2_B	Singly Bonded	Carbon Detected	(H-atoms Missing). C264 Check
315_ALERT_2_B	Singly Bonded	Carbon Detected	(H-atoms Missing). C293 Check
315_ALERT_2_B	Singly Bonded	Carbon Detected	(H-atoms Missing). C364 Check
315_ALERT_2_B	Singly Bonded	Carbon Detected	(H-atoms Missing). C464 Check
315_ALERT_2_B	Singly Bonded	Carbon Detected	(H-atoms Missing). C664 Check

Alerts concerning atoms with missing neighbor carbon atoms. This reflects partially or not refined amino acid side-chains carbon-carbon bonds and those atoms have been left without

hydrogen atoms.

340_ALERT_3_B Low Bond Precision on C-C Bonds				0.02216
Ang.				
416_ALERT_2_B Short Intra D-H..H-D	H772	..H783	.	1.56
Ang.				
	x,y,z =	1_555 Check		
416_ALERT_2_B Short Intra D-H..H-D	H270	..H281	.	1.52
Ang.				
	x,y,z =	1_555 Check		
416_ALERT_2_B Short Intra D-H..H-D	H208	..H485	.	1.73
Ang.				
	x,y,z =	1_555 Check		
420_ALERT_2_B D-H Without Acceptor	O71	--H71	.	Please
Check				
420_ALERT_2_B D-H Without Acceptor	O169	--H169	.	Please
Check				
420_ALERT_2_B D-H Without Acceptor	O370	--H370	.	Please
Check				
420_ALERT_2_B D-H Without Acceptor	O670	--H670	.	Please
Check				
910_ALERT_3_B Missing # of FCF Reflection(s) Below Theta(Min).				11
Note				
911_ALERT_3_B Missing FCF Refl Between Thmin & STh/L=				0.472
4936 Report				

Compound	Alert
9	
	082_ALERT_2_B High R1 Value 0.16 Report
	084_ALERT_3_B High wR2 Value (i.e. > 0.25) 0.43 Report
	090_ALERT_3_B Poor Data / Parameter Ratio (Zmax > 18) 4.35
	Note

These alerts are inherent to the quality of the data.

241_ALERT_2_B High	'MainMol' Ueq as Compared to Neighbors of
S962 Check	
241_ALERT_2_B High	'MainMol' Ueq as Compared to Neighbors of
N301 Check	
241_ALERT_2_B High	'MainMol' Ueq as Compared to Neighbors of
C655 Check	
241_ALERT_2_B High	'MainMol' Ueq as Compared to Neighbors of
C665 Check	
241_ALERT_2_B High	'MainMol' Ueq as Compared to Neighbors of
N31A Check	
241_ALERT_2_B High	'MainMol' Ueq as Compared to Neighbors of
C59A Check	
241_ALERT_2_B High	'MainMol' Ueq as Compared to Neighbors of
S96 Check	
241_ALERT_2_B High	'MainMol' Ueq as Compared to Neighbors of
C20 Check	
241_ALERT_2_B High	'MainMol' Ueq as Compared to Neighbors of

C59 Check		
242_ALERT_2_B	Low	'MainMol' Ueq as Compared to Neighbors of
C348 Check		
242_ALERT_2_B	Low	'MainMol' Ueq as Compared to Neighbors of
C360 Check		
242_ALERT_2_B	Low	'MainMol' Ueq as Compared to Neighbors of
S695 Check		
242_ALERT_2_B	Low	'MainMol' Ueq as Compared to Neighbors of
N667 Check		
242_ALERT_2_B	Low	'MainMol' Ueq as Compared to Neighbors of
C699 Check		
242_ALERT_2_B	Low	'MainMol' Ueq as Compared to Neighbors of
C756 Check		
242_ALERT_2_B	Low	'MainMol' Ueq as Compared to Neighbors of
C762 Check		
242_ALERT_2_B	Low	'MainMol' Ueq as Compared to Neighbors of
N555 Check		
242_ALERT_2_B	Low	'MainMol' Ueq as Compared to Neighbors of
C440 Check		
242_ALERT_2_B	Low	'MainMol' Ueq as Compared to Neighbors of
C536 Check		
242_ALERT_2_B	Low	'MainMol' Ueq as Compared to Neighbors of
C564 Check		
242_ALERT_2_B	Low	'MainMol' Ueq as Compared to Neighbors of
N58A Check		
242_ALERT_2_B	Low	'MainMol' Ueq as Compared to Neighbors of
N85A Check		
242_ALERT_2_B	Low	'MainMol' Ueq as Compared to Neighbors of
C29A Check		
242_ALERT_2_B	Low	'MainMol' Ueq as Compared to Neighbors of
C53B Check		
242_ALERT_2_B	Low	'MainMol' Ueq as Compared to Neighbors of
N58 Check		
242_ALERT_2_B	Low	'MainMol' Ueq as Compared to Neighbors of
C15 Check		
242_ALERT_2_B	Low	'MainMol' Ueq as Compared to Neighbors of
C95 Check		

Alerts are a consequence of anisotropic refinement and are inherent to the quality of the data.

315_ALERT_2_B	Singly Bonded Carbon Detected (H-atoms Missing).
C966 Check	
315_ALERT_2_B	Singly Bonded Carbon Detected (H-atoms Missing).
C747 Check	
315_ALERT_2_B	Singly Bonded Carbon Detected (H-atoms Missing).
C567 Check	
315_ALERT_2_B	Singly Bonded Carbon Detected (H-atoms Missing).
C148 Check	

Alerts concerning atoms with missing neighbor carbon atoms. This reflects partially or not refined amino acid side-chains carbon-carbon bonds and those atoms have been left without hydrogen atoms.

341_ALERT_3_B	Low Bond Precision on C-C Bonds	0.05004
---------------	---------------------------------------	---------

Ang.						
410_ALERT_2_B	Short Intra H...H Contact	H49F	..H51A	.	1.82	
Ang.						
		x,y,z =	1_555 Check			
412_ALERT_2_B	Short Intra XH3 .. XHn	H33A	..H33F	.	1.72	
Ang.						
		x,y,z =	1_555 Check			
413_ALERT_2_B	Short Inter XH3 .. XHn	H33G	..H54C	.	1.97	
Ang.						
		x,1+y,z =	1_565 Check			
413_ALERT_2_B	Short Inter XH3 .. XHn	H52E	..H73H	.	1.91	
Ang.						
		1+x,1+y,z =	1_665 Check			
430_ALERT_2_B	Short Inter D...A Contact	O1X	..O26	.	2.74	
Ang.						
		-1+x,y,1+z =	1_456 Check			
430_ALERT_2_B	Short Inter D...A Contact	O4X	..O764	.	2.59	
Ang.						
		x,y,z =	1_555 Check			
430_ALERT_2_B	Short Inter D...A Contact	O5X	..O881	.	2.74	
Ang.						
		x,y,z =	1_555 Check			
430_ALERT_2_B	Short Inter D...A Contact	O5X	..O765	.	2.78	
Ang.						
		x,y,z =	1_555 Check			
430_ALERT_2_B	Short Inter D...A Contact	O6X	..N162	.	2.63	
Ang.						
		-1+x,y,1+z =	1_456 Check			
430_ALERT_2_B	Short Inter D...A Contact	O6X	..O7X	.	2.78	
Ang.						
		x,y,z =	1_555 Check			
430_ALERT_2_B	Short Inter D...A Contact	O9X	..O281	.	2.57	
Ang.						
		-1+x,y,1+z =	1_456 Check			
911_ALERT_3_B	Missing FCF Refl Between Thmin & STh/L=				0.427	
	2967 Report					

Atomic coordinates and structure factors have been uploaded to the Cambridge Crystallographic Data Centre (CCDC) with accession code 2002474, 2010173 and 2010131 are available free upon request.

Table 4: Crystal data and refinement details for compound **1**, **7** and **9**.

Compound	1	7	9
Formula	$C_{55}H_{57}CaN_{14}O_{22}S_3$	$C_{58.3}H_{54.5}N_{15.6}O_{18.8}S_3$	$C_{102.7}H_{88.7}Ca_{0.7}N_{25.7}O_{35.2}S_6$
M [g/mol]	1659.17	1371.56	2463.73
d_{min} [Å]	0.8	1.06	1.17
Crystal system	Hexagonal	Triclinic	Triclinic
Space group	$P6_5$	$P1$	$P1$
a [Å]	17.90824(9)	26.4540(2)	26.6387(9)
b [Å]	17.90824(9)	27.9371(2)	28.6958(6)
c [Å]	46.5216(2)	30.9544(3)	36.1958(12)
α [°]	90	90.943(6)	84.231(2)
β [°]	90	92.550(6)	71.432(3)
γ [°]	120	91.431(6)	87.031(2)
Volume [Å ³]	12920.9 (11)	22843.4 (3)	26089.9(14)
Z	6	8	6
$\rho/g\text{ mm}^{-3}$	1.279	0.798	0.941
Color and Shape	yellow hexagonal prism	Yellow needle	Yellow needle
Size (mm)	0.15 x 0.02 x 0.02	0.4 x 0.04 x 0.02	0.04 x 0.04 x 0.15
μ/mm^{-1}	0.262	0.270	0.406
Total reflections	160150	95050	110283
Unique data [$F_o > 2\sigma F_o$]	17481	44786	25313
R_{int}	0.057	0.0354	0.1016
Parameters/restraints	842/20	5927/559	7146/5020
R1, wR2	0.1215, 0.3576	0.0699, 0.2171	0.1634, 0.4346
Goodness-of-fit	1.714	0.984	1.142
Total potential solvent accessible void volume from SQUEEZE/ Å ³	4276.5	11665	11531
CCDC number	2002474	2010173	2010131

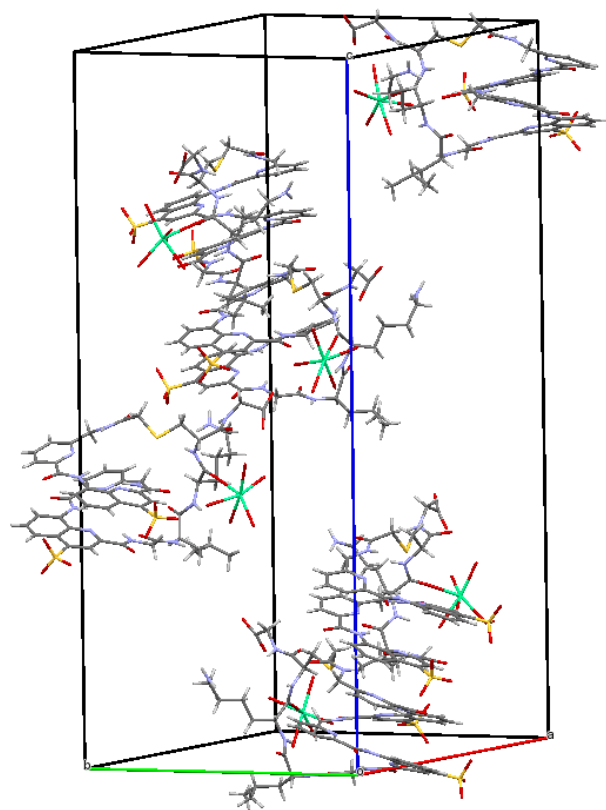


Figure S9: Crystal packing arrangement of six identical molecules of compound *D-1* in the unit cell.

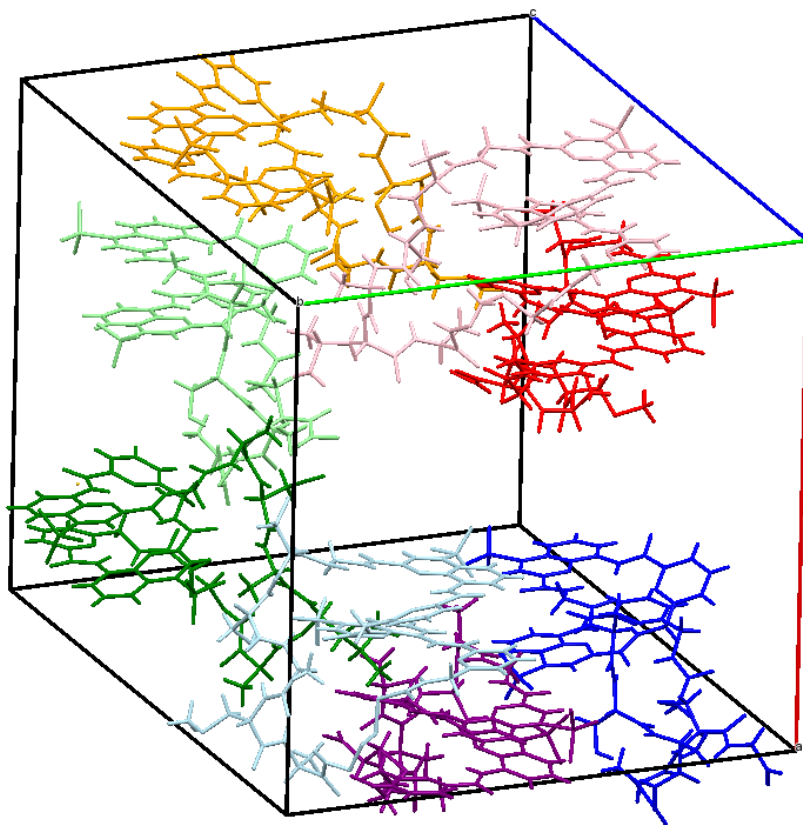


Figure S10: Crystal packing arrangement of eight individual molecules of compound **7** in one unit cell. For visualization, the different conformers have been stained in different colors.

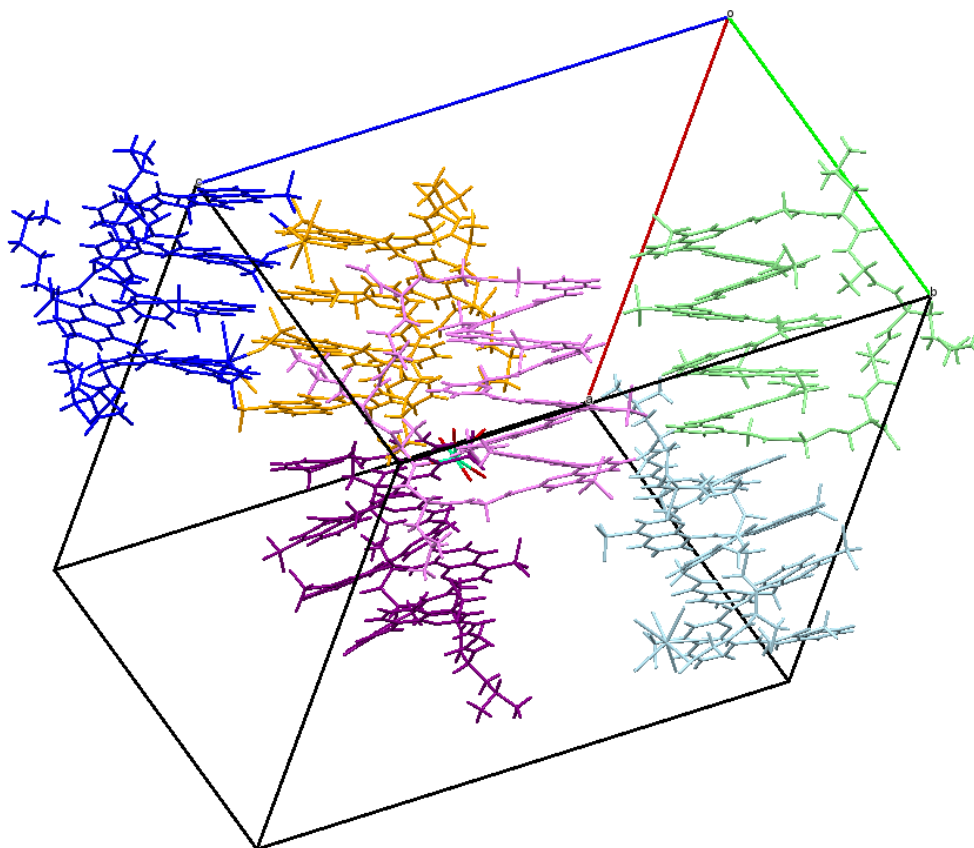


Figure S11: X-ray structure of the cocrystallization of compound *L*-**9** and *D*-**9** showing six individual molecules in one unit cell. For visualization, the conformers have been stained in different colors. Compound *L*-**9** (*P*-helicity) is shown in green, light blue and purple. Compound *D*-**9** (*M*-helicity) is shown in dark blue, orange and pink.

Table 1: Peptide loop dihedral angles (phi and psi) obtained from peptide-Foldamer-hybrid macrocycle x-ray structures from N to C terminus (top to bottom).

Comp.	1			3			7			9		
	Aa	Dihedral-angle (deg)		Aa	Dihedral-angle (deg)		Aa	Dihedral-angle (deg)		Aa	Dihedral-angle (deg)	
		ϕ	ψ									
N	Leu	-75.2	-61.4	Phe	-95.2	6.00	Glu	-148	58.5	Leu	-119	7.2
	Lys	-149	130	Lys	-63.4	149	Ser	-89.2	112	Ala	-79.2	174
	Cys	-71.4	-50.0	Lys	-66.1	150	Ala	-56.3	-50.9	Lys	-124	-20.9
				Lys	-56.5	145	Leu	-68.5	-28.1	Ala	-136	142
				Cys	-56.0	142	Ala	-85.1	-38.6	Cys	-78.4	127
C							Cys	-137	176			

7.6. Biodegradation assay of foldamer-peptide hybrids in the presents of Pronase E, Trypsin or alpha-Chymotrypsin

Methods

The stability of foldamer-peptide hybrids in protease-rich medium was tested in a 96-well polypropylene plate at room temperature. Therefore, the linear and the cycle sequences were incubated with pronase E, trypsin or α -chymotrypsin respectively over a monitored range of time. To each well, an aqueous buffer (40 μ L; 10 mM TRIS, pH 7.5 for pronase E and trypsin or 10 mM TRIS pH 8.0 for α -chymotrypsin), an enzyme solution (1.7 μ L, 1.0 mg/mL pronase E, 0.1 mg/mL for trypsin and α -chymotrypsin) and a solution of foldamer-peptide-hybrid (8.3 μ L; 2.0 mM in the enzyme-specific buffer) was added in that order.^{14,15} The concentration of the foldamer-peptide-hybrid solution was determined by relying on UV calibration curve and UV absorbance.

As blank experiments, two control wells were performed meaning in one well no foldamer-peptide hybrid stock solution was added and in the second well, the enzyme was missing. During the incubation time, the 96-well plate was recovered with aluminum foil to prevent fast evaporation.

At defined time points, the reaction was quenched with a 5% aqueous TFA solution (200 μ L), and the progress of foldamer-peptide hybrid's degradation was monitored by using RP-HPLC.

Compounds **3** and **16** were analyzed on a C18-analytical column (linear gradient 15% to 65% mobile phase B, 7 min, 50 °C). **1** and **14** were analyzed on a C8-analytical column (linear gradient 10% to 35% D, 35% to 100% in 3 min, 7 min, 50 °C, NH₄OAc-NH₄OH buffer 15 mM pH 5.5). **4** and **15** were analyzed on a C18-analytical column (linear gradient 15% to 45% mobile phase B for 7 min, 45% to 100% in 3 min, 50 °C).

All RP-HPLC analyses were performed in duplicates. Peaks and their chromatographic parameters were analyzed by Chromeleon 7 software with the Cobra Wizard data processing tool. The relative area in % for the intact, undigested foldamer-peptide-hybrid was plotted against the incubation time.

LC-MS studies for foldamer-peptide-hybrids after incubation with proteases

To identify the fragments formed after incubation with proteases, the 96-well plate used for enzyme degradation studies was placed on the LC autosampler and each well was analyzed by RP-LCMS. 5 μ L

¹⁴ J. D. Sadowsky, J. K. Murray, Y. Tomita and S. H. Gellman, *ChemBiochem*, 2007, **8**, 903-916.

¹⁵ E. Teyssieres, J. P. Corre, S. Antunes, C. Rougeot, C. Dugave, G. Jouvion, P. Claudon, G. Mikaty, C. Douat, P. L. Goossens and G. Guichard, *J Med Chem*, 2016, **59**, 8221-8232.

of the in well solution was injected on a C18 column Kinetex® (2.1 x 50 mm, 2.6 µm, Phenomenex) (5% for 1 min, 5 to 100% B in 5 min, 50 °C; mobile phase A: 0.1% formic acid in water, mobile phase B: 0.1% formic acid in acetonitrile, 0.5 mL/min). The corresponding total ion count (TIC) profile from the TOF-MS detector gave the corresponding m/z values which allowed the identification of the foldamer-peptide hybrid fragments.

In the case of compound **16**, the starting material and a degradation product co-eluted. The quantification was thus carried out by measuring the extracted ion count (EIC) on the RP-LCMS. Therefore, the sample solutions after incubation with a given protease were injected on the LC-MS and the EIC ratio between signal 1533.6800 +- 0.5 m/z (starting material) and 1405.6220 +- 0.5 m/z (degradation product) was measured. By combining the UV trace ($\lambda = 254$ nm) of the signal (which corresponded to the sum of the UV signal of the two compounds) and selectively quantifying the two compounds by EIC, the degradation of compound **16** over time could be monitored.

microTOF II parameters:

Source	End Plate Offset	500 V
	Capillary	4500 V
	Nebulizer	3.0 bar
	Dry Gas	8.0 L/min
	Dry Temp	200 °C
Tune	Capillary Exit	240.0 V
	Skimmer 1	80.0 V
	Hexapole	23.0 V
	Hexapole RF	450.0 V
	Skimmer 2	23.0 V

For the reference experiment, a sample solution (40 µl) (after protease degradation, 40 min incubation time), was enriched with starting compound (5 µL, 2.0 mM solution). The mixture sample was analyzed by RP-LCMS with the above-mentioned parameters and the two EIC signals were compared with a reference solution (40 µL protease degradation sample + 5 µL water). After calculating the correlation between UV signal, enriched UV signal, EIC signal, and enriched EIC signal, a correcting factor was obtained which was used when determining the quantity of starting material in the degradation experiment.

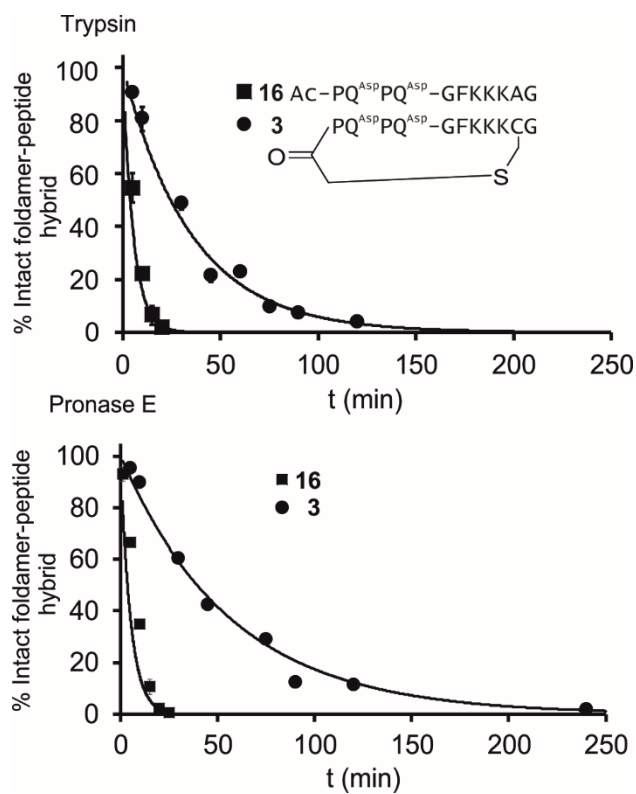


Figure S12: Enzymatic degradation of foldamer-peptide-hybrid compounds in the presence of Trypsin or Pronase E. The decreasing abundance of intact macrocyclic compound **3** (circles) is shown with its non-cyclic reference compound **16** (squares).

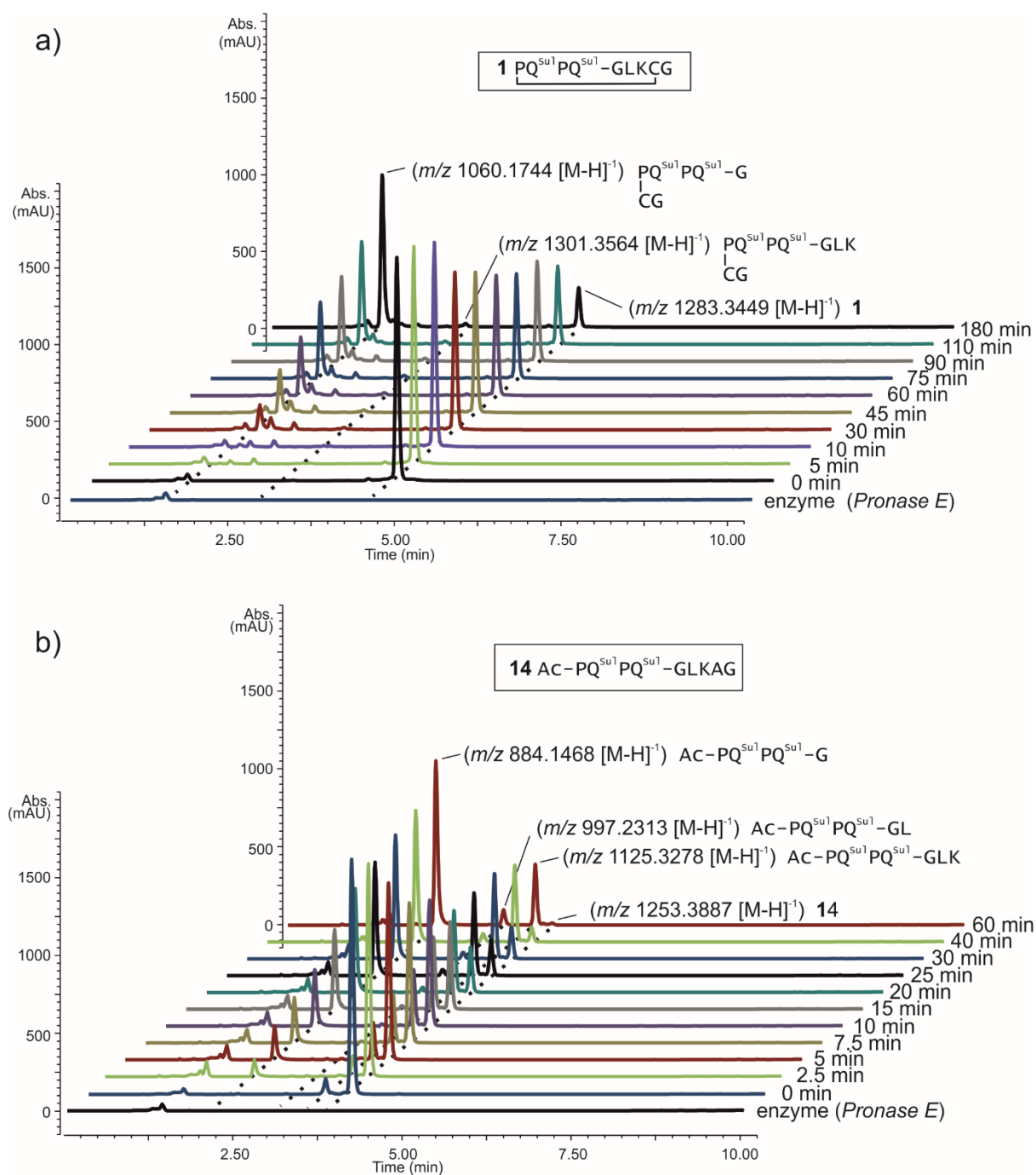


Figure S13: Overlaid chromatograms during the incubation of compound **1** in the presence of Pronase E (a) and **14** (b) Analytical HPLC (linear gradient 10% to 35% D in 7 min, 35% to 100% in 3 min, 50 °C, $\text{NH}_4\text{OAc-NH}_4\text{OH}$ buffer 15 mM pH 5.5, $\lambda=254$ nm). Peptide-foldamer-hybrid fragments formed during the degradation process determined by LC-MS.

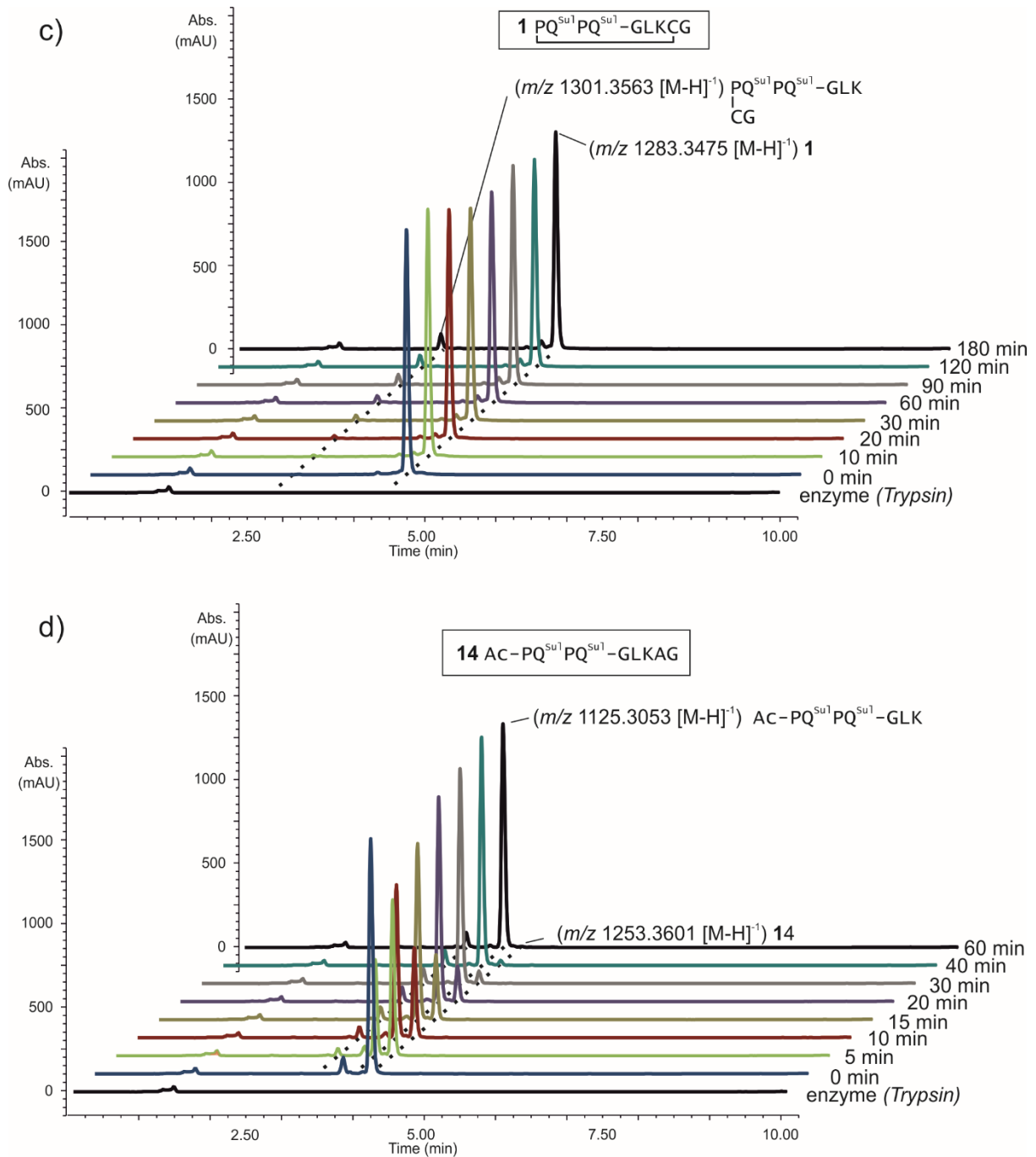


Figure S14: Overlaid chromatograms during the incubation of compound **1** in the presence of Trypsin (c) and **14** (d) Analytical HPLC (linear gradient 10% to 35% D in 7 min, 35% to 100% in 3 min, 50 °C, $\text{NH}_4\text{OAc-NH}_4\text{OH}$ buffer 15 mM pH 5.5, $\lambda=254$ nm). Peptide-foldamer-hybrid fragments formed during the degradation process and determined by LC-MS.

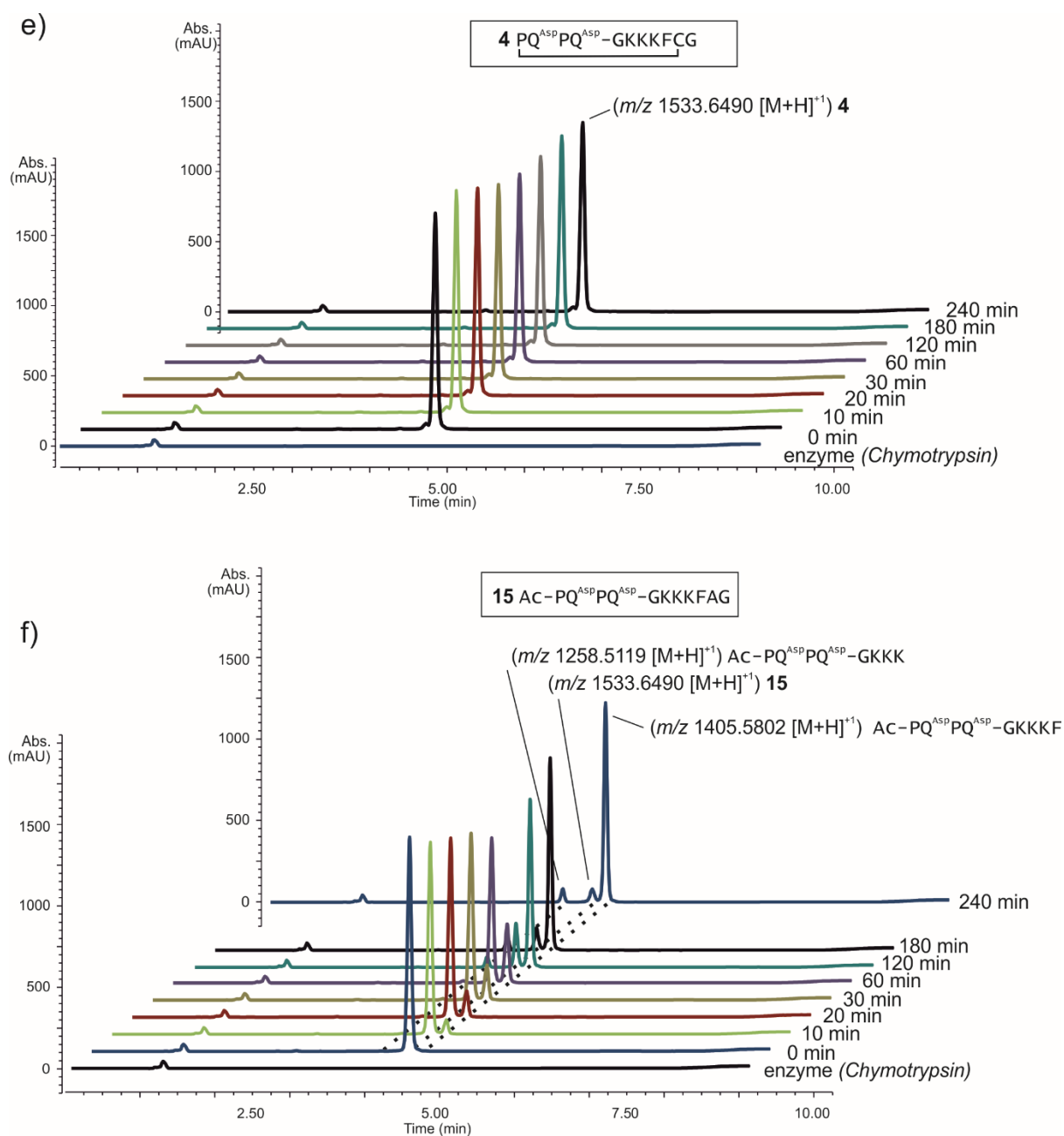


Figure S15: Overlaid chromatograms during the incubation of compound **4** in the presence of α -Chymotrypsin (e) and **15** (f). Analytical HPLC (linear gradient 15% to 45% B in 7 min, 45% to 100% in 3 min, 50 °C, 0.1% TFA, $\lambda=254$ nm). Peptide-foldamer-hybrid fragments formed during the degradation process and determined by LC-MS

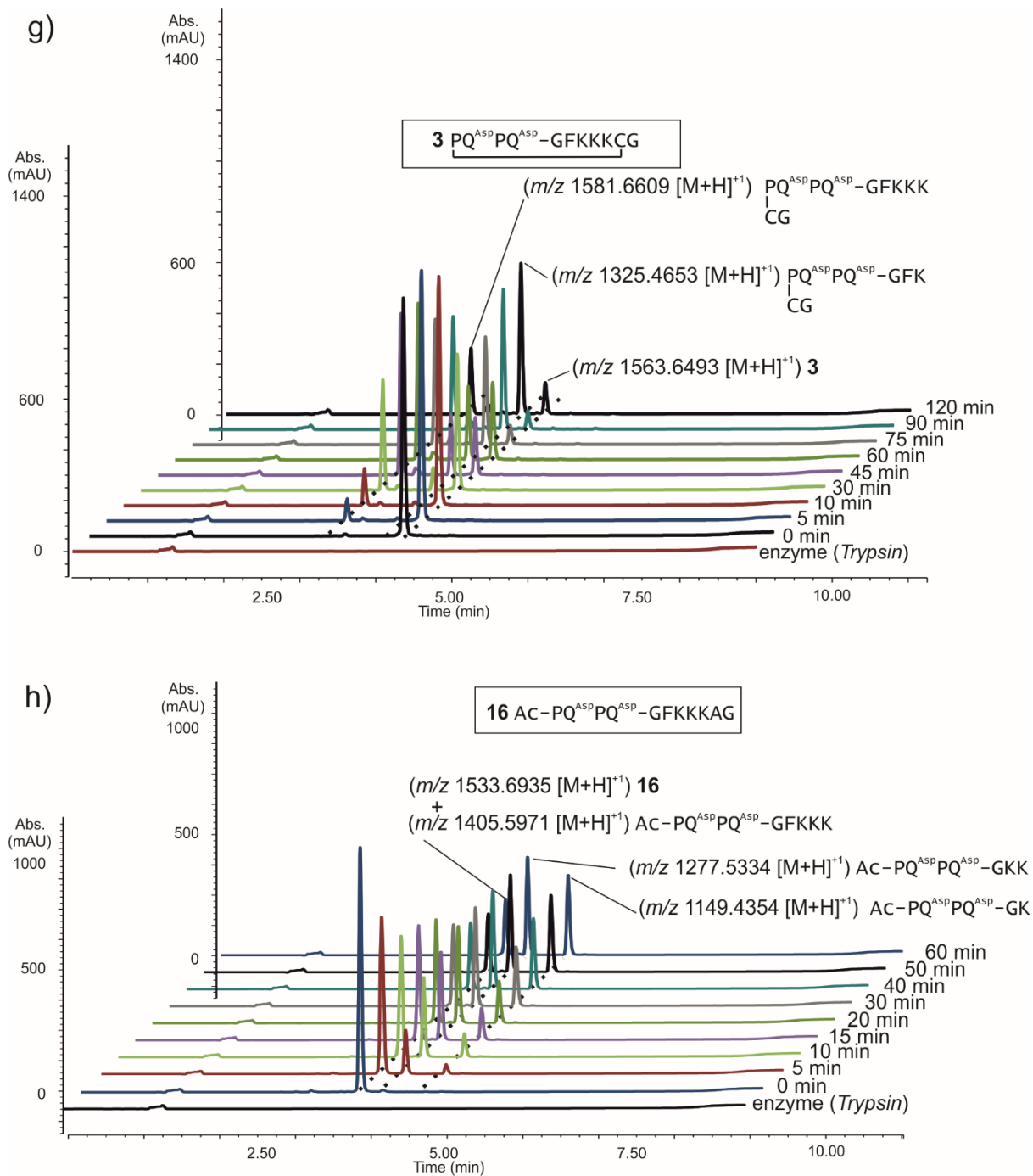


Figure S16: Overlaid chromatograms during the incubation of compound **3** in the presence of Trypsin (g) and **16** (h). Analytical HPLC (linear gradient 15% to 65% B in 7 min, 65% to 100% in 2 min, 50 °C, 0.1% TFA, $\lambda=254$ nm). Peptide-foldamer-hybrid fragments formed during the degradation process and determined by LC-MS.

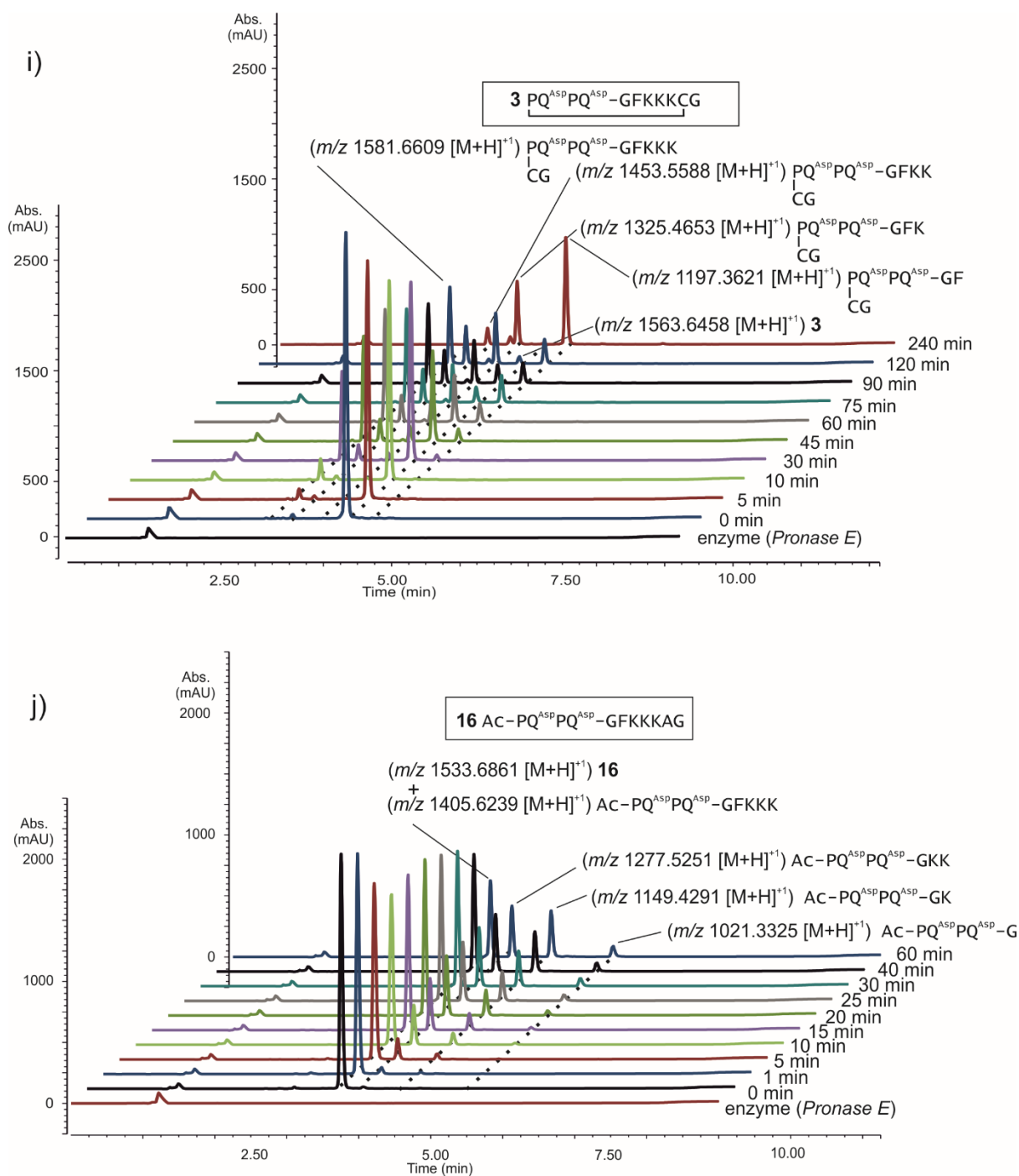
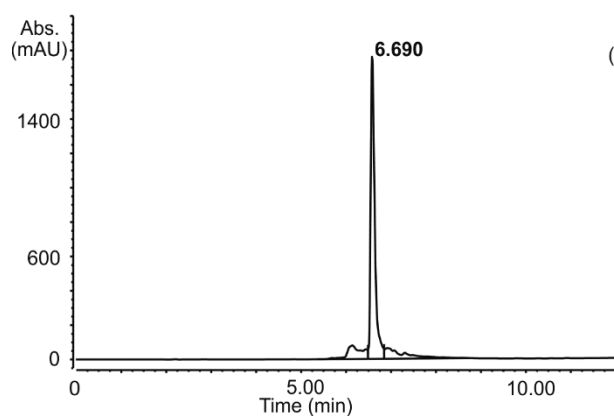


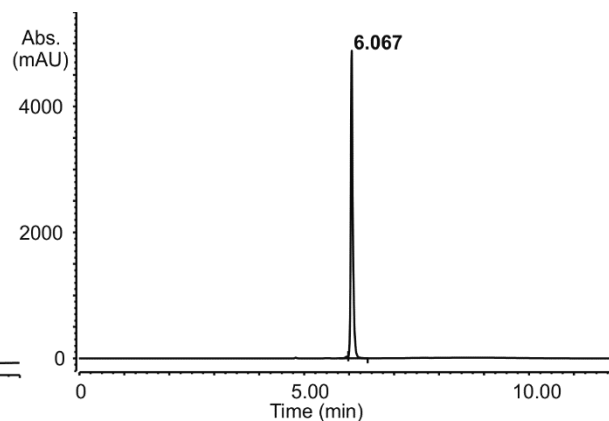
Figure S17: Overlaid chromatograms during the incubation of compound **3** (i) and **16** (j) in the presence of *Pronase E*. Analytical HPLC (linear gradient 15% to 65% B in 7 min, 65% to 100% in 2 min, 50 °C, 0.1% TFA, $\lambda=254$ nm). Peptide-foldamer-hybrid fragments formed during the degradation process and determined by LC-MS.

7.7. ^1H NMR spectra and HPLC profiles

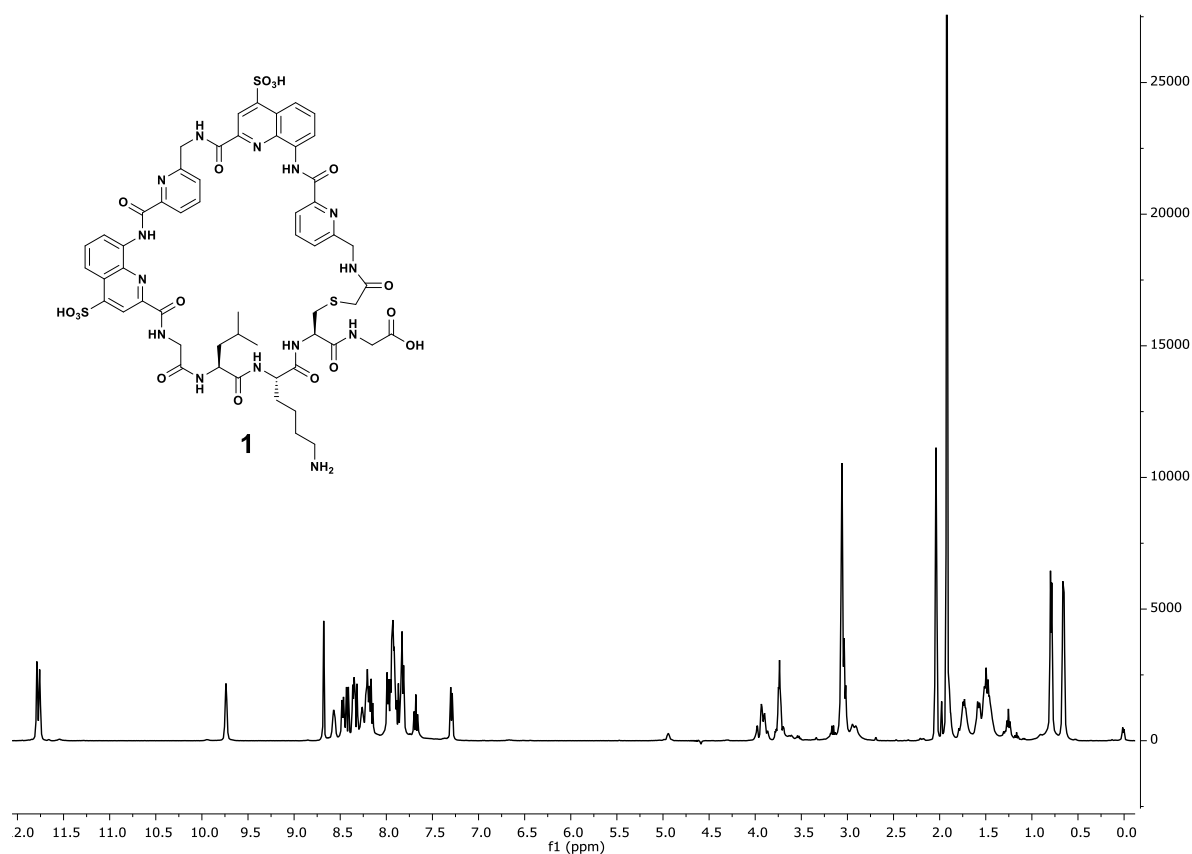
Compound **1**.



Analytical RP-HPLC profile of **1** crude from SPS. (20 to 80 vol. % B over 10 min, 25 °C, $\lambda=300$ nm)

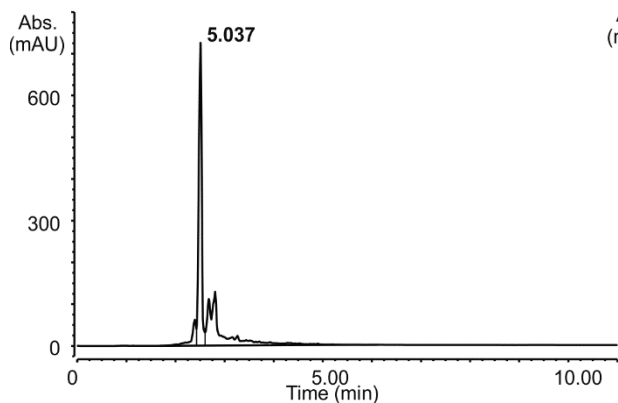


Analytical RP-HPLC profile of **1**. (10 to 80 vol. % B over 10 min, 25 °C, $\lambda=254$ nm)

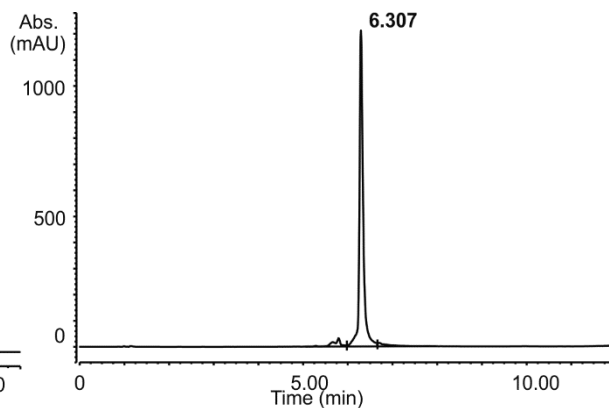


^1H NMR Spectrum (500 MHz, 12.5 mM ammonium acetate buffer at pH 8.5 with 25% acetonitrile- d_3 , water suppression, 25 °C) of **1**.

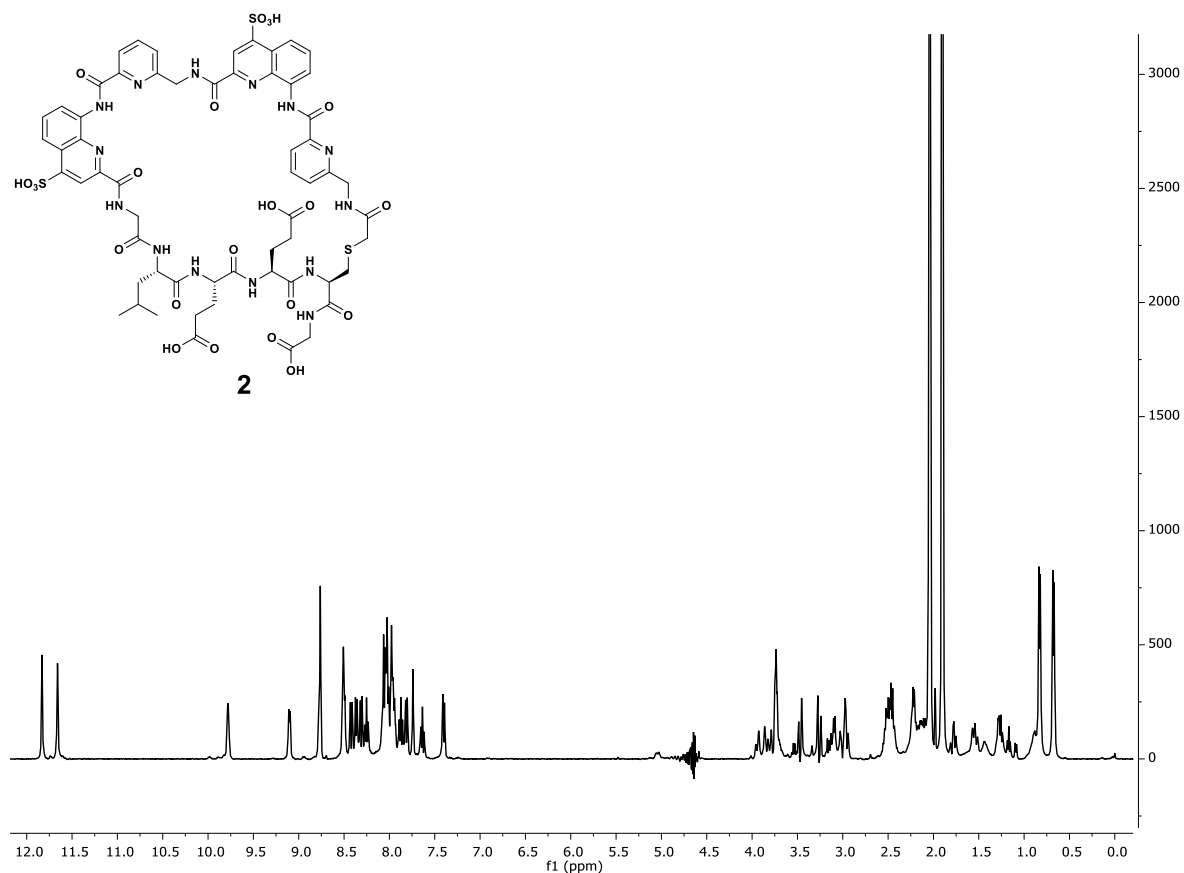
Compound 2.



Semi-preparative RP-HPLC profile of **2** crude from SPS. (5 to 35 vol. % B over 10 min, 25 °C, $\lambda=300$ nm)

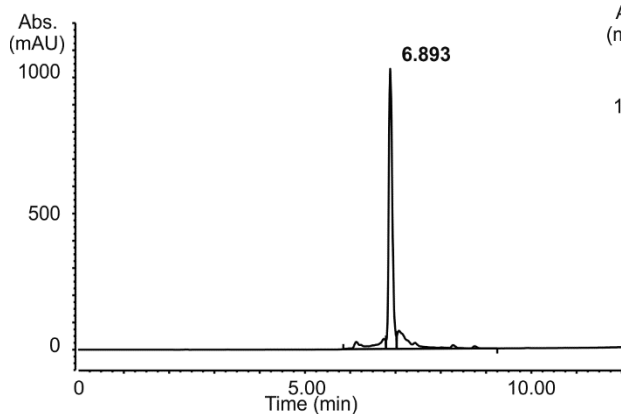


Analytical RP-HPLC profile of **2**. (10 to 45 vol. % B over 10 min, 25 °C, $\lambda=254$ nm)

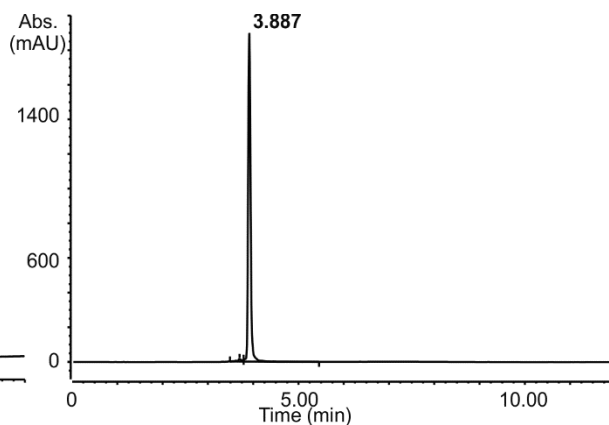


¹H NMR Spectrum (500 MHz, 12.5 mM ammonium acetate buffer at pH 8.5 with 25% acetonitrile-*d*₃, water suppression, 25 °C) of **2**.

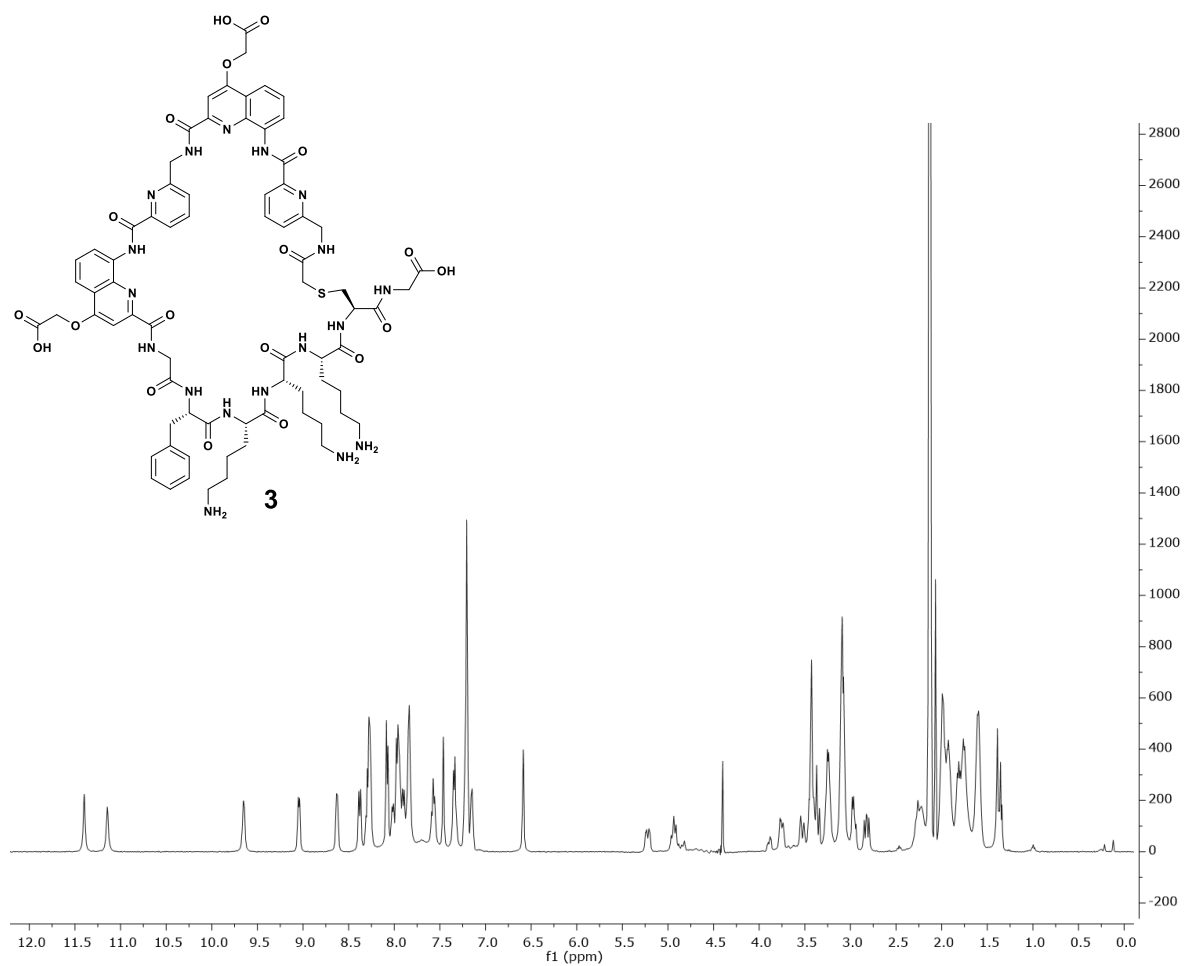
Compound 3.



Analytical RP-HPLC profile of **3** crude from SPS. (20 to 80 vol. % D over 10 min, 25 °C, $\lambda=254$ nm)

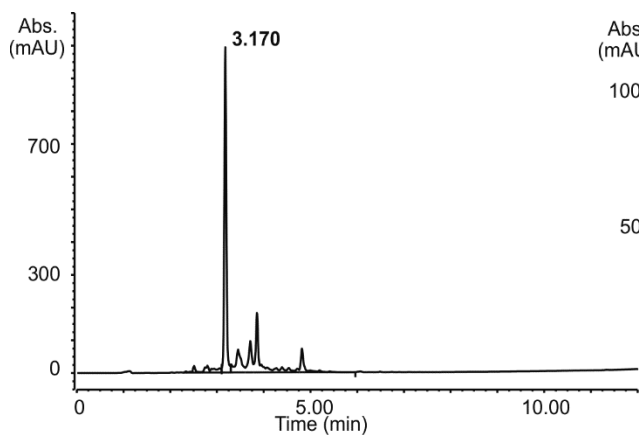


Analytical RP-HPLC profile of **3**. (10 to 80 vol. % D over 10 min, 25 °C, $\lambda=254$ nm)

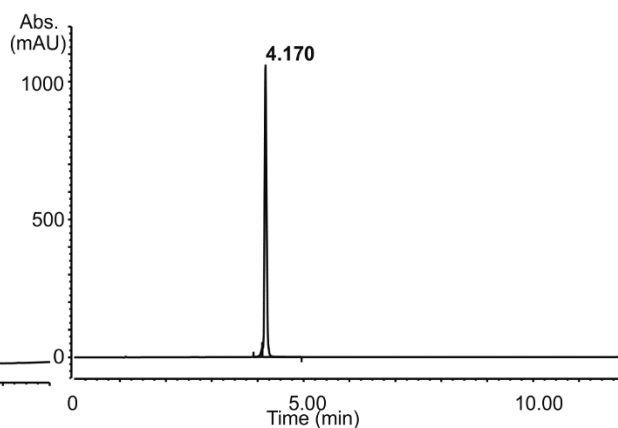


^1H NMR Spectrum (500 MHz, water/acetonitrile- d_3 (3:1, v/v), water suppression, 25 °C) of **3**.

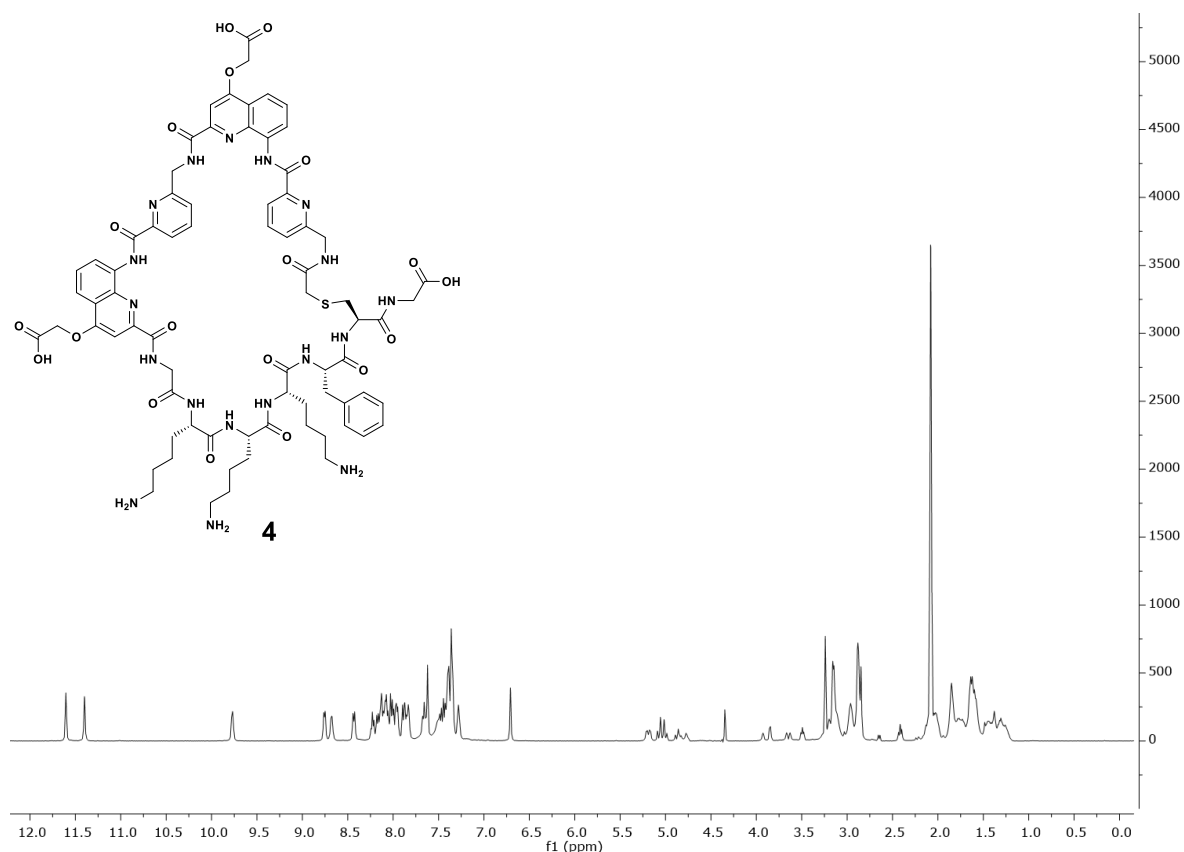
Compound 4.



Analytical RP-HPLC profile of **4** crude from SPS. (20 to 80 vol. % B over 10 min, 50 °C, $\lambda=254$ nm)

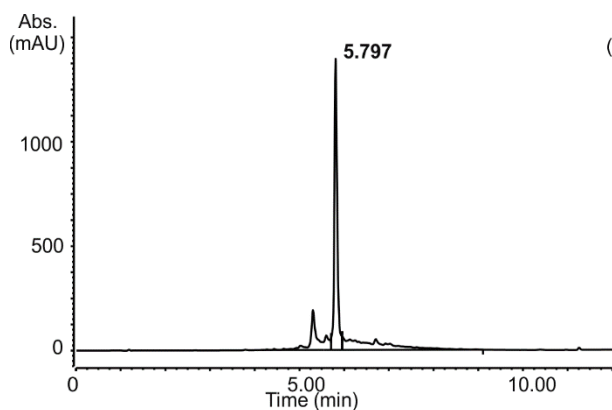


Analytical RP-HPLC profile of **4**. (10 to 80 vol. % D over 10 min, 50 °C, $\lambda=300$ nm)

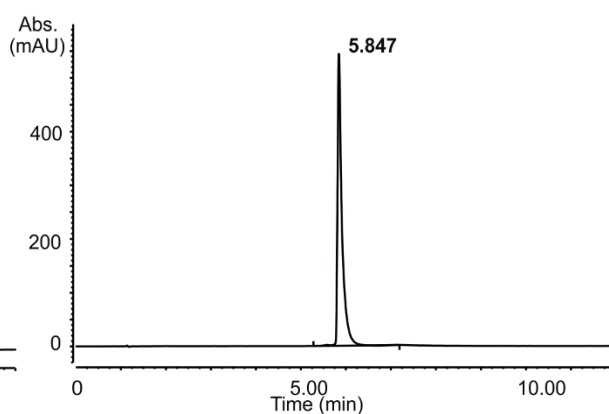


^1H NMR Spectrum (500 MHz, water/acetonitrile- d_3 (3:1, v/v), water suppression, 25 °C) of **4**.

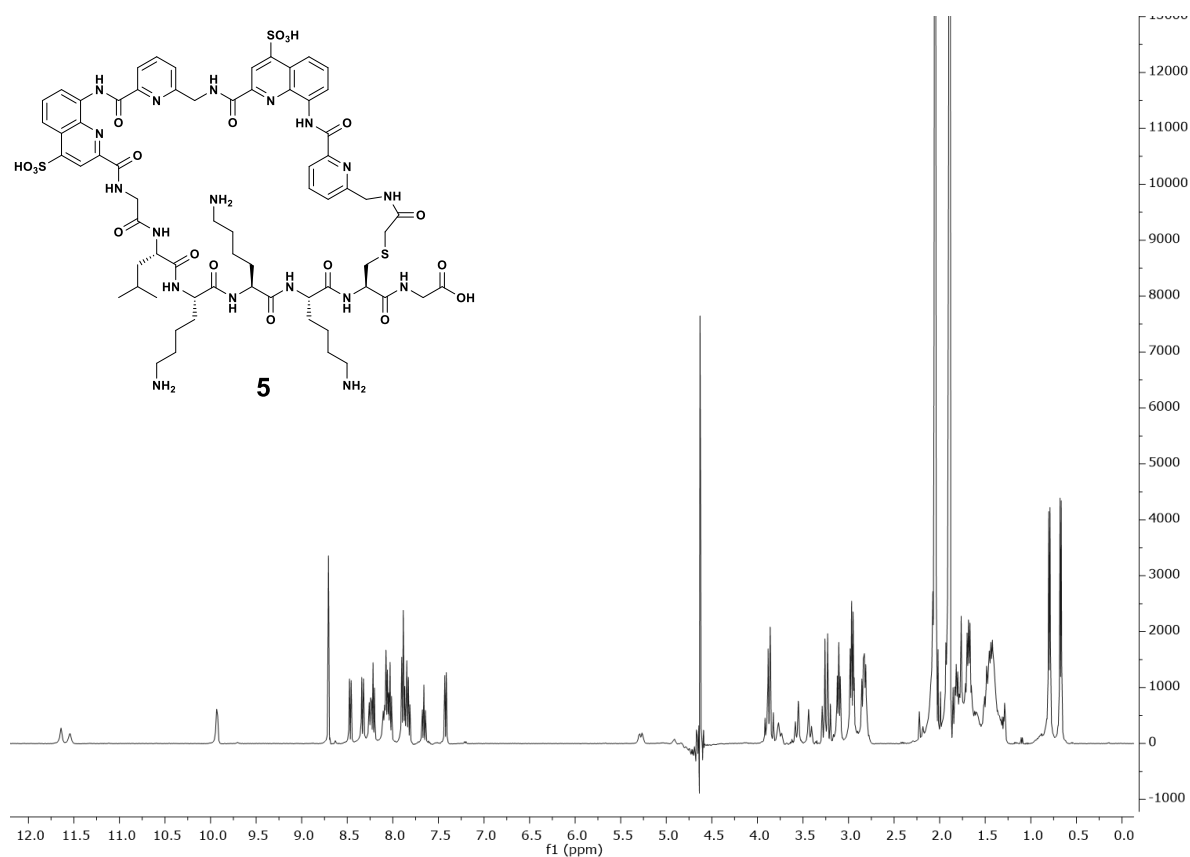
Compound 5.



Analytical RP-HPLC profile of **5** crude from SPS. (10 to 45 vol. % B over 10 min, 25 °C, $\lambda=254$ nm)

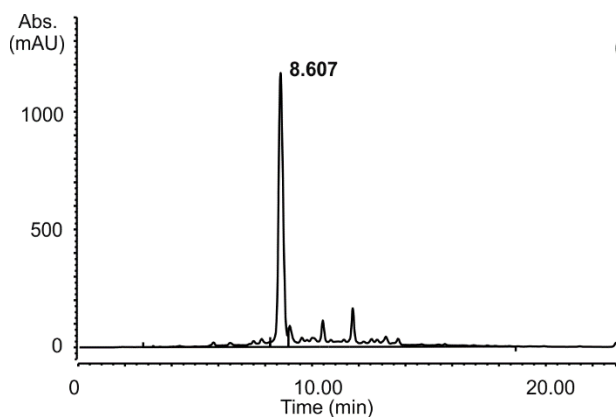


Analytical RP-HPLC profile of **5**. (10 to 50 vol. % D over 10 min, 25 °C, $\lambda=254$ nm)

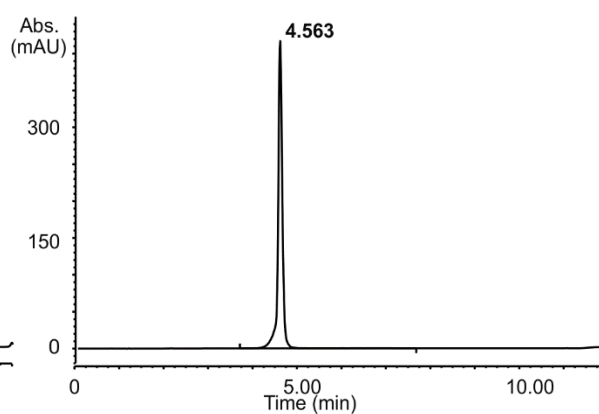


^1H NMR Spectrum (500 MHz, 12.5 mM ammonium acetate buffer at pH 8.5 with 25% acetonitrile- d_3 , water suppression, 25 °C) of **5**.

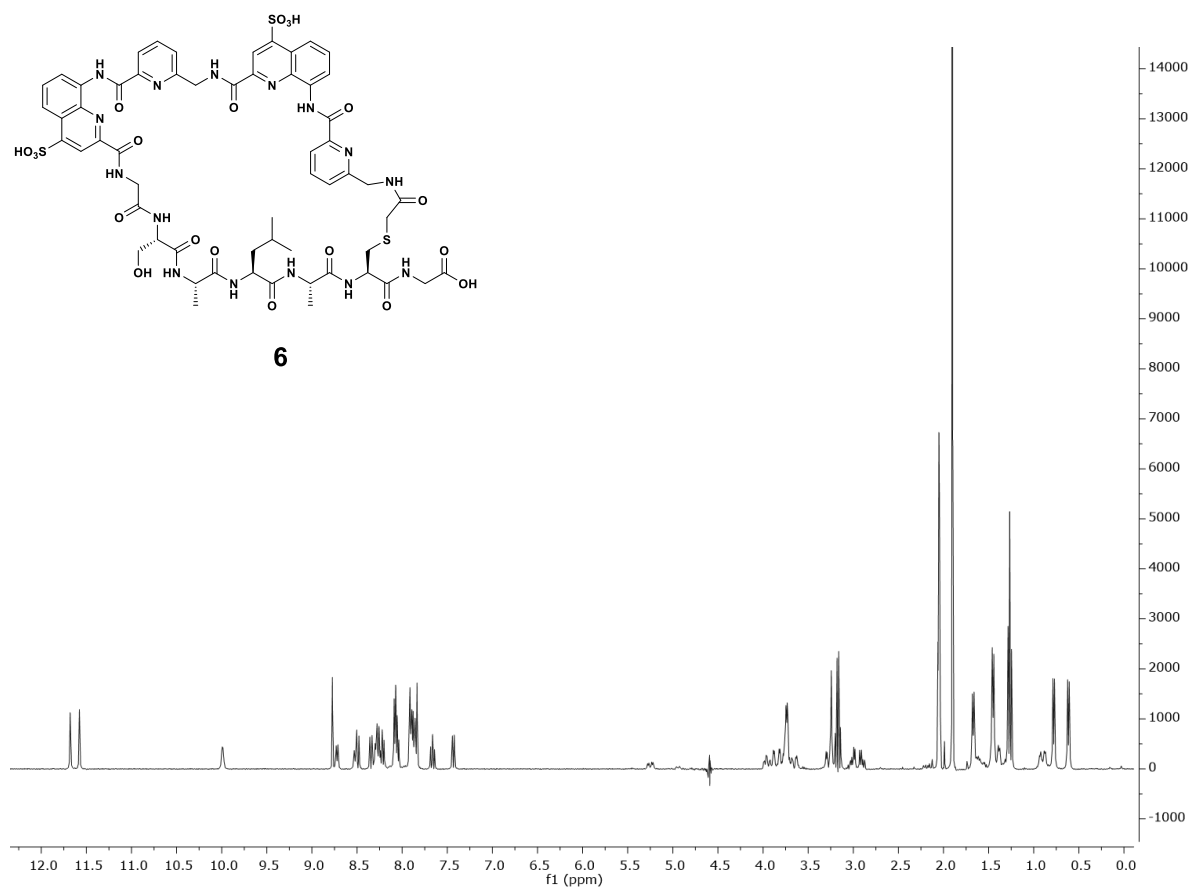
Compound 6.



Semi-preparative RP-HPLC profile of **6** crude from SPS. (10 to 28 vol. % D over 20 min, 25 °C, $\lambda=300$ nm)

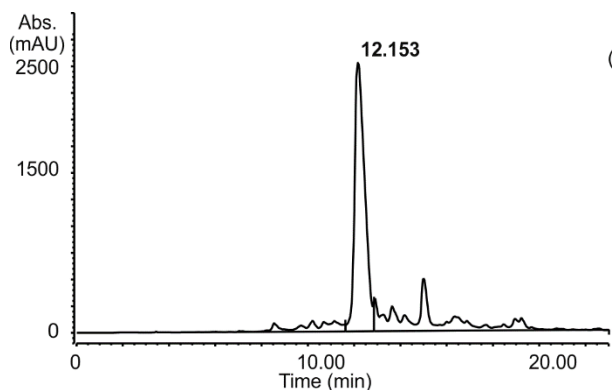


Analytical RP-HPLC profile of **6**. (10 to 30 vol. % D over 10 min, 25 °C, $\lambda=254$ nm)

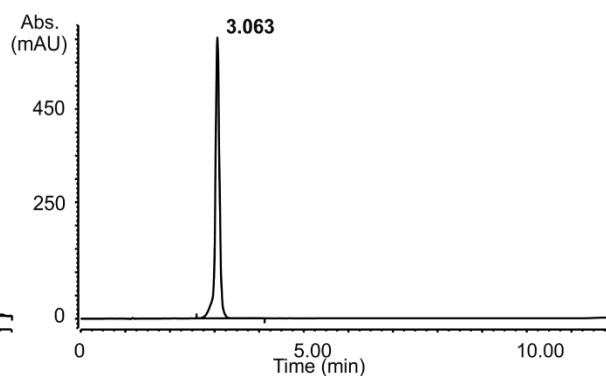


^1H NMR Spectrum (400 MHz, 12.5 mM ammonium acetate buffer at pH 8.5 with 25% acetonitrile- d_3 , water suppression, 25 °C) of **6**.

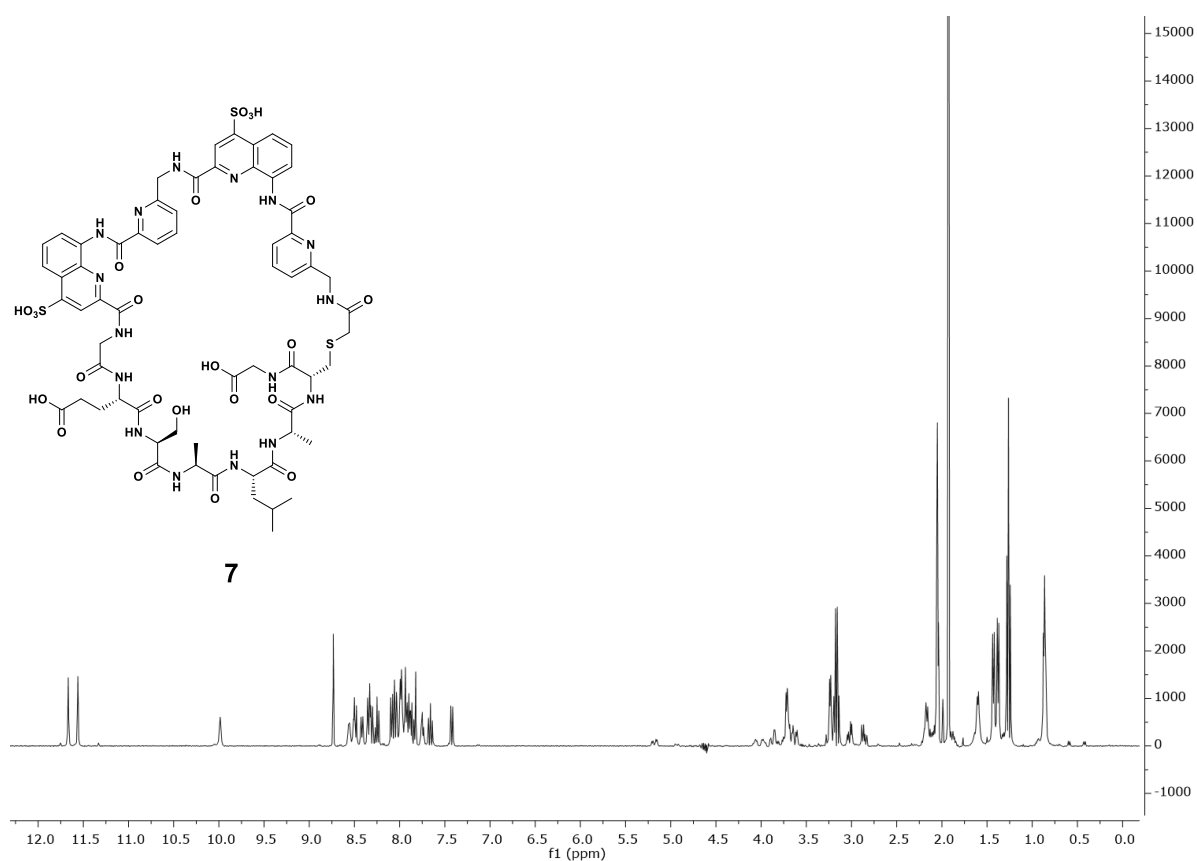
Compound 7.



Semi-preparative RP-HPLC profile of **7** crude from SPS. (5 to 20 vol. % D over 20 min, 25 °C, $\lambda=300$ nm)

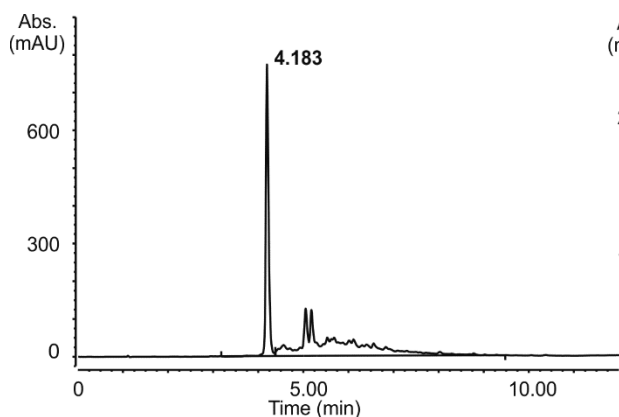


Analytical RP-HPLC profile of **7**. (10 to 30 vol. % D over 10 min, 25 °C, $\lambda=254$ nm)

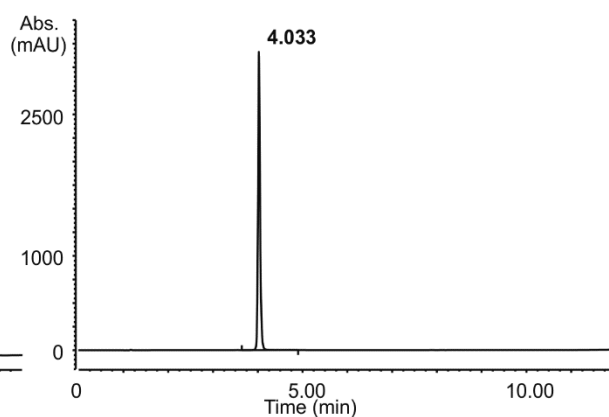


¹H NMR Spectrum (400 MHz, 12.5 mM ammonium acetate buffer at pH 8.5 with 25% acetonitrile *d*₃, water suppression, 25 °C) of **7**.

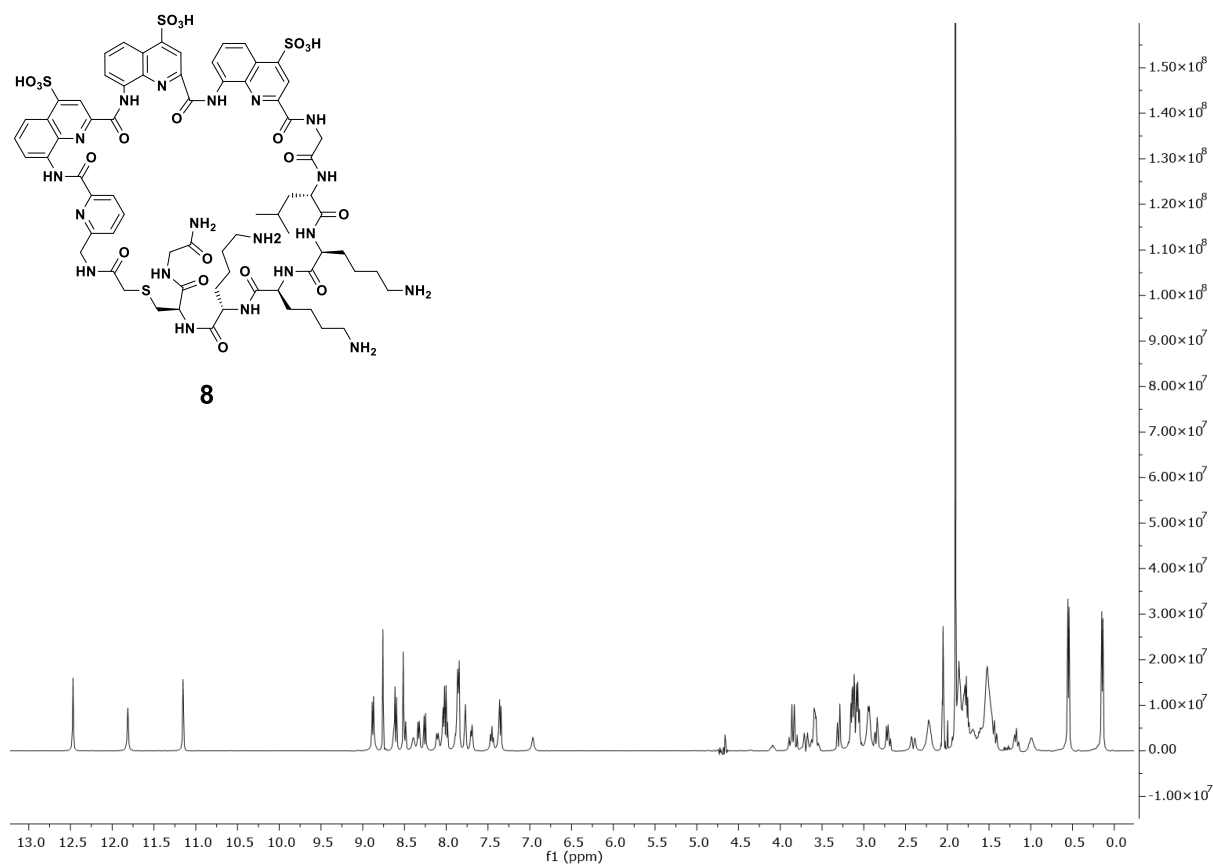
Compound 8.



Analytical RP-HPLC profile of **8** crude from SPS. (10 to 45 vol. % B over 10 min, 25 °C, $\lambda=254$ nm)

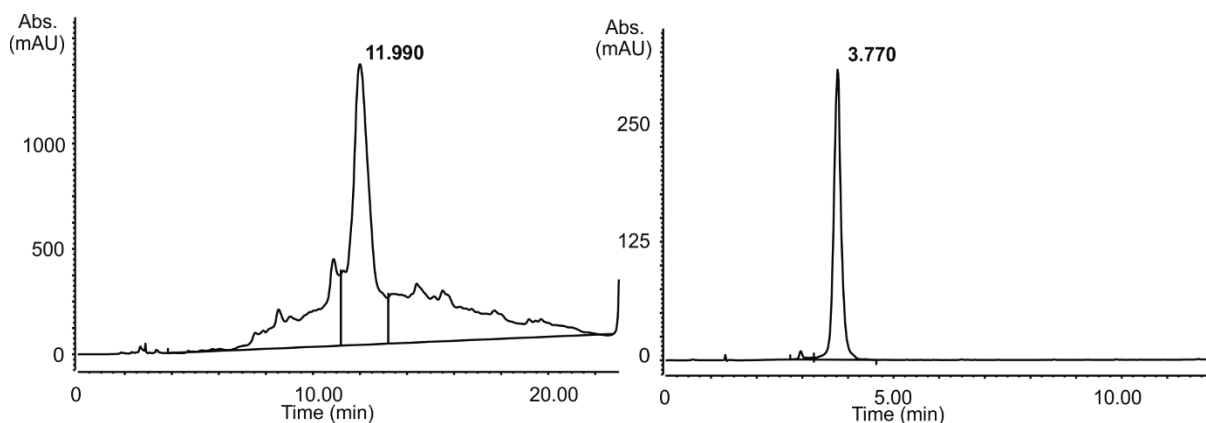


Analytical RP-HPLC profile of **8**. (10 to 45 vol. % B over 10 min, 25 °C, $\lambda=254$ nm)



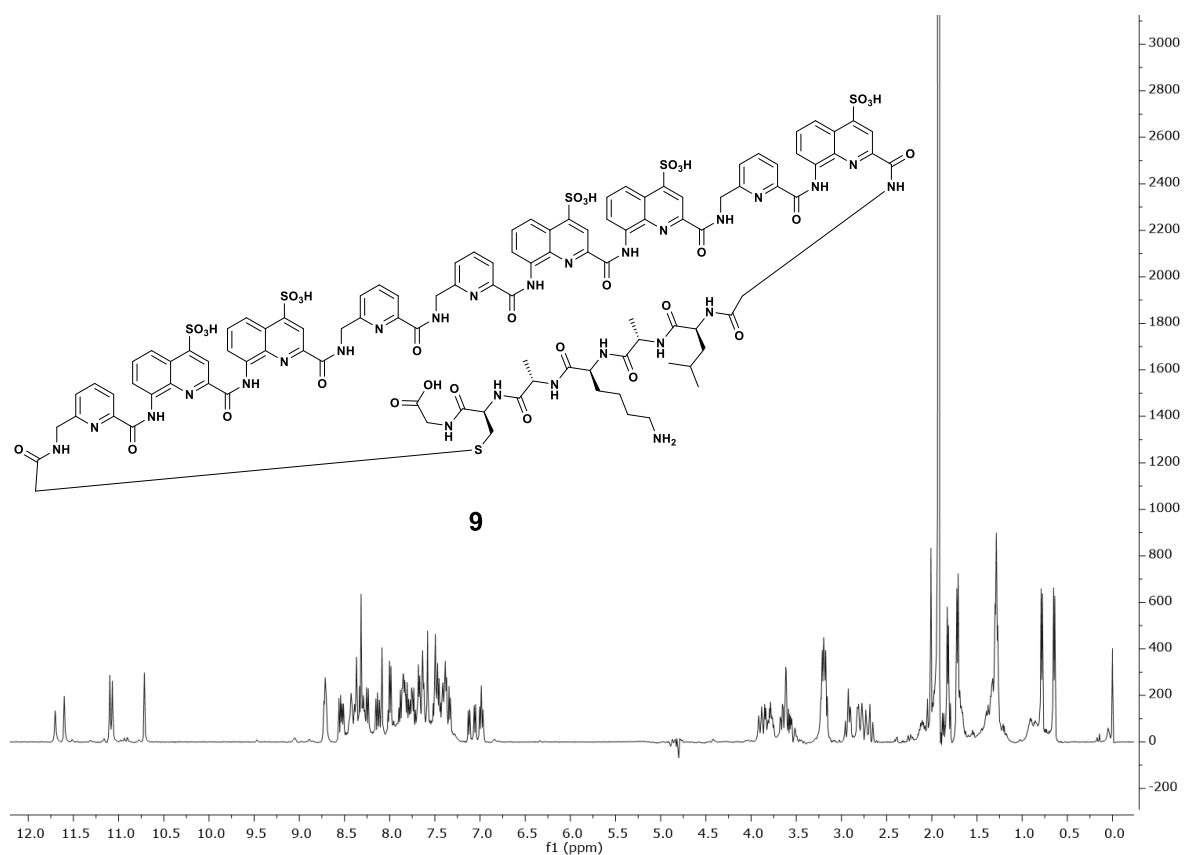
^1H NMR Spectrum (500 MHz, 12.5 mM ammonium acetate buffer at pH 8.5 with 25% acetonitrile d_3 , water suppression, 25 °C) of **8**.

Compound 9.



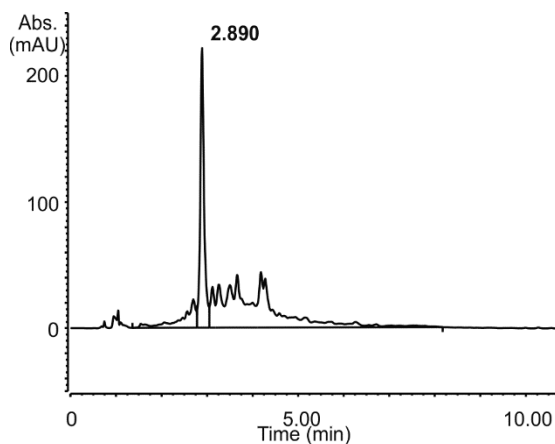
Semi-preparative RP-HPLC profile of **9** crude from SPS. (8 to 25 vol. % D over 20 min, 25 °C, $\lambda=300$ nm)

Analytical RP-HPLC profile of **9**. (5 to 50 vol. % D over 10 min, 25 °C, $\lambda=254$ nm)

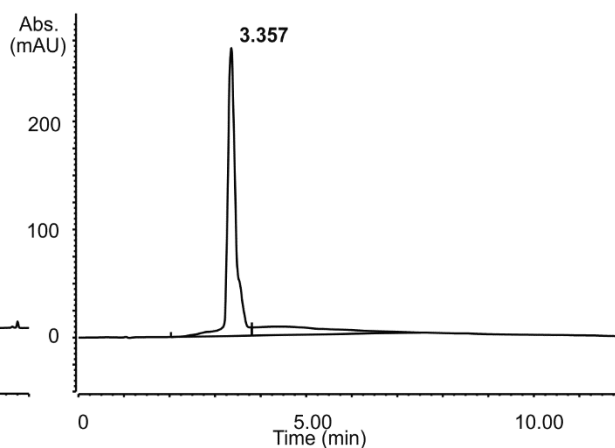


^1H NMR Spectrum (500 MHz, 12.5 mM ammonium acetate buffer at pH 8.5 with 10% D_2O , water suppression, 25 °C) of **9**.

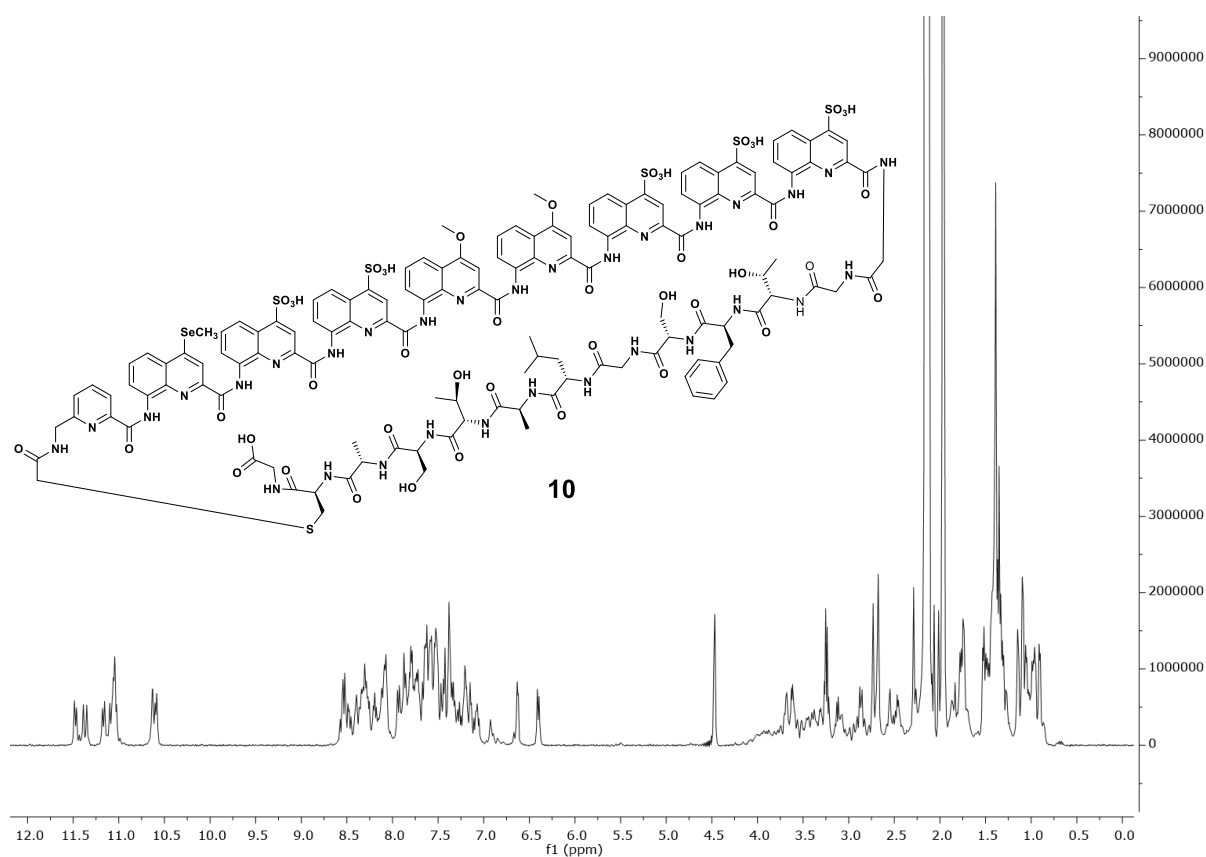
Compound 10.



Analytical RP-HPLC profile of **10** crude from SPS. (10 to 45 vol. % D over 10 min, 50 °C, $\lambda=254$ nm)

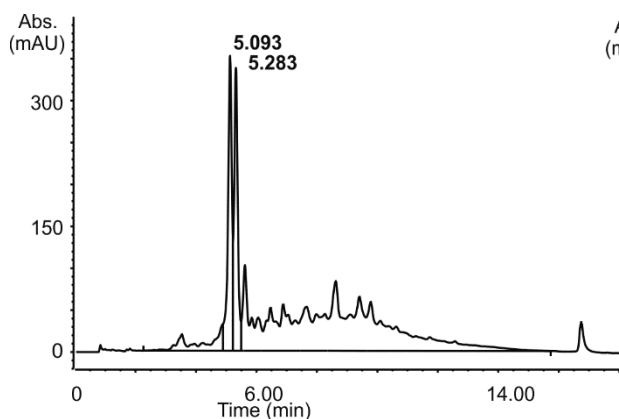


Analytical RP-HPLC profile of **10**. (10 to 80 vol. % D over 10 min, 50 °C, $\lambda=254$ nm)

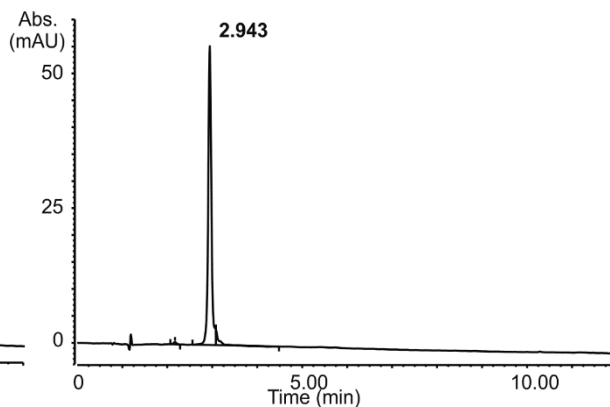


^1H NMR Spectrum (500 MHz, 12.5 mM ammonium acetate buffer at pH 8.5 with 50% acetonitrile d_3 , water suppression, 25 °C) of **10**.

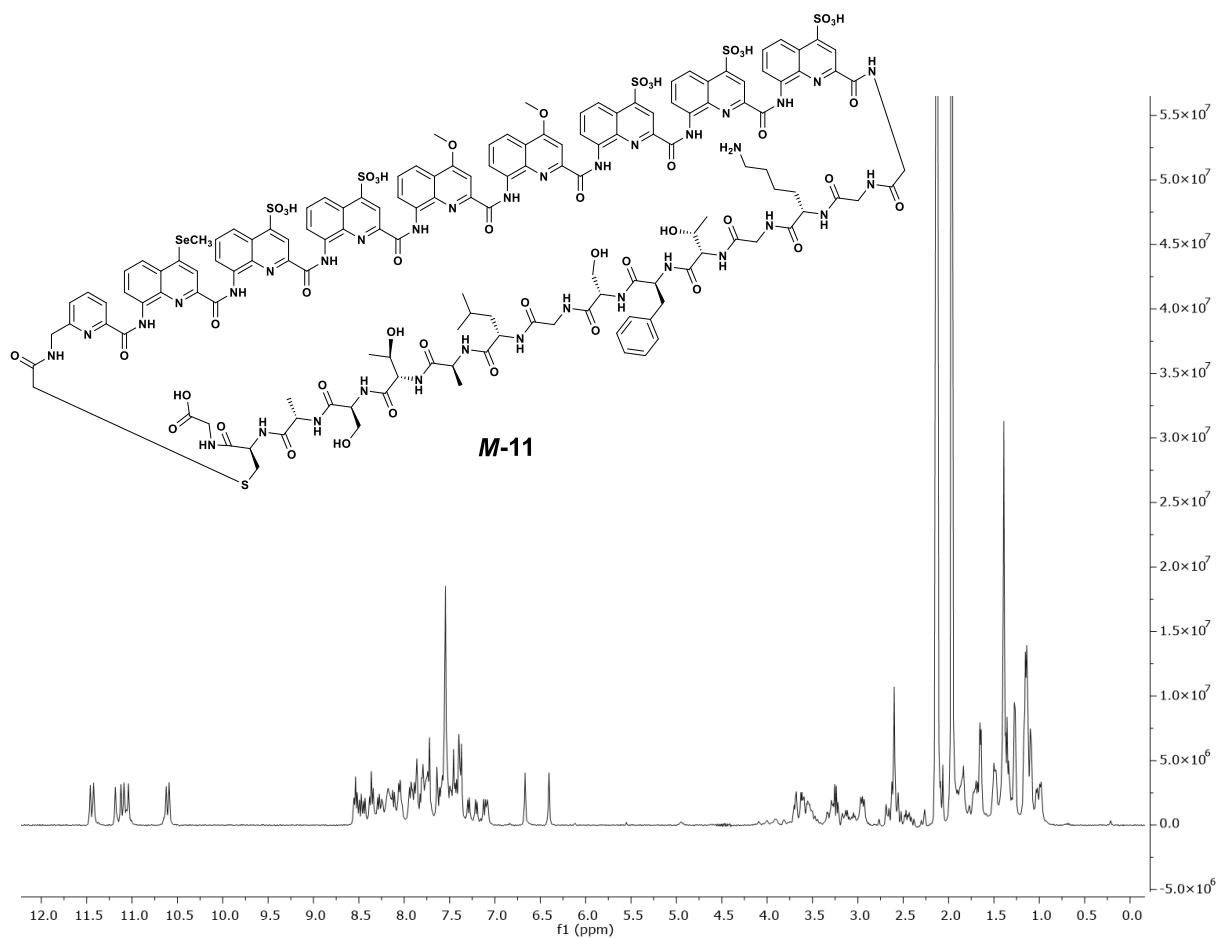
Compound **M-11**.



Semi-preparative RP-HPLC profile of **11** crude from SPS. (10 to 35 vol. % D over 15 min, 50 °C, $\lambda=300$ nm)

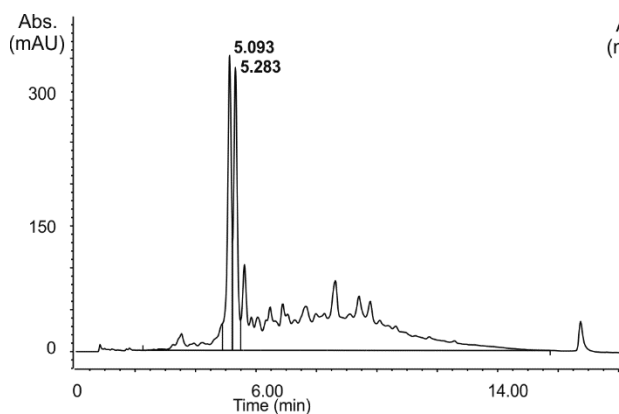


Analytical RP-HPLC profile of **M-11**. (10 to 45 vol. % D over 10 min, 50 °C, $\lambda=300$ nm)

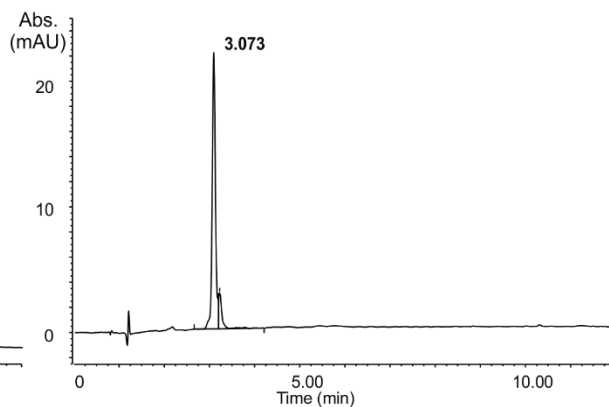


^1H NMR Spectrum (500 MHz, 12.5 mM ammonium acetate buffer at pH 8.5 with 50% acetonitrile d_3 , water suppression, 25 °C) of **M-11**.

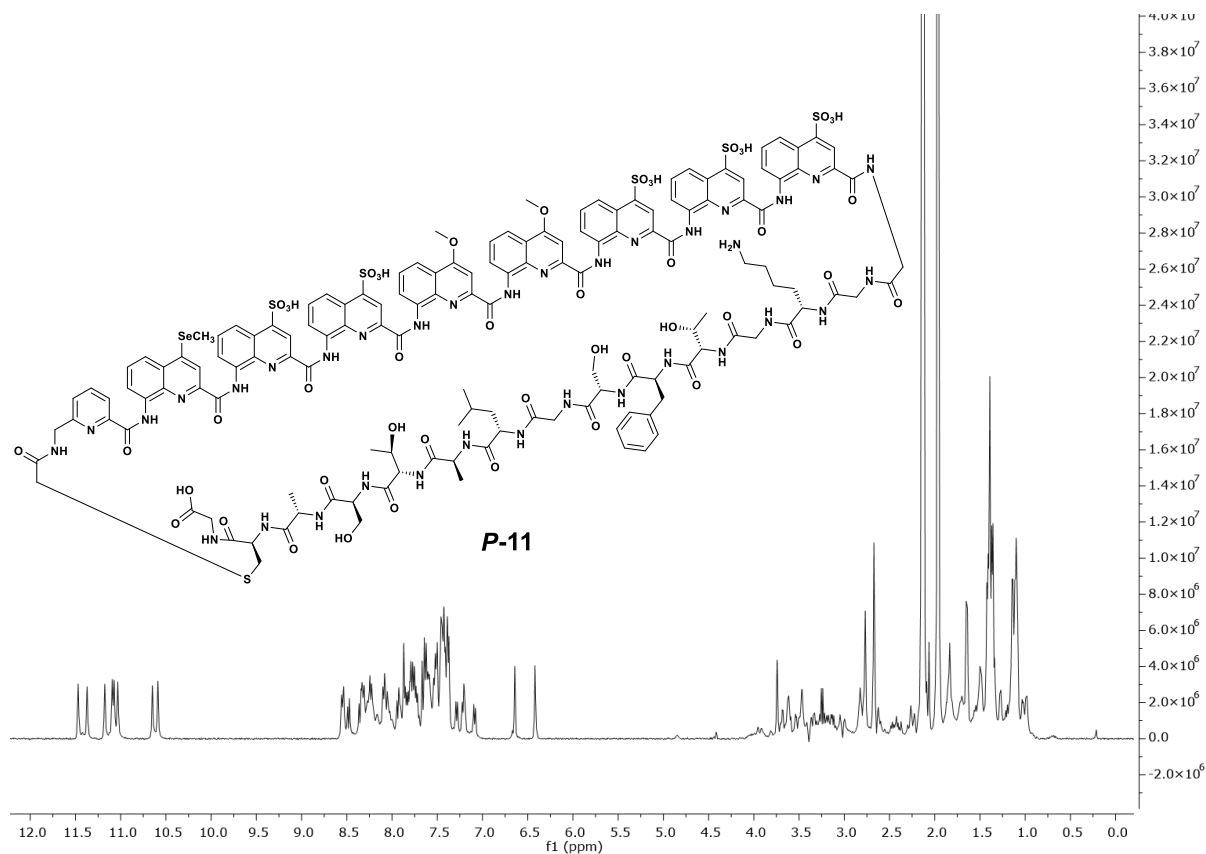
Compound **P-11**.



Semi-preparative RP-HPLC profile of **11** crude from SPS. (10 to 35 vol. % D over 15 min, 50 °C, $\lambda=300$ nm)

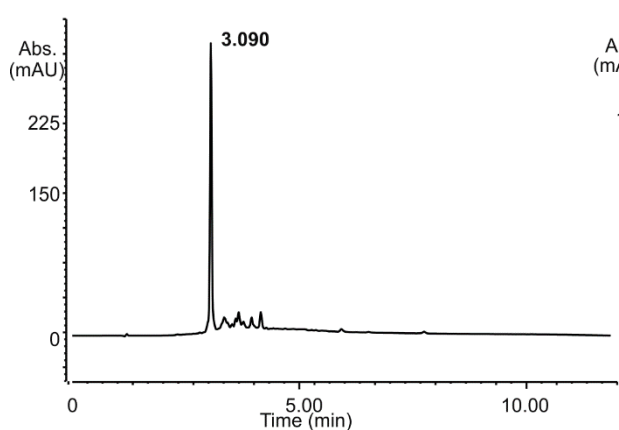


Analytical RP-HPLC profile of **P-11**. (10 to 45 vol. % D over 10 min, 50 °C, $\lambda=300$ nm)

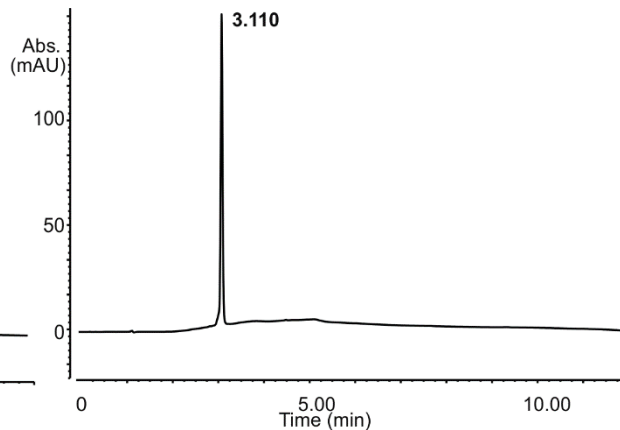


^1H NMR Spectrum (500 MHz, 12.5 mM ammonium acetate buffer at pH 8.5 with 50% acetonitrile d_3 , water suppression, 25 °C) of **P-11**.

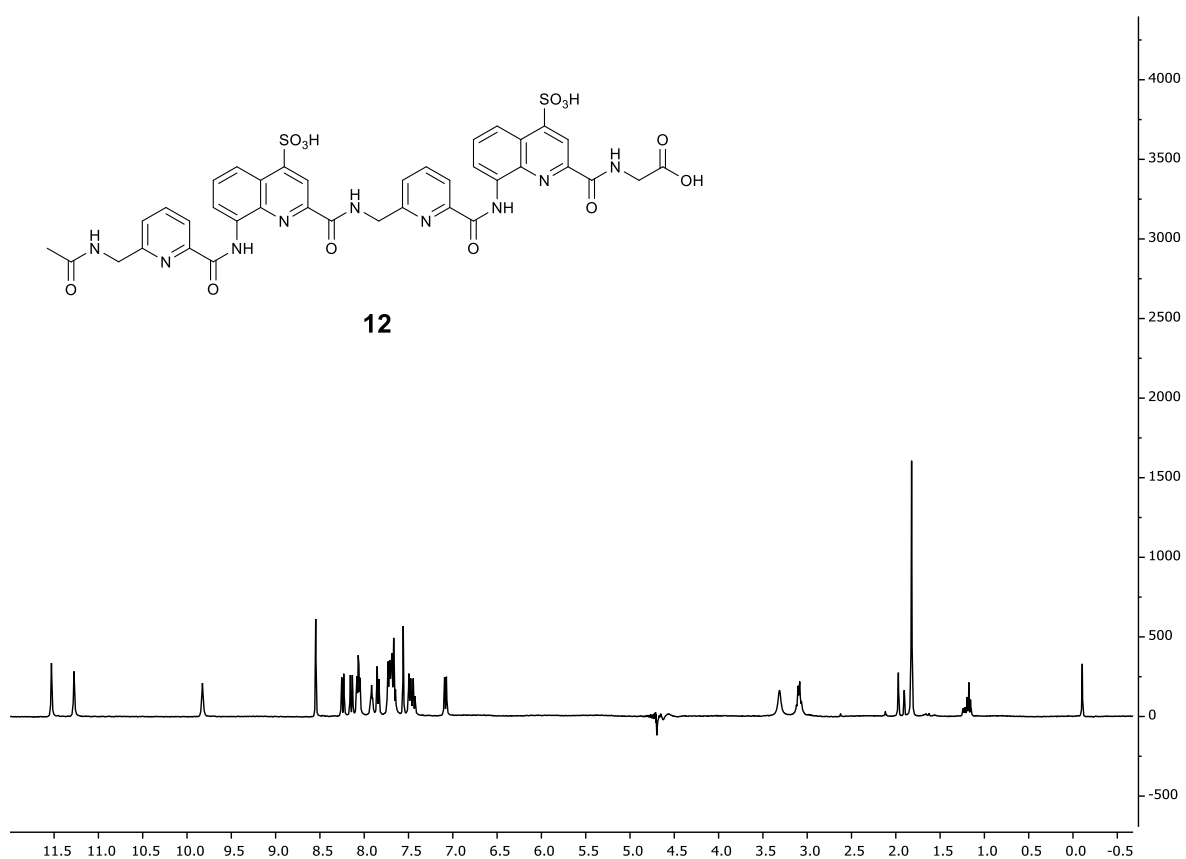
Compound **12**.



Analytical RP-HPLC profile of **12** crude from SPS. (10 to 100 vol. % D over 10 min, 25 °C, $\lambda=300$ nm)

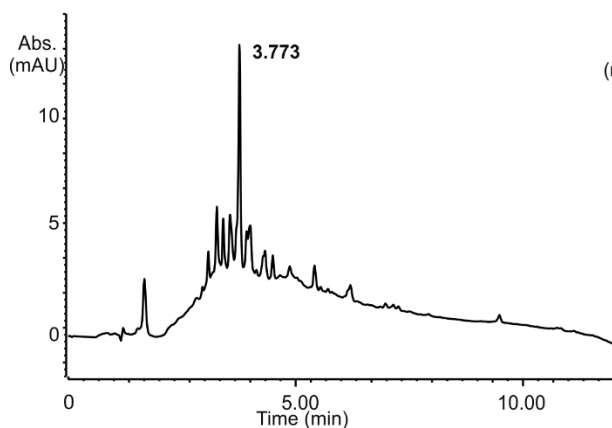


Analytical RP-HPLC profile of **12**. (10 to 100 vol. % D over 10 min, 25 °C, $\lambda=300$ nm)

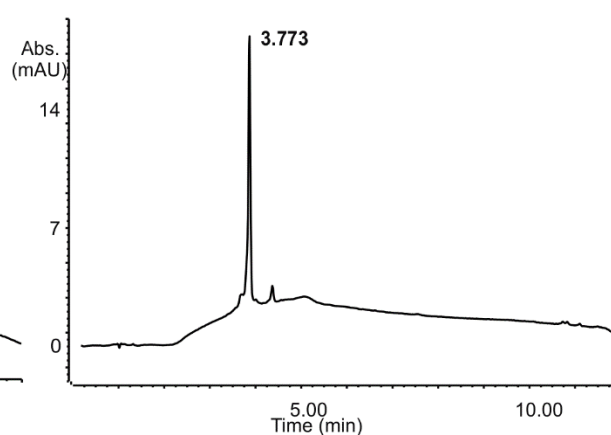


^1H NMR Spectrum (400 MHz, 50 mM NaHCO_3 buffer with 10% D_2O , water suppression, 25 °C) of **12**.

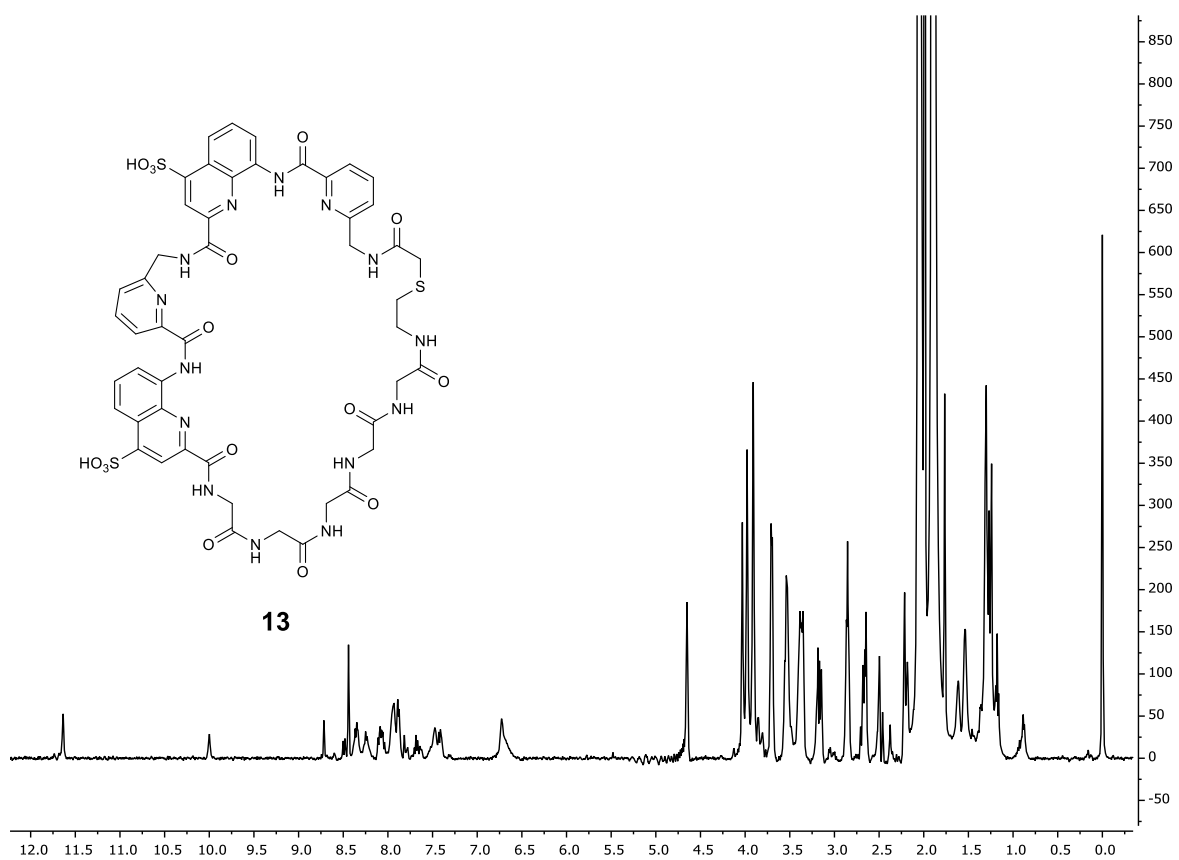
Compound 13.



Analytical RP-HPLC profile of **13** crude from SPS. (10 to 100 vol. % D over 10 min, 25 °C, $\lambda=300$ nm)

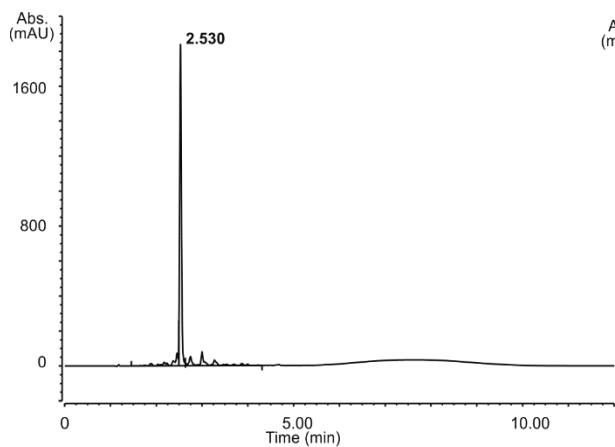


Analytical RP-HPLC profile of **13**. (10 to 100 vol. % D over 10 min, 25 °C, $\lambda=300$ nm)

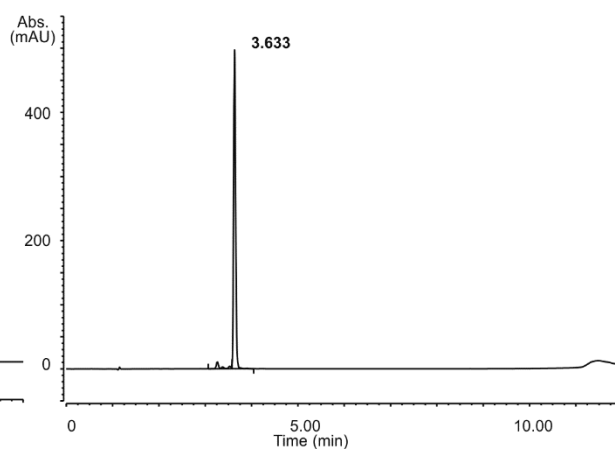


^1H NMR Spectrum (400 MHz, 12.5 mM ammonium acetate buffer at pH 8.5 with 25% acetonitrile d_3 , water suppression, 25 °C)

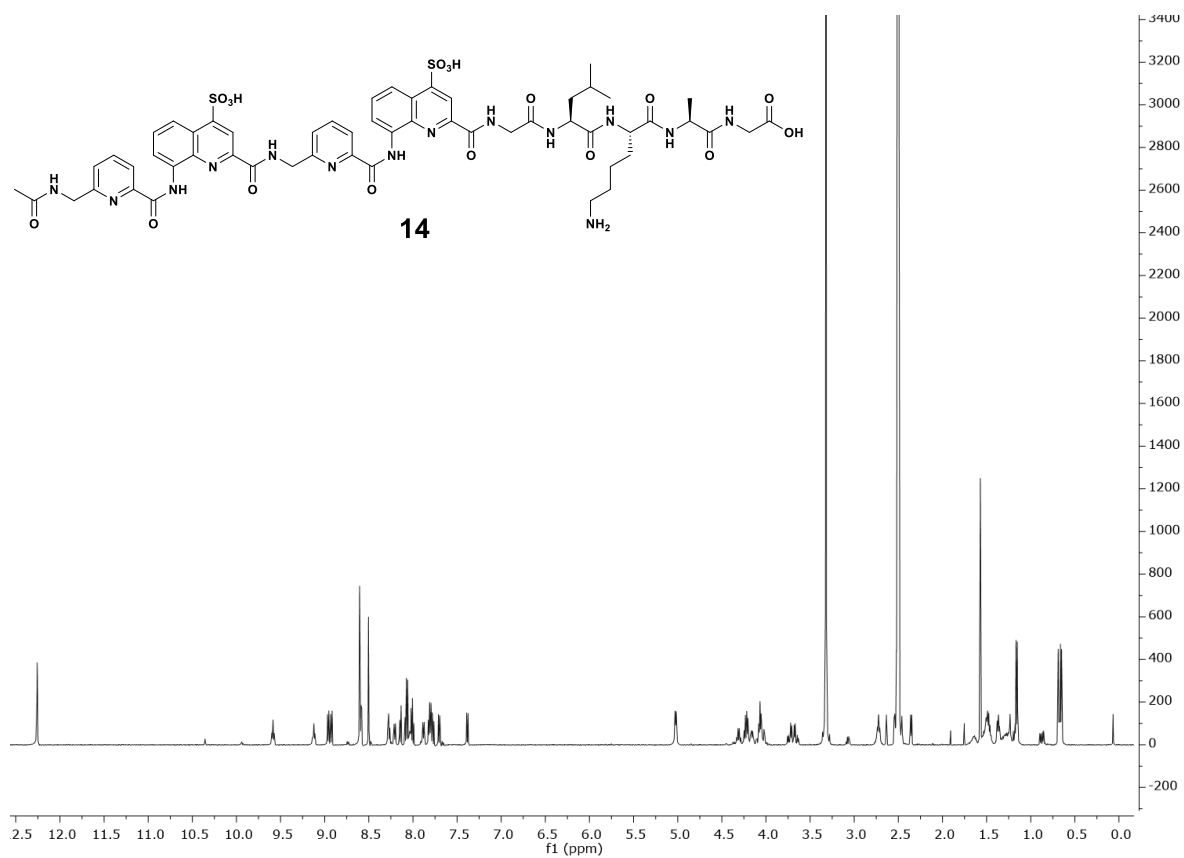
Compound 14.



Analytical RP-HPLC profile of **14** crude from SPS. (10 to 100 vol. % D over 15 min, 25 °C, $\lambda=300$ nm)

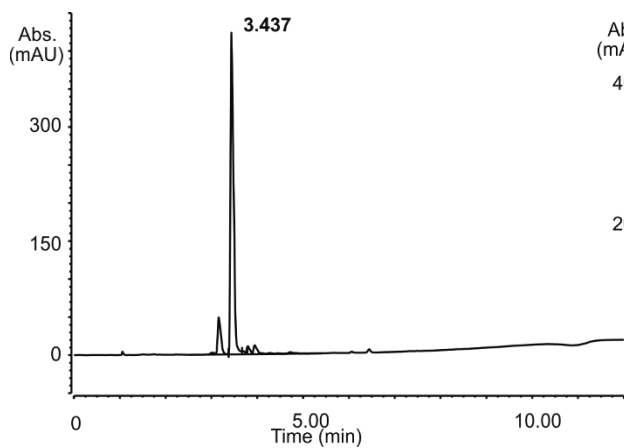


Analytical RP-HPLC profile of **14**. (10 to 45 vol. % D over 10 min, 25 °C, $\lambda=300$ nm)

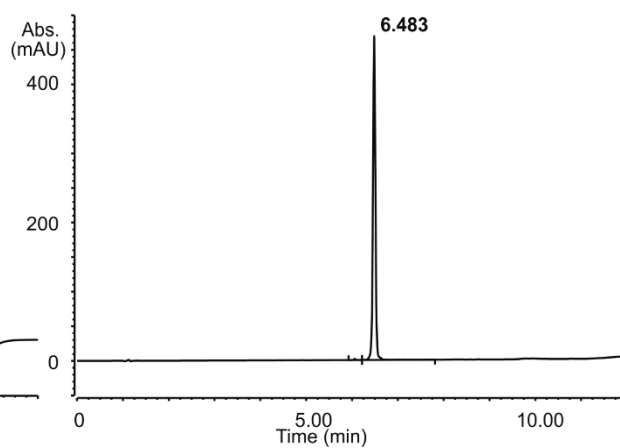


^1H NMR Spectrum (500 MHz, $\text{DMSO-}d_6$, 25 °C) of **14**.

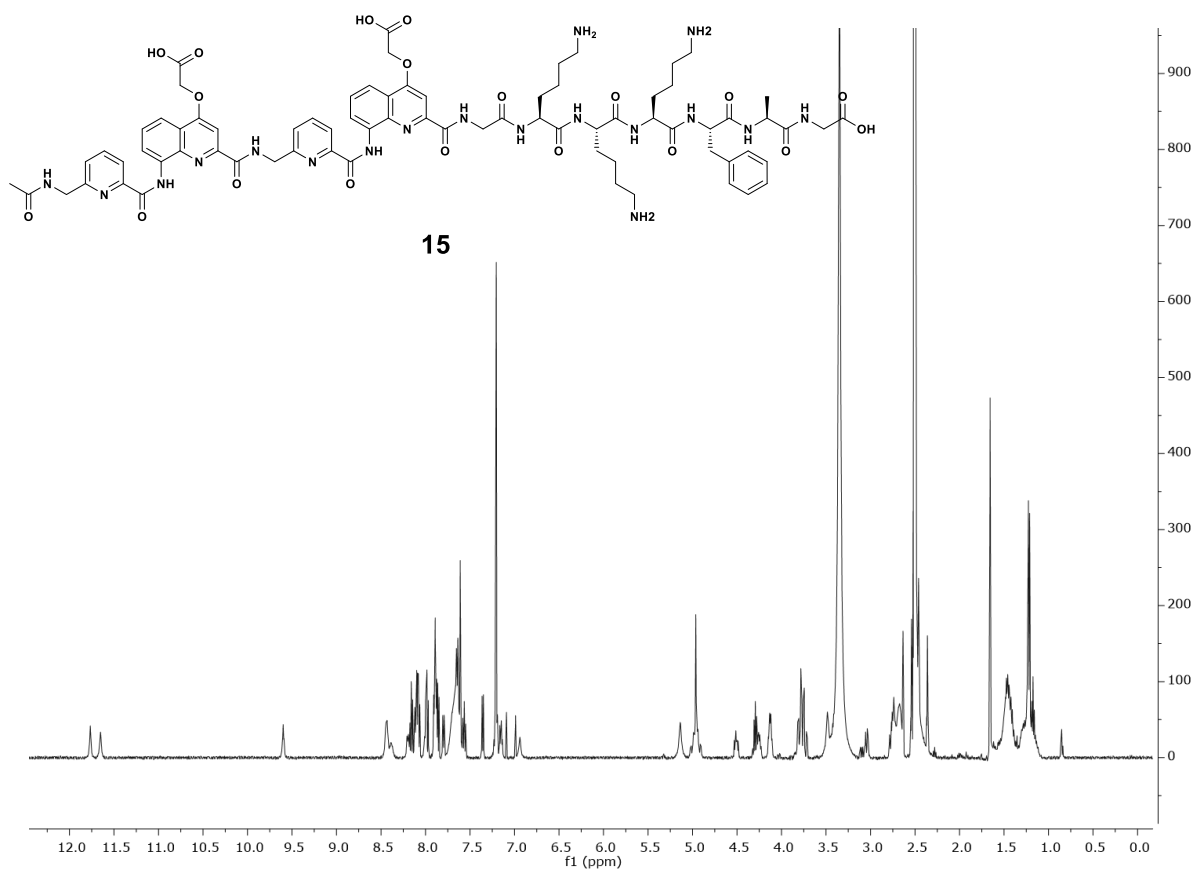
Compound 15.



Analytical RP-HPLC profile of **15** crude from SPS. (10 to 100 vol. % B over 10 min, 50 °C, $\lambda=254$ nm)

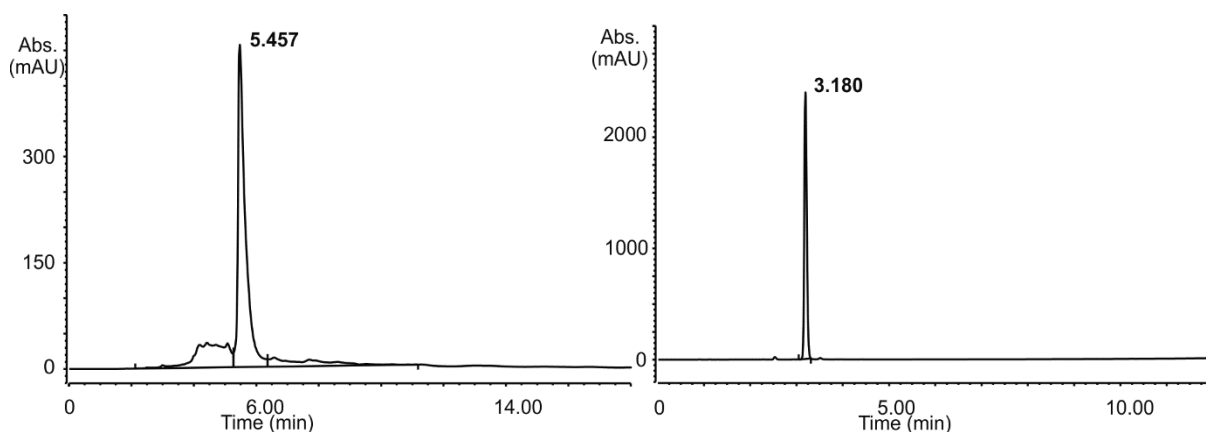


Analytical RP-HPLC profile of **15**. (10 to 45 vol. % B over 10 min, 50 °C, $\lambda=254$ nm)



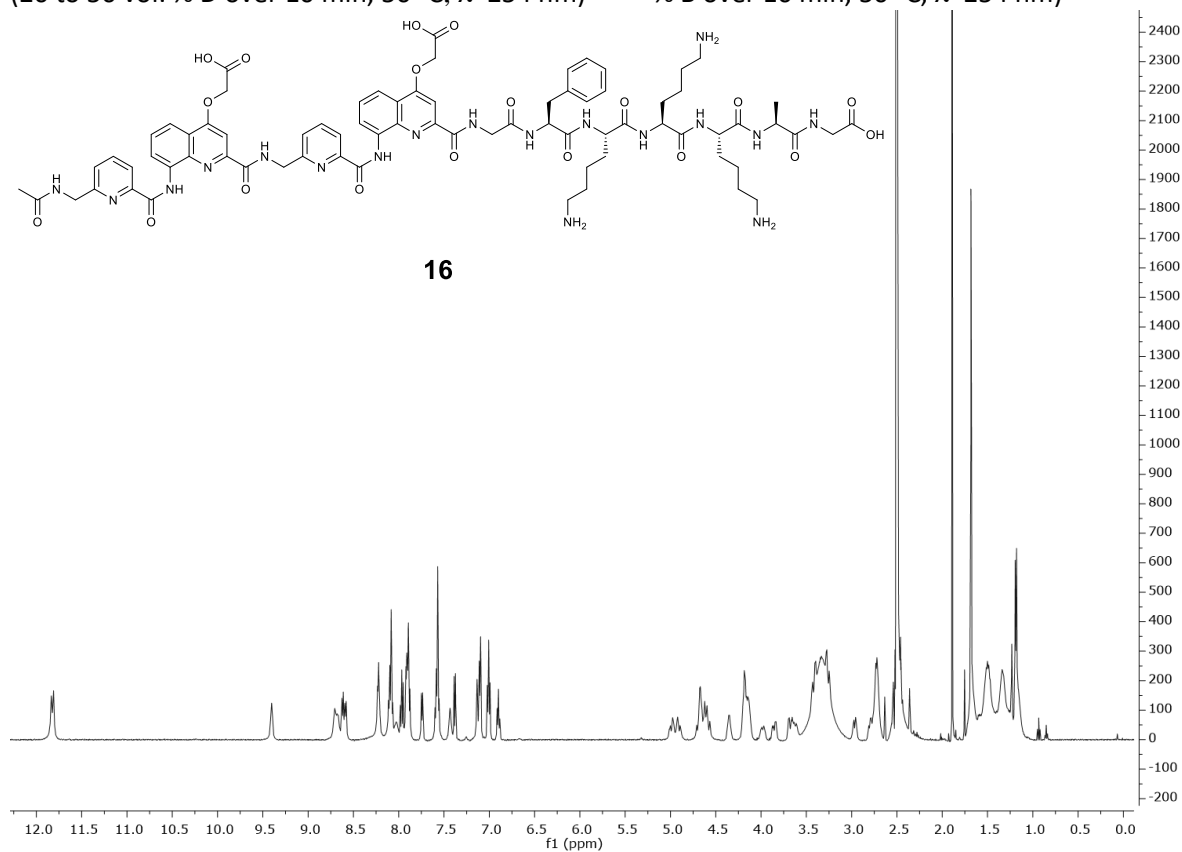
^1H NMR Spectrum (500 MHz, $\text{DMSO-}d_6$, 25 °C) of **15**.

Compound 16.



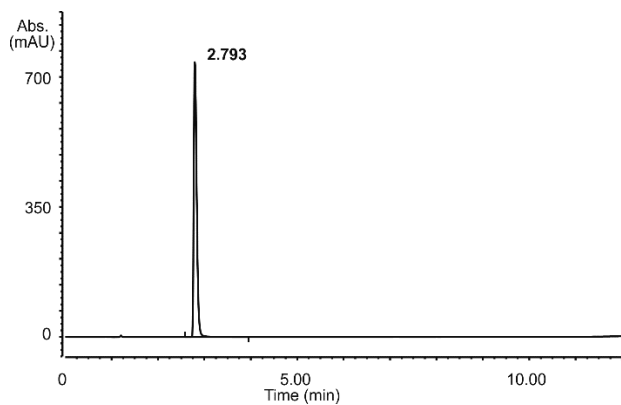
Analytical RP-HPLC profile of **16** crude from SPS.
(20 to 50 vol. % D over 10 min, 50 °C, λ=254 nm)

Analytical RP-HPLC profile of **16**. (20 to 80 vol.
% B over 10 min, 50 °C, λ=254 nm)

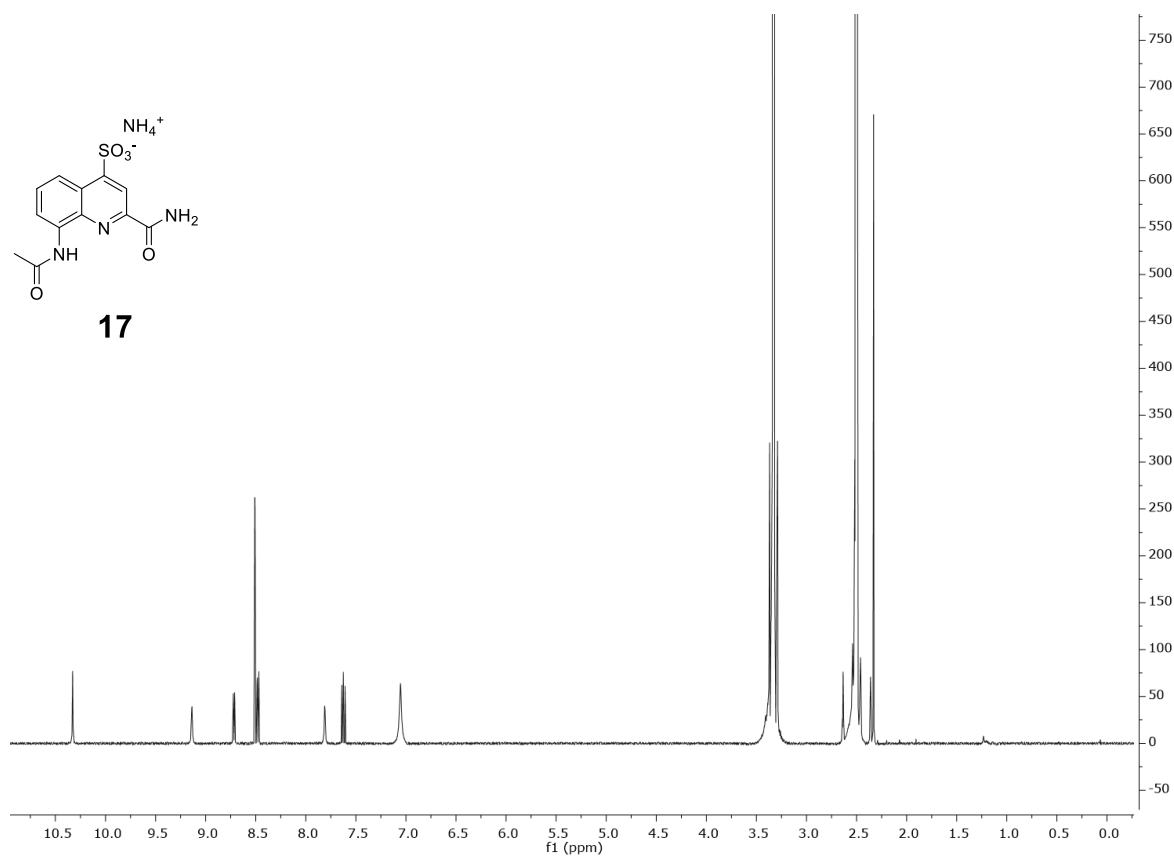


¹H NMR Spectrum (500 MHz, DMSO-*d*₆, 25 °C) of **16**.

Compound **17**.



Analytical RP-HPLC profile of **17**. (5 to 50 vol. % D over 10 min, 50 °C, $\lambda=254$ nm)



¹H NMR Spectrum (500 MHz, DMSO-*d*₆, 25 °C) of **17**.

8. Main Text: Display Selection of a Hybrid Foldamer-Peptide Macrocycle

Authors: Sebastian Dengler, Ryan T. Howard, Vasily Morozov, Christos Tsiamantas, Zhiwei Liu, Christopher Dobrzanski, Vojislava Pophristic, Wei-En Huang, Sophie Brameyer, Céline Douat, Hiroaki Suga and Ivan Huc

Published: An earlier version of this manuscript was posted preprint on *ChemRxiv* on 03.02.2022.

DOI: [10.26434/chemrxiv-2022-5rlmv](https://doi.org/10.26434/chemrxiv-2022-5rlmv)

Author contribution: The project was conceptualized and supervised by I. Huc in collaboration with H. Suga. R. T. Howard performed CD studies, fluorescence polarization, SPR experiment, assisted with chemical synthesis, protein expression and purification, and protein-hybrid co-crystallization. V. Morozov performed protein expression and purification, solved and refined the structure. C. Tsiamantas performed *in vitro* translation and RaPID selection. Z. Liu, C. Dobrzanski and V. Pophristic planned and executed molecular dynamics simulation setup, binding mode analysis, and the role for Tyr11 in M foldamer macrocycles and the destabilization of the α -helix with P foldamer and V10A mutation. S. Brameyer assisted with SPR experiments. C. Douat co-supervised the project and assisted with chemical synthesis. The manuscript was written by R. T. Howard, V. Morozov, C. Tsiamantas, C. Douat, and I. Huc. Most of the chemical synthesis and analytical characterization was performed by me.

Display Selection of a Hybrid Foldamer-Peptide Macrocycle

Sebastian Dengler,^{+[a]} Ryan T. Howard,^{+[a]} Vasily Morozov,^{+[a]} Christos Tsiamantas,^{+[b]} Zhiwei Liu,^[c] Christopher Dobrzanski,^[c] Vojislava Pophristic,^[c] Wei-En Huang,^[b] Sophie Brameyer,^[d] Céline Douat,^[a] Hiroaki Suga,^{*[b]} and Ivan Huc^{*[a]}

[a] S. Dengler,^[+] Dr. R. T. Howard,^[+] Dr. V. Morozov,^[+] Dr. C. Douat, Prof. I Huc
Department of Pharmacy and Center for Integrated Protein Science, Ludwig-Maximilians-Universität
Butenandtstr. 5–13, 81377 München (Germany)
E-mail: ivan.huc@cup.lmu.de

[b] Dr. C. Tsiamantas,^[+] Wei-En Huang, Prof. H Suga
Department of Chemistry, School of Science, The University of Tokyo
7-3-1 Hongo, Bunkyo, Tokyo, 113-0033 (Japan)
E-mail: hsuga@chem.s.u-tokyo.ac.jp

[c] Prof. Z. Liu, Dr. C. Dobrzanski, Prof. V. Pophristic
Department of Chemistry & Biochemistry, Rowan University
201 Mullica Hill Road • Glassboro, New Jersey 08028 (USA)

[d] Dr. S. Brameyer
Biozentrum, Microbiology, Ludwig-Maximilians-Universität
Großhaderner Str. 2-4, 82152 Martinsried (Germany)

[+] These authors contributed equally to this work.

Supporting information for this article is given via a link at the end of the document.

Abstract: Expanding the chemical diversity of peptide macrocycle libraries for display selection is desirable to improve their potential at binding biomolecular targets. We now have implemented a considerable expansion through a large aromatic helical foldamer inclusion. A helical aromatic foldamer was identified that undergoes flexizyme-mediated tRNA acylation and is capable of initiating ribosomal translation with yields sufficiently high to perform an mRNA display selection of macrocyclic foldamer-peptide hybrids. A hybrid macrocycle binder to the C-lobe of the E6AP HECT domain was selected that showed highly converged peptide residues. A crystal structure and molecular dynamics simulations revealed that both the peptide and foldamer are helical in an intriguing reciprocal stapling fashion. The strong residue convergence could be rationalized based on their involvement in specific interactions with the target protein. The foldamer stabilizes the peptide helix through stapling and through contacts with key residues. These results altogether represent a significant extension of the chemical space amenable to display selection and highlight possible benefits of inserting an aromatic foldamer into a peptide macrocycle for the purpose of protein recognition.

Introduction: Peptide and protein display technologies based on nucleic acid sequence encoding are a powerful way to identify potent and selective ligands for biomolecular targets. Such technologies have demonstrated their clinical potential in the development of a range of approved antibody therapies from phage display platforms,¹ and the discovery of peptidic drugs such as ecallantide² and romiplostim.³ Many modern display technologies leverage the incorporation of non-natural modifications into peptide libraries to expand the chemical diversity of these molecules beyond the natural catalogue⁴ and allow the discovery of peptides with desirable pharmacological profiles, including resistance to proteolytic degradation, cell permeability, and novel modes of binding.⁵ Incorporation of these non-natural modifications, e.g. for the purpose of macrocyclization, has been achieved through either post-synthetic modification,⁶ exploitation of the ribosome's promiscuity,⁷ or genetic engineering of library host organisms.⁸ The remarkable tolerance of the ribosome to accept amino acids with abiotic modifications has recently been highlighted by the incorporation of aromatic oligoamide foldamers (AOFs) into the nascent peptide chain (Figure 1a). Pyridine (P) and quinoline (Q)

containing oligomers were charged onto tRNA by flexizymes and ribosomally incorporated into the polypeptide chain affording AOF-peptide hybrids with up to five P/Q-units as translation initiators,⁹ or up to three P/Q-units as sidechain appendages.¹⁰ Functionalization of the N-terminus as a chloroacetamide also allowed for spontaneous macrocyclization with a downstream cysteine thiol.^{9a, 10} The main interest of introducing AOF segments within a peptide macrocycle lies in their inherent folding information. The propensity of Q_n and (PQ)_n oligomers to adopt stable helical conformations is well-documented.¹¹ Within a hybrid macrocycle, folding of the helical aromatic segment prevails and alters the peptide conformation, for example by stretching the peptide backbone.^{9a, 12} It also confers resistance towards proteolytic degradation of the peptide.¹² In addition, AOFs themselves have potential for directly interacting with proteins¹³ and they exist as natural products.¹⁴ It was therefore a logical next step to challenge ribosomal translation not just with the production of one AOF-peptide macrocycle, but with an entire DNA-encoded library of such macrocycles.

Here we show that FIT-synthesized macrocyclic AOF-peptide hybrids are compatible with mRNA display selection using the random nonstandard peptides integrated discovery (RaPID) platform. Translation initiators containing the foldamer element were optimized for tRNA acylation and translation efficiency, and one initiator was successfully utilized in a selection experiment, generating the first biologically evolved AOF-peptide hybrid macrocycle against a protein target, the catalytic C-lobe of the E6AP HECT domain (Figure S4).¹⁵ This E3 ligase was chosen as a proof-of-concept bait protein given its use in a previously successful peptide affinity selection campaign with the RaPID platform.¹⁶ A crystal structure of the macrocycle-protein complex revealed that both the peptide and foldamer are helical in an intriguing reciprocal stapling fashion.

Results and Discussion: We first set out to identify a foldamer giving sufficiently high yields of both flexizyme-mediated tRNA acylation and ribosomal peptide initiation for the purpose of display selection.

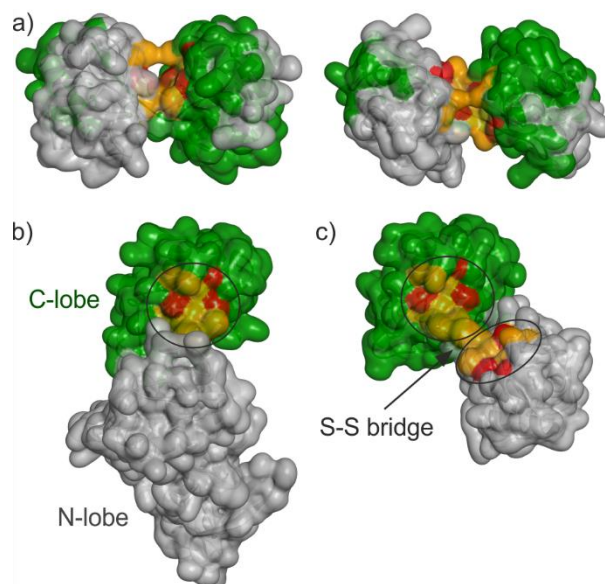
Table 1. Yields of tRNA acylation and peptide translation with foldamer initiators.

Initiator	N-terminus	Acylation (%)	Translation ^[a] (%)
1	Ac	0	-
2	Ac	16	5
3	Ac	75	12
4	Ac	14	<i>N/D</i> ^[b]
5	Ac	85	12
6	Ac	14	13
7	CIAC	38	8 ^[c]
8	CIAC	35	2 ^[c]
9	CIAC	67	6 ^[c]

[a] relative to the same reaction with canonical amino acids only (no reprogramming). [b] Smearing did not allow accurate quantification. [c] The template used for quantification is different from that used for other entries.

Next-generation sequencing of the recovered DNA libraries hinted at an influence of the abiotic segment. The short library converged into a practically unique sequence with a randomized region of seven amino acid residues (Figure 2d, middle, Figure S6). With the longer library, no such convergence was observed (Figure S6). To assess selectivity for C-lobe and the necessity of the foldamer segment, we conducted independent rounds of selection with only the top mRNA sequence of each library. Challenging the translation products of these sequences against beads with and without C-lobe (so-called clone assay) resulted in the binding and recovery of material only when C-lobe was present, suggesting binding of these sequences to the target (Figure 2d right, Figure S7). When the experiment was conducted substituting the CIAC-foldamer-GF-tRNA^{Met} initiator with CIAC-Trp-tRNA^{Met}, binding of the shorter peptide macrocycle was abolished, highlighting a direct or indirect, but essential role of the foldamer in the binding interactions. The effect was lower in the case of the peptide from the larger macrocycle library. Given these results, further studies focused on a hit from the enriched species of smaller macrocycle library.

Foldamer-peptide macrocycle **10** (Figure 2d), an analogue of the top hit from library NNK4–9, was then chemically synthesized, first by automated solid-phase synthesis of the peptide segment, followed by automated solid-phase foldamer synthesis to install the PQ^{Dap}PQ^{Ala} tetramer. Subsequent manual incorporation of the N-terminal chloroacetamide was performed on-resin before cleavage and side chain deprotection, thioether macrocyclization, and purification by reverse-phase HPLC. As shown in Figure 2e and 2f, the binding of **10** to C-lobe was demonstrated by surface plasmon resonance (SPR), with C-lobe immobilized on the SPR chip through its histidine tag, in the same manner it was immobilized during RaPID selection. A K_D of $0.92 \pm 0.26 \mu\text{M}$ was extracted from curve fitting of the sensorgrams with a 1:1 binding isotherm. However, when C-lobe was not immobilized, attempts to measure K_D values using e.g. biotinylated or fluorescein-labelled derivatives of **10** (Scheme



S1) were hampered by protein aggregation. C-lobe solutions were notably viscous and no reliable K_D values could be extracted neither by SPR with an immobilized macrocycle nor by fluorescence polarization. C-lobe has been reported to dimerize via domain swapping (Figure 3a).^{15b} Yet is unknown whether this dimerization mode contributes to the observed aggregation and viscosity.

Figure 3. a) Two views of the swapped-domain dimer of the C-lobe of the E6AP HECT domain (PDB #6TGK).^{15b} One C-lobe is shown in green and the other in gray. The red and orange patches highlight amino acids involved in foldamer-peptide macrocycle binding in the structure shown in c). In the swapped-dimer, these residues are found in a different arrangement; b) Structure of the E6AP HECT domain (PDB #1C4Z).^{15a} The C-lobe and N-lobe are shown in green and gray, respectively. The red and orange patches within the circle highlight the same amino acids as in a). c) Structure of the disulfide-bridged dimer of the C-lobe of the E6AP HECT domain (PDB #7QPB, this work). The two C-lobes shown in gray and green have the same structure as the C-lobe of the native HECT domain. Each has a macrocycle binding site shown by the encircled orange and red residues, but only one macrocycle binds to the C-lobe shown in green in the structure (see Figure 4).

The ¹H NMR spectrum of **10** exhibited characteristics of a helically-folded foldamer component (Figure S8).¹² In presence of 25% acetonitrile in water the circular dichroism (CD) spectrum of **10** was flat in the quinoline absorption region (300-400 nm, Figure S8) indicating no preference for either *P* or *M* foldamer helicity. In water containing 0.5% DMSO, a weak positive band was observed indicating some handedness bias in favor of the *P* helix. However, the band intensity, and thus the extent of handedness bias, was weak in comparison to that observed with PQPQ-peptide macrocycles with shorter peptide loops,^{9a, 12} suggesting modest handedness bias. Upon adding C-lobe to **10**, the CD spectrum at 300-400 nm remained unchanged (Figure S9). This may reflect that the *P* and *M* conformers of **10** bind equally well to C-lobe, or that complex formation is hampered by aggregation.

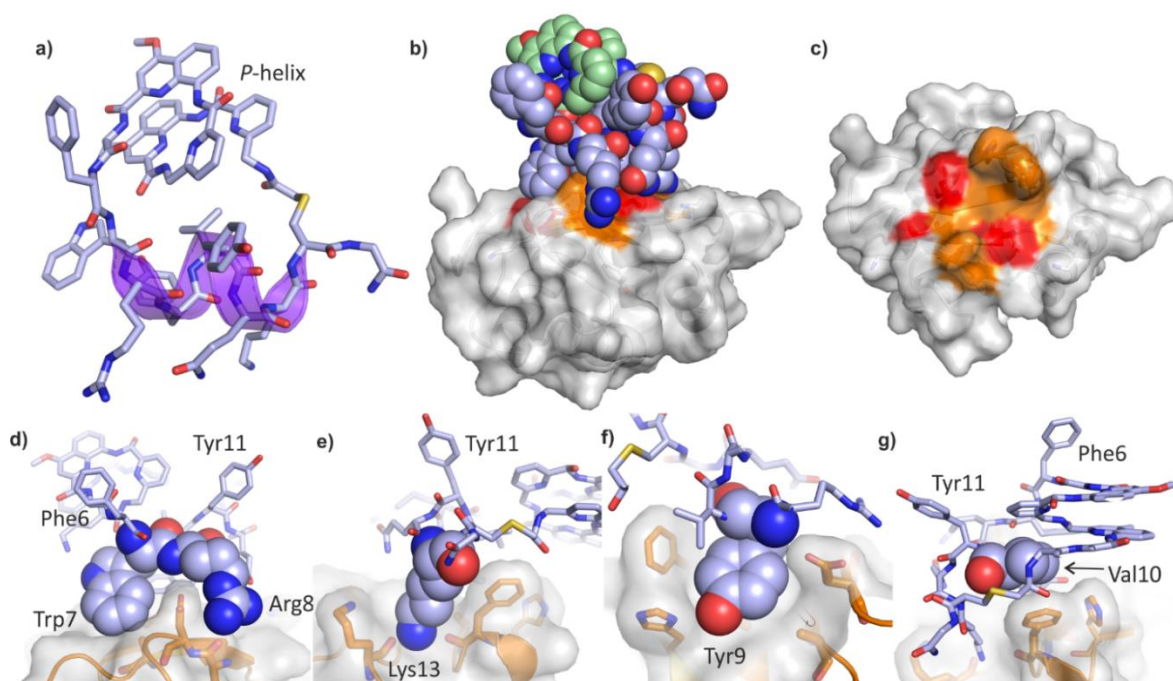


Figure 4. Crystal structure of the complex between C-lobe and macrocycle **10** (PDB #7QPB). a) View of the macrocycle alone showing the peptide and foldamer helices. b) Overall view of the complex. Macrocycle **10** is shown in space filling representation. Carbon atoms in green belong to the foldamer. c) Top view of the macrocycle binding site on the protein. Hydrogen bonds, salt-bridges, and hydrophobic contacts are highlighted in orange and longer distance hydrophobic contacts are shown in red. d–g) Specific macrocycle-protein contacts. Residues of interest are shown in space filling representation. Residues of **10** are numbered starting from the N-terminus of the foldamer segment (P1, Q2, P3, Q4, Gly5, Phe6... Cys14, Gly15).

We next attempted to decipher the interactions between **10** and C-lobe. The complex was successfully crystallized and its structure in the solid state was solved in space group *C2* at 2.3 Å resolution (Figures S10-17). The asymmetric unit contains two molecules of **10** and four of C-lobe. The protein has the same structure as the C-lobe of an intact E6AP HECT domain whose coordinates were used for molecular replacement (Figure 3b, PDB #1C4Z).^{15a} The four proteins are in fact two disulfide-bridged dimers (Figure 3c, Figure S13). Oxidation of Cys820 presumably occurred during crystallization. Yet this dimerization is unrelated to the domain swapping dimerization mentioned above^{15b} (Figure 3a) as it does not alter the native C-lobe fold.

The macrocycle **10** was found in a remarkable conformation in which both the peptide and foldamer segments are helically folded (Figure 4a, Figure S14), as if stapling each other. The peptide forms a slightly distorted α -helix, e.g. with some bifurcated hydrogen bonds (Figure S15). With only eight residues involved (WRVYVQKC), the peptide helix would not be expected to be stable without an intramolecular staple.¹⁸ The PQQQ helix matches well with earlier structures.^{9a, 12} In contrast with its conformation in solution, the foldamer helix is exclusively *P* in the solid state, indicating induction of handedness during crystallization. Crystal packing is relatively tight. As shown in detail in the supporting information, each macrocycle **10** makes contacts with four distinct proteins (Figures S10-13, S16-17). However, most of the peptide residues that converged during display selection, *i.e.* the α -helix, form an extended and intimate

binding area with one of these four proteins (Figure 4b,c), whereas other contacts are limited and mostly concern the peptide residues that were not selected and one Q unit of the foldamer. It can therefore be inferred that the largest contact area – ca 400 Å² – constitutes the actual binding region. The proximity between the binding region and the disulfide bridge makes it impossible for two macrocycles to simultaneously bind a C-lobe disulfide dimer (Figure S13), shedding light on the 2:1 C-lobe-macrocycle stoichiometry in the crystal. The protein-macrocycle interface of the complex involves extended hydrophobic contacts (with Gly755, Gly756, Ala805, Ile 803, Phe821, Val823), salt bridges and hydrogen bonds (Figure S16). Several of the highly converged peptide residues show high shape and interaction complementarity with the protein surface, notably Trp7, Arg8, Tyr9, Val10 and Lys13 (Figure 4d-g). The most converged residue, Arg8, is clamped by Asp754 and Glu752 of C-lobe. Val10 occupies the core of the macrocycle and is in contact with both C-lobe and the foldamer. Altogether, the high convergence of the selection is largely explained by the involvement of the converged residues into a well-defined α -helical fold that forms extended, tight, and shape-complementary contacts with the selection target. As the only exception, Tyr11 displays high selection convergence yet it points away from the cognate C-lobe in the crystal structure. MD simulations were used to shed further light on the macrocycle-protein interactions (Figure 5, Figures S18–25). The complex found in the solid state was used as a starting point of MD runs. The complex underwent little change for some time. Upon prolonged simulation, the main interactions could be disrupted and other configurations were observed. In particular, direct

contacts of the foldamer to the hydrophobic protein area occurred while the α -helix was still folded but exposed to water (Figure 5d). Such configuration might play a role as pre-associated states along the coordinates that lead to tight complex formation.

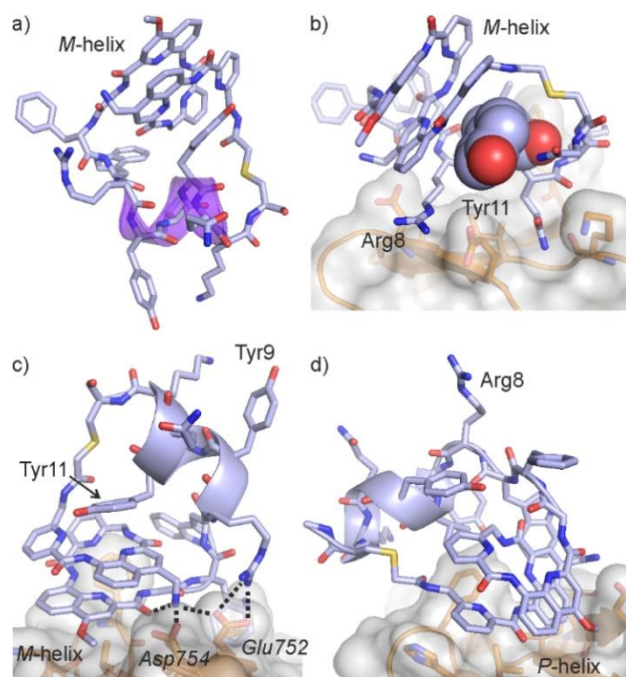


Figure 5. Representative snapshots of MD simulations of **10** in complex with C-lobe. a) View of *M*-helical **10** (the protein has been removed for clarity). b) Binding of *M*-helical **10** C-lobe in a mode similar to that of the crystal structure. c) Alternate binding mode of *M*-helical **10** showing extensive protein-foldamer contacts. d) Same as c) but with *P*-helical **10**. The α -helix of **10** is shown as a solid ribbon in a), c) and d). Some remarkable hydrogen bonds are shown as dashed lines.

MD runs of a V10A mutant showed a destabilization of the α -helix (Figure S25, Table S2), highlighting the structural contribution of Val10 to the stabilization of the macrocycle conformation. A model of the macrocycle with an *M* foldamer helix was also built (Figure 5a) and energy minimized in complex with C-lobe while keeping the α -helix essentially intact.

MD runs showed that the complex was kept in place with the same key peptide-protein interactions observed in the solid state for at least as long as with the *P* helix. The macrocycle with the *M* helix then also explored alternate configurations involving hydrophobic foldamer-protein contacts (Figure 5c). A notable feature was the tight and persistent stacking of Tyr11 on the *M* foldamer helix at the core of the macrocycle (Figure 5b, S24), in a role similar to that of Val10 with the *P* foldamer helix. Conversely, with the *M* foldamer helix, the V10A mutation did not result in a collapse of the α -helix (Figure S25, Table S2). These results thus suggest that Tyr11 and Val10 may play a similar role of macrocycle conformation stabilizer through the mediation of foldamer-peptide contacts. The role of Val10 is critical to the *P*-helical foldamer conformation whereas Tyr11 stabilizes the structure with the *M*-helical foldamer.

Conclusion: We have presented the first successful display selection of a macrocyclic peptide containing a large aromatic helical foldamer segment against a protein target, the C-lobe of the E6AP HECT domain. Selection was made possible by the sufficient yields of tRNA acylation and expression, despite the size – equivalent to a decapeptide – of the foldamer-containing initiator unit, highlighting the great tolerance of the ribosome to non-natural appendages during peptide translation. Display selection showed remarkable convergence toward a rather short peptide (seven residues) among the various peptide lengths available in the two libraries used (5-9 and 10-15 residues). The observed affinity between macrocycle **10** and C-lobe ($K_d = \sim 1 \mu\text{M}$) was not as high as we aimed, compared with many of RaPID peptides that frequently deliver nanomolar or sub-nanomolar binders, and cell studies were not undertaken. However, a crystallographic structure and MD simulations provide a basis to improve the foldamer and the peptide to enhance interactions. The structure and simulations revealed an unexpected macrocycle conformation in which both the peptide and foldamer are helical, as if stapling each other. The stapling of an α -helix by a foldamer helix is a new concept that will deserve further investigation to assess its potential general applicability. Structural studies also shed light on the role of the selected peptide residues. Most were found to be involved in tight contacts and interactions with the protein target. Others mediate foldamer-peptide contacts within the macrocycle. The foldamer thus appears to stabilize the peptide α -helix not only by firmly holding its two ends but also via other contacts with residues of the α -helix. In the conformation bound to C-lobe, the foldamer helix protrudes as a large and rigid handle that can in principle be modified to further enhance functions, including to promote further contacts with the protein target or with other protein partners, or to improve bioavailability such as e.g. cell penetration. A key advantage of the aromatic foldamer unit would then be that it can be decorated with various substituents without altering its shape nor the shape and function of the peptide residues. New selection experiments against other protein targets are in progress to further explore these possible benefits.

Acknowledgements: We thank Dr. Sunbum Kwon for assistance with chemical synthesis and Dr. Sonia Lorenz for providing the expression vector for C-lobe. We are grateful to the European Synchrotron Radiation Facility (ESRF, Grenoble, France) for providing the beamtime (proposal mx2279), and Local Contact at the ESRF for providing assistance in using beamline ID23-1.¹⁹ We thank University of the Sciences and West Pharmaceutical Services, Inc. for providing computational resources used for MD simulations.

Associated Content: One pdf file with supporting information Figures, experimental procedures and methods for calculations as well as characterization of new compounds. Two excel spreadsheets containing extended data set about CD and SPR measurements and mRNA display selection. **Keywords:** Foldamer • Macrocyclic Peptide • Display selection • Protein recognition

Author Information

Corresponding Author

* Prof. I Huc - Department of Pharmacy and Center for Integrated Protein Science, Ludwig-Maximilians-Universität, Butenandtstr. 5–13, 81377 München (Germany)

E-mail: ivan.huc@cup.lmu.de

* Prof. H Suga - Department of Chemistry, School of Science, The University of Tokyo 7-3-1 Hongo, Bunkyo, Tokyo, 113-0033 (Japan)

E-mail: hsuga@chem.s.u-tokyo.ac.jp

Present Addresses

† Vertex Pharmaceuticals (Europe) Ltd, Milton Park, Abingdon, OX14 4RW, United Kingdom.

‡ Orbit Discovery, The Oxford Science Park, Schrödinger Building, Oxford, OX4 4GE, United Kingdom.

Author Contributions

The manuscript was written through contributions of all authors. All authors have given approval to the final version of the manuscript. #These authors contributed equally.

Funding Sources

This work was supported by the Deutsche Forschungsgemeinschaft (DFG) via project HU1766/2-1 and CRC1309-C7 (project ID 325871075) to I.H. and by the JSPS Grant-in-Aid for Specially Promoted Research via project JP21H05618 to H.S. We thank Daniel Gill and Binhao Teng for contributing some building block precursors.

- [1] Barderas, R.; Benito-Peña, E. The 2018 Nobel Prize in Chemistry: phage display of peptides and antibodies. *Anal. Bioanal. Chem.* **2019**, *411*, 2475-2479.
- [2] Bernstein, J. A.; Qazi, M. Ecallantide: its pharmacology, pharmacokinetics, clinical efficacy and tolerability. *Expert Rev. Clin. Immunol.* **2010**, *6*, 29-39.
- [3] Molineux, G.; Newland, A. Development of romiplostim for the treatment of patients with chronic immune thrombocytopenia: from bench to bedside. *Br. J. Haematol.* **2010**, *150*, 9-20.
- [4] Muttenthaler, M.; King, G. F.; Adams, D. J.; Alewood, P. F. Trends in peptide drug discovery. *Nat. Rev. Drug Discov.* **2021**, *20*, 309-325.
- [5] (a) Guillen Schlippe, Y. V.; Hartman, M. C.; Josephson, K.; Szostak, J. W. In vitro selection of highly modified cyclic peptides that act as tight binding inhibitors. *J. Am. Chem. Soc.* **2012**, *134*, 10469-10477. (b) Imanishi, S.; Katoh, T.; Yin, Y.; Yamada, M.; Kawai, M.; Suga, H. In vitro selection of macrocyclic D/L-hybrid peptides against human EGFR. *J. Am. Chem. Soc.* **2021**, *143*, 5680-5684. (c) Kong, X.-D.; Moriya, J.; Carle, V.; Pojer, F.; Abriata, L. A.; Deyle, K.; Heinis, C. De novo development of proteolytically resistant therapeutic peptides for oral administration. *Nat. Biomed. Eng.* **2020**, *4*, 560-571. (d) Tsiamantas, C.; Otero-Ramirez, M. E.; Suga, H. Discovery of functional macrocyclic peptides by means of the RaPID system. *Cyclic Peptide Design* **2019**, 299-315.
- [6] (a) Rhodes, C. A.; Pei, D. Bicyclic peptides as next-generation therapeutics. *Eur. J. Chem.* **2017**, *23*, 12690-12703. (b) Tsutsumi, H.; Kuroda, T.; Kimura, H.; Goto, Y.; Suga, H. Posttranslational chemical installation of azoles into translated peptides. *Nat. Commun.* **2021**, *12*, 1-8. (c) Oppewal, T. R.; Jansen, I. D.; Hekelaar, J.; Mayer, C. A strategy to select macrocyclic peptides featuring asymmetric molecular scaffolds as cyclization units by phage display. *J. Am. Chem. Soc.* **2022**, *144*, 3644-3652.
- [7] (a) Katoh, T.; Suga, H. In vitro selection of foldamer-like macrocyclic peptides containing 2-aminobenzoic acid and 3-aminothiophene-2-carboxylic acid. *J. Am. Chem. Soc.* **2022**, *144*, 2069-2072. (b) Katoh, T.; Tajima, K.; Suga, H. Consecutive elongation of D-amino acids in translation. *Cell Chem. Biol.* **2017**, *24*, 46-54. (c) Kawakami, T.; Murakami, H.; Suga, H. Messenger RNA-programmed incorporation of multiple N-methyl-amino acids into linear and cyclic peptides. *Chem. Biol.* **2008**, *15*, 32-42.
- [8] (a) Oller-Salvia, B.; Chin, J. W. Efficient Phage Display with Multiple Distinct Non-Canonical Amino Acids Using Orthogonal Ribosome-Mediated Genetic Code Expansion. *Angew. Chem., Int. Ed.* **2019**, *58*, 10844-10848. (b) Oller-Salvia, B.; Chin, J. W. Efficient phage display with multiple distinct non-canonical amino acids using orthogonal ribosome-mediated genetic code expansion. *Angew. Chem.* **2019**, *131*, 10960-10964.
- [9] (a) Rogers, J. M.; Kwon, S.; Dawson, S. J.; Mandal, P. K.; Suga, H.; Huc, I. Ribosomal synthesis and folding of peptide-helical aromatic foldamer hybrids. *Nat. Chem.* **2018**, *10*, 405-412. (b) Tsiamantas, C.; Kwon, S.; Douat, C.; Huc, I.; Suga, H. Optimizing aromatic oligoamide foldamer side-chains for ribosomal translation initiation. *ChemComm* **2019**, *55*, 7366-7369.
- [10] (a) Tsiamantas, C.; Kwon, S.; Rogers, J. M.; Douat, C.; Huc, I.; Suga, H. Ribosomal incorporation of aromatic oligoamides as peptide sidechain appendages. *Angew. Chem.* **2020**, *132*, 4890-4894. (b) Tsiamantas, C.; Kwon, S.; Rogers, J. M.; Douat, C.; Huc, I.; Suga, H. Ribosomal Incorporation of Aromatic Oligoamides as Peptide Sidechain Appendages. *Angew. Chem., Int. Ed.* **2020**, *59*, 4860-4864.
- [11] (a) Baptiste, B.; Douat-Casassus, C.; Laxmi-Reddy, K.; Godde, F.; Huc, I. Solid phase synthesis of aromatic oligoamides: application to helical water-soluble foldamers. *J. Org. Chem. Res.* **2010**, *75*, 7175-7185. (b) Jiang, H.; Léger, J.-M.; Huc, I. Aromatic δ -peptides. *J. Am. Chem. Soc.* **2003**, *125*, 3448-3449. (c) Kudo, M.; Maurizot, V.; Kauffmann, B.; Tanatani, A.; Huc, I. Folding of a linear array of α -amino acids within a helical aromatic oligoamide frame. *J. Am. Chem. Soc.* **2013**, *135*, 9628-9631.
- [12] Dengler, S.; Mandal, P. K.; Allmendinger, L.; Douat, C.; Huc, I. Conformational interplay in hybrid peptide-helical aromatic foldamer macrocycles. *Chem. Sci.* **2021**, *12*, 11004-11012.
- [13] (a) Azzarito, V.; Miles, J. A.; Fisher, J.; Edwards, T. A.; Warriner, S. L.; Wilson, A. J. Stereocontrolled protein surface recognition using chiral oligoamide proteomimetic foldamers. *Chem. Sci.* **2015**, *6*, 2434-2443. (b) Hegedus, Z.; Grison, C. M.; Miles, J. A.; Rodriguez-Marin, S.; Warriner, S. L.; Webb, M. E.; Wilson, A. J. A catalytic protein-proteomimetic complex: using aromatic oligoamide foldamers as activators of RNase S. *Chem. Sci.* **2019**, *10*, 3956-3962. (c) Jewginski, M.; Granier, T.; Langlois d'Estaintot, B. a.; Fischer, L.; Mackereth, C. D.; Huc, I. Self-assembled protein-aromatic foldamer complexes with 2: 3 and 2: 2: 1 stoichiometries. *J. Am. Chem. Soc.* **2017**, *139*, 2928-2931. (d) Kumar, S.; Birol, M.; Schlamadinger, D. E.; Wojcik, S. P.; Rhoades,

- E.; Miranker, A. D. Foldamer-mediated manipulation of a pre-amyloid toxin. *Nat. Commun.* **2016**, *7*, 1-11. (e) Kumar, S.; Hamilton, A. D. α -helix mimetics as modulators of A β self-assembly. *J. Am. Chem. Soc.* **2017**, *139*, 5744-5755. (f) Vallade, M. I.; Jewginski, M.; Fischer, L.; Buratto, J. r. m.; Bathany, K.; Schmitter, J.-M.; Stupfel, M.; Godde, F. d. r.; Mackereth, C. D.; Huc, I. Assessing Interactions between Helical Aromatic Oligoamide Foldamers and Protein Surfaces: A Tethering Approach. *Bioconjugate Chem.* **2018**, *30*, 54-62. (g) Ziach, K.; Chollet, C.; Parissi, V.; Prabhakaran, P.; Marchivie, M.; Corvaglia, V.; Bose, P. P.; Laxmi-Reddy, K.; Godde, F.; Schmitter, J.-M. Single helically folded aromatic oligoamides that mimic the charge surface of double-stranded B-DNA. *Nat. Chem.* **2018**, *10*, 511-518. (h) Ahmed, J.; Fitch, T. C.; Donnelly, C. M.; Joseph, J. A.; Ball, T. D.; Bassil, M. M.; Son, A.; Zhang, C.; Ledreux, A.; Horowitz, S.; et al. Foldamers reveal and validate therapeutic targets associated with toxic α -synuclein self-assembly. *Nat. Commun.* **2022**, *13*, 2273.
- [14] Seedorf, T.; Kirschning, A.; Solga, D. Natural and synthetic oligoarylamides: privileged structures for medical applications. *Eur. J. Chem.* **2021**, *27*, 7321-7339.
- [15] (a) Huang, L.; Kinnucan, E.; Wang, G.; Beaudenon, S.; Howley, P. M.; Huibregtse, J. M.; Pavletich, N. P. Structure of an E6AP-UbcH7 complex: insights into ubiquitination by the E2-E3 enzyme cascade. *Science* **1999**, *286*, 1321-1326. (b) Ries, L. K.; Liess, A. K.; Feiler, C. G.; Spratt, D. E.; Lowe, E. D.; Lorenz, S. Crystal structure of the catalytic C-lobe of the HECT-type ubiquitin ligase E6AP. *Protein Sci.* **2020**, *29*, 1550-1554.
- [16] Yamagishi, Y.; Shoji, I.; Miyagawa, S.; Kawakami, T.; Katoh, T.; Goto, Y.; Suga, H. Natural product-like macrocyclic N-methyl-peptide inhibitors against a ubiquitin ligase uncovered from a ribosome-expressed de novo library. *Chem. Biol.* **2011**, *18*, 1562-1570.
- [17] Vallade, M.; Sai Reddy, P.; Fischer, L.; Huc, I. Enhancing aromatic foldamer helix dynamics to probe interactions with protein surfaces. *Eur. J. Org. Chem.* **2018**, *2018*, 5489-5498.
- [18] Harrison, R. S.; Shepherd, N. E.; Hoang, H. N.; Ruiz-Gómez, G.; Hill, T. A.; Driver, R. W.; Desai, V. S.; Young, P. R.; Abbenante, G.; Fairlie, D. P. Downsizing human, bacterial, and viral proteins to short water-stable alpha helices that maintain biological potency. *Proc. Natl. Acad. Sci. U. S. A.* **2010**, *107*, 11686-11691.
- [19] Nurizzo, D.; Mairs, T.; Guizarro, M.; Rey, V.; Meyer, J.; Fajardo, P.; Chavanne, J.; Biasci, J.-C.; McSweeney, S.; Mitchell, E. The ID23-1 structural biology beamline at the ESRF. *J. Synchrotron Radiat.* **2006**, *13*, 227-238.

9. Supporting Information: Display Selection of a Hybrid Foldamer-Peptide Macrocycle

Display Selection of a Hybrid Foldamer-Peptide Macrocycle

*Sebastian Dengler^{#[a]} Ryan T. Howard^{#[a]} Vasily Morozov^{#[a]} Christos Tsiamantas^{#[b]}
Zhiwei Liu,^[c] Christopher Dobrzanski,^[c] Vojislava Pophristic,^[c] Wei-En Huang,^[b] Sophie
Brameyer,^[d] Céline Douat,^[a] Hiroaki Suga,^{*[b]} and Ivan Huc^{*[a]}.*

^[a]Department of Pharmacy and Center for Integrated Protein Science, Ludwig-Maximilians-Universität, Butenandtstr. 5–13, 81377 München (Germany)

^[b]Department of Chemistry, School of Science, The University of Tokyo, 7-3-1 Hongo, Bunkyo, Tokyo, 113-0033 (Japan)

^[c]Department of Chemistry & Biochemistry, Rowan University, 201 Mullica Hill Road • Glassboro, New Jersey 08028 (USA)

^[d]Biozentrum, Microbiology, Ludwig-Maximilians-Universität, Großhaderner Str. 2-4, 82152 Martinsried (Germany)

9.1. Supporting figures

Figure S1

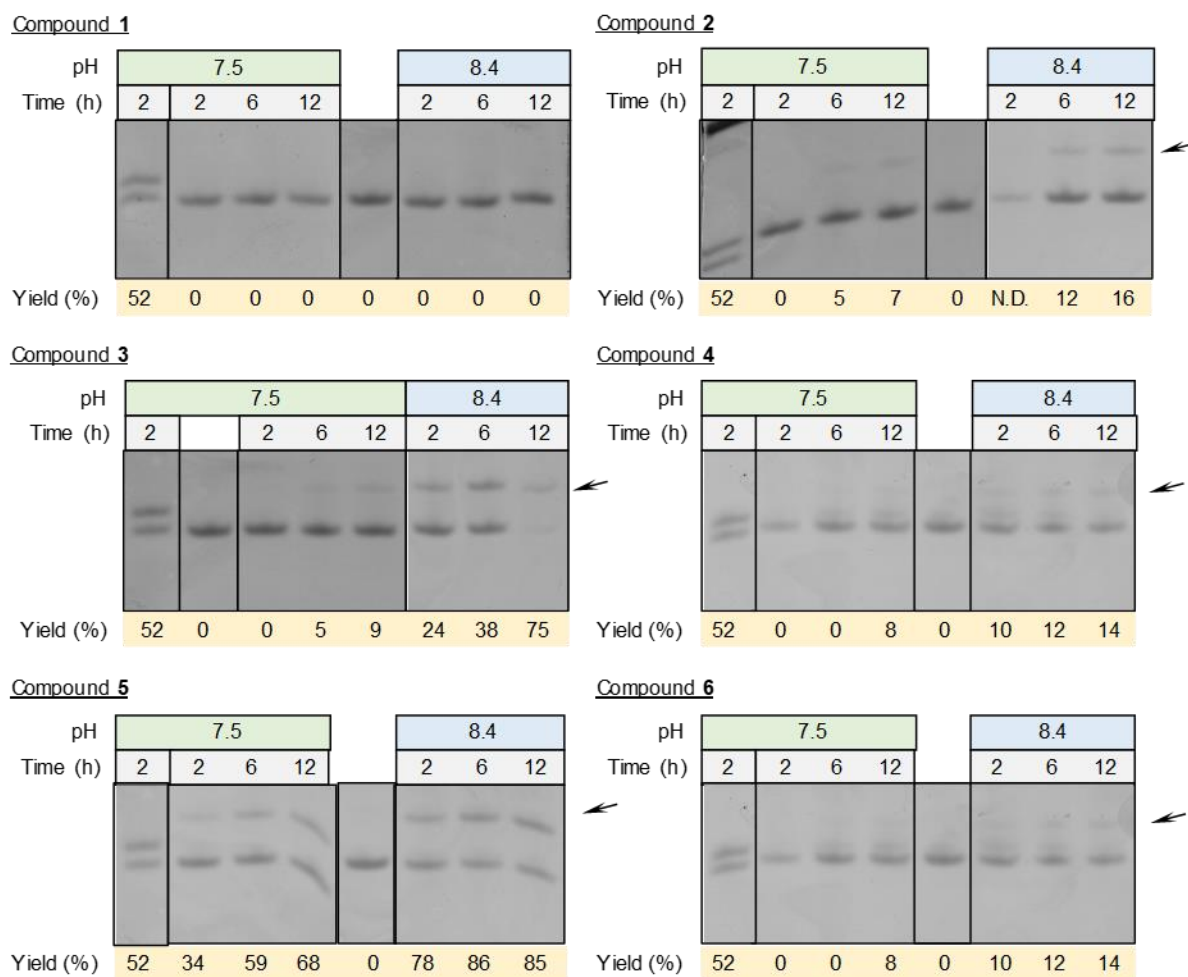


Figure S1 part 1. Assessment of tRNA acylation was carried out using mhRNA (microhelix RNA, a tRNA mimic) over the course of 24 hours, at two different pH values, 7.5 and 8.4, in green and blue, respectively. mhRNA acylated with the foldamer substrate is shown with an arrow while the lower band corresponds to “free” mhRNA. Acid-PAGE gels corresponding to the N-acetylated compounds 1–6 are shown. In all cases the first band corresponds to the acylation of ClAc-Trp-CME which is used as a control. The band which is not labelled is a reaction in which DMSO has been added instead of the activated substrate.

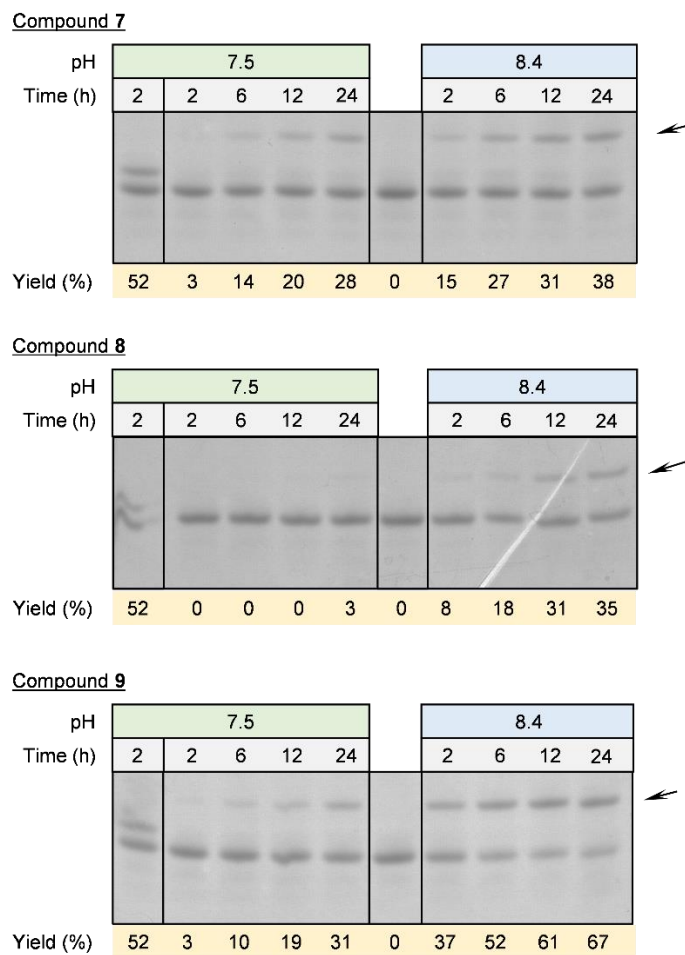


Figure S1 part 2. Assessment of tRNA acylation was carried out using mHRNA (microhelix RNA, a tRNA mimic) over the course of 24 hours, at two different pH values, 7.5 and 8.4, in green and blue, respectively. mHRNA acylated with the foldamer substrate is shown with an arrow while the lower band corresponds to “free” mHRNA. Acid-PAGE gels corresponding to the N-chloroacetylated compounds **7–9** are shown. In all cases the first band corresponds to the acylation of ClAc-Trp-CME which is used as a control. The band which is not labelled is a reaction in which DMSO has been added instead of the activated substrate.

Figure S2

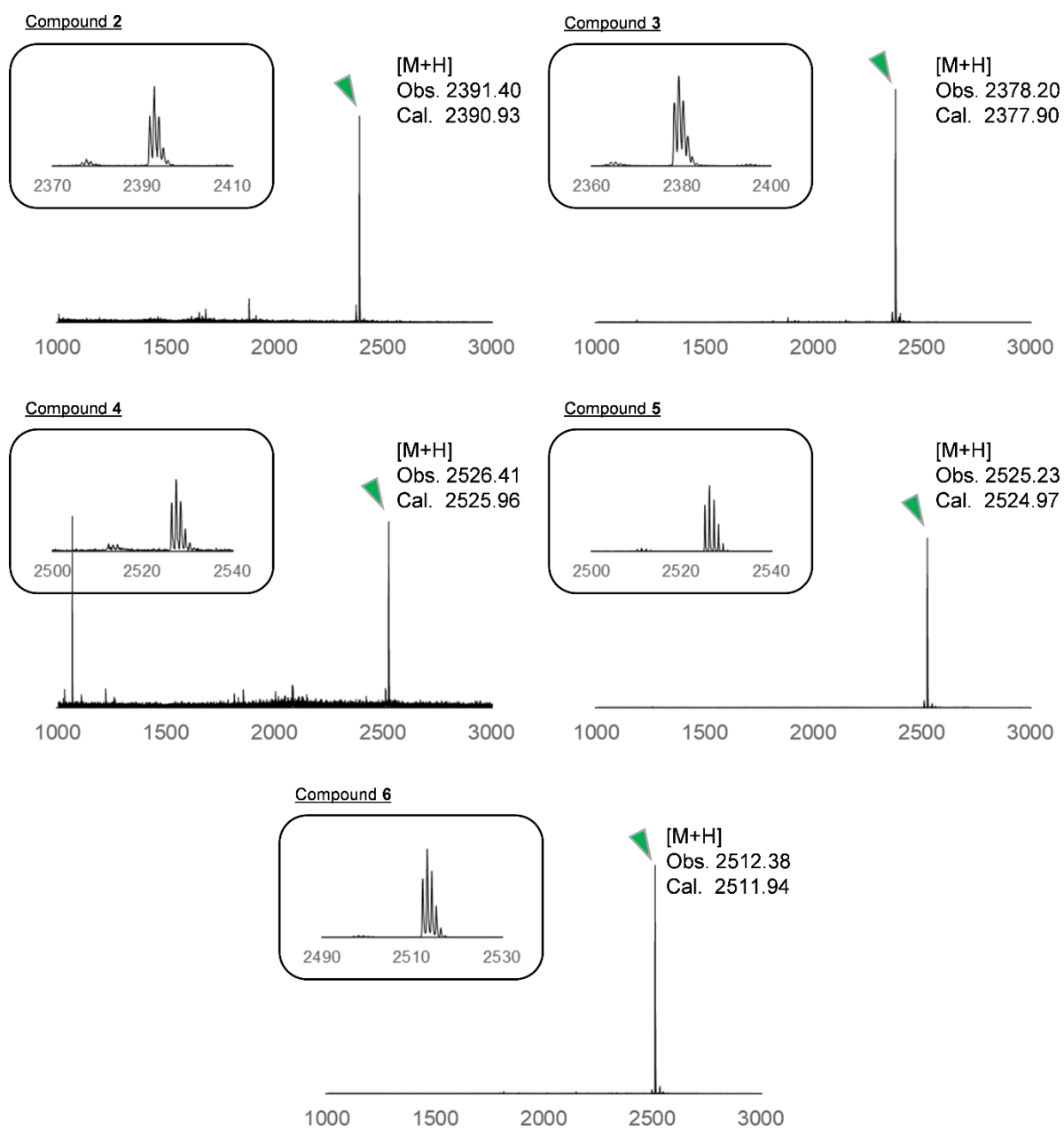


Figure S2 part 1. MALDI-TOF spectra of the translation reactions, demonstrating the successful incorporation of the foldamer substrates into peptide sequences. N-acetylated compounds **2–6** substituted the initiator Met residue in the MGGTTY-flag sequence. The peaks ($[M+H]^+$) corresponding to the desired peptide sequences are shown with the green arrow. Flag stands for an octapeptide with the sequence DYKDDDDK.

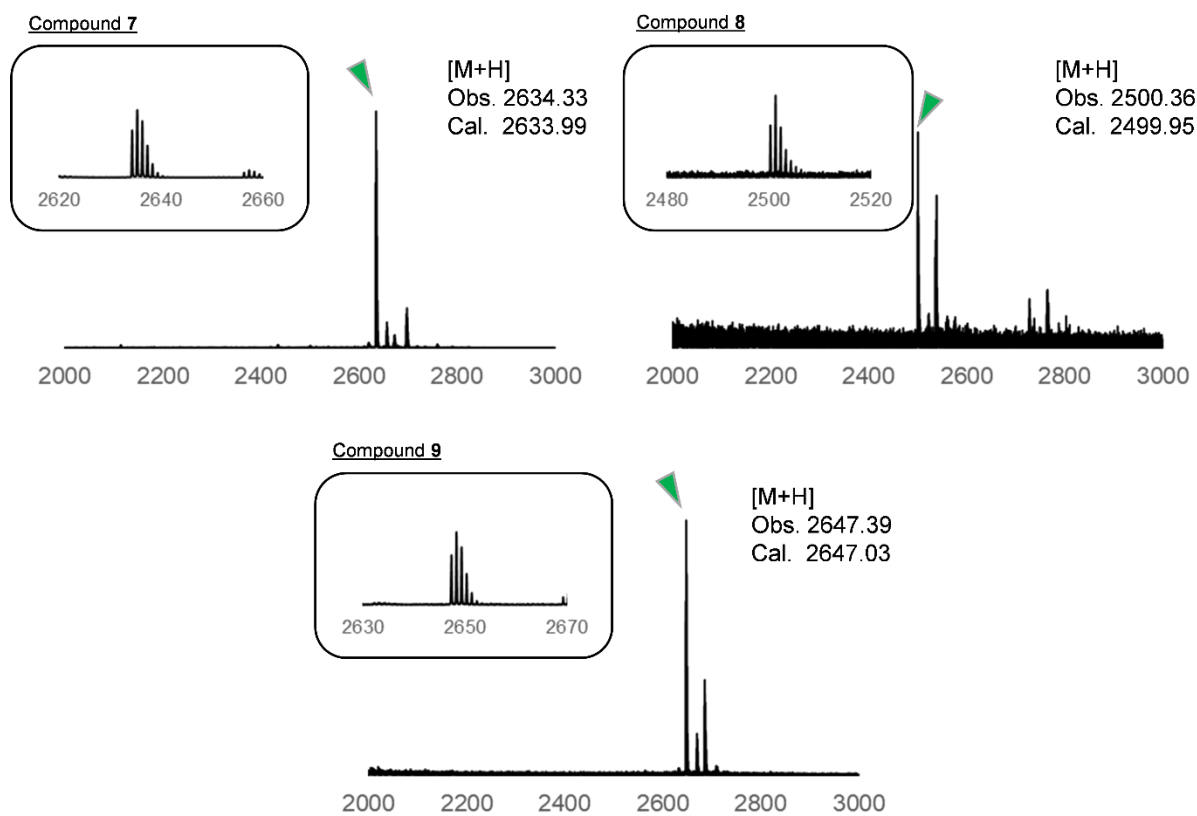


Figure S2 part 2. MALDI-TOF spectra of the translation reactions, demonstrating the successful incorporation of the foldamer substrates into peptide sequences. N-chloroacetylated compounds **7–9** substituted the initiator Met residue in MYAATAACA-flag with which the ClAc functionality of the downstream Cys residue readily cyclizes. The peaks corresponding to the desired peptide sequences are shown with the green arrow. Flag stands for an octapeptide with the sequence DYKDDDDK.

Figure S3

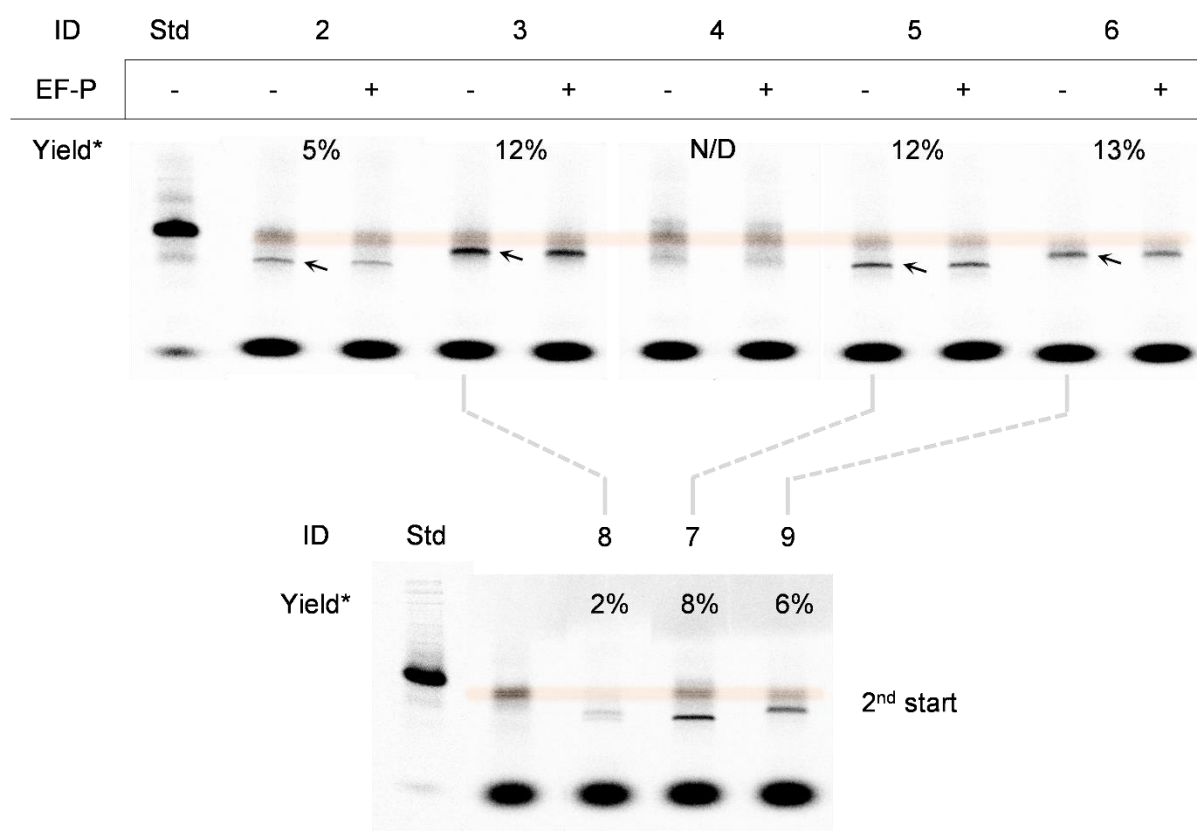
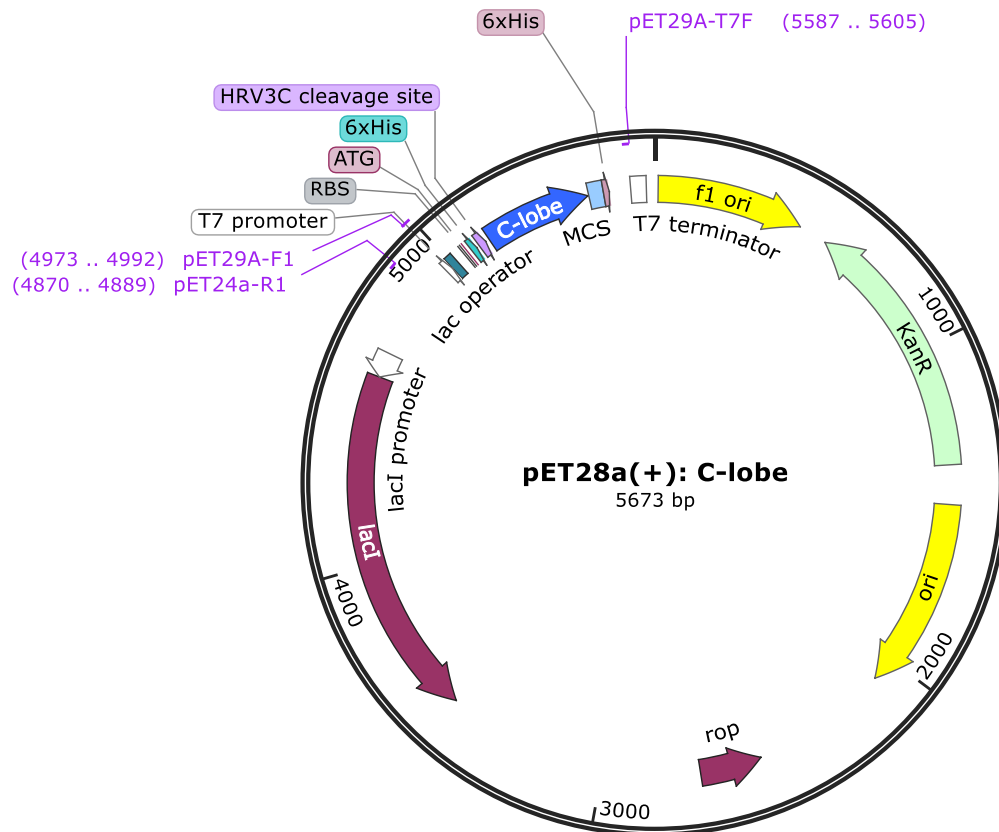


Figure S3. Quantification of the translation reactions by means of radioisotopes. Upper part: Substrates **2–6** were incorporated into the MGGTTY-flag sequence, with and without elongation factor P (EF-P), a translation factor that was previously shown to facilitate the incorporation of “difficult” amino acids. In our case this factor had no effect on the incorporation efficiency. Lower part: Substrates **7–9** were incorporated in the MYAATAACA-flag sequence to yield macrocyclic foldamer-peptide hybrids. Lane 2 (unlabelled) corresponds to a translation reaction in which “uncharged” $\text{tRNA}^{\text{fMet}}_{\text{CAU}}$ (initiator tRNA) was added instead, demonstrating that the observed band corresponds to a peptide sequence lacking the initiating (foldamer) residue (highlighted in orange). Std stands for standard and it is a reaction in which Met has been added, allowing a direct comparison of the foldamer-initiated sequences with their “natural” counterparts. Yields are a comparison of the concentration of the foldamer-peptide hybrid and its “natural” counterpart. The intense band at the bottom of the gels corresponds to unreacted ^{14}C Asp.

Figure S4



ATGGGCAGCAGCCATCATCATCATCATCACAGCAGCGGCCTGGAAGTTCTGTTCCAGGGGCCCATATGGCTA
 GCAATCTAGATTTCCAAGCACTAGAAGAACTACAGAATATGACGGTGGCTATACCAGGGACTCTGTTCTGAT
 TAGGGAGTTCTGGGAAATCGTTCATTCATTTACAGATGAACAGAAAAGACTCTTCTTGCAGTTTACAACGGGC
 ACAGACAGAGCACCTGTGGGAGGACTAGGAAAATTAAGATGATTATAGCCAAAATGGCCAGACACAGA
 AAGTTACCTACATCTCATACTTGCTTTAATGTGCTTTACTTCCGGAATACTCAAGCAAAGAAAACTAAAG
 AGAGATTGTTGAAGGCCATCACGTATGCCAAAGATTGGCATGCTGTAA

MGSSHHHHHSSGLEVLFQ|GPHMASNLDFQALEETTEYDGGYTRDSVLIREFWEIVHSFTDEQKRLFLQFTTGTD
 RAPVGGGLGKLMIIAKNGPDTERLPTSHTCFNVLLPEYSSKEKLLKERRLLKAITYAKGFGL

Figure S4. pET28a(+) plasmid map (top), coding sequence (middle), and “C-lobe” protein expression product (bottom) used in this study; | indicates the HRV3C protease cleavage site.

Figure S5

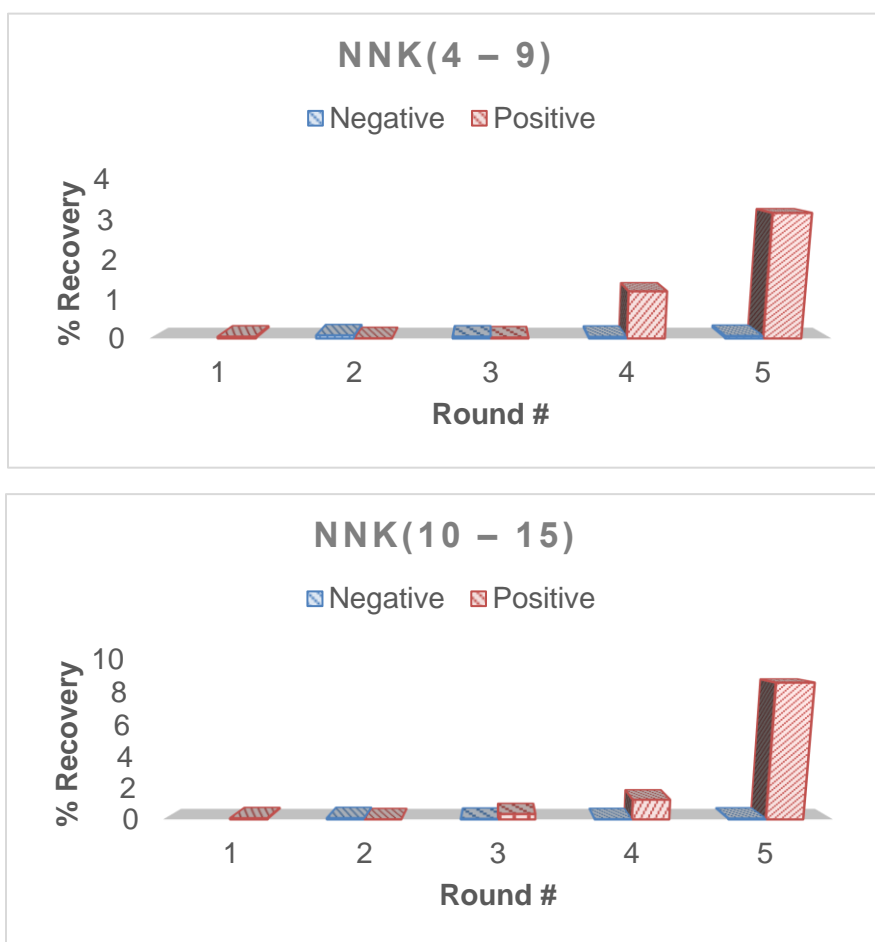


Figure S5. The recovery (%) for the 5 rounds of the selection experiment for the NNK4–9 (top) and NNK 10–15 (bottom) libraries as determined by qPCR for both positive (protein-modified beads, shown also in **Figure 2d**) and negative (non-modified beads).

Figure S6

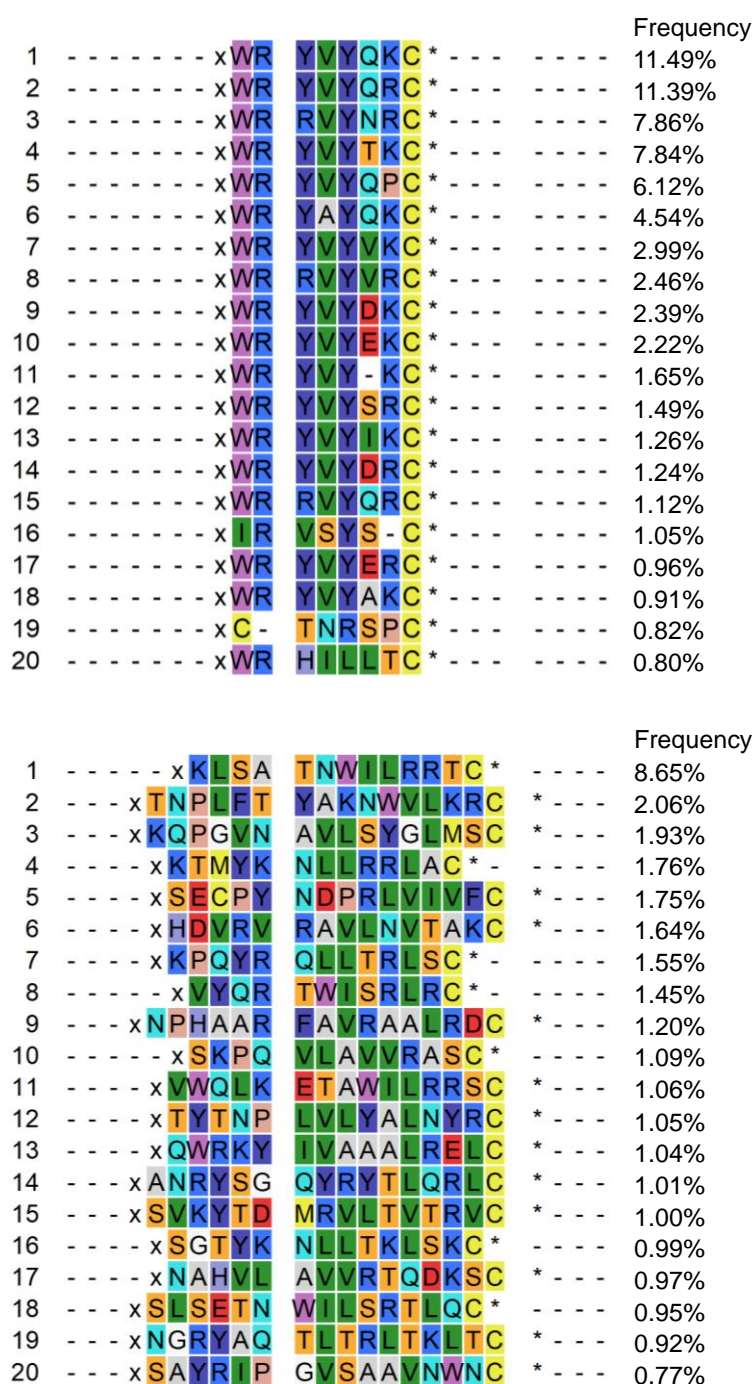


Figure S6. A clustal alignment of the 20 most abundant sequences for both libraries, NNK4–9 (top) and 10–15 (bottom), in which: (x) stands for the Foldamer-G-F- segment, (*) for the G-S-G-S-G-S linker followed by the *amber* stop codon (TAG) and (-) in the middle of the sequence (sequences 11,16 & 19 in short library) indicates the appearance of the *amber* stop codon (TAG). The number on the right indicates the appearance frequency (number of reads/total number of reads x 100). Alignment of the top 50 sequences can be found in **Extended Data 1**.

Figure S7

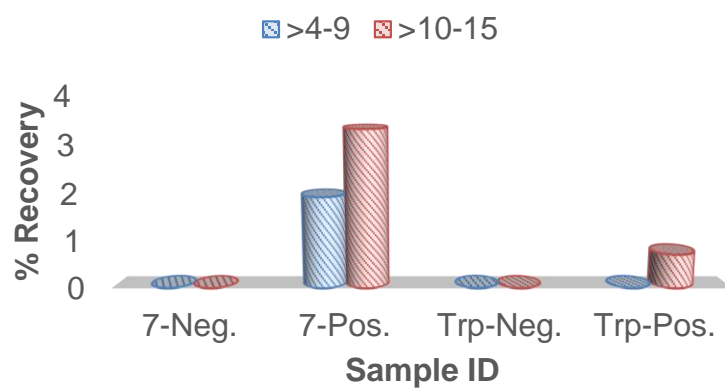


Figure S7. The top sequences of each library from the sequencing data, linked to their genotype, were exposed to protein-modified (Pos) and unmodified beads (Neg), and recovery determined by qPCR, highlighting the selectivity attributed to the scaffold from the abiotic residue (7-Neg vs 7-Pos). In a subsequent experiment, the abiotic initiator was substituted with Trp (capable of undergoing cyclization). While in the large peptide some binding could be retained, in the case of the shorter peptide was completely abolished, hinting on the significance of the peptide's foldamer-imposed orientation.

Figure S8

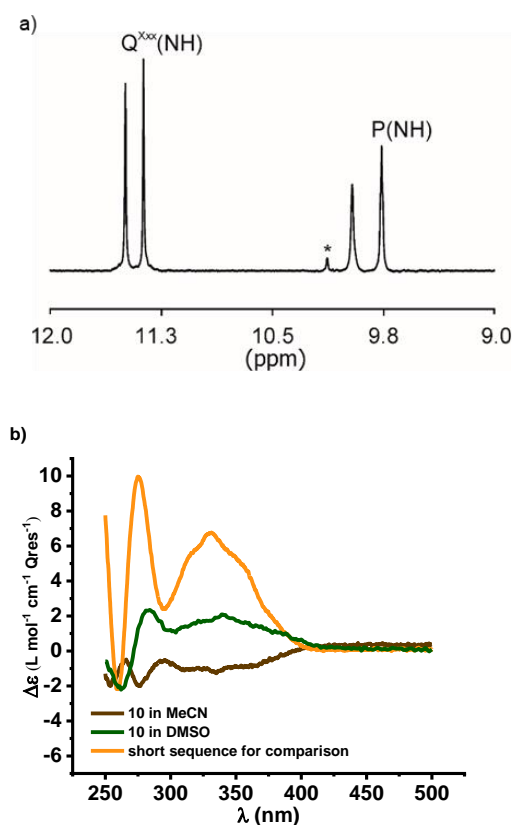


Figure S8. (a) Part of the ^1H NMR spectrum of **10** between 12.0–9.0 ppm in CD_3CN (25% (v/v) in H_2O , water suppression). The helically-folded, downfield-shifted protons of the quinoline amides are at ~ 11.5 ppm, and one of the two pyridine amides is at ~ 9.7 ppm. This significant downfield shift of amide proton resonances is a result of a strong hydrogen-bonded structure which is a typical indicator for helical folding.¹ The adjacent signal at ~ 10.0 ppm belongs to the Trp7 N–H signal, and the asterisk (*) denotes an impurity. (b) CD spectrum of **10** at 25 °C in different solvents: recorded at a concentration of 242 μM in $\text{H}_2\text{O}/\text{MeCN}$ (75:25 v/v); recorded at a concentration of 15 μM in 20 mM PBS buffer pH 7.4, containing 0.5% DMSO used for the initial dissolution of **10**. CD Exact experimental parameters (incl. path length and other machine settings) are described fully in **Extended Data 2**. CD spectrum of a previously reported macrocyclic peptide-foldamer hybrid ($\text{CH}_2\text{--C(O)--PQ}^{\text{ASP}}\text{PQ}^{\text{ASP}}\text{GlyPhe(Lys)}_3\text{CysGly--OH}$, compound **3** from Dengler *et al*; italics represent elements connected by thioether macrocyclization)² with *P* handedness bias is included for comparison.

Figure S9

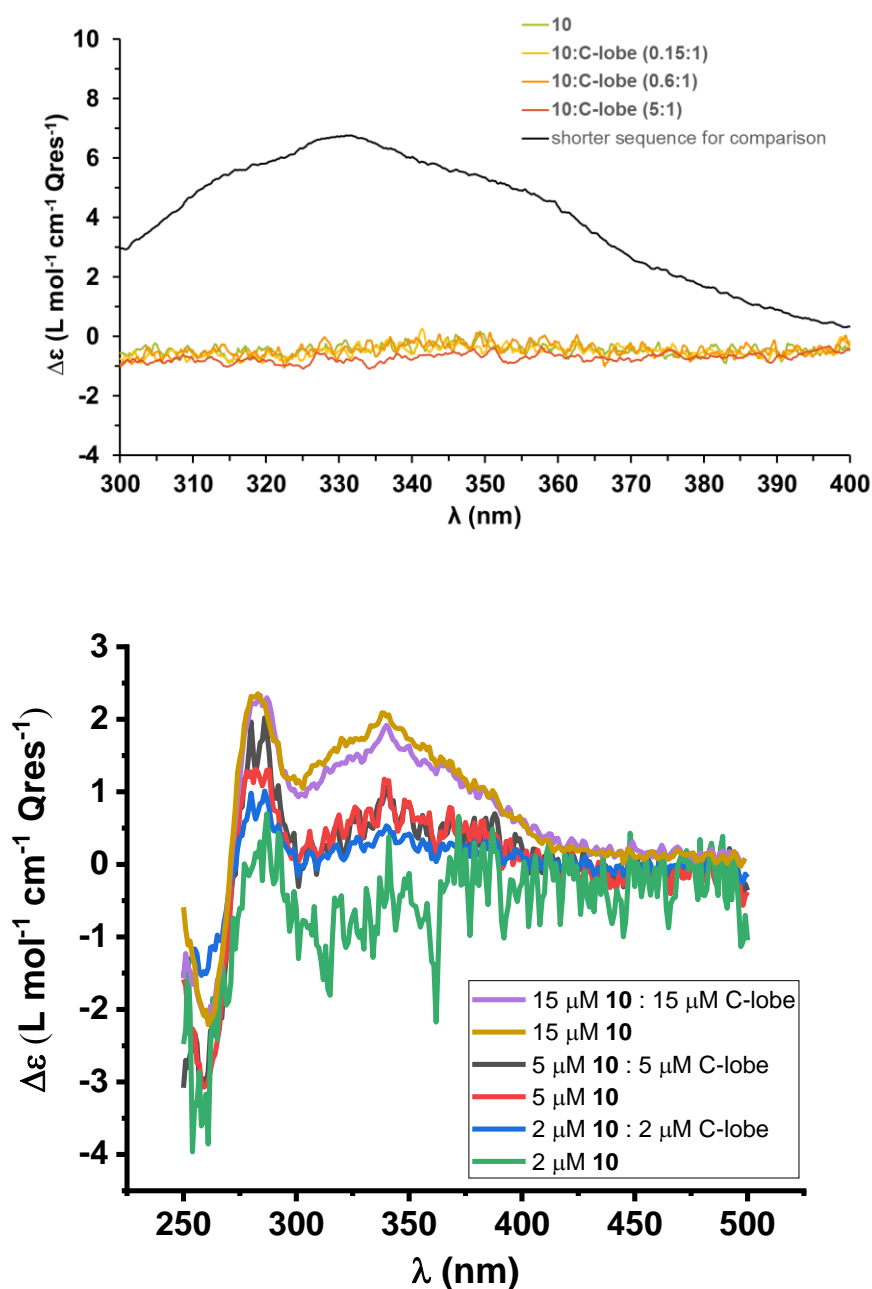
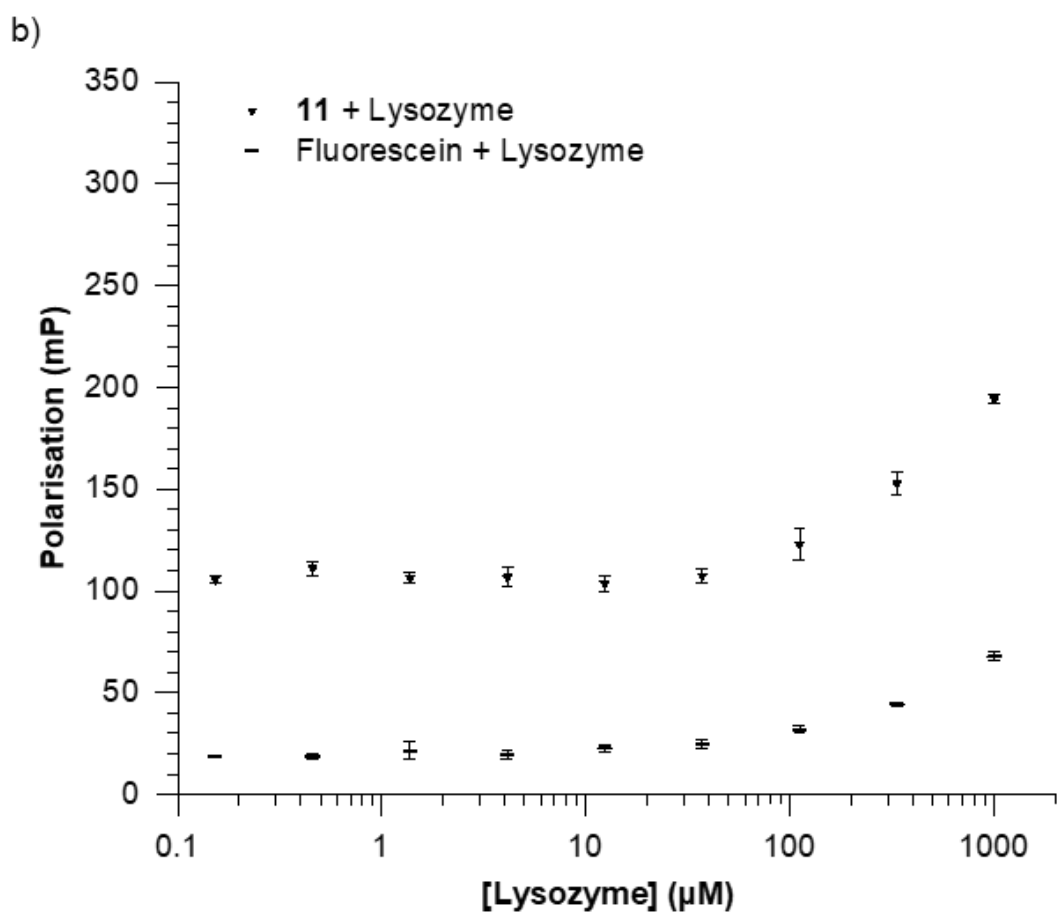
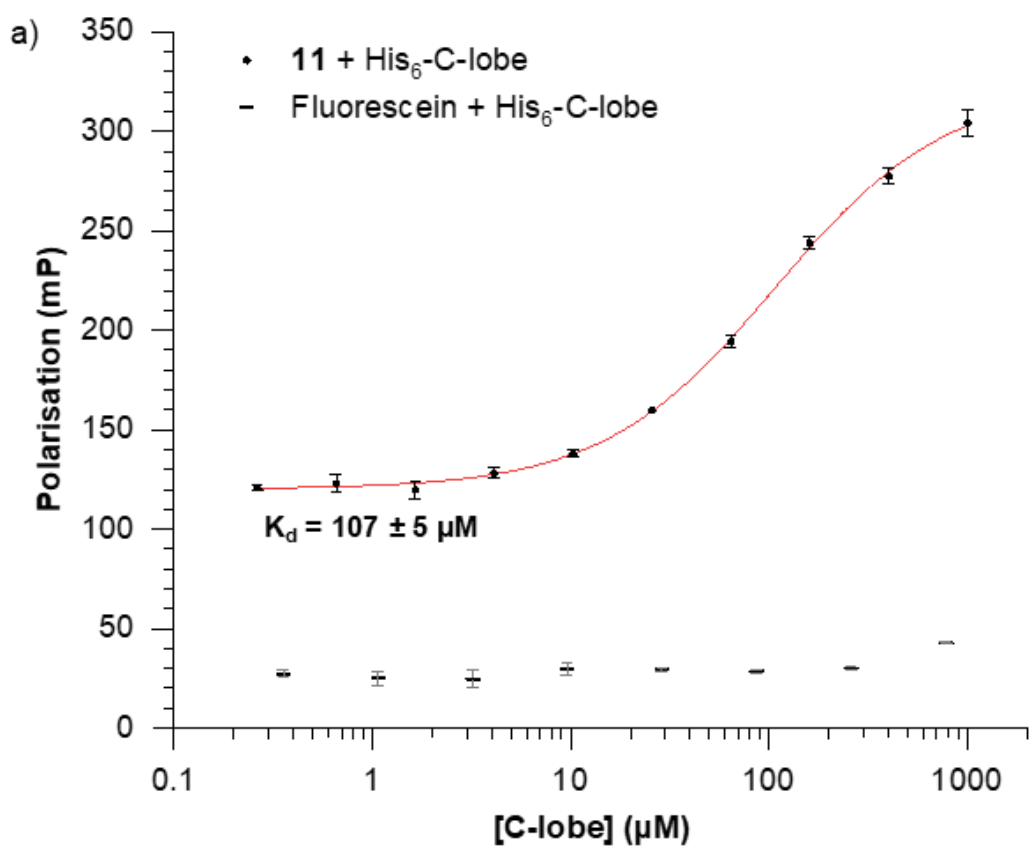


Figure S9. (Top) CD spectrum of **10** with the indicated equivalents of cleaved C-lobe at 10 °C. The solution was prepared by addition of **10** from a stock solution in DW (top panel) or DMSO (bottom panel) to buffered protein solution. No change in the CD spectrum of **10** between 300–400 nm is observed. Exact experimental parameters (incl. buffer conditions, path length, and other machine settings) are described fully in **Extended Data 2**. The CD spectrum of the previously reported macrocyclic peptide-foldamer hybrid described in **Figure S9** with *P* handedness bias is included for comparison.

Figure S10



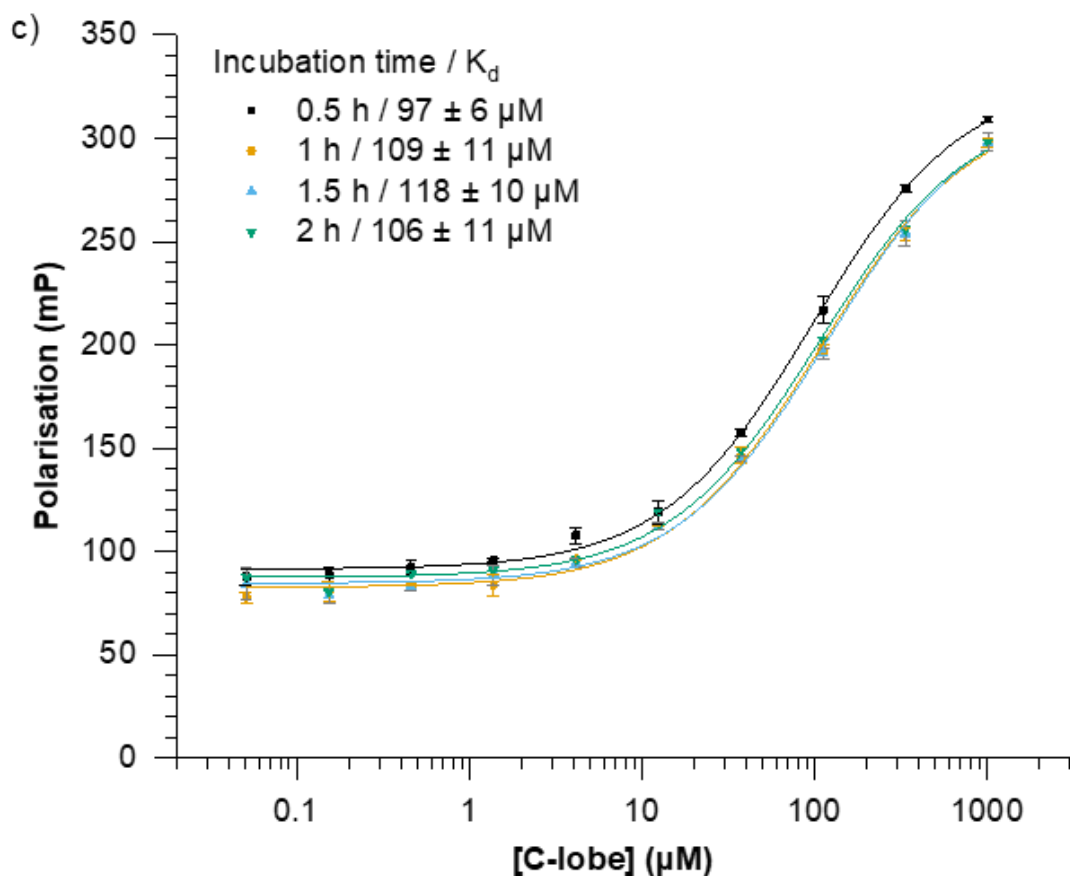


Figure S10. Extended fluorescence polarization data. All experiments were run in technical triplicate in RaPID selection buffer (Tris-HCl (50 mM) pH 7.6, NaCl (150 mM), DTT (5 mM), Tween-20 (0.05% (v/v)), NaN_3 (0.05% (w/v))) with 20 nM of the respective fluorescent tracer and blanked against a buffer-only control. All error bars represent standard deviation of $n = 3$ technical replicates. Full data and fitting results can be found in **Extended Data 2**. (a) **Figure 2e** re-drawn with visible error bars. (b) Fluorescence polarization of **11** or fluorescein with varying concentrations of lysozyme. (c) Biological replicate 2 (black) of the fluorescence polarization of **11** with varying concentrations of His₆-C-lobe, including measurements taken after longer incubation times (colors): minimal variation in data points and fitted K_d were observed suggesting binding had reached equilibrium.

Figure S11

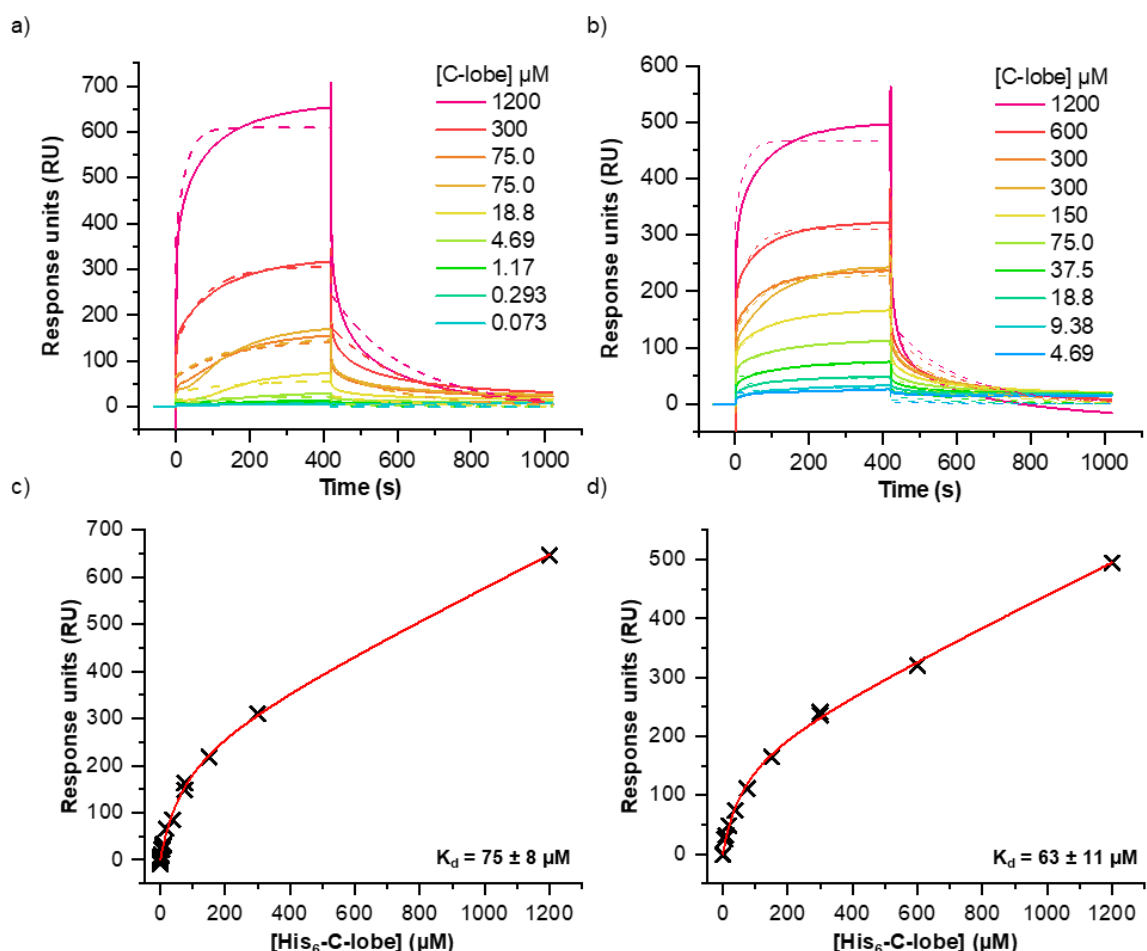


Figure S11. (a–b) SPR sensorgrams (a: replicate 1, b: replicate 2, also shown in **Figure 2f**) of the interaction between the His₆-tagged C-lobe of the HECT domain of E6AP (analyte) and biotinylated macrocycle **12** (surface-bound ligand, biotin-functionalized analogue of **10**). Measurements were recorded on a Biacore T200 using a streptavidin sensor chip in SPR analysis buffer (Tris-HCl (50 mM) pH 7.5, NaCl (150 mM), DTT (1 mM), NaN₃ (0.05% (v/v)), Tween-20 (0.05% (v/v))) and spectra were plotted after subtraction from the signal on the reference flow cell. Data (solid lines) were fit (dashed lines) using Biacore T200 Evaluation Software 3.1. (c–d) Maximum response unit values plotted against protein concentration (c: replicate 1, d: replicate 2) and fit to the quadratic binding isotherm with a factor to account for non-specific binding. K_d was found to be consistent across replicates. Full data and fitting results can be found in **Extended Data 2**.

Figure S12

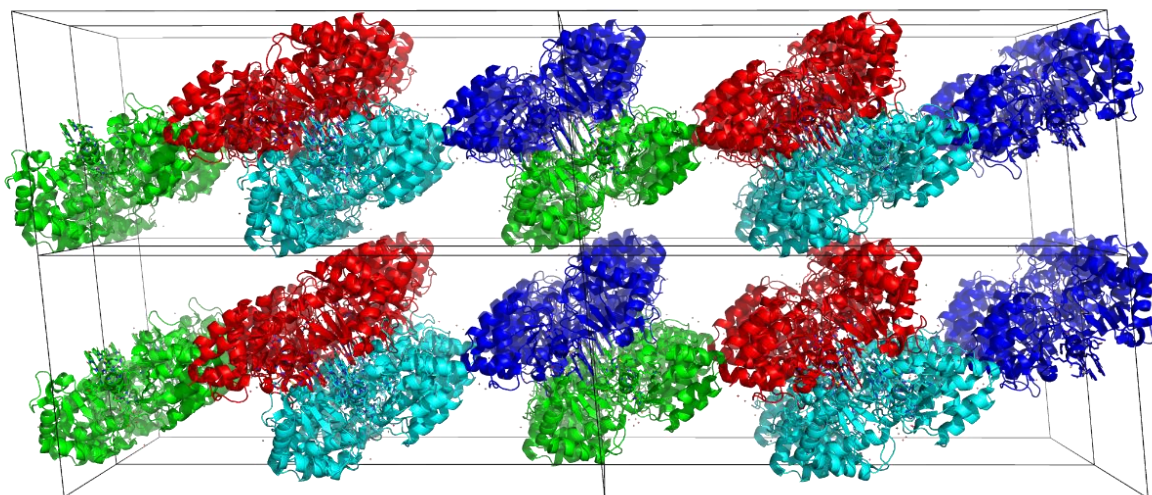


Figure S12. The crystal lattice of the C-lobe and ligand **10** complex. The asymmetric units in the unit cells are shown in green, red, cyan, and blue.

Figure S13

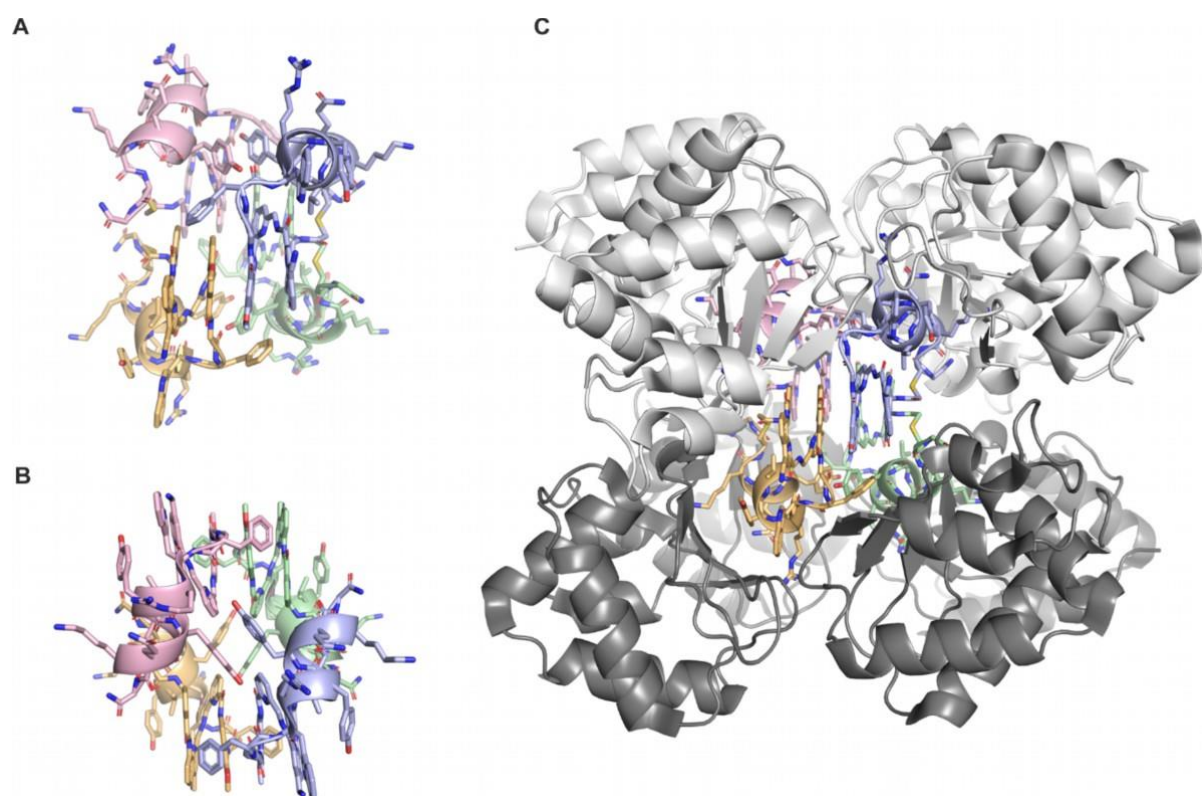
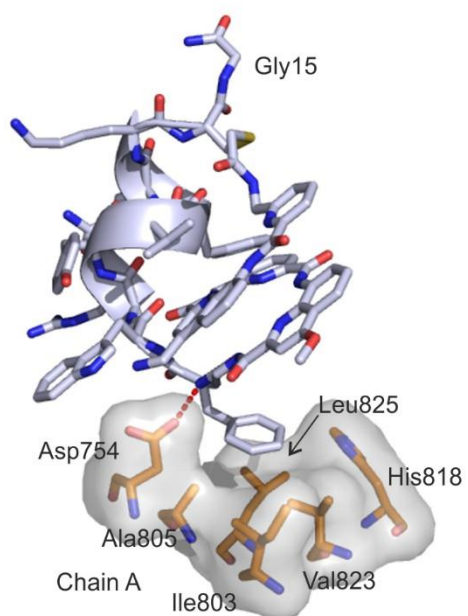


Figure S13. Crystal packing of the C-lobe and ligand **10** complex. Two views of a cluster of four macrocycles **10** showing stacking between (A) foldamers and (B) between Tyr11 residues. C) Cube formed by eight C-lobe proteins surrounding the cluster of four macrocycles.

Figure S14

A



B

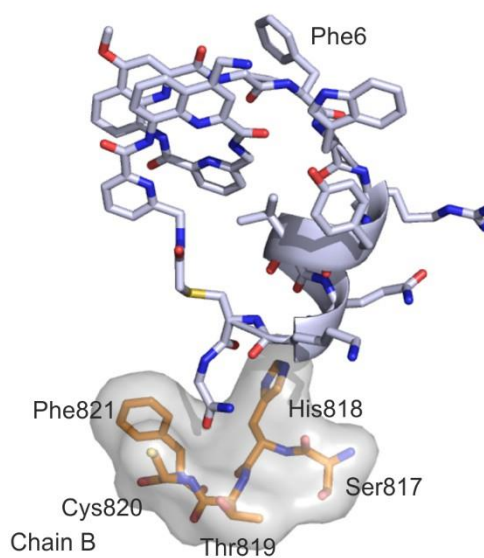


Figure S14. Representation of the contacts between the residues Phe6 and Gly15 in **10** and the C-lobe surface of chains A and B in the asymmetric unit, respectively.

Figure S15

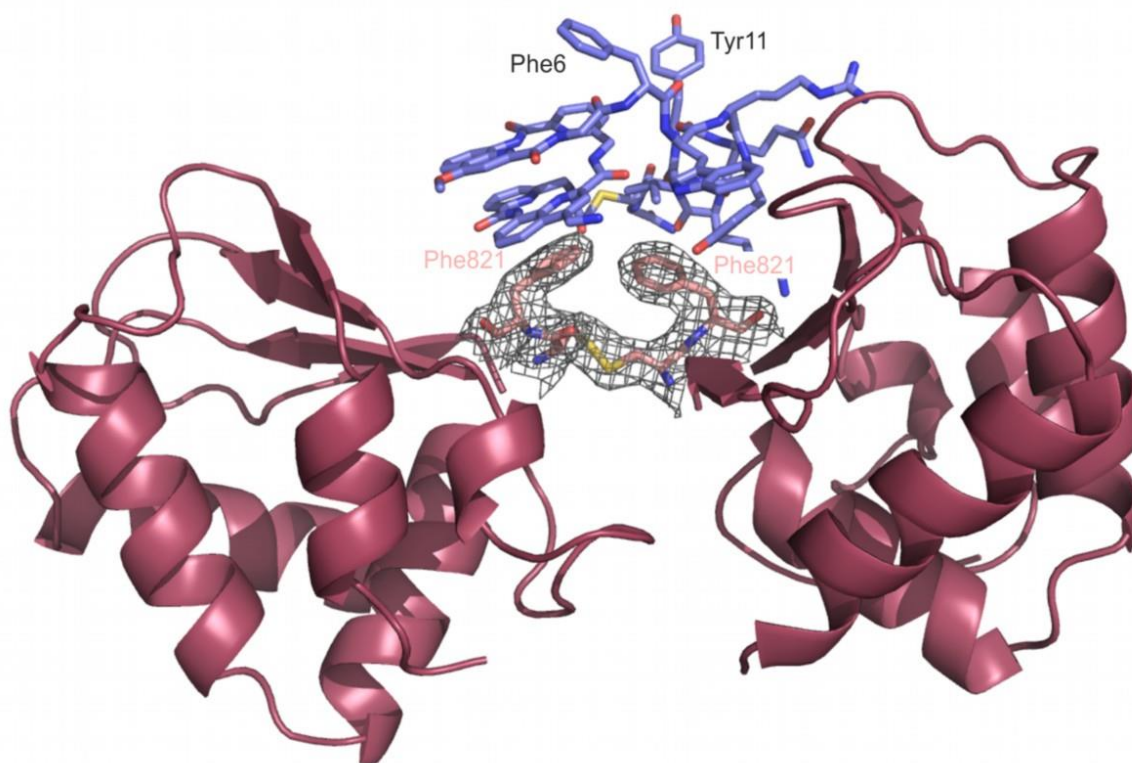


Figure S15. The disulfide bridge between Cys820 of chain C and Cys820 of the symmetry-related chain A' (right) in the crystal packing. The stacking of Phe821 (chain A') and foldamer units of the macrocyclic ligand **10** prevents binding of a second macrocycle on the cognate site of A' and promotes the 2:1 protein-ligand stoichiometry in the crystal. The Cys820 and Phe821 amino acid residues are shown with the 2Fo-2Fc electron density map at 1.0 σ for the disulfide.

Figure S16

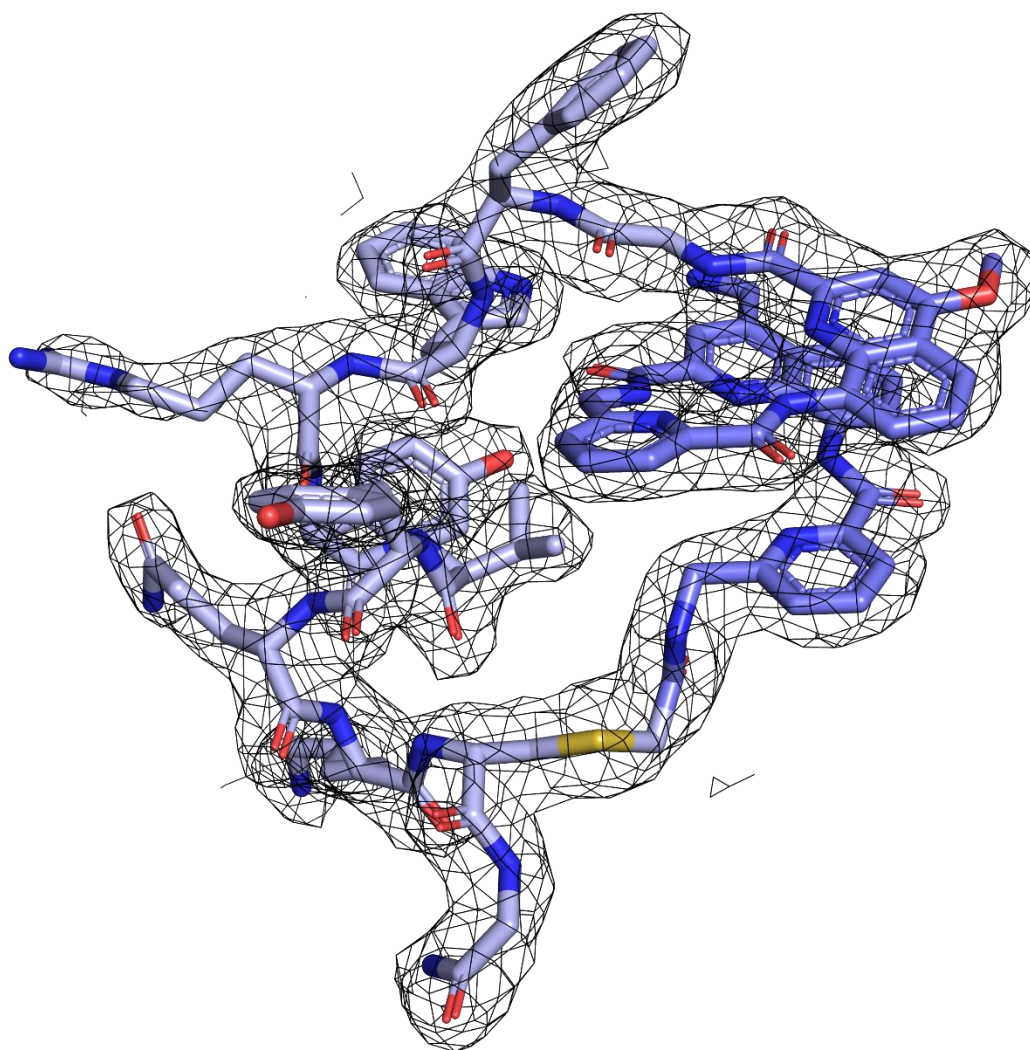


Figure S16. The weighted 2Fo-Fc electron density maps (black mesh) for the bound ligand **10** in the crystal structure are shown contoured at 1.0 σ .

Figure S17

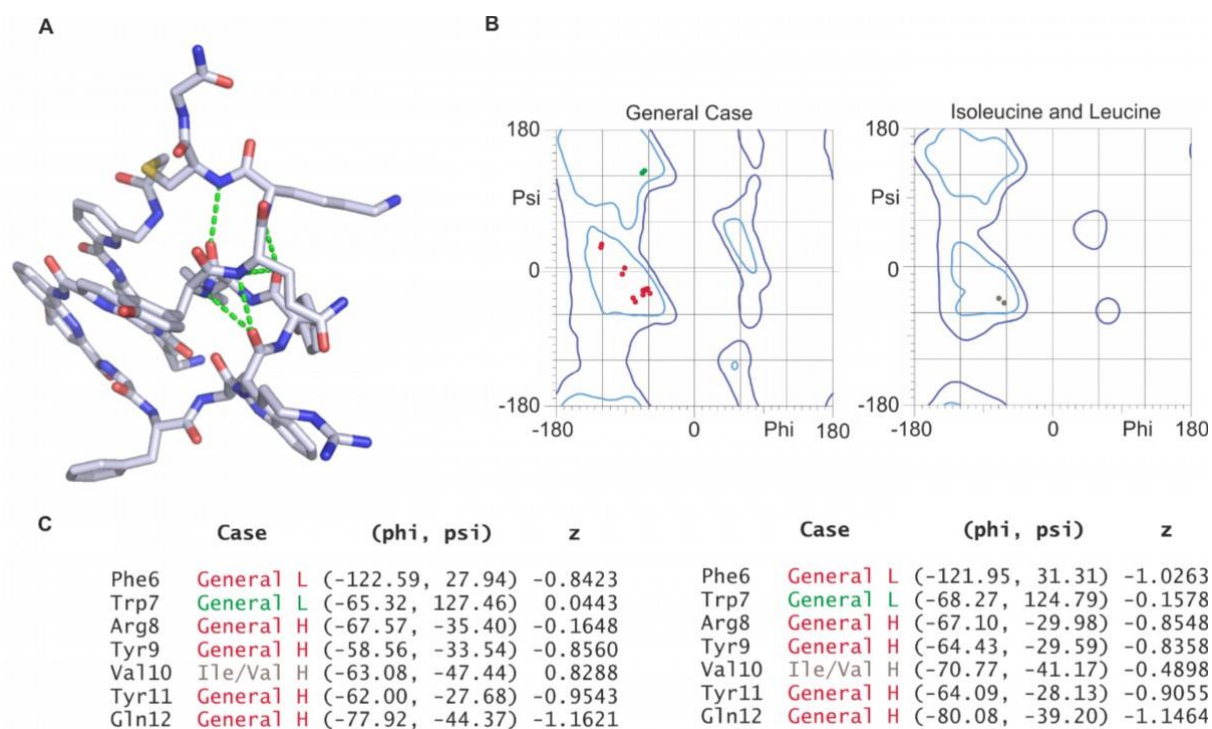


Figure S17. a) Intramolecular hydrogen bond network of the α -helix in **10**; B) Ramachandran plots obtained from MolProbity and C) Tables of Phi, Psi and Z data for each of the residues involved in the α -helix conformation and corresponding to the two hybrid molecules of **10** present in the asymmetric unit.

Figure S18

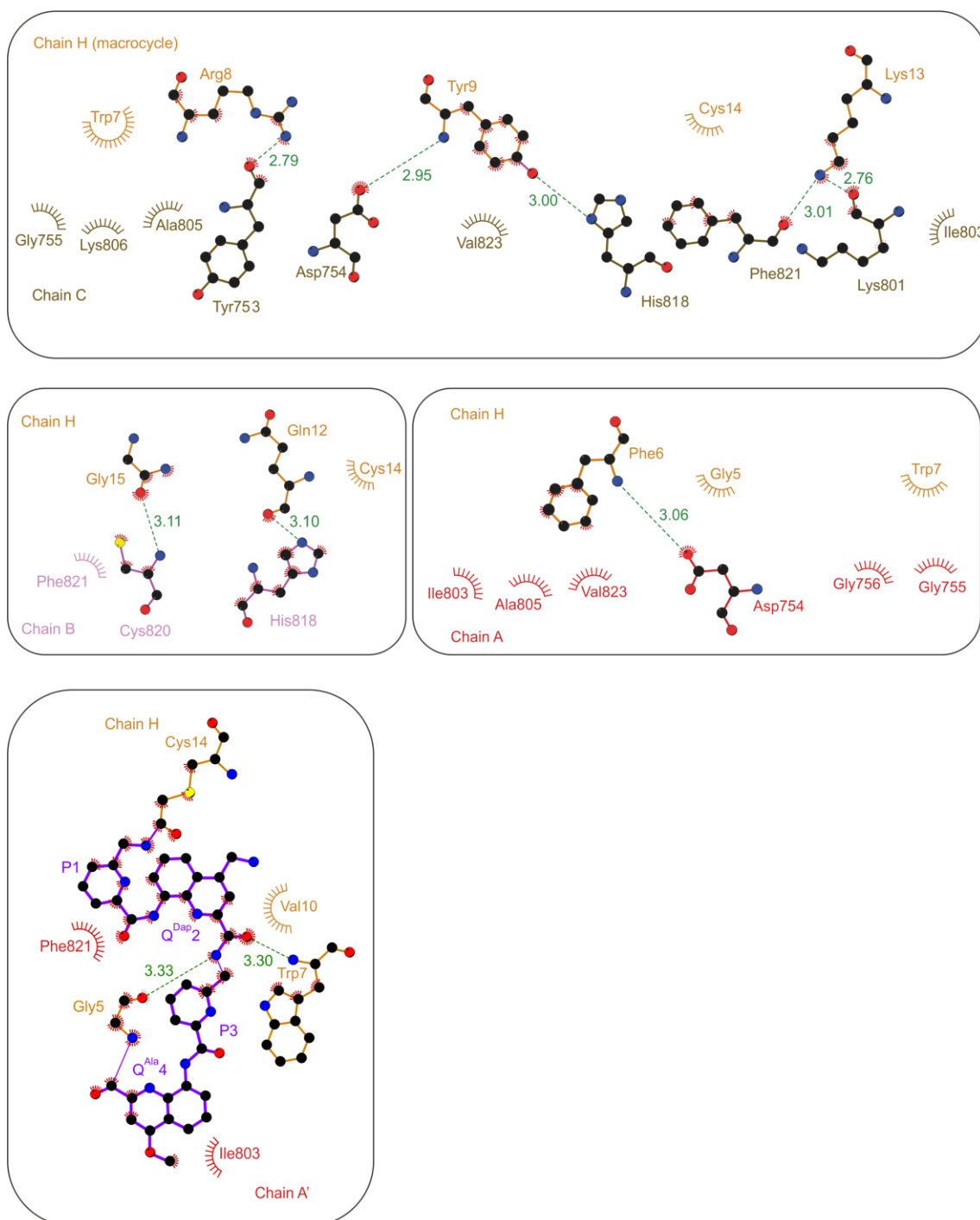


Figure S18. LigPlot representation of the crystal contacts between macrocycle **10** (chain H) and four distinct C-lobe protein chains (chains A, A', C and B). The top panel shows contacts between protein residues of chain C and the peptide residues that were converged during the display selection, constituting a binding area of 396 Å². The middle left panel show contacts between protein residues of chain B and the Gly15, Gln12, and Cys14 residues of the ligand, contact area of 5 Å². The middle right panel shows contacts between protein residues of chain A and Phe6, Gly5, and Trp7 of the ligand, contact area of 201 Å². The bottom panel shows interactions between the chain A' and the ligand **10**, contact area of 173 Å². The plots were generated using LigPlot v.14.5 software and the 7QP B PDB file.^[3]

Figure S19

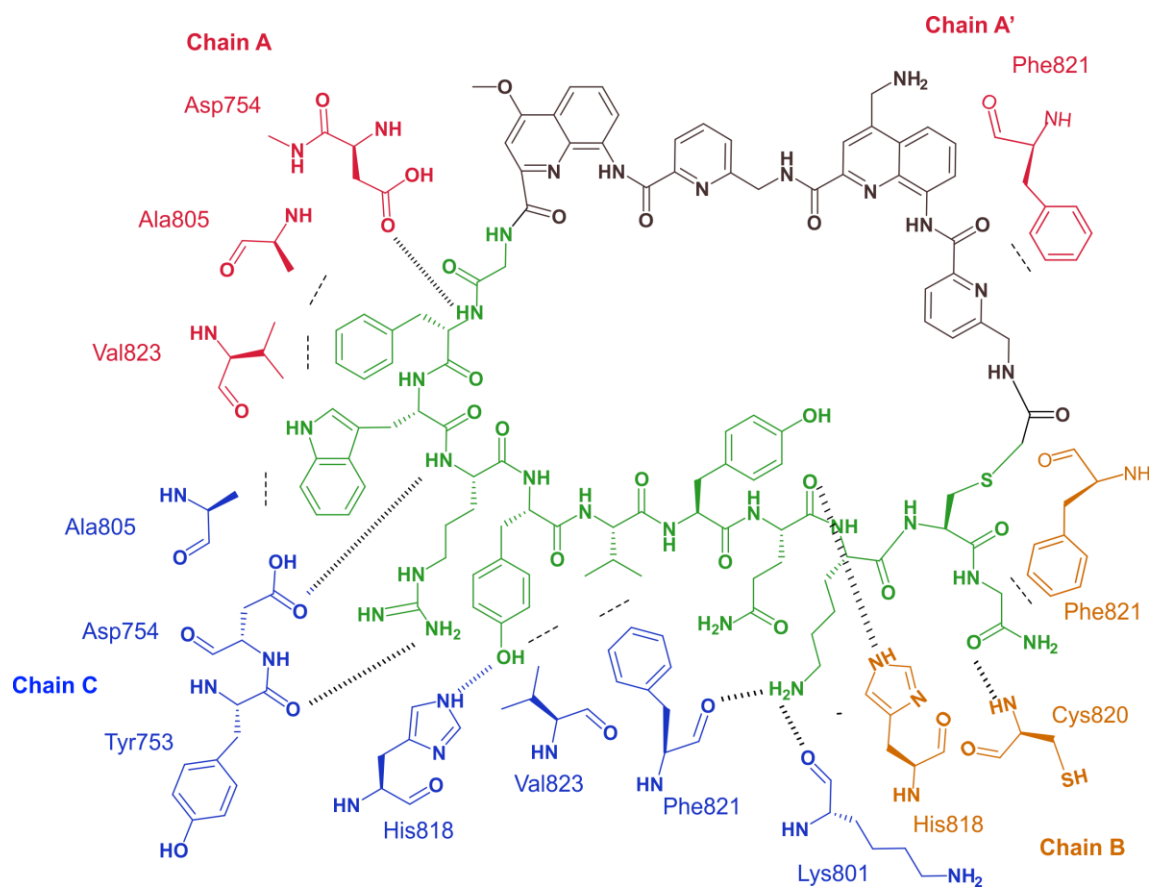


Figure S19. Overview of contacts between macrocycle **10** (chain H) and four C-lobe protein chains of the crystal lattice (A, A', B, C). The actual macrocycle binding site is on chain C. For more details, see **Figure S18**.

Figure S20

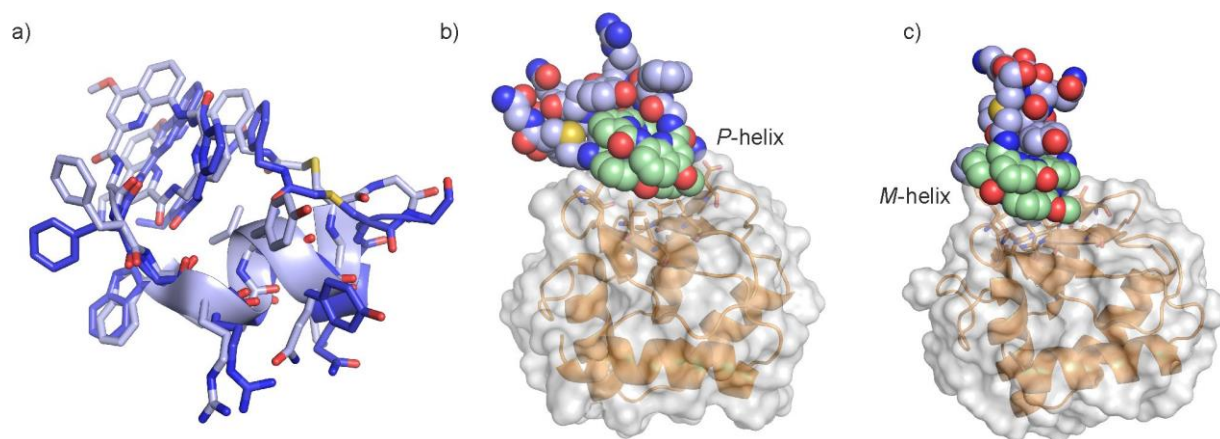


Figure S20. a) Overlay of **10** with a *P*-helical foldamer as found in complex with C-lobe in the crystal structure (dark blue) and of **10** with an *M*-helical foldamer as found in a snapshot of an MD simulation of its complex with C-lobe (gray). b) Snapshot of an MD simulation of **10** with a *P*-helical foldamer (green) showing a binding mode where the foldamer is in contact with the protein. c) Snapshot of an MD simulation of **10** with an *M*-helical foldamer (green) showing a binding mode where the foldamer is in contact with the protein.

Figure S21

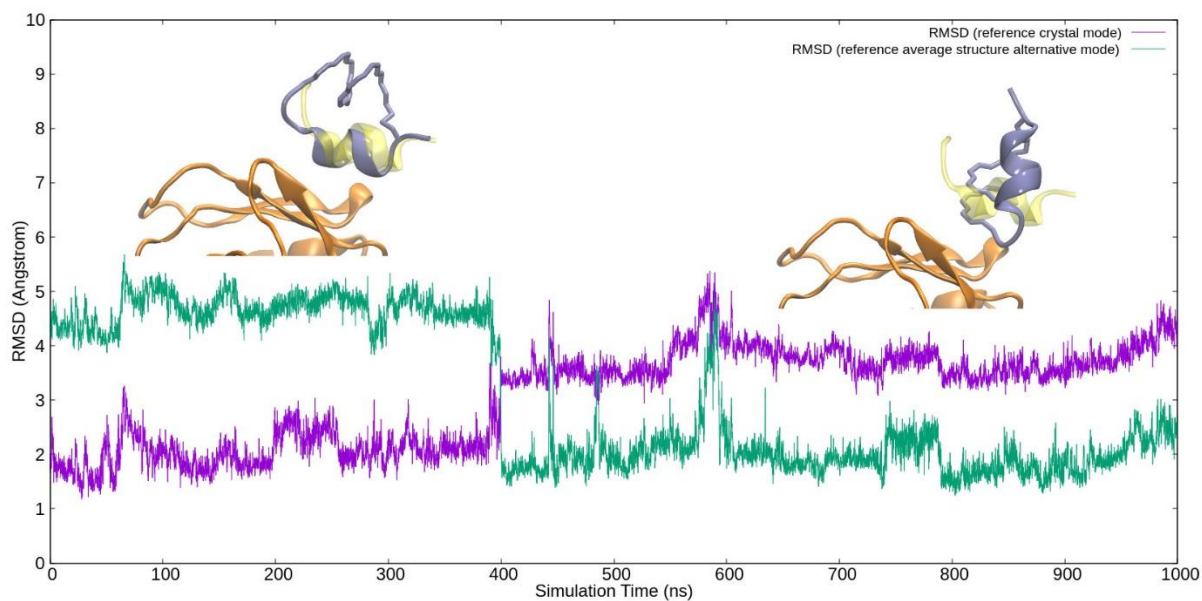


Figure S21. Root mean square displacement (RMSD) along a 1000 ns MD simulation trajectory for a *M 10* with C-lobe complex. Purple line is RMSD with respect to the crystal structure (C-lobe and α -helix backbone atoms included in RMSD calculation). Green line is RMSD with respect to an average structure of all conformations in the alternative binding mode (as shown in **Figure 4c** of the main text, C-lobe, α -helix and foldamer backbone atoms included in RMSD calculation). Two snapshots represent the structures of crystal mode (left) and alternative mode (right, with foldamer helix in contact with the protein), in which the α -helix in crystal structure is shown in a transparent yellow representation as reference.

Figure S22

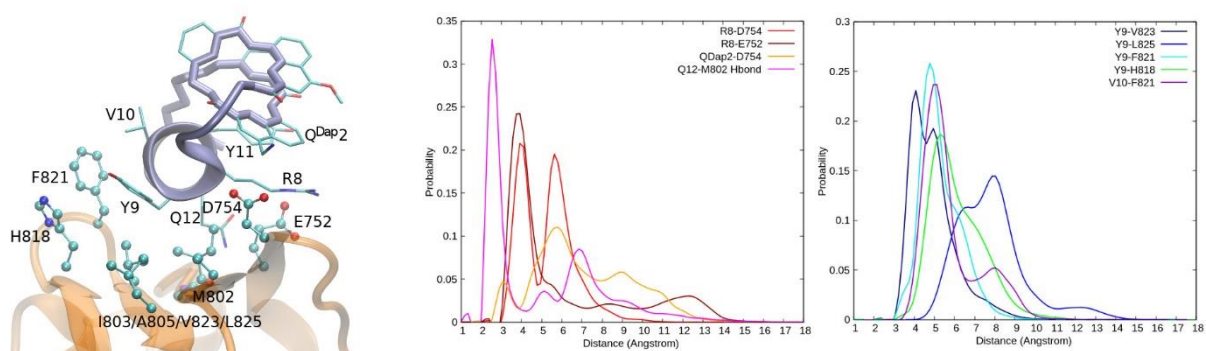


Figure S22. Snapshot and distance histograms for the *M 10*-C-lobe complex at the binding mode similar to the crystal structure. Left: Representative snapshot. Middle: Salt bridge and hydrogen bond (Hbond) distance histograms, in which the side chain N atom in Q^{Dap2} and guanidinium C atom in Arg8 of the macrocycle, and the carboxylate C atoms in Glu752 or Asp754 of C-lobe are used in the distance calculation. Hbond distance is between Gln12 side chain N of the macrocycle and Met802 backbone O atom of C-lobe. Right: Distance histograms for other contacts, in which the centers of masses of hydrophobic side chain groups of C-lobe (Val823, Leu825, Phe821, His818) and the macrocycle (Tyr9, Val10) are used in calculating the residue-residue distance. The probability of occurrence is normalized by the total number of conformations in this binding mode.

Figure S23

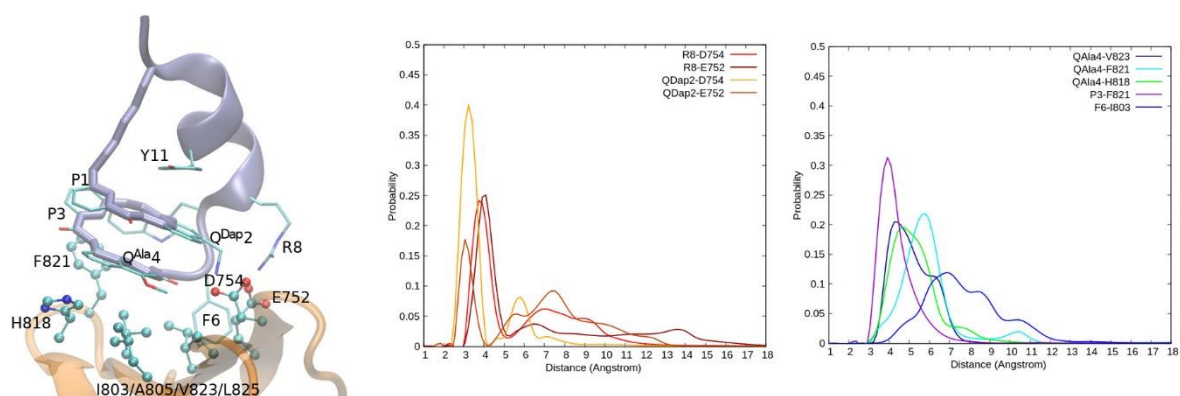


Figure S23. Snapshot and distance histograms for the *M* 10-C-lobe complex at an alternative binding mode as shown in **Figure 4c** in the main text. Left: Representative snapshot. Middle: Salt bridge distance histograms, in which the side chain N atom in Q^{Dap} and guanidine C atom in Arg8 of the macrocycle, and the carboxylate C atoms in Glu752 or Asp754 of C-lobe are used in the distance calculation. Right: Distance histograms for other contacts, in which the centers of masses of hydrophobic side chain groups of C-lobe (Val823, Phe821, His818, Ile803) and of the macrocycle (Q^{Ala}4, P3, Phe6) are used in calculating the residue-residue distance. The probability of occurrence is normalized by the total number of conformations in this binding mode.

Figure S24

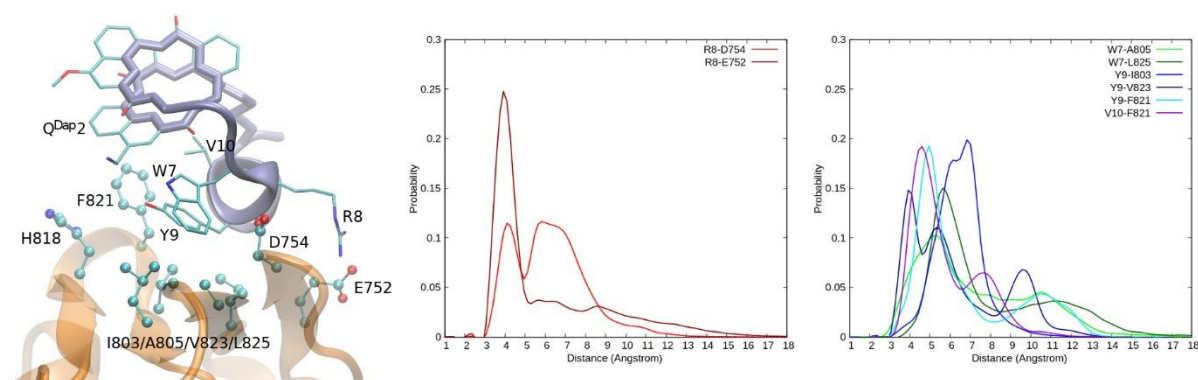


Figure S24. Snapshot and distance histograms for the *P* 10-C-lobe complex at the binding mode resembling the crystal structure. Left: Representative snapshot. Middle: Salt bridge distance histograms, in which the guanidine C atom in Arg8 of the macrocycle and the carboxylate C atoms of Glu752 or Asp754 are used in the distance calculation. Right: Distance histograms for other contacts, in which the centers of masses of hydrophobic side chains of C-lobe (Ile803, Ala805, Val823, Leu825, Phe821) and of macrocycle residues (Trp7, Tyr9, Val10) are used in calculating the residue-residue distance. The probability of occurrence is normalized by the total number of conformations in this binding mode.

Figure S25

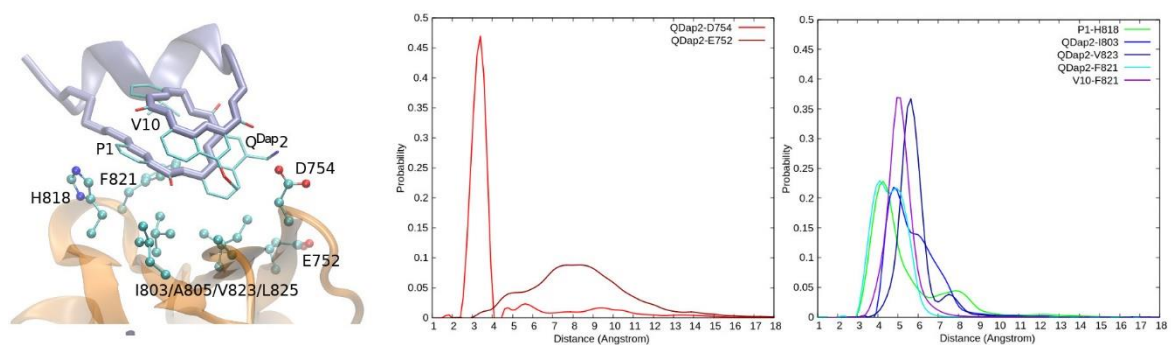


Figure S25. Snapshot and distance histograms for the *P 10*-C-lobe complex at an alternative binding mode as shown in **Figure 4d** in the main text. Left: Representative snapshot. Middle: Salt bridge distance histograms, in which the side chain N atom in Q^{Dap} and the carboxylate C atoms in Glu752 or Asp754 are used in the distance calculation. Right: Distance histograms for other contacts, in which the centers of masses of hydrophobic side chain groups of C-lobe (Ile803, Val823, His818, Phe821) and foldamer residues (P1, Q^{Dap2} , Val10) are used in calculating the residue-residue distance. The probability of occurrence is normalized by the total number of conformations in this binding mode.

Figure S26

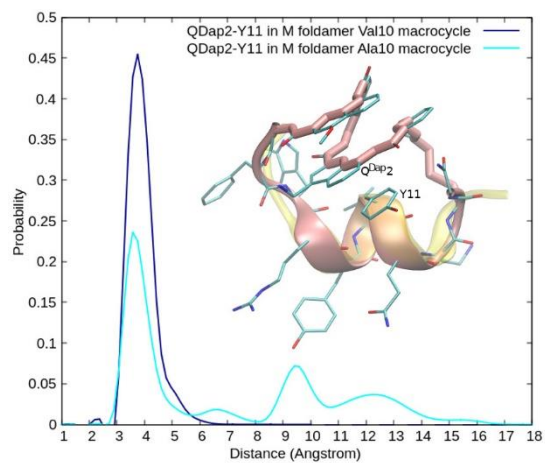


Figure S26. Histogram of the distance between COMs of aromatic rings of Q^{Dap2} and Tyr11 for *M* 10 foldamer macrocycles. The insert in the graph is a snapshot showing stacking of Tyr11 and Q^{Dap2} in the *M* Foldamer macrocycle. All MD trajectories are included (i.e. including all binding modes).

Figure S27

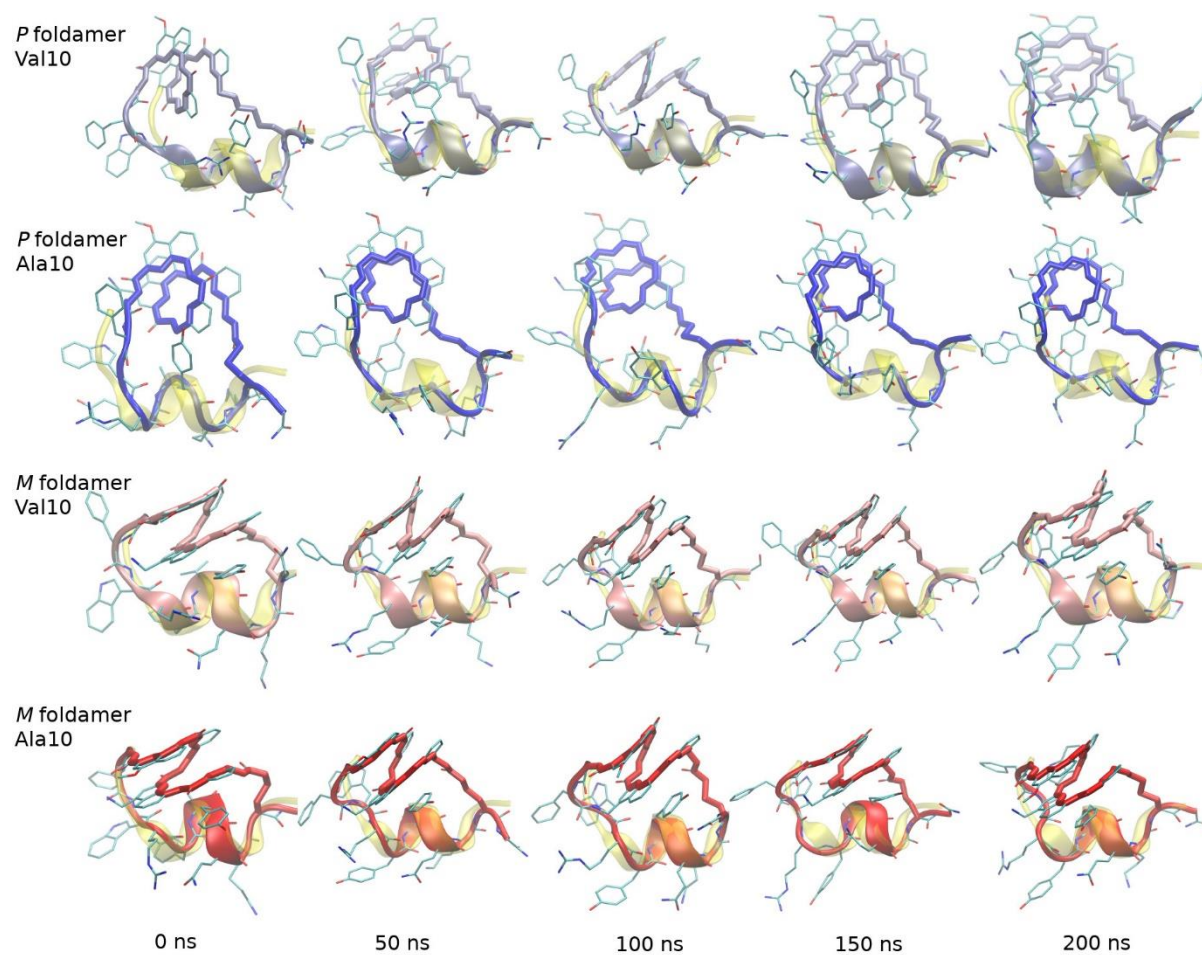


Figure S27. Snapshots of **10** in the first 200ns with C-lobe removed for clarity on macrocycle structures. The α -helix in transparent yellow is the crystal structure, used here as a reference.

9.2. Biochemistry and Structural Biology

Materials and general methods

All chemicals were purchased from Sigma-Aldrich at molecular biology grade or higher unless otherwise indicated. The pET28a(+) vector containing isoform I of human E6AP₇₄₁₋₈₅₂ (“C-lobe”) with an N-terminal HRV3C protease-cleavable His₆-tag^[4] (sequence and plasmid map: **Figure S4**) was a kind gift from Dr. Sonja Lorenz (Max Planck Institute for Biophysical Chemistry) and sequence fidelity was confirmed by Sanger sequencing. One Shot™ BL21(DE3) Chemically Competent *E. coli* (C600003) and HisPur™ Ni-NTA Superflow Agarose (25217) were purchased from ThermoFisher Scientific. Econo-Column® gravity flow columns (7372551) were purchased from BioRad. Color Prestained Protein Standard (P7718S) was purchased from New England Biolabs.

Exclusively ultrapure water from an OmniaTap system (Stakpure) was used. Bacterial culture media and equipment were sterilized by autoclaving. Bacterial cultures were grown using a MaxQ-6000 shaking incubator (ThermoFisher Scientific). UV-Vis determination of protein concentration (280 nm), protein purity (260/280 nm), and OD₆₀₀ were all measured on a NanoDrop™ One^C (ThermoFisher Scientific). Bacterial centrifugation was carried out on an Avanti JXN-26 Centrifuge (Beckman Coulter) using a JLA-8.1000 or JA-25.50 rotor. Probe sonication was carried out on a UP200St Ultrasonic Processor fitted with a S26d14 Sonotrode (Hielscher Ultrasonics) using 5 cycles of 2 min on (100% amplitude, 90% pulse) and 5 min rest.

Sodium-dodecyl sulfate-polyacrylamide gel electrophoresis (SDS-PAGE) was carried out on a BioRad system, including a PowerPac™ HC High-Current Power Supply and a Mini-PROTEAN® Tetra Vertical Electrophoresis Cell. 2× 10-, 12-, or 15-well gels with a 15% resolving gel and 4% stacking gel were prepared as follows:

Reagent	Resolving gel (15%)	Stacking gel (4%)
H ₂ O	3.625 mL	3.25 mL
Resolving/Stacking Buffer (SureCast, Thermo)	2.5 mL	1.25 mL
Acrylamide 30% (SureCast, Thermo)	3.75 mL	0.5 mL
Ammonium Persulfate (10% (w/v) in H ₂ O)	100 µL	25 µL
<i>N,N,N',N'</i> -tetramethylethylenediamine (TEMED)	10 µL	5 µL

Gel samples were prepared by mixing 3:1 with sample loading buffer (4×: Tris-HCl (200 mM) pH 6.8, bromophenol blue (0.04% (w/v)), glycerol (24% (v/v)), SDS (8% (w/v)), β-mercaptoethanol (20% (v/v))) and boiling for 10 min. Gels were run at 85 V for 10 min then 180 V for 50 min and stained with Coomassie Brilliant Blue.

Size-exclusion chromatography (SEC) was carried out in a cold cabinet (Unichromat 1500) maintained at 15 °C on a custom Knauer fast protein liquid chromatography (FPLC) system coupled with a HiLoad® 16/600 Superdex® 75 pg column (Cytiva, 28989333). The column eluent was monitored by UV detection at 200, 220, 260, and 280 nm with a diode array detector and fractions were collected by a Foxy R1 Fraction Collector (Teledyne ISCO). Protein concentration and buffer exchange were performed using spin concentrators of various volume capacities (Amicon, 3 kDa MWCO) according to manufacturer’s instructions. Dialysis was performed using 3 kDa MWCO Slide-A-Lyzer™ G2 dialysis cassettes of various volume capacities (ThermoFisher Scientific) according to manufacturer’s instructions.

Protein expression and purification

Isoform I of human E6AP_{741–852} (“C-lobe”) was expressed from a pET28a(+) vector with an N-terminal HRV3C protease-cleavable His₆-tag (**Figure S4**). The protein was expressed recombinantly from *E. coli* BL21(DE3) cells overnight at 18 °C in LB broth supplemented with kanamycin (50 µg mL⁻¹; Janssen) and induced at an OD₆₀₀ of 0.6 with isopropyl-β-D-1-thiogalactopyranoside (IPTG, 0.5 mM). All subsequent steps were performed at 4 °C where possible. The cells were harvested by centrifugation (7,548 × g, 20 min), resuspended in lysis buffer (17.5 mL per 1 L culture; 50 mM Tris-HCl, pH 8.0, 100 mM NaCl, 5 mM imidazole, 1 mM DL-dithiothreitol (DTT), 0.1% (v/v) Triton X-100, 4% (v/v) glycerol), and lysed by probe sonication. The lysate was cleared by centrifugation (43,667 × g, 40 min) and incubated for 30 min with pre-equilibrated HisPur™ Ni-NTA Superflow Agarose (~2.5 mL slurry per 1 L culture). The agarose resin was applied to a gravity column, washed with wash buffer (100 mL; 50 mM Tris-HCl, pH 8.0, 400 mM NaCl, 5 mM imidazole, 1 mM DTT), and His₆-tagged protein eluted with elution buffer (50 mM Tris-HCl, pH 8.0, 400 mM NaCl, 250 mM imidazole, 1 mM DTT) by monitoring the absorption of the eluent at 280 nm. The purity of the eluent was determined by SDS-PAGE.

For isolation of protein with its associated His-tag, the eluate from the Ni-NTA column was further purified by SEC at a flow rate of 0.3–0.8 mL·min⁻¹ in SEC buffer (50 mM Tris-HCl, pH 7.4, 150 mM NaCl, 1 mM DTT) over Superdex 75 pg. Fractions corresponding to the protein of interest were analysed by SDS-PAGE for purity, combined, and concentrated.

For isolation of protein without its associated His-tag, the eluate from the Ni-NTA column was digested overnight by addition of HRV3C protease (Merck 71493; 20U per 1 mL crude protein) during dialysis into SEC buffer at 4 °C. The digested protein was incubated with Ni-NTA agarose as described above and eluted from the column with SEC buffer. The eluate was concentrated and purified further by SEC as described above.

In vitro translation

Preparation of eFx and tRNA^{fMet}_{CAU}

All oligonucleotides were purchased from Operon (Japan). DNA templates were assembled using reported protocols and after transcription, using T7 RNA polymerase, they resulted in the desired sequences.^[5–8]

Microhelix

Microhelix RNA (mhrRNA) was purchased from GeneDesign (Japan), being a mimic of the acceptor stem of tRNA (the site of aminoacylation), originally based on the acceptor stem of *E. coli* Asn tRNA.

Aminoacylation of mhrRNA

3 µL H₂O, 1 µL mhrRNA (250 µM), 1 µL eFx (250 µM) and 1 µL HEPES-KOH pH 8.4 (500 mM) were mixed, heated to 95 °C for 2 min and cooled to room temperature for 5 min. 2 µL MgCl₂ (3 M) was added and left for 5 min at room temperature. Solution was placed on ice until cold and the aminoacylation was initiated by adding 2 µL cyanomethyl substrate (25 µM) in DMSO. Reaction was incubated on ice for 2–12 hours, depending on the substrate; final concentrations: 25 µM microhelix, 25 µM eFx and 5 mM cyanomethyl ester in 50 mM HEPES-KOH pH 8.4, 600 mM MgCl₂, 20% DMSO. The reaction was stopped by pelleting any insoluble substrate, collecting the substrate, adding 4 reaction volumes (40 µL) of 0.3 M NaOAc pH 5.2, and the product precipitated using 10 reaction volumes of EtOH (100 µL). The pellet was washed with 0.1 M NaOAc pH 5.2, 70% EtOH and

analyzed by 20% denaturing acid PAGE (50 mM sodium acetate, 6 M urea). The RNA was stained with ethidium bromide and analyzed on an FLA-5100 (Fuji, Japan) and results are shown in **Figure S1**.

Aminoacylation of tRNA^{fMet}_{CAU} with foldamer substrates

25 μ M tRNA^{fMet}_{CAU}, 25 μ M eFx and 5 mM cyanomethyl ester substrate were incubated in 50 mM HEPES-KOH pH 8.4, 600 mM MgCl₂ in 20% DMSO using the time originating from the “Aminoacylation of mhRNA” for each substrate (**Figure S1**).

Model mRNA templates (encoding for fMGGGTYT-flag & fMYAATAACA-flag)

The following primers were purchased by Eurofins genomics (Japan):

Template encoding for fMYAATAA-flag

P1: GCGTAATACGACTCACTATAG

P2: TAATACGACTCACTATAGGGTTAACTTTAAACAAGGAGAAAAACATGTAC

P3:

CGTCGTCGTCCTTGTAGTCAGCACAAAGCAGCGGTAGCAGCGTACATGTTTTCTCCTTGTTAAAG

P4: CGAAGCTTACTTGTCGTCGTCGTCCTTGTAGTC

Template encoding for fMGGGTYTCA-flag

P1: GCGTAATACGACTCACTATAG

P2': TAATACGACTCACTATAGGGTTAACTTTAAACAAGGAGAAAAACATGGGC

P3': CGTCGTCGTCCTTGTAGTCGTCGTCGTCGTCGTCCTTGTTAAAG

P4: CGAAGCTTACTTGTCGTCGTCGTCCTTGTAGTC

P2^(') was annealed with P3^(') and extended using *Taq* DNA polymerase. The resulting product was diluted 200 times with PCR reaction buffer and amplified by using P1 and P4 as the 5'- and 3'-primers, respectively. The DNA product was transcribed by T7 RNA polymerase and purified by 10% denaturing PAGE. The mRNA template was dissolved in water and its concentration was adjusted to 10 μ M.

In vitro translation and MALDI-TOF-MS

A custom-made *in vitro* translation mixture was used, with the final concentrations of individual components: 1.2 μ M ribosome, 0.1 μ M T7 RNA polymerase, 4 μ g mL⁻¹ creatine kinase, 3 μ g mL⁻¹ myokinase, 0.1 μ M pyrophosphatase, 0.1 μ M nucleotidediphosphatase kinase, 2.7 μ M IF1, 0.4 μ M IF2, 1.5 μ M IF3, 30 μ M EF-Tu, 30 μ M EFTs, 0.26 μ M EF-G, 0.25 μ M RF2, 0.17 μ M RF3, 0.5 μ M RRF, 0.6 μ M MTF, 0.73 μ M AlaRS, 0.03 μ M ArgRS, 0.38 μ M AsnRS, 0.02 μ M CysRS, 0.06 μ M GlnRS, 0.23 μ M GluRS, 0.09 μ M GlyRS, 0.02 μ M HisRS, 0.4 μ M IleRS, 0.04 μ M LeuRS, 0.03 μ M MetRS, 0.68 μ M PheRS, 0.16 μ M ProRS, 0.04 μ M SerRS, 0.09 μ M ThrRS, 0.03 μ M TrpRS, 0.02 μ M ValRS, 0.13 μ M AspRS, 0.11 μ M LysRS, 0.02 μ M TyrRS. Additionally, 50 mM HEPES-KOH (pH 7.6), 100 mM potassium acetate, 2 mM GTP, 2 mM ATP, 1 mM CTP, 1 mM UTP, 20 mM creatine phosphate, 12 mM Mg(OAc)₂, 2 mM spermidine, 2 mM DTT, and 1.5 mg mL⁻¹ *E. coli* total tRNA (Roche).

- For MALDI-TOF analysis (**Figure S2**): 5 of the 20 canonical amino acids were included at 500 μ M, including Met, Asp, Tyr, Lys and Ala. Solutions containing the above plus 1.5 μ M mRNA template and 25 μ M foldamer-tRNA^{Pro1E2}_{GGU} (prepared using eFx, above) were incubated for 30 min at 37 °C. The foldamer-peptide hybrid was isolated using anti-FLAG M2 affinity agarose gel (Sigma)

and eluted using 0.2% TFA. Solution was mixed, 1:1, with a half-saturated solution (80% MeCN, 19.5% H₂O, 0.5% AcOH) of α -cyano-4-hydrocinnamic acid prior to spotting on a MALDI plate. Foldamer-peptide MALDI-TOF-MS analysis was performed by an UltrafleXtreme (Bruker Daltonics) in reflector/positive mode.

- For radioisotope quantification (**Figure S3**): 4 of the 20 canonical amino acids were included at 500 μ M: Met, Tyr, Lys and Ala. 50 μ M [¹⁴C]Asp was added. *In vitro* translation was carried out as above. Translation reactions were stopped by adding an equal volume of stop solution [0.9 M Tris-HCl (pH 8.45), 8% SDS, 30% glycerol and 0.001% xylene cyanol] and incubating at 95 °C for 2 min. Then, the samples were analyzed by 15% tricine SDS-PAGE and autoradiography analyzed using a Typhoon FLA 7000 imager (GE Healthcare). Peptide yield was normalized by intensity of [¹⁴C]Asp band. Note that FLAG-tag purification is not carried out during this experiment.

RaPID selection protocol

Two RNA libraries, consisting of 4–9 and 10–15 NNK codons, were prepared as previously described.^[9] Briefly, RNA molecules were synthesized by T7 RNA polymerase reactions from DNA templates assembled by PCR and purified by PAGE. Furthermore, puromycin-linked mRNA was prepared by incubation with puromycin-linked oligonucleotide and T4 RNA ligase and was purified by phenol/chloroform extraction and ethanol precipitation. Oligonucleotides for both libraries and puromycin-linked oligonucleotide were previously reported.^[10]

Ribosomal synthesis of the macrocyclic peptide libraries was performed as previously described.^[9] In brief, for the initial selection, 1.2 mM puromycin-linked mRNA library was translated in a Met-deficient FIT reaction containing 25 mM of 7-tRNA_{fMet} for 30 min at 37 °C. The reaction was incubated at 25 °C for 12 min before disruption of the ribosome–mRNA complex by incubation at 37 °C for 30 min in the presence of 20 mM EDTA. The resulting peptide-linked mRNAs were then reverse-transcribed using RNase H-reverse transcriptase (Promega) for 1 h at 42 °C. The mixture was desalted by means of Sephadex G-25. Subsequently, brief passage of the reaction over His-Tag Dynabeads (Life Technologies) thrice was carried out to remove translation proteins from the library. Affinity screening was performed by three serial passages (counterselections, 30 min each at 4 °C) of the library over His-Tag Dynabeads (Life Technologies), followed by affinity selection against 200 nM His₆-C-lobe immobilized on the same beads for 30 min at 4 °C. cDNA was eluted from the beads by heating to 95 °C for 5 min and fractional recovery from the final counterselection (negative control) and affinity selection step were assessed by quantitative PCR using Sybr Green I on a LightCycler thermal cycler (Roche) and results are shown in **Figure 2d** and **Figure S5**. Enriched DNA libraries were recovered by PCR and used as input for transcription reactions to generate the mRNA library for the subsequent round of screening. After five iterative rounds of library synthesis, affinity selection, and recovery, the final DNA library was sequenced to identify C-lobe binders.

For high-throughput sequencing of the selections carried out, DNA samples were PCR-amplified with nesting primers,^[10] purified using a Nucleospin column (Machery-Nagel), and sequenced using a MiSeq high-throughput sequencer (Illumina). Data analysis was performed using CLC sequence viewer 8 software (Qiagen). Results for the top 20 hits from each library are shown in **Figure S6**, and for the top 50 hits is shown in **Extended Data 1**.

Clone assay: In this experiment we demonstrate the effect of the foldamer initiator on the binding to the protein modified beads, for the two different library sizes. mRNA sequences encoding for the top hits from the sequencing data underwent an additional round of selection. Peptides, linked to their

genotype, were exposed sequentially to unmodified (Neg) and protein-modified (Pos) beads and recovery was again determined by qPCR in a manner similar to the selection experiment. In a subsequent experiment, the abiotic initiator was substituted with Trp (capable of undergoing cyclization) and the resulting peptides were treated as their “abiotic” counterparts. The results are shown in **Figure 2d** and **Figure S7**.

Circular dichroism (CD)

CD data were recorded on a Jasco J-810 spectrometer with 1 or 2 mm quartz cuvette. Exact experimental parameters, including sample solvent conditions, path length, and other machine settings, and all data and subsequent calculations, are described sample by sample in **Extended Data 2**. The exact concentration of macrocycle **10** in each sample was determined by taking the average absorbance value between 374.8–375.2 nm (\bar{A}_{375}) and applying it to the Beer-Lambert law:

$$[\mathbf{10}] (\mu\text{M}) = \frac{\bar{A}_{375} \cdot 10^6}{\varepsilon_{375} \cdot l}$$

Where ε_{375} is the extinction coefficient at 375 nm contributed by the Q monomers as previously reported ($2 \times 2,678 \text{ M}^{-1} \text{ cm}^{-1}$), and l is the path length (cm) of the cuvette. The raw CD data in millidegrees (mdeg) was converted to molar extinction per number of quinoline (Q) residues ($\Delta\varepsilon$) by the following equation:

$$\Delta\varepsilon (L \text{ mol}^{-1} \text{ cm}^{-1} Q_{res}^{-1}) = \frac{mdeg}{[\mathbf{10}] \cdot 10^{-6} \cdot l \cdot 32980 \cdot n_{Q_{res}}}$$

Where $n_{Q_{res}}$ is the number of Q residues in the compound.

Protein-macrocycle crystallization

For co-crystallisation of C-lobe with compound **10**, the solutions of these components were kept at 4 °C and pre-mixed as follows. HRV3C-cleaved C-lobe was buffer exchanged into NaN_3 (0.05% (v/v)) in H_2O , concentrated, and mixed (final concentration: 6.7 mg mL^{-1}) with 1.1 eq. compound **10** in H_2O . The mixture was centrifuged ($17,000 \times g$, 5 min, 4 °C) and the complex crystallized using the hanging drop technique in polyethylene glycol (PEG) 8,000 (7.2% (w/v)), sodium cacodylate (0.06 mM), $\text{Ca}(\text{OAc})_2$ (0.06 mM), pH 5.5 at 4 °C with a complex solution to reservoir solution ratio of 1:1. The plate-like crystals were mounted in nylon loops, cryoprotected with glycerol (15% (v/v)) and flash cooled in liquid nitrogen.

Data collection and structure refinement

X-ray diffraction data were collected at beamline ID23-1 of the European Synchrotron Radiation Facility (ESRF, Grenoble) on a Dectris Eiger2 X 16M detector.^[11] Data was processed using XDS package and the structure was solved by molecular replacement in Phase-MR using the C-lobe from the E6AP-UBCH7 complex as a search model (PDB ID: 1C4Z).^[12] The structure was further refined in iterative rounds of manual model building and refinement in Coot^[13] and Phenix.^[14] Jligand^[15] was used to produce restrain files for the foldamer-peptide hybrid, and the ligand was modelled into clearly feasible electron density map at the final stages of refinement. The structure was validated with MolProbity and deposited in the PDB under accession code 7QPB. The statistics of data collection and structure refinement are summarized in **Table S1**.

Table S1. Data collection and refinement statistics

Wavelength	
Resolution range	29.53 - 2.342 (2.426 - 2.342)
Space group	C 1 2 1
Unit cell	149.91 59.05 67.3 90 95.466 90
Total reflections	84596 (8078)
Unique reflections	24491 (2402)
Multiplicity	3.5 (3.4)
Completeness (%)	0.98 (0.97)
Mean I/sigma(I)	11.91 (1.91)
Wilson B-factor	50.30
R-merge	0.06614 (0.6111)
R-meas	0.07841 (0.7249)
CC1/2	0.998 (0.673)
CC*	0.999 (0.897)
Reflections used in refinement	24488 (2402)
Reflections used for R-free	1225 (120)
R-work	0.2152 (0.2840)
R-free	0.2632 (0.3344)
CC(work)	0.939 (0.770)
CC(free)	0.912 (0.679)
Number of non-hydrogen atoms	3753
macromolecules	3586
ligands	110
Protein residues	422
RMS(bonds)	0.015
RMS(angles)	1.05
Ramachandran favored (%)	98
Ramachandran allowed (%)	2.3
Ramachandran outliers (%)	0
Rotamer outliers (%)	0.26
Clashscore	3.31
Average B-factor	52.79
macromolecules	53.19
ligands	41.55

solvent	49.32
---------	-------

Statistics for the highest-resolution shell are shown in parentheses.

Fluorescence polarization

In an F-bottom, black 96-well plate (Greiner, 738-0026), a serial dilution in triplicate of the indicated protein was prepared in RaPID selection buffer (Tris-HCl (50 mM) pH 7.6, NaCl (150 mM), DTT (5 mM), Tween-20 (0.05% (v/v)), NaN₃ (0.05% (w/v))). Compound **11** or 5(6)-carboxyfluorescein (Sigma-Aldrich, 21877) was added to each well to a final concentration of 20 nM and a final well volume of 200 μ L. Buffer-only and fluorophore-only (no protein) controls were also included on the plate. The plates were incubated at 4 °C for a minimum of 30 min before measurement. Polarization data were measured on a TECAN Infinite M1000 Pro at ambient temperature with the following parameters: $\lambda_{\text{ex}} = 475$ nm (bandwidth = 5 nm), $\lambda_{\text{em}} = 525$ nm (bandwidth = 5 nm), gain/z-position calculated from well with highest protein concentration (**Extended Data 2**), flashes = 12, settle time = 50 ms, G-factor (calibrated from 1 nM fluorescein standard in 10 mM NaOH) = 1.084. For the calculation of K_d values, dose-response data were fit in OriginPro 2019b software to the quadratic 1:1 binding model^[16] using the following equation. Full data and fitting results can be found in **Extended Data 2**.

$$\text{Polarization} = \text{BOTTOM} + (\text{TOP} - \text{BOTTOM}) \left(\frac{([\mathbf{11}] + K_d + [P]) - \sqrt{(A_0 + K_d + [P])^2 - 4[\mathbf{11}][P]}}{2[\mathbf{11}]} \right)$$

Where $[P]$ is total protein concentration (μ M), *BOTTOM* is minimum polarization (mP, unbound), *TOP* is maximum polarization (mP, fully bound), K_d is the dissociation constant (μ M), and $[\mathbf{11}]$ is total **11** concentration (μ M), constrained to 0.02.

Surface plasmon resonance (SPR)

SPR assays were performed on a Biacore T200 (Cytiva) using a carboxymethyl dextran sensor chip pre-coated with streptavidin (SA Sensor Chip Series S; Cytiva). All experiments were carried out at a constant temperature of 25 °C in SPR analysis buffer (Tris-HCl (50 mM) pH 7.5, NaCl (150 mM), DTT (1 mM), NaN₃ (0.05% (w/v)), Tween-20 (0.05% (v/v))). Before immobilizing **12**, the chip was equilibrated by three injections of NaCl (1 M), NaOH (50 mM) at a flow rate of 10 μ L min⁻¹. Then **12** (10 nM) was injected at a flow rate of 10 μ L min⁻¹ for a total contact time of 240 s on flow cell 2. The chips were then washed by injecting NaCl (1 M), NaOH (50 mM), propan-2-ol (50% (v/v)). 170 response units (RU) of **12** were bound per flow cell. Analyses of the kinetics of interaction of His₆-C-lobe with **12** was performed at a flow rate of 30 μ L min⁻¹ in SPR analysis buffer at 25°C. Various concentrations of the His₆-C-lobe (0.073–1200 μ M), dissolved in running buffer, were passed over the flow cells for 420 s, and the complexes formed were allowed to dissociate for 600 s before the next cycle started. After each cycle, the surface was regenerated by injection of NaCl (2.5 M) for 30 s, followed by SDS (0.05% (w/v)) for 30 s at a flow rate of 30 μ L min⁻¹. Sensorgrams were recorded using the Biacore T200 Control Software 2.0.2 and analyzed with the Biacore T200 Evaluation Software 3.1. The surface of flow cell 1 was not coated and used to obtain blank sensorgrams for subtraction of the bulk refractive index background. The referenced sensorgrams were normalized to a baseline of 0. Peaks in the sensorgrams at the beginning and the end of the injection are due to the run-time difference between the flow cells for each chip. For the calculation of K_d values,

maximum response units for each sensorgram curve were plotted against concentration and fit in OriginPro 2019b software to the quadratic 1:1 binding model^[16] using the following equation, including a linear factor to account for non-specific binding and/or aggregation. Full data and fitting results can be found in **Extended Data 2**.

$$RU = BOTTOM + B[P] + (TOP - BOTTOM) \left(\frac{(A_0 + K_d + [P]) - \sqrt{(A_0 + K_d + [P])^2 - 4A_0[P]}}{2A_0} \right)$$

Where RU is SPR response units, $[P]$ is total protein concentration (μM), $BOTTOM$ is the minimum RU value (unbound), constrained to 0, TOP is the maximum RU value (fully bound) B is a linear coefficient, K_d is the dissociation constant (μM), and A_0 is a factor relating to total ligand concentration.

Molecular dynamics simulation setup

We carried out MD simulations on four macrocycle-C-lobe complexes. These are the two by two combinations of the M or P foldamer helix, with the α -helix or its V10A mutant. We built the initial structures of all four systems by adopting the positions and structures of C-lobe and α -helix in the crystal structure. The macrocycle with a foldamer helix was built using previously developed arylamide building blocks,^[17] in combination with amino acid residues, including a modified cysteine residue, with the AMBER20 software package.^[18] The α -helix structure (in both M and P macrocycles), as well as the P foldamer helix structure, were adjusted to reproduce and align with the crystal structure. Before solvation and equilibration, the foldamer helix also undergoes minimization while C-lobe and α -helix are kept fixed.

Each macrocycle-C-lobe complex was then solvated by explicit TIP3P water molecules in a periodic box measuring about 70 Å along each side. The ff14SB force field^[19] was used for amino acid residues. The general AMBER force field (GAFF),^[20] with improved torsional parameters,^[17] was used for the aromatic foldamer. Following a standard RESP^[21] charge fitting procedure, we also created a new cysteine unit with modified side chain to connect to the N-terminus of the foldamer helix. All systems were equilibrated using the same procedure involving minimization with solvent, heating and NPT simulation at 1 atm and 300K. Production runs using the NVT ensemble at 300K were then carried out for 500 to 1500 ns per run. For each system, 2-3 production runs were carried out in parallel using slightly different equilibrated structures (extracted at different times of the NPT equilibration run). The trajectories were then analyzed mainly using the cpptraj program in the AMBER20 package in terms of RMSD, distance, hydrogen bonding etc. as discussed.

Binding mode analysis

Binding mode analysis was carried out using a combination of visual inspection, RMSD calculations with respect to different reference structures (crystal structure or average structure of sections of trajectories with alternative binding mode), as well as analysis of specific residue to residue distances. **Figure S21** illustrates an example of a MD trajectory exhibits two binding modes. We then consolidated the conformations (*i.e.* sections of MD trajectories from all runs for the system) that belong to each binding mode for further analysis of the binding interactions. **Figure S22–S25** illustrate different binding modes found in the MD simulations of the P and M foldamer with Val10 α -helix macrocycle-C-lobe complexes. Residues that contribute to binding between macrocycle and C-lobe are shown and labelled specifically in the snapshot. Also shown in **Figure S22–S25** are distance histograms illustrating formation of salt bridges, as well as contacts between the aromatic and/or hydrophobic groups of the macrocycle and protein surface.

Role of Tyr11 in *M* foldamer macrocycles

The distance histogram in **Figure S26** clearly shows the persistent stacking of Tyr11 with Q^{Dap2} in the *M* foldamer macrocycle with Val10. The stacking is not so constant in the macrocycle with the V10A mutant.

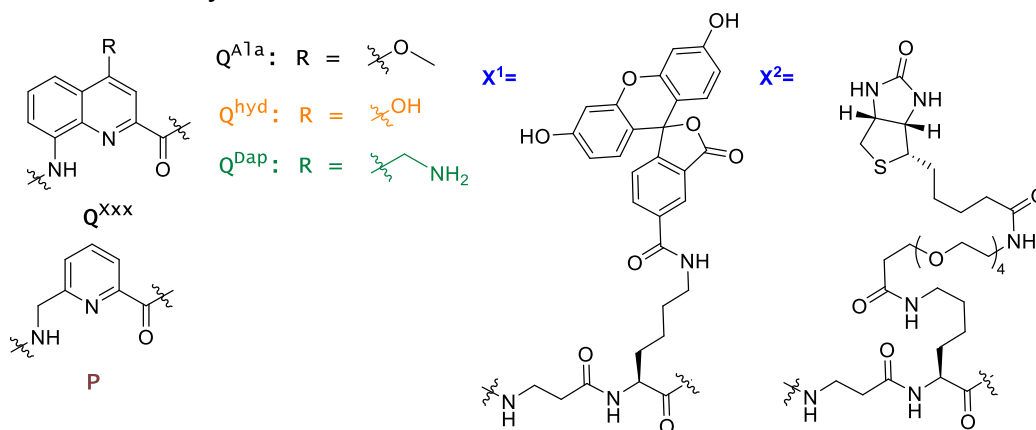
Destabilization of the α -helix in macrocycle with *P* foldamer and V10A mutation

Secondary structure analysis (**Table S2**) gives evidence on a significant destabilization of the α -helix (unwinding as shown in row 2 of **Figure S27**) upon the V10A mutation. For each 10-C-lobe, the analysis is carried out on all MD trajectories, thus including all binding modes. The fraction of helicity is based on average over time and all parallel runs of each system. The same mutation has a moderate effect on the *M* macrocycle helix.

Table S2. Fraction of helicity (3-10 and α -helix) obtained from residue by residue secondary structure analysis.^[22]

Macrocycles	<i>P</i> foldamer Val10 Total (3-10/ α)	<i>M</i> foldamer Val10 Total (3-10/ α)	<i>P</i> Foldamer V10A Total (3-10/ α)	<i>M</i> foldamer V10A Total (3-10/ α)
Trp7	0.01 (0.01/0.00)	0.00	0.00	0.00
Arg8	0.67 (0.07/ 0.60)	0.84 (0.00/ 0.84)	0.19 (0.06/0.14)	0.59 (0.03/ 0.56)
Tyr9	0.68 (0.07/ 0.61)	0.88 (0.01/ 0.87)	0.22 (0.06/0.16)	0.61 (0.03/ 0.58)
Val10 or Ala10	0.78 (0.14/ 0.64)	0.92 (0.02/ 0.90)	0.62 (0.41 /0.21)	0.81 (0.15/ 0.66)
Tyr11	0.87 (0.21/ 0.66)	0.95 (0.05/ 0.90)	0.69 (0.43 /0.26)	0.87 (0.20/ 0.67)
Gln12	0.57 (0.21/ 0.36)	0.75 (0.07/ 0.68)	0.62 (0.42 /0.20)	0.66 (0.21/ 0.45)
Lys13	0.44 (0.14/ 0.31)	0.53 (0.06/ 0.47)	0.47 (0.21/0.16)	0.46 (0.16/ 0.30)
Cys14	0.15 (0.02/0.13)	0.31 (0.02/0.29)	0.08 (0.00/0.08)	0.14 (0.03/0.11)

9.3. Chemical synthesis



Foldamer-peptide hybrid sequences evaluated for *in vitro* translation

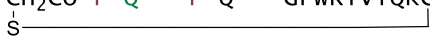
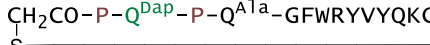
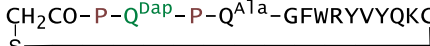


- | | |
|--|--|
| 1: AC-Q ^{Ala} -P-Q ^{Ala} -GF-CME | 4: AC-P-Q ^{Ala} -P-Q ^{Ala} -GF-CME |
| 2: AC-Q ^{Dap} -P-Q ^{Ala} -GF-CME | 5: AC-P-Q ^{Dap} -P-Q ^{Ala} -GF-CME |
| 3: AC-Q ^{Hyd} -P-Q ^{Ala} -GF-CME | 6: AC-P-Q ^{Hyd} -P-Q ^{Ala} -GF-CME |

Foldamer-peptide hybrid sequences used as initiators for RaPID selection against protein target

- 7: C[AC-P-Q^{Dap}-P-Q^{Ala}-GF-CME
- 8: C[AC-Q^{Hyd}-P-Q^{Ala}-GF-CME
- 9: C[AC-P-Q^{Hyd}-P-Q^{Ala}-GF-CME

Macrocyclic foldamer-peptide hybrids

- 10: CH₂CO-P-Q^{Dap}-P-Q^{Ala}-GFWRYVYQKCG-CONH₂

- 11: CH₂CO-P-Q^{Dap}-P-Q^{Ala}-GFWRYVYQKCGSG-X¹-CONH₂

- 12: CH₂CO-P-Q^{Dap}-P-Q^{Ala}-GFWRYVYQKCGSG-X²-CONH₂


Scheme S1. Foldamer-peptide hybrid sequences synthesized in the context of this study. The α -amino acid residues are written in one-letter code e.g. GF stands for Gly-Phe dipeptide and P in brown color stands for the pyridine unit.

Materials

Fmoc-Q^{Ala}-OH, Fmoc-Q^{OH}-OH, Fmoc-Q^{Dap}-OH and P monomers were prepared following reported synthetic protocols.^[23-25]

If not otherwise mentioned, chemical reagents were purchased from Sigma-Aldrich. Fmoc-*N*-protected amino acids, benzotriazol-1-yl-oxytripyrrolidinophosphonium hexafluorophosphate

(PyBOP), benzotriazol-1-yloxytris(dimethylamino)phosphonium hexafluorophosphate (BOP), 2-(1*H*-benzotriazol-1-yl)-1,1,3,3-tetramethyl-uronium-hexafluorophosphate (HBTU) and Biotin-PEG₄-COOH were purchased from IRIS Biotech. Solvents were purchased from Fisher Scientific (cyclohexane, ethyl acetate, dichloromethane (DCM), methanol and acetone, analytical grade), IRIS (*N*-methyl-2-pyrrolidinone (NMP)) or Carlo Erba (*N,N*-dimethylformamide (DMF) peptide grade) and used without further purification. Anhydrous tetrahydrofuran (THF) and anhydrous dichloromethane were obtained from MBRAUN SPS-800 solvent purification system. *N,N'*-diisopropylethylamine (DIPEA) was distilled over CaH₂ prior to use. Exclusively ultrapure water was used. Rink amide MBHA resin was purchased from CEM. SASRIN resin was purchased from IRIS biotech. H-(*L*)-Phe-2-CT-resin was purchased from Novabiochem. Silica column chromatography was performed on silica gel (230-400 mesh, 40-63 μm, Merck) and thin-layer chromatography (TLC) was performed on silica gel 60-F254 plates (Merck).

9.4. General methods for solid-phase synthesis

9.5. Solid-phase peptide synthesis (SPPS)

The peptide segments of compounds **1-9** were synthesized manually in a syringe reactor equipped with a filter on pre-loaded H-(*L*)-Phe-Chlorotrityl resin (manufacturer's loading: 0.54 mmol.g⁻¹; scale between 11 and 100 μmol). Fmoc-Gly-OH (3 eq. relative to resin loading) was coupled in the presence of HBTU (2.9 eq.) and DIPEA (6 eq.) in DMF at r.t. for 1 h and coupling was repeated once for 2 h.

The peptide segment for compounds **10-12** (**P10-P12** respectively) was synthesized using a Liberty Blue CEM[®] synthesizer at a scale of 100 μmol. Microwave couplings were performed twice at 50°C for 10 min with Fmoc-*N*-α-amino acid (5 eq. relative to the resin loading, 0.5 mmol), PyBOP (5 eq., 0.5 mmol), and DIPEA (10 eq. 1.0 mmol) in DMF (4 mL in total). Fmoc deprotection was performed twice with 20% (v/v) piperidine in DMF (2.0 mL) at 75°C (1 × 30 s and 1 × 180 s). The resin was washed with DMF (2 × 2 mL) after the two consecutive deprotection steps and one time with DMF (3 mL) in between coupling and deprotection steps.

9.6. Solid-phase foldamer synthesis (SPFS) for compounds 1-9, 11-12

SPFS for compounds **1-9** (including acid chloride activation, HBTU coupling and Fmoc deprotection) was undertaken according to reported protocols.^[26]

9.7. Solid-phase foldamer synthesis (SPFS) of F10

The SPFS of foldamer fragment of **10** (**F10**) was carried out on a Discover-Bio CEM[®] microwave oven in open vessel mode as previously described^[21] on Fmoc-Gly-SASRIN resin (manufacturer's loading: 0.79 mmol g⁻¹) by using the *in situ* activation strategy on a 200 μmol scale.

9.8. Fragment condensation

F10 was next coupled *via* a fragment condensation approach (Figure S2) on the resin-bound peptide **P10** on a 0.050 mmol scale. To remove any remaining moisture, **F10** was lyophilized prior to coupling. **F10** (50 mg, 0.047 mmol, 0.94 eq.) was then dissolved in dry NMP (0.4 mL) and dry THF (1.0 mL) together with DIPEA (35 μL, 0.2 mmol, 4 eq.) and BOP (44 mg, 0.1 mmol, 2 eq.). After pre-activation for 3 min, the coupling solution was added to the resin-bound H-Phe-peptide **P10** under N₂ atmosphere. The mixture was stirred for 24 h at r.t. by monitoring the progress of the reaction via HPLC analysis. The resin solution was filtered off and washed with DMF (3 × 3 mL). To facilitate HPLC purification, remaining unreacted resin-bound H-Phe-peptide **P10** was acetylated (**Method 9.9**).

9.9. N-terminal acetylation

Unreacted N-terminal aliphatic amines were acetylated with a solution of acetic anhydride in DCM (50% (v/v), 1 mL per 100 mg resin). The resin was incubated with this reaction mixture for 10 min with mechanical shaking at r.t. For the N-terminal aromatic amines of the Q monomers, the reaction time was extended to 16 h at r.t. and DIPEA (5 eq.) was added to the reaction mixture.

9.10. N-terminal chloroacetylation

For N-terminal chloroacetylation, the resin was incubated with a solution of chloroacetic anhydride (10 eq.) together with DIPEA (20 eq.) in dry DCM or DMF for 15 min at r.t. with mechanical shaking. This step was repeated once without washing in between. For the aromatic amine of Q monomers, the reaction time was extended to 30 min (twice). The resin solution was filtered off, washed with DCM and dried under a stream of nitrogen.

9.11. Cleavage of resin-bound oligomers

For Cys-containing foldamer-peptide hybrids (**10a–12a**), the Rink amide resin was treated with the cleavage cocktail (10-15 mL per gram of resin) consisting of trifluoroacetic acid (TFA)/triisopropylsilane (TIS)/ethane-1,2-dithiol (EDT)/H₂O (92.5:2.5:2.5:2.5, v/v/v/v) at r.t. for 120 min. Precipitation and subsequent centrifugation of the foldamer-peptide hybrids and fragments were performed in cold Et₂O. The precipitates were dried under a stream of nitrogen, dissolved in an acetonitrile/water mixture and lyophilized.

For the cleavage of protected foldamer fragments (**1a–9a**), the corresponding chlorotrityl or SASRIN resin was treated with a solution (20 mL per gram of resin) of hexafluoroisopropanol (HFIP) in dry DCM (60% (v/v)) for 60 min at r.t. This cleavage step was repeated once giving a better recovery yield without loss of purity of the crude. Foldamer fragment **F10** was cleaved with a solution of HFIP in dry DCM (30:70, v/v) for 2 x 60 min at r.t.

9.12. Cyanomethyl ester (CME) installation

The CME ester was installed on the crude cleavage products of foldamer-Gly-Phe-OH fragments (precursors of **1-6** and **7-9**). The foldamer-Gly-Phe-OH was dissolved in anhydrous DMF directly followed by the addition of freshly distilled DIPEA (6 eq.) or pre-dried potassium carbonate (6 eq.) and bromo acetonitrile (6 eq.). The reaction mixture was stirred for 2 h at r.t. under inert N₂ atmosphere. The progression of the reaction was monitored by TLC (EtOAc/cyclohexane mixtures). The crude protected CME adducts were extracted with EtOAc and washed once with 5% (v/v) citric acid in water and twice with saturated aqueous (sat. aq.) NaCl. The organic layer was dried over MgSO₄, filtered over cotton, and concentrated under reduced pressure. The remaining DMF was azeotroped with toluene (3x) and crude CME esters were purified by silica column chromatography (ethylacetate/cyclohexane mixtures or MeOH/DCM mixtures, yields: 37%-89%).

9.13. Boc/*tert*-Bu deprotection of CME containing foldamer-peptide hybrids

Deprotection of Boc and *t*Bu protecting groups was performed by dissolving the foldamer-Gly-Phe-CEM esters in a mixture of TFA:DCM:TIS (50:48:2 v/v/v) and stirring at r.t. for 2 h. The solvents were removed by evaporation and the pure solid compounds were obtained after trituration in Et₂O.

9.14. General methods for NMR, HRMS, HPLC analysis and purification

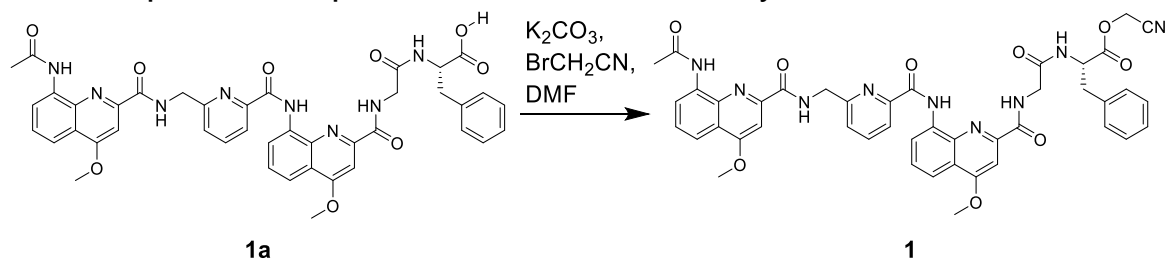
¹H NMR spectra were recorded on Avance III HD 400 MHz Bruker BioSpin and Avance III HD 500 MHz Bruker BioSpin spectrometers. All chemical shifts are reported in ppm and calibrated against residual

solvent signals of DMSO- d_6 (δ 2.50 ppm) and $CDCl_3$ (δ 7.26 ppm). In the case of 1H NMR spectra recorded in H_2O/CH_3CN , 3-(trimethylsilyl)propionic-2,2,3,3- d_4 acid sodium salt (TPS) was added to the medium and calibrated against δ 0.00. Coupling constants (J) are reported in Hz. Signal multiplicities were abbreviated as *s*, singlet; *d*, doublet; *t*, triplet; *q*, quartet, and *m*, multiplet.

High-resolution electrospray mass spectra for compounds **1–9** were recorded on a Thermo Finnigan LTQ FT Ultra Fourier Transform Ion Cyclotron Resonance Mass Spectrometer by direct infusion of the analyte dissolved in either DCM or aqueous media in positive or negative ionization mode. Mass spectra for compounds **10–12** were recorded on a Bruker microTOF II by direct infusion from aqueous media in either positive or negative ionization mode. The instrument was calibrated in positive and negative mode by direct infusion of a calibration solution (Agilent Technologies ESI-L Low Concentration Tuning Mix).

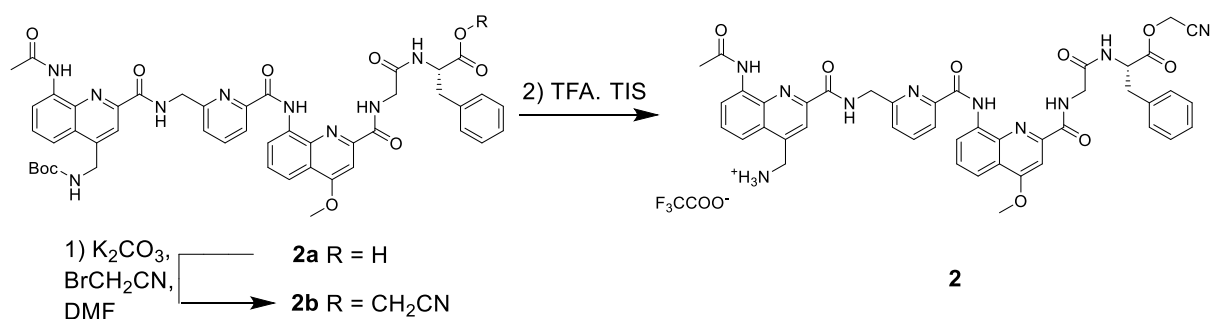
RP-HPLC analyses, as well as semi-preparative purification, were performed on an Ultimate 3000 HPLC System (ThermoFisher Scientific). Preparative RP-HPLC purification was performed on a Waters system with a 2707 Autosampler, a 2489 UV/Visible detector, a 2545 Quaternary Gradient Module and a Fraction Collector III. For analytical analysis, a Nucleodur C18 Gravity column (4 × 100 mm, 5 μ m, Macherey-Nagel) was used, and semi-preparative purifications were performed on a Nucleodur C18 Gravity column (10 × 250 mm, 5 μ m, Macherey-Nagel). A Nucleodur C8 Gravity column (4 × 50 mm, 5 μ m, Macherey-Nagel) was also used in analytical mode and for semi-preparative purification, the Nucleodur C8 Gravity column (10 × 100 mm, 5 μ m, Macherey-Nagel) was employed. Semi-preparative purification was performed with an automated fraction collector system from ThermoFisher Scientific. Preparative purifications were performed on a VP 125/21 Nucleodur C18 HTec column (21 × 125 mm, 5 μ m, Macherey-Nagel). When using acidic conditions 0.1% (v/v) TFA was added to the aqueous mobile phase (referred to as mobile phase A) and to acetonitrile (referred to as mobile phase B). For analytical RP-HPLC analysis, a flow rate of 1.0 mL.min⁻¹ was applied, semi-preparative purification on RP-HPLC was performed at a flow rate of 5.0 mL.min⁻¹, and preparative purification was performed at 25 mL.min⁻¹. The column eluent was monitored by UV detection at 214, 254, and/or 300 nm with a diode array detector.

9.15. Experimental procedures for chemical synthesis



Compound 1a: Compound **1a** was prepared on a preloaded H-(L)-Phe-2-CT resin (0.60 mmol/g) using SPPS (**Method 9.5**) and SPFS (**Method 9.6**) synthesis protocols on an 0.011 mmol scale. After final acetylation (**Method 9.9**) and resin cleavage (**Method 9.11**) with HFIP:DCM (60:40, v/v), a crude brown powder was recovered in 44% yield (3.9 mg) and was used directly in subsequent reactions without further purification steps.

Compound 1: Compound **1** was synthesized from carboxylic acid **1a** (3.9 mg, 4.9 μmol) using the general cyanomethyl installation protocol (**Method 9.12**). The obtained crude residue was purified by silica gel column chromatography using a mixture of EtOAc and cyclohexane starting from 50% to 100% (v/v) EtOAc. After evaporating the corresponding fractions, compound **3** was obtained as a white solid (1.7 mg, 41%). ^1H NMR (500 MHz, Chloroform-*d*) δ 11.93 (s, 1H), 9.60 (s, 1H), 9.46 (s, 1H), 9.06 (dd, $J = 7.7, 1.3$ Hz, 1H), 8.67 (d, $J = 7.7$ Hz, 1H), 8.59 (t, $J = 5.5$ Hz, 1H), 8.31 (dd, $J = 7.6, 1.1$ Hz, 1H), 7.98 – 7.94 (m, 2H), 7.84 (dd, $J = 16.3, 8.1$ Hz, 2H), 7.74 (s, 1H), 7.64 (t, $J = 8.1$ Hz, 1H), 7.55 (s, 1H), 7.50 – 7.45 (m, 1H), 7.18 (p, $J = 3.6$ Hz, 3H), 6.92 – 6.86 (m, 2H), 4.96 – 4.90 (m, 1H), 4.76 (dd, $J = 15.0, 6.2$ Hz, 1H), 4.69 (d, $J = 15.6$ Hz, 1H), 4.61 – 4.52 (m, 1H), 4.45 (d, $J = 15.7$ Hz, 1H), 4.36 (dd, $J = 17.0, 6.4$ Hz, 1H), 4.29 – 4.21 (m, 1H), 4.15 (s, 3H), 4.13 (s, 3H), 2.94 (dd, $J = 14.0, 5.5$ Hz, 1H), 2.82 (dd, $J = 14.0, 7.6$ Hz, 1H), 1.88 (s, 3H). HRMS (ESI⁺): m/z calculated for $\text{C}_{44}\text{H}_{39}\text{N}_9\text{O}_9$ $[\text{M}+\text{H}]^+$ 838.2944 found 838.2945.

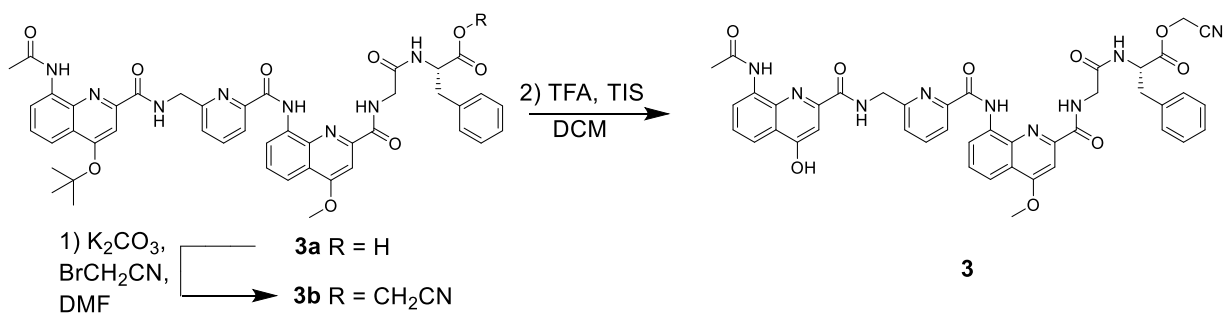


Compound 2a: Compound **2a** was prepared on a preloaded H-(L)-Phe-2-CT resin (0.60 mmol/g) using SPPS (**Method 9.5**) and SPFS (**Method 9.6**) synthesis protocols on an 0.011 mmol scale. After final acetylation (**Method 9.9**) and resin cleavage (**Method 9.11**) with HFIP:DCM (60:40, v/v), a crude brown powder was recovered in 42% yield (4.1 mg) and was used directly in subsequent reactions without further purification steps.

Compound 2b: Compound **2b** was synthesized from carboxylic acid **2a** (4.1 mg, 4.6 μmol) using the general cyanomethyl installation protocol (**Method 9.12**). The obtained crude residue was purified

by silica gel column chromatography using a mixture of EtOAc in cyclohexane starting from 30% to 100% (v/v) EtOAc. After evaporating the corresponding fractions, compound **2b** was obtained as a white solid (3.8 mg, 89%). ¹H NMR (500 MHz, CDCl₃/DMSO) δ 11.75 (s, 1H), 9.67 (s, 1H), 9.45 (t, *J* = 6.1 Hz, 1H), 8.83 (dd, *J* = 7.7, 1.3 Hz, 1H), 8.49 (dd, *J* = 15.6, 8.2 Hz, 2H), 8.39 (d, *J* = 6.0 Hz, 1H), 8.10 (s, 1H), 8.05 (dd, *J* = 7.6, 1.2 Hz, 1H), 7.76 – 7.72 (m, 2H), 7.67 (dd, *J* = 7.7, 1.2 Hz, 1H), 7.49 (dd, *J* = 8.5, 1.2 Hz, 1H), 7.43 – 7.38 (m, 1H), 7.38 – 7.34 (m, 2H), 6.98 – 6.96 (m, 3H), 6.71 – 6.65 (m, 2H), 6.14 (s, 1H), 4.62 (d, *J* = 5.6 Hz, 2H), 4.55 (dd, *J* = 9.0, 5.0 Hz, 1H), 4.48 (dd, *J* = 15.0, 8.0 Hz, 2H), 4.28 (d, *J* = 6.2 Hz, 1H), 4.23 (d, *J* = 15.7 Hz, 1H), 4.12 (d, *J* = 5.2 Hz, 2H), 3.93 (s, 3H), 2.65-2.55 (m, 2H), 1.60 (s, 3H), 1.30 (s, 9H). HRMS (ESI⁺): *m/z* calculated for C₄₉H₄₈N₁₀O₁₀ [M+H]⁺ 937.3628 found 937.3626.

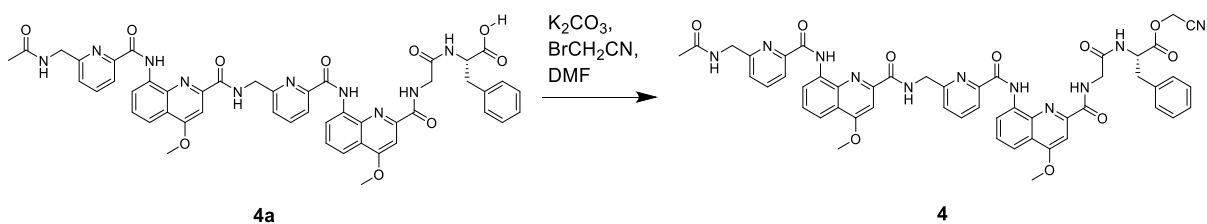
Compound 2: Compound **2** was synthesized from cyanomethyl ester **2b** (1.4 mg, 1.5 μmol) using the general deprotection protocol (**Method 9.13**) in a TFA:DCM:TIS mixture. The obtained white powder was used without further purification (0.7 mg, 0.7 μmol, 50%). ¹H NMR (500 MHz, DMSO-*d*₆) δ 12.12 (s, 1H), 10.23 (s, 1H), 10.18 (t, *J* = 6.1 Hz, 1H), 8.96 (dd, *J* = 7.7, 1.3 Hz, 1H), 8.90 (t, *J* = 6.2 Hz, 1H), 8.79 (d, *J* = 7.6 Hz, 1H), 8.74 (dd, *J* = 7.8, 1.2 Hz, 1H), 8.51 (s, 3H), 8.37 (s, 1H), 8.19 (dd, *J* = 7.6, 1.2 Hz, 1H), 8.13 (t, *J* = 7.7 Hz, 1H), 7.92 (dd, *J* = 8.4, 1.4 Hz, 1H), 7.86 (dd, *J* = 8.5, 1.3 Hz, 1H), 7.79 – 7.69 (m, 4H), 7.61 (s, 1H), 7.11 – 7.05 (m, 5H), 4.92 – 4.82 (m, 4H), 4.69 (s, 2H), 4.59 (td, *J* = 8.1, 6.0 Hz, 1H), 4.23 (dd, *J* = 16.9, 6.3 Hz, 1H), 4.17 (s, 3H), 4.16 – 4.12 (m, 1H), 2.96 (dd, *J* = 13.7, 6.0 Hz, 1H), 2.90 (dd, *J* = 13.8, 8.6 Hz, 1H), 2.13 (s, 3H). HRMS (ESI⁺): *m/z* calculated for C₄₄H₄₁N₁₀O₈ [M+H]⁺ 837.3103 found 837.3100.



Compound 3a: Compound **3a** was prepared on a preloaded H-(L)-Phe-2-CT resin (0.60 mmol/g) using SPPS (**Method 9.5**) and SPFS (**Method 9.6**) synthesis protocols on an 0.011 mmol scale. After final acetylation (**Method 9.9**) and resin cleavage (**Method 9.11**) with HFIP/DCM (60:40, v/v), a crude brown powder was recovered in 54% yield (5.0 mg) and was used directly in subsequent reactions without further purification steps.

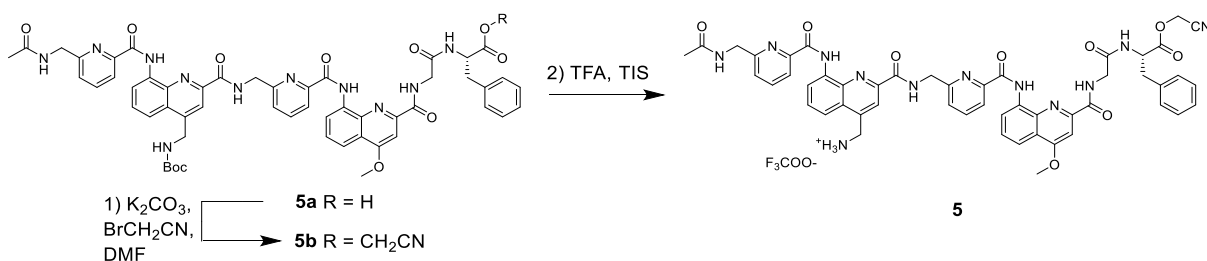
Compound 3b: Compound **3b** was synthesized from carboxylic acid **3a** (5.0 mg, 5.0 μmol) using the general cyanomethyl installation protocol (**Method 9.12**). The obtained crude residue was purified by silica gel column chromatography using a mixture of EtOAc in cyclohexane starting from 50% to 100% (v/v) EtOAc. After evaporating the corresponding fractions, compound **3b** was obtained as a white solid (1.2 mg, 37%). ^1H NMR (500 MHz, Chloroform-*d*) δ 11.97 (s, 1H), 9.61 (s, 1H), 9.43 (t, J = 6.1 Hz, 1H), 9.07 (dd, J = 7.7, 1.3 Hz, 1H), 8.69 – 8.60 (m, 2H), 8.30 (dd, J = 7.7, 1.1 Hz, 1H), 7.99 – 7.93 (m, 2H), 7.89 – 7.85 (m, 2H), 7.83 (dd, J = 7.7, 1.2 Hz, 1H), 7.64 (t, J = 8.1 Hz, 1H), 7.56 (s, 1H), 7.49 – 7.44 (m, 1H), 7.20 – 7.15 (m, 3H), 6.89 (dd, J = 6.5, 2.8 Hz, 2H), 6.41 (d, J = 8.8 Hz, 1H), 4.92 (ddd, J = 8.7, 7.5, 5.6 Hz, 1H), 4.76 – 4.68 (m, 2H), 4.62 (dd, J = 14.8, 5.9 Hz, 1H), 4.37 (d, J = 15.6 Hz, 1H), 4.35 – 4.25 (m, 2H), 4.13 (s, 3H), 2.93 (dd, J = 14.1, 5.7 Hz, 1H), 2.82 (dd, J = 14.0, 7.5 Hz, 1H), 1.88 (s, 3H), 1.71 (s, 9H). HRMS (ESI⁺): m/z calculated for $\text{C}_{47}\text{H}_{45}\text{N}_9\text{O}_9$ $[\text{M}+\text{H}]^+$ 880.3413 found 880.3416

Compound 3: Compound **3** was synthesized from cyanomethyl ester **3b** (1.2 mg, 1.3 μmol) using the general deprotection protocol (**Method 9.13**) in a TFA:DCM:TIS mixture. The obtained white powder was used without further purification (0.5 mg, 0.6 μmol , 54%). ^1H NMR (500 MHz, DMSO-*d*₆) δ 12.16 (s, 1H), 11.93 (s, 1H), 10.10 (s, 1H), 10.06 (t, J = 6.2 Hz, 1H), 8.97 (dd, J = 7.7, 1.3 Hz, 1H), 8.88 (t, J = 6.2 Hz, 1H), 8.79 (d, J = 7.5 Hz, 1H), 8.65 (dd, J = 7.8, 1.3 Hz, 1H), 8.18 (dd, J = 7.6, 1.2 Hz, 1H), 8.12 (t, J = 7.7 Hz, 1H), 7.93 (dd, J = 8.4, 1.3 Hz, 1H), 7.81 (dd, J = 8.4, 1.4 Hz, 1H), 7.76 – 7.71 (m, 2H), 7.65 (s, 2H), 7.52 (t, J = 8.1 Hz, 1H), 7.11 – 7.04 (m, 5H), 4.86 (d, J = 4.4 Hz, 2H), 4.84 – 4.79 (m, 2H), 4.59 (td, J = 8.0, 6.4 Hz, 1H), 4.25 (dd, J = 17.0, 6.4 Hz, 1H), 4.17 (s, 3H), 4.17 – 4.12 (m, 1H), 2.99 – 2.84 (m, 2H), 2.12 (s, 3H). HRMS (ESI⁻): m/z calculated for $\text{C}_{43}\text{H}_{37}\text{N}_9\text{O}_9$ $[\text{M}-\text{H}]^-$ 822.2641 found 822.2641.



Compound 4a: Compound **4a** was prepared on a preloaded H-(L)-Phe-2-CT resin (0.60 mmol/g) using SPPS (**Method 9.5**) and SPFS (**Method 9.6**) synthesis protocols on an 0.011 mmol scale. After final acetylation (**Method 9.9**) and resin cleavage (**Method 9.11**) with HFIP:DCM (60:40, v/v), a crude brown powder was recovered in 25% yield (2.5 mg) and was used directly in subsequent reactions without further purification steps.

Compound 4: Compound **4** was synthesized from carboxylic acid **4a** (2.5 mg, 2.7 μ mol) using the general cyanomethyl installation protocol (**Method 9.12**). The obtained crude residue was purified by silica gel column chromatography using a mixture of MeOH in DCM starting from 1% to 6% (v/v) MeOH. After evaporating the corresponding fractions, compound **4** was obtained as a white solid (2.0 mg, 76%). $^1\text{H NMR}$ (500 MHz, Chloroform-*d*) δ 11.73 (s, 1H), 11.63 (s, 1H), 9.51 (d, $J = 5.3$ Hz, 1H), 8.58 (ddd, $J = 14.6, 7.7, 1.3$ Hz, 2H), 8.32 (s, 1H), 8.19 (d, $J = 7.6$ Hz, 1H), 8.03 (t, $J = 7.7$ Hz, 1H), 8.00 (d, $J = 7.6$ Hz, 1H), 7.97 (dd, $J = 8.5, 1.3$ Hz, 1H), 7.93 (dd, $J = 8.4, 1.3$ Hz, 1H), 7.86 (t, $J = 7.7$ Hz, 1H), 7.76 (s, 1H), 7.71 (d, $J = 7.7$ Hz, 1H), 7.61 – 7.57 (m, 1H), 7.51 – 7.46 (m, 1H), 7.29 (d, $J = 9.7$ Hz, 1H), 7.23 (d, $J = 4.9$ Hz, 1H), 7.12 – 7.06 (m, 3H), 6.96 (dd, $J = 6.7, 2.9$ Hz, 2H), 6.44 (d, $J = 7.7$ Hz, 1H), 6.36 (s, 1H), 5.04 (d, $J = 5.0$ Hz, 2H), 4.82 – 4.77 (m, 1H), 4.65 (d, $J = 15.6$ Hz, 1H), 4.54 (d, $J = 15.6$ Hz, 1H), 4.21 (s, 3H), 4.09 (s, 3H), 3.93 (t, $J = 5.9$ Hz, 2H), 3.90 – 3.83 (m, 1H), 3.75 (dd, $J = 16.0, 5.1$ Hz, 1H), 3.02 – 2.93 (m, 2H), 1.77 (s, 3H). HRMS (ESI $^+$): m/z calculated for $\text{C}_{51}\text{H}_{45}\text{N}_{11}\text{O}_{10}$ $[\text{M}+\text{H}]^+$ 972.3424 found 972.3419.

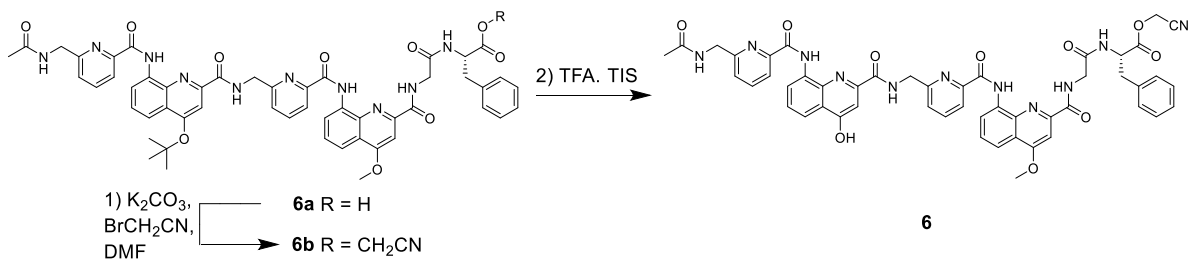


Compound 5a: Compound **5a** was prepared on a preloaded H-(L)-Phe-2-CT resin (0.60 mmol/g) using SPPS (**Method 9.5**) and SPFS (**Method 9.6**) synthesis protocols on an 0.011 mmol scale. After final acetylation (**Method 9.9**) and resin cleavage (**Method 9.11**) with HFIP:DCM (60:40, v/v), a crude brown powder was recovered in 27% yield (3.0 mg) and was used directly in subsequent reactions without further purification steps.

Compound 5b: Compound **5b** was synthesized from carboxylic acid **5a** (3.0 mg, 3.0 μ mol) using the general cyanomethyl installation protocol (**Method 9.12**). The obtained crude residue was purified

by silica gel column chromatography using a mixture of MeOH in DCM starting from 1% to 5% (v/v) MeOH. After evaporating the corresponding fractions, compound **5b** was obtained as a white solid (1.5 mg, 48%). ¹H NMR (500 MHz, DMSO-*d*₆) δ 11.83 (s, 1H), 11.78 (s, 1H), 9.53 (d, *J* = 5.8 Hz, 1H), 8.57 (d, *J* = 7.3 Hz, 1H), 8.54 (dd, *J* = 7.8, 3.4 Hz, 2H), 8.46 (t, *J* = 5.9 Hz, 1H), 8.19 (s, 1H), 8.14 – 8.10 (m, 2H), 8.06 (d, *J* = 7.5 Hz, 1H), 7.99 (t, *J* = 7.7 Hz, 1H), 7.90 (d, *J* = 7.6 Hz, 1H), 7.86 (dd, *J* = 8.5, 1.6 Hz, 2H), 7.79 (d, *J* = 7.7 Hz, 1H), 7.63 (dt, *J* = 11.7, 7.9 Hz, 3H), 7.37 (dd, *J* = 7.7, 1.1 Hz, 1H), 7.20 (s, 1H), 7.12 – 7.07 (m, 5H), 4.97 (d, *J* = 5.4 Hz, 2H), 4.85 (d, *J* = 1.0 Hz, 2H), 4.75 (d, *J* = 5.9 Hz, 2H), 4.50 (q, *J* = 7.2 Hz, 1H), 4.10 (s, 3H), 3.84 (qd, *J* = 16.8, 5.7 Hz, 2H), 3.62 (d, *J* = 5.8 Hz, 2H), 2.91 (dd, *J* = 7.3, 3.9 Hz, 2H), 1.64 (s, 3H), 1.44 (s, 9H). HRMS (ESI⁻): *m/z* calculated for C₅₆H₅₄N₁₂O₁₁ [M-H]⁻ 1069.3962 found 1069.3979.

Compound 5: Compound **5** was synthesized from cyanomethyl ester **5b** (1.5 mg, 1.4 μmol) using the general deprotection protocol (**Method 9.13**) in a TFA:DCM:TIS mixture. The obtained white powder was used without further purification (0.6 mg, 0.6 μmol, 40 %). ¹H NMR (500 MHz, DMSO-*d*₆) δ 11.77 (s, 1H), 11.76 (s, 1H), 9.61 (t, *J* = 5.2 Hz, 1H), 8.55 – 8.46 (m, 7H), 8.40 (s, 1H), 8.17 – 8.11 (m, 2H), 8.06 (d, *J* = 7.5 Hz, 1H), 8.01 (t, *J* = 7.7 Hz, 1H), 7.91 (dd, *J* = 10.3, 8.0 Hz, 2H), 7.85 (dd, *J* = 8.4, 1.3 Hz, 1H), 7.80 (d, *J* = 7.9 Hz, 1H), 7.71 (t, *J* = 8.1 Hz, 1H), 7.62 (t, *J* = 8.1 Hz, 1H), 7.38 (d, *J* = 7.7 Hz, 1H), 7.12 – 7.06 (m, 6H), 4.99 (d, *J* = 5.1 Hz, 2H), 4.86 (s, 2H), 4.72 (s, 2H), 4.48 (q, *J* = 7.2 Hz, 1H), 4.09 (s, 4H), 3.89 – 3.78 (m, 2H), 3.57 (d, *J* = 5.9 Hz, 2H), 2.96 – 2.86 (m, 2H), 1.67 (s, 3H). HRMS (ESI⁺): *m/z* calculated for C₅₁H₄₈N₁₂O₉ [M+H]⁺ 971.3583 found 971.3587.

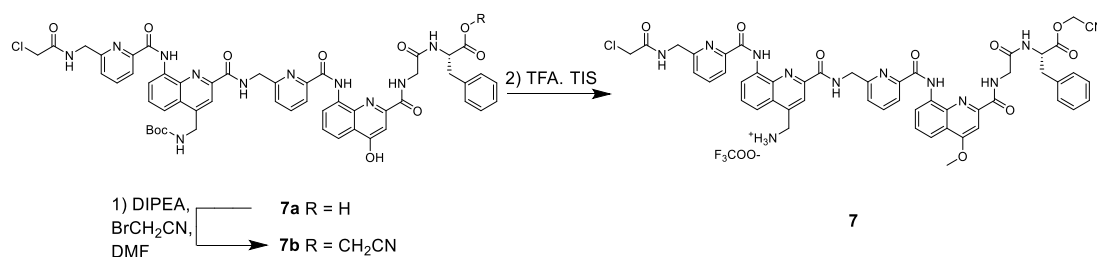


Compound 6a: Compound **6a** was prepared on a preloaded H-(L)-Phe-2-CT resin (0.60 mmol/g) using SPPS (**Method 9.5**) and SPFS (**Method 9.6**) synthesis protocols on an 0.011 mmol scale. After final acetylation (**Method 9.9**) and resin cleavage (**Method 9.11**) with HFIP:DCM (60:40, v/v), a crude brown powder was recovered in 28% yield (3.0 mg) and was used directly in subsequent reactions without further purification steps.

Compound 6b: Compound **6b** was synthesized from carboxylic acid **6a** (3.0 mg, 3.1 μmol) using the general cyanomethyl installation protocol (**Method 9.12**). The obtained crude residue was purified by silica gel column chromatography using a mixture of MeOH in DCM starting from 1% to 5% (v/v) MeOH. After evaporating the corresponding fractions, compound **4b** was obtained as a white solid (1.5 mg, 48%). ¹H NMR (500 MHz, Chloroform-*d*) δ 11.79 (s, 1H), 11.66 (s, 1H), 9.45 (t, *J* = 5.2 Hz, 1H), 8.63 (dd, *J* = 7.7, 1.3 Hz, 1H), 8.57 (dd, *J* = 7.7, 1.3 Hz, 1H), 8.34 (t, *J* = 5.6 Hz, 1H), 8.20 (dd, *J* = 7.6, 1.0 Hz, 1H), 8.02 (t, *J* = 7.2 Hz, 1H), 8.00 – 7.96 (m, 2H), 7.92 (dd, *J* = 8.5, 1.3 Hz, 1H), 7.90 (s, 1H), 7.83 (t, *J* = 7.7 Hz, 1H), 7.70 (dd, *J* = 7.8, 1.0 Hz, 1H), 7.59 (dd, *J* = 8.4, 7.7 Hz, 1H), 7.48 – 7.43 (m, 1H), 7.10 – 7.05 (m, 3H), 6.96 – 6.91 (m, 2H), 6.45 (d, *J* = 7.8 Hz, 1H), 6.31 (t, *J* = 5.4 Hz, 1H), 5.05 (t, *J* = 4.5 Hz, 2H), 4.78 (dt, *J* = 7.8, 6.1 Hz, 1H), 4.60 (d, *J* = 15.6 Hz, 1H), 4.49 (d, *J* = 15.6 Hz, 1H), 4.09 (s, 3H), 3.91

(dd, $J = 5.6, 4.3$ Hz, 2H), 3.85 (dd, $J = 16.2, 5.4$ Hz, 1H), 3.74 (dd, $J = 16.4, 5.3$ Hz, 1H), 2.99 – 2.90 (m, 2H), 1.76 (s, 8H), 1.74 (s, 3H). HRMS (ESI⁺): m/z calculated for C₅₄H₅₁N₁₁O₁₁ [M+H]⁺ 1014.3893 found 1014.3894.

Compound 6: Compound **6** was synthesized from cyanomethyl ester **6b** (1.5 mg, 1.5 μmol) using the general deprotection protocol (**Method 9.13**) in a TFA:DCM:TIS mixture. The obtained white powder was used without further purification (0.5 mg, 0.5 μmol, 35 %). ¹H NMR (500 MHz, DMSO-*d*₆) δ 12.06 (s, 1H), 11.89 (s, 1H), 11.73 (s, 1H), 9.49 (t, $J = 5.3$ Hz, 1H), 8.62 (d, $J = 7.3$ Hz, 1H), 8.51 (ddd, $J = 16.7, 7.7, 1.3$ Hz, 2H), 8.46 (t, $J = 5.7$ Hz, 1H), 8.15 – 8.05 (m, 3H), 7.97 (t, $J = 7.7$ Hz, 1H), 7.90 – 7.82 (m, 3H), 7.80 – 7.75 (m, 1H), 7.65 (s, 1H), 7.62 (t, $J = 8.0$ Hz, 1H), 7.50 (t, $J = 8.0$ Hz, 1H), 7.35 (dd, $J = 7.8, 1.1$ Hz, 1H), 7.21 (s, 1H), 7.15 – 7.06 (m, 6H), 4.93 (d, $J = 5.4$ Hz, 2H), 4.86 (d, $J = 0.9$ Hz, 2H), 4.49 (q, $J = 7.3$ Hz, 1H), 4.08 (s, 3H), 3.92 (dd, $J = 17.0, 5.8$ Hz, 1H), 3.83 (dd, $J = 17.1, 5.6$ Hz, 1H), 3.59 (d, $J = 6.0$ Hz, 2H), 2.93 (dd, $J = 13.8, 6.5$ Hz, 1H), 2.88 (dd, $J = 13.7, 8.0$ Hz, 1H), 1.63 (s, 3H). HRMS (ESI⁻): m/z calculated for C₅₀H₄₃N₁₁O₁₀ [M-H]⁻ 956.3122 found 956.3123.

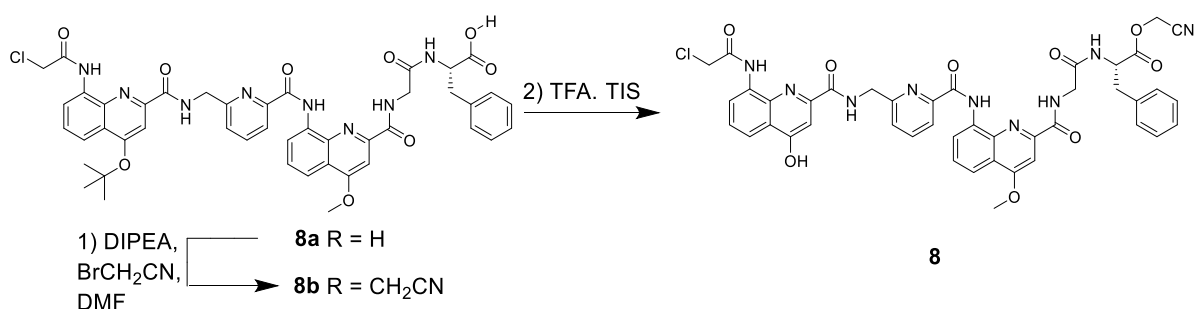


Compound 7a: Compound **7a** was prepared from H-(L)-Phe-2-CT resin on a 0.1 mmol scale (185 mg, manufacturer's loading: 0.54 mmol g⁻¹) using SPPS (**Method 9.5**) and SPFS (**Method 9.6**) synthesis protocols followed by final chloroacetylation (**Method 9**). The crude product obtained from resin cleavage (**Method 9.11**) was used directly in subsequent reaction without further purification (100 mg, 94%). ¹H NMR (500 MHz, DMSO-*d*₆) δ 12.67 (s, 1H), 11.78 (s, 1H), 11.75 (s, 1H), 9.54 (t, $J = 5.2$ Hz, 1H), 8.52 – 8.49 (m, 2H), 8.43 (t, $J = 5.8$ Hz, 1H), 8.22 (d, $J = 7.8$ Hz, 1H), 8.18 (s, 1H), 8.14 (t, $J = 7.7$ Hz, 1H), 8.05 (t, $J = 7.7$ Hz, 2H), 8.01 (t, $J = 7.7$ Hz, 1H), 7.91 (dd, $J = 7.6, 1.1$ Hz, 1H), 7.85 (dt, $J = 8.5, 1.8$ Hz, 2H), 7.79 (dd, $J = 7.8, 1.0$ Hz, 1H), 7.67 – 7.64 (m, 1H), 7.63 – 7.59 (m, 2H), 7.38 (dd, $J = 7.8, 1.1$ Hz, 1H), 7.16 (s, 1H), 7.10 – 7.05 (m, 5H), 4.97 (t, $J = 4.5$ Hz, 2H), 4.75 (d, $J = 5.9$ Hz, 2H), 4.43 – 4.34 (m, 1H), 4.09 (s, 3H), 3.93 (s, 2H), 3.89 – 3.81 (m, 1H), 3.75 (dd, $J = 16.8, 5.6$ Hz, 1H), 3.67 (d, $J = 5.9$ Hz, 2H), 2.92 (dd, $J = 13.7, 5.7$ Hz, 1H), 2.83 (dd, $J = 13.7, 7.7$ Hz, 1H), 1.44 (s, 9H). HRMS (ESI⁻): m/z calculated for C₅₃H₅₀ClN₁₁O₁₁ [M-H]⁻ 1064.3464 found 1064.3445.

Compound 7b: Compound **7b** was synthesized from carboxylic acid **7a** (100 mg, 0.1 mmol) the general cyanomethyl installation protocol (**Method 9.12**). The obtained crude residue was purified by silica gel column chromatography using a mixture of acetone in DCM starting from 20% to 40% (v/v) acetone. After evaporating the corresponding fractions, compound **8b** was obtained as a white solid (52 mg, 52%). ¹H NMR (500 MHz, DMSO-*d*₆) δ 11.78 (s, 1H), 11.75 (s, 1H), 9.55 (t, $J = 5.3$ Hz, 1H), 8.57 (d, $J = 7.3$ Hz, 1H), 8.53 – 8.48 (m, 3H), 8.40 (t, $J = 5.8$ Hz, 1H), 8.19 (s, 1H), 8.14 (t, $J = 7.7$ Hz, 1H), 8.06 (d, $J = 7.6$ Hz, 1H), 8.01 (t, $J = 7.7$ Hz, 1H), 7.92 – 7.89 (m, 1H), 7.85 (dt, $J = 8.4, 1.5$ Hz, 2H), 7.80 (dd, $J = 7.8, 1.0$ Hz, 1H), 7.67 – 7.59 (m, 3H), 7.38 (dd, $J = 7.7, 1.1$ Hz, 1H), 7.15 – 7.07 (m, 6H), 4.96 (d, $J = 5.4$ Hz, 2H), 4.86 (d, $J = 1.2$ Hz, 2H), 4.75 (d, $J = 5.9$ Hz, 2H), 4.50 (q, $J = 7.2$ Hz, 1H), 4.09 (s,

3H), 3.93 (s, 2H), 3.88 – 3.75 (m, 2H), 3.65 (d, $J = 5.9$ Hz, 2H), 2.97 – 2.88 (m, 2H), 1.44 (s, 9H). HRMS (ESI⁻): m/z calculated for C₅₆H₅₃ClN₁₂O₁₁ [M-H]⁻ 1103.3573 found 1103.3564.

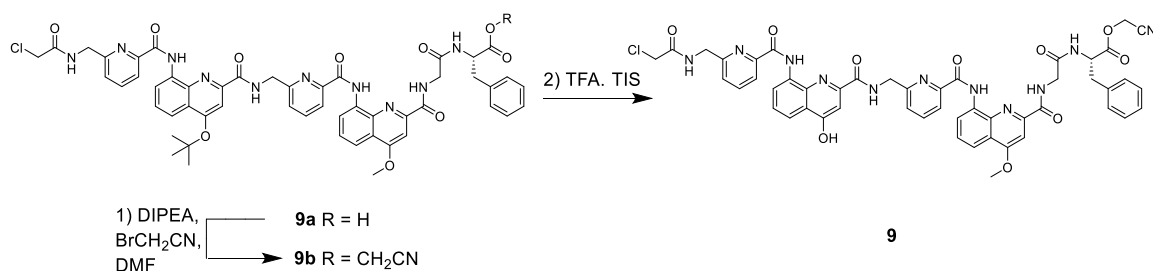
Compound 7: For the synthesis of compound **7**, the total **7b** was directly submitted to the general deprotection protocol (**Method 9.13**) in a TFA:DCM:TIS mixture. The obtained white powder was used without further purification (43 mg, 0.042 mmol, 91%). ¹H NMR (500 MHz, DMSO-*d*₆) δ 11.72 (s, 1H), 11.71 (s, 1H), 9.61 (t, $J = 5.0$ Hz, 1H), 8.56 (s, 3H), 8.52 – 8.43 (m, 5H), 8.40 (s, 1H), 8.16 (t, $J = 7.7$ Hz, 1H), 8.07 – 8.01 (m, 2H), 7.91 (td, $J = 7.6, 1.1$ Hz, 2H), 7.83 (ddd, $J = 12.6, 8.1, 1.2$ Hz, 2H), 7.73 – 7.67 (m, 1H), 7.64 – 7.59 (m, 1H), 7.40 (dd, $J = 7.8, 1.0$ Hz, 1H), 7.14 – 7.05 (m, 6H), 4.98 (d, $J = 5.0$ Hz, 2H), 4.87 (d, $J = 1.0$ Hz, 2H), 4.72 (d, $J = 5.8$ Hz, 2H), 4.48 (td, $J = 7.7, 6.5$ Hz, 1H), 4.08 (s, 3H), 3.95 (s, 2H), 3.86 – 3.76 (m, 2H), 3.59 (d, $J = 5.8$ Hz, 2H), 2.92 (qd, $J = 13.8, 7.1$ Hz, 2H). HRMS (ESI⁻): m/z calculated for C₅₁H₄₅ClN₁₂O₉ [M-H]⁻ 1005.3194 found 1005.3209.



Compound 8a: Compound **8a** was prepared from H-(L)-Phe-2-CT resin on a 0.1 mmol scale (210 mg, manufacturer's loading: 0.54 mmol g⁻¹) using SPPS (**Method 9.5**) and SPFS (**Method 9.6**) synthesis protocols followed by final chloroacetylation (**Method 9.11**). The crude product obtained from resin cleavage (**Method 9.11**) was used directly in subsequent reaction without further purification. ¹H NMR (500 MHz, DMSO-*d*₆) δ 12.70 (s, 1H), 12.14 (s, 1H), 10.39 (s, 1H), 9.92 (t, $J = 6.0$ Hz, 1H), 8.96 (dd, $J = 7.7, 1.3$ Hz, 1H), 8.83 (t, $J = 6.1$ Hz, 1H), 8.58 (dd, $J = 7.8, 1.3$ Hz, 1H), 8.51 (d, $J = 8.0$ Hz, 1H), 8.19 (dd, $J = 7.7, 1.1$ Hz, 1H), 8.14 (t, $J = 7.7$ Hz, 1H), 8.05 (d, $J = 7.6$ Hz, 1H), 7.92 (dd, $J = 8.4, 1.3$ Hz, 1H), 7.86 (dd, $J = 8.5, 1.3$ Hz, 1H), 7.81 – 7.77 (m, 2H), 7.75 – 7.70 (m, 1H), 7.62 – 7.55 (m, 2H), 7.09 – 7.02 (m, 5H), 4.91 – 4.81 (m, 2H), 4.48 (td, $J = 8.1, 5.6$ Hz, 1H), 4.36 – 4.27 (m, 2H), 4.26 – 4.19 (m, 1H), 4.15 (s, 3H), 4.09 (dd, $J = 17.0, 5.9$ Hz, 1H), 2.93 (dd, $J = 13.8, 5.6$ Hz, 1H), 2.82 (dd, $J = 13.8, 8.2$ Hz, 1H), 1.62 (s, 9H). HRMS (ESI⁻): m/z calculated for C₄₅H₄₂ClN₈O₉ [M-H]⁻ 873.2769 found 873.2763.

Compound 8b and 8: Compound **8b** was synthesized from carboxylic acid **8a** (43 mg, 0.05 mmol) using the general cyanomethyl installation protocol (**Method 9.12**). For the synthesis of compound **8**, the obtained crude residue **8b** was directly submitted to the general deprotection protocol (**Method 9.13**) in a TFA:DCM:TIS mixture. The crude compound was dissolved in DCM in which impurities precipitated within 24 h. The mixture was filtered and the filtrate was evaporated, redissolved and purified by semi-preparative HPLC using a gradient from 55–80% over 15 min at 25 °C on an RP-18 column. (16 mg, 37 %). ¹H NMR (500 MHz, DMSO-*d*₆) δ 12.15 (s, 1H), 12.04 (s, 1H), 10.37 (s, 1H), 9.89 (t, $J = 6.1$ Hz, 1H), 8.95 (dd, $J = 7.7, 1.3$ Hz, 1H), 8.83 (t, $J = 6.1$ Hz, 1H), 8.76 (d, $J = 7.4$ Hz, 1H), 8.57 (dd, $J = 7.8, 1.3$ Hz, 1H), 8.18 (dd, $J = 7.6, 1.1$ Hz, 1H), 8.12 (t, $J = 7.7$ Hz, 1H), 7.92 (dd, $J = 8.5, 1.3$ Hz, 1H), 7.87 (dd, $J = 8.4, 1.3$ Hz, 1H), 7.76 – 7.71 (m, 2H), 7.65 (s, 1H), 7.58 (s, 1H), 7.55 (t, $J = 8.1$ Hz, 1H), 7.11 – 7.04 (m, 5H), 4.87 (d, $J = 1.5$ Hz, 2H), 4.85 (d, $J = 6.1$ Hz, 2H), 4.56 (td, J

= 7.9, 6.6 Hz, 1H), 4.36 (d, $J = 1.4$ Hz, 2H), 4.20 (dd, $J = 17.0, 6.3$ Hz, 1H), 4.15 (s, 3H), 4.11 (dd, $J = 17.0, 5.9$ Hz, 1H), 2.95 (dd, $J = 13.7, 6.4$ Hz, 1H), 2.89 (dd, $J = 13.8, 8.2$ Hz, 1H). HRMS (ESI⁻): m/z calculated for C₄₃H₃₆ClN₉O₉ [M-H]⁻ 856.2252 found 856.2244.

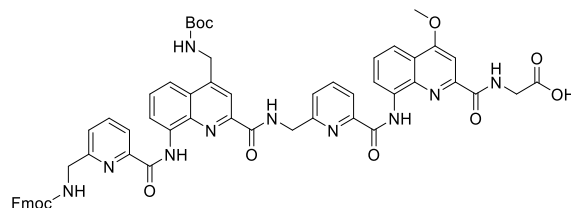


Compound 9a: Compound **9a** was prepared from H-(L)-Phe-2CT resin on a 0.1 mmol scale (185 mg, manufacturer's loading: 0.54 mmol g⁻¹) using SPSS (**Method 9.5**) and SPFS (**Method 9.6**) synthesis protocols followed by final chloroacetylation (**Method 9.7**). The crude product obtained from resin cleavage (**Method 9.11**) was used directly in subsequent reaction without further purification (110 mg, 98%). ¹H NMR (500 MHz, Chloroform-*d*) δ 11.72 (s, 1H), 11.52 (s, 1H), 9.53 (t, $J = 5.1$ Hz, 1H), 8.53 (d, $J = 7.6$ Hz, 1H), 8.46 – 8.41 (m, 1H), 8.31 (t, $J = 5.4$ Hz, 1H), 8.13 (d, $J = 7.6$ Hz, 1H), 7.94 (dd, $J = 14.8, 7.8$ Hz, 3H), 7.86 (dd, $J = 8.4, 1.3$ Hz, 1H), 7.82 (s, 1H), 7.79 (t, $J = 7.7$ Hz, 1H), 7.62 (d, $J = 7.8$ Hz, 1H), 7.54 (t, $J = 8.1$ Hz, 1H), 7.42 (t, $J = 5.5$ Hz, 1H), 7.38 (t, $J = 8.1$ Hz, 1H), 7.20 (d, $J = 7.7$ Hz, 1H), 7.12 (s, 1H), 7.05 – 6.99 (m, 5H), 6.74 (d, $J = 7.4$ Hz, 1H), 5.03 – 4.97 (m, 2H), 4.66 (q, $J = 6.5$ Hz, 1H), 4.02 (s, 3H), 3.98 (t, $J = 4.0$ Hz, 1H), 3.90 (dd, $J = 16.8, 5.1$ Hz, 1H), 3.85 (s, 2H), 3.79 (dd, $J = 15.9, 5.0$ Hz, 1H), 3.70 (dd, $J = 15.9, 5.2$ Hz, 1H), 3.04 – 2.96 (m, 1H), 2.93 – 2.86 (m, 1H), 1.71 (s, 9H). HRMS (ESI⁻): m/z calculated for C₅₂H₄₈ClN₁₀O₁₀ [M-H]⁻ 1007.3249 found 1007.3232.

Compound 9b: Compound **9b** was synthesized from carboxylic acid **9a** (110 mg, 0.1 mmol) the general cyanomethyl installation protocol (**Method 9.12**). The obtained crude residue was purified by silica gel column chromatography using a mixture of acetone in DCM starting from 20% to 40% (v/v) acetone. After evaporating the corresponding fractions, compound **9b** was obtained as a white solid (49 mg, 47%). ¹H NMR (500 MHz, DMSO-*d*₆) δ 11.83 (s, 1H), 11.62 (s, 1H), 9.55 (t, $J = 5.1$ Hz, 1H), 8.66 (d, $J = 7.3$ Hz, 1H), 8.47 (t, $J = 5.9$ Hz, 1H), 8.43 (ddd, $J = 7.7, 2.9, 1.4$ Hz, 2H), 8.34 (t, $J = 5.6$ Hz, 1H), 8.16 (t, $J = 7.7$ Hz, 1H), 8.07 (dd, $J = 7.7, 1.0$ Hz, 1H), 7.99 (t, $J = 7.7$ Hz, 1H), 7.87 – 7.80 (m, 4H), 7.79 (s, 1H), 7.62 – 7.57 (m, 1H), 7.53 – 7.49 (m, 1H), 7.37 (dd, $J = 7.8, 1.0$ Hz, 1H), 7.17 – 7.10 (m, 5H), 7.08 (s, 1H), 5.00 – 4.89 (m, 2H), 4.88 (s, 2H), 4.50 (td, $J = 7.8, 6.6$ Hz, 1H), 4.06 (s, 3H), 3.92 (s, 2H), 3.82 (qd, $J = 17.1, 5.6$ Hz, 2H), 3.56 (d, $J = 5.9$ Hz, 2H), 2.93 (qd, $J = 13.8, 7.3$ Hz, 2H), 1.69 (s, 9H). HRMS (ESI⁻): m/z calculated for C₅₄H₄₉ClN₁₁O₁₀ [M-H]⁻ 1046.3358 found 1046.3349.

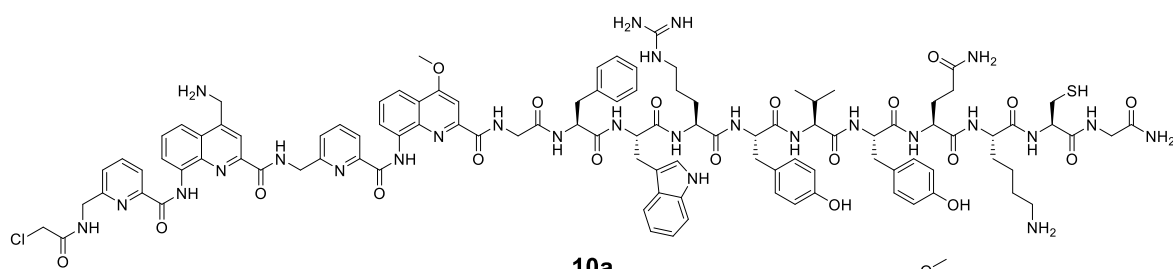
Compound 9: For the synthesis of compound **9**, the total **9b** was directly submitted to the general deprotection protocol (**Method 9.13**) in a TFA:DCM:TIS mixture. The obtained white powder was used without further purification (47 mg, 0.042 mmol, 87 %). ¹H NMR (500 MHz, DMSO-*d*₆) δ 12.05 (s, 1H), 11.86 (s, 1H), 11.67 (s, 1H), 9.51 (t, $J = 5.2$ Hz, 1H), 8.63 (d, $J = 7.3$ Hz, 1H), 8.51 – 8.45 (m, 3H), 8.40 (t, $J = 5.7$ Hz, 1H), 8.14 (t, $J = 7.7$ Hz, 1H), 8.07 (d, $J = 7.4$ Hz, 1H), 8.00 (t, $J = 7.7$ Hz, 1H), 7.91 – 7.81 (m, 3H), 7.79 (d, $J = 7.8$ Hz, 1H), 7.64 (s, 1H), 7.61 (t, $J = 8.1$ Hz, 1H), 7.48 (t, $J = 8.0$ Hz, 1H), 7.37 (d, $J = 7.7$ Hz, 1H), 7.16 (s, 1H), 7.15 – 7.07 (m, 5H), 4.92 (d, $J = 5.3$ Hz, 2H), 4.87 (d, $J = 1.1$ Hz, 2H),

4.49 (q, $J = 7.4$ Hz, 1H), 4.07 (s, 3H), 3.91 (s, 2H), 3.90 – 3.78 (m, 2H), 3.61 (d, $J = 5.9$ Hz, 2H), 2.92 (qd, $J = 13.8, 7.3$ Hz, 2H). HRMS (ESI⁻): m/z calculated for C₅₀H₄₁ClN₁₁O₁₀ [M-H]⁻ 990.2732 found 990.2721.

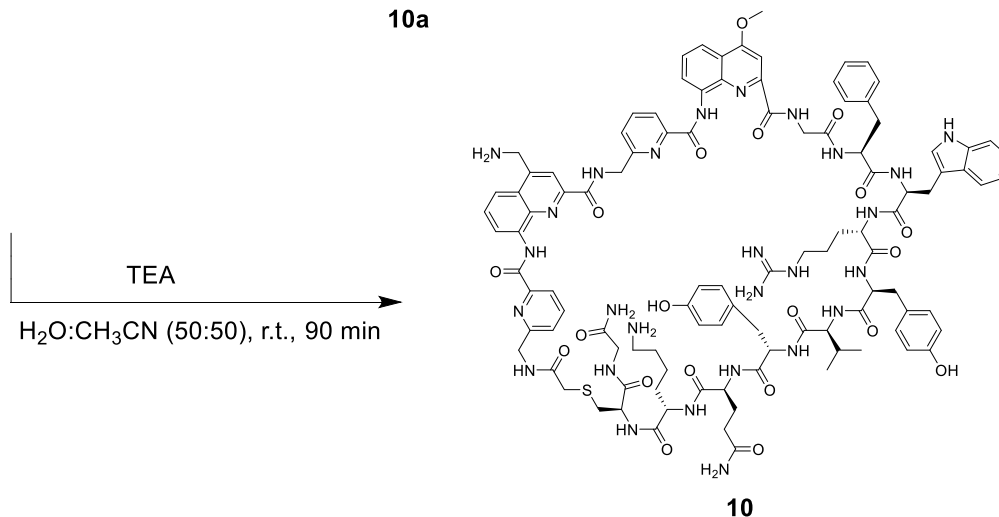


F10

Foldamer fragment F10: **F10** was synthesized on a preloaded Fmoc-Gly-SASRIN resin (loading: 0.61 mmol/g) using the general SPFS procedure (**Method 9.7**) on a 0.2 mmol scale. **F10** was recovered in 70% yield (150 mg) after cleavage (**Method 9.11**) using 6 mL of HFIP/DCM (30:70, v/v) mixture for 1 h at r.t. and was used without any further purification. ¹H NMR (500 MHz, DMSO-*d*₆) δ 12.67 (s, 1H), 11.86 (s, 1H), 11.77 (s, 1H), 9.60 (d, $J = 6.0$ Hz, 1H), 8.52 (d, $J = 7.7$ Hz, 1H), 8.47 (d, $J = 7.8$ Hz, 1H), 8.43 (d, $J = 6.2$ Hz, 1H), 8.17 (s, 1H), 8.10 (t, $J = 7.6$ Hz, 1H), 8.02 (dd, $J = 14.4, 7.3$ Hz, 2H), 7.92 (d, $J = 7.5$ Hz, 1H), 7.88 – 7.81 (m, 2H), 7.79 (d, $J = 7.7$ Hz, 1H), 7.75 (d, $J = 7.6$ Hz, 2H), 7.70 (t, $J = 6.1$ Hz, 1H), 7.64 (t, $J = 8.0$ Hz, 2H), 7.58 (t, $J = 8.1$ Hz, 1H), 7.44 (d, $J = 7.5$ Hz, 2H), 7.32 (t, $J = 7.7$ Hz, 3H), 7.17 (dd, $J = 14.7, 7.4$ Hz, 3H), 5.00 (d, $J = 5.2$ Hz, 2H), 4.74 (d, $J = 5.9$ Hz, 2H), 4.19 – 4.16 (m, 1H), 4.12 (d, $J = 6.9$ Hz, 2H), 4.08 (s, 3H), 4.03 (t, $J = 6.9$ Hz, 1H), 3.87 (d, $J = 6.0$ Hz, 2H), 3.62 (d, $J = 6.0$ Hz, 2H), 1.45 (s, 9H). HRMS (ESI⁻) m/z calculated for C₅₈H₅₃N₁₀O₁₁ [M+H]⁺ 1065.3890 found 1065.4042.



10a

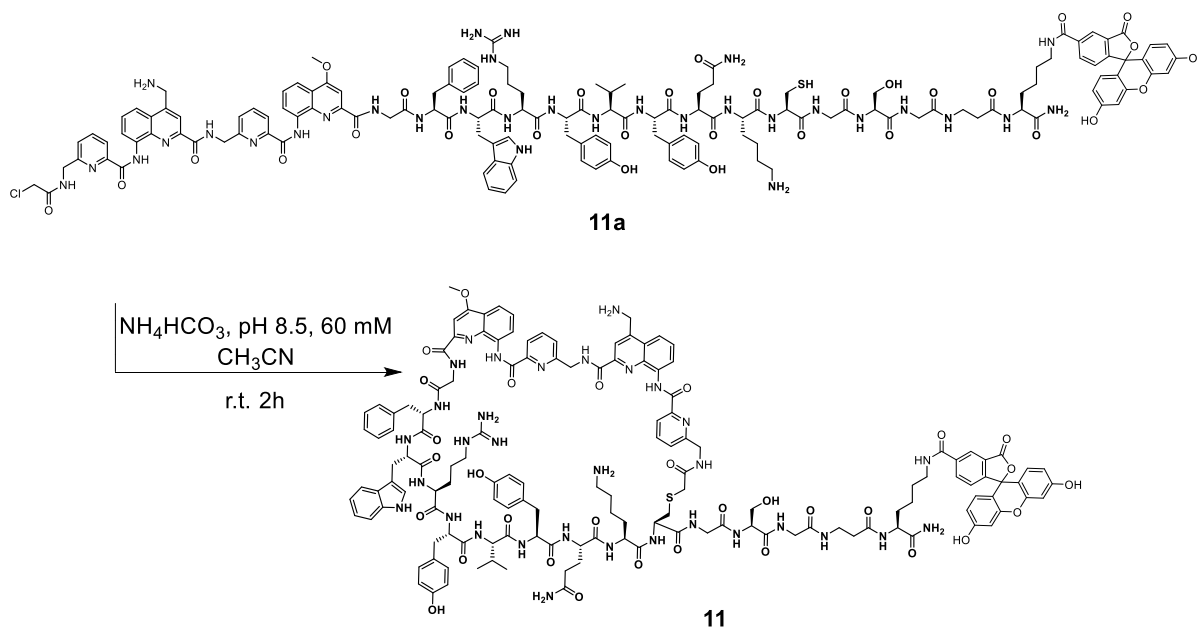


10

Compound 10a: Resin-bound Fmoc-Phe-Trp(Boc)-Arg(Pbf)-Tyr(*t*Bu)-Val-Tyr(*t*Bu)-Gln(Trt)-Lys(Boc)-Cys(Trt)-Gly-NH- was first prepared from Rink amide resin (0.33 mmol/g) using a CEM Liberty Blue

microwave automated peptide synthesizer (**Method 9.5**) on a 0.1 mmol scale. Fragment condensation (**Method 9.8**) with foldamer fragment **F10** was next performed on a 50 μmol scale of deprotected resin-bound peptide. After Fmoc deprotection (piperidine (20% (v/v)) in DMF, 2 mL, 2 \times 5 min), final chloroacetylation (**Method 9**) and TFA cleavage (**Method 9.11**), crude **10a** (118 mg, 94%) was directly engaged in the macrocyclization reaction without further purification. HRMS (ESI⁺): m/z calculated for $\text{C}_{105}\text{H}_{123}\text{ClN}_{27}\text{O}_{20}\text{S}$ [M+H]⁺ 2149.8875 found 2149.9112

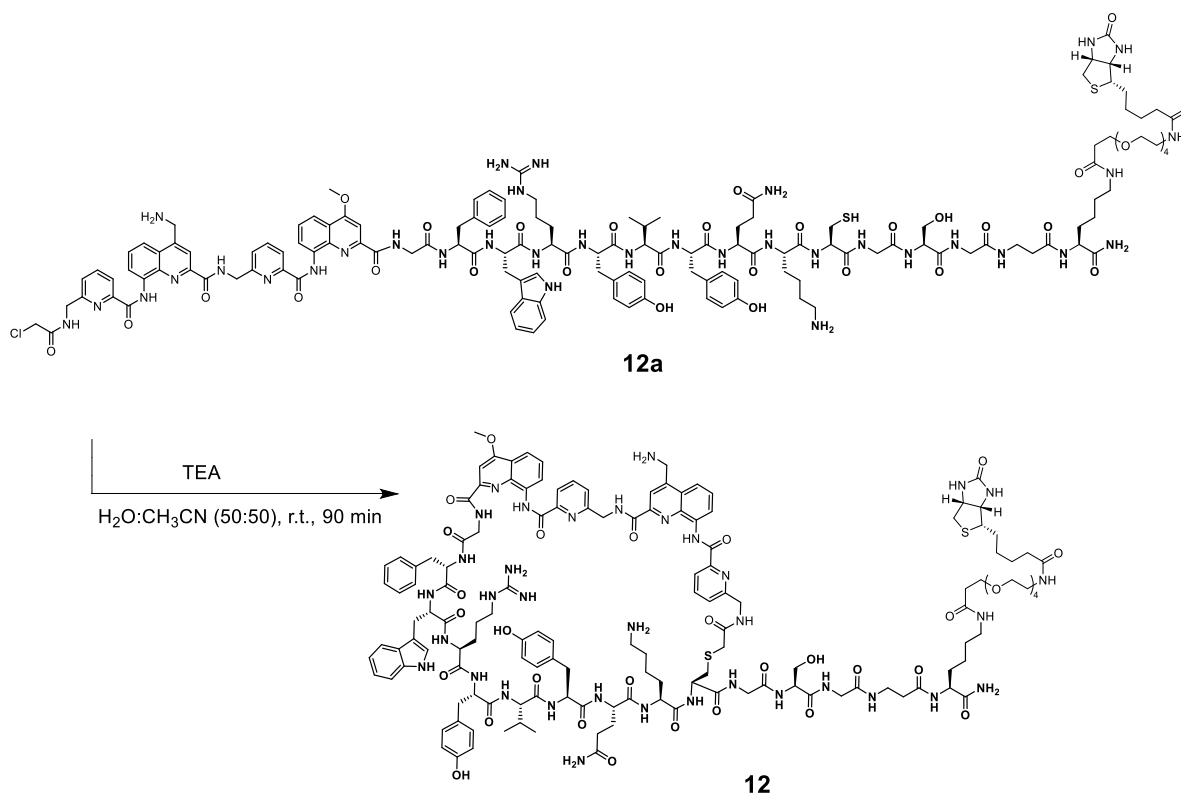
Compound 10: Total compound **10** was dissolved in 88 mL CH_3CN (50% (v/v) in H_2O) to a 0.5 mM dilution and triethylamine (6 mL, 0.5 M) was added. After 90 min at r.t. without agitation and monitoring the reaction by HPLC, the reaction mixture was concentrated under reduced pressure and acidified with an equimolar volume of TFA. Remaining solvents were evaporated by lyophilization and the crude macrocycle was purified by using semi-preparative RP-HPLC with a gradient from 30–50% solvent B over 15 minutes at 50 °C on a 250 mm C18 column to give **10** as a colorless solid. For further studies, 2 \times lyophilization from HCl (0.1 M) provided compound **10** as an HCl salt. (12 mg, 10%). ¹H NMR was performed in CD_3CN (25% (v/v) in H_2O) with water suppression. ¹H NMR (500 MHz, Acetonitrile- d_3) δ 11.49 (s, 1H), 11.37 (s, 1H), 9.96 (s, 1H), 9.76 (t, $J = 4.4$ Hz, 1H), 8.37 (d, $J = 7.1$ Hz, 1H), 8.28 (s, 1H), 8.25 (s, 1H), 8.14 (d, $J = 8.6$ Hz, 1H), 8.07 (t, $J = 8.1$ Hz, 4H), 8.00 (d, $J = 8.2$ Hz, 1H), 7.97 – 7.89 (m, 5H), 7.84 – 7.79 (m, 2H), 7.76 (d, $J = 7.5$ Hz, 1H), 7.62 (dt, $J = 19.8, 8.7$ Hz, 3H), 7.52 (dd, $J = 14.6, 8.1$ Hz, 3H), 7.42 (d, $J = 10.9$ Hz, 2H), 7.40 – 7.34 (m, 3H), 7.32 (d, $J = 9.3$ Hz, 3H), 7.20 (dd, $J = 23.5, 8.6$ Hz, 1H), 7.04 (m, 9H), 6.96 – 6.89 (m, 6H), 6.85 – 6.77 (m, 1H), 6.74 – 6.65 (m, 6H), 6.62 (s, 1H), 4.80–4.40 (water suppression region), 3.97 (s, 2H), 3.84 (qd, $J = 17.1, 6.5$ Hz, 2H), 3.65 – 3.52 (m, 2H), 3.30 – 3.16 (m, 4H), 3.16 – 3.01 (m, 4H), 3.01 – 2.82 (m, 11H), 2.82 – 2.64 (m, 4H), 2.34 – 2.16 (m, 3H), 1.95 (q, $J = 8.1, 7.5$ Hz, 1H), 1.87 – 1.58 (m, 5H), 1.48 – 1.14 (m, 5H), 0.98 (s, 1H), 0.78 (m, 8H). HRMS (ESI⁺): m/z calculated for $\text{C}_{105}\text{H}_{122}\text{N}_{27}\text{O}_{27}\text{S}$ [M+H]⁺ 2113.9108 found 2113.9446.



Compound 11a: Peptide Fmoc-Phe-Trp(Boc)-Arg(Pbf)-Tyr(tBu)-Val-Tyr(tBu)-Gln(Trt)-Lys(Boc)-Cys(Trt)-Gly-Ser(Trt)-Gly- β Ala-Lys(Alloc)-NH- was first prepared from Rink amide resin (0.33 mmol/g)

using a CEM Liberty Blue microwave automated peptide synthesizer on a 0.1 mmol scale. The foldamer segment was then coupled with standard SPFS (**Method 9.6**) on a 0.033 mmol scale. After Fmoc deprotection (piperidine (20% (v/v)) in DMF, 2 mL, 2× 5 min), and chloroacetylation (**Method 9.7**), the Alloc protecting group was removed with Pd(PPh₃)₄ (0.1 eq., 3.8 mg, 3.3 μmol) and phenylsilane (20 eq., 81 μL, 660 μmol) in DCM (2 mL), 2× each for 30 min. Fluorescein was installed on the free amine with compound **13** (3 eq., 47 mg, 100 μmol) in DMF (1.5 mL) for 16 h at r.t. After final TFA cleavage (**Method 9.11**), crude **11a** (75 mg, 79%) was purified by using preparative RP-HPLC with a gradient from 25–45% solvent B over 10 min at r.t. on a 125 mm C18 column to give **11a** as a yellow solid after lyophilization (8 mg, 10%). HRMS (ESI⁺): *m/z* calculated for C₁₄₀H₁₅₉ClN₃₂O₃₁S [M+2H]²⁺ 1426.6240 found 1426.6235.

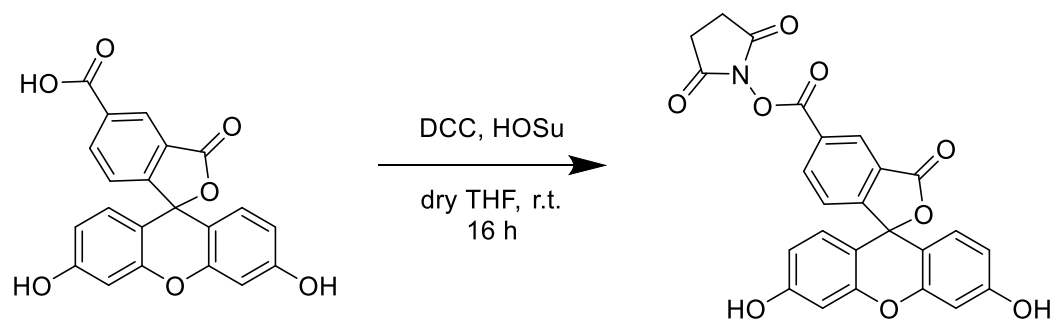
Compound 11: Compound **11a** (8 mg) was dissolved in 21 mL H₂O together with 7 mL acetonitrile to a 0.1 mM dilution and the solvent was freed from oxygen by freeze-pump-thaw. Independently, a solution of 21 mL of NH₄HCO₃ (60 mM, pH 8.5) and 7 mL acetonitrile was prepared, oxygen removed by Freeze-Pump-Thaw and the Foldamer solution added via syringe under inert gas atmosphere. The mixture was quickly stirred and left without agitation for 2 h at r.t. The reaction was quenched with TFA, solvents were evaporated by lyophilization and the crude macrocycle was purified by using preparative RP-HPLC with a gradient from 25–45% solvent B over 10 min at r.t. on a 125 mm C18 column to give **11** as a yellow solid. For further studies, 2× lyophilization from HCl (0.1 M) provided compound **11** as an HCl salt (1 mg, 13%). ¹H NMR was performed in CD₃CN (50% (v/v) in aq. HCl (0.1 M)) with water suppression. HRMS (ESI⁺): *m/z* calculated for C₁₄₀H₁₅₈N₃₂O₃₁S [M+2H]²⁺ 1408.0757 found 1408.0915.



Compound 12a: Peptide Fmoc-Phe-Trp(Boc)-Arg(Pbf)-Tyr(tBu)-Val-Tyr(tBu)-Gln(Trt)-Lys(Boc)-Cys(Trt)-Gly-Ser(Trt)-Gly-βAla-Lys(Alloc)-NH- was first prepared from Rink amide resin (0.33 mmol/g) using a CEM Liberty Blue microwave automated peptide synthesizer on a 0.1 mmol scale. The foldamer segment was then coupled with standard SPFS (**Method 9.6**) on a 0.025 mmol scale. The

resin was transferred to a syringe reactor and the Alloc protecting group was removed with Pd(PPh₃)₄ (0.1 eq., 2.9 mg, 2.5 μmol) and phenylsilane (20 eq., 62 μL, 500 μmol) in DCM (2 mL), 2× each for 30 min. Biotin-PEG₄-COOH (1.5 eq., 18.4 mg, 37.5 μmol) was coupled to the free amine with BOP (1.7 eq., 18.8 mg, 42.5 μmol) and DIPEA (3 eq., 13 μL, 75 μmol) in DMF (3 mL) for 16 h at r.t. After Fmoc deprotection, final chloroacetylation (**Method 8**) and TFA cleavage (**Method 9.11**), crude **12a** (72 mg, 97%) was directly engaged in the macrocyclization reaction without further purification. HRMS (ESI⁺): *m/z* calculated for C₁₄₀H₁₈₂ClN₃₅O₃₂S₂ [M+2H]²⁺ 1483.1483 found 1483.1458.

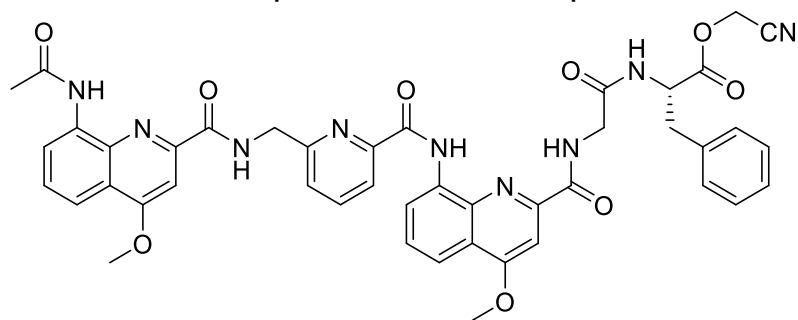
Compound 12: Compound **12a** was dissolved in CH₃CN (40 mL, 50% (v/v) in H₂O) to a 0.5 mM dilution and triethylamine (100 μL, 18 mM) was added. After stirring at r.t. for 90 min and monitoring the reaction by HPLC, the reaction mixture was acidified with an equimolar volume of TFA and concentrated under reduced pressure. Remaining solvents were evaporated by lyophilization and the crude macrocycle was purified by using preparative RP-HPLC with a gradient from 28–40% solvent B over 20 min at r.t. on a 125 mm C18 column to give **12** as a white solid. For further studies, 2× lyophilization from HCl (0.1 M) provided compound **12** as an orange HCl salt. (4.80 mg, 1.51 μmol, 6%). ¹H NMR was performed in CD₃CN (50% (v/v) in H₂O) with water suppression. HRMS (ESI⁺): *m/z* calculated for C₁₄₀H₁₈₂ClN₃₅O₃₂S₂ [M+2H]²⁺ 1465.1600 found 1465.1919.



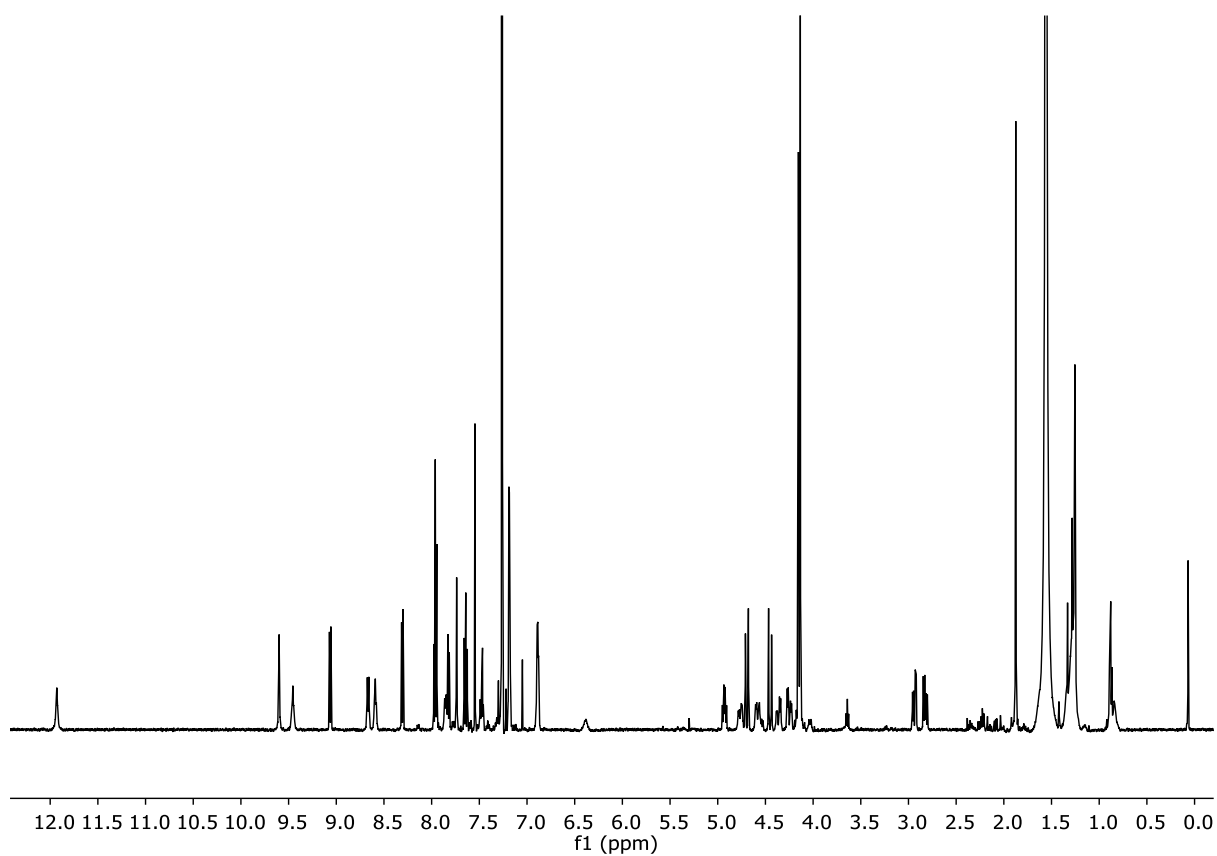
13

Compound 13: 5-Carboxyfluorescein (250 mg, 0.66 mmol) was suspended in dry THF (2.5 mL) and a solution of *N*-hydroxysuccinimide (1.3 eq., 99 mg, 0.86 mmol) dissolved in dry THF (0.5 mL) was added, followed by the addition of a solution of *N,N'*-dicyclohexylcarbodiimide (1.3 eq., 177 mg, 0.86 mmol) in dry THF (0.5 mL). After 16 h stirring at r.t. the mixture was filtered and the precipitate washed with Et₂O (2 × 10 mL) and EtOAc (1 × 10 mL). The filtrate was concentrated under reduced pressure and remaining solvents azeotroped with toluene (3 × 5 mL) providing **13** as an orange solid (270 mg, 90%). ¹H NMR (400 MHz, DMSO-*d*₆) δ 10.18 (s, 2H), 8.54 (d, *J* = 1.7 Hz, 1H), 8.43 (dd, *J* = 8.1, 1.6 Hz, 1H), 7.56 (d, *J* = 8.1 Hz, 1H), 6.71 (s, 1H), 6.70–6.68 (m, 3H), 6.55 (d, *J* = 2.3 Hz, 1H), 6.53 (d, *J* = 2.3 Hz, 1H), 2.93 (s, 4H). HRMS (ESI⁺): *m/z* calculated for C₂₅H₁₅NO₉ [M+H]⁺ 474.0820 found 474.1079.

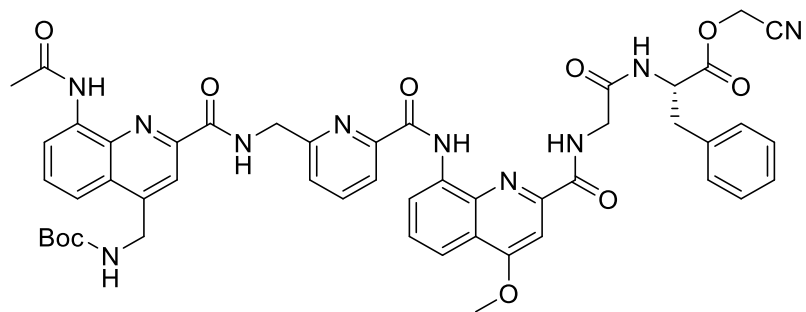
9.16. ¹H NMR spectra and HPLC profiles



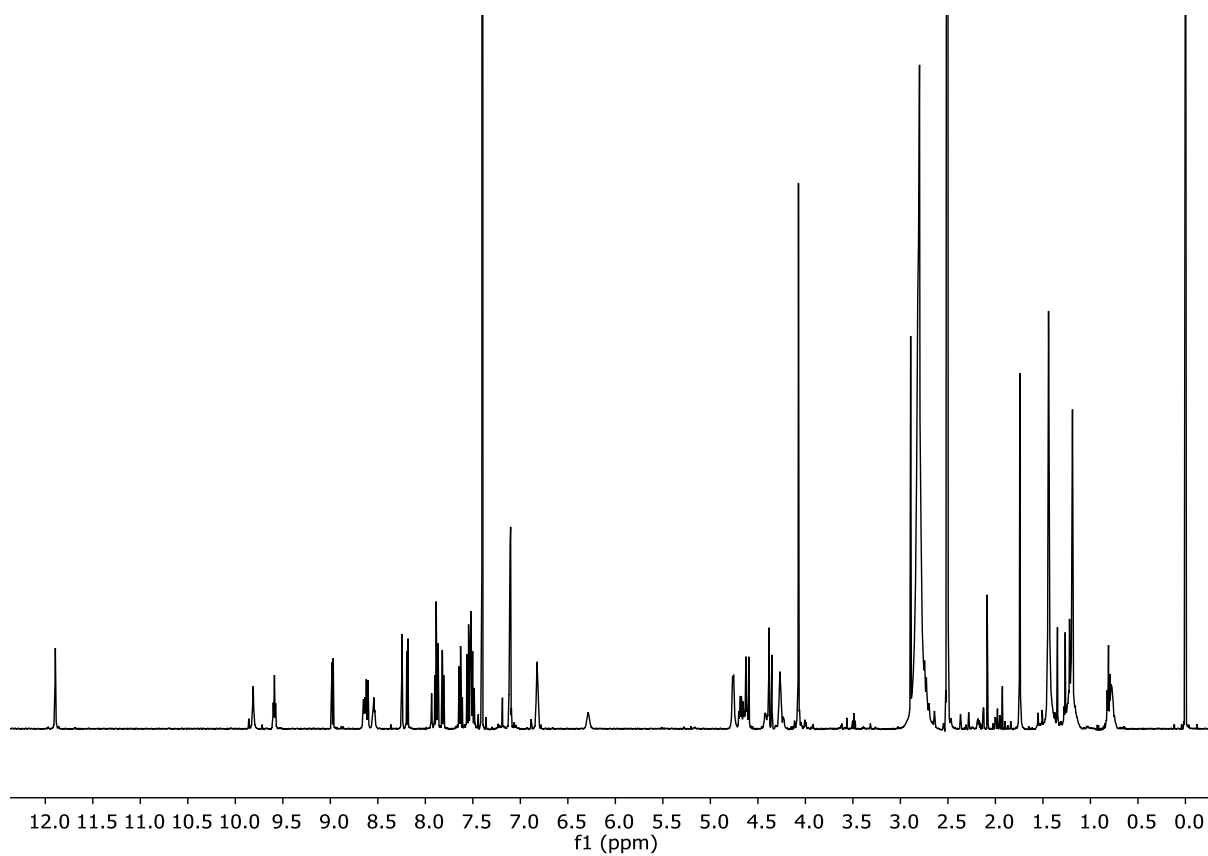
1



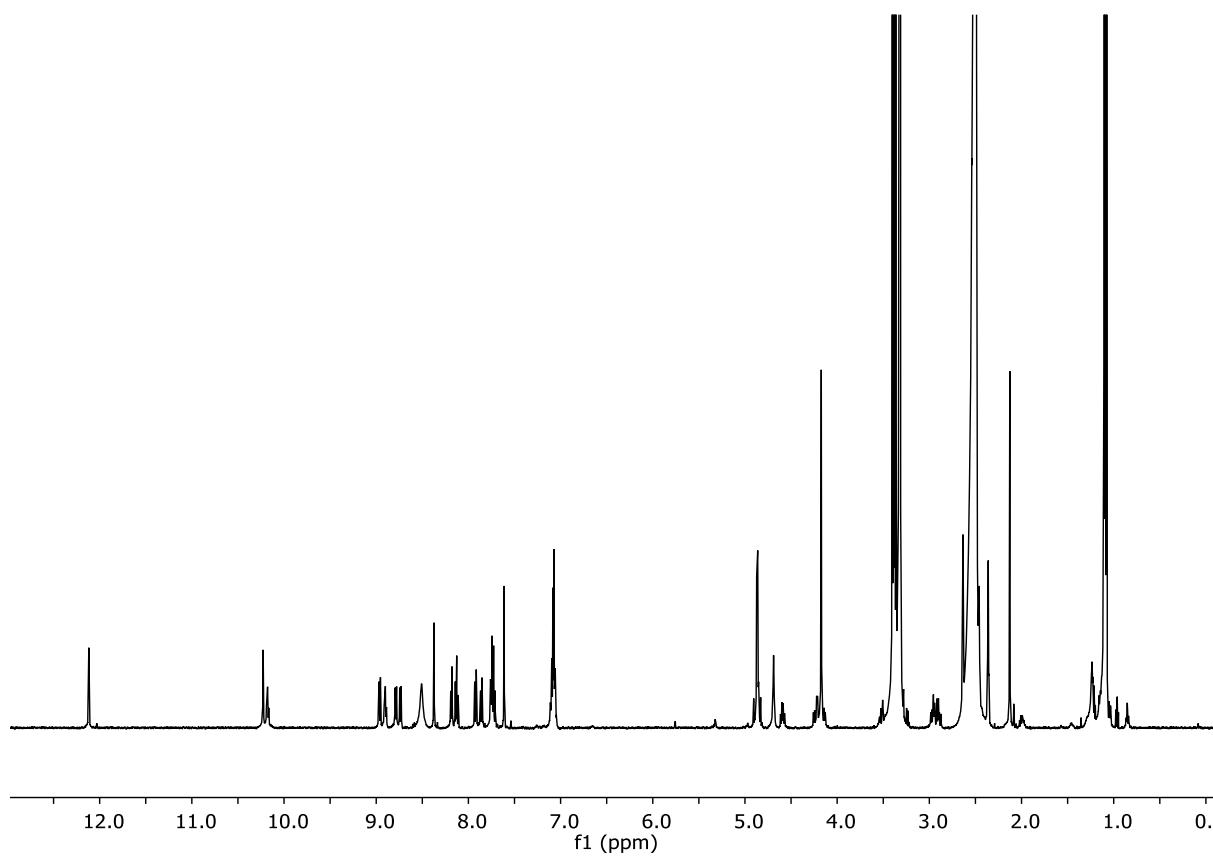
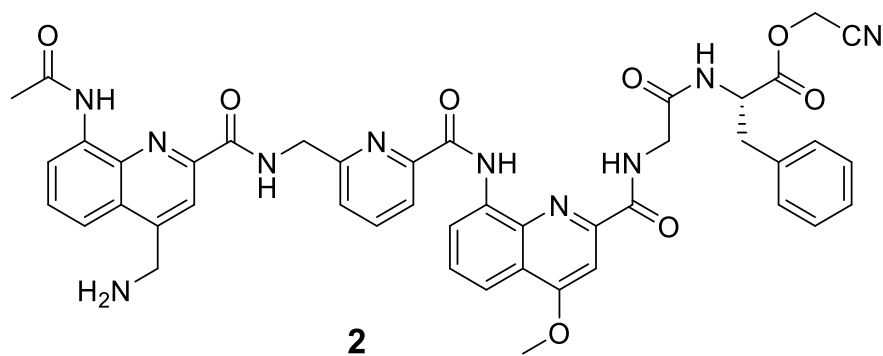
¹H NMR spectrum (500 MHz, CDCl₃, 25 °C) of **1**.



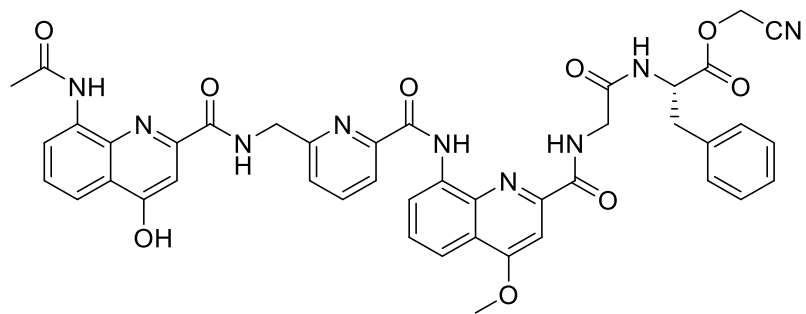
2b



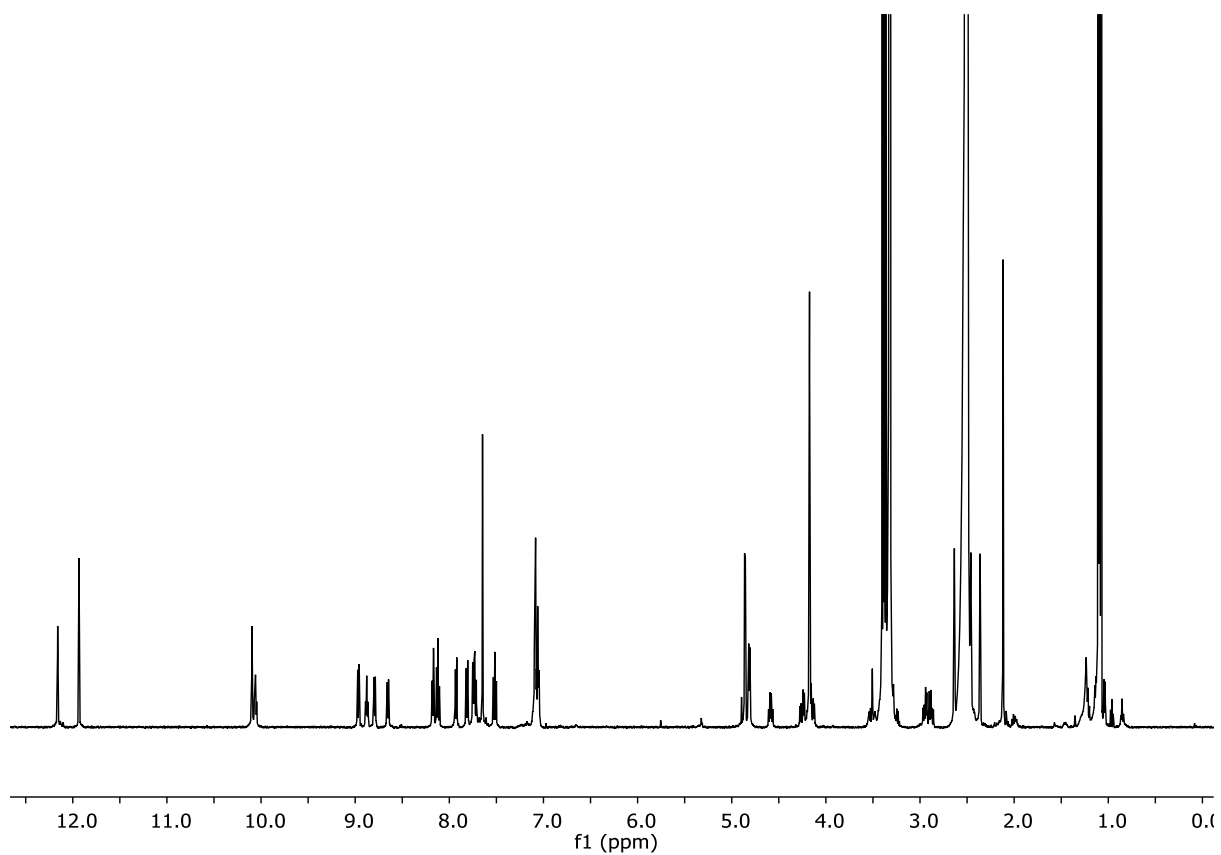
¹H NMR spectrum (500 MHz, CDCl₃, 25 °C) of **2b**.



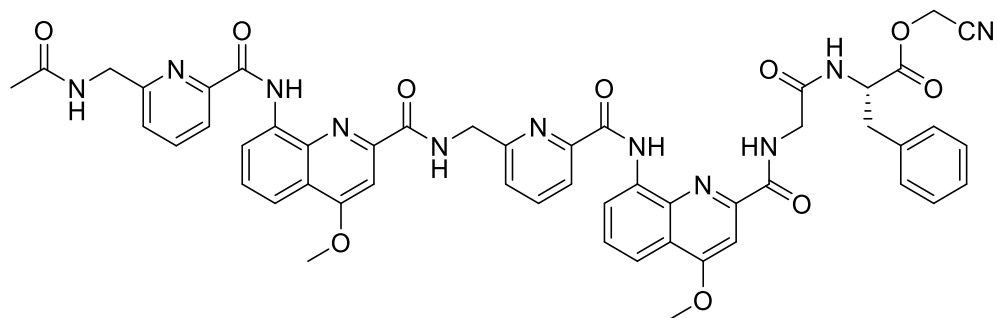
¹H NMR spectrum (500 MHz, DMSO-*d*₆, 25 °C) of **2**.



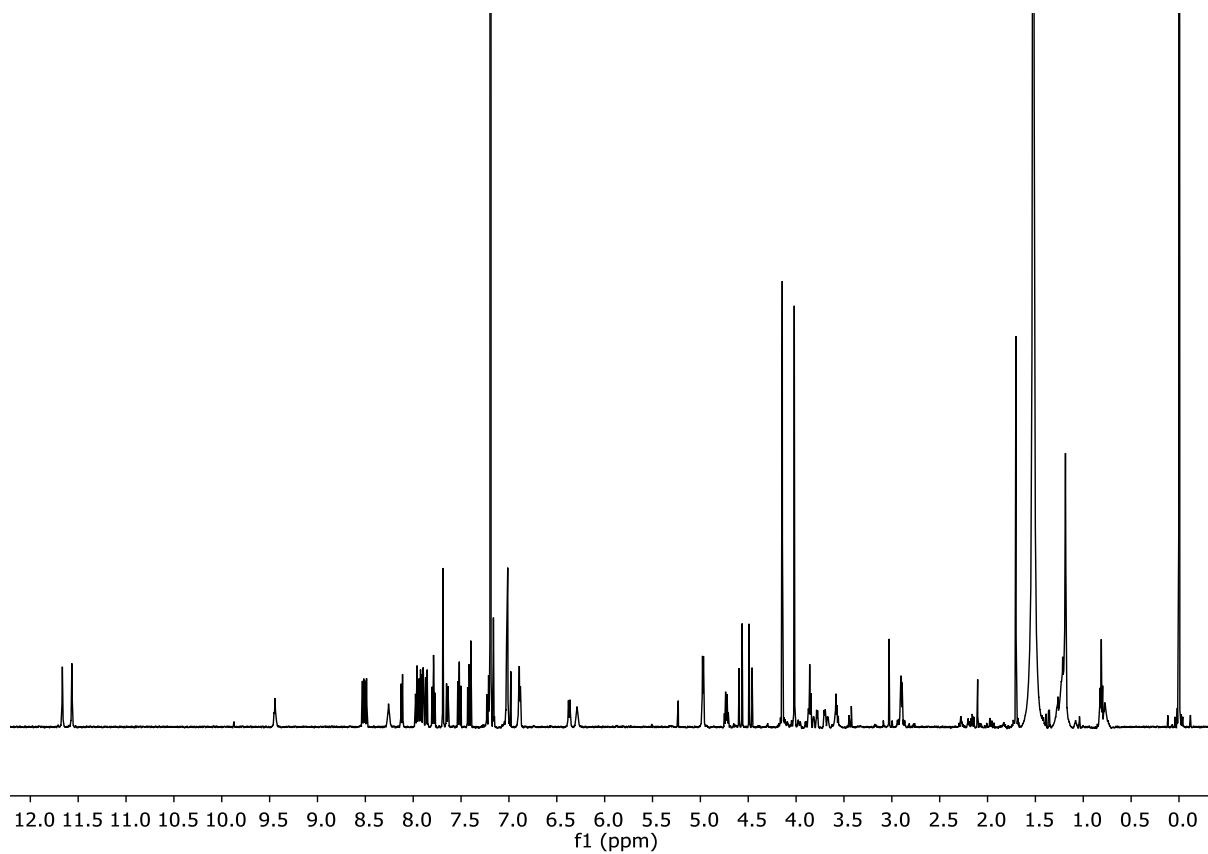
3



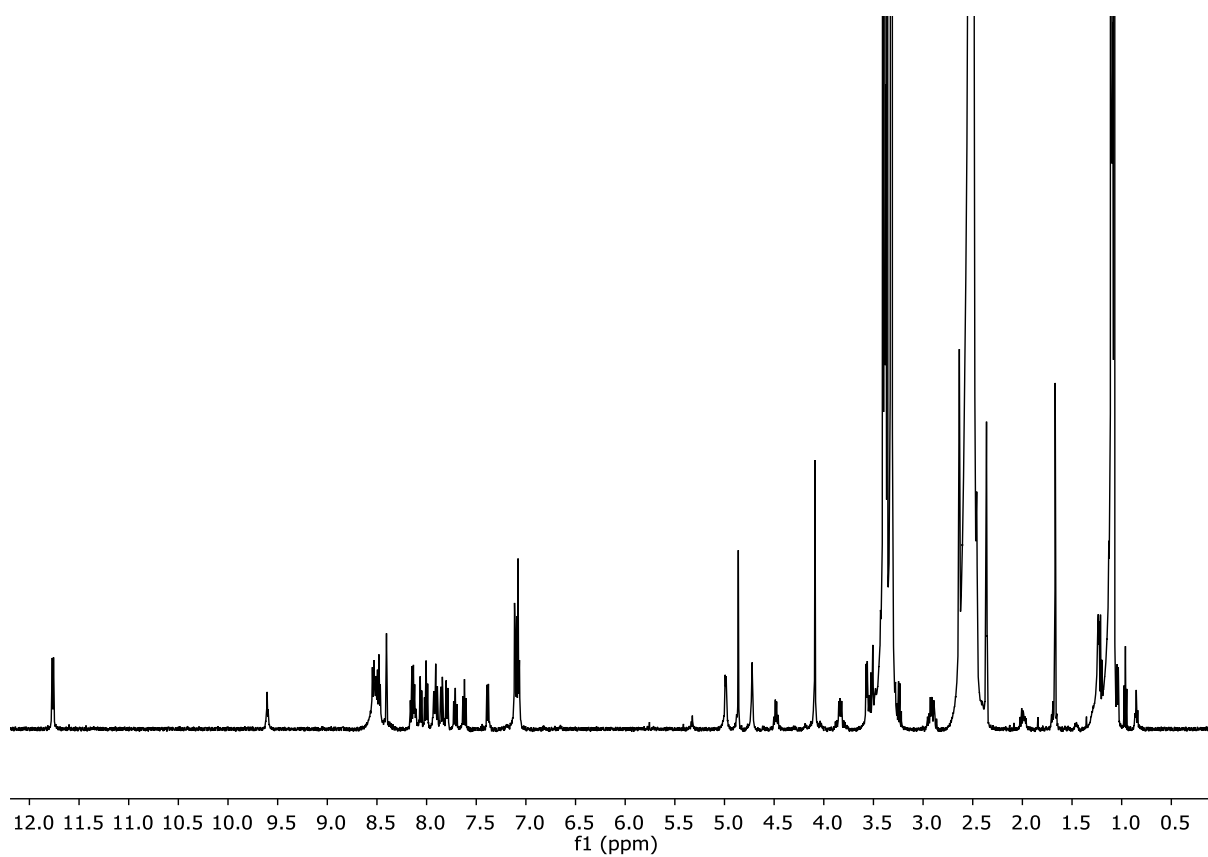
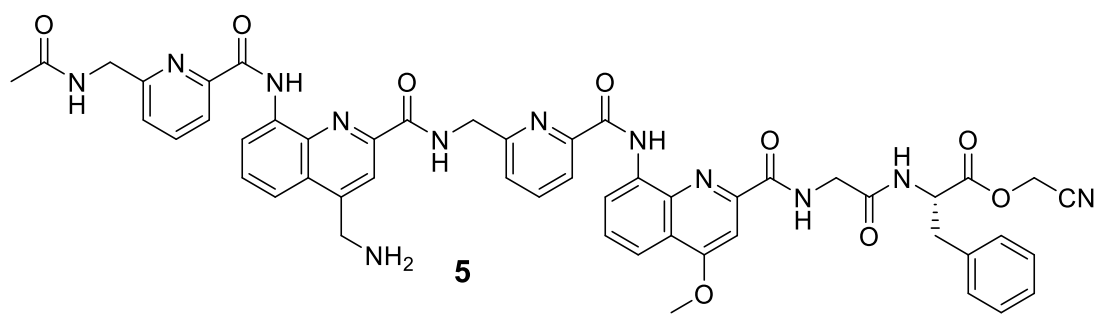
¹H NMR spectrum (500 MHz, DMSO-*d*₆, 25 °C) of **3**.



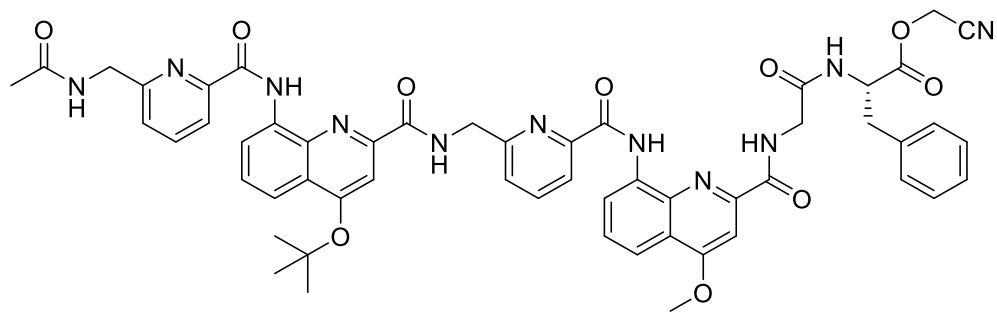
4



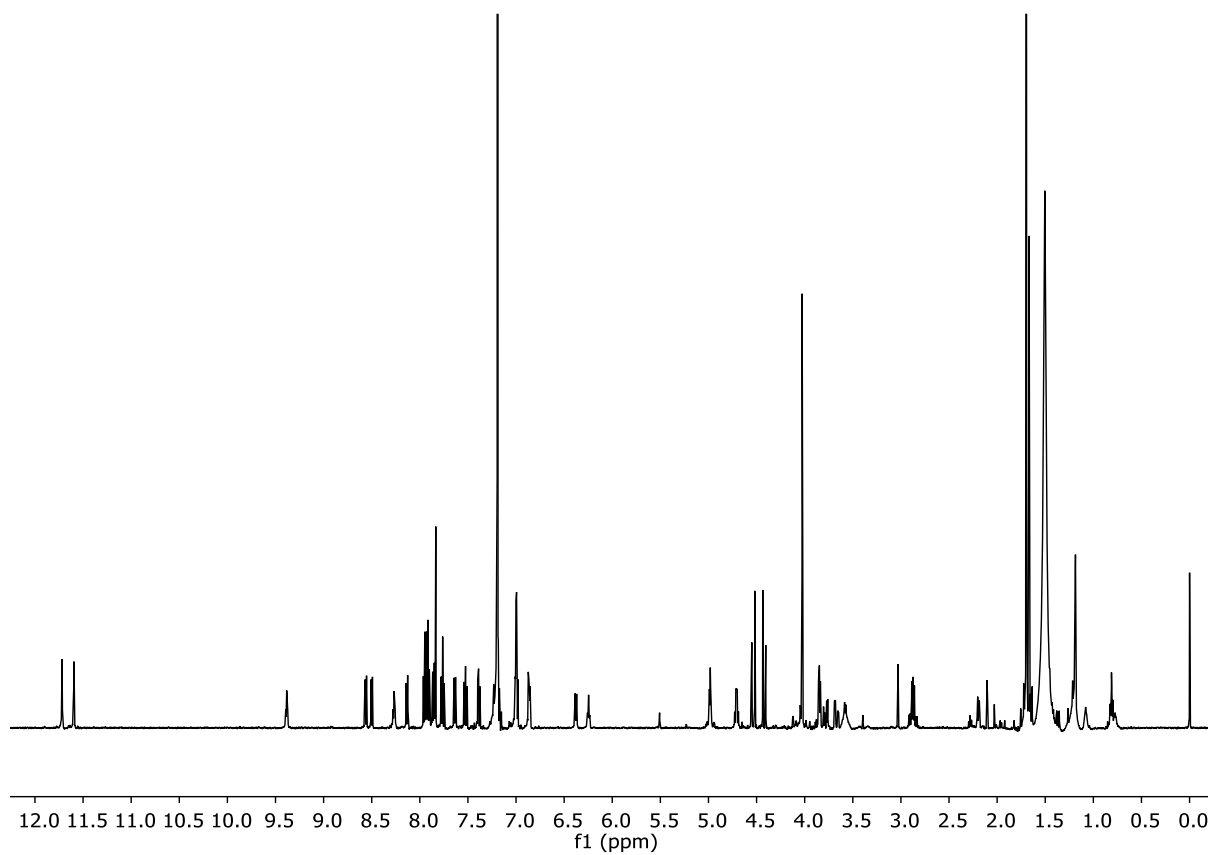
¹H NMR spectrum (500 MHz, CDCl₃, 25 °C) of **4**.



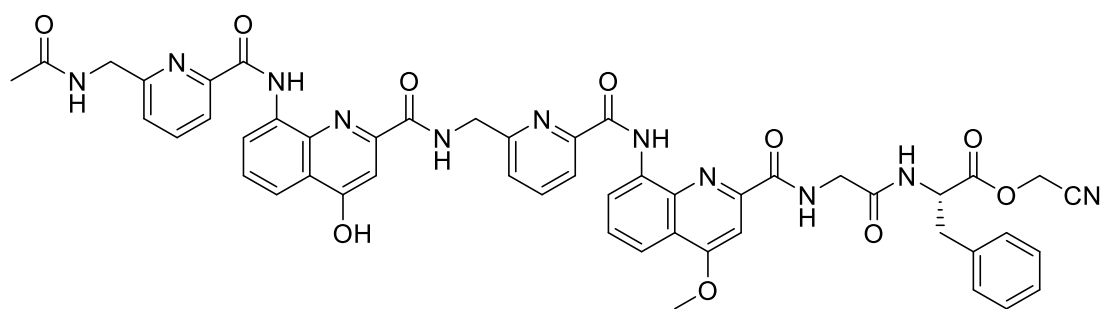
¹H NMR spectrum (500 MHz, DMSO-*d*₆, 25 °C) of **5**.



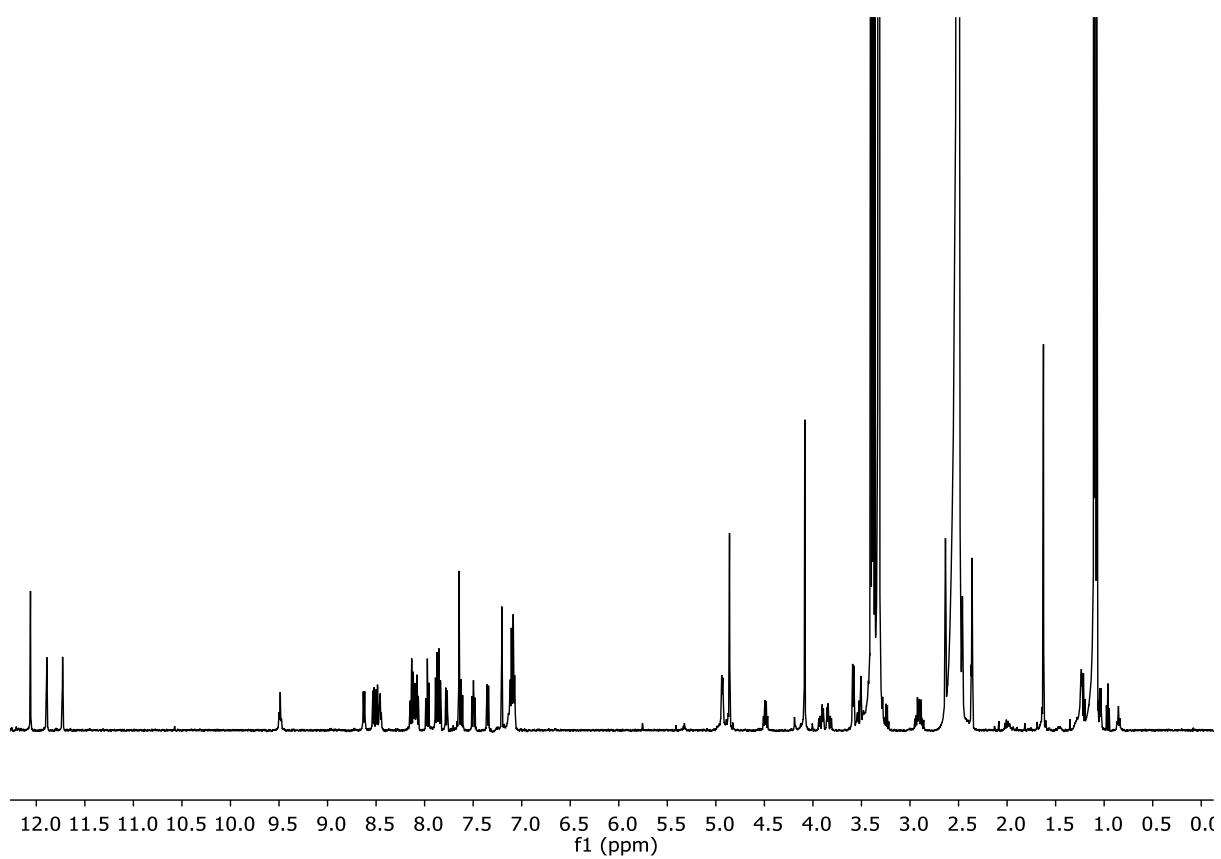
6b



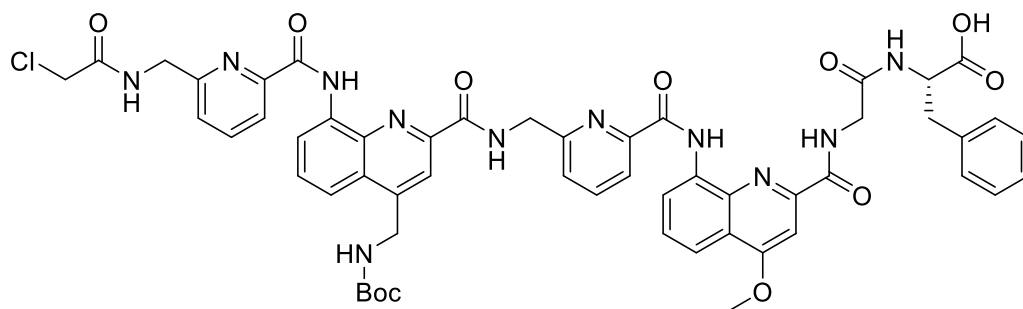
¹H NMR spectrum (500 MHz, CDCl₃, 25 °C) of **6b**.



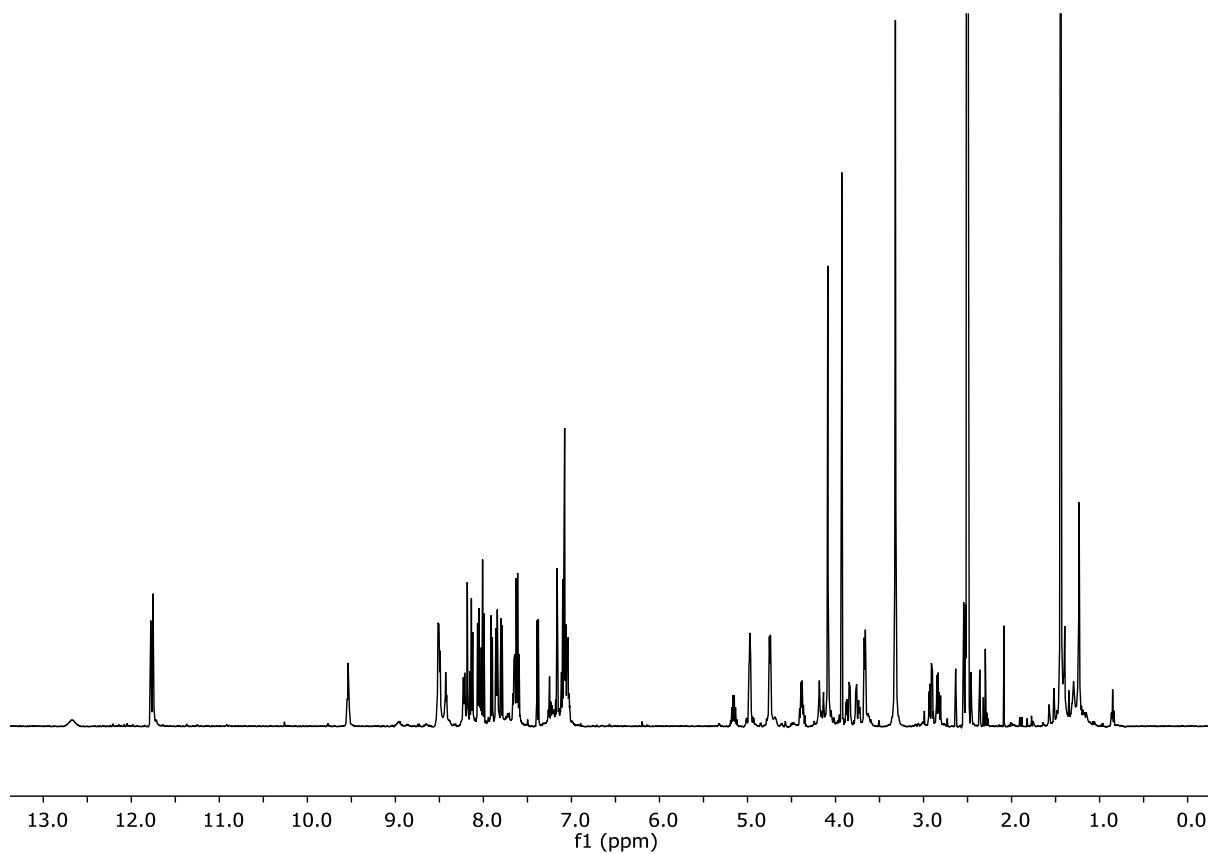
6



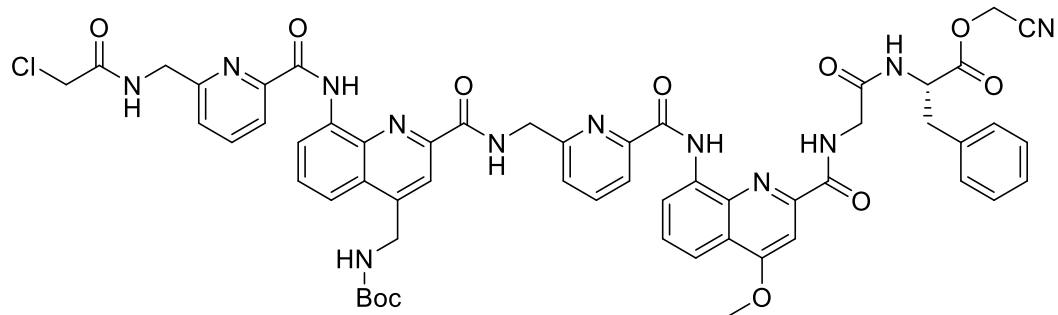
^1H NMR spectrum (500 MHz, $\text{DMSO-}d_6$, 25 °C) of 6.



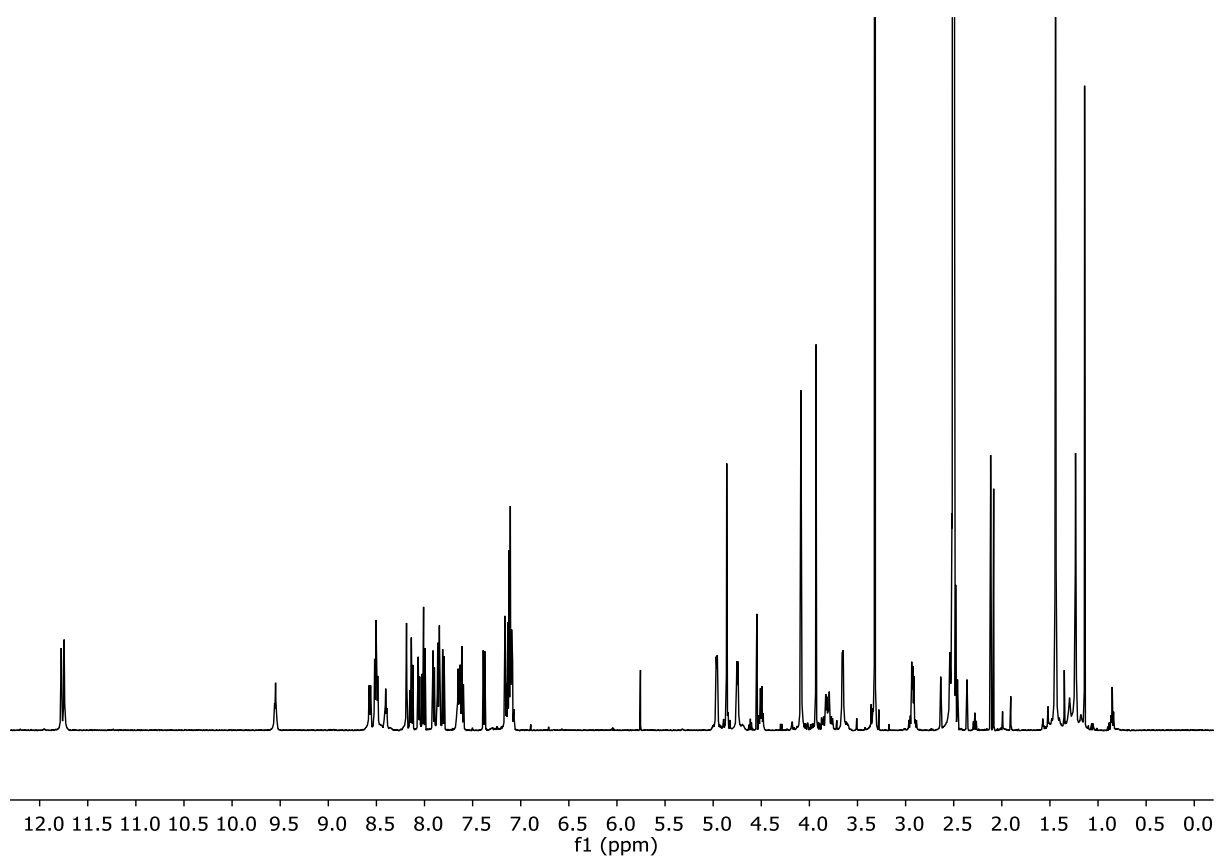
7a



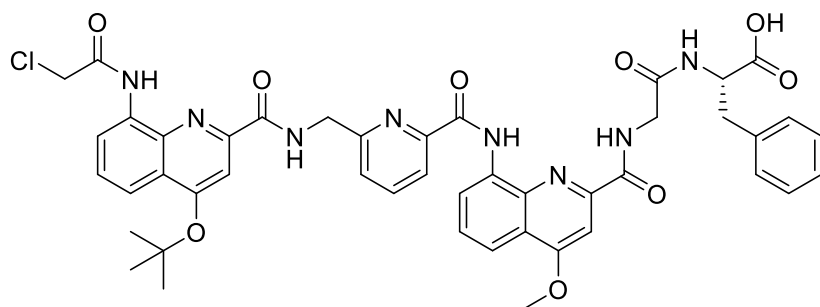
¹H NMR spectrum (500 MHz, DMSO-*d*₆, 25 °C) of **7a**.



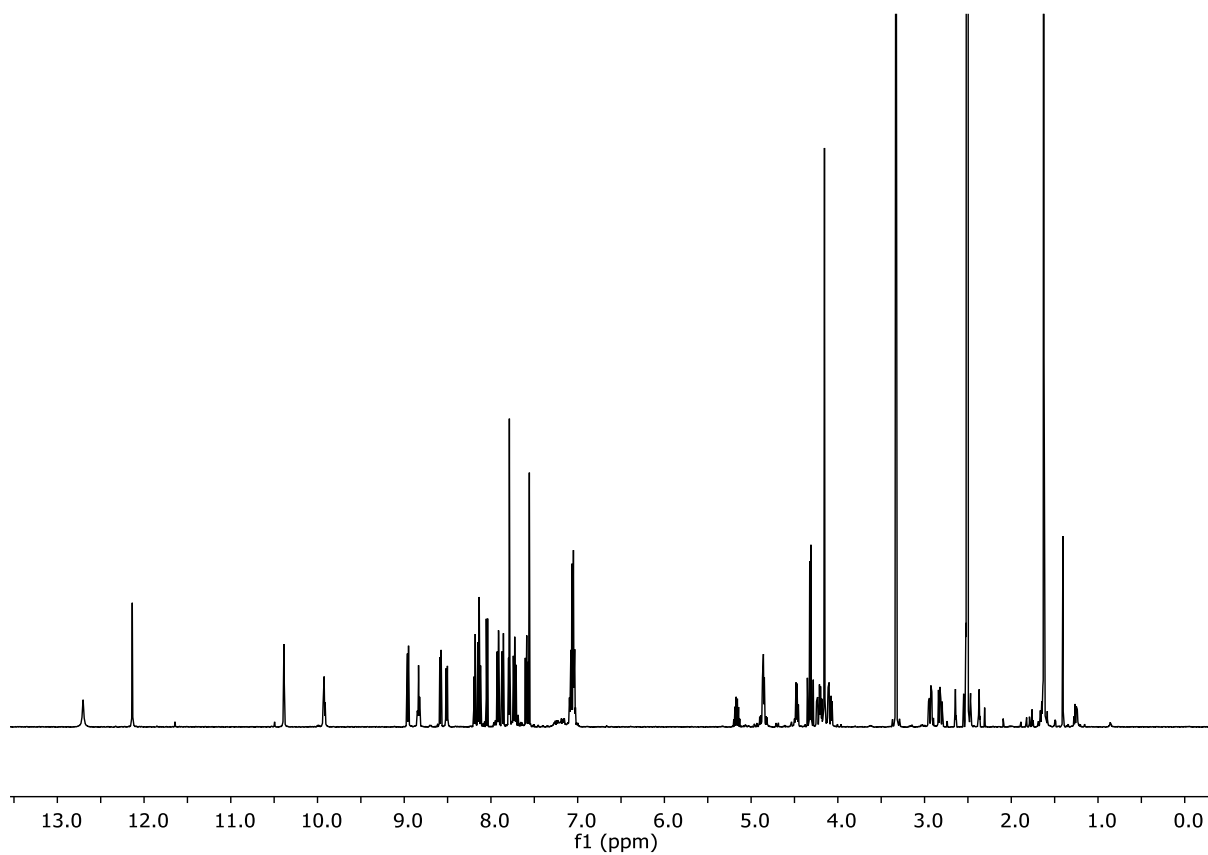
7b



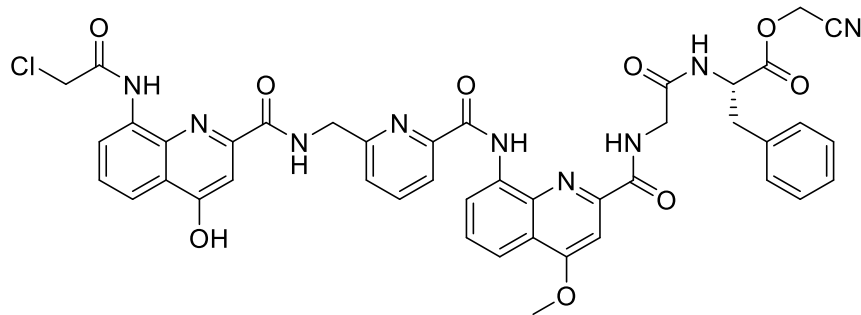
^1H NMR spectrum (500 MHz, $\text{DMSO-}d_6$, 25 °C) of **7b**.



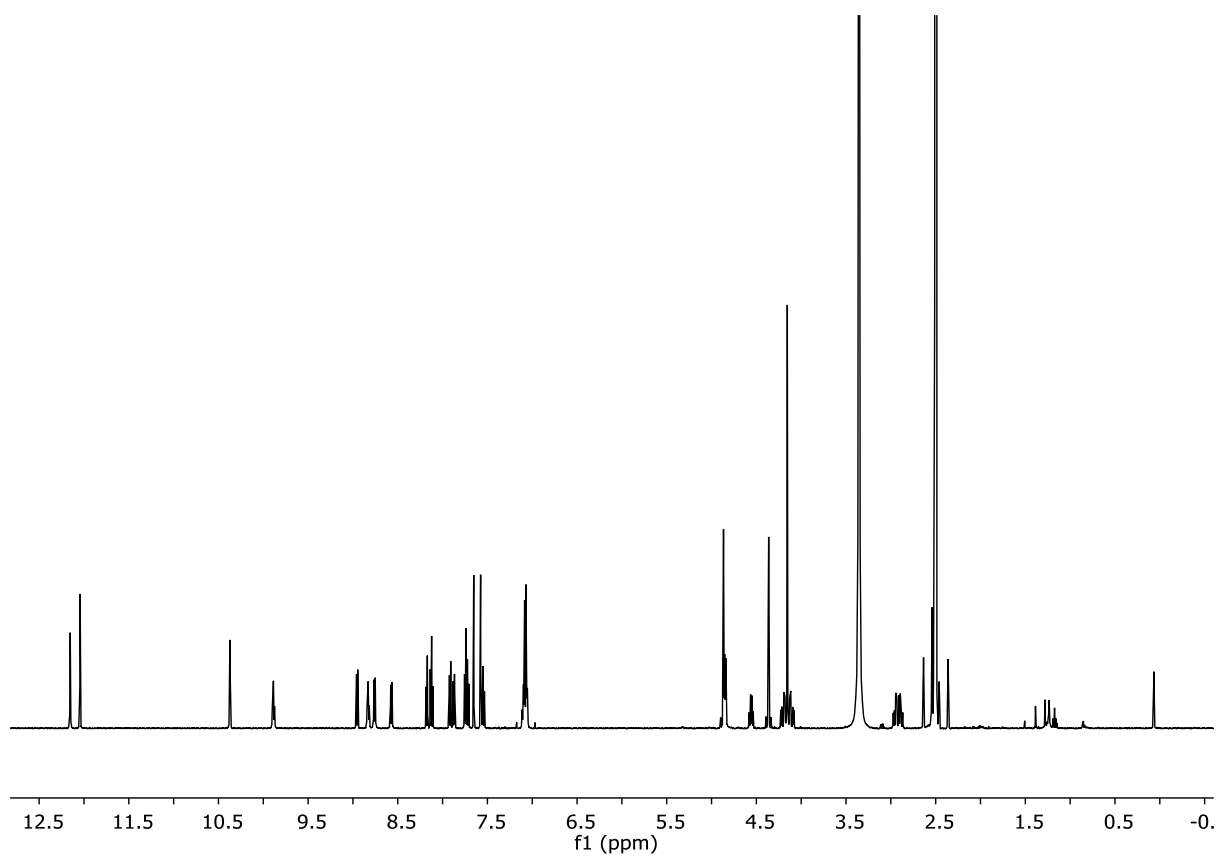
8a



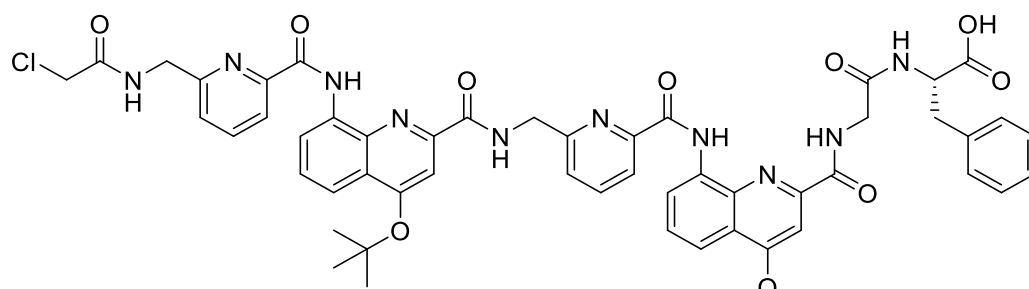
¹H NMR spectrum (500 MHz, DMSO-*d*₆, 25 °C) of **8a**.



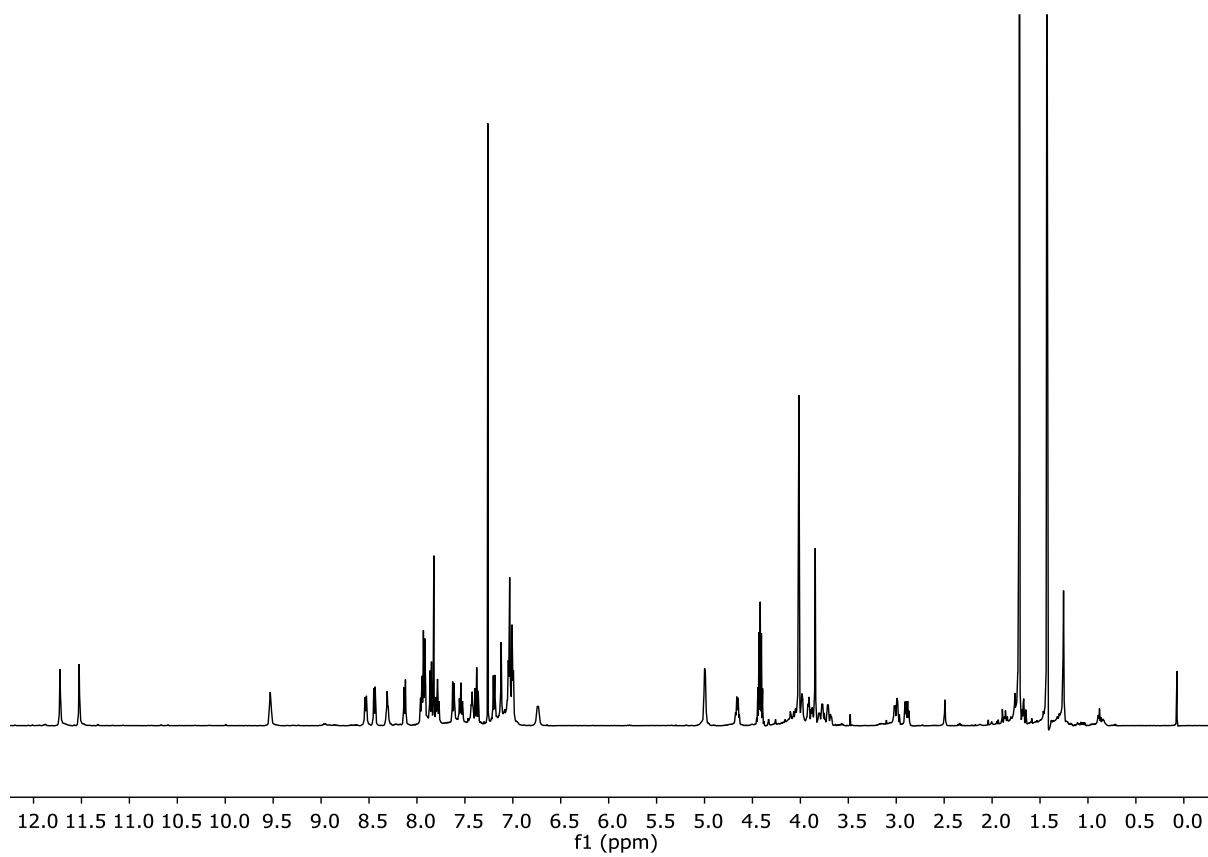
8



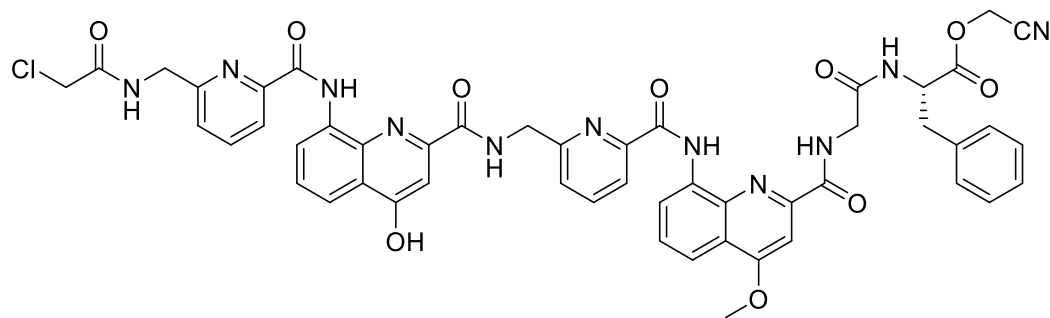
¹H NMR spectrum (500 MHz, DMSO-*d*₆, 25 °C) of **8**.



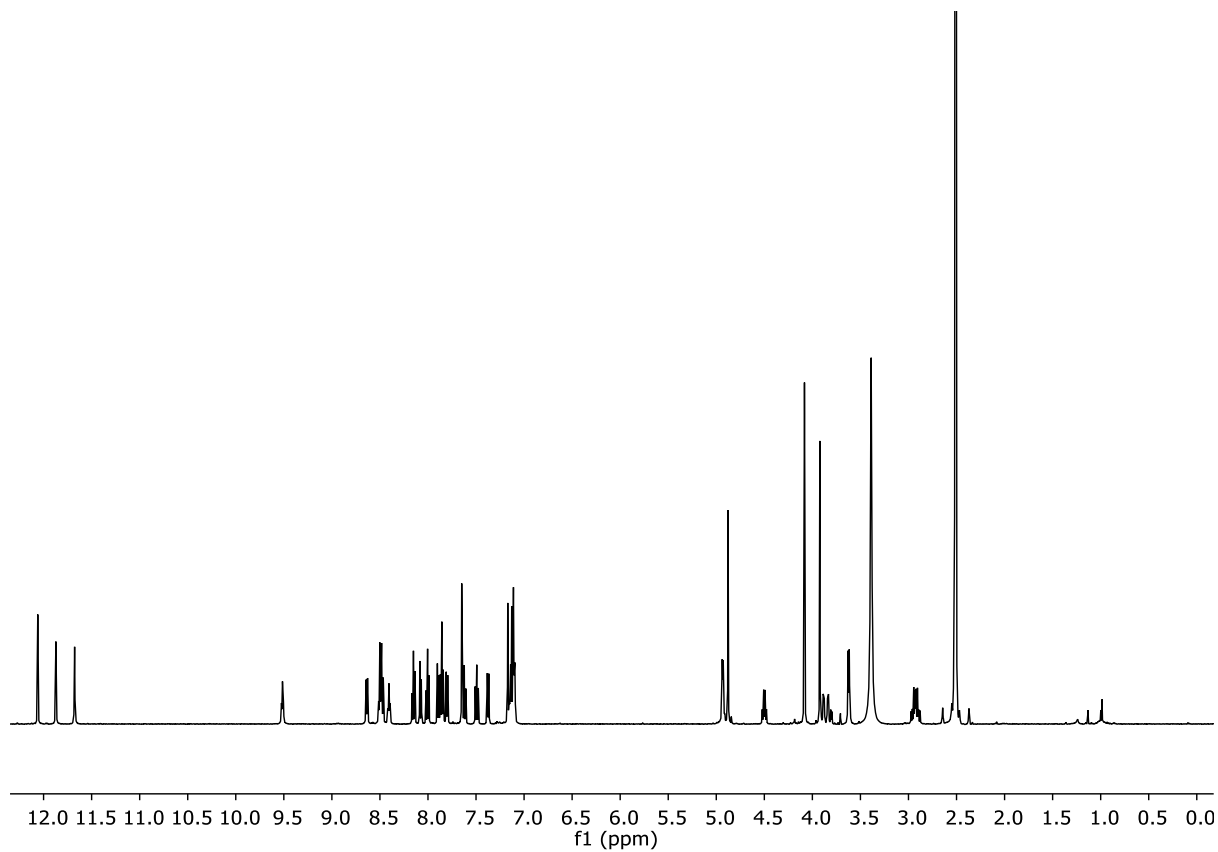
9a



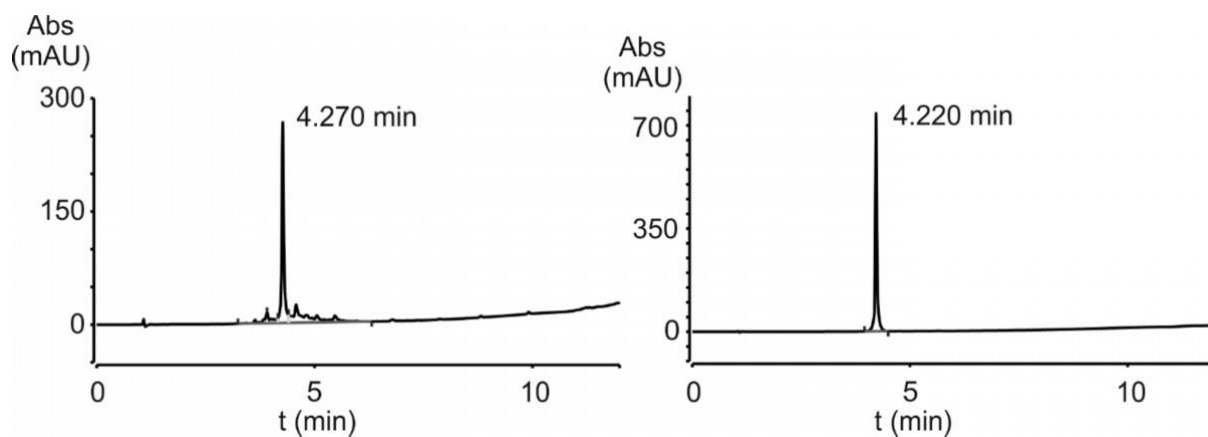
^1H NMR spectrum (500 MHz, CDCl_3 , 25 °C) of **9a**.



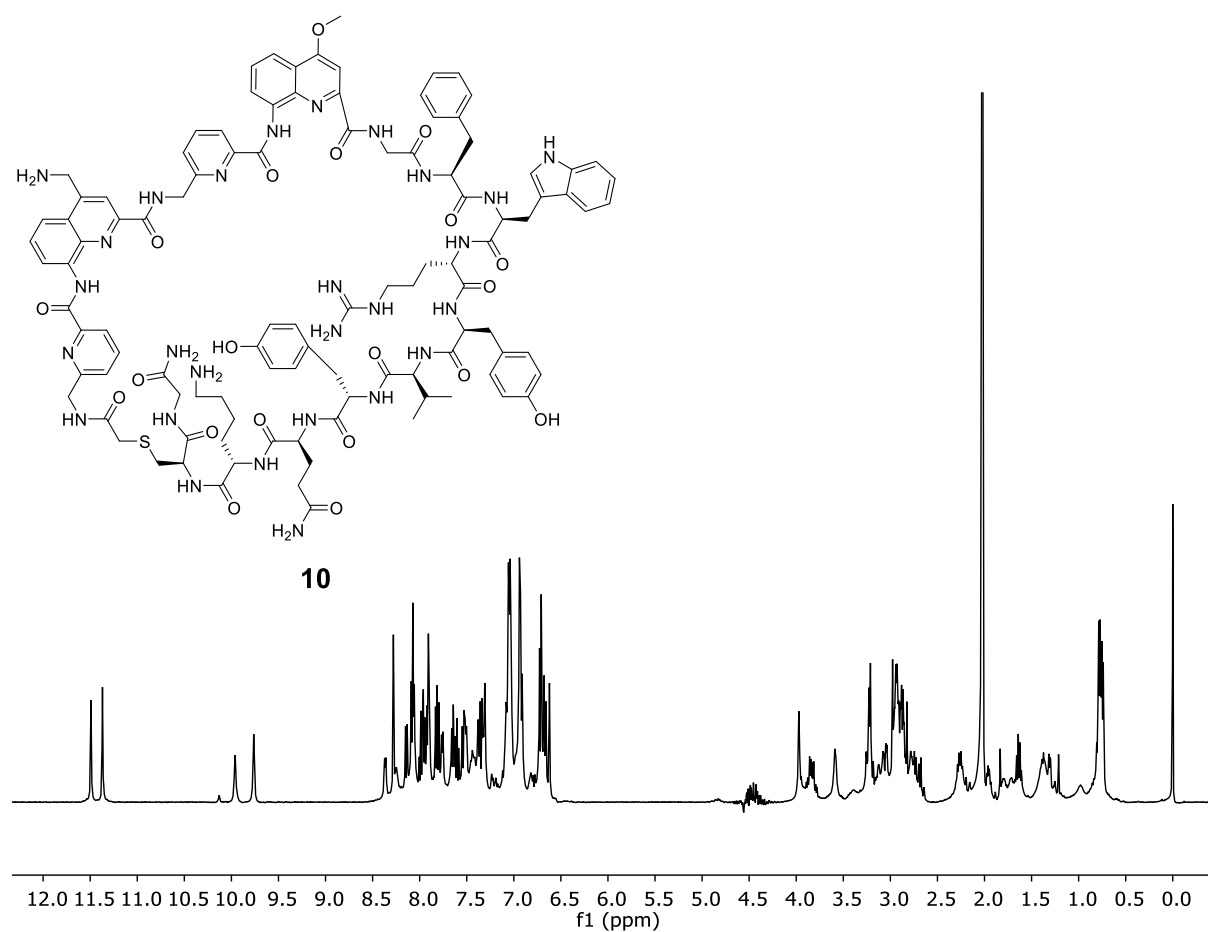
9



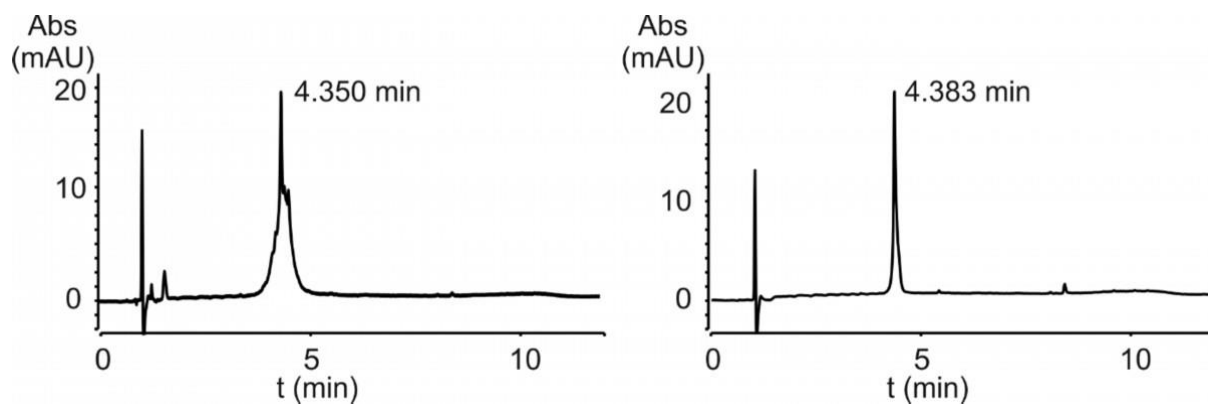
¹H NMR spectrum (500 MHz, DMSO-*d*₆, 25 °C) of **9**.



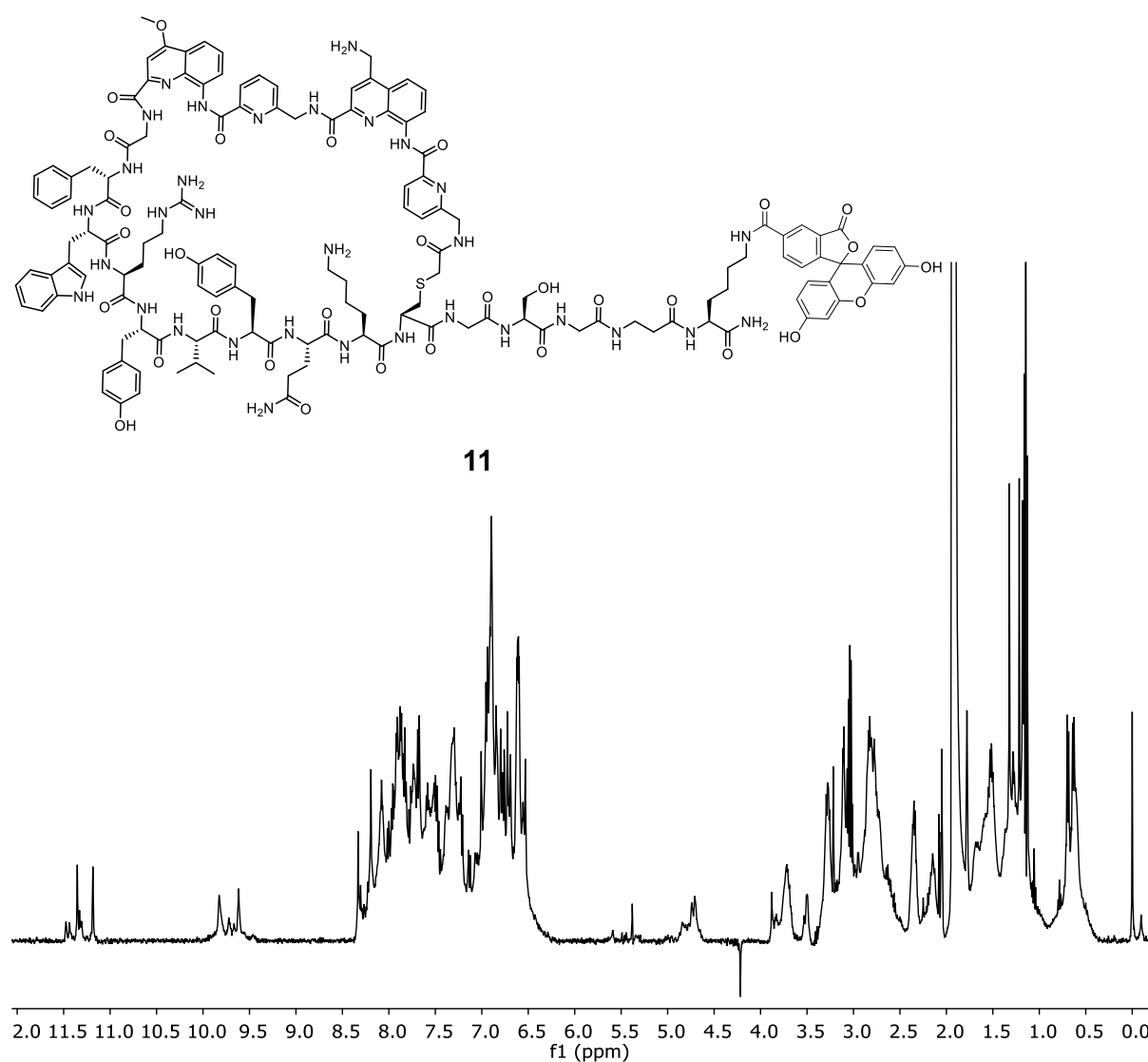
Analytical RP-HPLC profiles of **10** as a crude (left) and purified (right). RP-HPLC gradient: 10–100% (v/v) B over 10 min, 50 °C, $\lambda = 254$ nm).



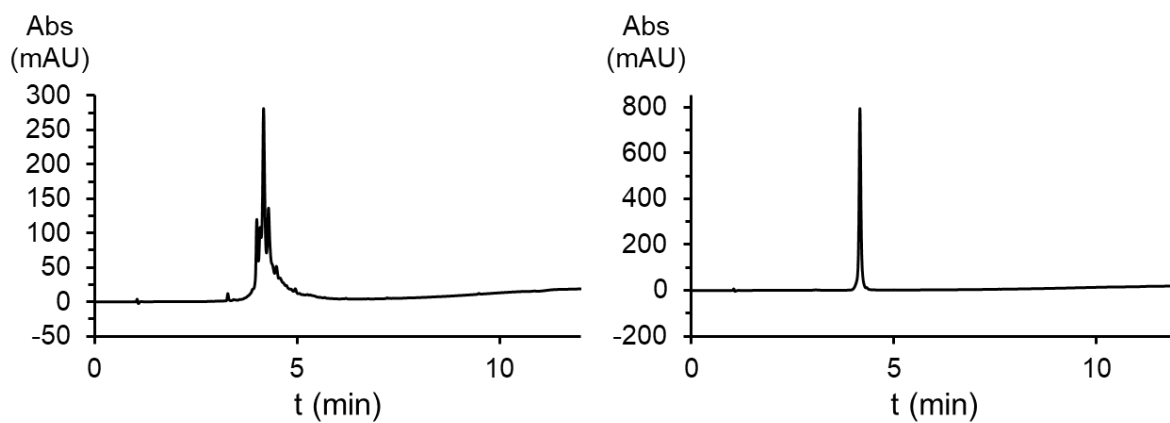
^1H NMR spectrum (500 MHz, water with 25% (v/v) acetonitrile- d_3 , water suppression, 25 °C) of **10**.



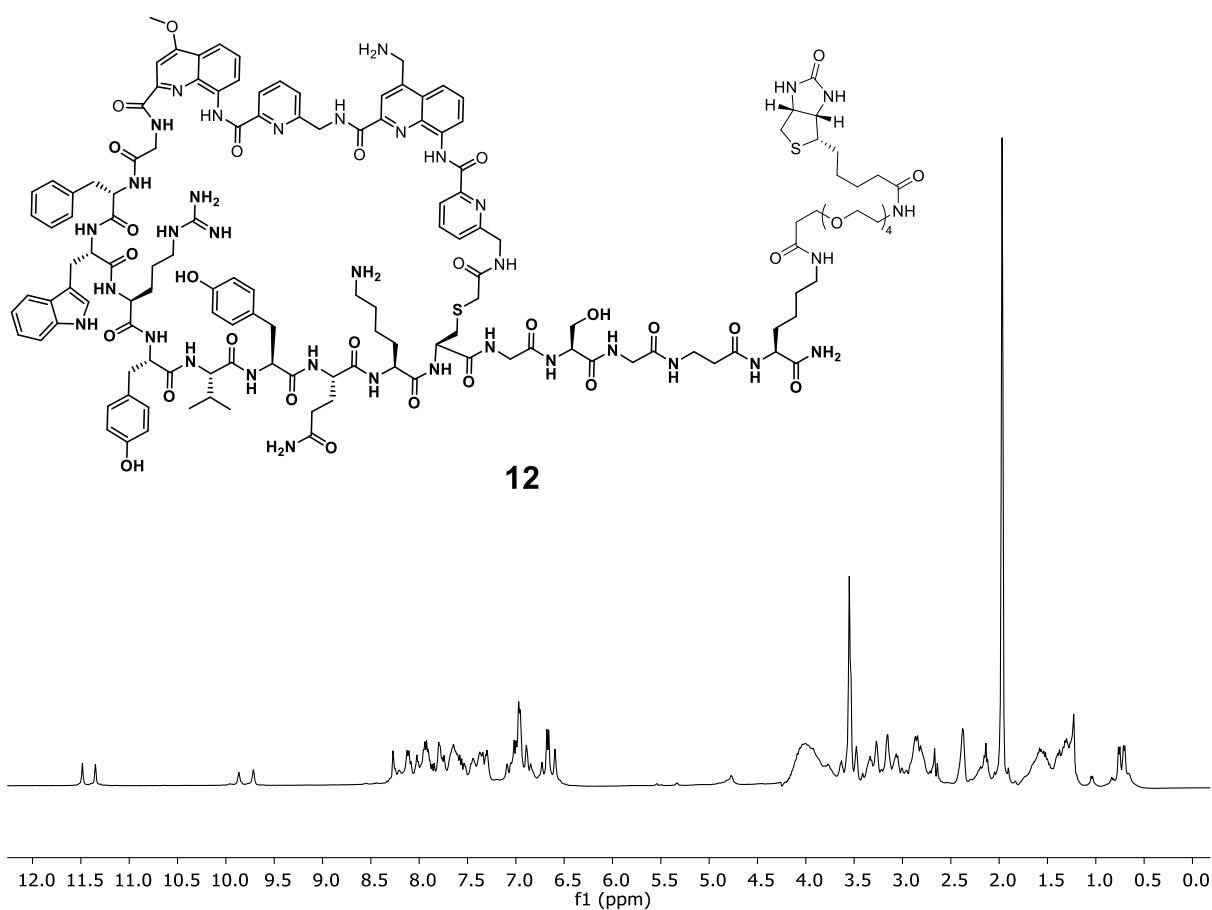
Analytical RP-HPLC profile of **11** as a crude (left) and purified (right). RP-HPLC gradient: 10–100% (v/v) B over 10 min, 50 °C, $\lambda = 254$ nm).



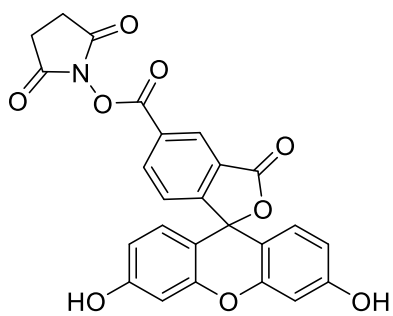
^1H NMR spectrum (500 MHz, 0.1 M HCl with 50% (v/v) acetonitrile- d_3 , water suppression, 25 °C) of **11**.



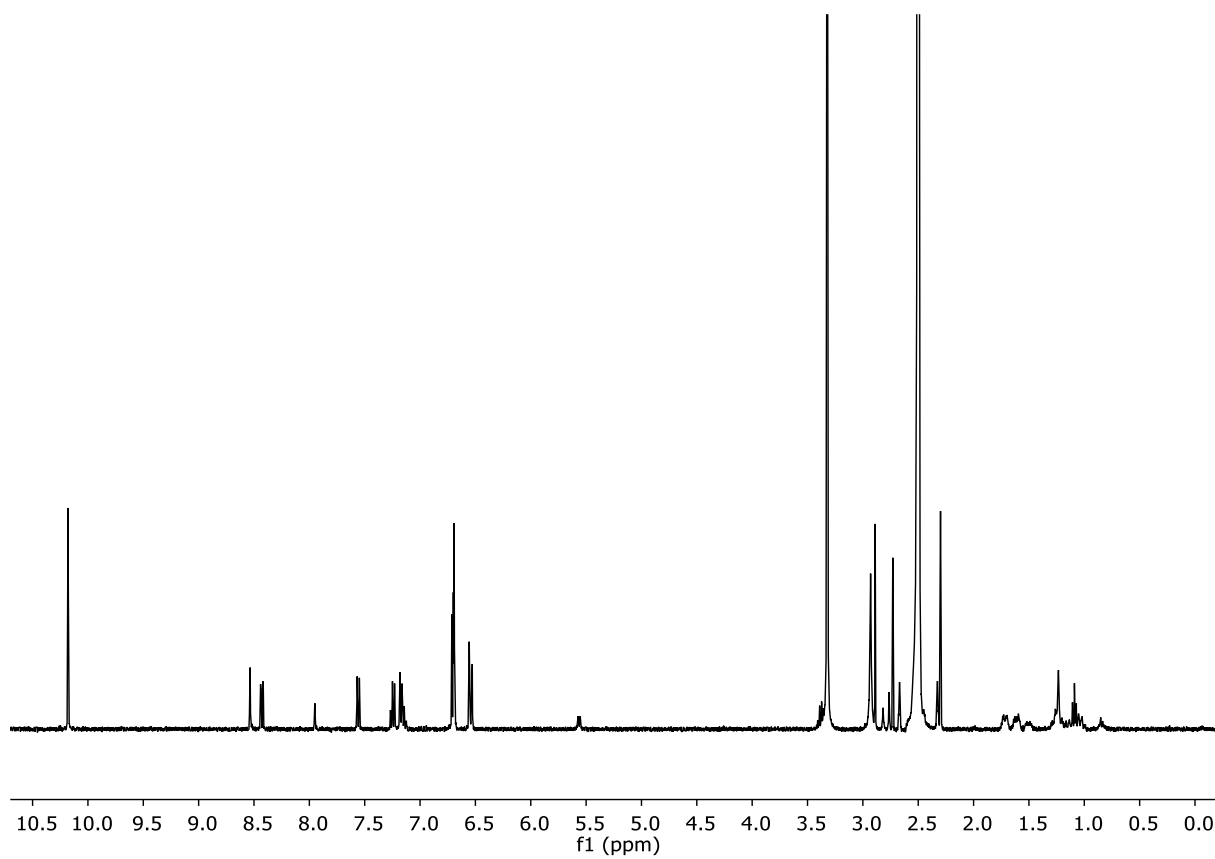
Analytical RP-HPLC profiles of **12** as a crude (left) and purified (right). RP-HPLC gradient: 10–100% (v/v) B over 10 min, 50 °C, $\lambda = 254$ nm).



^1H NMR spectrum (500 MHz, water with 50% (v/v) acetonitrile- d_3 , water suppression, 25 °C) of **12**.



13



¹H-NMR Spectrum (400 MHz, DMSO-*d*₆, 25°C) of **13**.

9.17. Supporting references

- [1] H. Jiang, J.-M. Léger, I. Huc, *J. Am. Chem. Soc.* **2003**, *125*, 3448–3449.
- [2] S. Dengler, P. K. Mandal, L. Allmendinger, C. Douat, I. Huc, *Chem. Sci.* **2021**, *12*, 11004–11012.
- [3] A. C. Wallace, R. A. Laskowski, J. M. Thornton, *Protein Eng.* **1995**, *8*, 127–34.
- [4] L. K. Ries, A. K. L. Liess, C. G. Feiler, D. E. Spratt, E. D. Lowe, S. Lorenz, *Protein Sci.* **2020**, *29*, 1550–1554.
- [5] H. Murakami, A. Ohta, H. Ashigai, H. Suga, *Nat. Methods* **2006**, *35*, 357–359.
- [6] Y. Goto, A. Ohta, Y. Sako, Y. Yamagishi, H. Murakami, H. Suga, *ACS Chem. Biol.* **2008**, *3*, 120–129.
- [7] T. Katoh, I. Wohlgemuth, M. Nagano, M. V. Rodnina, H. Suga, **2016**, DOI 10.1038/ncomms11657.
- [8] T. Katoh, Y. Iwane, H. Suga, *Nucleic Acids Res.* **2017**, *45*, 12601–12610.
- [9] Y. Hayashi, J. Morimoto, H. Suga, *ACS Chem. Biol.* **2012**, *7*, 607–613.
- [10] D. J. Ford, N. M. Duggan, S. E. Fry, J. Ripoll-Rozada, S. M. Agten, W. Liu, L. Corcilius, T. M. Hackeng, R. Van Oerle, H. M. H. Spronk, A. S. Ashhurst, V. Mini Sasi, J. A. Kaczmarek, C. J. Jackson, P. J. B. Pereira, T. Passioura, H. Suga, R. J. Payne, *J. Med. Chem.* **2021**, *64*, 7853–7876.
- [11] D. Nurizzo, T. Mairs, M. Guijarro, V. Rey, J. Meyer, P. Fajardo, J. Chavanne, J.-C. Basci, S. McSweeney, E. Mitchell, *J. Synchrotron Radiat.* **2006**, *13*, 227–238.
- [12] L. Huang, E. Kinnucan, G. Wang, S. Beaudenon, P. M. Howley, J. M. Huibregtse, N. P. Pavletich, *Science* **1999**, *286*, 1321–1326.
- [13] P. Emsley, B. Lohkamp, W. G. Scott, K. Cowtan, *Acta Crystallogr. Sect. D Biol. Crystallogr.* **2010**, *66*, 486–501.
- [14] D. Liebschner, P. V. Afonine, M. L. Baker, G. Bunkóczi, V. B. Chen, T. I. Croll, B. Hintze, L.-W. Hung, S. Jain, A. J. McCoy, N. W. Moriarty, R. D. Oeffner, B. K. Poon, M. G. Prisant, R. J. Read, J. S. Richardson, D. C. Richardson, M. D. Sammito, O. V. Sobolev, D. H. Stockwell, T. C. Terwilliger, A. G. Urzhumtsev, L. L. Videau, C. J. Williams, P. D. Adams, *Acta Crystallogr. Sect. D Struct. Biol.* **2019**, *75*, 861–877.
- [15] E. Potterton, P. Briggs, M. Turkenburg, E. Dodson, *Acta Crystallogr. Sect. D Biol. Crystallogr.* **2003**, *59*, 1131–1137.
- [16] I. Jarmoskaite, I. AlSadhan, P. P. Vaidyanathan, D. Herschlag, *Elife* **2020**, *9*, 1–34.
- [17] Z. Liu, A. M. Abramyan, V. Pophristic, *New J. Chem.* **2015**, *39*, 3229–3240.
- [18] D. A. Case, H. M. Aktulga, K. Belfon, I. Y. Ben-Shalom, S. R. Brozell, D. S. Cerutti, T. E. Cheatham III, V. W. D. Cruzeiro, T. A. Darden, R. E. Duke, G. Giambasu, M. K. Gilson, H. Gohlke, A. W. Goetz, R. Harris, S. Izadi, S. A. Izmailov, K. Kasavajhala, A. Kovalenko, R. Kransy, T. Kurtzman, T. S. Lee, S. LeGrand, P. Li, C. Lin, J. Liu, T. Luchko, R. Luo, V. Man, K. M. Merz, Y. Miao, O. Mikhailovskii, G. Monard, H. Nguyen, A. Onufriev, F. Pan, S. Pantano, R. Qi, D. R. Roe, A. Roitberg, C. Sagui, S. Schott-Verdugo, J. Shen, C. L.

- Simmerling, N. R. Skrynnikov, J. Smith, J. Swails, R. C. Walker, J. Wang, L. Wilson, R. M. Wolf, X. Wu, Y. Xiong, Y. Xue, D. M. York, P. A. Kollman (2020), AMBER 2020, University of California, San Francisco.
- [19] J. A. Maier, C. Martinez, K. Kasavajhala, L. Wickstrom, K. E. Hauser, C. Simmerling, *J. Chem. Theory Comput.* **2015**, *11*, 3696–3713.
- [20] J. Wang, R. M. Wolf, J. W. Caldwell, P. A. Kollman, D. A. Case, *J. Comput. Chem.* **2004**, *25*, 1157–1174.
- [21] J. Wang, P. Cieplak, P. A. Kollman, *J. Comput. Chem.* **2000**, *21*, 1049–1074.
- [22] W. Kabsch, C. Sander, *Biopolymers* **1983**, *22*, 2577–2637.
- [23] J. Buratto, C. Colombo, M. Stupfel, S. J. Dawson, C. Dolain, B. Langlois d’Estaintot, L. Fischer, T. Granier, M. Laguerre, B. Gallois, I. Huc, *Angew. Chem.* **2014**, *126*, 902–906.
- [24] S. De, B. Chi, T. Granier, T. Qi, V. Maurizot, I. Huc, *Nat. Chem.* **2018**, *10*, 51–57.
- [25] M. Vallade, P. Sai Reddy, L. Fischer, I. Huc, *Eur. J. Org. Chem.* **2018**, *2018*, 5489–5498.
- [26] J. M. Rogers, S. Kwon, S. J. Dawson, P. K. Mandal, H. Suga, I. Huc, *Nat. Chem.* **2018**, *10*, 405–412.

10. Main Text: Differential Peptide Multi-Macrocyclizations at the Surface of a Helical Foldamer Template

Authors: Sebastian Dengler, Céline Douat and Ivan Huc

Published: *Angew. Chem. Int. Ed.* **2022**, 61, e202211138

DOI: <https://doi.org/10.1002/anie.202211138>

Author contribution: The project was conceptualized and supervised by I. Huc. C. Douat co-supervised the work. The manuscript was written by C. Douat, I. Huc, and me. Most of the experimental work was performed by me.

VIP **Foldamers** Very Important Paper

How to cite:

International Edition: doi.org/10.1002/anie.202211138

German Edition: doi.org/10.1002/ange.202211138

Differential Peptide Multi-Macrocyclizations at the Surface of a Helical Foldamer Template

Sebastian Dengler, Céline Douat, and Ivan Huc*

Abstract: Hybrid sequences comprising a peptide with several Cys residues and an aromatic foldamer helix with several chloroacetamide functions at its surface were synthesized. Such products may in principle form numerous macromulticyclic thioether products by intramolecularly combining all Cys residues and all chloroacetamide functions. However, we show that the reactive sites on the structurally defined helix can be placed at such locations that the peptide selectively stitches itself to form a series of different macrocycles within mostly one preferred product. Reactions were monitored by HPLC and products with two, three or four macrocycles were identified using LC-MS and NMR. The series of selective macrocyclizations define a sort of reaction trail where reaction sites otherwise identical are involved successively because of their precise positioning in space. The trails can be predicted to a large extent based on structural considerations and the assumption that smaller macrocycles form faster.

Introduction

The importance of cyclic and macrocyclic molecules in chemistry cannot be overstated. It generally stems from the benefits provided by their limited conformational freedom. Innumerable cyclization methods have been reported and the key role played by stereochemical and conformational preorganization in these reactions has been thoroughly highlighted.^[1,2] Macrocyclic peptides are a large subclass of cyclic molecules with a high potential to bind protein target surfaces.^[3] Multiple peptide macrocyclization reactions have been validated^[4,5] some of which, e.g. the simple substitution of a chloromethylene function by the thiol of a Cys residue to form a thioether, are so efficient that they can be

performed reliably and concomitantly on libraries of trillions of different peptides for display selection.^[3,6]

At the exclusion of ladder polymers where the same cyclization step is repeated many times,^[7] preparing molecules with multiple cycles generally requires elaborate strategies. The careful positioning of reactive functions on a small molecule may lead to a reaction cascade that produces several different rings at once.^[8] Bimacrocycles of variable size and composition can be efficiently produced from peptides containing three Cys residues and a 1,3,5-tris-bromomethyl platform, thanks to the C_3 -symmetry of the platform which yields the same product regardless of which Cys residue reacts first, second or third.^[9] Typical synthetic and biosynthetic strategies to produce multimacrocyclic molecules rely on independent cyclization steps involving different reaction groups, which can be cumbersome. Yet some notable exceptions exist. For example, chemical and stereochemical preferences in disulfide bridge formation, including the fact that disulfides are subject to exchange reactions, have allowed for the direct preparation of complex multicycles.^[9b,10] In proteins as well, specific arrays of disulfide bridges may form, directed by both structural control (folding) and disulfide exchange (mediated by protein disulfide isomerases).^[11]

Here, we report that a series of different peptide macrocycles may form selectively at the surface of a structurally well-defined aromatic oligoamide foldamer helix derived from δ -amino acids. In contrast with the above examples of multimacrocyclization, the functionalities involved are all identical—up to four thiols and four chloroacetamides—and reactions are irreversible. Selective macrocyclizations take place at the expense of the multiple intramolecular products that may in principle be expected. Selectivity is predictable and appears to be guided by ring size, with the smallest ring forming first, reducing the size of the subsequent smallest ring, and by the structural organization imparted by the aromatic helix which places some reactive centers out of the reach of others. The outcome is a sort of reaction trail^[12] along which a flexible peptide chain stitches itself in a certain order to bridge reactive centers at the surface of a well-defined molecular scaffold. The products consist of a compact hydrophobic core (the aromatic helix) surrounded by peptide loops. They are reminiscent of protein structures and might thus find use as multivalent protein binders.

[*] S. Dengler, Dr. C. Douat, Prof. Dr. I. Huc
Department of Pharmacy and Center for Integrated Protein Science,
Ludwig-Maximilians-Universität
Butenandtstr. 5–13, 81377 München (Germany)
E-mail: ivan.huc@cup.lmu.de

© 2022 The Authors. Angewandte Chemie International Edition published by Wiley-VCH GmbH. This is an open access article under the terms of the Creative Commons Attribution Non-Commercial License, which permits use, distribution and reproduction in any medium, provided the original work is properly cited and is not used for commercial purposes.

Results and Discussion

Design and synthesis

We have previously reported the formation of helical aromatic oligoamide foldamer/peptide hybrid macrocycles via the substitution of an N-terminal chloroacetamide on the foldamer helix by a Cys thiol near the C-terminus of the peptide (Figure 1, left).^[13] Interest for these compounds followed the discovery that they may be produced—when the foldamer is short enough—by ribosomal peptide translation through reprogramming the initiation step with a foldamer-functionalized tRNA, paving the way to display selection experiments.^[14] Aromatic foldamers containing 4-substituted 8-amino-2-quinoline carboxylic acid units (Q^{Xxx} , Figure 2a) adopt particularly stable helical conformations in water.^[15] Within the macrocycles, the folding propensity of the aromatic segments was shown to influence peptide conformation and enhance peptide resistance toward proteolytic degradation and, in a reciprocal effect, the chirality of the peptides was shown to bias foldamer helix handedness.^[13,14]

Encouraged by this background, we set out to test whether a large peptide loop may be connected more than once to the rigid foldamer helix, *de facto* further reducing its conformational freedom and creating several different macrocycles (Figure 1). For this purpose, we prepared a series of foldamer-peptide hybrids in which the peptide contains a variable number of Cys residues separated by loops of different sizes, and the foldamer displays chloroacetamides as side chain appendages at different positions of the helix, and investigated their cyclization. Systematic

variations of the peptide sequences were not considered for this study. Nevertheless, the peptides were designed so as to contain diverse sequences, keeping some polar residues to preserve water solubility and avoiding synthetically demanding residues (e.g. Pro, Val, His). A generic structure is shown in Figure 2b. To simplify the presentation, the foldamer units are numbered from the C-terminus while the α -amino acid residues (AAs) are numbered from the N-terminus. Thus, all sequences comprise a Q^{Asp1} -Gly1 linkage at the foldamer-peptide junction. All sequences also comprise a B^{Rme4} unit near the middle of the foldamer segment. This chiral residue quantitatively biases helix handedness towards its left-handed conformation.^[16] Typically, induced CD bands indicate handedness bias and a single set of signals on 1H NMR spectra as well as a single HPLC peak confirm full handedness control.^[13] The foldamer segment generally consisted of Q^{Asp} and Q^{Dap} charged residues to provide solubility in both basic and acidic aqueous media and was acetylated or acylated with a short diethylene-glycol-containing acid at the N-terminus. A new Alloc-protected Fmoc- $Q^{Dap(Alloc)}$ -OH monomer was synthesized to anchor chloroacetamide functions at the final stage of solid phase synthesis.

Synthetic methods and protocols are described in detail in the Supporting Information. Typically, the Cys-containing peptide was first prepared via conventional Fmoc-based chemistry under microwave irradiation and phosphonium-based coupling conditions (i.e. PyBOP and DIPEA) on a low loading Fmoc-Gly-Wang resin (scale 50–100 μ mol). From there, solid phase foldamer synthesis can be continued with Fmoc- Q^{Xxx} monomers, including some $Q^{Dap(Alloc)}$, and Appel coupling conditions.^[15a,17] We also validated the

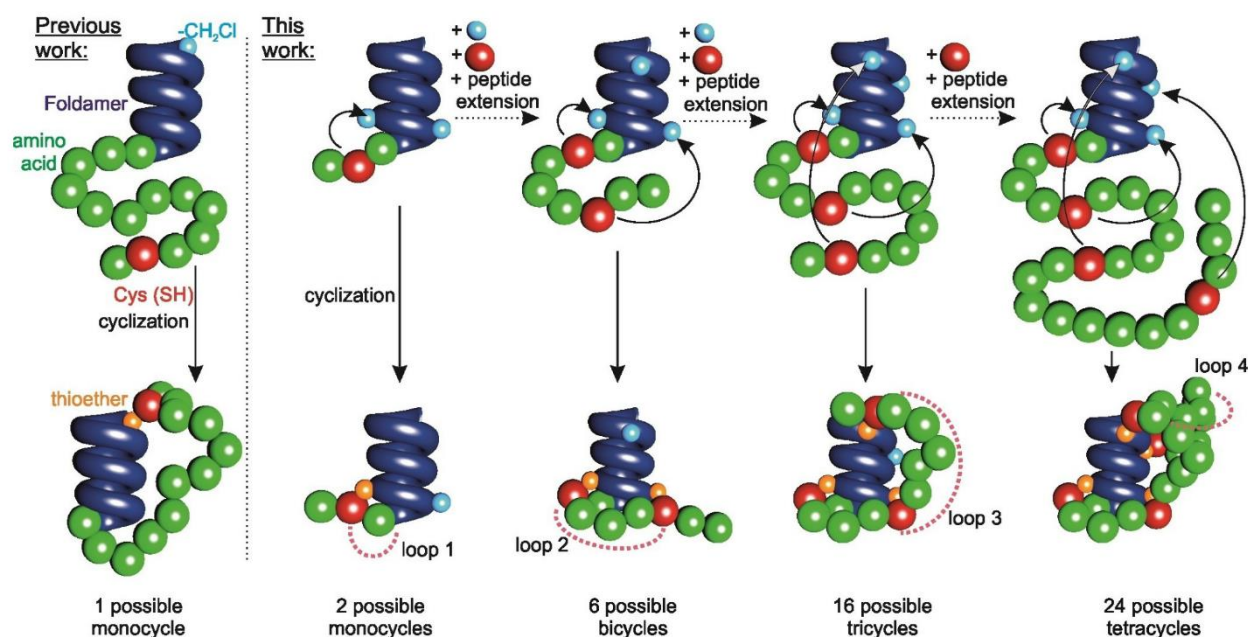


Figure 1. Schematic illustration of selective macrocyclizations of helical aromatic foldamer-peptide hybrids. The foldamer is shown as a blue helix tube and the peptide as a string of balls. Upon careful positioning of chloroacetamide electrophiles on the helix and of Cys thiols in the peptide sequence, i.e. through the adjustment of peptide loop size, selective reaction trails^[12] can be programmed to form multicyclic products.

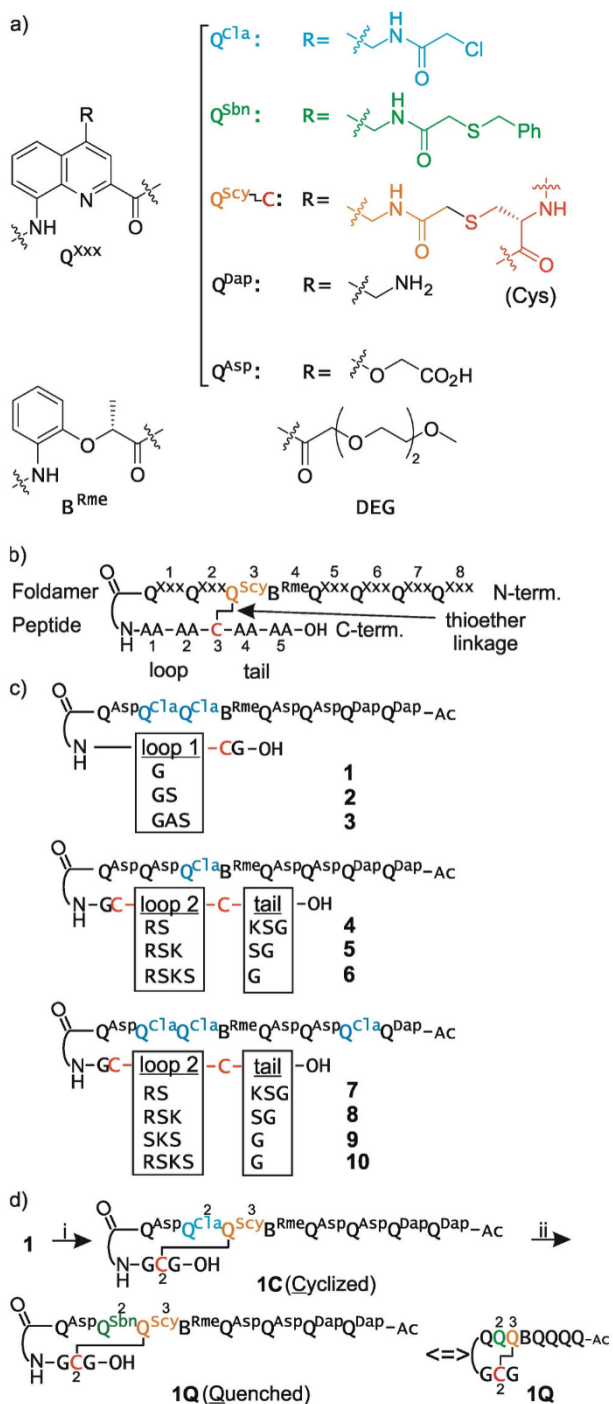


Figure 2. a) Foldamer building blocks. b) Generic cyclic foldamer-peptide hybrid defining sequence numbering, peptide loops, and tail. c) Sequences with variable loop sizes investigated for the preparation of mono and bicyclic structures. Amino acids are designated by the single letter code. d) Representative reaction scheme from **1** towards monocycle **1C** and its quenched derivative **1Q**. (i) aqueous basic conditions; (ii) addition of benzyl mercaptan. A simplified depiction of **1Q** is also shown and used in other figures. Note that Q within the foldamer segment refers to a color-coded Q^{xxx} quinoline-based monomer (as in (a)), not to glutamine (Q, Gln) which may also be present in the peptide or the letter Q used in the quenched products (e.g. **1Q**).

possibility to presynthesize and purify a protected Fmoc-foldamer-Gly-OH segment on SASRIN[®] resin and ligate it directly to the resin-bound free amine peptide (see ESI section 2.4.3.3.). With the protected foldamer-peptide hybrid still on the resin, Alloc protections were selectively removed and the corresponding Q^{Dap} monomers were converted into Q^{Clax} units (Figure 2a) with chloroacetic anhydride. After TFA cleavage and side chain deprotection, the purification of the hybrid oligomers was carried out by semi-preparative RP-HPLC in acidic media (hence the importance of solubility). At pH 2, the thiols and chloroacetamides did not react. The linear foldamer-peptide hybrids were recovered in good to moderate yields with purity over 95 %.

Cyclizations were triggered under basic conditions (TEA buffer pH 10 or $NaHCO_3$ buffer pH 8.5),^[18] converting Q^{Clax} units into Q^{Scy} connected to a Cys residue by a thioether. Low concentrations (25–100 μ M) favored intramolecular processes. Oxygen was removed in most cases by freeze-pump-thaw cycles and tris(2-carboxyethyl)phosphine (TCEP) was further added to avoid disulfide formation. Acetonitrile was added to enhance solubility. Urea (8 M) was sometimes used as a chaotropic additive (see below). Progression of the cyclizations could be monitored by RP-HPLC and mass spectrometry (LC-ESI-MS, see Figures S2, S4–S17, S20–S26, S29–S31). Conversion yields were estimated by integrating HPLC peak areas against an internal reference. After cyclization, unreacted chloroacetamides could be quenched with benzyl mercaptan yielding hydrophobic Q^{Sbn} units. Fmoc- Q^{Sbn} -OH was also synthesized and incorporated directly in some sequences to ascertain compound identification (Figures S3, S18, S19, S27, S28). Sequences 4–6 which possess an excess number of Cys residues were also quenched using a chloroacetamide solution (Figures S6–8).

Monocycle formation

Examination of molecular models showed that the side chain in position 4 of Q3 was the closest to the N-terminal residues of the peptide and might react first if the smallest ring size is favored during macrocyclization. The side chain of Q2 and possibly Q1, Q5, and Q7 would be the next nearest sites. More remote positions were expected to be out of reach of AAs close to the N-terminus. Thus, sequences 1–3 were designed to test the selectivity of macrocyclization between a Cys residue in positions 2, 3 or 4 and chloroacetamides on Q^{Clax2} and Q^{Clax3} . Cyclization was complete after only five minutes. While **2** and **3** generated two products (**2C-a** and **2C-b**, and **3C-a** and **3C-b**, respectively), **1** yielded a single product **1C** (Figures 2d, 3a–c). Separation of the peaks and MS analysis confirmed that all compounds corresponded to a cyclic adduct. The unreacted chloroacetamide functions were quenched with benzyl mercaptan. The products (**1Q**, **2Q-a/b**, **3Q-a/b**) were all separated and identified by LC-ESI-MS analysis. Thus, selective cyclization occurs only with **1** which has the shortest loop1, consisting of a single Gly residue. Proof that Cys2 has cyclized with Q^{Clax3} in **1C** and **1Q** was obtained by

independently synthesizing a reference sequence (**R1**) using Q^{Cl^a3} and Q^{S^{bn}2} instead of Q^{Cl^a3} and Q^{Cl^a2}. After cyclization, ¹H NMR and HPLC analyses confirmed **R1** to be identical to **1Q** (Figures S3d, S3). This shortest loop1 was kept in all subsequent designs.

A second series of sequences was then prepared containing Q^{Cl^a3} and Cys2, and also a second Cys residue in positions 5, 6 or 7 (**4–6** in Figure 2c). Cyclization was again quick. A single product was observed with **5** and **6**, and two with **4** (Figure 3a–c). In these early experiments, TCEP had not been added initially. As a consequence, intramolecular cyclization was followed by intermolecular disulfide bridge formation, as confirmed by LC–MS analysis. Subsequent addition of TCEP reduced the disulfides and all products showed a mass consistent with one thioether and one free thiol function. The latter could be quenched with excess chloroacetamide. We inferred that the Cys2/Q^{Cl^a3} reaction remains clean even in the presence of a second Cys residue provided that the latter is at least three amino acids apart (as in **5** and **6**). Compound **4** has a shorter loop2 and Cys5 apparently competes with Cys2.

Bicycle formation

Careful examination of molecular models then suggested that a Cys residue in position 6 or 7 left free after the Cys2/Q^{Cl^a3} reaction might reach a chloroacetamide on Q2, with Q7 being just a little more remote and other Q units being further away. The rationale was again that the smallest ring would form the fastest. Compounds **7–10** were then prepared, all having Q^{Cl^a2}, Q^{Cl^a3} and Q^{Cl^a7} reactive centers, and two Cys residues, one in position 2 and the other in

position 5, 6 or 7, as in **4–6**. The cyclization of **7**, with the smallest loop2, was nonselective, consistent with the behavior of **4** (Figure 3a,b). The major product **7C-a** has the mass expected for a bicycle, yet a monocyclic product (**7C-b**) was also detected. The monocycle was interpreted as resulting from a Cys5/Q^{Cl^a3} reaction, that leaves Cys2 unable to reach Q^{Cl^a2} or Q^{Cl^a7}.

The cyclization of **8**, **9** and **10** progressed selectively towards a bicycle, as identified by LC–MS (Figure 3a–c). The remaining, unreacted chloroacetamide function was then quenched with benzyl mercaptan to yield **8Q**, **9Q** and **10Q** which were all isolated in pure form by RP–HPLC (Figures S10–12). Based on the models, the bicyclization pattern of **8–10**, as well as the major bicyclization product of **7**, were thought to result from a Cys2/Q^{Cl^a3} reaction followed by a CysX/Q^{Cl^a2} with X=5–7, leaving Q^{Cl^a7} free to react with benzyl mercaptan. This reaction trail leads to a sort of crossing of the thioether bridges (Figure 3c, left).

The reaction trail was ascertained by the NMR structural assignment of **9Q** (Supporting Information section 1.2). Key for the assignment were NOESY correlations involving the amide NH of the side chain in Q^{S^{bn}} and Q^{S^{cy}} units. Thus, a correlation between the side chain NH of Q^{S^{cy}3} and the Cys2 NH, and a correlation between the side chain NH of Q^{S^{cy}2} and the Cys7 NH were observed. Consistently, the side chain NH of Q^{S^{bn}7} correlated with the benzylic CH₂. NMR assignment also revealed characteristic signals suggesting that the peptide has a defined conformation (Figure S43).

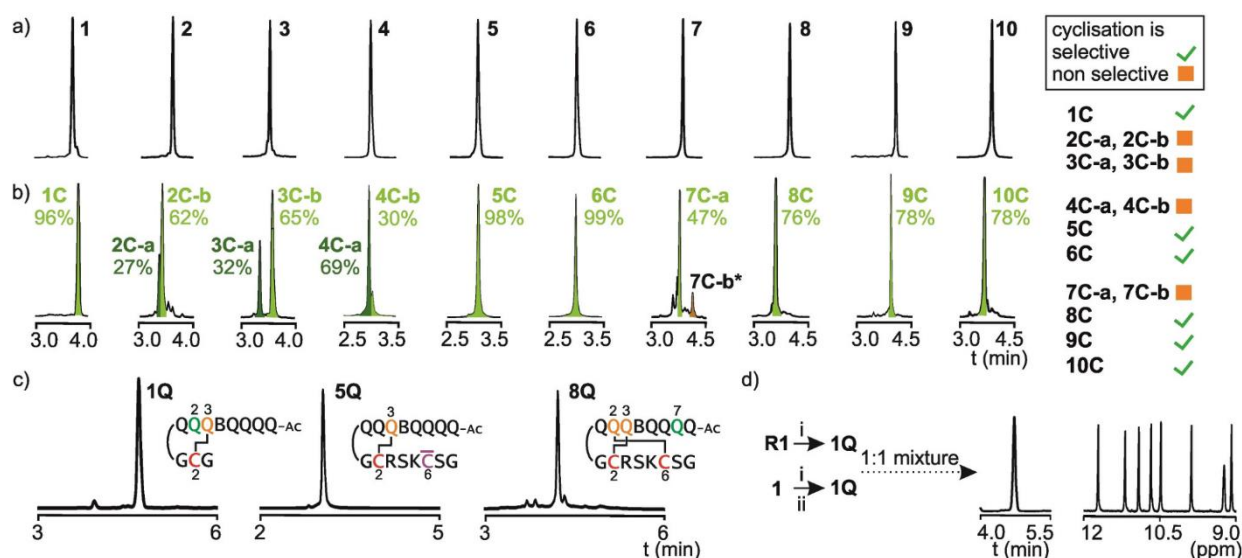


Figure 3. HPLC chromatograms of compounds **1–10** before (a) and after cyclization (b). Percentages indicate yields calculated by peak integration and comparison with an internal standard. c) HPLC chromatograms and schematic formula of quenched products **1Q**, **5Q** and **8Q**. Q^{xxx} units are color-coded as in Figure 2a. Green indicates a benzyl thioether side chain (Q^{S^{bn}}). Purple C indicates Cys(CH₂CONH₂) from the quenching of Cys residue with chloroacetamide. d) HPLC chromatogram and excerpt of the ¹H NMR spectrum (aromatic NH resonances) of a 1 : 1 mixture of **1Q** produced by quenching of **1C**, and **1Q** produced by cyclization of **R1**.

Tricycle formation

In summary of the above, **8–10** may form two macrocycles with high selectivity leaving Q^{Cl}7 free for a subsequent reaction. Triple cyclization was therefore attempted by adding one Cys residue further in the peptide sequence. Sequences **11–14** were then designed (Figure 4a). They all comprise the same loop1 (-Gly-) and loop2 (-Ser-Lys-Ser-) expected to promote Cys2/Q^{Cl}3 and Cys6/Q^{Cl}2 reactions, and a third loop of variable size before a cysteine in position 9, 10, 11 or 12. This Cys residue was expected to react with Q^{Cl}7. Anticipating the next increment, **11–14** also comprise a fourth chloroacetamide electrophile on Q^{Cl}6. This unit is located on the other side of the helix and in principle out of reach of cysteines in position 8 to 11, at the condition the peptide is already stitched to the foldamer by Cys2 and

Cys6, i.e. that the smallest macrocycles have formed first. Compounds **11–14** contain seven aromatic units instead of eight for **1–10** because Q8 was considered to be unneeded at this stage.

Cyclization of **11** and **12** showed two main products whose mass corresponded to a tricycle (Figure 4b). Due to their short loop3, we hypothesized that Cys9 (in **11**) and Cys10 (in **12**) reacted with Q^{Cl}2 in competition with Cys6, leaving the latter to react with Q^{Cl}7 (Figure 4c). In contrast, **13** and **14** yielded one main tricycle (Figure 4b). However, in comparison with the mono- and bicycle series, the chromatograms of **11C–14C** were less clean and isolated yields were lower. MS analysis revealed that all four starting materials contained impurities, despite showing one HPLC peak. To improve purity, subsequent sequences (precursors of tetracycles in the next section) were prepared via fragment condensation approach with the side chain protected Fmoc-foldamer-Gly-OH pre-synthesized on a Fmoc-Gly-SASRIN[®] resin and purified before condensation. In the case of **11–14**, accurate analysis of the reactions was hampered by the starting material impurities. Nevertheless, bicyclic products were detectable even after long incubation, suggesting that some “dead-ends” were met when reactions take a undesirable trail.

The progression of the macrocyclization of **14** was monitored by LC-MS in small time increments over 6 h (see Figure S17). Remarkably, a main monocycle and a main bicycle were observed to form successively, supporting the hypothesis that the smallest rings form faster and that Cys2, Cys6 and Cys12 residues react in this order. The reaction was overall slower than with bicycles. About 3 h were needed before chromatograms stopped evolving. After 6 h, cyclization reactions of **11–14** were quenched with benzyl mercaptan. Pure quenched trimacrocycles **11Q-a**, **11Q-b**, **12Q-a**, **13Q** and **14Q** could be isolated by preparative RP-HPLC and analyzed. Reference sequence **R14** was synthesized in which the foldamer and peptide were kept the same as in **14**, except for Q^{Sb}6 which was already installed instead of Q^{Cl}6. **R14** was then cyclized, and the isolated product proved to be identical to **14Q**, proving that Q^{Cl}6 had not been involved, as anticipated (Figure 4d). This analysis also revealed that **14Q** contained about 8% of another product (Figure 4d, ¹H NMR spectrum and S33). LC-MS did not indicate any obvious mass suggesting that another tricycle may have formed even with the longest loop3 and co-eluted with the main product.

Intrigued by the possible consequences of multi-macrocycle formation on the peptide conformation, we compared the CD spectra of linear **14** and cyclic **14Q**. Both spectra are dominated by CD bands belonging to the quinoline chromophores of the left-handed foldamer helix (Figure S49). A negative band near 390 nm and another near 260 nm were the most notable. Upon subtracting the CD spectra of **14** and **14Q**, a slight band remained near 260 nm, suggesting that the foldamer conformation is slightly different in the two compounds so that perfect subtraction of its contribution to the CD spectrum cannot be achieved. Another band was visible near 220 nm after subtraction, but it is not possible to tell whether it comes from variations in

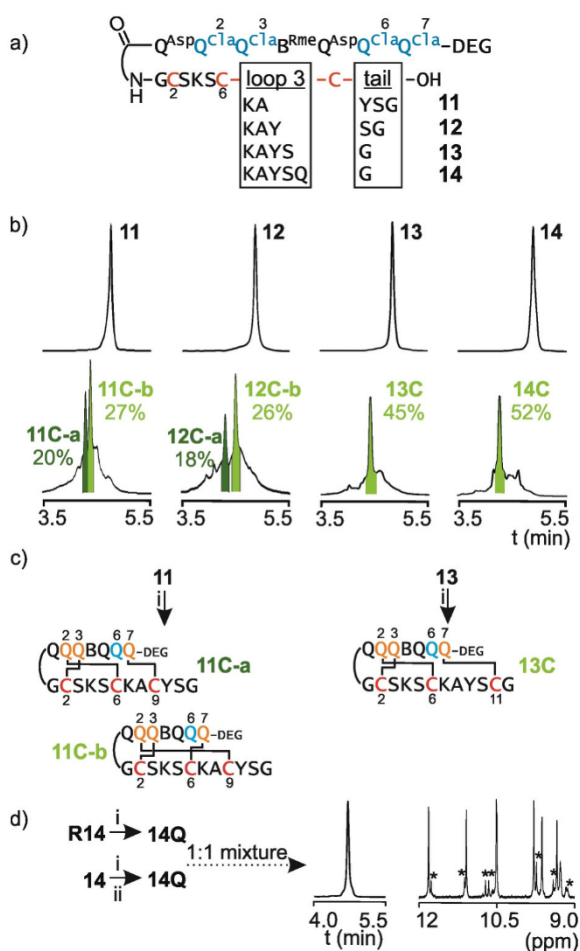


Figure 4. a) Foldamer-peptide hybrid sequences with four chloroacetamides and three Cys residues with variable loop3 sizes. b) HPLC chromatograms before and after cyclization. Percentages are yields calculated by peak integration and comparison with an internal standard. c) Cyclization trail of **11C** and **13C**. d) HPLC chromatogram and excerpt of the ¹H NMR spectrum (aromatic NH resonances) of a 1:1 mixture of **14Q** obtained from the cyclization of **R14** and of **14Q** obtained by quenching **14C**. Stars indicate signals belonging to an isomer of trimacrocycle **14Q**.

the peptide contribution to the CD spectrum, or whether it also results from slight changes in the foldamer conformation since both the foldamer and the peptide absorb at 220 nm.

Tetracycle formation

To target Q^{Cla6} in a fourth macrocycle, sequences **15–17** were designed (Figure 5a). They possess the same loop3 as **14** (-Lys-Ala-Tyr-Ser-Gln-), before Cys12, peptide loop4, and a fourth Cys residue. Because of the remote location of Q^{Cla6} from Q7, a relatively long loop4 was designed with either six, eight, or ten AAs, bringing the fourth Cys residue to position 19, 21 or 23, respectively. Considering that Q^{xxx} and B^{Rmc} aromatic δ -amino acids are similar in size to a dipeptide, **15–17** are equivalent to 34-amino acid peptides. To enhance the overall purity of the resin-bound peptide fragment, a single coupling cycle was performed and coupling time was extended to 30 min at room temperature using a 10 equivalent excess of Fmoc-AA-OH with respect to the resin loading. Initial cyclizations in the bicarbonate buffer showed unexpectedly complex HPLC chromatograms. We suspected that folding and aggregation of the long peptides may be a source of complications. Indeed much sharper chromatograms were obtained upon performing reactions in the presence of chaotropic agents such as urea. Precursors **15–17** all yielded three tetracycles (e.g. **15C-a** to **15C-c**) distinguishable by LC-MS (Figures 5b, S21, S23, S25). Subsequent quenching with benzyl mercaptan resulted in a shift to higher retention times of most other chromatographic peaks (Figures 5b, quenched and S20, S22, S24), suggesting that they contained orphan Q^{Cla} units. MS analysis of the quenched products validated this hypothesis. The persistence of orphan Q^{Cla} units is a good indication that the helical template behaves as a rigid object even in the presence of the chaotropic agent: intramolecular reactions that require unfolding of the foldamer helix are disfavored. In the case of **15** and **16**, the three isomeric tetracycles could be isolated as pure or slightly cross-contaminated products (Figures S20, S22). Since all three isomers have the same molecular composition, their different retention times are noteworthy and suggest significant variations in their 3D arrangement, i.e. in the way they expose functionalities to the solvent and the stationary phase. This is a result of the peptide chain winding around the foldamer helix by different trails resulting in different cyclization patterns.

Cyclizations were monitored at small time increments by HPLC and LC-MS (Figures S20–S25). Figure 5c shows the example of **15**. The successive appearance of the mono-, bi- and tricycles before accumulation of the tetracycles was clearly evidenced. Given the outcome of tricyclization reactions (previous section), the Cys2/ Q^{Cla3} , Cys6/ Q^{Cla2} , Cys12/ Q^{Cla7} , CysX/ Q^{Cla6} (X = 19, 21 or 23) reaction sequence was presumed to be favored, generating two sequence crossings of thioether bridges (Figure 5d, right). Models helped formulate hypotheses regarding the nature of the two other products. The allowed and forbidden reactions

(because the peptide is too short to reach a certain Q^{Cla} unit) were systematically examined (Figure S46). For example, if another Cys residue than Cys2 reacts with Q^{Cla3} , Cys2 necessarily remains an orphan site. After the first Cys2/ Q^{Cla3} reaction, Cys6 may react with Q^{Cla7} instead of Q^{Cla2} (Figure 5d, right). This pattern was not detected for compounds **9** and **10**, but appeared for **11–14** and appears to be more significant with **15–17**. It thus seems that the ability of Cys6 to quickly reach Q^{Cla2} decreases upon elongating the peptide beyond Cys6, although the additional AAs are not involved in the loop. If Cys6 reacts with Q^{Cla7} , Cys12 can only react with Q^{Cla2} as the remaining Q^{Cla6} is out of reach. The last remaining Cys21 then reacts with the remaining Q^{Cla6} . A third plausible tetracycle may form after the Cys2/ Q^{Cla3} , Cys6/ Q^{Cla2} reactions when Cys21 reacts with Q^{Cla7} before Cys12 does, leaving Q^{Cla6} as the only option for Cys12 even though this pathway is not a priori favored (Figure 5d, middle). In summary, only three tetracycles form out of 24 formal possibilities, and one of the three is favored over the other two. Figure 5e shows the structural formula of the presumably dominant form of **15C** and provides a visual measure on the large macrocycles that spontaneously form based on structural preferences.

Recapitulation of a more selective trail via Q^{Cla1}

We then assessed a second cyclization trail via Q^{Cla1} instead of Q^{Cla7} . This choice was again guided by reasonable predictions based on the relative distances between foldamer units and the assumption that smaller cycles form faster. We first verified that the Cys2/ Q^{Cla3} plus Cys6/ Q^{Cla2} (or Cys7/ Q^{Cla2}) reaction sequence could be performed selectively in presence of Q^{Cla1} . Compounds **18** and **19** which possess two Cys residues and three Q^{Cla} units were synthesized for this purpose (Figure 6a). After 3 h of reaction in a bicarbonate buffer, a major bicyclic product was observed in both cases (**18C** and **19C** in Figures 6b, S26, S29). The unreacted chloroacetamide was quenched with benzyl mercaptan to yield **18Q** and **19Q**, respectively. Separately, reference macrocycle **R18** was synthesized with the same peptide as **18** and a Q^{Sbn1} - Q^{Cla2} - Q^{Cla3} segment, that is, with a benzyl thioether already installed on Q1. The cyclization of **R18** yields a product analytically identical to **18Q** (Figures 6d, S28), indicating that Q^{Cla1} had remained free in **18C** (Figure 6c, left).

Finally, a tetracycle was targeted from precursor **20** (Figure 6a). This sequence comprises the same peptide segment as **15** with Cys residues in 2, 6, 12 and 19, as well as four chloroacetamides at Q1, Q2, Q3 and at the N-terminus. Cyclization in the presence of urea was monitored by LC-MS (Figure S31). The chromatogram did not evolve after 24 h and the reaction was stopped after 48 h. One major tetracycle was detected and isolated (Figure 6b, right). Its NMR spectrum demonstrates that it is a unique well-defined product (see Supporting Information section 3). A second, minor, tetracyclic product was not isolated (star in Figure 6b). A slightly broadened HPLC peak corresponding to a tricycle dead end was also observed. Further analysis (e.g.

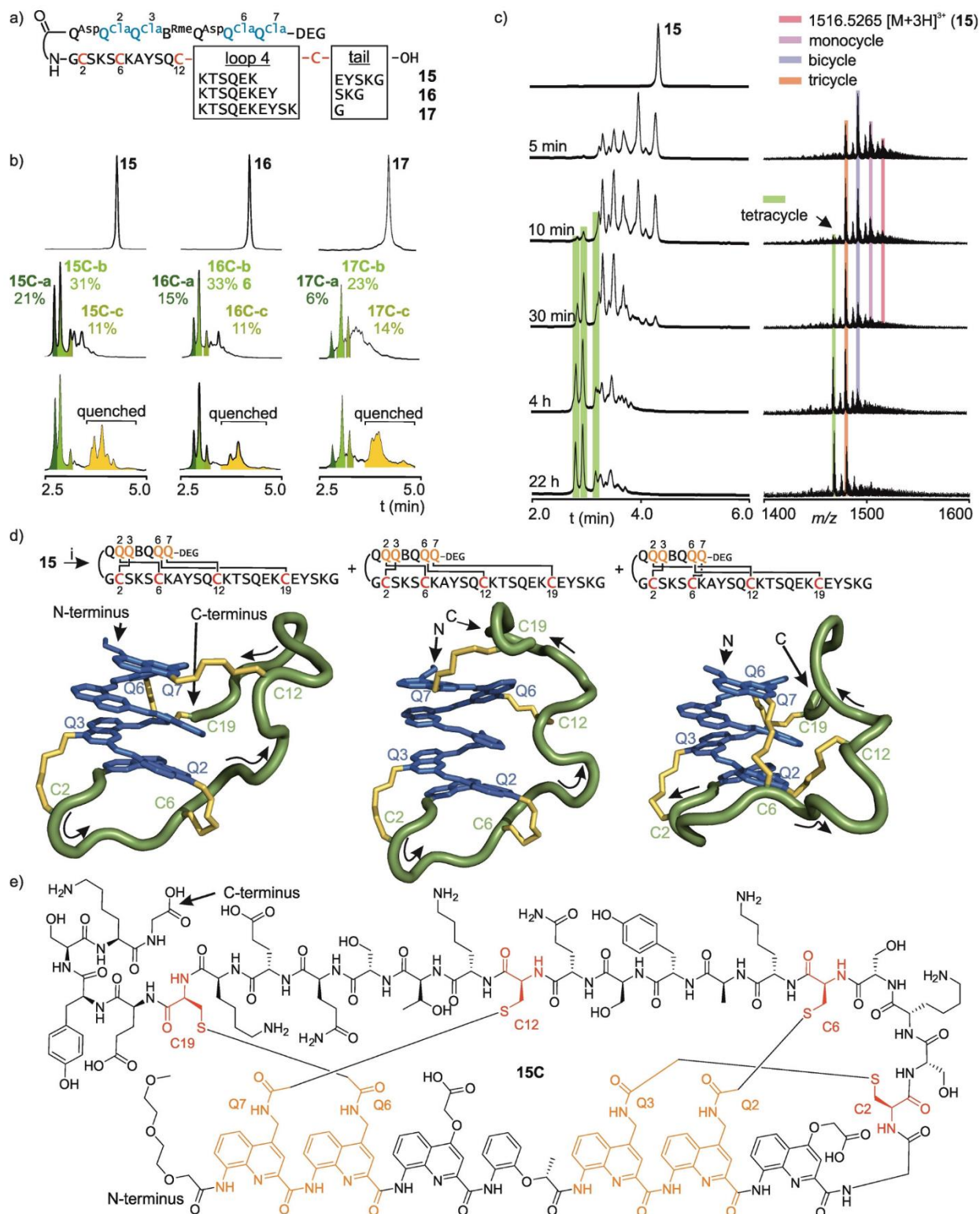


Figure 5. a) Foldamer-peptide hybrid sequences with four chloroacetamides and four Cys residues with variable loop4 sizes. b) From top to bottom: HPLC chromatograms before cyclization, after cyclization and after quenching with benzyl mercaptan. Tetracycles are marked with different green colors. Quenched sequences are marked with yellow. Percentages are yields calculated by peak integration and comparison with an internal standard. c) Parallel HPLC and ESI-MS monitoring of the cyclization of **15**. MS spectra correspond to the mass spectrum acquisition for the time segment 2.5–5.0 min of the chromatogram. HPLC peaks of tetracyclic products are marked in green. d) Plausible structures of three **15C** products. The foldamer is represented in blue, the peptide main chain is schematized as a green tube, and thioether-containing linkages are shown in yellow. Arrows indicate N- to C-terminus orientation. e) Structural formula of **15C**.

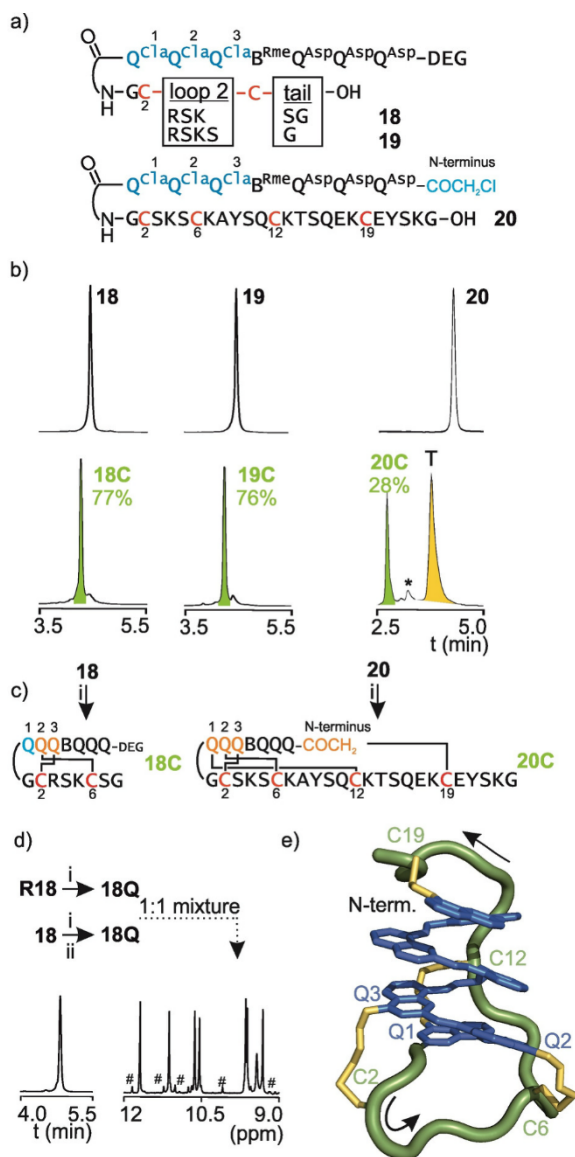


Figure 6. a) Foldamer-peptide hybrid sequences with chloroacetamides on Q1 b) HPLC chromatograms before (top) and after cyclization (bottom). Bicycles **18C**, bicycle **19C** and tetracycle **20C** are marked in green. Remaining dead-end tricycles (T) are marked in orange. The star indicates a second minor tetracycle. Percentages are yields calculated by peak integration and comparison with an internal standard. c) Preferred cyclization trails of **18** and **20**. d) HPLC chromatogram and excerpt of the ^1H NMR spectrum (aromatic NH resonances) of a 1:1 mixture of **18Q** obtained from the cyclization of either **R18** or by quenching **18C**. # indicate signals belonging to an impurity. e) Plausible structure of **20C**. The foldamer is colored in blue, the peptide main chain is schematized as a green tube, and thioether-containing linkages are shown in yellow. Arrows indicate N- to C-terminus orientation. The C-terminal EYKSG segment is omitted for clarity.

isolation and NMR spectroscopy) was not performed to determine whether this peak corresponds to one product to several products of identical mass. Given the demonstrated Cys2/Q^{Cla}3 and Cys6/Q^{Cla}2 selectivity, and the fact that Cys12 can hardly reach the N-terminal chloroacetamide, the

connectivity shown in Figures 6c and 6e with three sequence crossings can be reasonably proposed for **20C**. The chromatographic behavior of these compounds confirms a trend noted in earlier experiments: when comparing the retention time of a given acyclic precursor to that of the products that form successively (first monocycles, then bicycles, then tricycles, etc.), one notes that migration on the reverse-phase faster the macrocyclization is advanced, as if stitching the peptide progressively shields the hydrophobic aromatic foldamer helix from exposure to water.

Conclusion

The concept of reaction trails has been introduced where a peptide can selectively covalently link itself at up to four sites of a structurally defined rigid helical aromatic foldamer scaffold. Selective differential multimacrocyclization proceeds with good efficiency despite similar reaction partners being involved at each step, which in principle would allow for the formation of numerous isomeric products. The most outstanding feature of the multicyclic products is that the macrocycles produced are different in size and geometry: both the peptide and aromatic foldamer segments contained in each macrocycle of a given multicyclic product differ. The efficiency of the process rests on the fact that shorter cycles form faster, and on the structural stability of the scaffold. The trails can be to a large extent predicted and designed. By comparison with shape persistent macrocycles^[19] and multicycles^[20] whose formation is often favored by the preorganization of the non-cyclic precursor, the macrocycles formed here may be coined semi-shape persistent: only part of their non-cyclic precursor is structurally defined, yet this is sufficient to promote selective cyclization.

Multiple directions for further development can be envisaged from this point including, but not limited to, challenging shorter loops, introducing repeat cyclic motifs (constant peptide loop size and constant number of units between reactive quinoline side chains), or investigating the dependence on stereochemistry. Regarding this latter aspect, using a *P* foldamer helix instead of an *M* helix to cyclize *L*-peptides amounts to cyclizing *D*-peptides on the *M*-helix, that is, to offer the same loop size and trail, but with the possibility to improve or worsen selectivity because the relative stereochemistry of the peptide and helix is different. Other lines of development include using the macromulti-cycles for multivalent protein recognition and, eventually, their incorporation in display selection experiments. Progress along these lines will be reported in due course.

Acknowledgements

We thank the Deutsche Forschungsgemeinschaft (DFG) for financial support via project HU1766/2-1 and CRC1309-C7 (project ID 325871075). We thank Daniel Gill and Binhao Teng for contributing some building block precursors as well as Lars Allmendinger for assistance with NMR measure-

ments. Open Access funding enabled and organized by Projekt DEAL.

Conflict of Interest

The authors declare no conflict of interest.

Data Availability Statement

The data that support the findings of this study are available from the corresponding author upon reasonable request.

Keywords: Aromatic Foldamer • Helical Conformation • Macrocycle • Peptide • Reaction Trail

- [1] a) V. Martí-Centelles, M. D. Pandey, M. I. Burguete, S. V. Luis, *Chem. Rev.* **2015**, *115*, 8736–8834.
- [2] S. Ma, in *Handbook of Cyclization Reactions*, Wiley-VCH, Weinheim, **2010**.
- [3] a) A. A. Vinogradov, Y. Yin, H. Suga, *J. Am. Chem. Soc.* **2019**, *141*, 4167–4181; b) W. Liu, S. J. de Veer, Y.-H. Huang, T. Sengoku, C. Okada, K. Ogata, C. N. Zdenek, B. G. Fry, J. E. Swedberg, T. Passioura, D. J. Craik, H. Suga, *J. Am. Chem. Soc.* **2021**, *143*, 18481–18489.
- [4] For selected reviews: a) C. J. White, A. K. Yudin, *Nat. Chem.* **2011**, *3*, 509–524; b) L. Reguera, D. G. Rivera, *Chem. Rev.* **2019**, *119*, 9836–9860; c) Y. H. Lau, P. de Andrade, Y. Wu, D. R. Spring, *Chem. Soc. Rev.* **2015**, *44*, 91–102; d) C. Bechtler, C. Lamers, *RSC Med. Chem.* **2021**, *12*, 1325–1351.
- [5] a) T. R. Oppewal, I. D. Jansen, J. Hekelaar, C. Mayer, *J. Am. Chem. Soc.* **2022**, *144*, 3644–3652; b) Y. Wu, H. F. Chau, W. Thor, K. H. Y. Chan, X. Ma, W. L. Chan, N. J. Long, K. L. Wong, *Angew. Chem. Int. Ed.* **2021**, *60*, 20301–20307; *Angew. Chem.* **2021**, *133*, 20463–20469; c) J. E. Montgomery, J. A. Donnelly, S. W. Fanning, T. E. Speltz, X. Shangguan, J. S. Coukos, G. L. Greene, R. E. Moellering, *J. Am. Chem. Soc.* **2019**, *141*, 16374–16381; d) Y. H. Lau, Y. Wu, M. Rossmann, B. X. Tan, P. De Andrade, Y. S. Tan, C. Verma, G. J. McKenzie, A. R. Venkitaraman, M. Hyvönen, D. R. Spring, *Angew. Chem. Int. Ed.* **2015**, *54*, 15410–15413; *Angew. Chem.* **2015**, *127*, 15630–15633; e) J. Ceballos, E. Grinhagena, G. Sangouard, C. Heinis, J. Waser, *Angew. Chem. Int. Ed.* **2021**, *60*, 9022–9031; *Angew. Chem.* **2021**, *133*, 9104–9113; f) M. S. Islam, S. L. Junod, S. Zhang, Z. Y. Buuh, Y. Guan, M. Zhao, K. H. Kaneria, P. Kafley, C. Cohen, R. Maloney, Z. Lyu, V. A. Voelz, W. Yang, R. E. Wang, *Nat. Commun.* **2022**, *13*, 350.
- [6] a) T. Katoh, T. Sengoku, K. Hirata, K. Ogata, H. Suga, *Nat. Chem.* **2020**, *12*, 1081–1088; b) S. Imanishi, T. Katoh, Y. Yin, M. Yamada, M. Kawai, H. Suga, *J. Am. Chem. Soc.* **2021**, *143*, 5680–5684; c) C. W. Lin, M. J. Harner, A. E. Douglas, V. Lafont, F. Yu, V. G. Lee, M. A. Poss, J. F. Swain, M. Wright, D. Lipovšek, *Angew. Chem. Int. Ed.* **2021**, *60*, 22640–22645; *Angew. Chem.* **2021**, *133*, 22822–22827.
- [7] a) X. Hou, Z. Wang, J. Lee, E. Wysocki, C. Oian, J. Schlak, Q. R. Chu, *Chem. Commun.* **2014**, *50*, 1218–1220; b) Y. C. Teo, H. W. H. Lai, Y. Xia, *Chem. Eur. J.* **2017**, *23*, 14101–14112; c) J. F. Reuther, J. L. Dees, I. V. Kolesnichenko, E. T. Hernandez, D. V. Ukrainsev, R. Guduru, M. Whiteley, E. V. Anslын, *Nat. Chem.* **2018**, *10*, 45–50.
- [8] K. C. Nicolaou, J. S. Chen, *Chem. Soc. Rev.* **2009**, *38*, 2993–3009.
- [9] a) S. Chen, D. Bertoldo, A. Angelini, F. Pojer, C. Heinis, *Angew. Chem. Int. Ed.* **2014**, *53*, 1602–1606; *Angew. Chem.* **2014**, *126*, 1628–1632; b) W. Liu, Y. Zheng, X. Kong, C. Heinis, Y. Zhao, C. Wu, *Angew. Chem. Int. Ed.* **2017**, *56*, 4458–4463; *Angew. Chem.* **2017**, *129*, 4529–4534; c) G. J. J. Richelle, S. Ori, H. Hiemstra, J. H. Van Maarseveen, P. Timmerman, *Angew. Chem. Int. Ed.* **2018**, *57*, 501–505; *Angew. Chem.* **2018**, *130*, 510–514.
- [10] a) C. Wu, J.-C. Leroux, M. A. Gauthier, *Nat. Chem.* **2012**, *4*, 1044–1049; b) H. Dong, J. Li, H. Liu, S. Lu, J. Wu, Y. Zhang, Y. Yin, Y. Zhao, C. Wu, *J. Am. Chem. Soc.* **2022**, *144*, 5116–5125.
- [11] P. J. Robinson, N. J. Bulleid, *Cells* **2020**, *9*, 1994.
- [12] Reaction trail describes the sequence of reactions needed to produce a desired product which is opposed to reaction pathway, which describes the successive steps at the molecular level which take place in a chemical reaction.
- [13] S. Dengler, P. K. Mandal, L. Allmendinger, C. Douat, I. Huc, *Chem. Sci.* **2021**, *12*, 11004–11012.
- [14] a) J. M. Rogers, S. Kwon, S. J. Dawson, P. K. Mandal, H. Suga, I. Huc, *Nat. Chem.* **2018**, *10*, 405–412; b) C. Tsiamantas, S. Kwon, C. Douat, I. Huc, H. Suga, *Chem. Commun.* **2019**, *55*, 7366–7369; c) C. Tsiamantas, S. Kwon, J. M. Rogers, C. Douat, I. Huc, H. Suga, *Angew. Chem. Int. Ed.* **2020**, *59*, 4860–4864; *Angew. Chem.* **2020**, *132*, 4890–4894.
- [15] a) B. Baptiste, C. Douat-Casassus, K. Laxmi-Reddy, F. Godde, I. Huc, *J. Org. Chem.* **2010**, *75*, 7175–7185; b) D. Bindl, P. K. Mandal, I. Huc, *Chem. Eur. J.* **2022**, *28*, e202200538; c) S. J. Dawson, Á. Mészáros, L. Pethő, C. Colombo, M. Csékei, A. Kotschy, I. Huc, *Eur. J. Org. Chem.* **2014**, 4265–4275; d) T. Qi, V. Maurizot, H. Noguchi, T. Charoenraks, B. Kauffmann, M. Takafuji, H. Ihara, I. Huc, *Chem. Commun.* **2012**, *48*, 6337–6339.
- [16] D. Bindl, E. Heinemann, P. K. Mandal, I. Huc, *Chem. Commun.* **2021**, *57*, 5662–5665.
- [17] X. Hu, S. J. Dawson, Y. Nagaoka, A. Tanatani, I. Huc, *J. Org. Chem.* **2016**, *81*, 1137–1150.
- [18] Initial experiments were carried out at pH 10 in TEA buffer. It was observed, that the ϵ -amine of Lys residues can act as nucleophiles at that pH. Switching to pH 8.5 prevented the side reaction.
- [19] W. Zhang, J. S. Moore, *Angew. Chem. Int. Ed.* **2006**, *45*, 4416–4439; *Angew. Chem.* **2006**, *118*, 4524–4548.
- [20] J. Lin, J. Wu, X. Jiang, Z. Li, *Chin. J. Chem.* **2009**, *27*, 117–122.

Manuscript received: July 28, 2022

Accepted manuscript online: August 22, 2022

Version of record online: ■■■, ■■■

11. Supporting Information: Differential Peptide Multi-Macrocyclizations at the Surface of a Helical Foldamer Template

11.1. Supporting Figures and Tables

RP-HPLC and LC-MS monitoring of reactions and product analysis

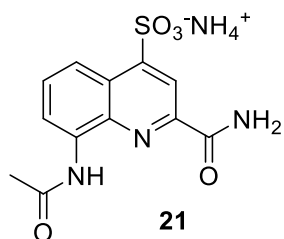


Figure S1 - Ac-Q^{Sul}-NH₂ monomer (**21**) used as an internal standard for RP-HPLC analyses

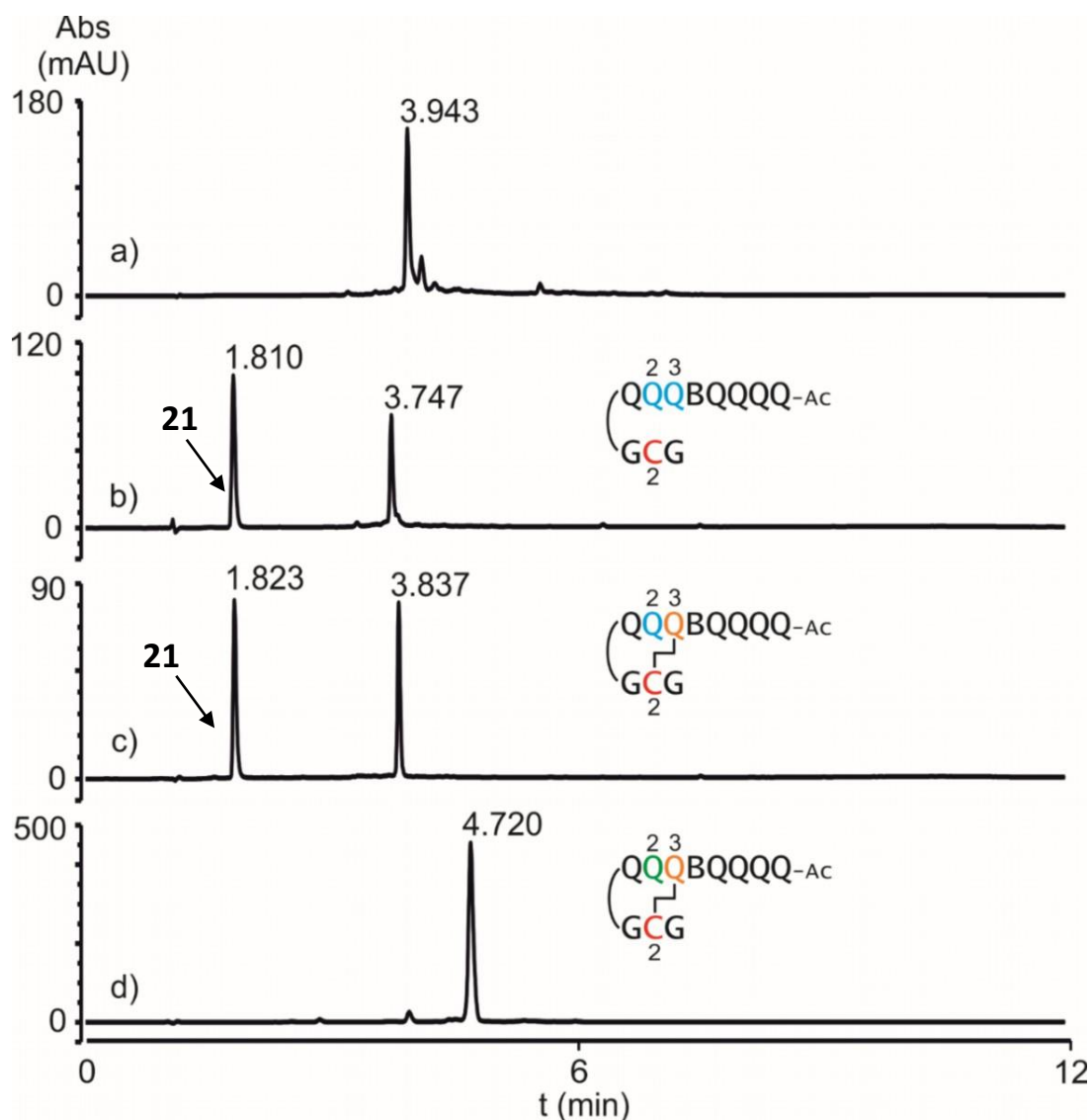


Figure S2 – RP-HPLC analysis of the synthesis, purification and cyclization of sequence **1**. Overlay of RP-HPLC profiles measured from each synthetic step of compound **1Q** synthesized from compound **1** measured with standard HPLC conditions. Compound **1** after SPS/SPFS as a crude (a), after purification co-injected with internal standard **21**(b), after cyclization and co-injected with **21** (**1C**, c) and after benzyl mercaptan installation (**1Q**, d). Chromatograms a), c) and d) obtained after the reaction without prior purification. a) and d) recorded at 300 nm, b) and c) at 375 nm.

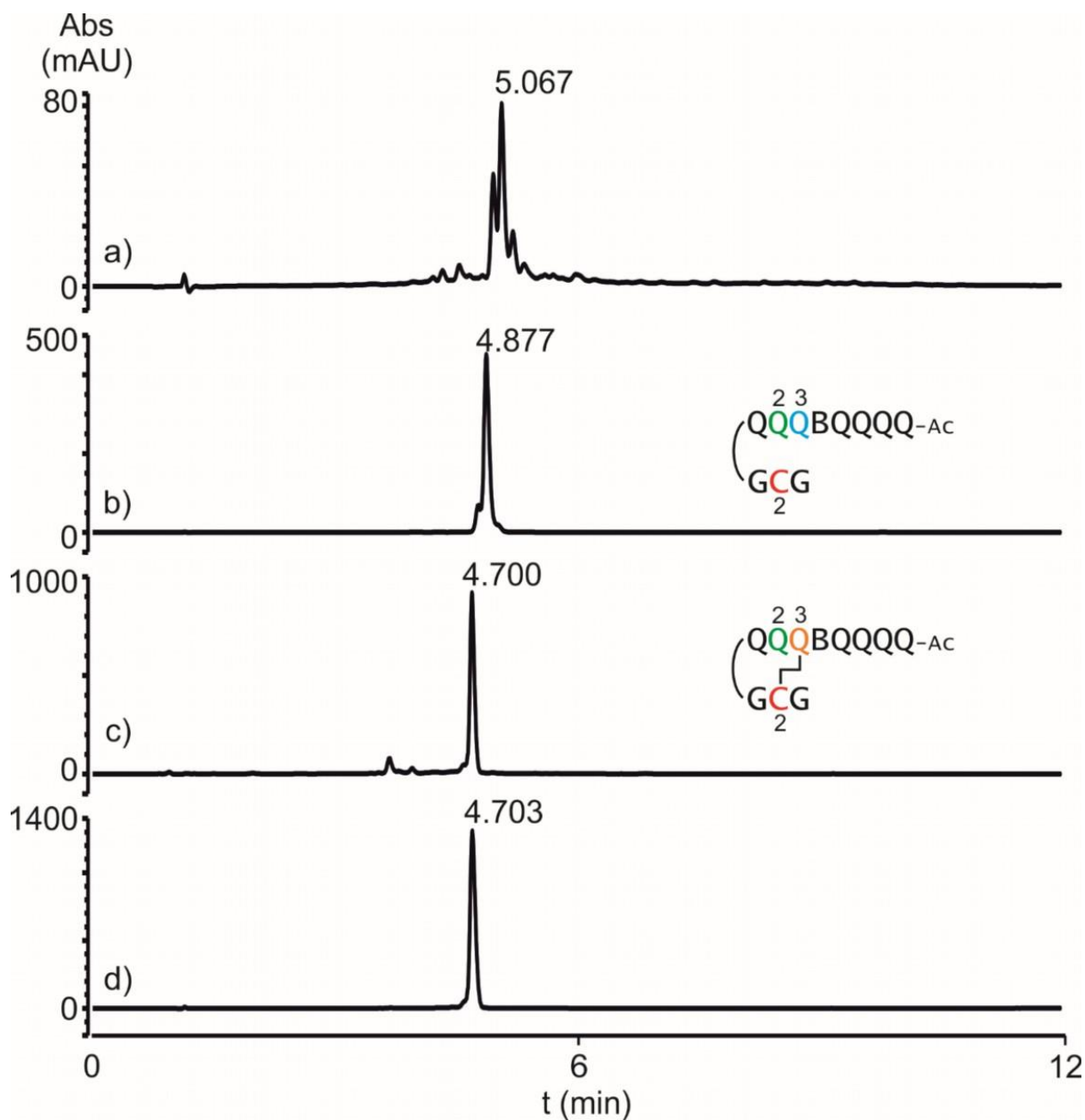


Figure S3 – RP-HPLC analysis of the synthesis, purification and cyclization of sequence R1: Overlay of RP-HPLC profiles measured from each synthetic step of compound **1Q** synthesized from compound **R1** measured with standard HPLC conditions. Compound **R1** after SPS/SPFS as a crude (a), after purification (b), after cyclization (**1Q**, c) and after final purification d). Chromatograms a), and c) obtained after the reaction without prior purification. All chromatograms were recorded at 300 nm.

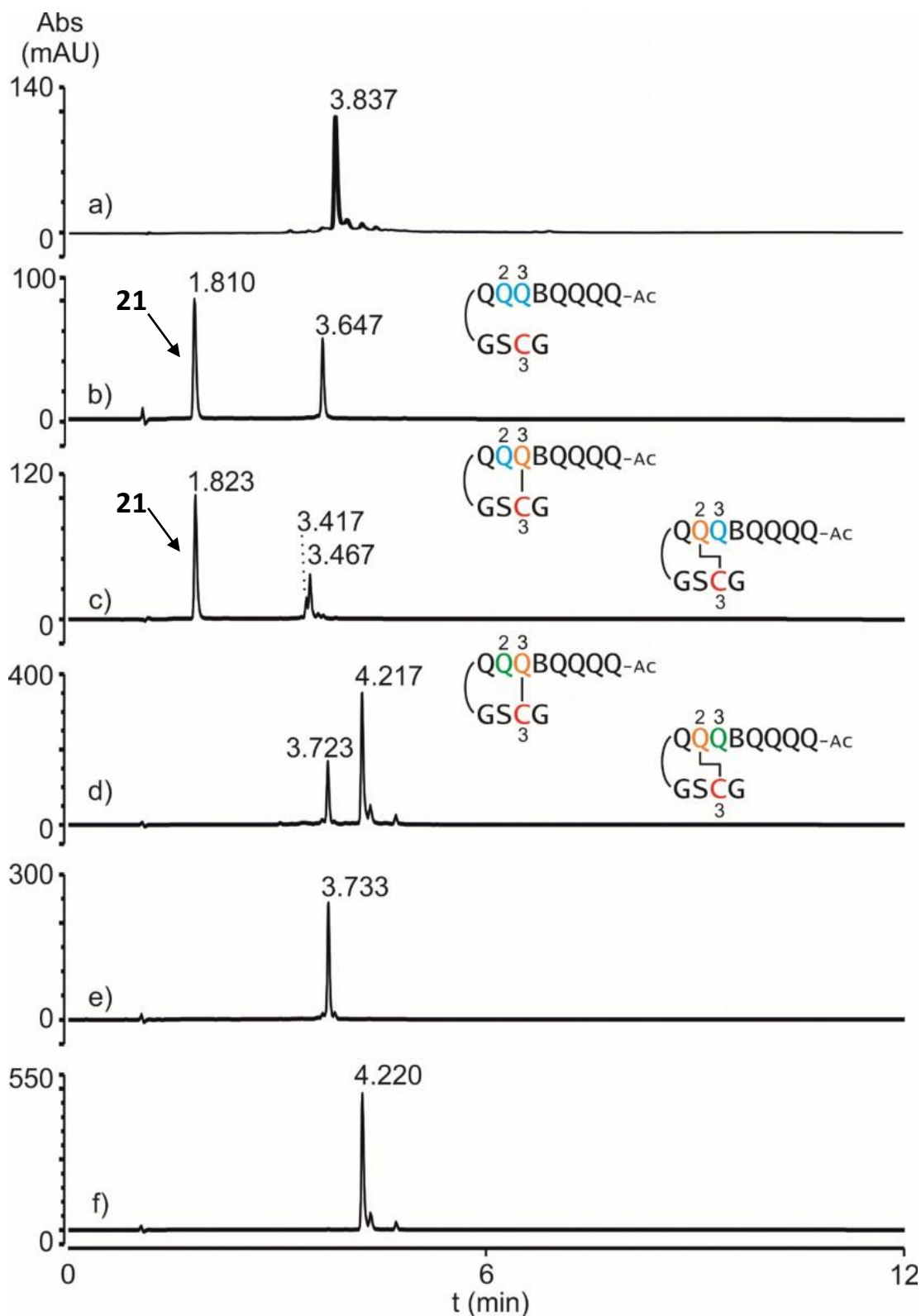


Figure S4 – RP-HPLC analysis of the synthesis, purification and cyclization of sequence 2. Overlay of RP-HPLC profiles measured from each synthetic step of compound 2Q measured with standard HPLC conditions. Compound 2 after SPS/SPFS as a crude (a), after purification co-injected with internal standard 21 (b), after cyclization co-injected with internal standard 21 (2C, c), after benzyl mercaptan installation (2Q, d) and final purification (2Q-a, e and 2Q-b, f). Chromatograms a), c) and d) obtained after the reaction without prior purification. a) recorded at 300 nm and b)-f) at 375 nm.

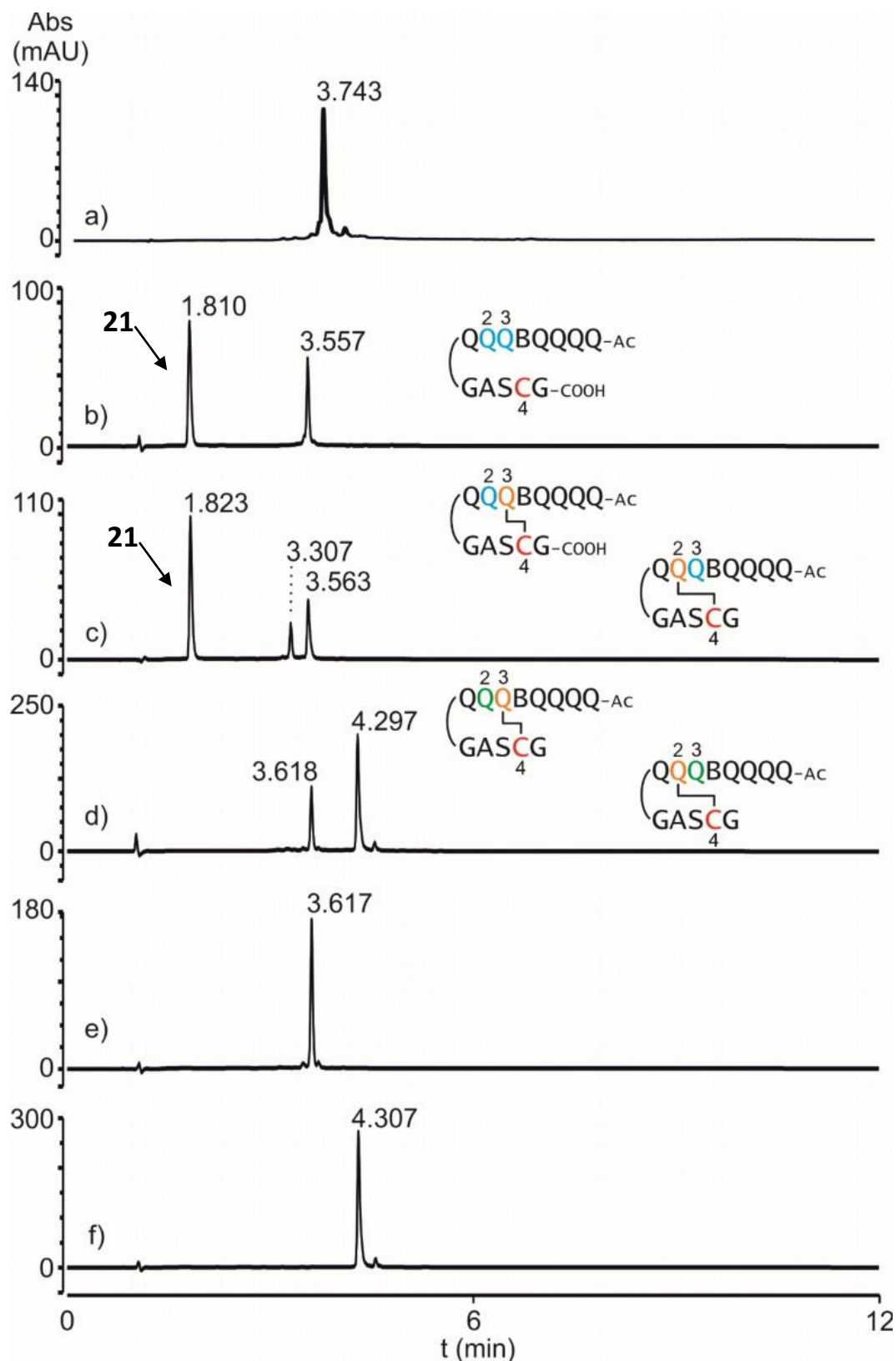


Figure S5 – RP-HPLC analysis of the synthesis, purification and cyclization of sequence 3. Overlay of RP-HPLC profiles measured from each synthetic step of compound **3Q** measured with standard HPLC conditions. Compound **3** after SPS/SPFS as a crude (a), after purification co-injected with internal standard **21** (b), after cyclization co-injected with internal standard **21** (**3C**, c), after benzyl mercaptan installation d) and final purification (**3Q**-a, e and **3Q**-b, f). Chromatograms a), c) and d) obtained after the reaction without prior purification. a) recorded at 300 nm and b)-f) at 375 nm.

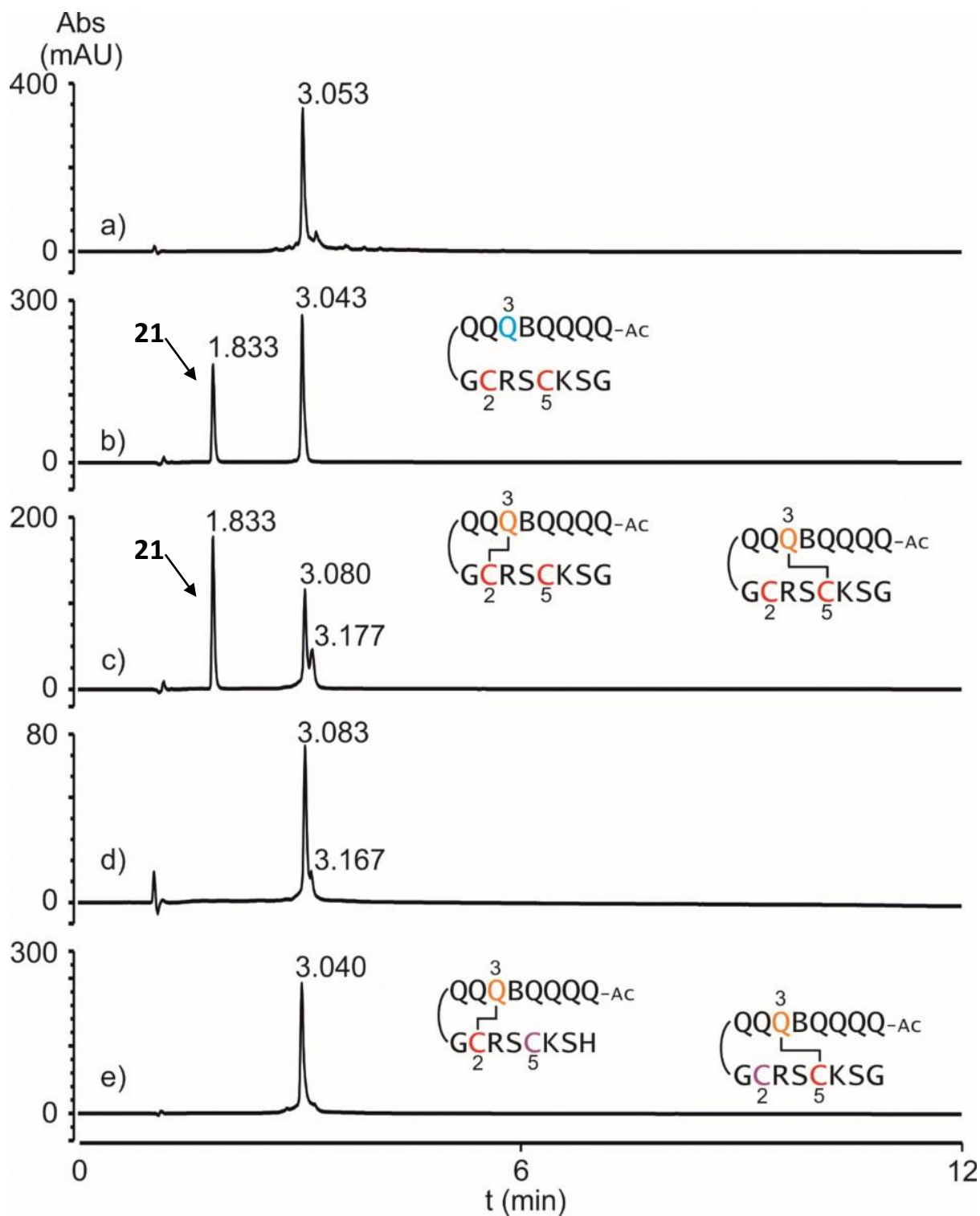


Figure S6 – RP-HPLC analysis of the synthesis, purification and cyclization of sequence 4. Overlay of RP-HPLC profiles measured from each synthetic step of compound 4Q measured with standard HPLC conditions. Compound 4 after SPS/SPFS as a crude (a), after purification co-injected with internal standard 21 (b), after cyclization co-injected with internal standard 21 (4C, c), after reduction of the disulfide impurity with TCEP (disappearance of disulfide proven by LC-MS) d) and acetamide installation (4Q, e). Chromatograms a), c), d) and e) obtained after the reaction without prior purification. All chromatograms were recorded at 375 nm.

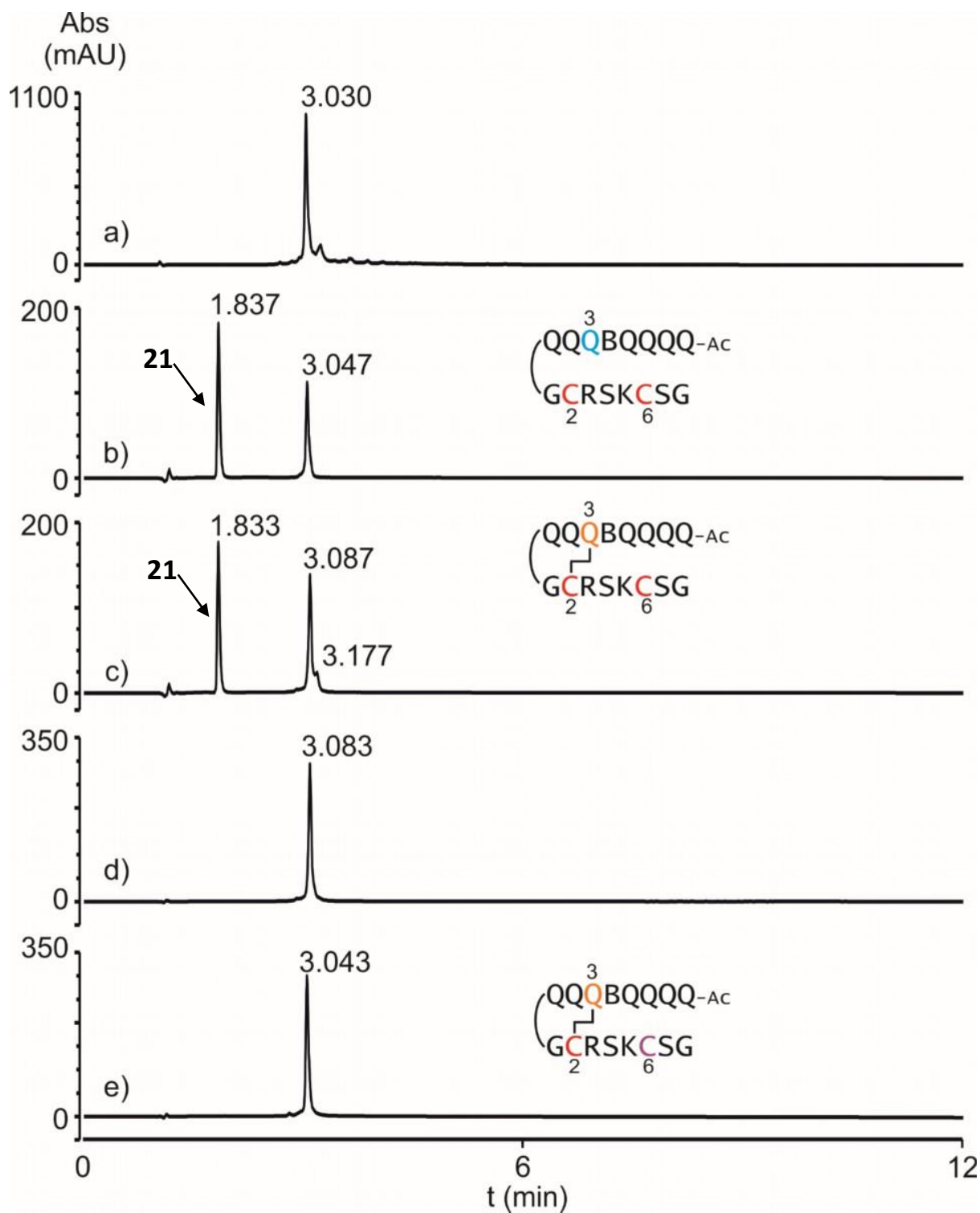


Figure S7 – RP-HPLC analysis of the synthesis, purification and cyclization of sequence 5. Overlay of RP-HPLC profiles measured from each synthetic step of compound 5Q measured with standard HPLC conditions. Compound 5 after SPS/SPFS as a crude (a), after purification co-injected with internal standard 21 (b), after cyclization co-injected with internal standard 21 (5C, c), after reduction of the disulfide impurity with TCEP (disappearance of disulfide proven by LC-MS) (d) and acetamide installation (5Q, e). Chromatograms a), c), d) and e) obtained after the reaction without prior purification. All chromatograms were recorded at 375 nm.

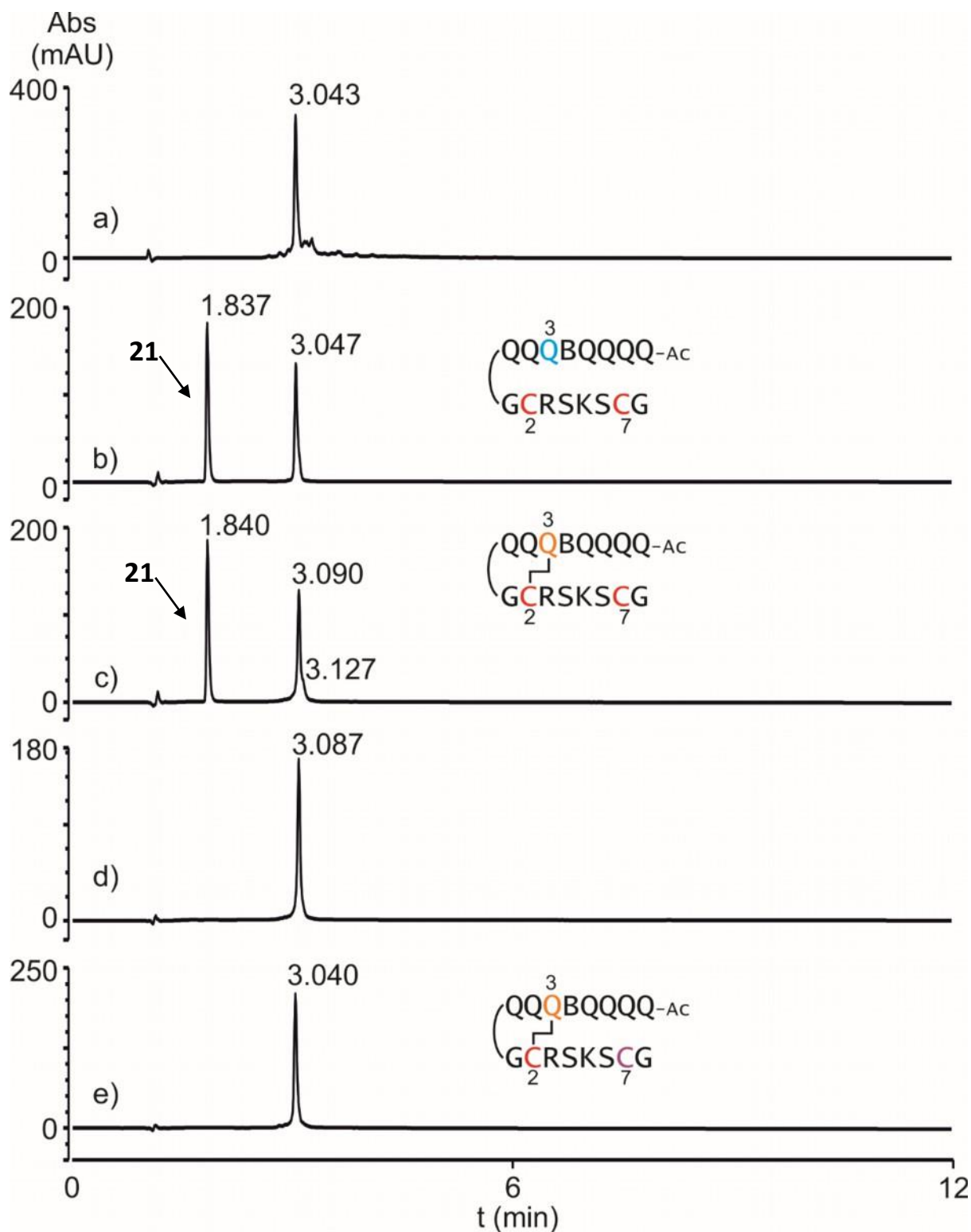


Figure S8 – RP-HPLC analysis of the synthesis, purification and cyclization of sequence 6. Overlay of RP-HPLC profiles measured from each synthetic step of compound **6** measured with standard HPLC conditions. Compound **6** after SPS/SPFS as a crude (a), after purification co-injected with internal standard **21** (**6C**, c), after cyclization co-injected with internal standard **21** (**6C**, c), after reduction of the disulfide impurity with TCEP (disappearance of disulfide proven by LC-MS, d) and acetamide installation (**6Q**, e). Chromatograms a), c), d) and e) obtained after the reaction without prior purification. All chromatograms were recorded at 375 nm.

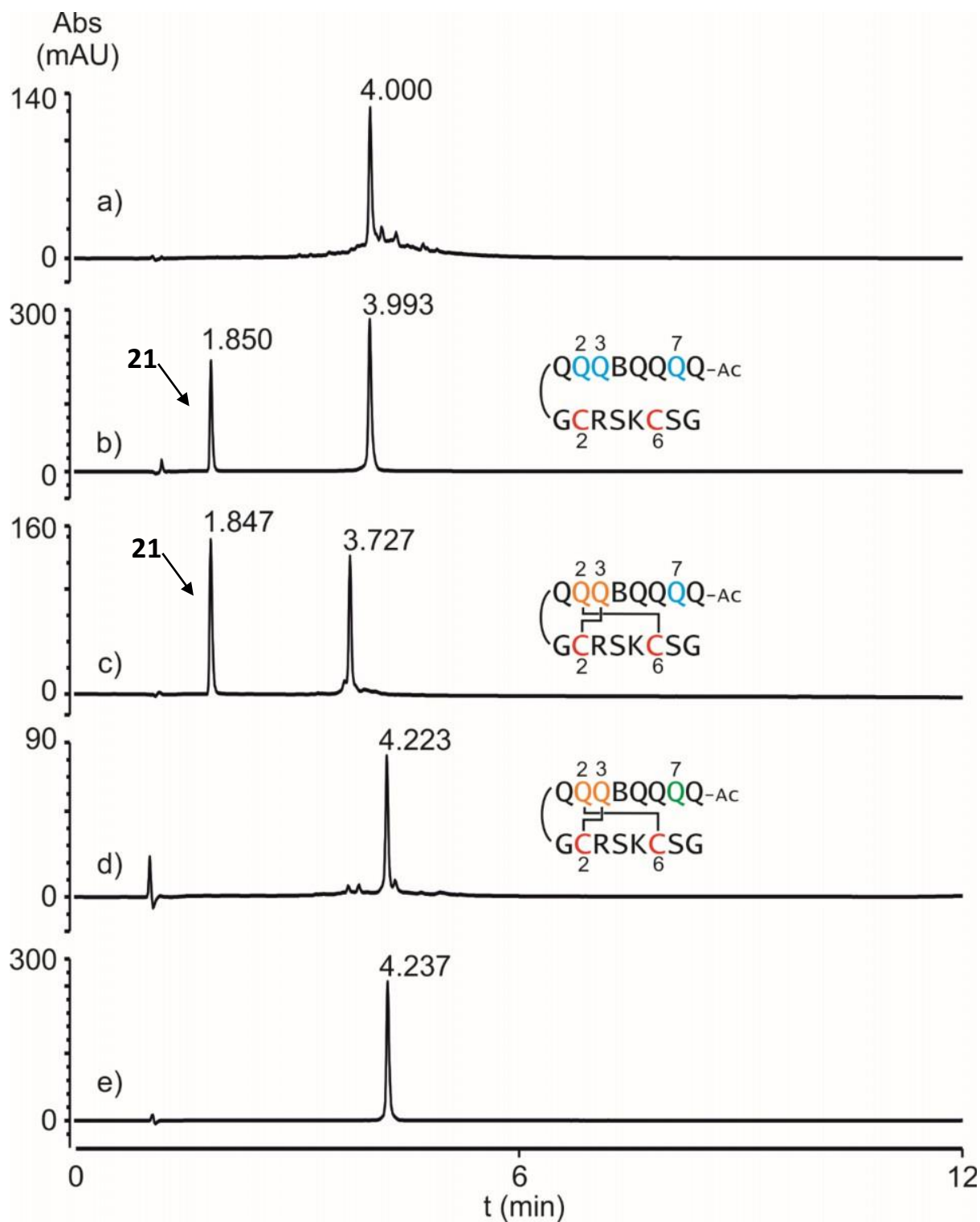


Figure S10 – RP-HPLC analysis of the synthesis, purification and cyclization of sequence 8. Overlay of RP-HPLC profiles measured from each synthetic step of compound **8Q** measured with standard HPLC conditions. Compound **8** after SPS/SPFS as a crude (a), after purification co-injected with internal standard **21** (b), after cyclization co-injected with internal standard **21** (**8C**, c), after benzyl mercaptan installation d) and final purification (**8Q**, e). Chromatograms a), c) and d) obtained after the reaction without prior purification. All chromatograms were recorded at 375 nm.

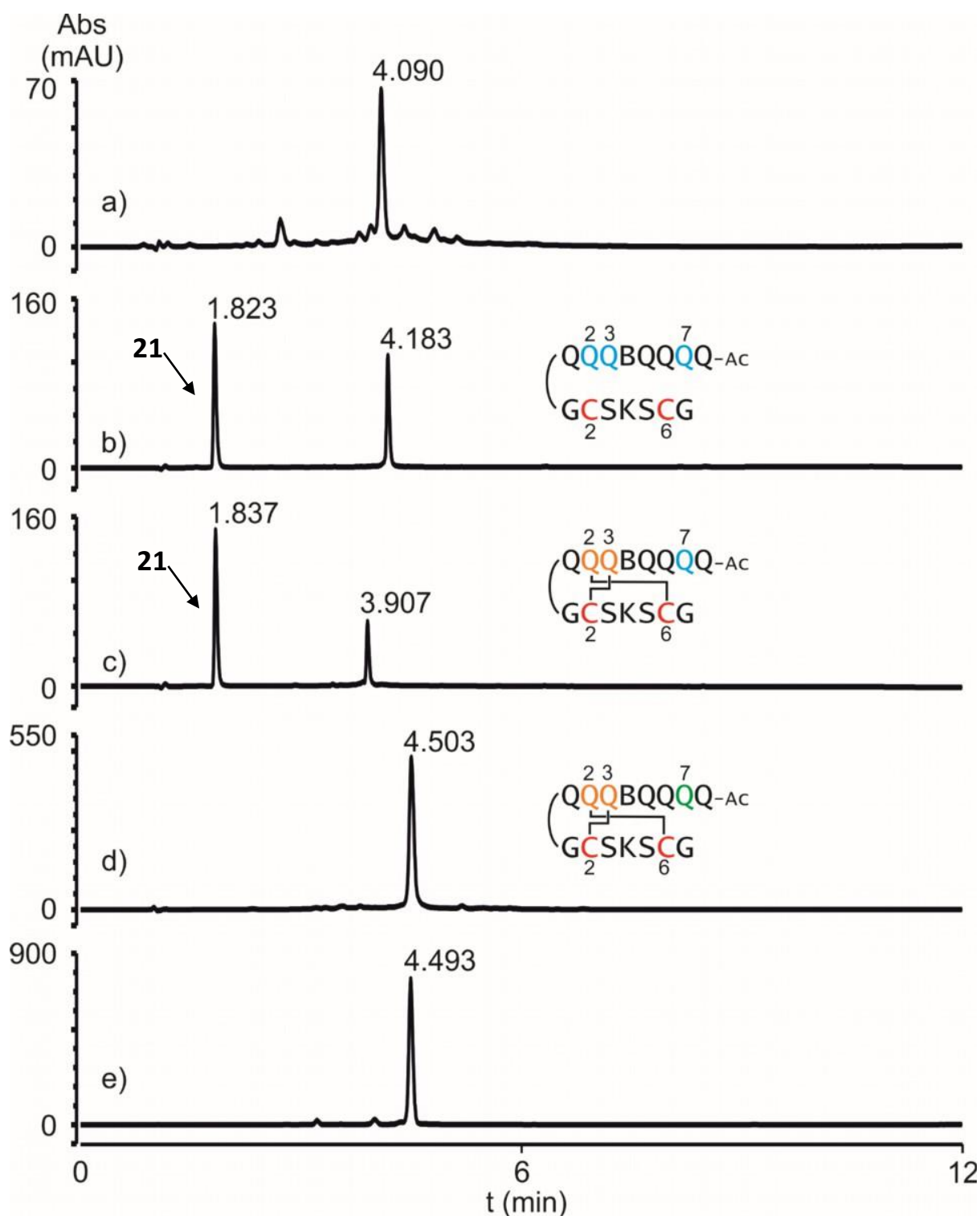


Figure S11 – RP-HPLC analysis of the synthesis, purification and cyclization of sequence 9. Overlay of RP-HPLC profiles measured from each synthetic step of compound **9Q** measured with standard HPLC conditions. Compound **9** after SPS/SPFS as a crude (a), after purification co-injected with internal standard **21** (b), after cyclization co-injected with internal standard **21** (9C, c), after benzyl mercaptan installation d) and final purification (**9Q**, e). Chromatograms a), c) and d) obtained after the reaction without prior purification. a), d) and e) were recorded at 300 nm and b-c) at 375 nm.

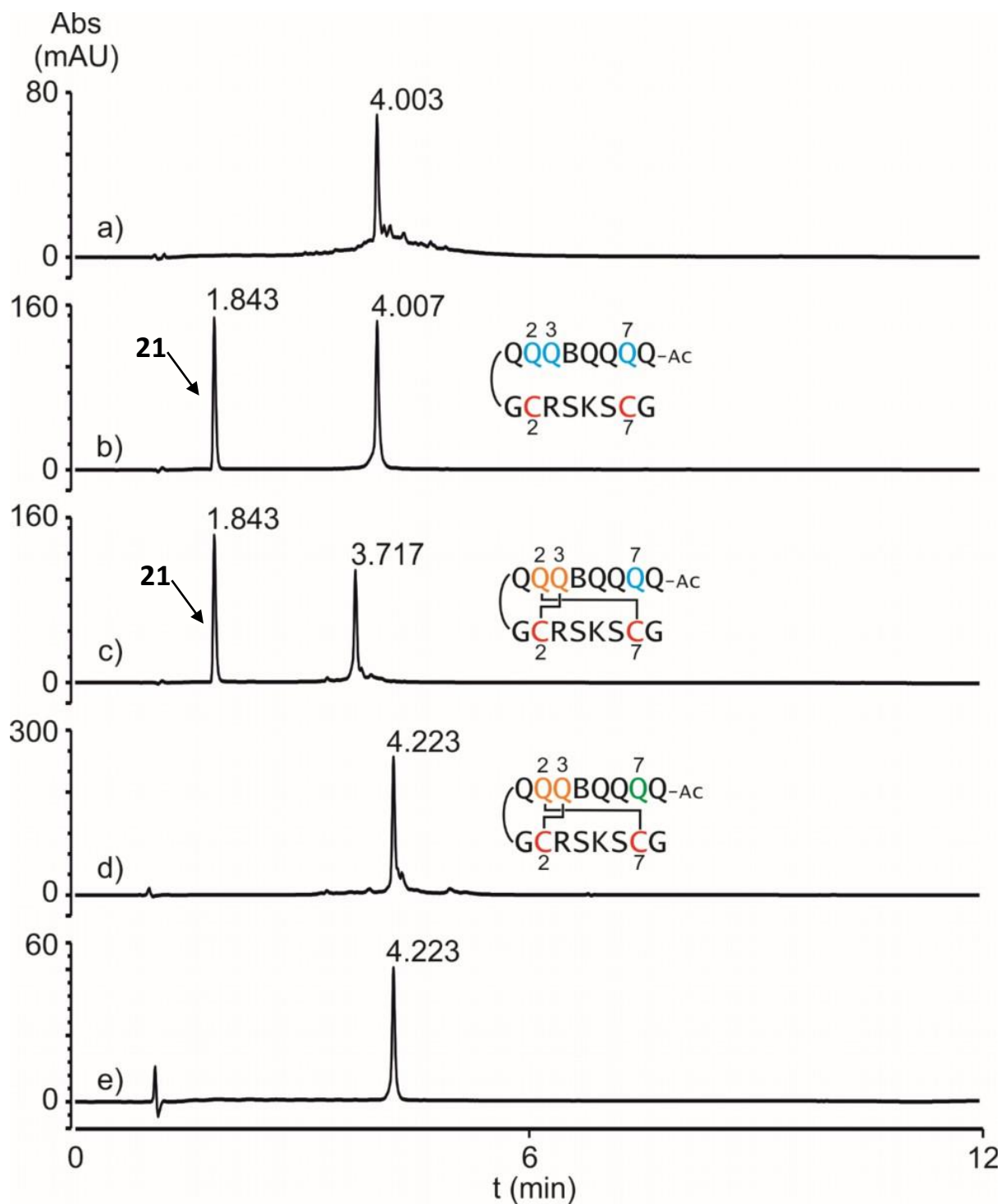


Figure S12 – RP-HPLC analysis of the synthesis, purification and cyclization of sequence 10. Overlay of RP-HPLC profiles measured from each synthetic step of compound **10Q** measured with standard HPLC conditions. Compound **10** after SPS/SPFS as a crude (a), after purification co-injected with internal standard **21** (b), after cyclization co-injected with internal standard **21** (**10C**, c), after benzyl mercaptan installation d) and final purification (**10Q**, e). Chromatograms a), c) and d) obtained after the reaction without prior purification. All chromatograms were recorded at 375 nm.

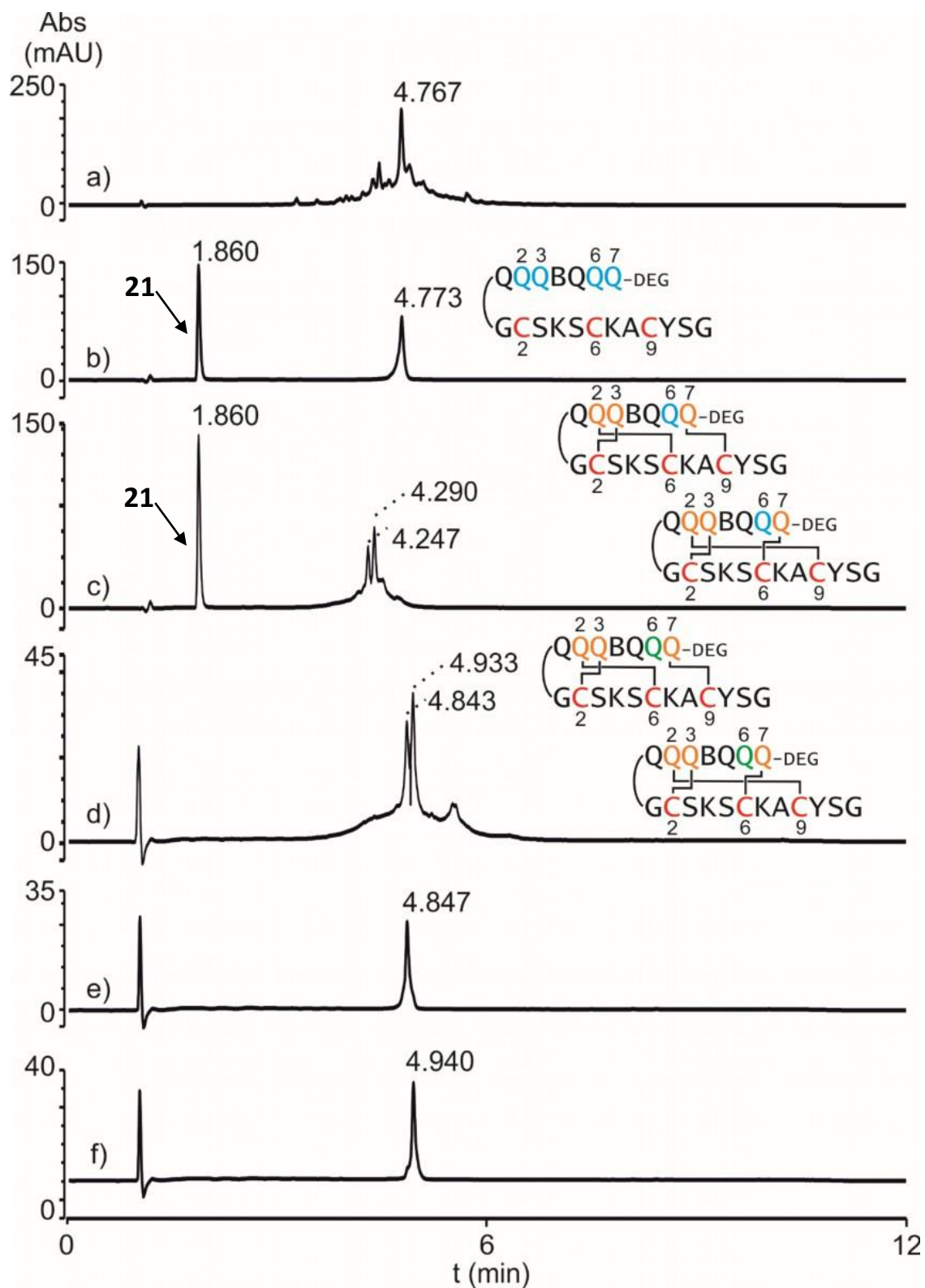


Figure 13 – RP-HPLC analysis of the synthesis, purification and cyclization of sequence 11. Overlay of RP-HPLC profiles measured from each synthetic step of compound **11Q** synthesized from compound **11** measured with standard HPLC conditions. Compound **11** after SPS/SPFS as a crude (a), after purification co-injected with internal standard **21** (b), after cyclization co-injected with internal standard **21** (**11C**, c), after benzyl mercaptan installation d) and final purification (**11Q-a**, e and **11Q-b**, f). Chromatograms a), c) and d) obtained after the reaction without prior purification. All chromatograms were recorded at 375 nm.

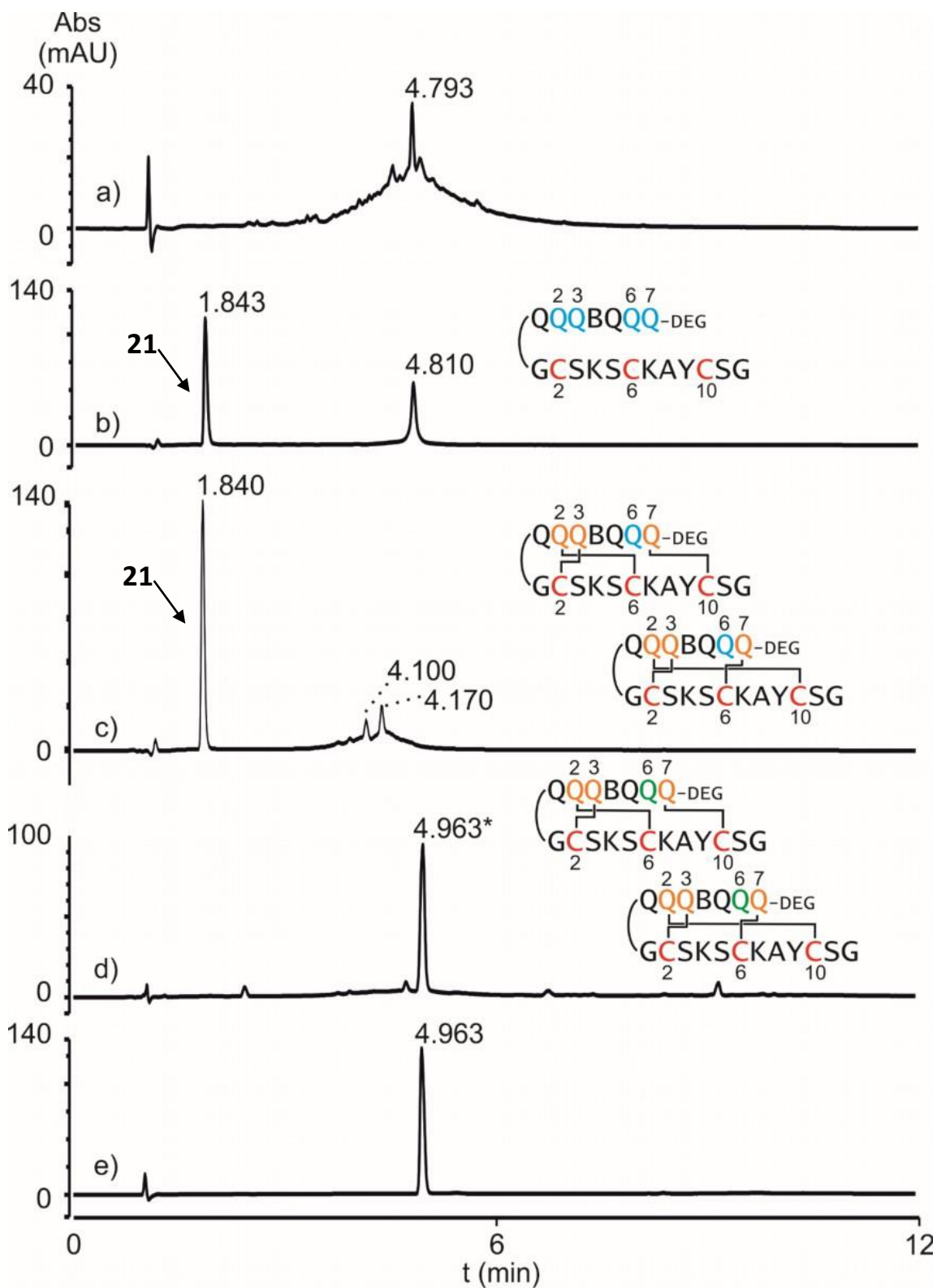


Figure S14 – RP-HPLC analysis of the synthesis, purification and cyclization of sequence 12. Overlay of RP-HPLC profiles measured from each synthetic step of compound **12Q** synthesized from compound **12** measured with standard HPLC conditions. Compound **12** after SPS/SPFS as a crude (a), after purification co-injected with internal standard **21** (b), after cyclization co-injected with internal standard **21** (**12C**, c), after benzyl mercaptan installation d) and final purification (**12Q-a**, e). Chromatograms a), c) and d) obtained after the reaction without prior purification. Single peak marked with * interpreted as co-elution of both conformers. All chromatograms were recorded at 375 nm.

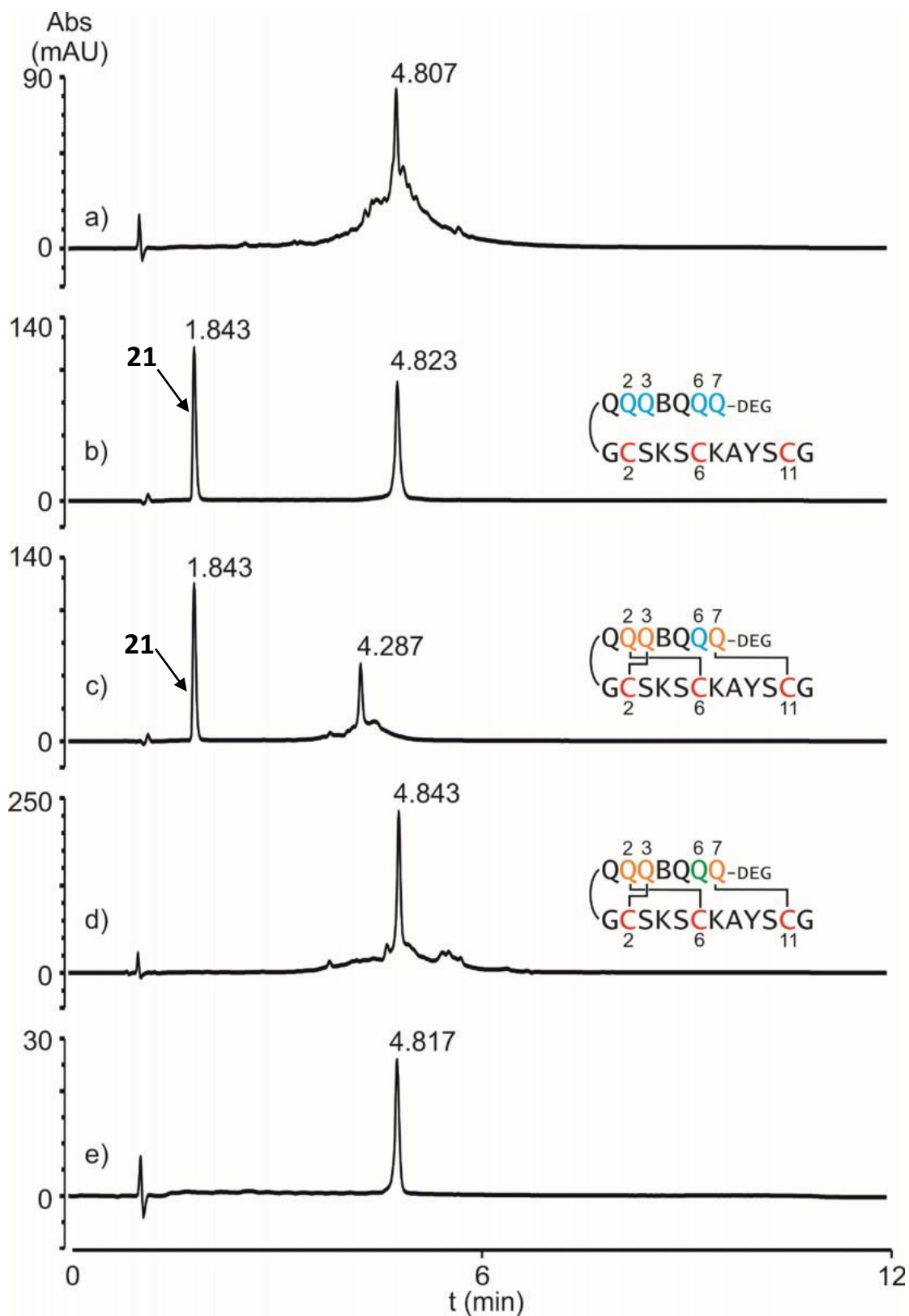


Figure S15 – RP-HPLC analysis of the synthesis, purification and cyclization of sequence 13. Overlay of RP-HPLC profiles of each synthetic step of compound **13Q** which were measured with standard HPLC conditions. Compound **13** after SPS/SPFS as a crude (a), after purification co-injected with internal standard **21** (b), after cyclization co-injected with internal standard **21** (**13C**, c), after benzyl mercaptan installation d) and final purification (**13Q**, e). Chromatograms a), c) and d) obtained after the reaction without prior purification. All chromatograms were recorded at 375 nm.

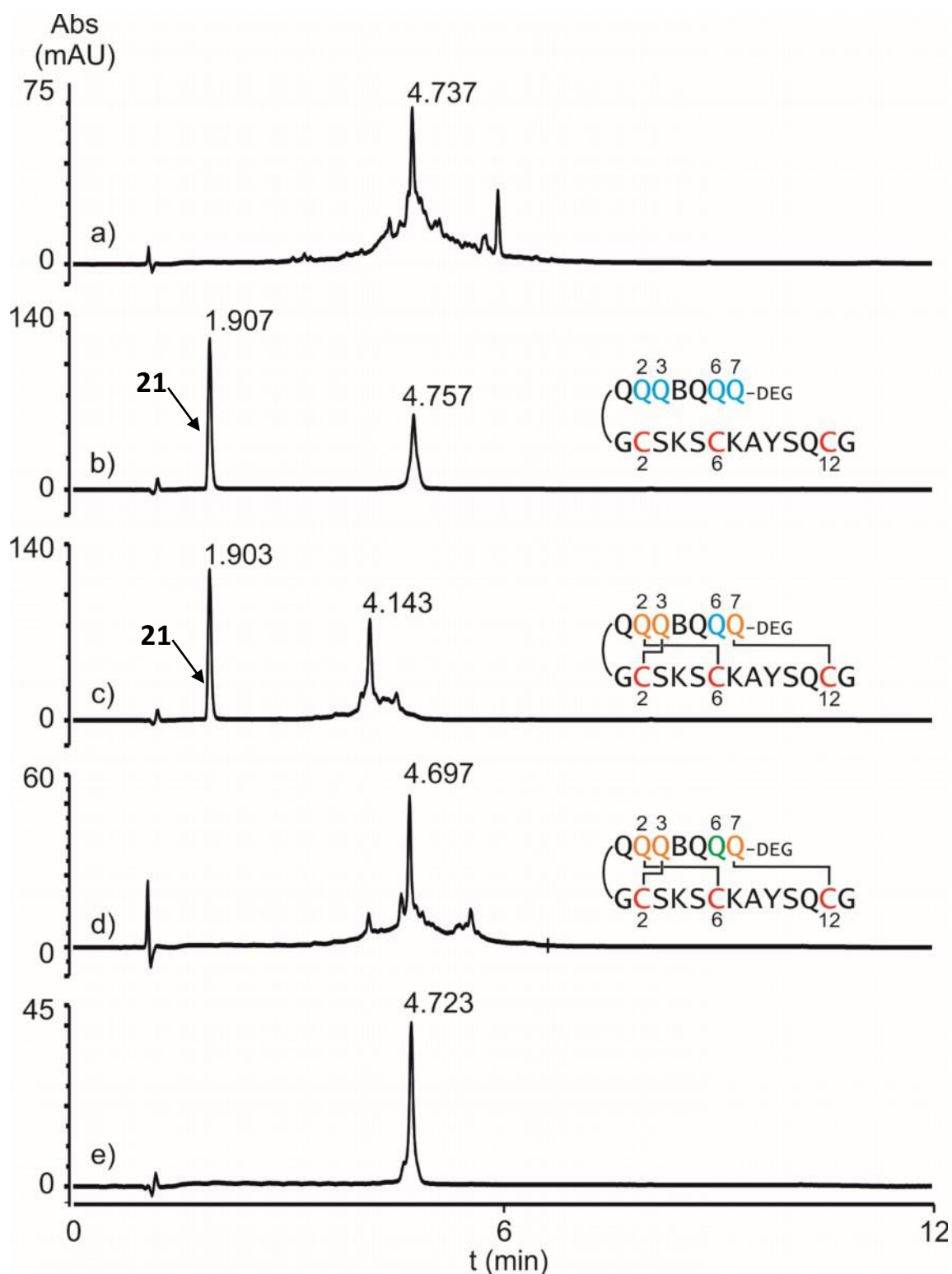


Figure S16 – RP-HPLC analysis of the synthesis, purification and cyclization of sequence 14. Overlay of RP-HPLC profiles from each synthetic step of compound **14Q** synthesized from **14** measured with standard HPLC conditions. Compound **14** after SPS/SPFS as a crude (a), after purification co-injected with internal standard **21** (b), after cyclization co-injected with internal standard **21** (**14C**, c), after benzyl mercaptan installation d) and final purification (**14Q**, e). Chromatograms a), c) and d) obtained after the reaction without prior purification. All chromatograms were recorded at 375 nm.

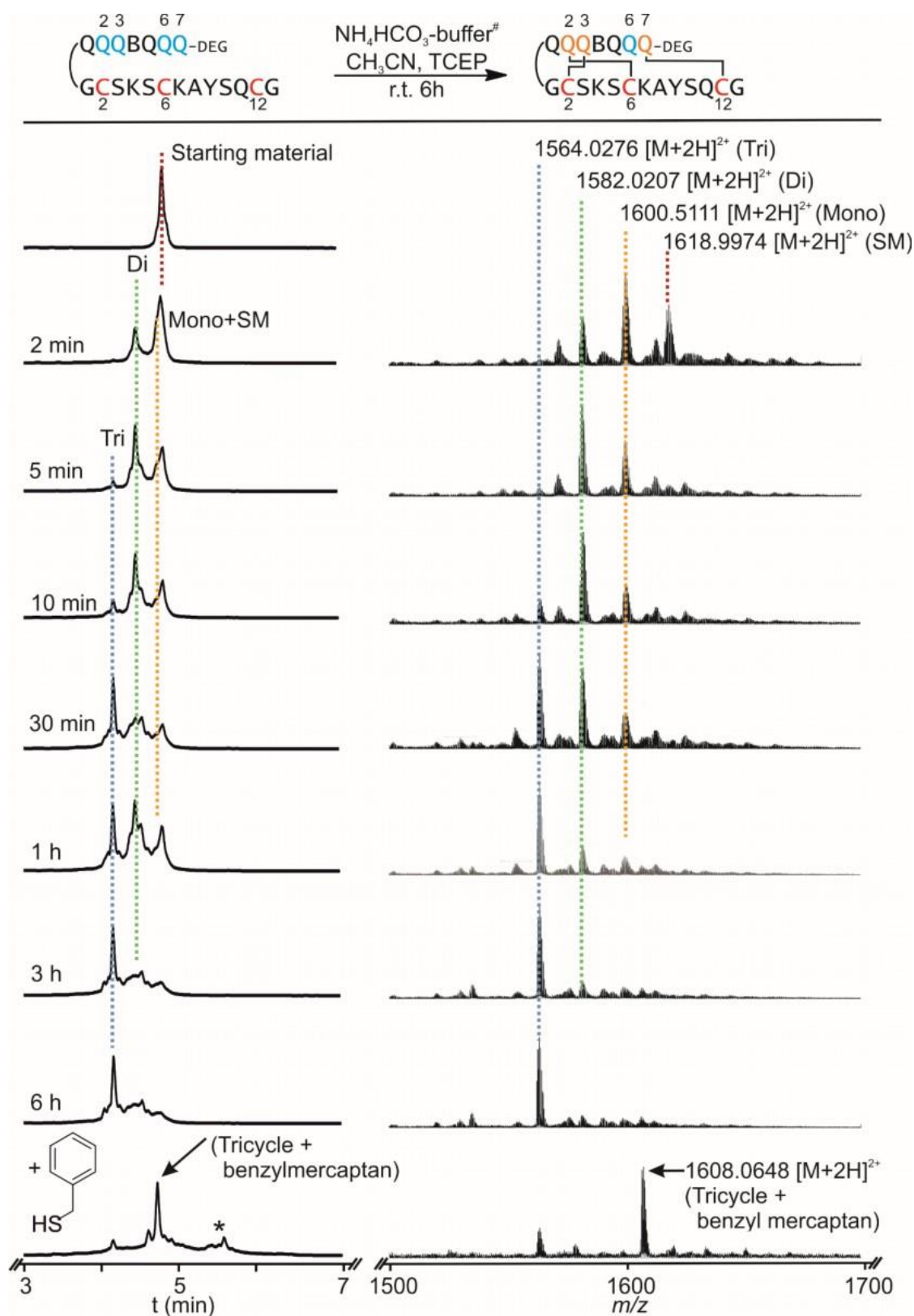


Figure S17 - Excerpts of the RP-HPLC and ESI-MS traces of the macrocyclization progression of 14C with final termination of the unreacted chloroacetamide group with benzyl mercaptan (*). The ESI-MS spectra reported correspond to the time segment 2.5 to 5 min. The resolution of the LC traces was not good enough to distinguish each peak intermediate on the base peak chromatogram (BPC) of the TOF detector. Sodium hydrogen carbonate buffer pH 8.5, 60 mM (#). Chromatograms were measured with standard HPLC conditions and recorded at 375 nm.

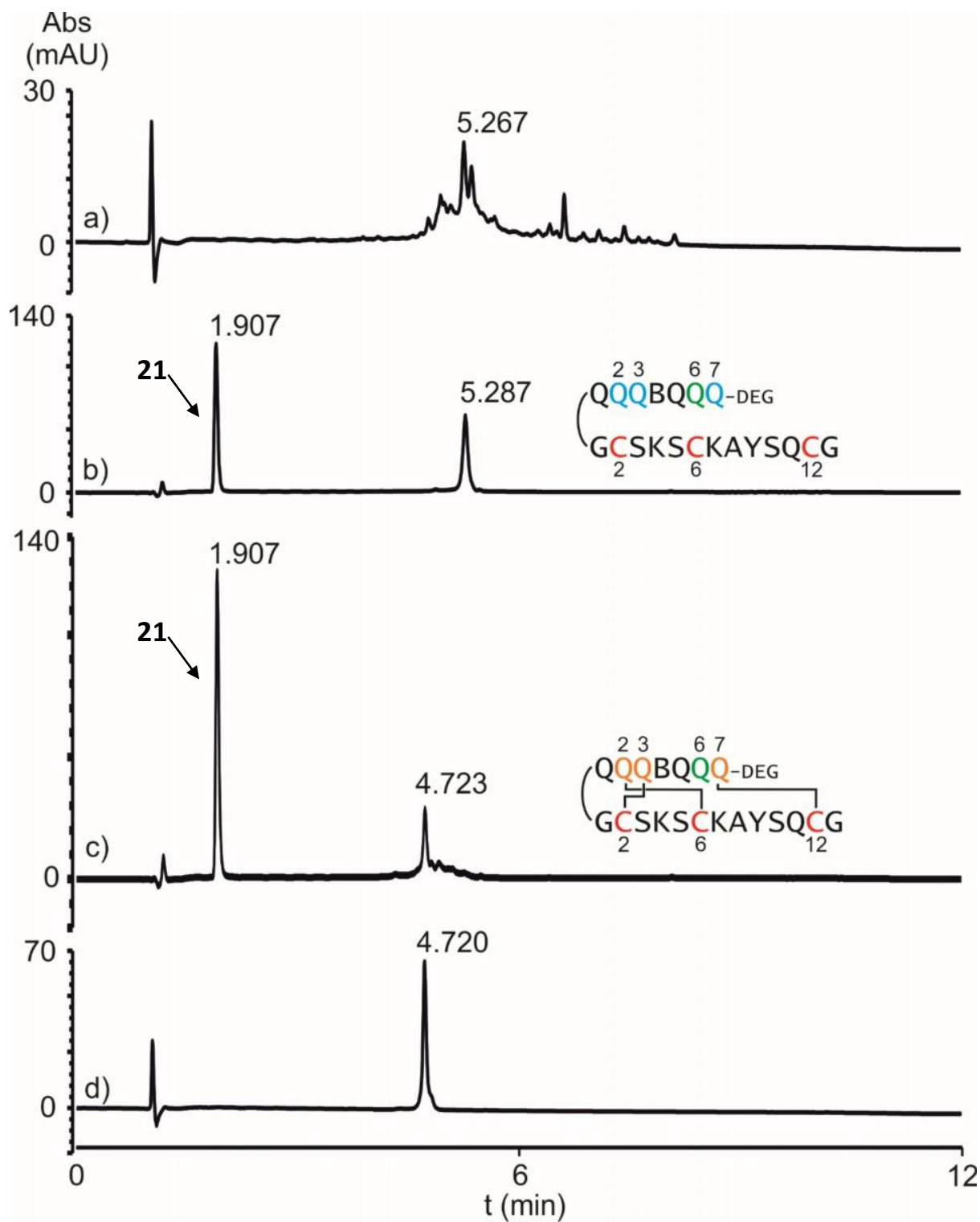


Figure S18 – RP-HPLC analysis of the synthesis, purification and cyclization of sequence 14. Overlay of RP-HPLC profiles from each synthetic step of compound **14Q** synthesized from **R14** measured with standard HPLC conditions. Compound **R14** after SPS/SPFS as a crude (a), after purification co-injected with internal standard **21** (b), after cyclization co-injected with internal standard **21** (**14Q**, c), and final purification (**14Q**, d). Chromatograms a), and c) obtained after the reaction without prior purification. All chromatograms were recorded at 375 nm.

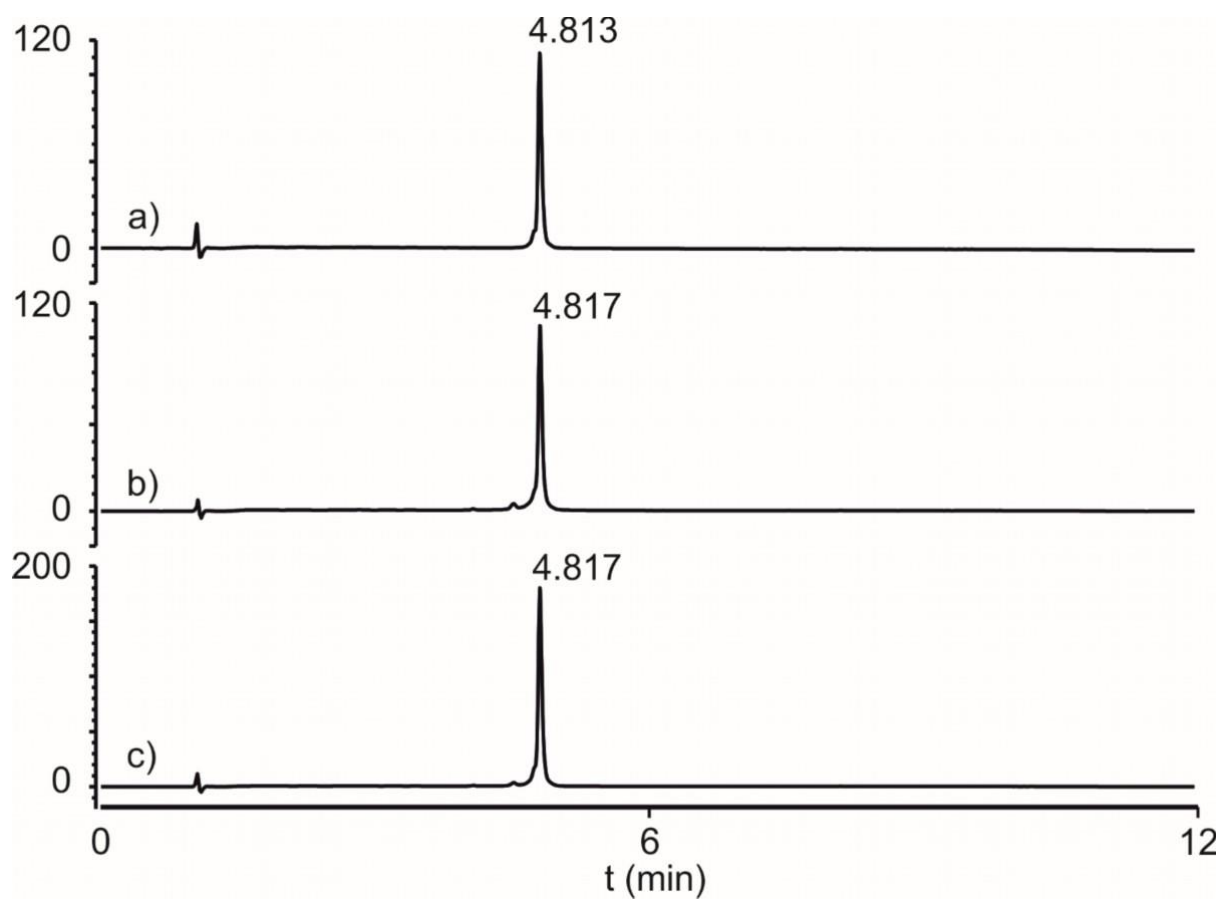


Figure S19 - RP-HPLC analysis of sequence 14. Overlay of RP-HPLC profiles from compound **14** obtained from the competition experiment (a), synthesized from the reference experiment (b) and as a co-injection (c). Chromatograms were measured with standard HPLC conditions. All chromatograms were recorded at 375 nm.

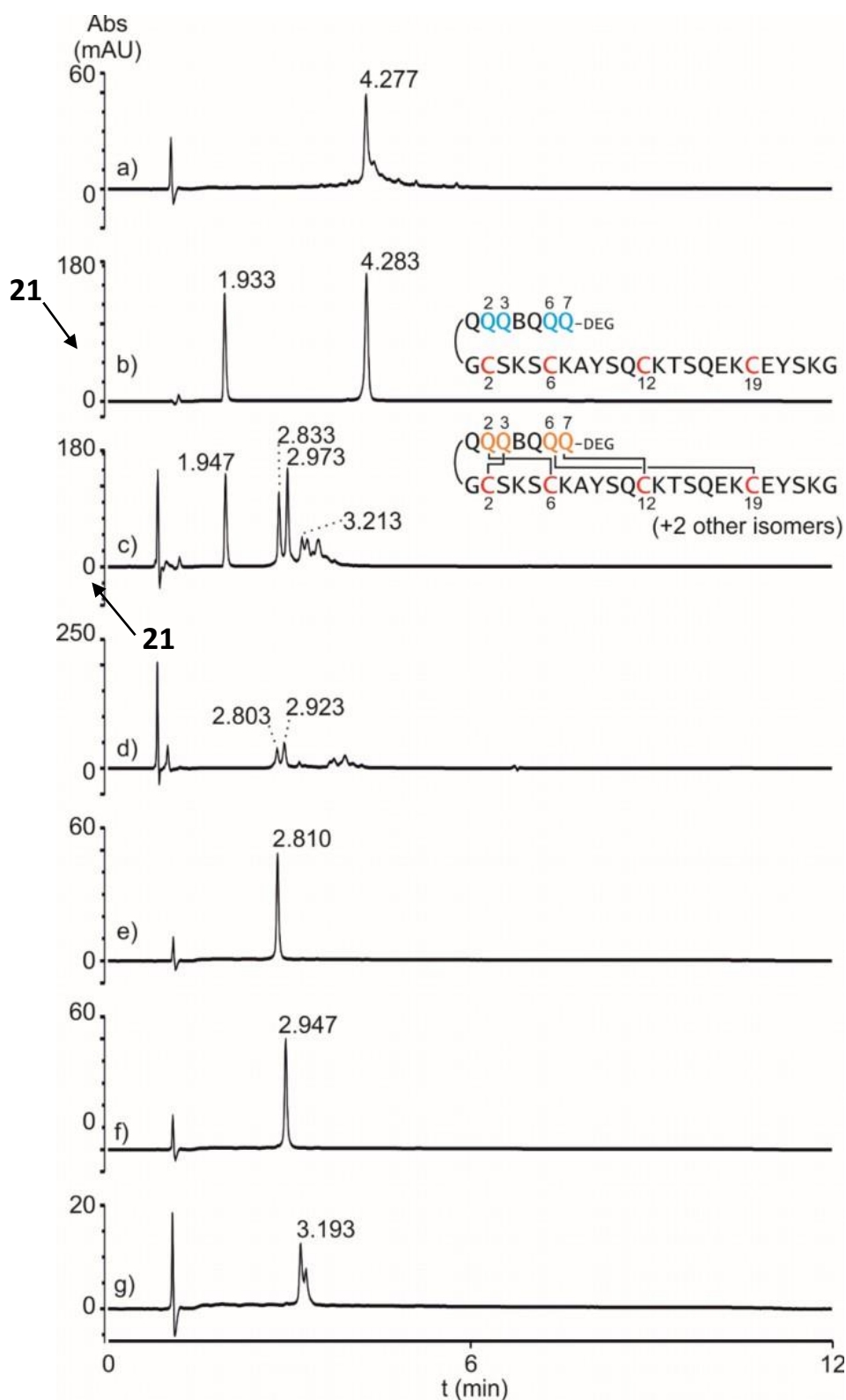


Figure S20 – RP-HPLC analysis of the synthesis, purification and cyclization of sequence 15. Overlay of RP-HPLC profiles from each synthetic step of compound **15C** synthesized from **15** measured with standard HPLC conditions. Compound **15** after SPS/SPFS as a crude (a), after purification co-injected with internal standard **21** (b), after cyclization co-injected with internal standard **21** (**15C**, c), and after addition of benzylmercaptan (d). The three isomers (**15C-a**, **15C-b** and **15C-c**) were separated in e) f) and g). Chromatograms a), c) and d) obtained after the reaction without prior purification. All chromatograms were recorded at 375 nm.

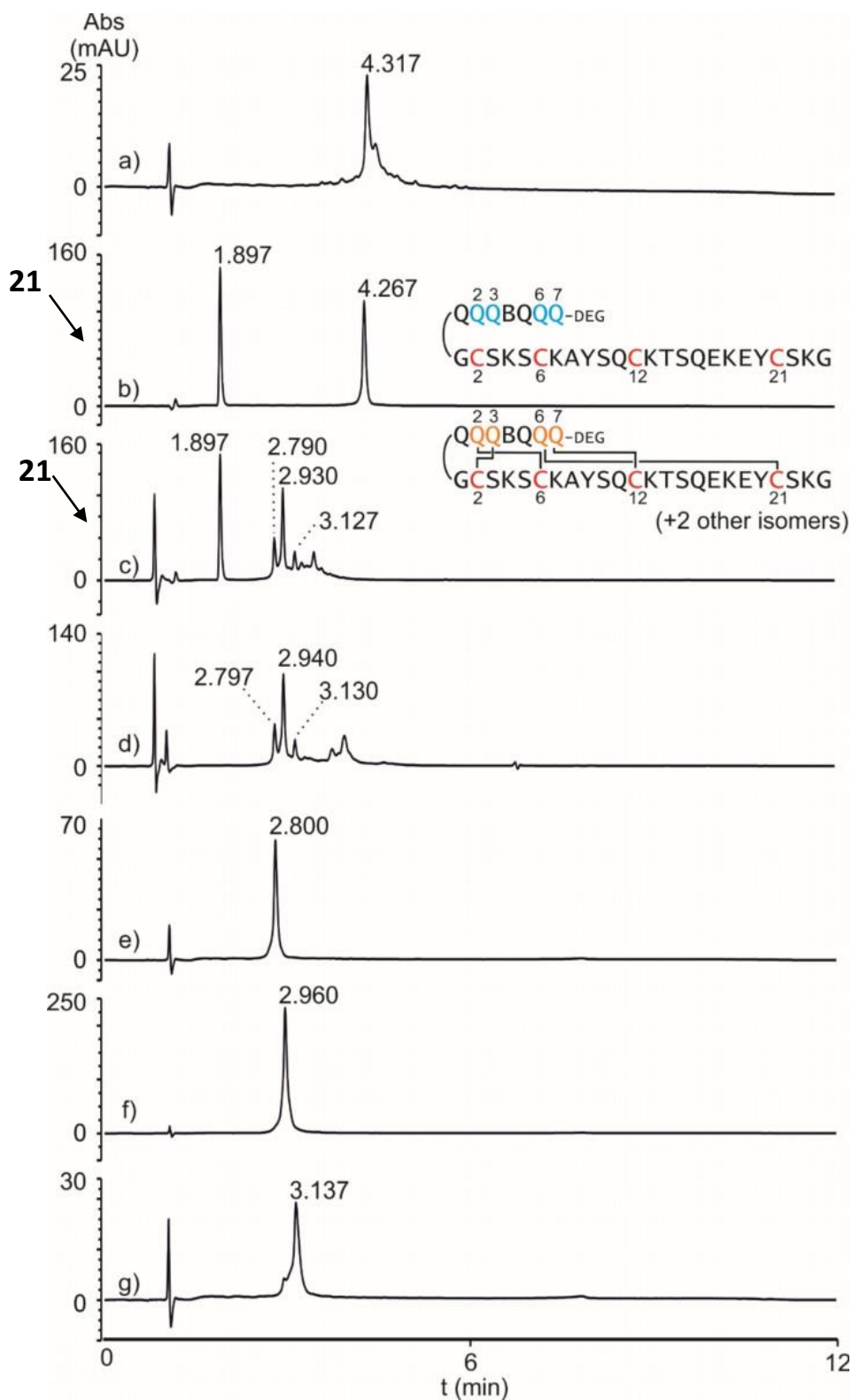


Figure S22 – RP-HPLC analysis of the synthesis, purification and cyclization of sequence 16. Overlay of RP-HPLC profiles from each synthetic step of compound **16C** synthesized from **16** measured with standard HPLC conditions. Compound **16** after SPS/SPFS as a crude (a), after purification co-injected with internal standard **21** (b), after cyclization co-injected with internal standard **21** (**16C**, c), and after addition of benzylmercaptan (d). The three main isomers (**16C-a**, **16C-b** and **16C-c**) were separated in e) f) and g). Chromatograms a), c) and d) obtained after the reaction without prior purification. All chromatograms were recorded at 375 nm.

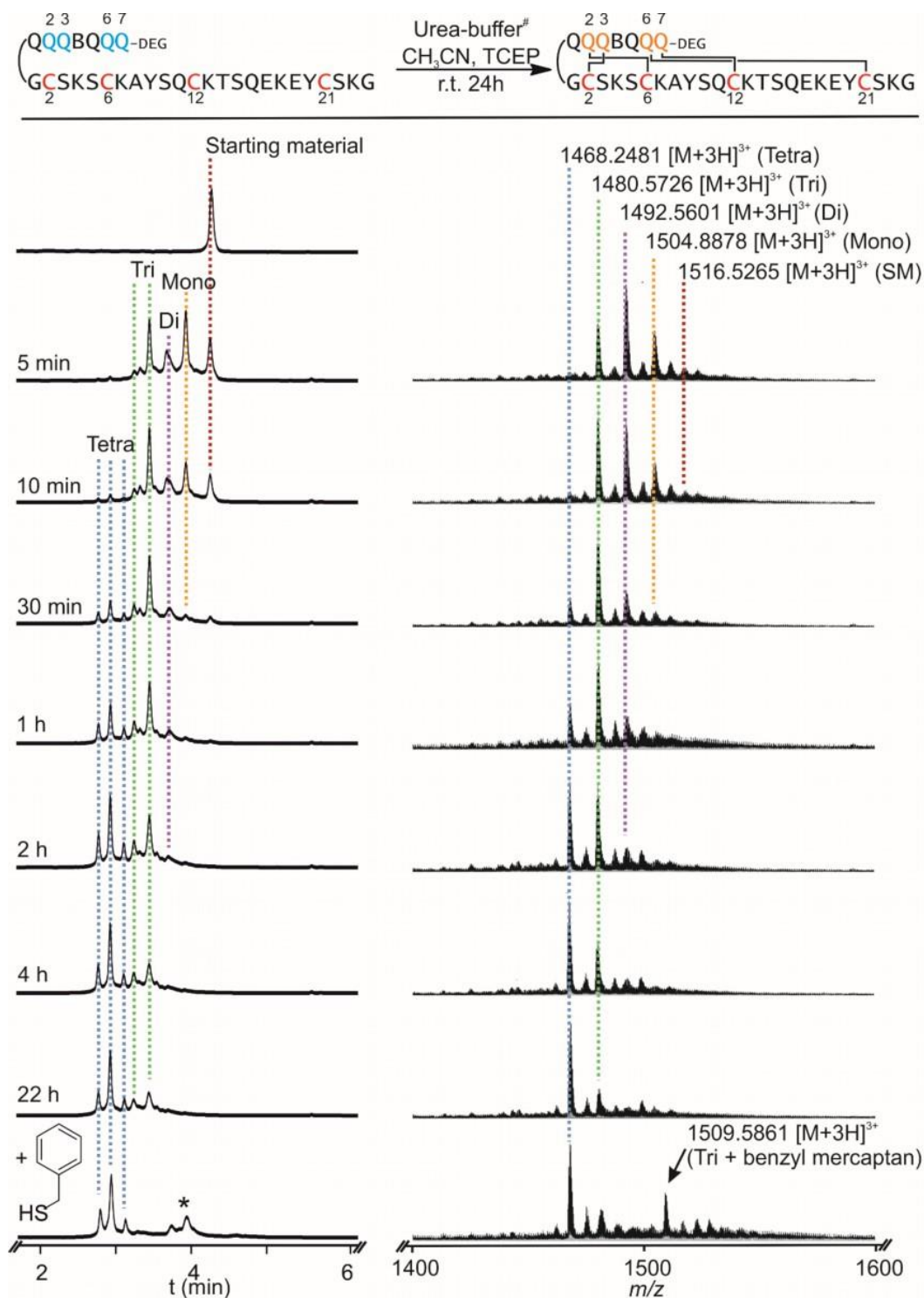


Figure S23 - Excerpts of the RP-HPLC and ESI-MS traces of the macrocyclization progression of 16C with final termination of the unreacted chloroacetamide group with benzyl mercaptan (*). The ESI-MS spectra reported correspond to the time segment 2.5 to 4.5 min. The resolution of the LC traces was not good enough to distinguish each peak intermediate on the base peak chromatogram (BPC) of the TOF detector. Urea buffer pH 8.5, 8 M (#). Chromatograms were measured with standard HPLC conditions and recorded at 375 nm.

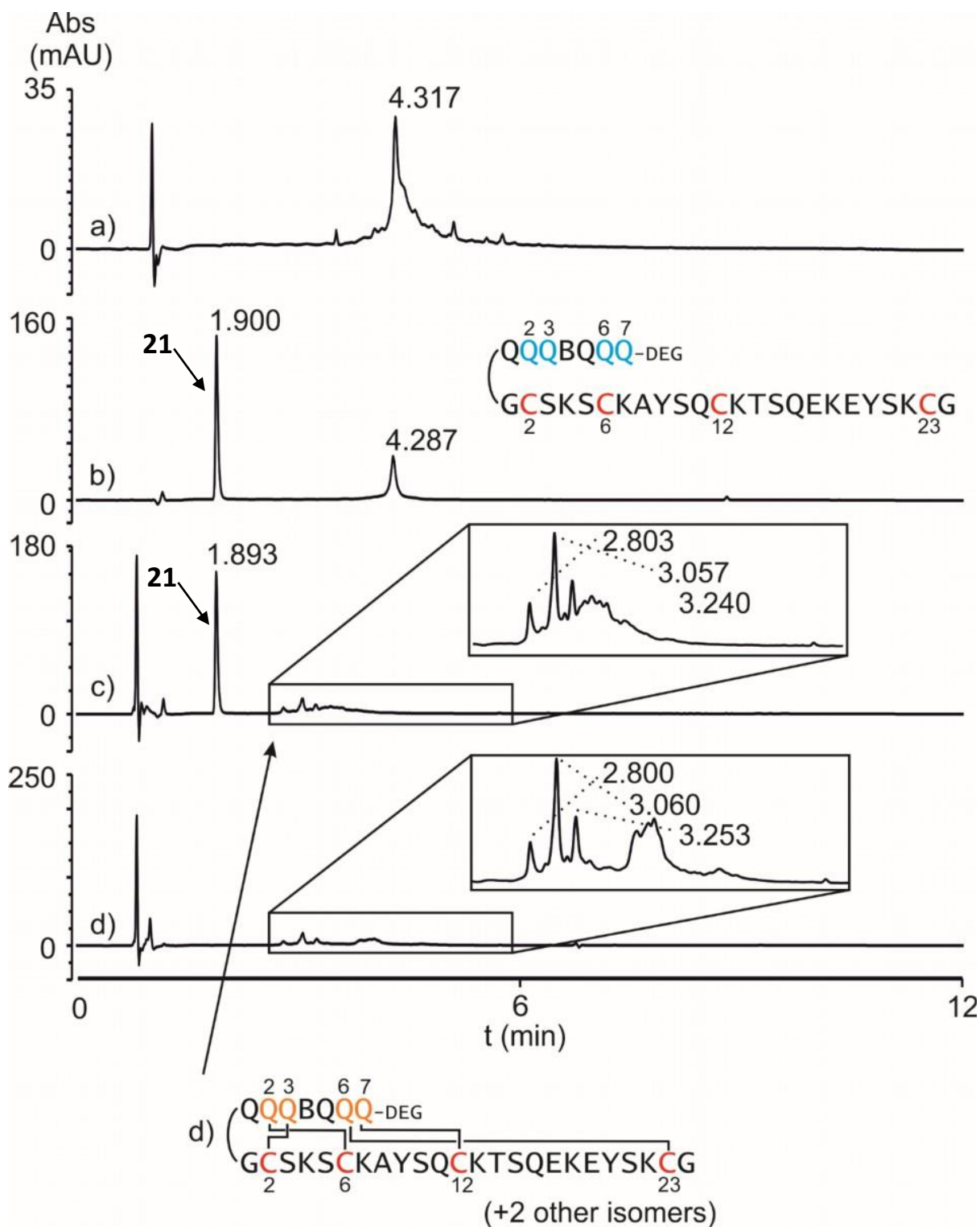


Figure S24 – RP-HPLC analysis of the synthesis, purification and cyclization of sequence 17. Overlay of RP-HPLC profiles from each synthetic step of compound **17C** synthesized from **17**. Compound **17** after SPS/SPFS as a crude (a), after purification co-injected with internal standard **21** (b), after cyclization co-injected with internal standard **21** (**17C**, c), and after addition of benzylmercaptan (d). Chromatograms a), c) and d) obtained after the reaction without prior purification. Due to low amounts, no final purification was carried out. Chromatograms were measured with standard HPLC conditions. All chromatograms were recorded at 375 nm.

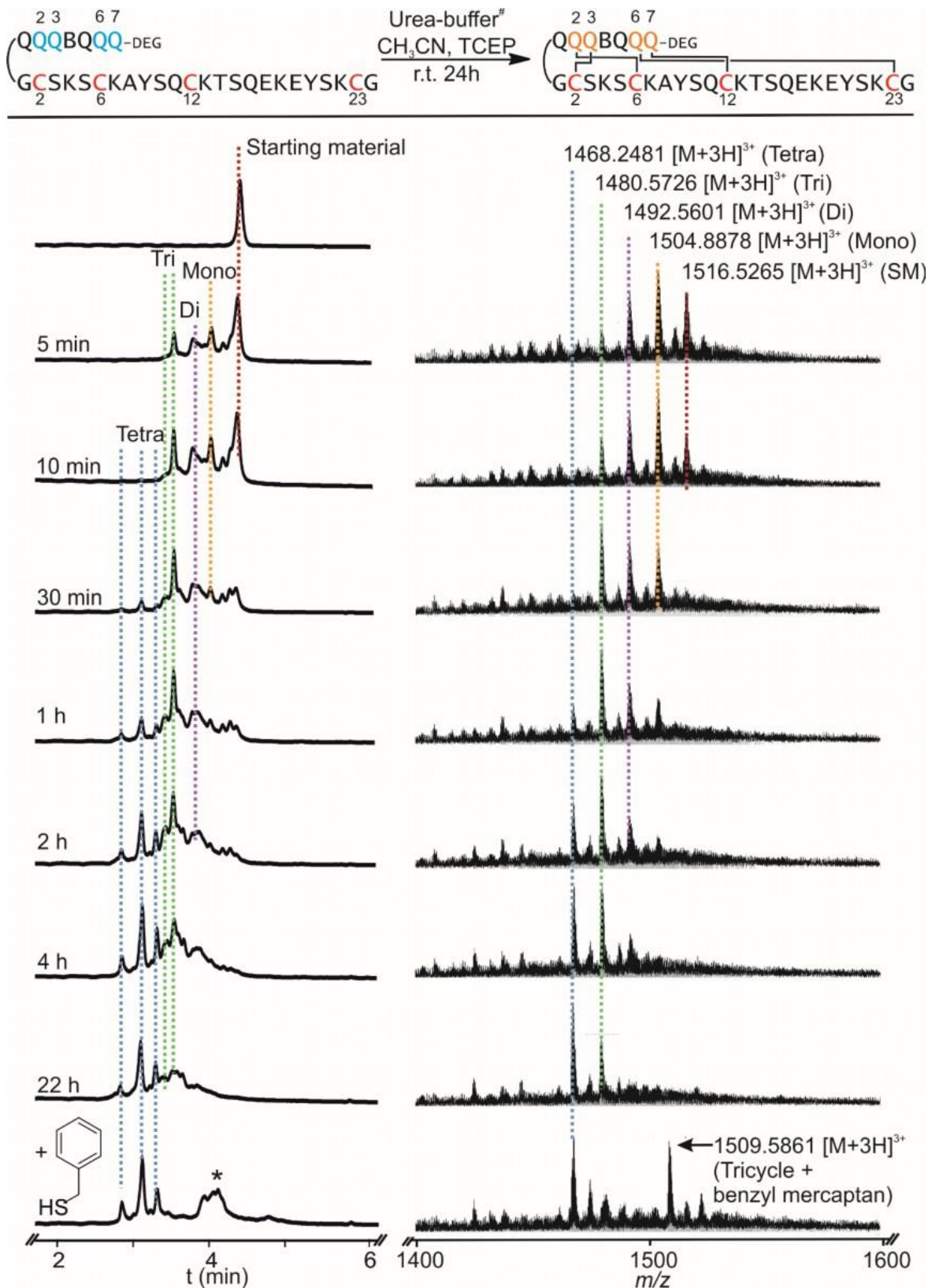


Figure 25 - Excerpts of the RP-HPLC and ESI-MS traces of the macrocyclization progression of 17C with final termination of the unreacted chloroacetamide group with benzyl mercaptan (*). The ESI-MS spectra reported correspond to the time segment 2.5 to 4.5 min. The resolution of the LC traces was not good enough to distinguish each peak intermediate on the base peak chromatogram (BPC) of the TOF detector. Urea buffer pH 8.5, 8 M (#). Chromatograms were measured with standard HPLC conditions and recorded at 375 nm.

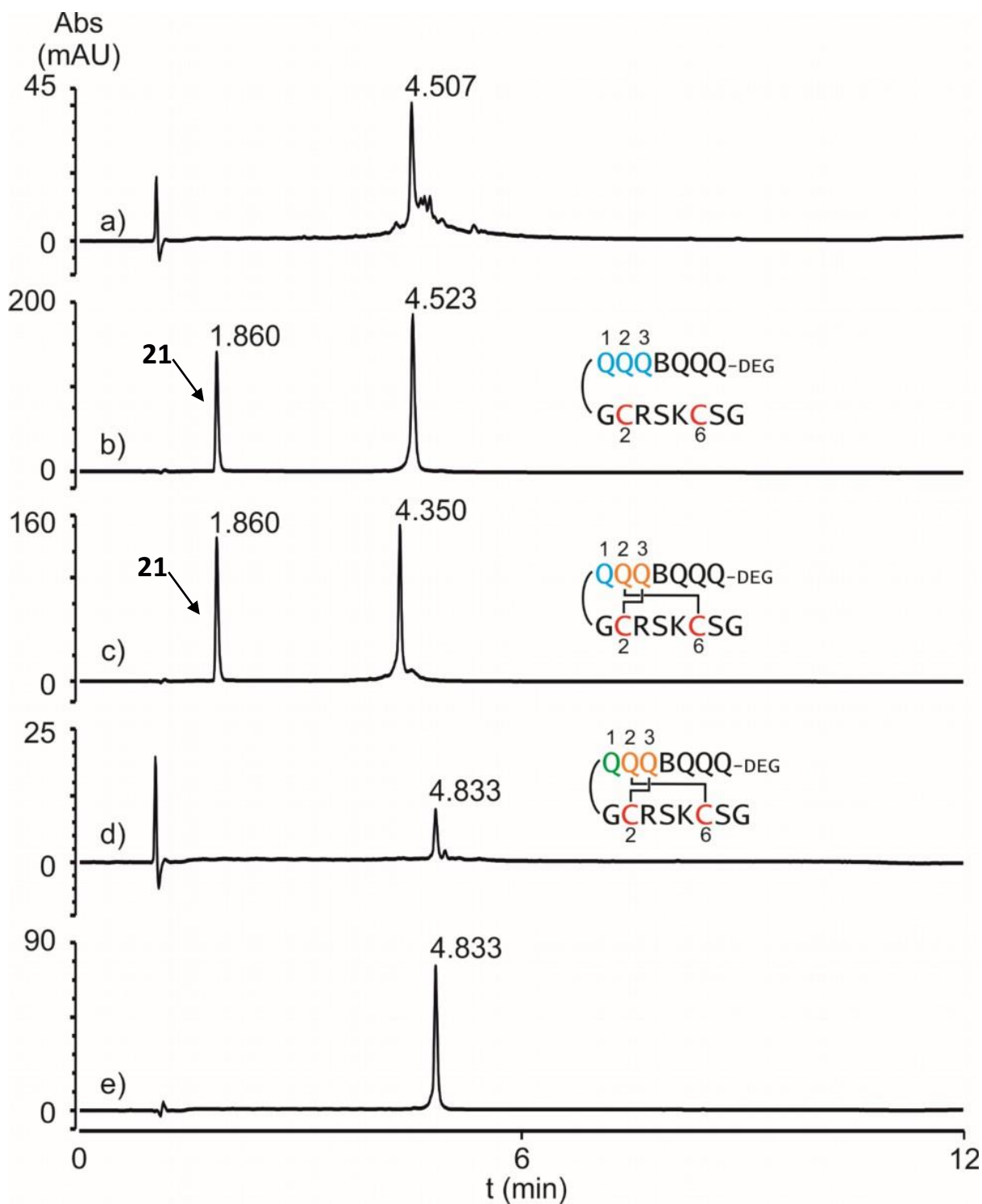


Figure S26 – RP-HPLC analysis of the synthesis, purification and cyclization of sequence 18. Overlay of RP-HPLC profiles from each synthetic step of compound **18Q** synthesized from **18**. Compound **18** after SPS/SPFS as a crude (a), after purification co-injected with internal standard **21** (b), after cyclization co-injected with internal standard **21** (**18C**, c), after benzyl mercaptan installation (**18Q**, d) and final purification (**18Q**, e). Chromatograms a), and c) obtained after the reaction without prior purification. Chromatograms were measured with standard HPLC conditions. All chromatograms were recorded at 375 nm.

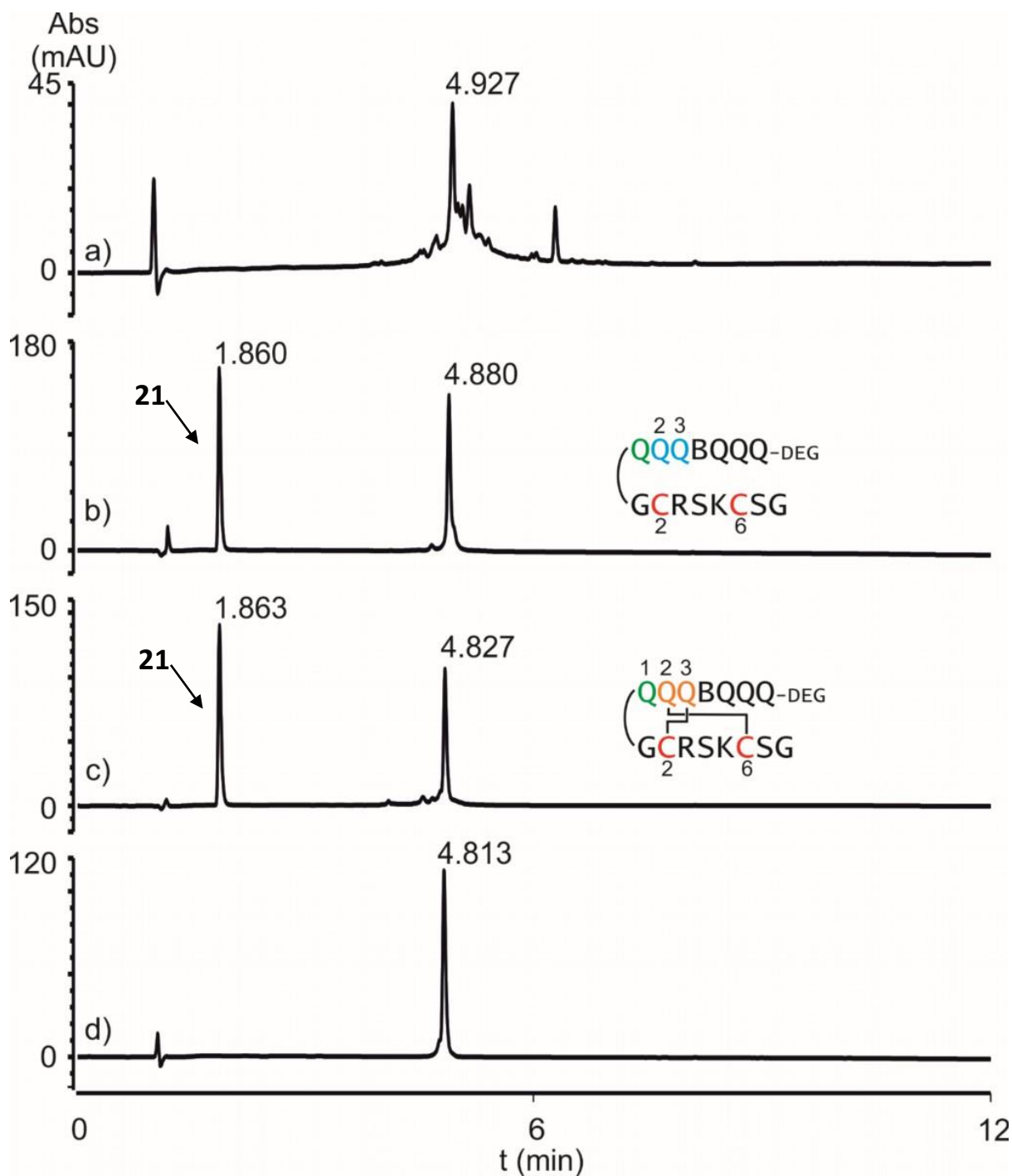


Figure S27 – RP-HPLC analysis of the synthesis, purification and cyclization of sequence R18. Overlay of RP-HPLC profiles from each synthetic step of compound **18Q** synthesized from **R18**. Compound **R18** after SPS/SPFS as a crude (a), after purification co-injected with internal standard 21 (b), after cyclization co-injected with internal standard 21 (**18Q**, c) and final purification (**18Q**, d). Chromatograms a), and c) obtained after the reaction without prior purification. Chromatograms were measured with standard HPLC conditions. All chromatograms were recorded at 375 nm.

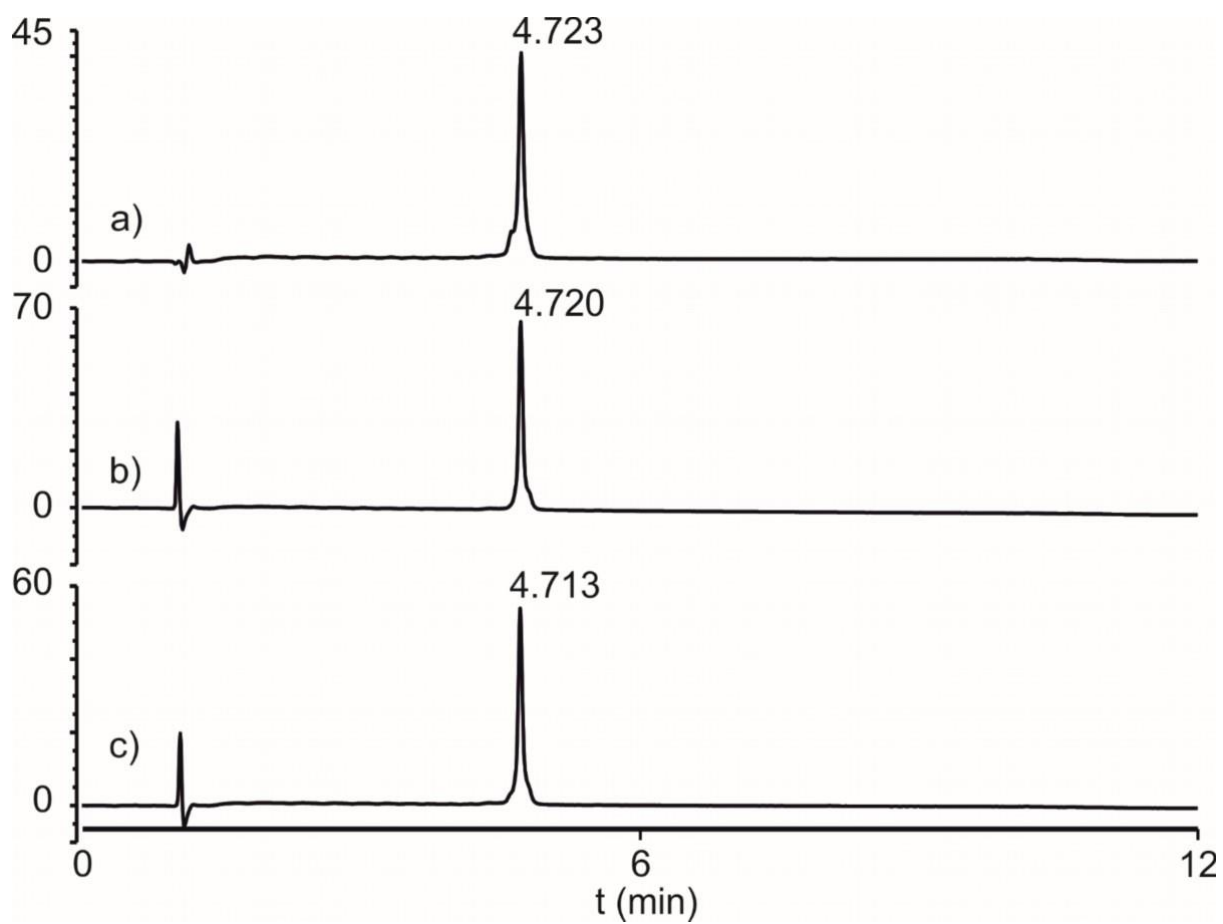


Figure S28 - RP-HPLC analysis of sequences 18. Overlay of RP-HPLC profiles measured from compound **18** obtained from the competition experiment (a), synthesized from the reference experiment (b) and as a co-injection (c). Chromatograms were measured with standard HPLC conditions. All chromatograms were recorded at 375 nm.

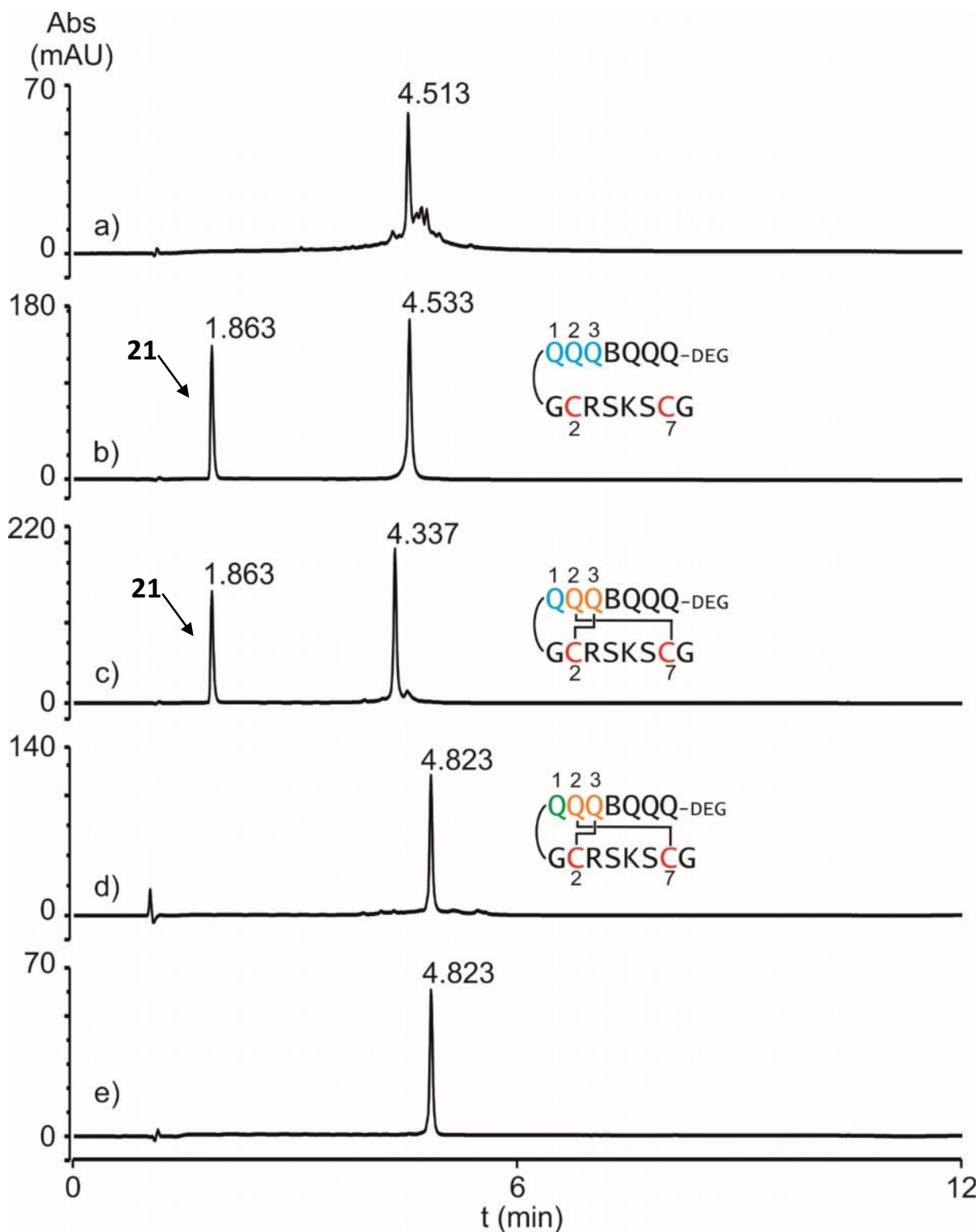


Figure S29 – RP-HPLC analysis of the synthesis, purification and cyclization of sequence 19. Overlay of RP-HPLC profiles measured from each synthetic step of compound 19Q. Compound 19 after SPS/SPFS as a crude (a), after purification co-injected with internal standard 21 (b), after cyclization co-injected with 21 (19C, c), after benzyl mercaptan installation d) and final purification (19Q, e). Chromatograms a), c) and d) were recorded after the reaction without prior purification. Chromatograms were measured with standard HPLC conditions. All chromatograms were recorded at 375 nm.

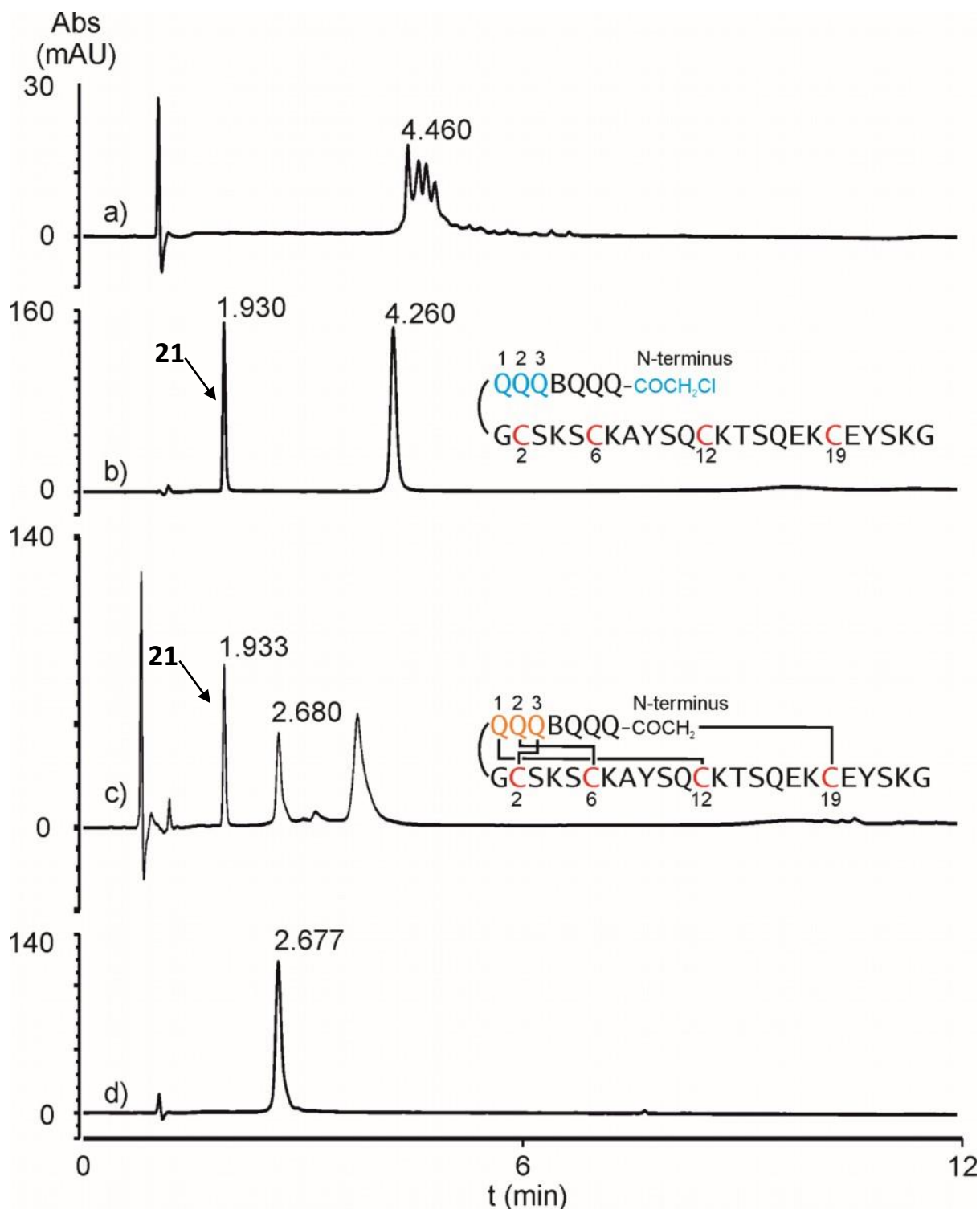


Figure S30 – RP-HPLC analysis of the synthesis, purification and cyclization of sequence 20. Overlay of RP-HPLC profiles measured from each synthetic step of compound **20Q**. Compound **20** after SPS/SPFS as a crude (a), after purification co-injected with internal standard b(b), after cyclization co-injected with **20** (**20C**, c), and final purification (**20C**, d). Chromatograms a), and c) were recorded after the reaction without prior purification. Chromatograms were measured with standard HPLC conditions. All chromatograms were recorded at 375 nm.

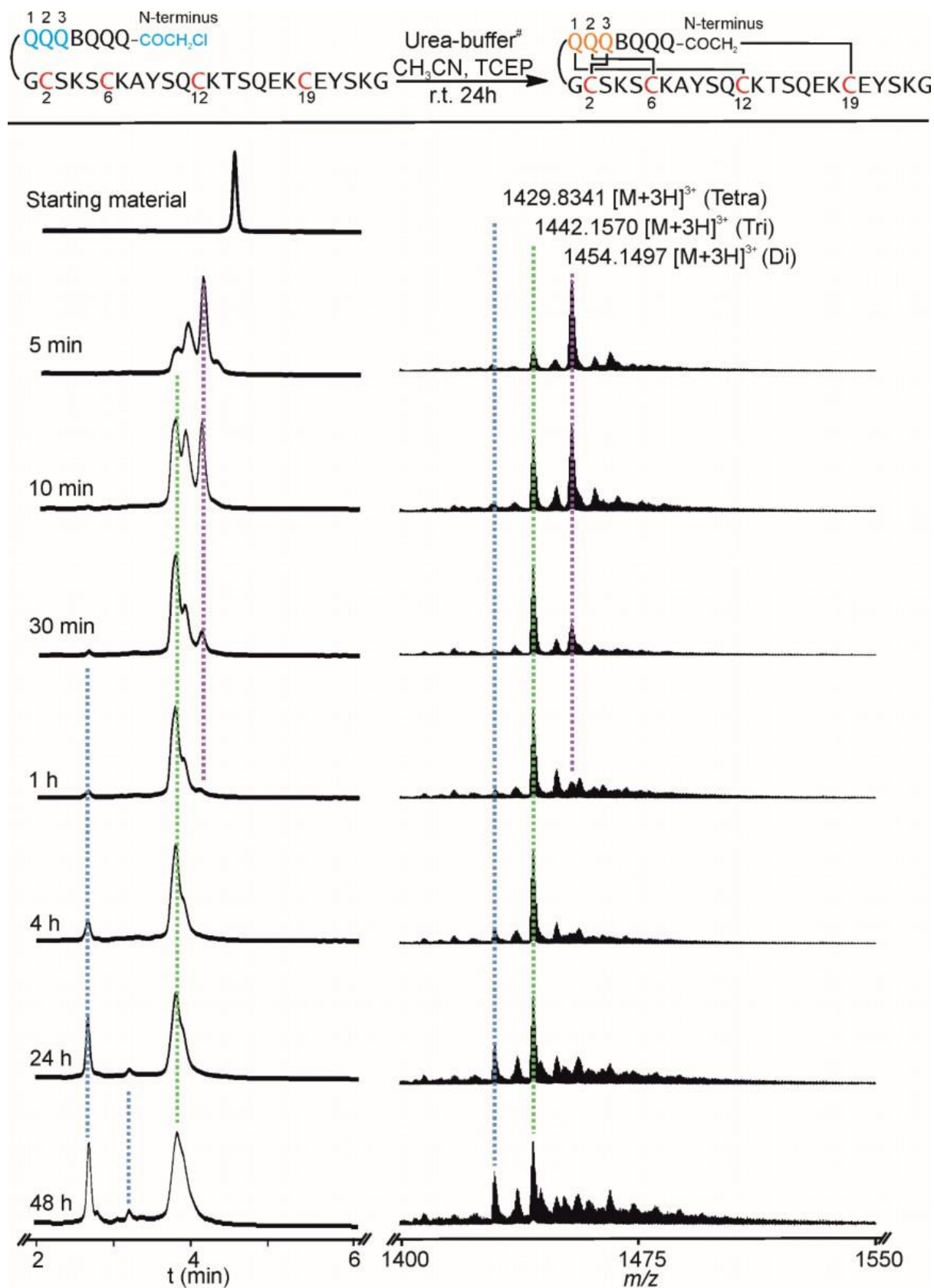


Figure S31 - Excerpts of the RP-HPLC and ESI-MS traces of the macrocyclization progression of 20C. The ESI-MS spectra reported correspond to the time segment 2.0 to 4.5 min. The resolution of the LC traces was not good enough to distinguish each peak intermediate on the base peak chromatogram (BPC) of the TOF detector. Urea buffer pH 8.5, 8 M (#). Chromatograms were measured with standard HPLC conditions and recorded at 375 nm.

NMR identification of products and structural study of **9Q**

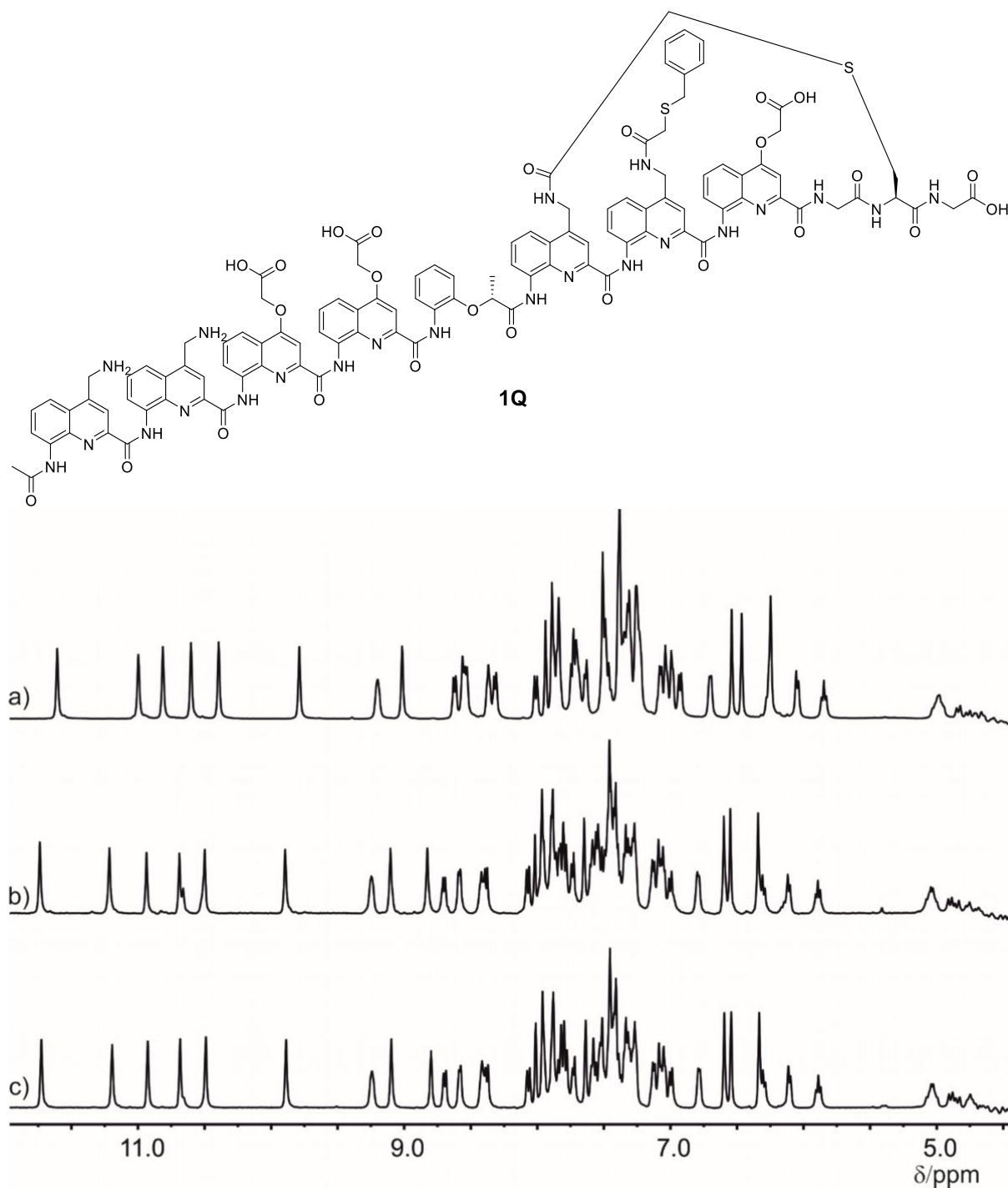


Figure S32 - NH and aromatic region of the ¹H NMR overlaid spectra of **1Q synthesized by two different routes.** ¹H NMR spectra recorded in a solvent mixture of NH₄OAc 3mM pH 8.5 in CD₃CN (50:50, v/v) (500 MHz, 25°C) with TMSP (3-(trimethylsilyl)propionic-2,2,3,3-d₄ acid sodium salt) of **1Q** synthesized from compound **1** (a); synthesized from compound **R1** (b) and the 1:1 mixture of the two products synthesized via (a) or (b) route (c).

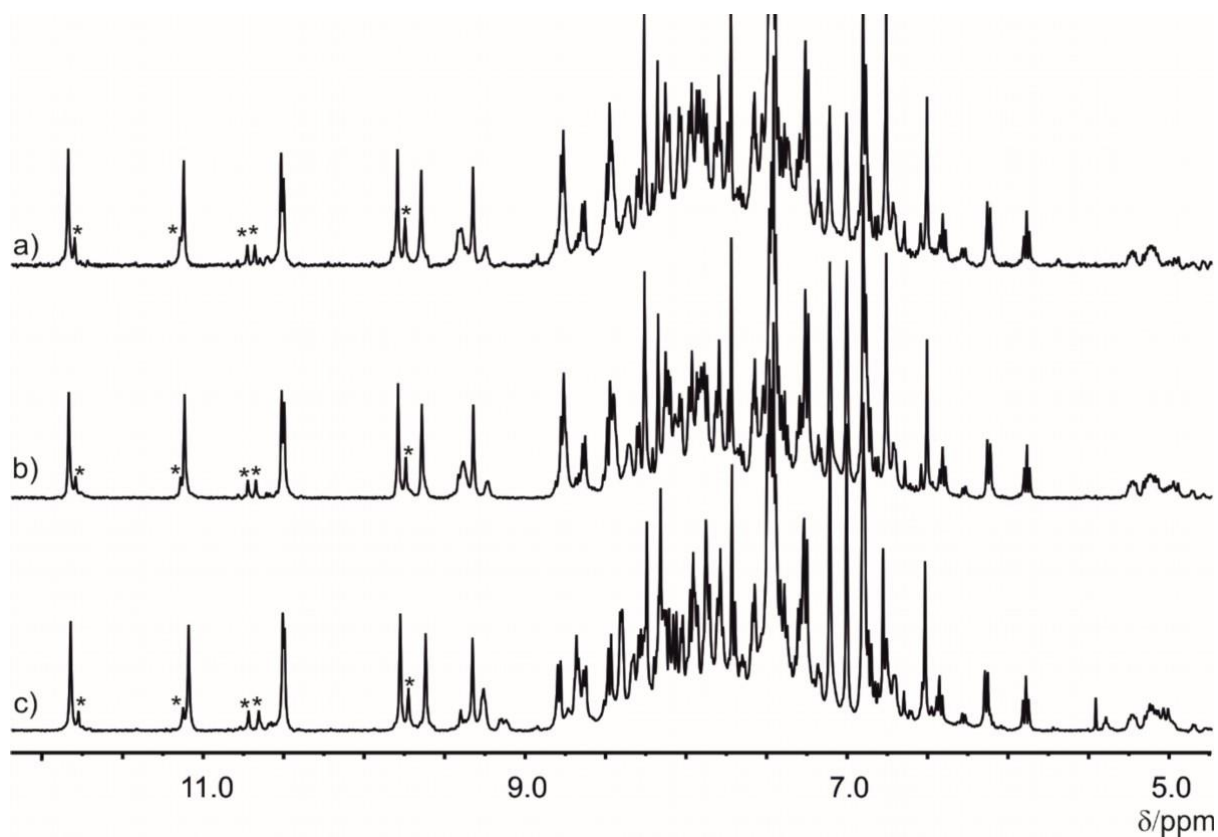
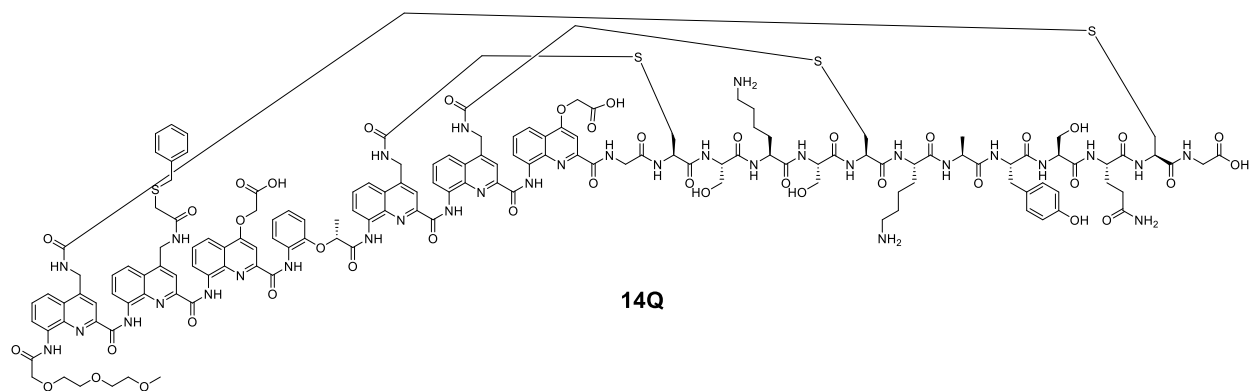


Figure S33 - NH and aromatic region of the ^1H NMR overlaid spectra of 14Q synthesized by two different routes. ^1H NMR spectra recorded in a solvent mixture of NH_4OAc 3mM pH 8.5 in CD_3CN (50:50, v/v) (500 MHz, 25°C) with TMS of **14Q** synthesized from compound **14** (a); from compound **R14** (b) and the 1:1 mixture of the two products synthesized via (a) or (b) route (c). Signals assigned with * are considered as a synthetic impurity (over insertion of a Ser residue was detected by LC-MS analysis). Yet the presence of a different conformer cannot be excluded.

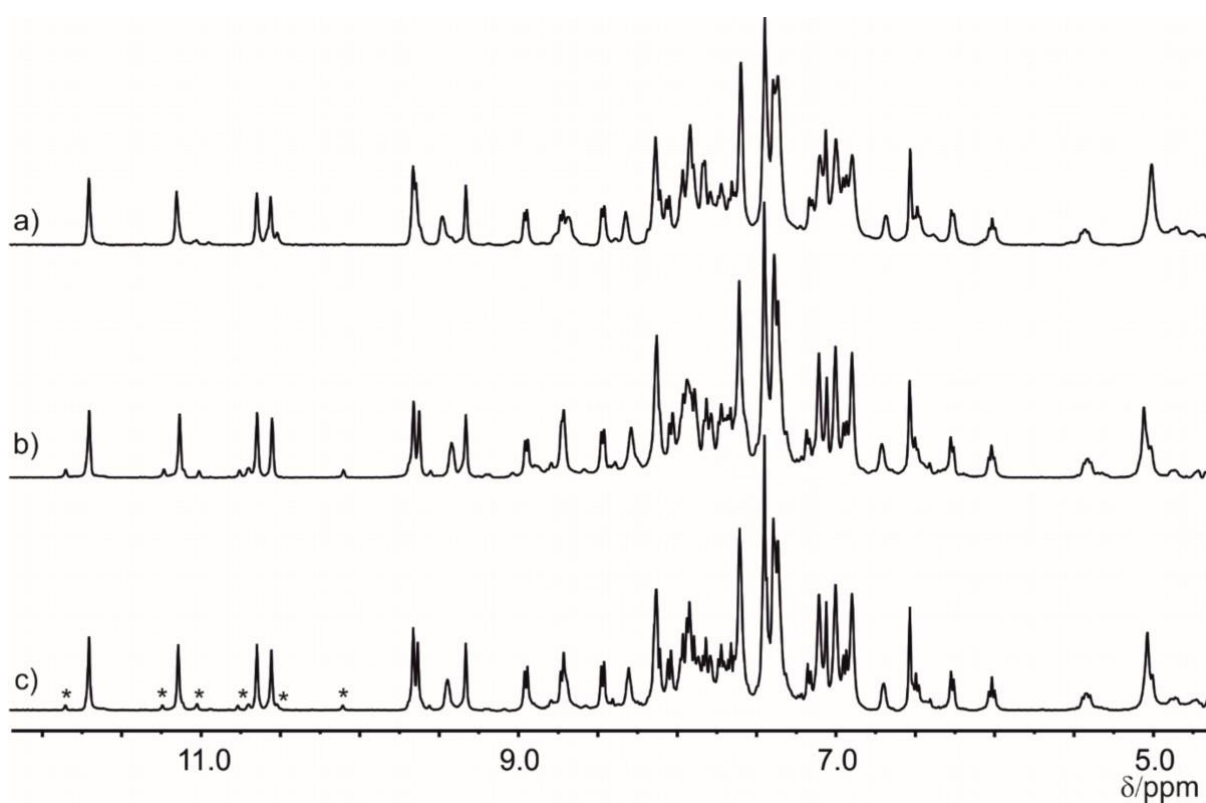
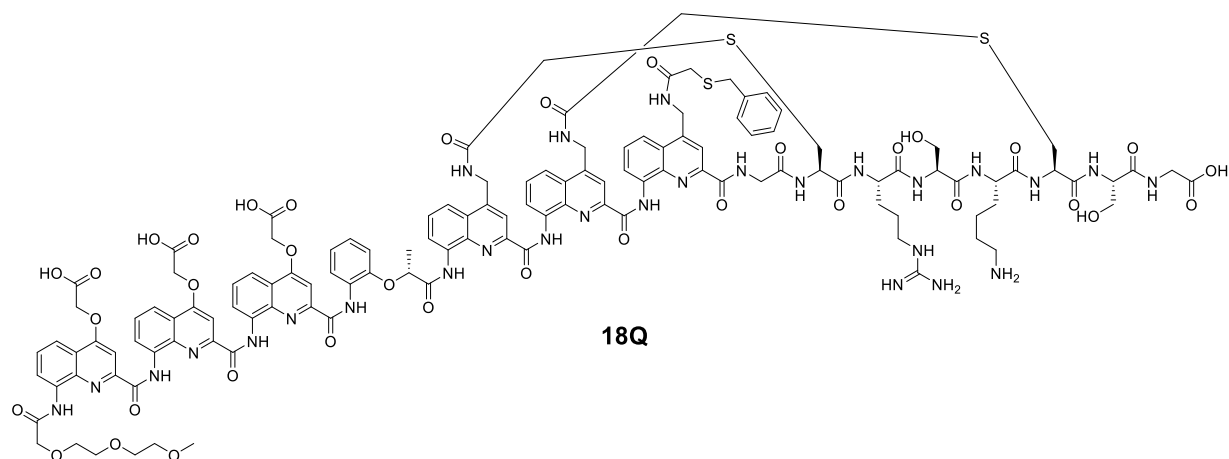


Figure S34 - NH and aromatic region of the ^1H NMR overlaid spectra of **18Q synthesized by two different routes.** ^1H NMR spectra recorded in a solvent mixture of NH_4OAc 3mM pH 8.5 in CD_3CN (50:50, v/v) (500 MHz, 25°C) with TMS of **18Q** synthesized from compound **18** (a); from compound **R18** (b) and the 1:1 mixture of the two products synthesized via (a) or (b) route (c). Signals assigned with * are considered as a synthetic impurity.

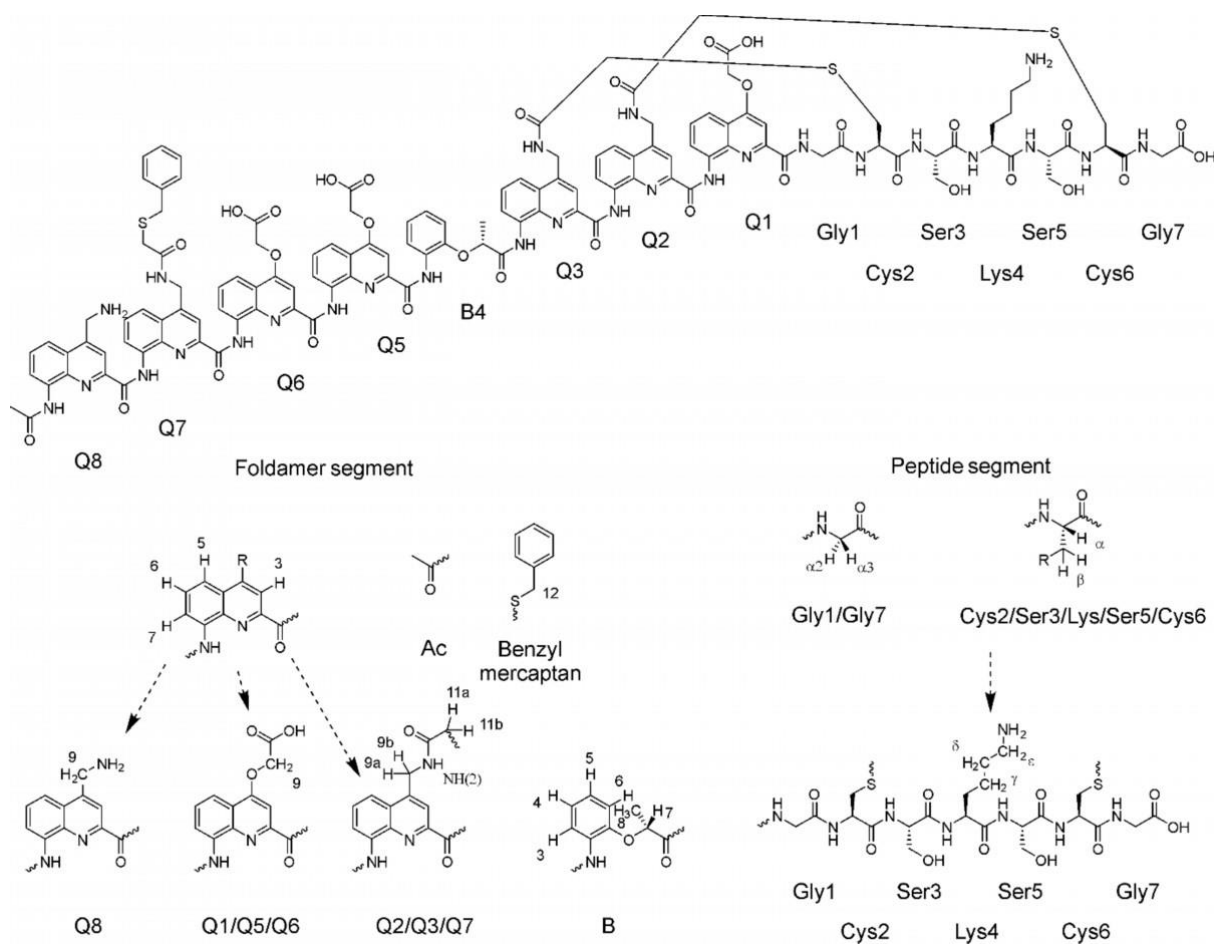


Figure 35 - Residue numbering of 9Q for full ^1H NMR assignment

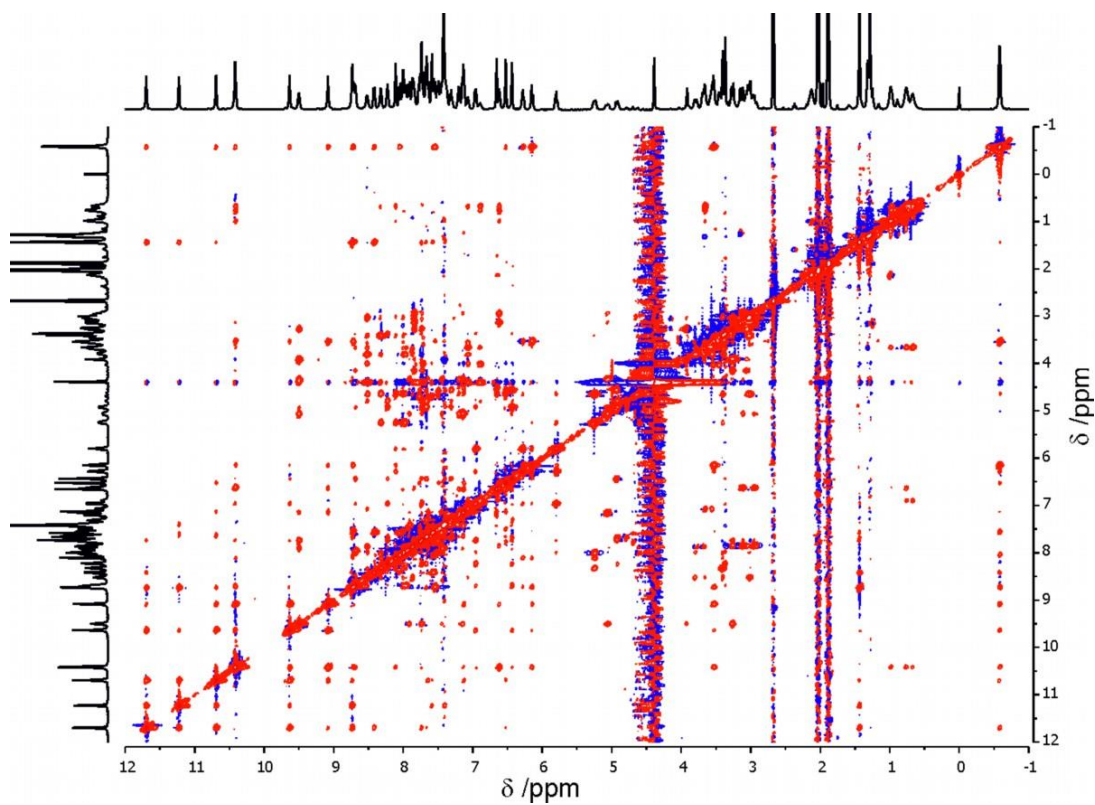


Figure S36 - ^1H NOESY spectrum of **9Q**. NMR solvent mixture of NH_4OAc (5mM pH 8.5) in CD_3CN (50:50, v/v) (500 MHz, 25°C) with TMSp.

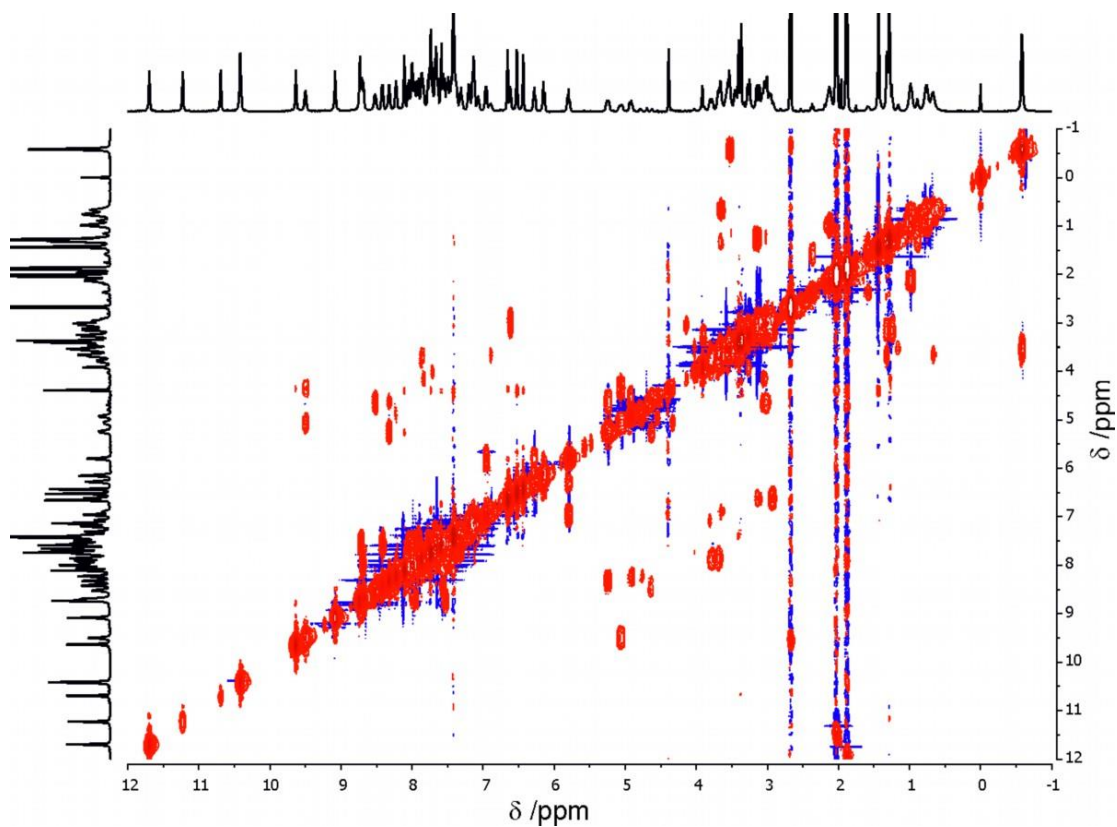


Figure S37 - ^1H COSY spectrum of **9Q**. NMR solvent mixture of NH_4OAc (5mM pH 8.5) in CD_3CN (50:50, v/v) (500 MHz, 25°C) with TMSp.

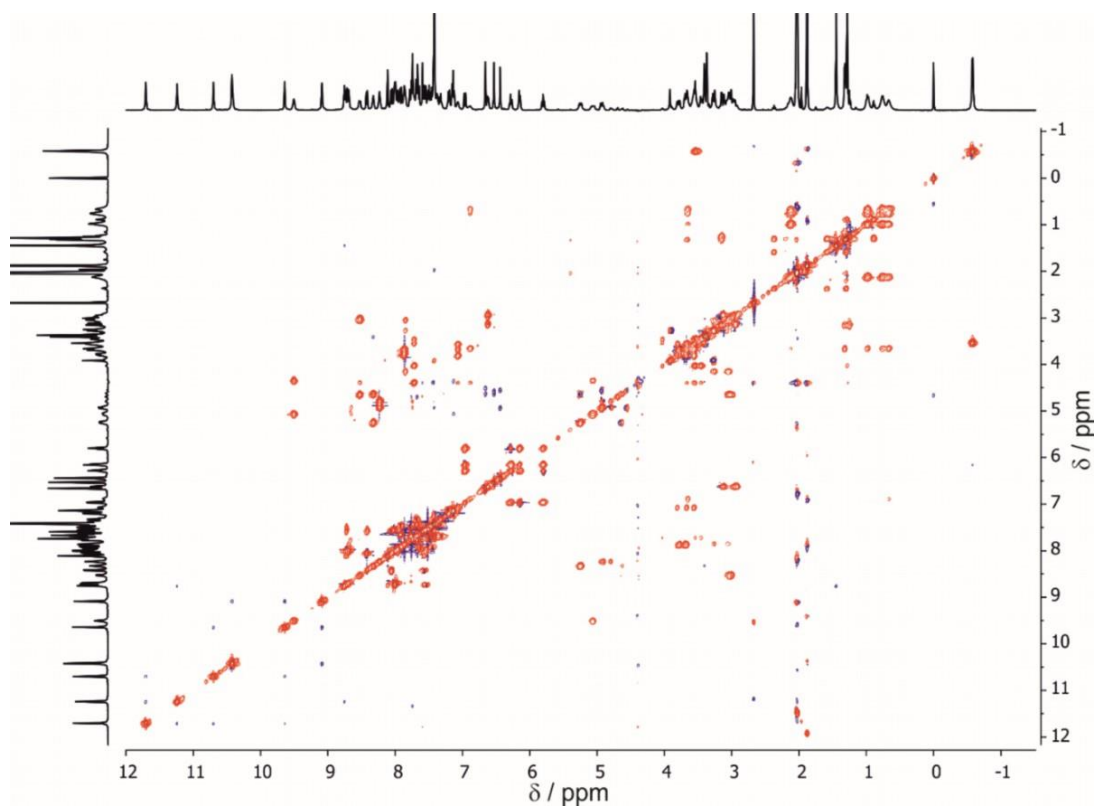


Figure S38 - ^1H TOCSY spectrum of **9Q**. NMR solvent mixture of NH_4OAc (5mM pH 8.5) in CD_3CN (50:50, v/v) (500 MHz, 25°C) with the addition of TMSP.

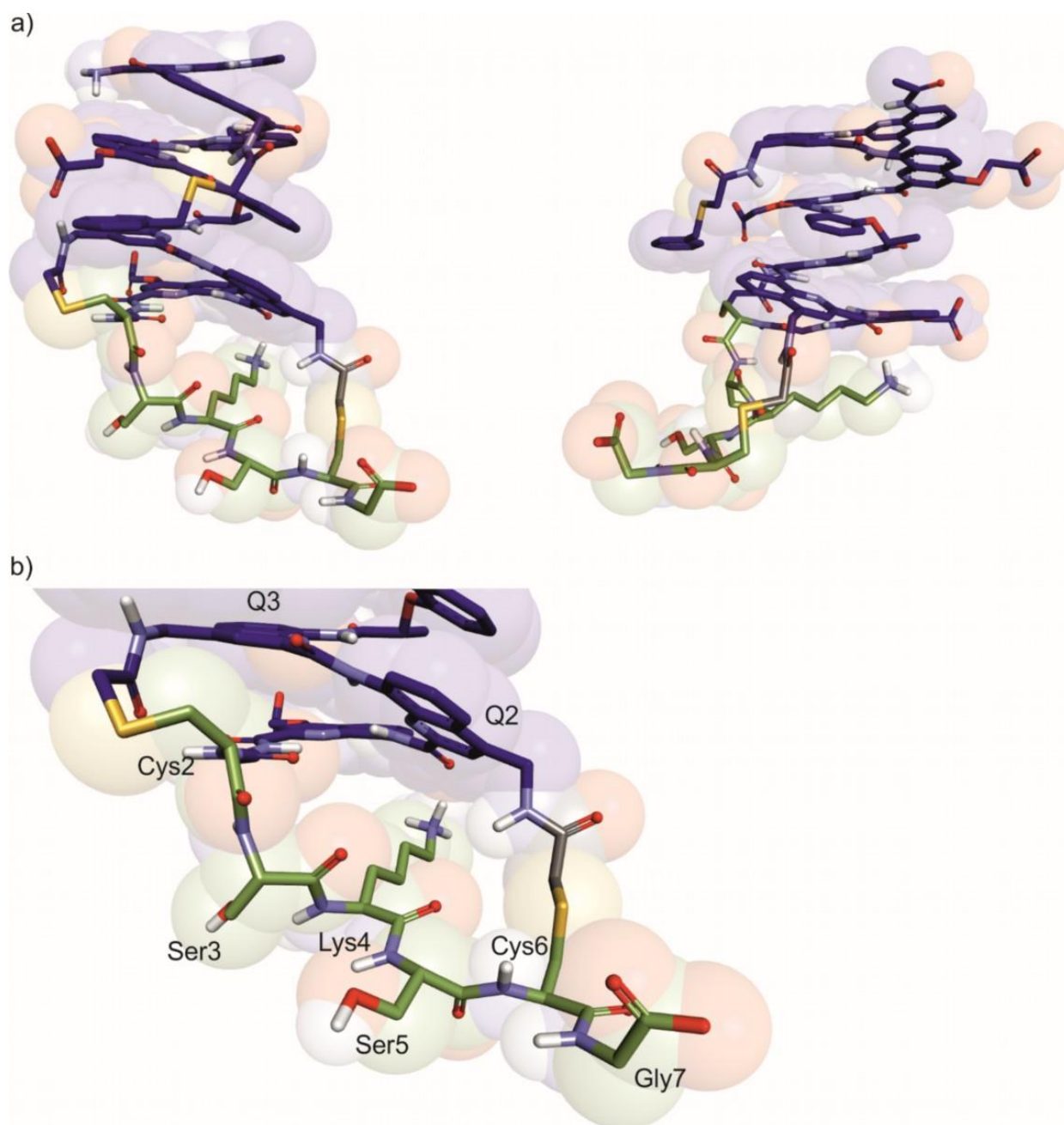


Figure S39 – Molecular models of 9Q. Molecular models obtained from MacroModel in the Maestro platform (force field potential: MMFFs, solvent: water, mini. method PRCG) of **9Q** a) from two different perspectives and b) zoom to the peptide region. Non-polar hydrogens are omitted for clarity. Foldamer carbon atoms are dyed in dark blue, peptide backbone carbon atoms in green.

Res.	H3	H4	H5	H6	H7	H8	H9	H11	NH	NH(2)	Ac	H12	Benz.
Q8	7.58		7.76	7.50	7.67		4.69		8.74		1.43		
Q7	7.74		7.68	7.32	7.40		4.92 (a), 4.79 (b)	3.40	11.22	8.23		3.92	7.45- 7.39
Q6	6.52		8.05	7.55	8.42		4.58		11.69				
Q5	6.43		7.92	7.45	7.64		4.56		10.69				
B	6.96	5.80	6.28	6.15	3.53	- 0.59			9.63				
Q3	7.74		7.14	7.20	7.13		5.05 (a), 4.34 (b)	3.92 (a), 3.27 (b)	9.08	9.50			
Q2	8.11		8.00	7.96	8.68		5.25 (a), 4.64 (b)	3.41 (a), 3.04 (b)	10.42	8.32			
Q1	6.65		8.01	7.54	8.72		4.51		10.41				

Table S1. ¹H chemical shift values in ppm for the foldamer segment of compound **9Q**

	α	β	γ	δ	ϵ	NH
Gly1	3.13 (2), 2.95 (3)					6.62
Cys2	4.14	3.05, 3.27				7.84
Ser3	4.03	3.45, 3.55				7.71
Lys4	3.66	0.67	0.76	0.99	2.12	6.90
Ser5	4.00	3.70				7.95
Cys6	4.64	3.04				8.52
Gly7	3.78 (2), 3.68 (3)					7.87

Table S2. ¹H chemical shift values in ppm for the peptide segment of compound **9Q**

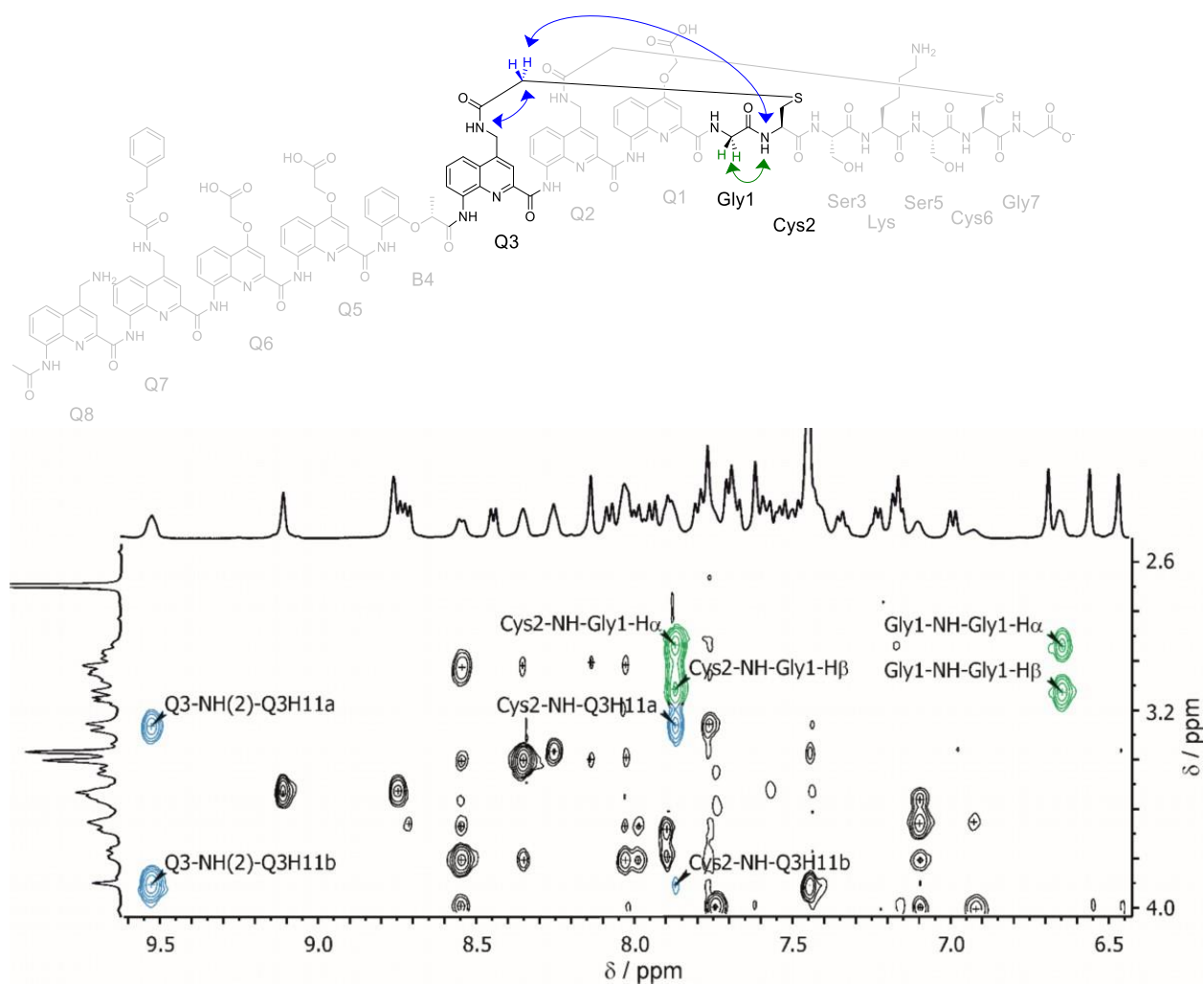


Figure S40 – Q3-macrocycle ^1H NOESY correlations. Excerpt of ^1H NOESY spectrum of **9Q** in a solvent mixture of NH_4OAc (5mM pH 8.5) in CD_3CN (50:50, v/v) (500 MHz, 25°C). Colored cross peaks relate to the correlation between Gly1 and Q3 side chain as part of a macrocycle.

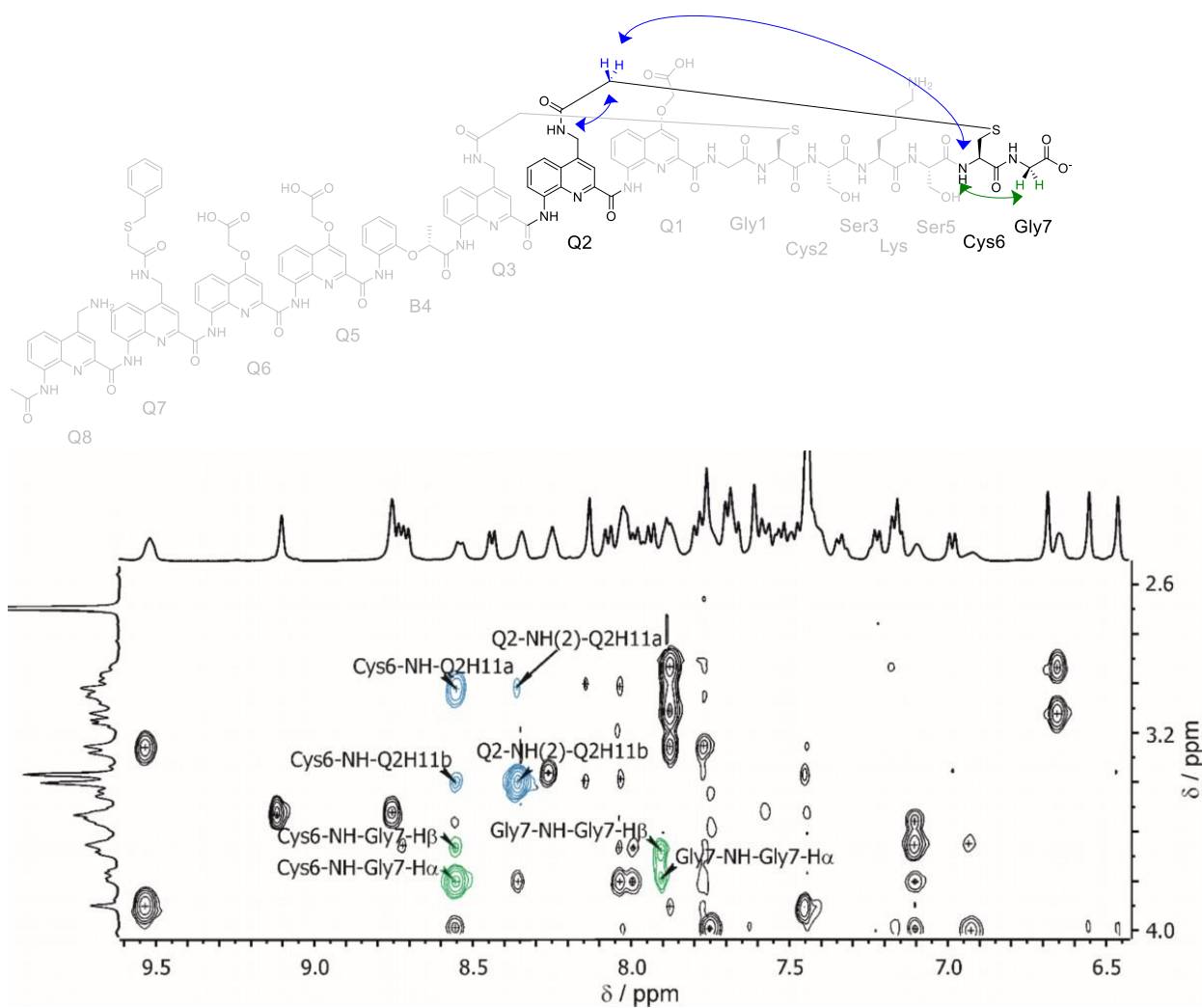


Figure S41 – Q2-macrocycle ^1H NOESY correlations. Excerpt of ^1H NOESY spectrum of **9Q** in a mixture of NH_4OAc (5mM pH 8.5) in CD_3CN (50:50, v/v) (500 MHz, 25°C). Colored cross peaks relate to the correlation between Gly7 and Q2 sidechain as part of a macrocycle.

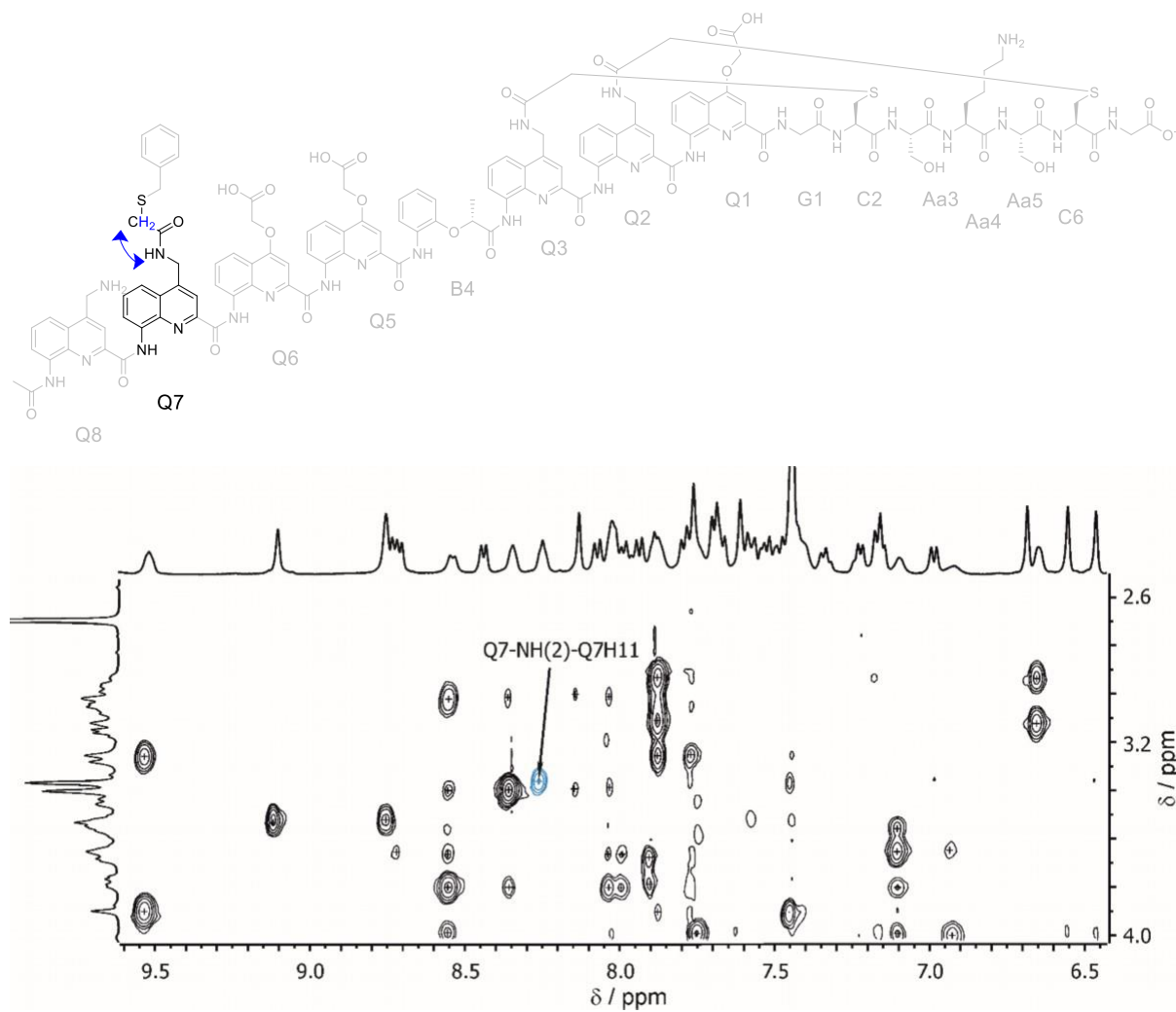


Figure S42 – Q7 NOESY correlation. Excerpt of ¹H NOESY spectrum of **9Q** in a mixture of NH₄OAc (5mM pH 8.5) in CD₃CN (50:50, v/v) (500 MHz, 25°C). Cross peaks correlation on Q7 side chain is depicted in blue.

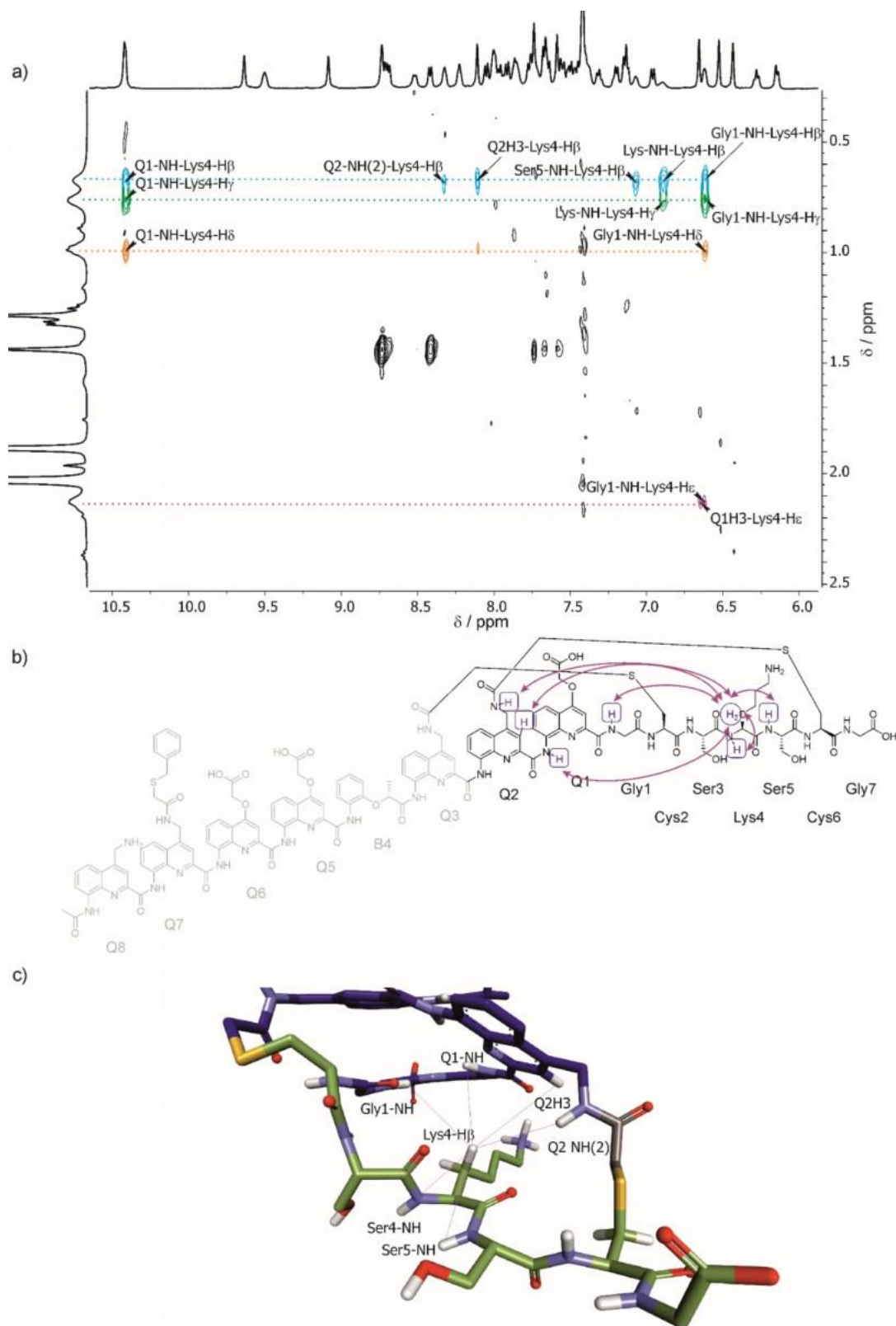


Figure S43 – Lys4 ^1H -NOESY correlations. a) Excerpt of ^1H NOESY spectrum of **9Q** in a solvent mixture of NH_4OAc (5mM pH 8.5) in CD_3CN (50:50, v/v) (500 MHz, 25°C). Colored cross peaks relate to the correlation between Lys4-H β (blue), Lys4-H γ (green), Lys4-H δ , and Lys4-H ϵ and neighboring aromatic and amide protons. b) Chemical structure of **9Q** and Lys4-H β correlations. c) Model of **9Q** and their correlations of signals shown for Lys4-H β exemplarily. NOE signals are depicted in purple lines.

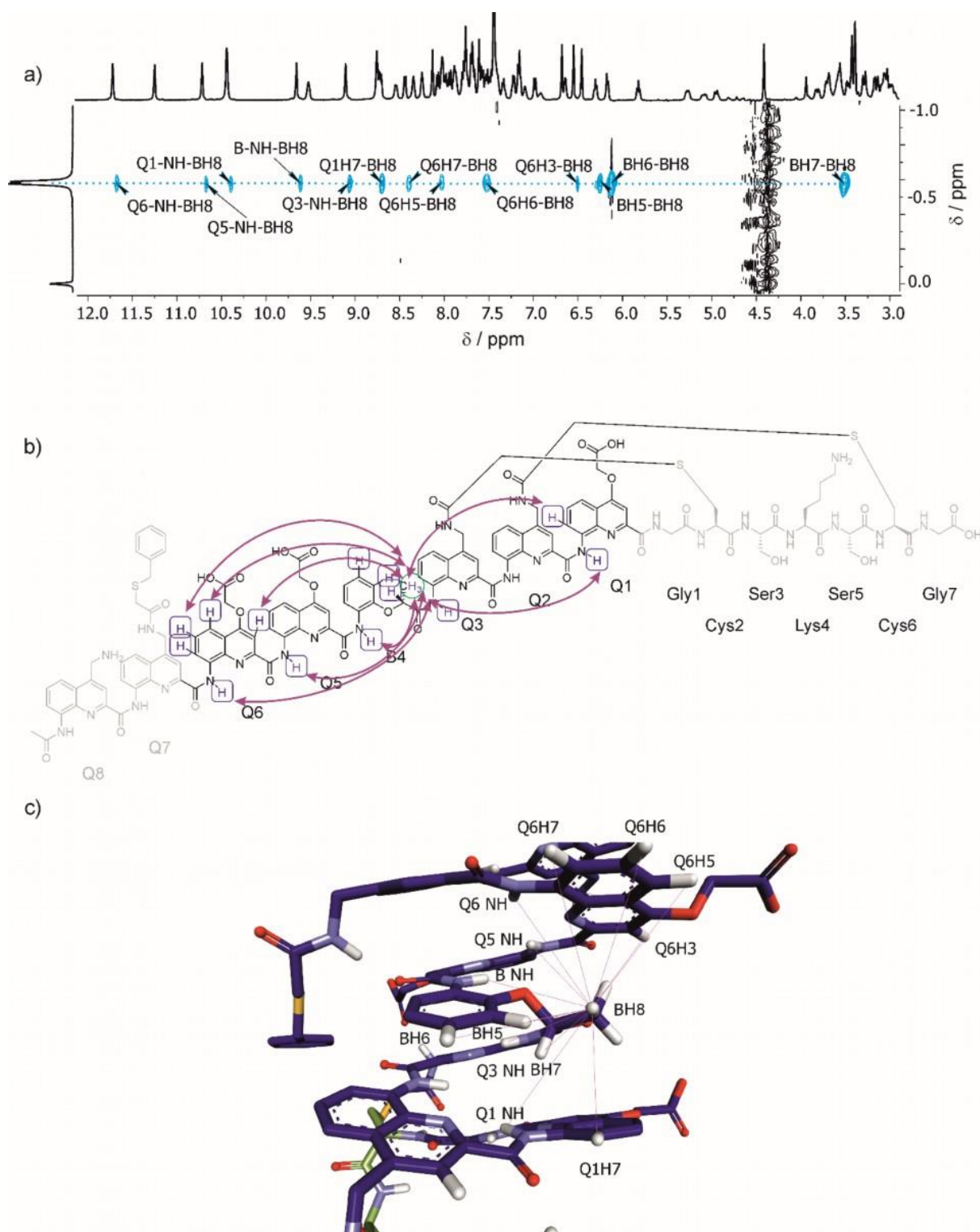


Figure S44 – BH8 ^1H -NOESY correlations. a) Excerpt of ^1H NOESY spectrum of **9Q** in a solvent mixture of NH_4OAc (5mM pH 8.5) in CD_3CN (50:50, v/v) (500 MHz, 25°C). Marked cross peaks relate to the correlation between BH8 and neighboring protons. Chemical structure of **9Q** and BH8 correlations. c) Model of **9Q** and their correlations of BH8 signals. NOE signals indicated by purple lines.

Reaction trail analysis of 16

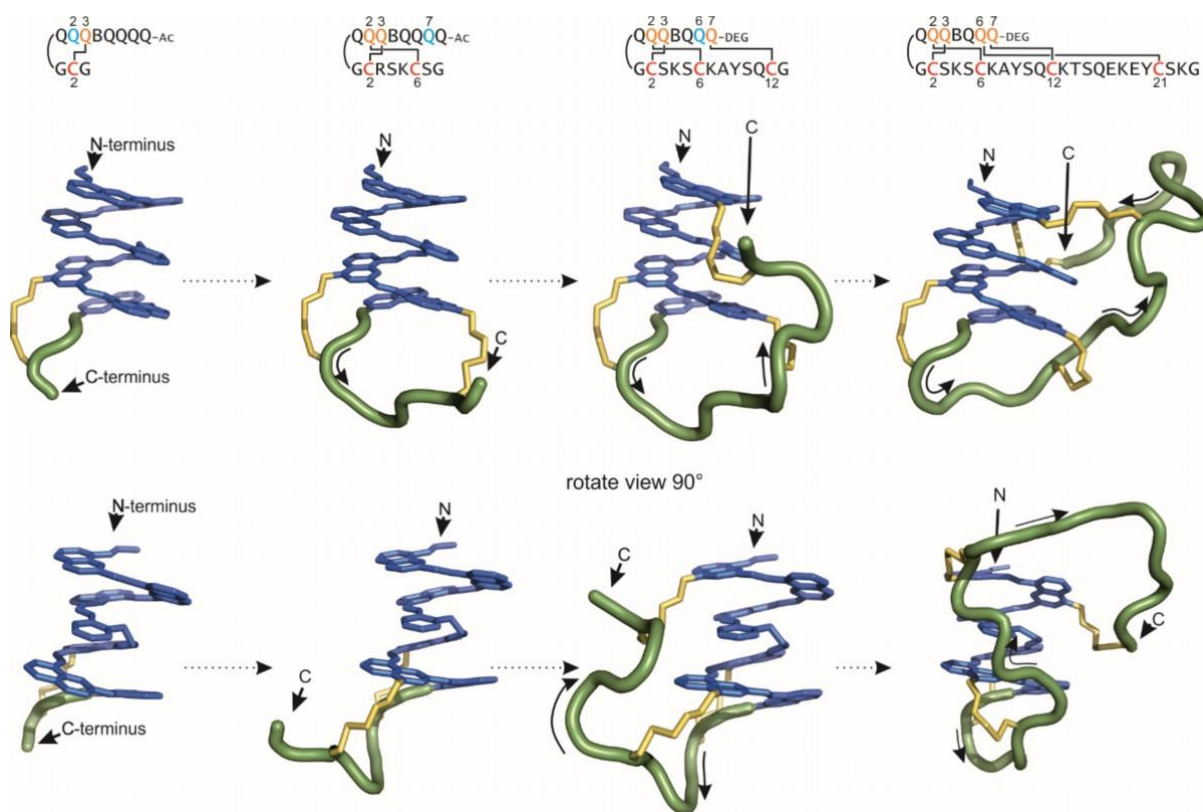


Figure S45 - Molecular models which illustrate the cyclization trail of the mono-, di-, tri- and tetracycle. Foldamer shown in blue, peptide loops in green, thioether linker in yellow. Arrows indicate N- to C-terminus.

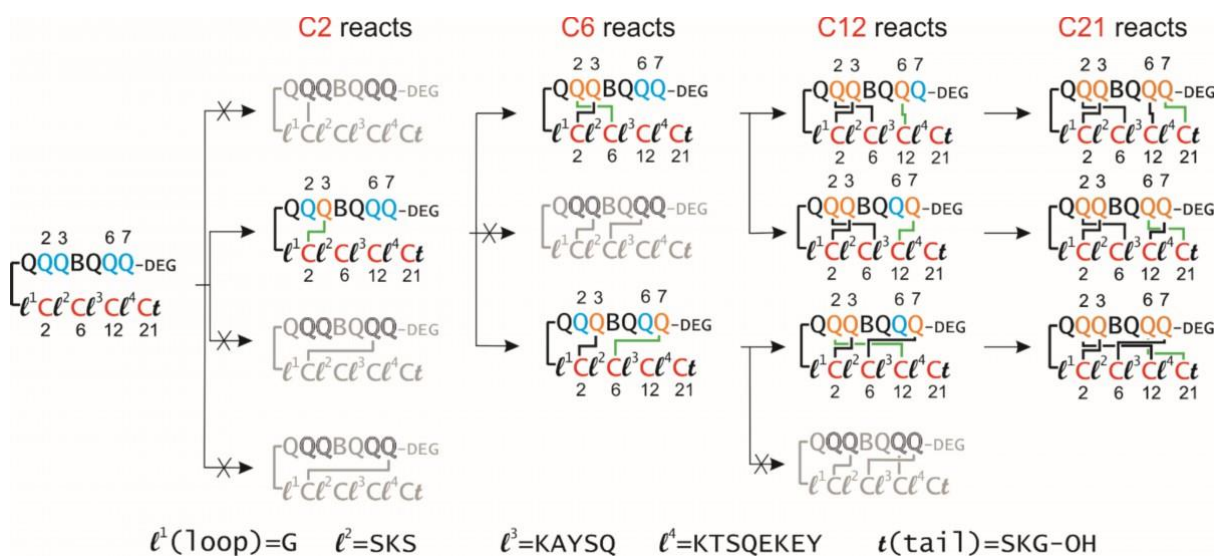


Figure S46 - Scheme of the cyclization trail of 16C. Colored schemes are plausible cyclization trails.

Synthetic schemes

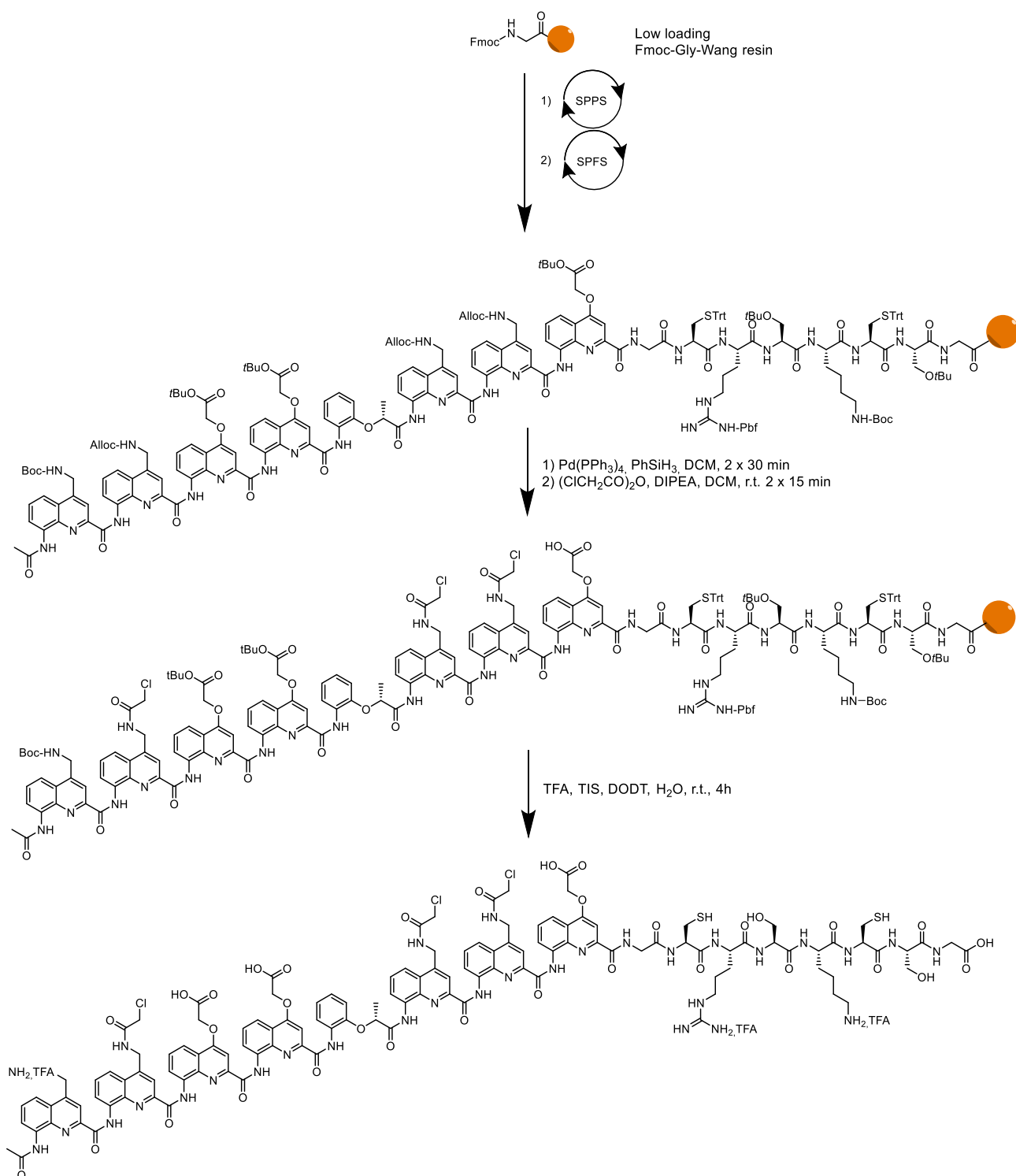


Figure S47 - General synthetic scheme exemplarily shown of linear Foldamer-peptide-hybrid 8 on solid support.

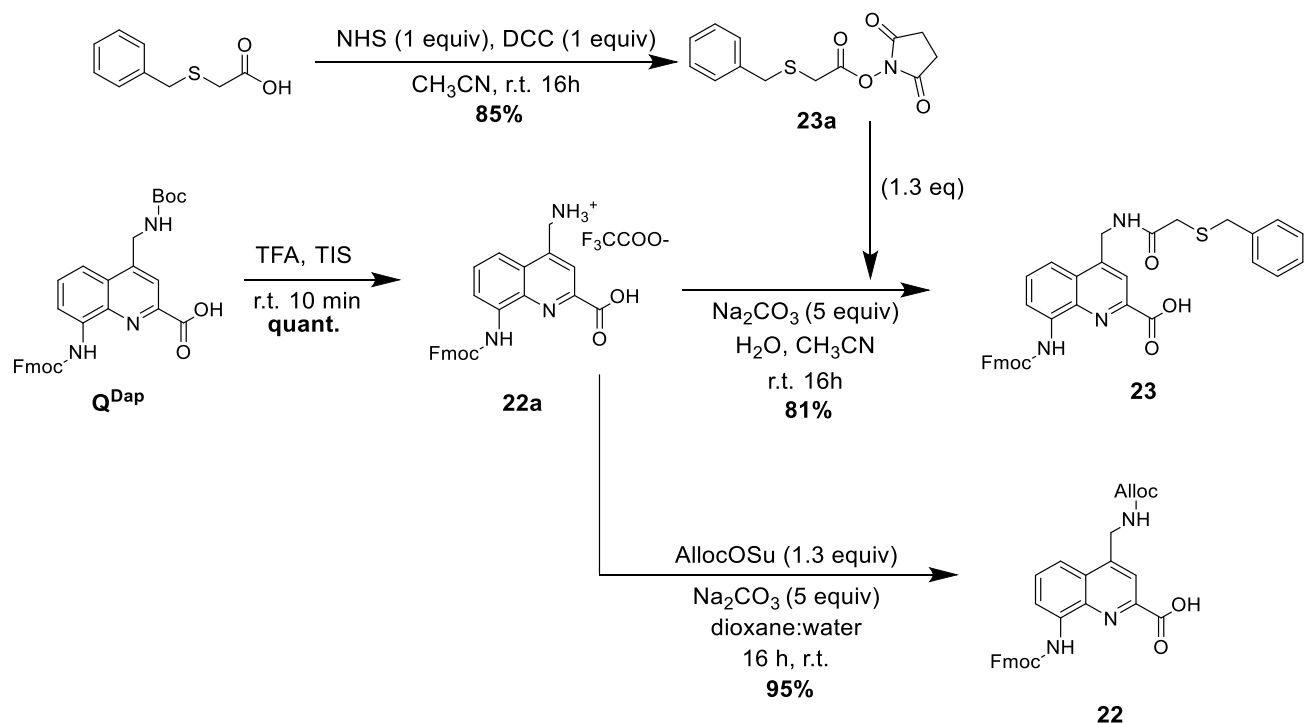


Figure S48 - Synthetic routes for the monomer Fmoc-Q(Dap-Alloc)-OH (22**) and Fmoc-Q(SBn)-OH (**23**)**

Circular dichroism (CD) spectra

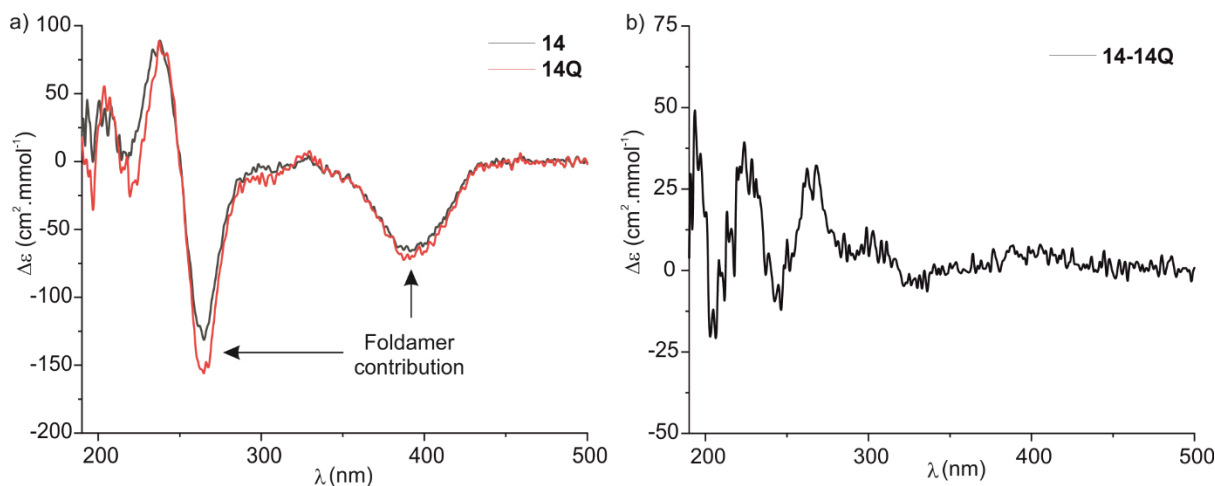


Figure S49 – CD spectrum from **14 and **14Q**.** a) Individual CD spectra for compound **14** (linear) and **14Q** (cyclic) and CD spectra obtained after subtracting the individual spectra of **14-14Q**.

11.2. Material and Methods

RP-HPLC analyses

Analytical RP-HPLC analyses, were performed on an Ultimate 3000 RP-HPLC System (ThermoFisher Scientific). For analytical analysis, a Nucleodur C18 Gravity column (4 x 100 mm, 5 μ m, Macherey-

Nagel) was used at a flow rate of 1 ml/min. Semi-preparative purification was performed on a Waters system equipped with a 2545 Quaternary Gradient Module with automated fraction collector system on a Nucleodur C18 Htec 5 μ m 125/21 column at a flow rate of 25 ml/min. When using acidic conditions 0.1 % TFA was added to the aqueous mobile phase (referred to as mobile phase A) and to acetonitrile (referred to as mobile phase B). The column eluent was monitored by UV detection at 214, 254, and 300 nm with a diode array detector.

For the quantification of the macrocyclization reaction, a solution of internal standard **21** (0.70 – 0.77 mM, 0.1 % TFA in H₂O/CH₃CN (90:10, v/v)) and a foldamer solution (1.5 – 0.5 mM, 0.1 % TFA in H₂O/CH₃CN (90:10, v/v)) was prepared and the concentration of each solution was determined by measuring the UV absorbance at 375 nm with the NanoDrop UV-spectrometer and a 1 cm cuvette. Prior to RP-HPLC analysis, both solutions were mixed in a 1:1 ratio. The peak areas of standard and analysis compounds were determined separately by integration and the correction factor (KF) was calculated from the purified non-cyclic foldamer-peptide hybrid compound. Identical analysis and re-processing were carried out after the macrocyclization step. The area of the macrocycle was determined by integration and the % of macrocyclization conversion was calculated via the previously determined KF value.

$$KF = \frac{F_A * C_{IS}}{F_{IS} * C_I}$$

C_{IS} = Concentration of the internal standard (IS)

C_I = Concentration of the analyte (A)

F_{IS} = Area of the IS

F_A = Area of A

If not otherwise specified following RP-HPLC profiles were recorded by using a gradient from 10 to 100 % CH₃CN (0.1% TFA) at 50°C. The concentrations of internal standards **21** and analytes were determined by UV-VIS spectroscopy before RP-HPLC analysis.

LCMS analyses

LCMS spectra were recorded on a Bruker microTOF II in either positive or negative ionization mode. The instrument was calibrated in positive and negative mode by direct infusion of a calibration solution (Agilent Technologies ESI-L Low Concentration Tuning Mix). The HPLC line was an Ultimate 3000 RP-HPLC System (ThermoFisher Scientific) equipped with a Nucleodur C18 Gravity column (2 x

50 mm, 1.8 μm , Macherey-Nagel) at a flow rate of 0.33 ml/min. 0.1 % formic acid was added to the aqueous mobile phase (solvent A) and to acetonitrile (solvent B). The column eluent was monitored by UV detection at 214, 254, and 300 nm with a diode array detector.

NMR analyses

^1H -NMR spectra were recorded on Avance III HD 400 MHz Bruker BioSpin and Avance III HD 500 MHz Bruker BioSpin spectrometers. All chemical shifts (δ) are reported in ppm and calibrated against residual solvent signals of DMSO- d_6 (δ 2.50 ppm) and CDCl_3 (δ 7.16 ppm). In the case of ^1H -NMR spectra recorded in $\text{H}_2\text{O}/\text{CH}_3\text{CN}$ or aqueous salt buffered systems, 3-(trimethylsilyl)propionic-2,2,3,3- d_4 acid sodium salt (TMSP) was added to the medium and calibrated against δ 0.00 ppm. Coupling constants (J) are reported in Hz. Signal multiplicities were abbreviated as *s*, singlet; *d*, doublet; *t*, triplet; *q*, quartet, and *m*, multiplet.

Molecular modeling

Models were simulated by using Maestro version 11.5 (Schrödinger Inc.). Energy minimized structures were obtained using MacroModel energy minimization with the following parameters: force field: MMFFs; Solvent: Water; Electrostatic treatment: Constant dielectric; Dielectric constant: 1.0; Charges from: Force field; Cutoff: Extended; Van der Waals: 8.0; Electrostatic: 20.0; H-bond: 4.0; Mini Method: TNCG; Maximum iterations: 2500; converge on: Gradient; Convergence threshold: 0.05. No other extended options.

As a starting point, the coordinates of the crystal structure of a previously described peptide-foldamer hybrid macrocycle (CCDC entry # 2010131) were imported. From the imported structure, the peptide was deleted and the helical foldamer part was modified to match the sequence included in the molecules synthesized in this study (*i.e.* DEG- or Ac-QQQBQQQ-OH). The C-terminal peptide was built on the foldamer as a growing alanine chain with cysteine residues at positions consistent with the sequences from the syntheses. Other amino acids than alanine and cysteine were not used. The initial non cyclic model was energy minimized. Acetamidomethyl-containing side chains were introduced at positions of interest on the foldamer helix. The cysteine thiol and acetamide were then joined by deleting the sulfide hydrogen and one acetyl hydrogen atom and replacing them by a sulfur-carbon single bond, thus creating a macrocycle. The initial length of this bond may be very long and can eventually be somewhat reduced by adjusting bond rotations in the peptide chain prior to creating the bond. Energy minimization was started again leading to a quick adjustment of the bond length and translating into conformational changes of the peptide and possibly of the helix. Observation of unfavorable conformational patterns in the energy minimized structure, and in

particular, even slight distortions of the foldamer conformation were interpreted as strain that would make the spontaneous formation of this cycle unfavorable. The process was repeated, placing the cysteine residue at different positions in the peptide sequence and the acetamidomethyl group on different quinoline rings of the foldamer. When a cysteine residue could cyclize without creating strain with different side chains, the nearest reaction site was considered to be favored. These iterations were repeated for bi-, tri- and tetra-cycles. The xyz coordinates of representative multicycles are provided as an extended data set excel file.

CD analysis

All CD curves were recorded on a Jasco J-810 spectrometer with 10 mm quartz cuvette. Following parameters were used: Wavelength range from 650 to 180 nm. Scan speed: 50 nm/min, accumulation: 2, response time: 1.0 s, bandwidth: 2, temperature: 25 °C, sensitivity: standard, data pitch: 1 nm, nitrogen gas flow rate: 500L/h. The sample solution was prepared in degassed ultrapure water/acetonitrile solvent mixture 90:10 (v/v). $[\theta]$ values were obtained by using the formula: $\Delta\epsilon = m^\circ / (C \cdot l \cdot 32980)$; $\Delta\epsilon = \text{cm}^2 \cdot \text{mmol}^{-1}$, $m^\circ = \text{CD value in milli degrees}$, $l = \text{cuvette pathlength in cm}$, $C = \text{sample concentration in mol/L}$.

Chemical Synthesis

General

Fmoc-Q^{Asp(OtBu)}-OH, Fmoc-Q^{Dap(Boc)}-OH and Fmoc-B^{Rme}-OH monomers were prepared by following the reported synthetic protocols.¹ If not otherwise mentioned, chemical reagents were purchased from Sigma-Aldrich, and solvents from Fisher Scientific and used without further purification. Anhydrous tetrahydrofuran (THF) and anhydrous dichloromethane (DCM) were obtained from MBRAUN SPS-800 solvent purification system. Anhydrous chloroform (CHCl₃) and N,N-diisopropylethylamine (DIPEA) were distilled over CaH₂ prior to use. Exclusively ultrapure water was used. DMF and NMP (peptide grade) were purchased from Carlo Erba. Rink amide MBHA, Cl-MPA ProTide®, and low-loading preloaded Fmoc-Gly-Wang resins were purchased from CEM. Fmoc-Gly-SASRIN resin was purchased from Novabiochem. Fmoc-N-protected amino acids, benzotriazol-1-yl-oxytripyrrolidinophosphonium hexafluorophosphate (PyBOP), benzotriazol-1-yl-oxytris(dimethylamino)-phosphonium hexafluorophosphate (BOP) and 2-(1H-Benzotriazol-1-yl)-1,1,3,3-tetramethyl-uronium-hexafluorophosphate (HBTU) were purchased from IRIS Biotech. 2-(benzylthio)acetic acid was purchased from ABCR. Silica column chromatography purifications were

performed on silica gel (230-400 mesh, 40-63 μm , Merck) and thin-layer chromatography was performed on silica gel 60-F254 plates (Merck).

General protocol for SPPS

The peptide segments were assembled by using a Liberty Blue CEM[®] synthesizer at a minimum scale of 50 μmol . Fmoc deprotection was performed twice with 20% piperidine in DMF at 75°C (1 \times 30 sec. and 1 \times 180 sec.). The coupling cycles of the peptide segments in sequences **1-14** contained two coupling steps under microwave irradiation at 50°C for 10 min with N-Fmoc- α -AA-OH (6 equiv. relative to the resin loading), PyBOP (6 equiv.), and DIPEA (12 equiv.) in DMF. In the case of the peptide segments present in sequences **15, 16, 17, 20** and **21**, the coupling step were performed once at RT for 15 min with N-Fmoc- α -amino acid (10 equiv. relative to the resin loading), PyBOP (10 equiv.), and DIPEA (20 equiv.) in DMF. After Fmoc deprotection step, the resin was washed with DMF (2 \times 2 ml) step and following the coupling step, one time with DMF (3 ml). When ProTide[®] resin was used, due to its high swelling property, after Fmoc deprotection the resin was extensively washed with DMF (4 \times 4 ml) and following the coupling step one time with 4 ml DMF.

General protocol for SPFS

The microwave-assisted solid-phase synthesis (SPS) of foldamer-peptide hybrids was carried out on a Discover-Bio CEM[®] microwave oven in an open vessel mode. The temperature of the reaction mixture within the reactor vessel was monitored with an optical fiber probe.

Solid-phase foldamer synthesis (SPFS) for compounds **1-14** and **16-19**.

SPFS for compounds **1-14, 16-19** was undertaken according to reported protocols:

✓ Fmoc Deprotection. The resin was suspended at room temperature in a solution of 20 % piperidine in DMF for 1 \times 3 min and 1 \times 7 min with one DMF washing in between the two cycles. The resin was next washed once with DMF (3 mL) and with dry THF (3 \times 3 mL) prior to perform the in situ coupling.

✓ Iterative in situ coupling of Fmoc-Q-OH on resin-bound peptide. To the pre-swollen resin in dry THF (1 ml) was added 2,4,6-Collidine (9.0 equiv. relative to the resin loading). Concurrently, the Fmoc-Q-OH was suspended in 1.25 ml anhydrous CHCl_3 together with triphenylphosphine (8 equiv). Trichloroacetonitrile (TCAN) was quickly added and the reaction mixture was vigorously mixed before to be added to the suspended resin within 60 sec. The reaction vessel was then placed under microwave irradiation (25 W, ramp to 50°C over 5 min, then hold at 50°C for 15 min). The resin was filtered off and washed with anhydrous THF (2 \times 3 mL). The coupling step was repeated once. The resin was then filtered off and washed with THF (3 \times 3 mL) and DMF (2 \times 3 mL).

Solid-phase foldamer synthesis (SPFS) of **F15** and **F20**

The SPFS of foldamer fragment of **15** (**F10**) and **20** (**F20**) was carried out on a Discover-Bio CEM® microwave oven in open vessel mode as previously described² on Fmoc-Gly-SASRIN resin by using the in situ activation procedure (see above) on a 200 μmol scale.

Fragment condensation to assemble hybrid 15 and 20 on solid support (exemplified with compound 15)

F15 was next coupled via a fragment condensation approach on the resin-bound peptide **P15** on a 50 μmol scale. To remove any remaining moisture, **F15** was lyophilized prior to coupling. **F15** (50 mg, 47 μmol, 0.94 eq.) was then dissolved in dry NMP (0.4 mL) and dry THF (1.0 mL) together with DIPEA (35 μL, 0.2 mmol, 4 eq.) and BOP (44 mg, 100 μmol, 2 eq.). After pre-activation for 3 min, the coupling solution was added to the resin-bound H-Phe-peptide **P10** under N₂ atmosphere. The mixture was stirred for 24 h at r.t. by monitoring the progress of the reaction via HPLC analysis. The resin solution was filtered off and washed with DMF (3 x 3 mL). To facilitate HPLC purification, remaining unreacted resin-bound H-Phe-peptide **P10** was acetylated (Method 3.2.5).

General protocol for N-terminal acetylation

Before performing the N-terminal acetylation step on the resin-bound NH₂-oligomer, the resin was transferred to a 5 ml syringe equipped with a filter and washed with DCM (3 x 3 ml). The resin was next treated with a solution of acetic anhydride in DCM (50:50, v/v) for 16 h at RT. The resin was then filtered off and washed with DCM (3 x 3 ml).

General protocol for Alloc deprotection

The resin was incubated with a solution of Pd(PPh₃)₄ (0.1 equiv. relative to the number of Alloc protecting group), phenylsilane (20 equiv.), and dry DCM (1.5 ml) for 30 min at RT. This deprotection step was repeated once without any washing in between. The resin was then filtered off and washed with DCM (3 x 3 ml).

On resin Q^{Dap} side-chain chloroacetylation, resin cleavage and purification

The chloroacetylation step, resin cleavage and purification of crude foldamer-peptide-hybrids were carried out by following the reported procedures.²

Monomer syntheses

Compound 22a: Fmoc-Q(Dap(Boc))-OH was prepared by established protocol.^{1a} It (0.27 mol, 2 g) was dissolved in 60 ml TFA together with 600 μl TIS and stirred at RT for 10 min. The solvent was narrowed down to 5 ml TFA by rotary evaporation and the solution was next precipitated in 120 ml cold diethylether. The suspension was centrifuged and the supernatant discarded. Compound **22a** was obtained as a colorless powder in quantitative yield and used without further purification. ¹H NMR (500 MHz, DMSO-d₆) δ 13.77 (s, 1H), 10.51 (s, 1H), 8.58 (s, 3H), 8.35 (s, 1H), 7.94 (dt, J = 7.6,

0.9 Hz, 2H), 7.85 (dd, $J = 8.5, 1.3$ Hz, 1H), 7.78 (m, 3H), 7.44 (tt, $J = 7.5, 0.9$ Hz, 2H), 7.37 (td, $J = 7.5, 1.2$ Hz, 2H), 4.65 (d, $J = 6.8$ Hz, 2H), 4.46 (t, $J = 6.7$ Hz, 1H). ^{13}C NMR (126 MHz, DMSO) δ 165.24, 153.49, 144.85, 143.69, 142.51, 140.84, 136.51, 136.37, 130.11, 127.81, 127.22, 126.91, 125.12, 120.28, 119.17, 116.75, 116.52, 66.45, 46.59, 38.75. HRMS (ESI⁺) m/z calcd for $[\text{M}+1\text{H}]^{+1}$ $\text{C}_{26}\text{H}_{21}\text{N}_3\text{O}_4$ 440.1605 found 440.1438.

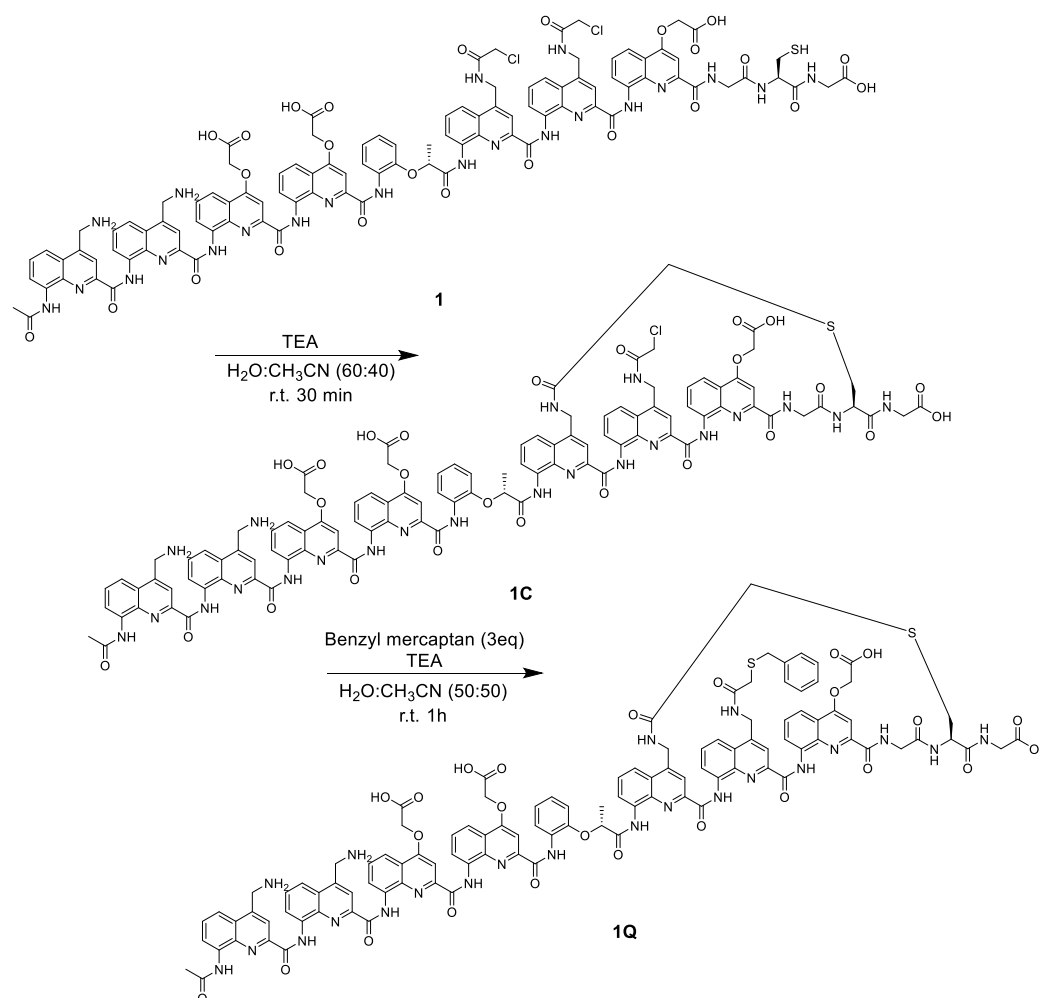
Compound 22: Compound **22a** (0.27 mmol) was dissolved in 54 ml dioxane and Na_2CO_3 (18 mmol, 1.9 g, 5 equiv.) was added together with 18 ml water to reach a concentration of 50 mM. *N*-(Allyloxycarbonyloxy)succinimide (4.7 mmol, 720 μl) was added dropwise to the reaction mixture. The reaction mixture was stirred at RT for 16h and acidified afterward with an aqueous solution of 5% HCl. The mixture was extracted with DCM (1 x 40ml, 2 x 20ml), the organic layers were combined, dried over MgSO_4 , filtered through a cotton plug and evaporated to dryness. The remaining oily liquid was co-evaporated with toluene (3 x 5 ml) and further dried under high vacuum overnight. Compound **22** was obtained in 95 % yield (1.8 g) as a light yellow solid and used without further purification. ^1H NMR (500 MHz, DMSO- d_6) δ 13.63 (s, 1H), 10.47 (s, 1H), 8.37 (s, 1H), 8.11 (d, $J = 6.3$ Hz, 2H), 7.93 (dt, $J = 7.6, 0.9$ Hz, 2H), 7.87 – 7.82 (m, 1H), 7.78 (dd, $J = 7.5, 1.0$ Hz, 2H), 7.70 (t, $J = 8.2$ Hz, 1H), 7.44 (tt, $J = 7.5, 0.8$ Hz, 2H), 7.36 (td, $J = 7.4, 1.2$ Hz, 2H), 5.95 (ddt, $J = 17.2, 10.5, 5.3$ Hz, 1H), 5.33 (dq, $J = 17.2, 1.7$ Hz, 1H), 5.21 (dq, $J = 10.4, 1.5$ Hz, 1H), 4.78 (d, $J = 6.1$ Hz, 2H), 4.62 (d, $J = 6.9$ Hz, 2H), 4.55 (dt, $J = 5.3, 1.6$ Hz, 2H), 4.45 (t, $J = 6.8$ Hz, 1H). ^{13}C NMR (126 MHz, DMSO) δ 165.24, 153.49, 144.85, 143.69, 142.51, 140.84, 136.51, 136.37, 130.11, 127.81, 127.22, 126.91, 125.12, 120.28, 119.17, 116.75, 116.52, 66.45, 46.59, 41.14. HRMS (ESI⁻) m/z calcd for $[\text{M}-1\text{H}]^{-1}$ $\text{C}_{30}\text{H}_{25}\text{N}_3\text{O}_6$ 522.1671 found 522.1995.

Compound 23a: For the synthesis of compound **23a**, 2-(benzylthio)acetic acid (700 mg, 3.8 mmol) and *N*-hydroxysuccinimide (442 mg, 3.8 mmol) were dissolved in acetonitrile (17 ml) and a solution of dicyclohexyl-carbodiimide (783 mg, 3.8 mmol) in acetonitrile (7 ml) was added within 5 minutes. After stirring at RT for 16 h under nitrogen atmosphere, solid dicyclohexylurea was removed, by filtration and the supernatant was evaporated to dryness. The compound was purified by silica gel flash column chromatography with 25% EtOAc in cyclohexane and obtained as a colorless solid after evaporation to dryness (900 mg, 85%). ^1H NMR (400 MHz, CDCl_3) δ 7.39 – 7.31 (m, 4H), 7.30 – 7.27 (m, 1H), 3.92 (s, 2H), 3.30 (s, 2H), 2.88 (s, 4H).

Compound 23: Compound **23** was synthesized by slowly adding compound **23a** (348 mg, 1.2 mmol) dissolved in 10 ml acetonitrile to a solution of **23** (556 mg, 1 mmol) together with Na_2CO_3 (530 mg, 5 mmol) in water (10 ml). After stirring at RT for 16 h the reaction was acidified with an aqueous solution of 5% HCl and the target compound **23** was recovered after filtration through a glass filter as a light yellow powder (490 mg, 81%). ^1H NMR (500 MHz, DMSO- d_6) δ 13.61 (s, 1H), 10.49 (s, 1H),

8.82 (t, $J = 6.0$ Hz, 1H), 8.37 (s, 1H), 8.17 (s, 1H), 7.93 (dt, $J = 7.6, 1.0$ Hz, 2H), 7.87 (dd, $J = 8.4, 1.2$ Hz, 1H), 7.78 (dd, $J = 7.5, 1.0$ Hz, 2H), 7.72 (t, $J = 8.2$ Hz, 1H), 7.44 (tt, $J = 7.5, 0.8$ Hz, 2H), 7.36 (td, $J = 7.4, 1.2$ Hz, 2H), 7.31 (d, $J = 4.2$ Hz, 5H), 4.86 (d, $J = 5.8$ Hz, 2H), 4.63 (d, $J = 6.9$ Hz, 2H), 4.46 (t, $J = 6.8$ Hz, 1H), 3.82 (s, 2H), 3.18 (s, 2H). ^{13}C NMR (126 MHz, DMSO- d_6) δ 169.82, 165.91, 153.98, 148.09, 145.49, 144.19, 141.30, 138.36, 137.08, 136.75, 130.08, 129.47, 128.84, 128.27, 127.84, 127.71, 127.40, 125.63, 120.74, 118.71, 117.20, 116.60, 66.91, 47.07, 40.13, 36.10, 34.37. HRMS (ESI $^+$) m/z calcd for $[\text{M}+\text{H}]^+$ $\text{C}_{35}\text{H}_{30}\text{N}_3\text{O}_5\text{S}$ 604.1901 found 604.1876.

Hybrid sequence synthesis and macrocyclizations reactions

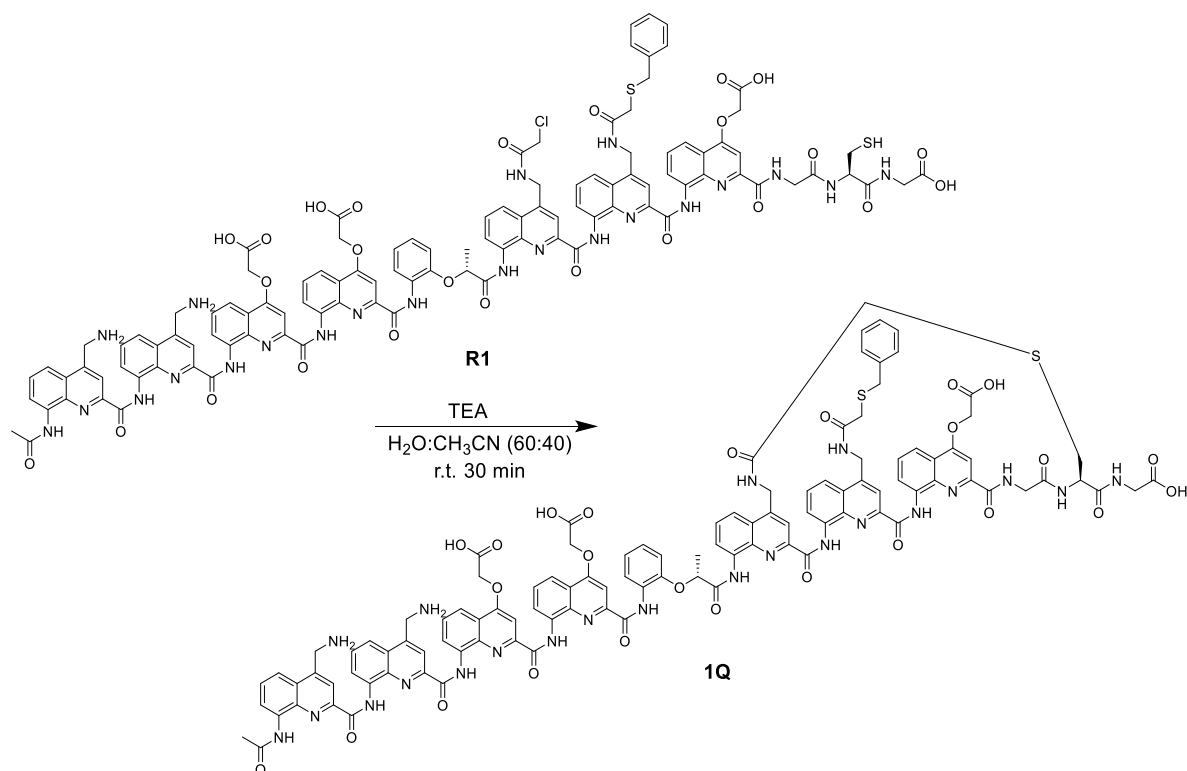


Compound 1: Foldamer-peptide **1** was built on a 25 μmol scale using Fmoc-Gly-preloaded Wang resin (0.33 mmol/g). After terminal acetylation, the Alloc protecting groups were removed, and directly followed by the chloroacetylation step. The resin was cleaved with TFA/TIS/ H_2O /EDT (92.5:2.5:2.5:2.5, v/v/v/v) and the crude product (30 mg, 51%, Figure S2a) was purified by semi-preparative RP-HPLC (gradient: from 25% to 40% solvent B over 15 minutes at 25°C) to give **1** in 14% yield (Figure S2 – RP-HPLC analysis of the synthesis, purification and cyclization of sequence 1. Overlay of RP-HPLC profiles measured from each synthetic step of compound 1Q synthesized from

compound **1** measured with standard HPLC conditions. Compound **1** after SPS/SPFS as a crude (a), after purification co-injected with internal standard **21(b)**, after cyclization and co-injected with **21 (1C, c)** and after benzyl mercaptan installation (**1Q, d**). Chromatograms a), c) and d) obtained after the reaction without prior purification. a) and d) recorded at 300 nm, b) and c) at 375 nm. HRMS (ESI⁺) *m/z* calcd (most abundant mass peak) for C₁₀₂H₈₈Cl₂N₂₂O₂₅S [M+2H]²⁺ 1062.2692 found 1062.2833

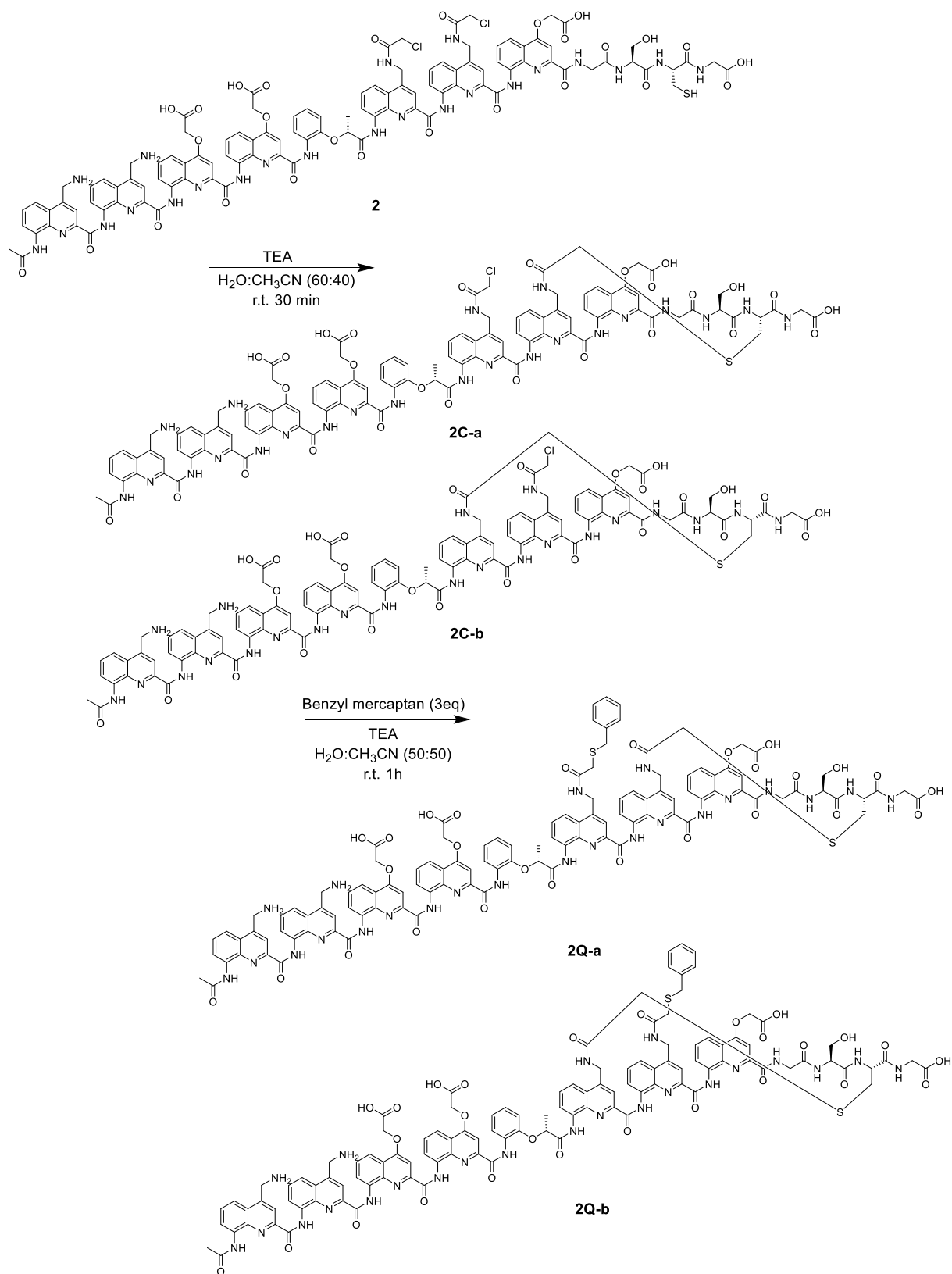
Compound 1C: After lyophilization, compound **1** (8 mg) was dissolved in a 1:1 mixture of acetonitrile in water (38 ml total) to reach a 0.1 mM concentration and the solvent was freed from oxygen. Freshly distilled TEA (1.32 ml, 0.25 mM) was added and the reaction was kept under nitrogen atmosphere without stirring. The progression of the macrocyclization was monitored by RP-HPLC. After 30 min, the reaction mixture was concentrated under reduced pressure and the remaining solvent lyophilized. The obtained crude product was used in the subsequent reaction without further purification (Figure S2c). C₁₀₂H₈₆ClN₂₂O₂₅S [M+H]⁺ 2086.5564 found 2086.5457

Compound 1Q: Compound **1C** (7 mg) was dissolved in a 1:1 mixture of acetonitrile in water (0.1 ml total) to reach a 50 mM concentration and TEA (2.8 μl, 6 equiv.) was added. While stirring, benzyl mercaptan (1.2 μl, 3 equiv.) was added and the reaction mixture was stirred at RT for 60 minutes. Solvents were removed, by lyophilization and the colorless product **1Q** (1.6 mg, Figure S2d) was obtained after semi-preparative RP-RP-HPLC purification using a gradient from 15% to 30% solvent D. ¹H NMR (500 MHz, CD₃CN) δ 11.67 (s, 1H), 11.10 (s, 1H), 10.88 (s, 1H), 10.64 (s, 1H), 10.44 (s, 1H), 9.85 (s, 1H), 9.24 (d, *J* = 6.9 Hz, 1H), 9.06 (s, 1H), 8.67 (d, *J* = 9.9 Hz, 2H), 8.56 (d, *J* = 7.0 Hz, 1H), 8.36 (q, *J* = 8.1, 7.2 Hz, 2H), 8.03 (d, *J* = 9.2 Hz, 1H), 7.98 (s, 1H), 7.92 (d, *J* = 8.9 Hz, 2H), 7.87 (d, *J* = 6.8 Hz, 2H), 7.76 (t, *J* = 9.2 Hz, 4H), 7.69 (d, *J* = 7.8 Hz, 1H), 7.58 (s, 1H), 7.54 (t, *J* = 6.1 Hz, 2H), 7.49 (t, *J* = 8.8 Hz, 2H), 7.41 (d, *J* = 8.7 Hz, 5H), 7.35 (dd, *J* = 16.5, 7.7 Hz, 6H), 7.26 (dd, *J* = 11.8, 6.8 Hz, 2H), 7.11 (t, *J* = 7.7 Hz, 1H), 7.04 (dd, *J* = 16.8, 7.8 Hz, 2H), 6.97 (d, *J* = 9.0 Hz, 1H), 6.74 (d, *J* = 7.4 Hz, 1H), 6.57 (s, 1H), 6.51 (s, 1H), 6.28 (d, *J* = 12.0 Hz, 2H), 6.08 (d, *J* = 8.4 Hz, 1H), 5.87 (t, *J* = 8.5 Hz, 1H), 5.01 (td, *J* = 18.2, 17.1, 7.8 Hz, 1H), 4.90 – 4.56 (m, 2H), 3.67 – 3.49 (m, 1H), 3.45 – 3.20 (m, 7H), 3.13 (q, *J* = 8.0 Hz, 1H), 1.41 (s, 4H), 1.35 – 1.19 (m, 3H), -0.60 (d, *J* = 6.7 Hz, 3H). HRMS (ESI⁻) *m/z* calcd (most abundant mass peak) for C₁₀₉H₉₁N₂₂O₂₅S₂ [M-H]⁻ 2172.5992 found 2172.6627.



Compound R1: Foldamer-peptide **R1** was on a 25 μmol scale using the low loading Fmoc-Gly-preloaded Wang resin (0.33 mmol/g). After terminal acetylation, the Alloc protecting group was removed, directly followed by chloroacetylation. The resin was cleaved with TFA/TIS/ H_2O /EDT (92.5:2.5:2.5:2.5, v/v/v/v) and the crude product (61 mg, 99%, Figure S3a) was purified by semi-preparative RP-HPLC (gradient: from 30% to 50% solvent B over 15 minutes at 25°C, Figure S4b). HRMS (ESI⁺) m/z calcd (most abundant mass peak) for $\text{C}_{109}\text{H}_{94}\text{ClN}_{22}\text{O}_{25}\text{S}_2$ $[\text{M}+\text{H}]^+$ 2210.5918 found 2210.5231.

Compound 1Q: After lyophilization, compound **R1** (13 mg) was dissolved in a 1:1 mixture of acetonitrile in water (54 ml total) to reach 0.1 mM concentration and the solvent was freed from oxygen. TEA (1.9 ml, 0.25 mM) was added and the reaction was kept under nitrogen atmosphere without stirring. The progression of the macrocyclization was monitored by RP-HPLC. After 20 min, the reaction mixture was concentrated under reduced pressure and the remaining solvent lyophilized. 7.3 mg light yellow product was obtained after purification by semi-preparative RP-HPLC (gradient: from 20% to 80% solvent B over 15 minutes at 25°C, Figure S3d). HRMS (ESI⁺) m/z calcd (most abundant mass peak) for $\text{C}_{109}\text{H}_{94}\text{N}_{22}\text{O}_{25}\text{S}_2$ $[\text{M}+2\text{H}]^{2+}$ 1087.8112 found 1087.8214.

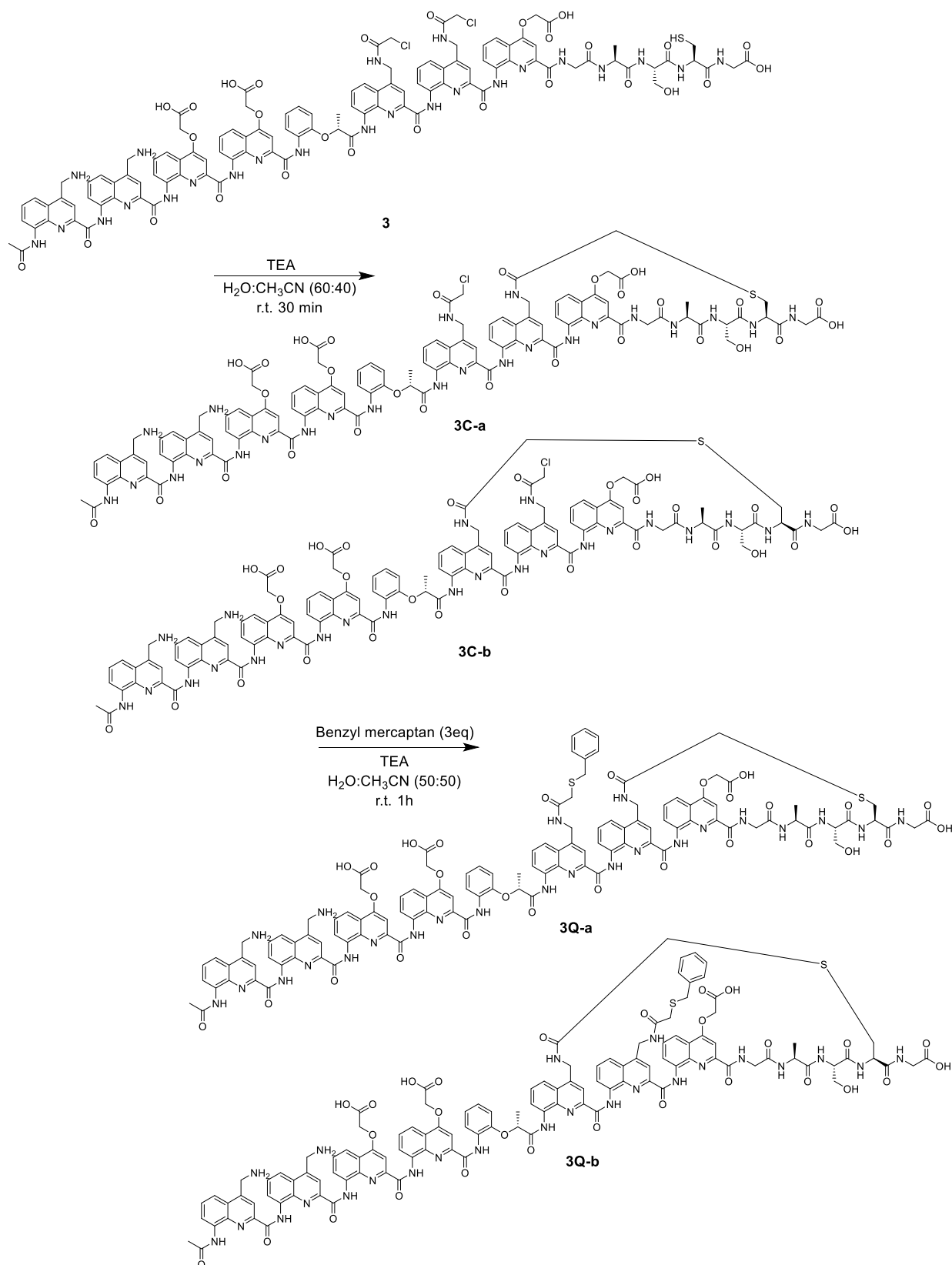


Compound 2: Foldamer-peptide **2** was built on a 25 μ mol scale using a low loading Fmoc-Gly-preloaded Wang resin (0.33 mmol/g). After terminal acetylation, the Alloc protecting group was removed, directly followed by chloroacetylation. The resin was cleaved with TFA/TIS/H₂O/DODT

(92.5:2.5:2.5:2.5, v/v/v/v) and the crude product (50 mg, 82%, see Figure S4a) was purified by semi-preparative RP-HPLC (gradient: from 25% to 40% solvent B over 15 minutes at 25°C, see Figure S4b). HRMS (ESI⁺) *m/z* calcd (most abundant mass peak) for C₁₀₅H₉₂Cl₂N₂₃O₂₇S [M+H]⁺ 2210.5676 found 2210.4959

Compound 2C: After lyophilization, compound **2** (14 mg) was dissolved in a mixture of acetonitrile (25 ml) in water (38 ml) to reach a 0.1 mM concentration and the solvent was freed from oxygen. TEA (2.1 ml, 0.25 mM) was added and the reaction was kept under nitrogen atmosphere without stirring. The progression of the macrocyclization was monitored by RP-HPLC. After 30 min, the reaction mixture was concentrated under reduced pressure and the remaining solvent lyophilized. The obtained crude product was used in the subsequent reaction without further purification (Figure S4c). HRMS (ESI⁺) *m/z* calcd (most abundant mass peak) for C₁₀₅H₉₁ClN₂₃O₂₇S [M+H]⁺ 2173.6137 found 2173.5875

Compound 2Q: Compound **2C** (14 mg) was dissolved in a 1:1 mixture of acetonitrile in water (0.13 ml total) to reach 50 mM concentration and TEA (5 μl, 6 equiv.) was added. While stirring, benzyl mercaptan (2.0 μl, 3 equiv.) was added and the reaction mixture was stirred at RT for 60 minutes. Solvents were removed, by lyophilization and the two conformational isomers were isolated by semi-preparative RP-RP-HPLC with a gradient from 15% to 35% solvent D (see Figure S4e and S4f). HRMS (ESI⁺) *m/z* calcd (most abundant mass peak) for C₁₁₂H₉₈N₂₃O₂₇S₂ [M+H]⁺ 2261.6490 found 2261.7231 for isomer (**2Q-a**) and 2261.7280 for isomer (**2Q-b**).

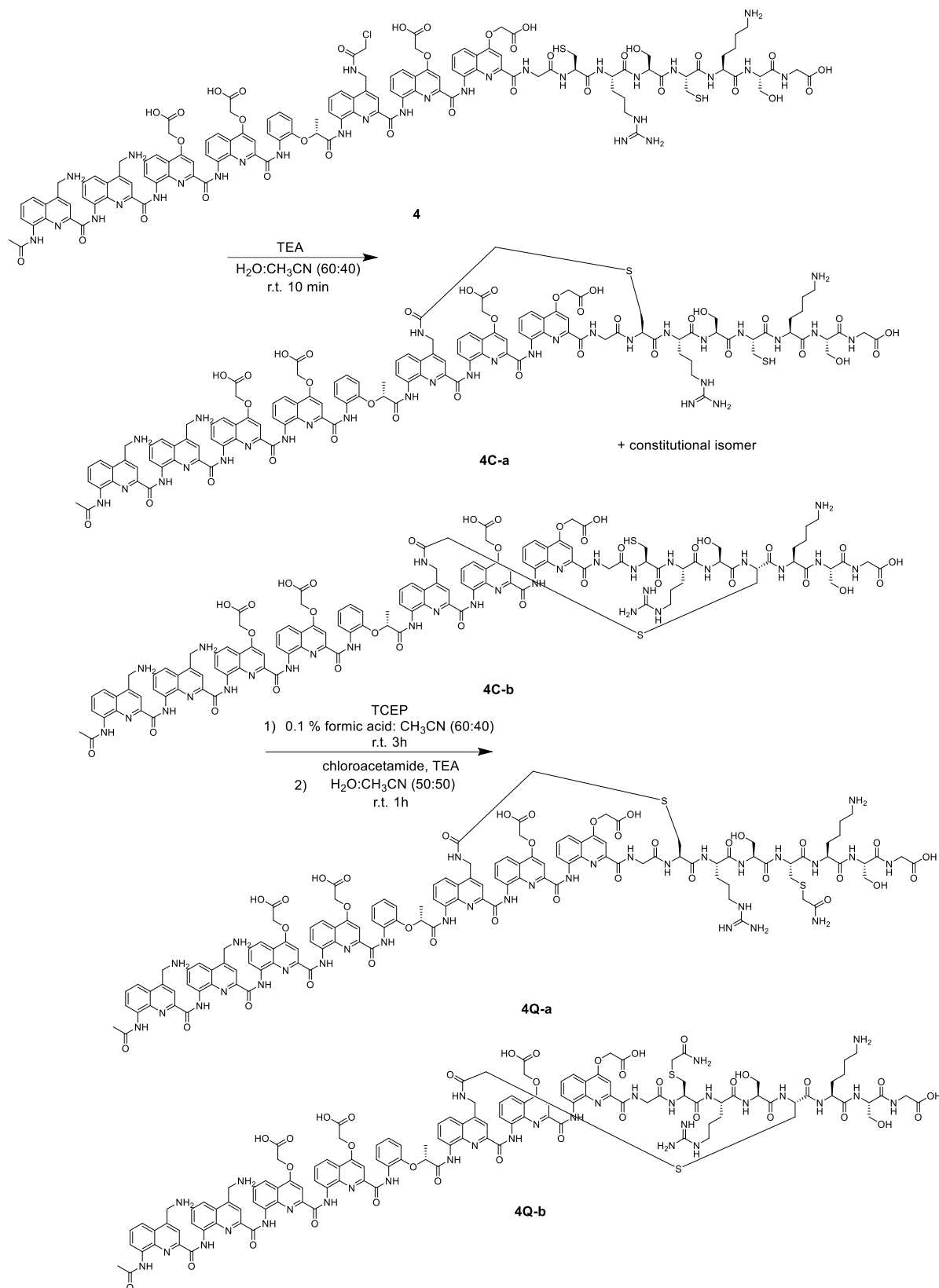


Compound 3: Foldamer-peptide **3** was built on a 25 μ mol scale using a low loading Fmoc-Gly-preloaded Wang resin (0.33 mmol/g). After terminal acetylation, the Alloc protecting group was removed, directly followed by chloroacetylation. The resin was cleaved with TFA/TIS/H₂O/DODT

(92.5:2.5:2.5:2.5, v/v/v/v) and the crude product (52 mg, 85%, Figure S5a) was purified by semi-preparative RP-HPLC (gradient: from 25% to 40% solvent B over 15 minutes at 25°C, Figure S5b). HRMS (ESI⁺) *m/z* calcd (most abundant mass peak) for C₁₀₈H₉₇Cl₂N₂₄O₂₈S [M+H]⁺ 2281.5348 found 2281.6053.

Compound 3C: After lyophilization, compound **3** (13 mg) was dissolved in mixture of acetonitrile (34 ml) in water (22 ml) to reach 0.1 mM concentration and the reaction mixture was freed from oxygen. TEA (1.9 ml, 0.25 mM) was added and the reaction was kept under nitrogen atmosphere without stirring. The progression of the macrocyclization was monitored by RP-HPLC. After 30 min, the reaction mixture was concentrated under reduced pressure and the remaining solvent lyophilized. The obtained crude product was used in the subsequent reaction without further purification (Figure S5c). HRMS (ESI⁺) *m/z* calcd (most abundant mass peak) for C₁₀₈H₉₆ClN₂₄O₂₈S [M+H]⁺ 2244.6490 found 2244.6337.

Compound 3Q: Compound **3C** (14 mg) was dissolved in a 1:1 mixture of acetonitrile in water (0.12 ml total) to reach 50 mM concentration and TEA (5 μl, 6 equiv.) was added. While stirring, benzyl mercaptan (2.0 μl, 3 equiv.) was added and the reaction mixture was stirred at RT for 60 minutes. Solvents were removed, by lyophilization and the two conformational isomers were isolated separately after using semi-preparative RP-RP-HPLC with a gradient from 15% to 35% solvent D (Figure S5e and S5f). HRMS (ESI⁺) *m/z* calcd (most abundant mass peak) for C₁₁₅H₁₀₃N₂₄O₂₈S₂ [M+H]⁺ 2332.6907 found 2332.7634 for isomer (**3Q-a**) and 2332.7661 for isomer (**3Q-b**).

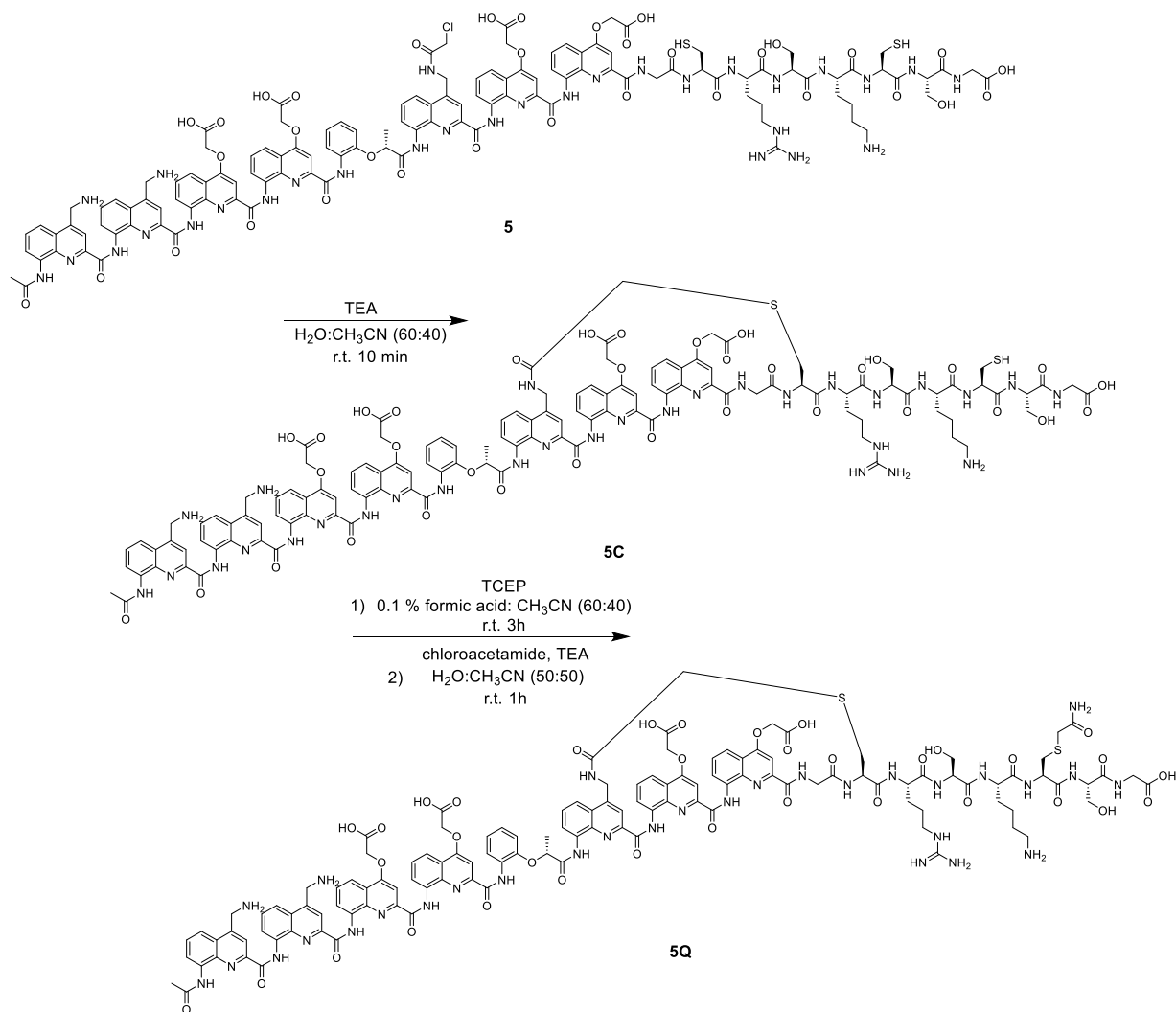


Compound 4: Foldamer-peptide **4** was built on a 25 μmol scale using a Fmoc-Gly-preloaded Wang resin (0.33 mmol/g). After terminal acetylation, the Alloc protecting group was removed, directly followed by chloroacetylation. The resin was cleaved with TFA/TIS/ H_2O /DODT (92.5:2.5:2.5:2.5, v/v/v/v) and the crude product (68 mg, 87%, Figure S6a) was purified by semi-preparative RP-HPLC

(gradient: from 15% to 30% solvent B over 8 minutes at 25°C, Figure S6b) to afford 28 mg of pure compound. HRMS (ESI⁺) *m/z* calcd (most abundant mass peak) for C₁₂₂H₁₂₄ClN₃₀O₃₄S₂ [M+H]⁺ 2652.8055 found 2652.8290

Compound 4C: After lyophilization, compound **4** (12 mg) was dissolved in a mixture of acetonitrile (18 ml) in water (27ml) to reach 0.1 mM concentration and the solvent was freed from oxygen by Freeze-Pump-Thaw. TEA (1.5 ml, 0.25 mM) was added and the reaction was kept under nitrogen atmosphere without stirring. The progression of the macrocyclization was monitored by RP-HPLC. After 60 min, the reaction mixture was concentrated under reduced pressure and the remaining solvent lyophilized. The obtained crude product was used in the subsequent reaction without further purification (Figure S6c). HRMS (ESI⁺) *m/z* calcd (most abundant mass peak) for C₁₂₂H₁₂₃N₃₀O₃₄S₂ [M+H]⁺ 2616.8288 found 2616.8594

Compound 4Q: To reduce inter molecular disulfides, compound **4C** (3.7 mg) was dissolved in a mixture of acetonitrile (0.28 ml) in water (0.42 ml, 0.1% formic acid) to reach a 2 mM concentration and TCEP (141 μl, 10mM, 1 equiv.) was added. The reaction mixture was stirred at RT and the progress of the reaction was monitored by RP-HPLC. The reaction was completed after 3h, chloroacetamide (280 μl, 10 mM, 2 equiv.) was added and the solution was basified with TEA (10 μl). The progression was monitored by RP-HPLC and completed after 6h (Figure S6d and S6e). Solvents were removed, by lyophilization. HRMS (ESI⁺) *m/z* calcd (most abundant mass peak) for C₁₂₄H₁₂₇N₃₁O₃₅S₂ [M+2H]²⁺ 1337.4288 found 1337.4685.

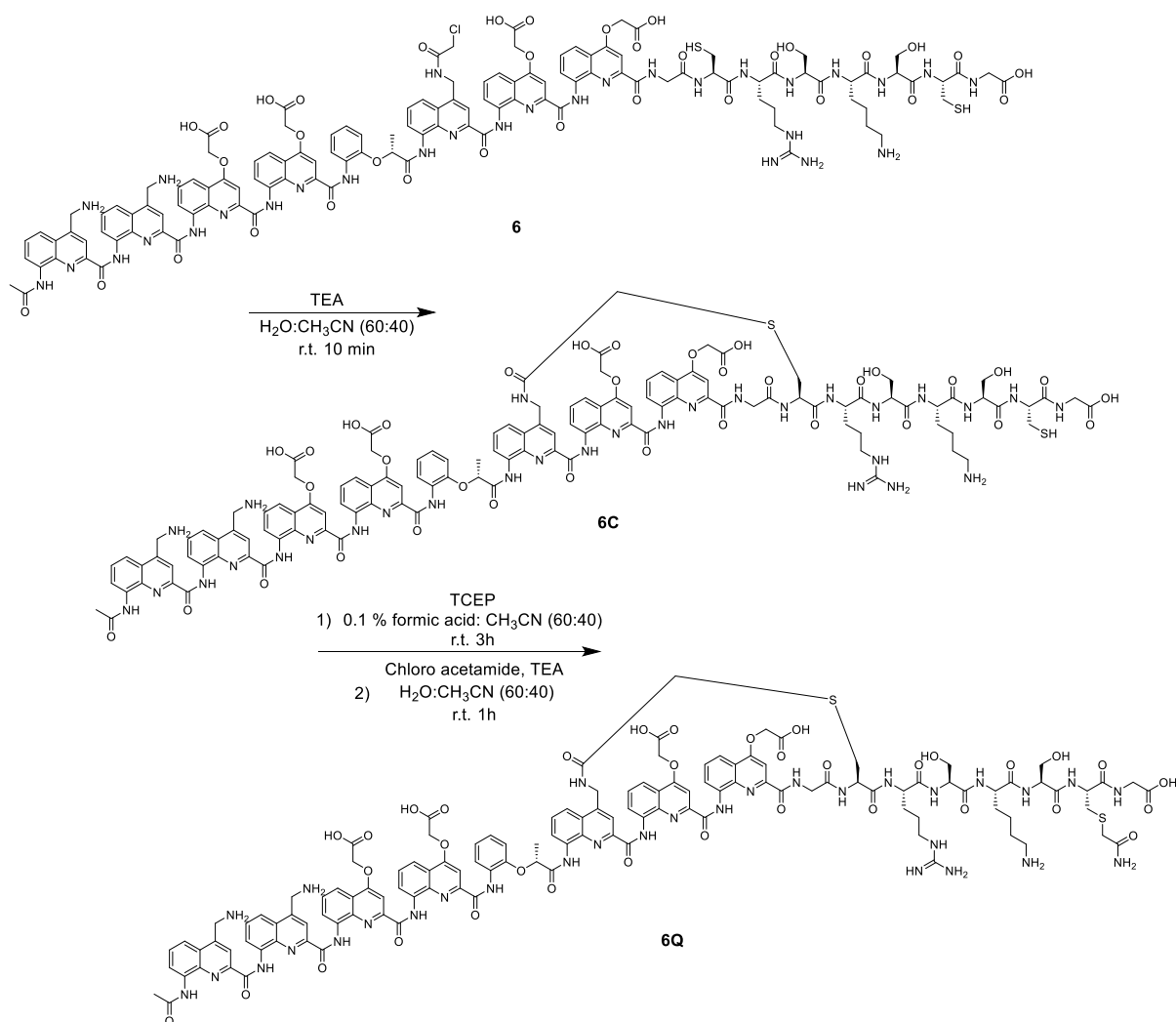


Compound 5: Foldamer-peptide **5** was built on a 25 μmol scale using a low loading Fmoc-Gly-preloaded Wang resin (0.33 mmol/g). After terminal acetylation, the Alloc protecting group was removed, directly followed by chloroacetylation. The resin was cleaved with TFA/TIS/ H_2O /DODT (92.5:2.5:2.5:2.5, v/v/v/v) and the crude product (70 mg, 90%, Figure S7a) was purified by semi-preparative RP-HPLC (gradient: from 15% to 30% solvent B over 8 minutes at 25°C, Figure S7b) to afford 18 mg of pure compound. HRMS (ESI⁺) m/z calcd (most abundant mass peak) for $\text{C}_{122}\text{H}_{124}\text{ClN}_{30}\text{O}_{34}\text{S}_2$ [M+H]⁺ 2652.8055 found 2652.8274.

Compound 5C: After lyophilization, compound **5** (9 mg) was dissolved in a mixture of acetonitrile (14 ml) in water (20 ml) to reach a 0.1 mM concentration and the solvent mixture was freed from oxygen. TEA (1.2 ml, 0.25 mM) was added and the reaction was kept under nitrogen atmosphere without stirring. The progression of the macrocyclization was monitored by RP-HPLC. After 30 min, the reaction mixture was concentrated under reduced pressure and the remaining solvent lyophilized. The obtained crude product was used in the subsequent reaction without further

purification (Figure S7c). HRMS (ESI⁺) *m/z* calcd (most abundant mass peak) for C₁₂₂H₁₂₃N₃₀O₃₄S₂ [M+H]⁺ 2616.8288 found 2616.8458.

Compound 5Q: To reduce inter molecular disulfides, compound **5C** (1.3 mg) was dissolved in a mixture of acetonitrile (0.2 ml) in water (0.5 ml, 0.1% formic acid) to reach a 0.5 mM concentration and TCEP (38 μl, 10mM, 1 equiv.) was added. The reaction mixture was stirred at RT and the progress of the reaction was monitored by RP-HPLC. The reaction was completed after 3h, chloroacetamide (45 μl, 10 mM, 2 eq) was added and the solution was basified with TEA (10 μl). The progression was monitored by RP-HPLC and was finished after 3h. Solvents were removed, by lyophilisation (Figure S7e). HRMS (ESI⁺) *m/z* calcd (most abundant mass peak) for C₁₂₄H₁₂₇N₃₁O₃₅S₂ [M+2H]²⁺ 1337.4288 found 1337.4722.

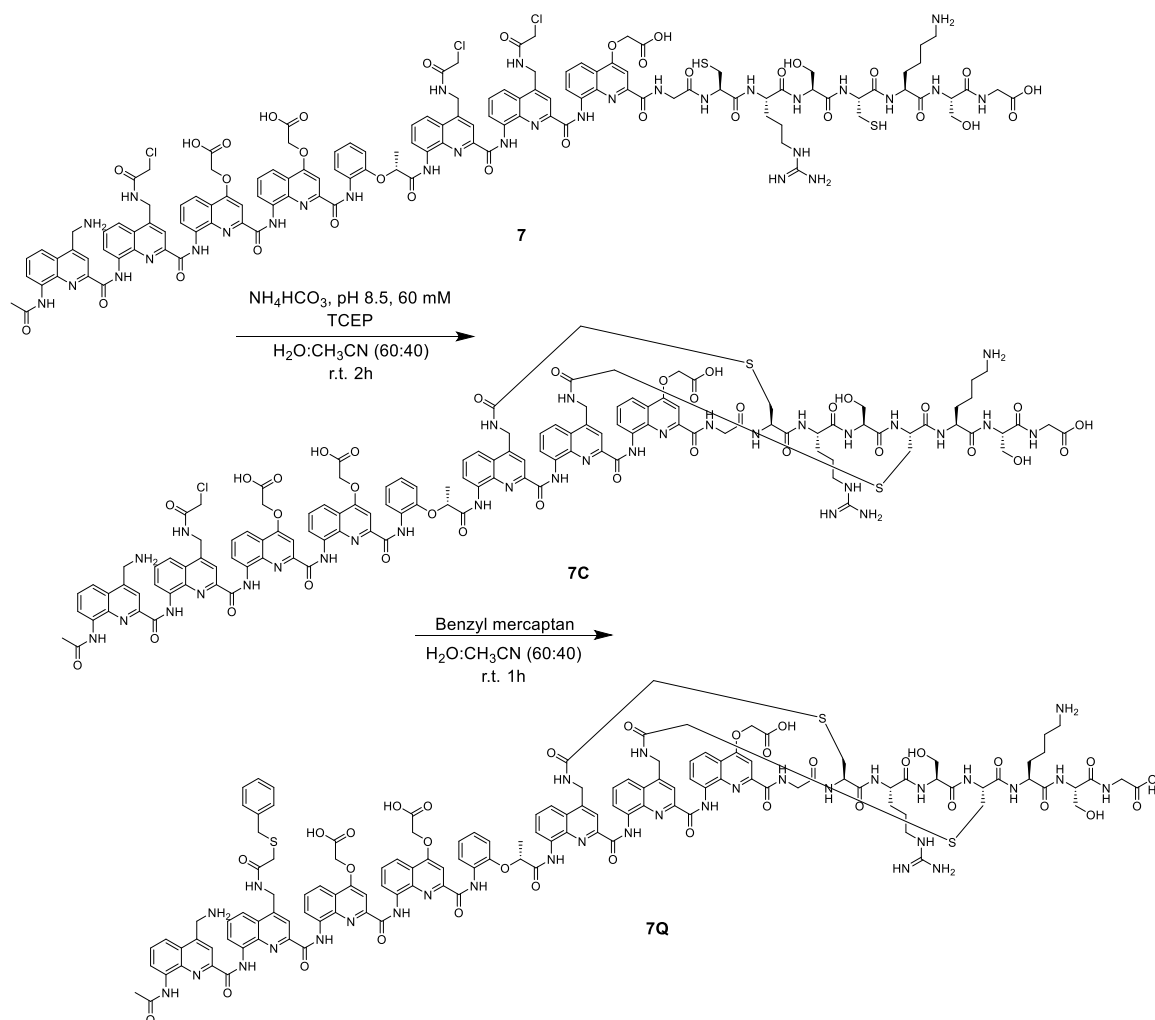


Compound 6: Foldamer-peptide **6** was built on a 25 μmol scale using a low loading Fmoc-Gly-preloaded Wang resin (0.33 mmol/g). After terminal acetylation, the Alloc protecting group was removed, directly followed by chloroacetylation. The resin was cleaved with TFA/TIS/H₂O/DODT

(92.5:2.5:2.5:2.5, v/v/v/v) and the crude product (69 mg, 88%, Figure S8a) was purified by semi-preparative RP-HPLC (gradient: from 15% to 30% solvent B over 8 minutes at 25°C) to afford 21 mg of pure compound (Figure S8b). HRMS (ESI⁺) *m/z* calcd (most abundant mass peak) for C₁₂₂H₁₂₄ClN₃₀O₃₄S₂ [M+H]⁺ 2652.8055 found 2652.8218

Compound 6C: After lyophilization, compound **6** (13.5 mg) was dissolved in a mixture of acetonitrile (21 ml) in water (30 ml) to reach a 0.1 mM concentration and the solvent mixture was freed from oxygen by Freeze-Pump-Thaw. Freshly distilled TEA (1.8 ml, 0.25 mM) was added and the reaction was kept under nitrogen atmosphere without stirring. The progression of the macrocyclization was monitored by RP-HPLC. After 30 min, the reaction mixture was concentrated under reduced pressure and the remaining solvent lyophilized. The obtained crude product was used in the subsequent reaction without further purification (Figure S8c). HRMS (ESI⁺) *m/z* calcd (most abundant mass peak) for C₁₂₂H₁₂₃N₃₀O₃₄S₂ [M+H]⁺ 2616.8288 found 2616.8203.

Compound 6Q: To reduce intermolecular disulfides, compound **6C** (3.2 mg) was dissolved in a mixture of acetonitrile (0.24 ml) in water (0.37 ml, 0.1% formic acid) to reach a 2 mM concentration and TCEP (122 μl, 10mM, 1 equiv.) was added. The reaction mixture was stirred at RT and the progress of the reaction was monitored by RP-HPLC. The reaction was completed after 3h, chloroacetamide (120 μl, 10 mM, 2 eq) was added and the solution was basified with TEA (10 μl). The progression was monitored by RP-HPLC and was completed after 3h. Solvents were removed, by lyophilisation (Figure S8e). HRMS (ESI⁺) *m/z* calcd (most abundant mass peak) for C₁₂₄H₁₂₇N₃₁O₃₅S₂ [M+2H]²⁺ 1337.4288 found 1337.4499.

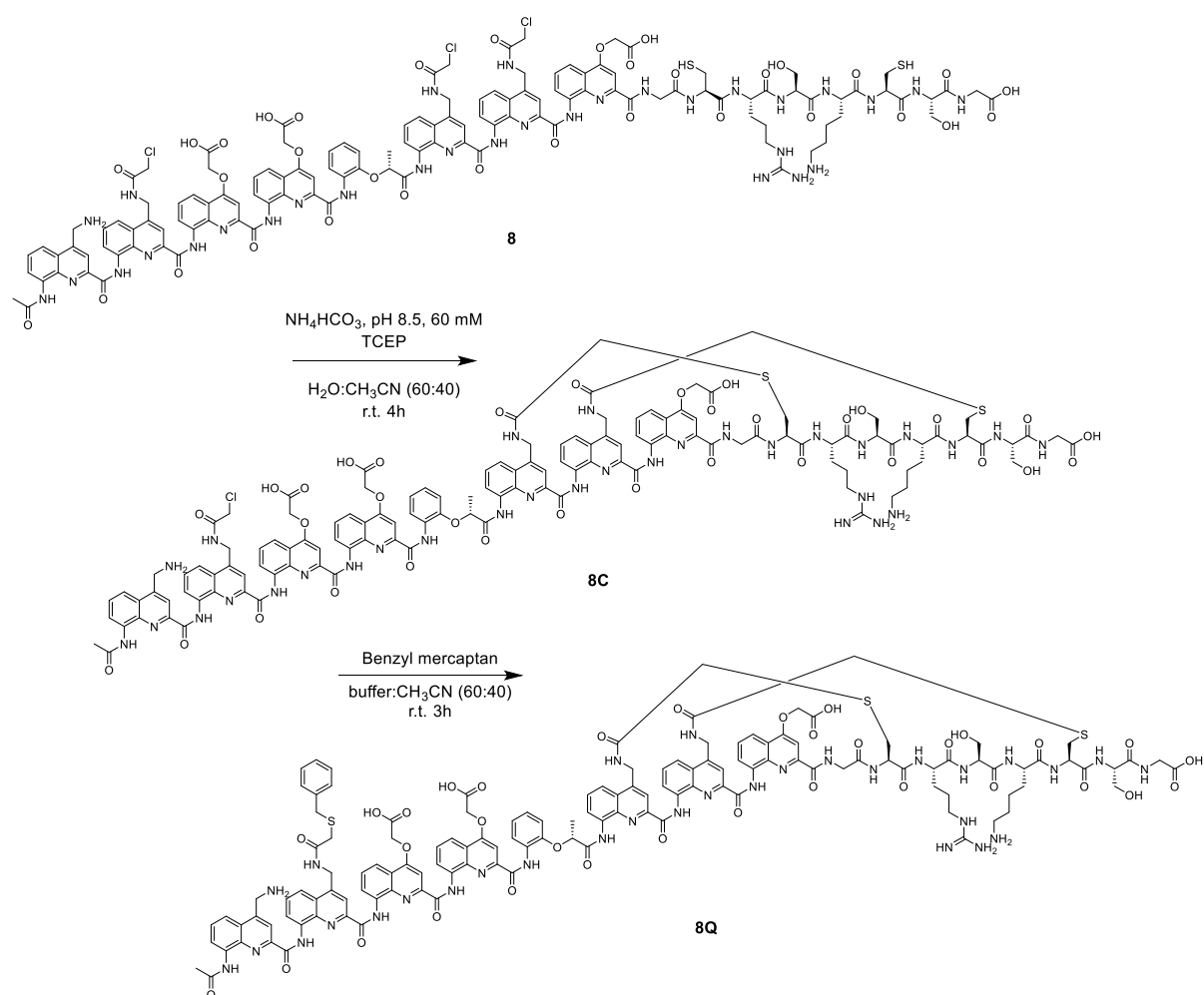


Compound 7: Foldamer-peptide **7** was built on a 25 μmol scale using a low loading Fmoc-Gly-preloaded Wang resin (0.33 mmol/g). After terminal acetylation, the Alloc protecting groups were removed, directly followed by chloroacetylation. The resin was cleaved with TFA/TIS/H₂O/DODT (92.5:2.5:2.5:2.5, v/v/v/v) and the crude product (64 mg, 82%, Figure S9a) was purified by semi-preparative RP-HPLC (gradient: from 25% to 45% solvent B over 8 minutes at 25°C) to afford 6 mg of pure compound (Figure S9b). HRMS (ESI⁺) *m/z* calcd (most abundant mass peak) for C₁₂₅H₁₂₇Cl₃N₃₁O₃₃S₂ [M+H]⁺ 2760.7752 found 2760.7947

Compound 7C: After lyophilization, compound **7** (1 mg) was dissolved in a mixture of acetonitrile (2.4 ml) in water (1.6 ml) to reach a 0.1 mM concentration and TCEP stock solution (4 μl , 10 mM, 1 equiv.) was added. The solvent mixture was freed from oxygen by Freeze-Pump-Thaw. Independently, a solvent mixture of NH₄HCO₃ (2.4 ml, 60 mM, pH 8.5) in acetonitrile (1.6 ml) was prepared and oxygen removed, by Freeze-Pump-Thaw. The Foldamer solution was added via syringe to NH₄HCO₃ solution under N₂ atmosphere. The mixture was quickly stirred and left without stirring for 2 h at RT. The progression of the macrocyclization was monitored by RP-HPLC. After 2 h, the reaction mixture was concentrated under reduced pressure and the remaining solvent lyophilized.

The obtained crude product was used in the subsequent reaction without further purification (Figure S9c). HRMS (ESI⁺) *m/z* calcd (most abundant mass peak) for C₁₂₅H₁₂₆ClN₃₁O₃₃S₂ [M+2H]²⁺ 1344.9144 found 1344.9769.

Compound 7Q: Compound **7C** (1 mg) was dissolved in a 1:1 mixture of NH₄HCO₃ (60 mM, pH 8.5) in acetonitrile (1 ml total) and benzylmercaptan (10.0 μl) was added. The reaction mixture was stirred at RT for 3 h. Solvents were removed by lyophilization. Pure compound was isolated after semi-preparative RP-RP-HPLC purification with a gradient from 25% to 45% solvent B over 10 min at RT (Figure S9e). HRMS (ESI⁺) *m/z* calcd (most abundant mass peak) for C₁₃₁H₁₃₁N₃₁O₃₃S₃ [M+2H]²⁺ 1388.4431 found 1388.5030.

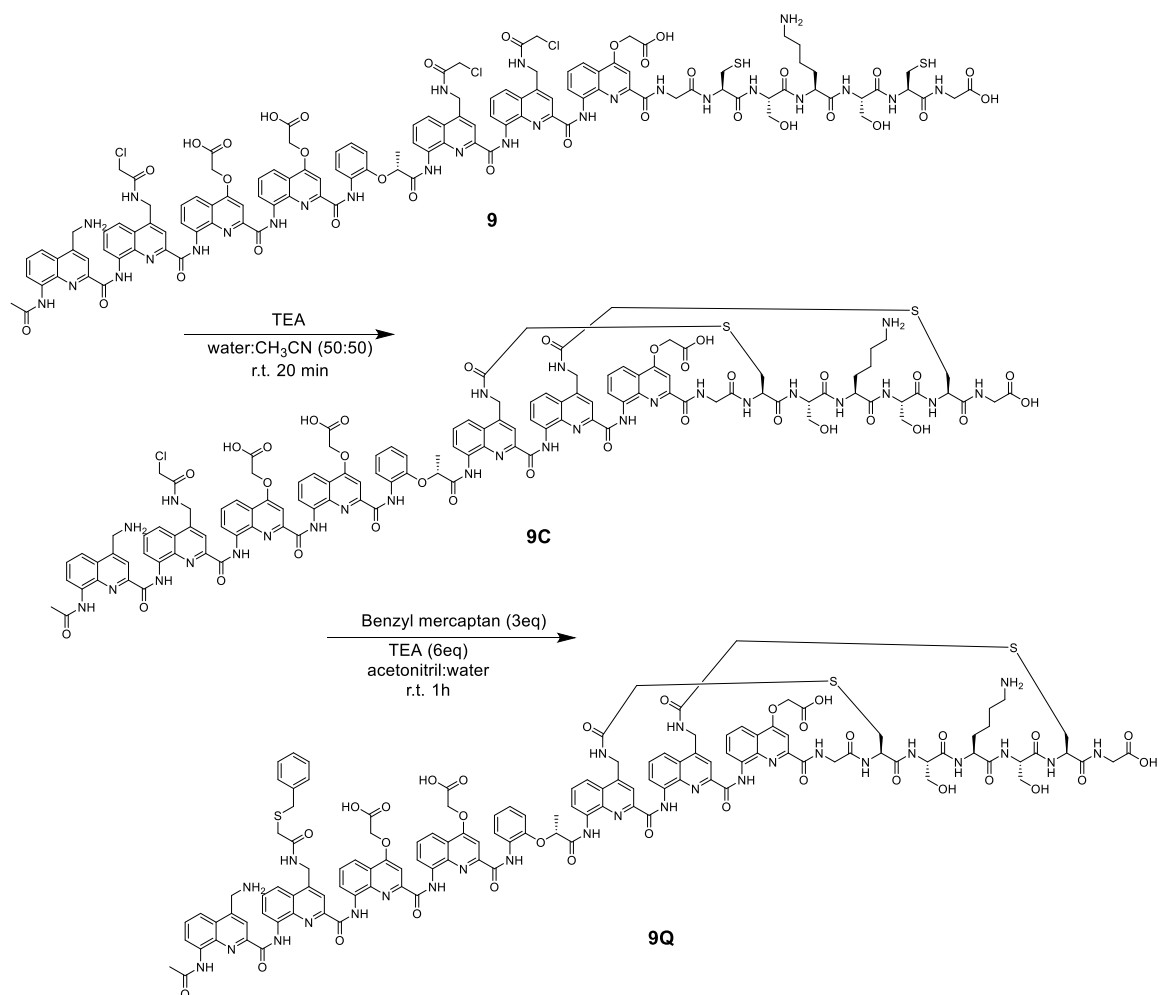


Compound 8: Foldamer-peptide **8** was built on a 25 μmol scale using a Low loading Fmoc-Gly-preloaded Wang resin (0.33 mmol/g). After terminal acetylation, the Alloc protecting groups were removed, directly followed by chloroacetylation. The resin was cleaved with TFA/TIS/H₂O/DODT (92.5:2.5:2.5:2.5, v/v/v/v) and the crude product (60 mg, 77%, Figure S10a) was purified by semi-preparative RP-HPLC (gradient: from 25% to 45% solvent B over 8 minutes at 25°C) to afford 6 mg of

pure compound (Figure S10b). HRMS (ESI⁺) *m/z* calcd (most abundant mass peak) for C₁₂₅H₁₂₇Cl₃N₃₁O₃₃S₂ [M+H]⁺ 2760.7752 found 2760.8162.

Compound 8C: After lyophilization, compound **8** (3 mg) was dissolved in a mixture of acetonitrile (4 ml) in water (6.0 ml) to reach a 0.1 mM concentration and TCEP stock solution (10 μl, 10 mM, 1 equiv.) was added. The solvent mixture was freed from oxygen by Freeze-Pump-Thaw. Independently, a solution of NH₄HCO₃ (6 ml, 60 mM, pH 8.5) in acetonitrile (4 ml) was prepared, oxygen removed, by Freeze-Pump-Thaw and the Foldamer solution added via syringe under inert gas atmosphere. The mixture was quickly stirred and left without stirring for 4 h at RT. The progression of the macrocyclization was monitored by RP-HPLC. After 4 h, the reaction mixture was quenched with TFA and the remaining solvent lyophilized. The obtained crude product was used in the subsequent reaction without further purification (Figure S10c). HRMS (ESI⁺) *m/z* calcd (most abundant mass peak) for C₁₂₅H₁₂₆ClN₃₁O₃₃S₂ [M+2H]²⁺ 1344.9144 found 1345.0008.

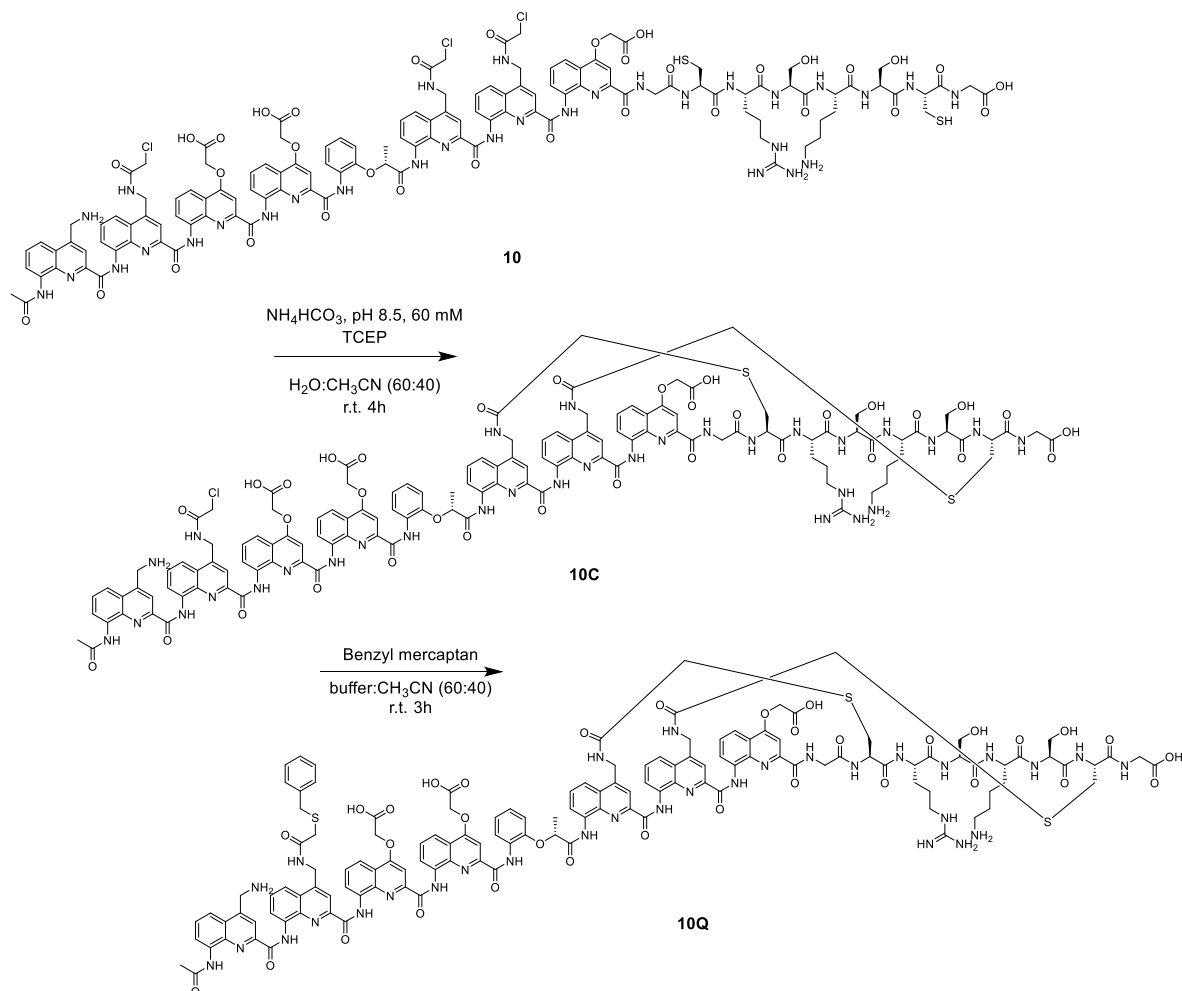
Compound 8Q: Compound **8C** (3 mg) was dissolved in mixture of NH₄HCO₃ buffer (0.15 ml, 60 mM, pH 8.5) in acetonitrile (0.1 ml) and benzyl mercaptan (1 μl) was added. The reaction mixture was stirred at RT for 3 h. Solvents were removed, by lyophilization. Pure compound was isolated after using semi-preparative RP-RP-HPLC with a gradient from 25% to 45% solvent B over 10 min at RT (Figure S10e). HRMS (ESI⁺) *m/z* calcd (most abundant mass peak) for C₁₃₁H₁₃₁N₃₁O₃₃S₃ [M+2H]²⁺ 1388.4431 found 1388.5030.



Compound 9: Foldamer-peptide **9** was built by relying on the CEM Liberty Blue microwave peptide synthesizer for the peptide segment and on the Liberty Bio for the stepwise assembly of the foldamer part on a 25 μmol scale using a Low loading Fmoc-Gly-preloaded Wang resin (0.33 mmol/g). After terminal acetylation, the Alloc protecting groups were removed, directly followed by chloroacetylation. The resin was cleaved with TFA/TIS/H₂O/EDT (92.5:2.5:2.5:2.5, v/v/v/v) and the crude product (38 mg, 50%, Figure S11a) was purified by semi-preparative RP-HPLC (gradient: from 35% to 45% solvent B over 15 minutes at 25°C (Figure S11b). HRMS (ESI⁺) m/z calcd (most abundant mass peak) for C₁₁₉H₁₁₅Cl₃N₂₇O₃₂S₂ [M+H]⁺ 2604.6709 found 2604.7563

Compound 9C: After lyophilization, compound **9** (8 mg) was dissolved in a 1:1 mixture of acetonitrile in water (30 ml total) to reach a 0.1 mM concentration and the solvent mixture was freed from oxygen. TEA (1.0 ml, 0.25 mM) was added and the reaction was kept under nitrogen atmosphere without stirring. The progression of the macrocyclization was monitored by RP-HPLC. After 30 min, the reaction mixture was concentrated under reduced pressure and the remaining solvent lyophilized. The obtained crude product was used in the subsequent reaction without further purification (Figure S11c). C₁₁₉H₁₁₃ClN₂₇O₃₂S₂ [M+H]⁺ 2531.7202 found 2531.7897.

Compound 9Q: 9C (7 mg) was dissolved in 1:1 mixture of acetonitrile in water (0.15 ml total) to reach a 50 mM concentration and TEA (3 μ l, 6 equiv.) was added. While stirring, benzylmercaptan (1.0 μ l, 3 equiv.) was added and the reaction mixture was stirred at RT for 60 minutes. Solvents were removed, by lyophilization and the colorless product (3.0 mg) was obtained after semi-preparative RP-HPLC purification with a gradient from 15% to 30% solvent D (Figure S11e). ^1H NMR (500 MHz, Acetonitrile- d_3) δ 11.70 (s, 1H), 11.23 (s, 1H), 10.69 (s, 1H), 10.42 (d, J = 5.2 Hz, 2H), 9.63 (s, 1H), 9.50 (s, 1H), 9.08 (s, 1H), 8.73 (s, 1H), 8.73 – 8.66 (m, 2H), 8.52 (d, J = 8.6 Hz, 1H), 8.42 (d, J = 8.1 Hz, 1H), 8.32 (s, 1H), 8.23 (d, J = 5.8 Hz, 1H), 8.11 (s, 1H), 8.05 (d, J = 9.1 Hz, 1H), 8.03 – 7.98 (m, 2H), 7.96 (t, J = 7.8 Hz, 1H), 7.91 (d, J = 9.1 Hz, 1H), 7.89 – 7.83 (m, 2H), 7.77 (d, J = 8.9 Hz, 1H), 7.74 (s, 2H), 7.71 (s, 1H), 7.66 (dd, J = 13.3, 8.1 Hz, 4H), 7.59 (s, 2H), 7.55 (d, J = 11.6 Hz, 2H), 7.53 – 7.45 (m, 3H), 7.42 (d, J = 4.9 Hz, 6H), 7.38 (s, 1H), 7.31 (t, J = 8.3 Hz, 1H), 7.20 (d, J = 7.9 Hz, 2H), 7.13 (t, J = 8.3 Hz, 2H), 7.07 (s, 1H), 6.96 (d, J = 9.0 Hz, 1H), 6.90 (s, 1H), 6.66 (s, 1H), 6.62 (s, 1H), 6.53 (s, 1H), 6.43 (s, 1H), 6.28 (t, J = 8.0 Hz, 1H), 6.15 (d, J = 8.3 Hz, 1H), 5.80 (t, J = 8.2 Hz, 1H), 5.24 (t, J = 10.4 Hz, 1H), 5.06 (dd, J = 17.3, 7.9 Hz, 1H), 4.93 (d, J = 13.0 Hz, 1H), 4.8-4.0 (water suppression region), 3.68 (d, J = 15.2 Hz, 2H), 3.54 (td, J = 15.1, 13.5, 7.6 Hz, 4H), 3.48 – 3.42 (m, 1H), 3.40 (s, 2H), 3.37 (d, J = 3.3 Hz, 2H), 3.26 (d, J = 13.9 Hz, 2H), 3.20 – 2.88 (m, 7H), 2.13 (s, 2H), 1.44 (s, 3H), 1.06 – 0.92 (m, 2H), 0.76 (s, 2H), 0.67 (s, 2H), -0.58 (d, J = 6.9 Hz, 4H). HRMS (ESI $^-$) m/z calcd (most abundant mass peak) for $\text{C}_{126}\text{H}_{118}\text{N}_{27}\text{O}_{32}\text{S}_3$ $[\text{M}-\text{H}]^-$ 2617.7637 found 2617.8408.

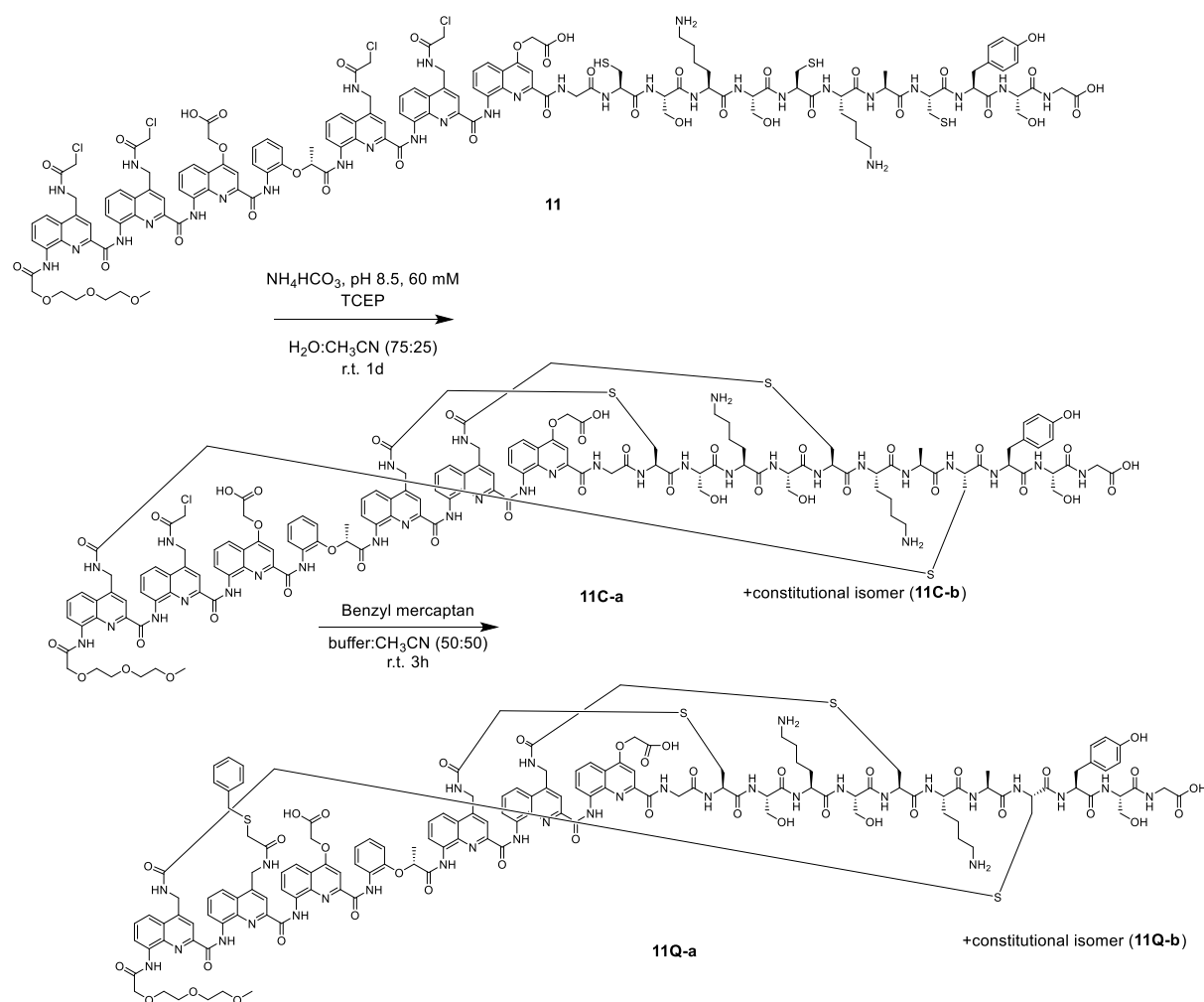


Compound 10: Foldamer-peptide **10** was built on a 25 μmol scale using a low loading Fmoc-Gly-preloaded Wang resin (0.33 mmol/g). After terminal acetylation, the Alloc protecting groups were removed, directly followed by chloroacetylation. The resin was cleaved with TFA/TIS/ H_2O /DODT (92.5:2.5:2.5:2.5, v/v/v/v) and the crude product (56 mg, 72%, Figure S12a) was purified by semi-preparative RP-HPLC (gradient: from 25% to 45% solvent B over 8 minutes at 25°C, Figure S12b) to afford 4 mg of pure compound. HRMS (ESI⁺) m/z calcd (most abundant mass peak) for $\text{C}_{125}\text{H}_{127}\text{Cl}_3\text{N}_{31}\text{O}_{33}\text{S}_2$ [M+H]⁺ 2760.7752 found 2760.8156

Compound 10C: After lyophilization, compound **10** (1.5 mg) was dissolved in a mixture of acetonitrile (2.4 ml) in water (3.6 ml) to reach a 0.1 mM concentration and TCEP stock solution (6 μl , 10 mM, 1 equiv.) was added. The solvent mixture was freed from oxygen by Freeze-Pump-Thaw. Independently, a solution of NH_4HCO_3 (3.6 ml, 60 mM, pH 8.5) in acetonitrile (2.4 ml) was prepared, oxygen removed, by Freeze-Pump-Thaw and the Foldamer solution added via syringe under inert gas atmosphere. The mixture was quickly stirred and left without stirring for 4 h at RT. The progression of the macrocyclization was monitored by RP-HPLC. After 4 h, the reaction mixture was quenched with TFA and the remaining solvent lyophilized. The obtained crude product was used in the

subsequent reaction without further purification (Figure S12b). HRMS (ESI⁺) *m/z* calcd (most abundant mass peak) for C₁₂₅H₁₂₆ClN₃₁O₃₃S₂ [M+2H]²⁺ 1344.9144 found 1344.9144

Compound 10Q: Compound **10C** (1.5 mg) was dissolved in a mixture of NH₄HCO₃ buffer (150 μl, 60 mM, pH 8.5) in acetonitrile (100 μl) and benzyl mercaptan (1 μl) was added. The reaction mixture was stirred at RT for 3 h. Solvents were removed, by lyophilization. Pure compound was isolated after semi-preparative RP-HPLC purification with a gradient from 25% to 45% solvent B over 10 min at RT (Figure S12e). HRMS (ESI⁺) *m/z* calcd (most abundant mass peak) for C₁₃₁H₁₃₁N₃₁O₃₃S₃ [M+2H]²⁺ 1388.4431 found 1388.5001.

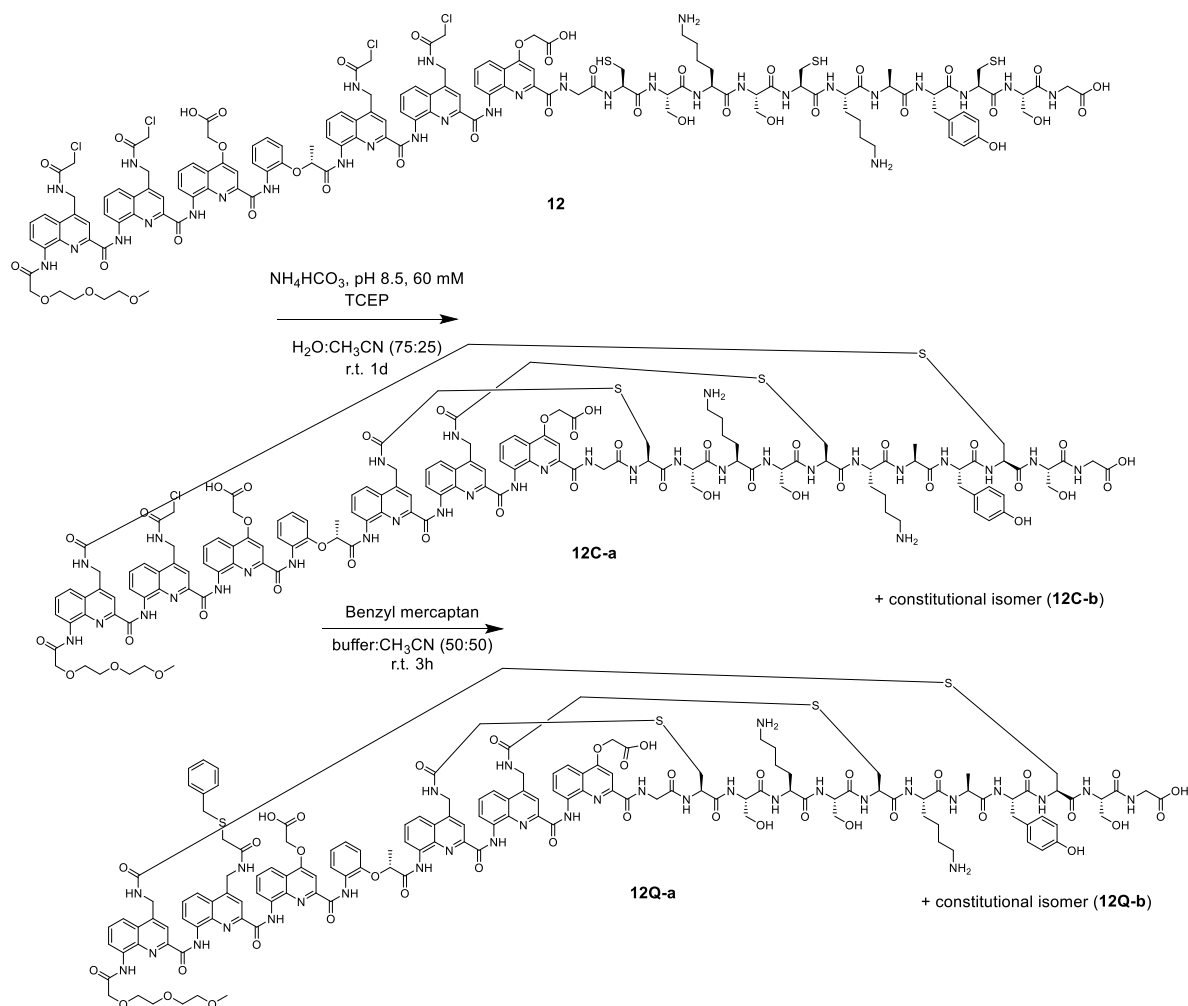


Compound 11: Foldamer-peptide **11** was built on a 25 μmol scale using a Low loading Fmoc-Gly-preloaded Wang resin (0.33 mmol/g). After terminal DEG installation, the Alloc protecting groups were removed, directly followed by chloroacetylation. The resin was cleaved with TFA/TIS/H₂O/DODT (92.5:2.5:2.5:2.5, v/v/v/v) and the crude product (83 mg, 81%, Figure S13a) was purified by semi-preparative RP-HPLC (gradient: from 25% to 45% solvent B over 10 minutes at 25°C)

to afford 4 mg of pure compound (Figure S14b). HRMS (ESI⁺) *m/z* calcd (most abundant mass peak) for C₁₃₈H₁₅₃Cl₄N₃₁O₃₉S₃ [M+2H]²⁺ 1554.9509 found 1555.0461.

Compound 11C: After lyophilization, compound **11** (3.0 mg) was dissolved in a mixture of acetonitrile (5 ml) in water (15 ml) to reach a 0.05 mM concentration and TCEP stock solution (10 μl, 10 mM, 0.1 equiv.) was added. The solvent mixture was freed from oxygen by Freeze-Pump-Thaw. Independently, a solution of NH₄HCO₃ (15 ml, 60 mM, pH 8.5) in acetonitrile (5 ml) was prepared, oxygen removed, by Freeze-Pump-Thaw and the foldamer solution added via syringe under inert gas atmosphere. The mixture was quickly stirred and left without stirring for 1d at RT. The progression of the macrocyclization was monitored by RP-HPLC. After 1d, the reaction mixture was quenched with formic acid and the remaining solvent lyophilized. The obtained crude product was used in the subsequent reaction without further purification (Figure S13c). HRMS (ESI⁺) *m/z* calcd (most abundant mass peak) for C₁₃₈H₁₅₀ClN₃₁O₃₉S₃ [M+2H]²⁺ 1499.9869 found 1500.0687 (**11C-a**) and 1500.0675 (**11C-b**).

Compound 11Q: Compound **11C** (1.5 mg) was dissolved in a 1:1 mixture of NH₄HCO₃ buffer (60 mM, pH 8.5) in acetonitrile (0.3 ml total) and benzyl mercaptan (4 μl) was added. The reaction mixture was stirred at RT for 3 h. Solvents were removed, by lyophilization. Pure compounds (two constitutional isomers) were isolated after semi-preparative RP-RP-HPLC purification with a gradient from 30% to 50% solvent B over 10 min at RT (Figure S13e and S13f). HRMS (ESI⁺) *m/z* calcd (most abundant mass peak) for C₁₄₅H₁₅₇N₃₁O₃₉S₄ [M+2H]²⁺ 1543.5156 found 1543.5291 (**11Q-a**) and 1543.5275 (**11Q-b**).

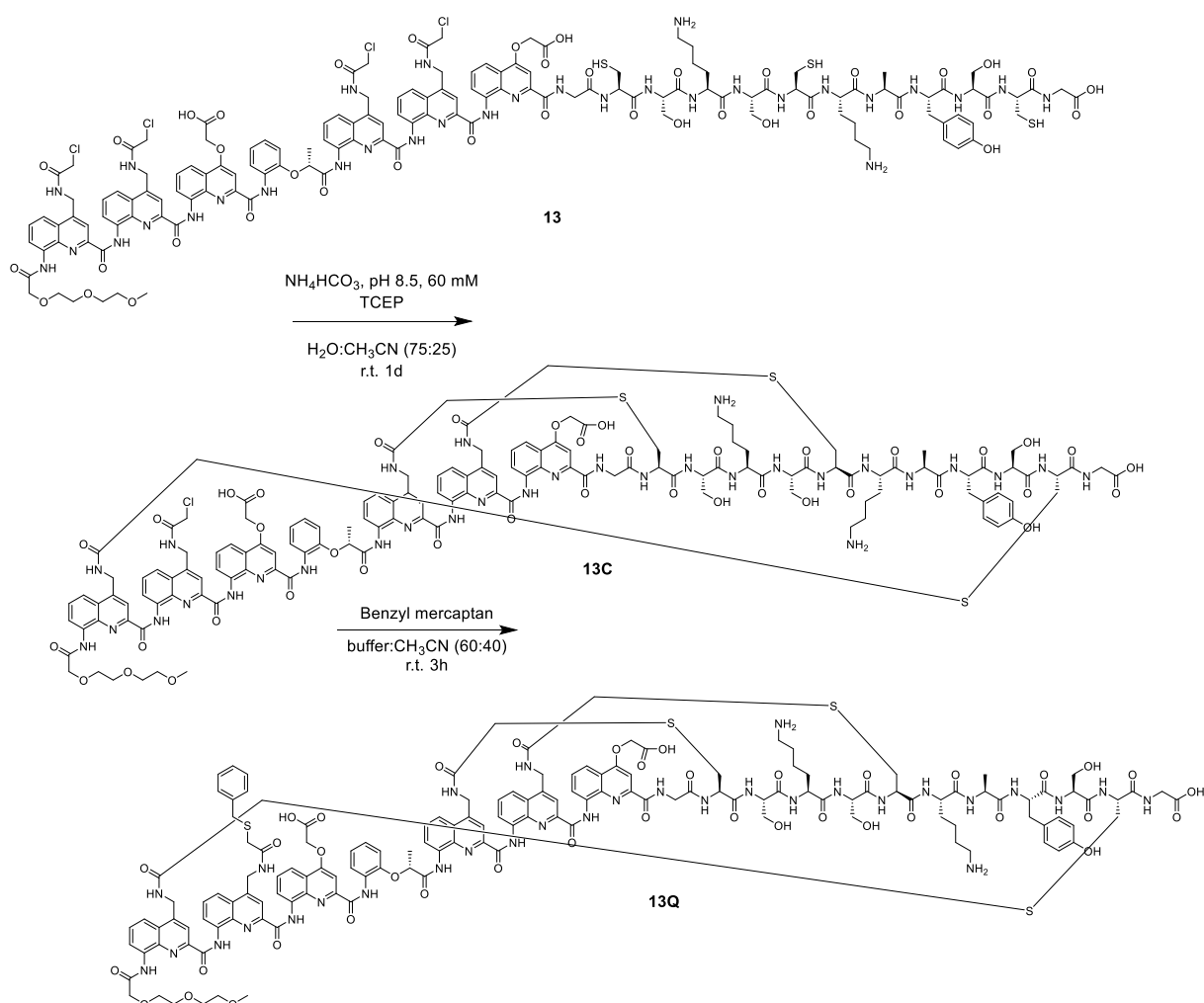


Compound 12: Foldamer-peptide **12** was built on a 25 μmol scale using a low loading Fmoc-Gly-preloaded Wang resin (0.33 mmol/g). After terminal DEG installation, the Alloc protecting groups were removed, directly followed by chloroacetylation. The resin was cleaved with TFA/TIS/H₂O/DODT (92.5:2.5:2.5:2.5, v/v/v/v) and the crude product (70 mg, 68%, Figure S15a) was purified by semi-preparative RP-HPLC (gradient: from 25% to 45% solvent B over 10 minutes at 25°C) to afford 2 mg of pure compound (Figure S15b). HRMS (ESI⁺) *m/z* calcd (most abundant mass peak) for C₁₃₈H₁₅₃Cl₄N₃₁O₃₉S₃ [M+2H]²⁺ 1554.9509 found 1554.4308

Compound 12C: After lyophilization, compound **12** (1.0 mg) was dissolved in a mixture of acetonitrile (2 ml) in water (8 ml) to reach a 0.05 mM concentration and TCEP stock solution (4 μl 10 mM, 0.1 equiv.) was added. The solvent mixture was freed from oxygen by Freeze-Pump-Thaw. Independently, a solution of NH₄HCO₃ (8 ml, 60 mM, pH 8.5) in acetonitrile (2 ml) was prepared, oxygen removed, by Freeze-Pump-Thaw and the Foldamer solution added via syringe under inert gas atmosphere. The mixture was quickly stirred and left without stirring for 1d at RT. The progression of the macrocyclization was monitored by RP-HPLC. After 1d, the reaction mixture was neutralized with formic acid and the remaining solvent lyophilized. The obtained crude product was used in the

subsequent reaction without further purification (Figure S15c). HRMS (ESI⁺) *m/z* calcd (most abundant mass peak) for C₁₃₈H₁₅₀ClN₃₁O₃₉S₃ [M+2H]²⁺ 1499.9869 found 1500.0080 (**12C-a**) and 1500.0078 (**12C-b**)

Compound 12Q: Compound **12C** (1.0 mg) was dissolved in 1:1 NH₄HCO₃ buffer (60 mM, pH 8.5) in acetonitrile (1.5 ml total) and benzyl mercaptan (20 μl) was added. The reaction mixture was stirred at RT for 3 h. Solvents were removed, by lyophilization. Pure compounds (two constitutional isomers) were isolated after semi-preparative RP-HPLC purification with a gradient from 30% to 50% solvent B over 10 min at RT (Figure S15e). HRMS (ESI⁺) *m/z* calcd (most abundant mass peak) for C₁₄₅H₁₅₇N₃₁O₃₉S₄ [M+2H]²⁺ 1544.0165 found 1543.9963. Both isomers most likely co-eluted.

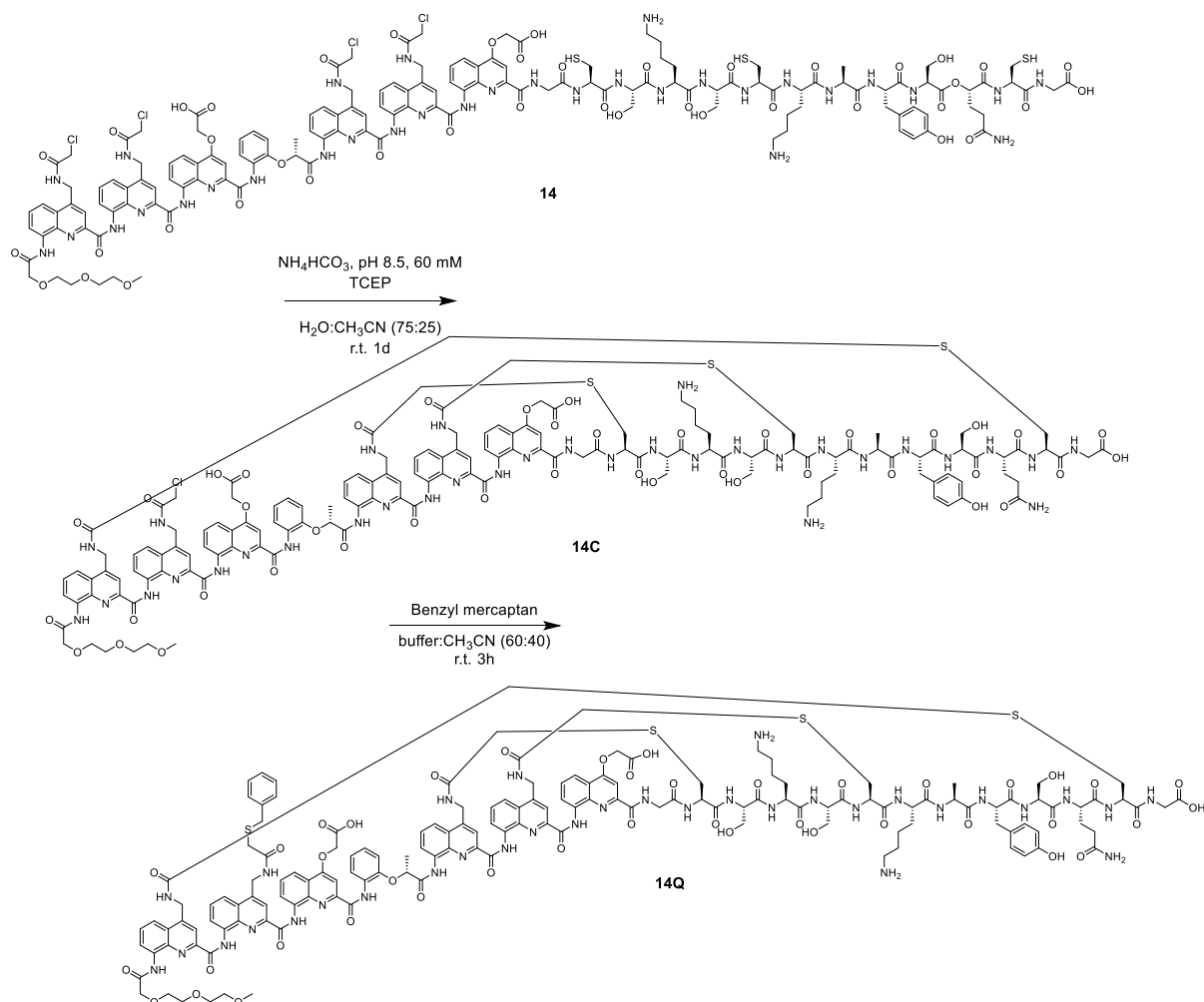


Compound 13: Foldamer-peptide **13** was built on a 25 μmol scale using a low loading Fmoc-Gly-preloaded Wang resin (0.33 mmol/g). After terminal DEG installation, the Alloc protecting groups were removed, directly followed by chloroacetylation. The resin was cleaved with TFA/TIS/H₂O/DODT (92.5:2.5:2.5:2.5, v/v/v/v) and the crude product (65 mg, 63%, Figure S16a) was purified by semi-preparative RP-HPLC (gradient: from 25% to 45% solvent B over 10 minutes at 25°C)

to afford 3 mg of pure compound (Figure S16b). HRMS (ESI⁺) *m/z* calcd (most abundant mass peak) for C₁₃₈H₁₅₃Cl₄N₃₁O₃₉S₃ [M+2H]²⁺ 1554.9509 found 1554.9518

Compound 13Q: After lyophilization, compound **13** (1.8 mg) was dissolved in a mixture of acetonitrile (3 ml) in water (9 ml) to reach a 0.05 mM concentration and TCEP stock solution (4 μl, 10 mM, 0.1 equiv.) and the solvent mixture was freed from oxygen by Freeze-Pump-Thaw. Independently, a solution of NH₄HCO₃ (9 ml, 60 mM, pH 8.5) in acetonitrile (3 ml) was prepared, oxygen removed, by Freeze-Pump-Thaw and the Foldamer solution added via syringe under inert gas atmosphere. The mixture was quickly stirred and left without stirring for 1d at RT. The progression of the macrocyclization was monitored by RP-HPLC. The reaction mixture was quenched with formic acid and the remaining solvent lyophilized. The obtained crude product was used in the subsequent reaction without further purification (Figure S16c). HRMS (ESI⁺) *m/z* calcd (most abundant mass peak) for C₁₃₈H₁₅₀ClN₃₁O₃₉S₃ [M+2H]²⁺ 1499.9869 found 1499.9807.

Compound 13Q: Compound **13C** was dissolved in 1:1 mixture of NH₄HCO₃ buffer (60 mM, pH 8.5) in acetonitrile (1.5 ml) and benzyl mercaptan (20 μl) was added. The reaction mixture was stirred at RT for 3 h. Solvents were removed, by lyophilization. Pure compound was isolated after semi-preparative RP-RP-HPLC purification with a gradient from 30% to 50% solvent B over 10 min at RT (Figure S16e). HRMS (ESI⁺) *m/z* calcd (most abundant mass peak) for C₁₄₅H₁₅₇N₃₁O₃₉S₄ [M+2H]²⁺ 1543.5156 found 1544.0290.

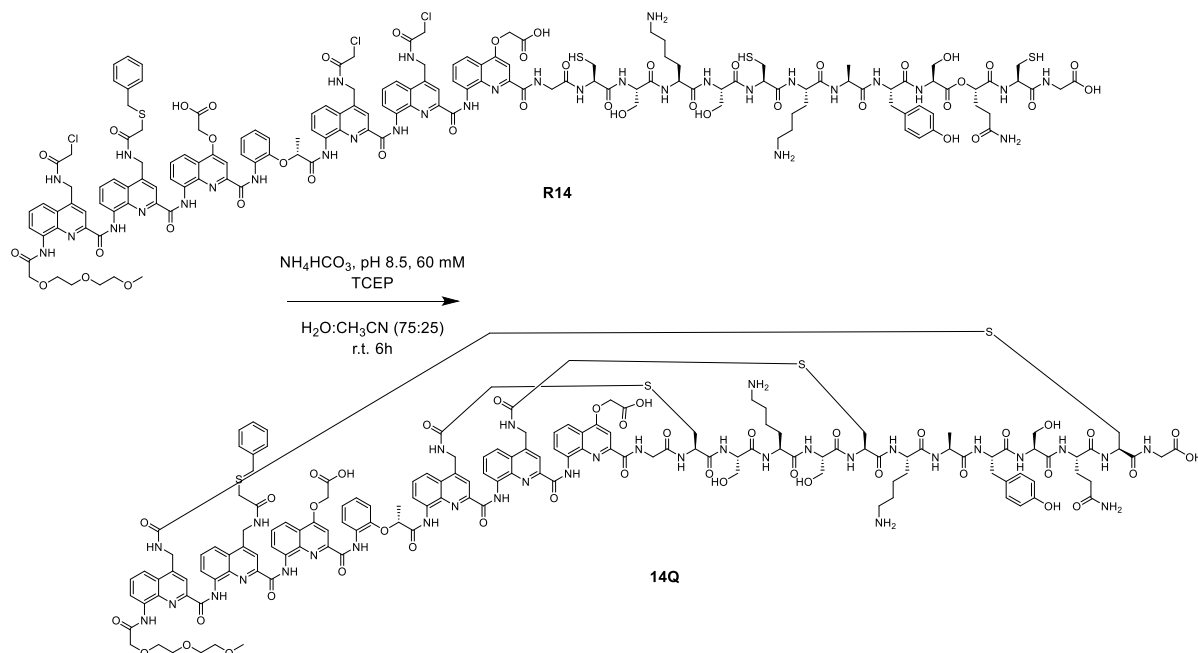


Compound 14: Foldamer-peptide **14** was built on a 25 μmol scale using a low loading Fmoc-Gly-preloaded Wang resin (0.33 mmol/g). After terminal DEG installation, the Alloc protecting groups were removed, directly followed by chloroacetylation. The resin was cleaved with TFA/TIS/ H_2O /DOTD (92.5:2.5:2.5:2.5, v/v/v/v) and the crude product (68 mg, 64%, Figure S17a) was purified by semi-preparative RP-HPLC (gradient: from 25% to 45% solvent B over 10 minutes at 25°C) to afford 5 mg of pure compound (Figure S17b). HRMS (ESI⁺) m/z calcd (most abundant mass peak) for $\text{C}_{143}\text{H}_{161}\text{Cl}_4\text{N}_{33}\text{O}_{41}\text{S}_3$ $[\text{M}+2\text{H}]^{2+}$ 1618.4806 found 1618.4738.

Compound 14C: After lyophilization, compound **14** (2.0 mg) was dissolved in a mixture of acetonitrile (3 ml) in water (9 ml) to reach a 0.05 mM concentration and TCEP stock solution (4 μl , 10 mM, 0.1 equiv.) was added. The solvent mixture was freed from oxygen by Freeze-Pump-Thaw. Independently, a solution of NH_4HCO_3 (9 ml, 60 mM, pH 8.5) in acetonitrile (3 ml) was prepared, oxygen removed, by Freeze-Pump-Thaw and the Foldamer solution added via syringe under inert N_2 atmosphere. The mixture was quickly stirred and left without stirring for 1d at RT. The progression of the macrocyclization was monitored by RP-HPLC. The reaction mixture was quenched with formic acid and the remaining solvent lyophilized. The obtained crude product was used in the subsequent

reaction without further purification (Figure S17c). HRMS (ESI⁺) *m/z* calcd (most abundant mass peak) for C₁₄₃H₁₅₈ClN₃₃O₄₁S₃ [M+2H]²⁺ 1564.0163 found 1564.0276.

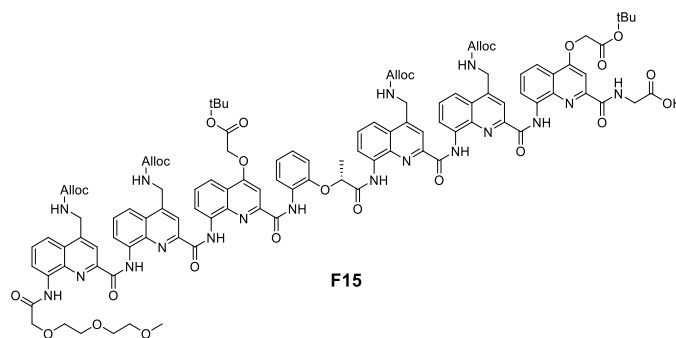
Compound 14Q: Compound **14C** was dissolved in 1:1 mixture of NH₄HCO₃ buffer (60 mM, pH 8.5) in acetonitrile (0.6 ml total), benzyl mercaptan (8 μl) was added and the reaction mixture was stirred at RT for 5 h. Solvents were removed, by lyophilization. Pure compound were isolated after semi-preparative RP-HPLC purification with a gradient from 30% to 50% solvent B over 10 min at RT (Figure S17e). HRMS (ESI⁺) *m/z* calcd (most abundant mass peak) for C₁₅₀H₁₆₅N₃₃O₄₁S₄ [M+2H]²⁺ 1608.0458 found 1608.0641.



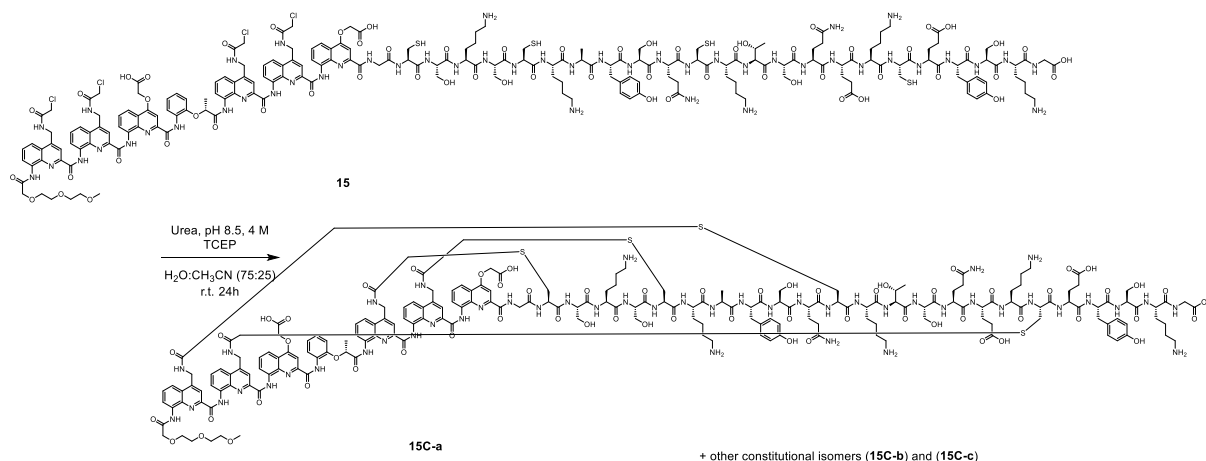
Compound R14: Foldamer-peptide **R14** was built on a 33 μmol scale using a low loading Fmoc-Gly-preloaded Wang resin (0.33 mmol/g). After terminal DEG installation, the Alloc protecting groups were removed, directly followed by chloroacetylation. The resin was cleaved with TFA/TIS/H₂O/EDT (92.5:2.5:2.5:2.5, v:v:v:v) and the crude product (73 mg, 66%, Figure S18a) was purified by semi-preparative RP-HPLC (gradient: from 33% to 40% solvent B over 10 minutes at 25°C) to afford 3 mg of pure compound (Figure S18b). HRMS (ESI⁺) *m/z* calcd (most abundant mass peak) for C₁₅₀H₁₆₈Cl₃N₃₃O₄₁S₄ [M+2H]²⁺ 1662.5087 found 1662.5291

Compound 14Q: After lyophilization, compound **R14** (2.0 mg) was dissolved in a mixture of acetonitrile (3 ml) in water (9 ml) to reach a 0.05 mM concentration and TCEP stock solution (4 μl, 10 mM, 0.1 equiv.) was added. The solvent mixture was freed from oxygen by Freeze-Pump-Thaw. Independently, a solution of NH₄HCO₃ (9 ml, 60 mM, pH 8.5) in acetonitrile (3 ml) was prepared, oxygen removed, by Freeze-Pump-Thaw and the Foldamer solution added via syringe under inert gas atmosphere. The mixture was quickly stirred and left without stirring for 6h at RT. The progression of

the macrocyclization was monitored by RP-HPLC. The reaction mixture was quenched with formic acid and the remaining solvent lyophilized. The obtained crude product was purified by semi-preparative RP-HPLC (gradient: from 30% to 50% solvent B over 10 minutes at 25°C) to afford 1 mg of pure compound (Figure S18d). ^1H NMR (500 MHz, CD_3CN) δ 11.84 (s, 1H), 11.12 (s, 1H), 10.51 (d, J = 8.2 Hz, 2H), 9.79 (s, 1H), 9.65 (s, 1H), 9.41 (d, J = 14.9 Hz, 1H), 9.33 (s, 1H), 8.77 (d, J = 9.4 Hz, 3H), 8.66 (dd, J = 20.3, 8.3 Hz, 2H), 8.49 (dd, J = 20.3, 11.5 Hz, 5H), 8.36 (s, 2H), 8.32 – 8.21 (m, 5H), 8.21 – 8.00 (m, 11H), 8.00 – 7.84 (m, 11H), 7.81 (q, J = 8.4, 6.4 Hz, 5H), 7.75 – 7.62 (m, 6H), 7.62 – 7.34 (m, 23H), 7.27 (dd, J = 18.8, 8.6 Hz, 7H), 7.11 (s, 4H), 7.01 (s, 4H), 6.96 – 6.76 (m, 10H), 6.74 (d, J = 24.5 Hz, 5H), 6.53 (d, J = 18.6 Hz, 2H), 6.41 (t, J = 8.7 Hz, 1H), 6.13 (d, J = 9.4 Hz, 1H), 5.89 (t, J = 8.5 Hz, 1H), 5.23 (s, 1H), 5.14 (d, J = 22.7 Hz, 1H), 5.0-4.1 (water suppression region), 3.89 (q, J = 12.4, 11.8 Hz, 7H), 3.62 (d, J = 47.7 Hz, 5H), 3.57 – 3.21 (m, 24H), 3.21 – 2.73 (m, 29H), 2.73 – 2.14 (m, 20H), 1.71 (q, J = 8.4 Hz, 6H), 1.56 – 1.07 (m, 21H), 0.90 (d, J = 35.1 Hz, 4H), -0.52 (d, J = 7.2 Hz, 3H). HRMS (ESI⁺) m/z calcd (most abundant mass peak) for $\text{C}_{150}\text{H}_{165}\text{N}_{33}\text{O}_{41}\text{S}_4$ $[\text{M}+2\text{H}]^{2+}$ 1608.0468 found 1608.0455.



Foldamer fragment F15: **F15** was synthesized on a preloaded Fmoc-Gly-SASRIN resin (0.72 mmol/g) using general SPFS procedure on a 100 μmol scale. Crude **F15** was recovered in 70% yield (150 mg) after cleavage using a mixture of HFIP in DCM (6 ml, 40:60, v/v) for 1h at RT. The obtained crude product was purified by semi-preparative RP-HPLC (gradient: from 72% to 87% solvent B over 10 minutes at 25°C) to afford 80 mg of pure compound. HRMS (ESI⁺) m/z calcd (most abundant mass peak) for $\text{C}_{110}\text{H}_{110}\text{N}_{18}\text{O}_{28}$ $[\text{M}+\text{H}]^+$ 2132.8064 found 2132.7844.



Compound 15: Foldamer-peptide **15** was built by relying on the CEM Liberty Blue microwave peptide synthesizer for the resin-bound Fmoc-Cys(Trt)-Ser(*t*Bu)-Lys(Boc)-Ser(*t*Bu)-Cys(Trt)-Lys(Boc)-Ala-Tyr(*t*Bu)-Ser(*t*Bu)-Gln(Trt)-Cys(Trt)-Lys(Boc)-Thr(*t*Bu)-Ser(*t*Bu)-Gln(Trt)-Glu(*t*Bu)-Lys(Boc)-Cys(Trt)-Glu(*t*Bu)-Tyr(*t*Bu)-Ser(*t*Bu)-Lys(Boc)-Gly peptide on a 100 μ mol scale using a low loading Fmoc-Gly-preloaded Wang resin (0.27 mmol/g). Fragment condensation with foldamer fragment **F15** was next performed on a 25 μ mol scale of resin-bound free amine peptide. Therefore **F15** (30 mg, 14 μ mol) was dissolved in mixture of DCM/THF (1.4 ml, 1:1, v:v) together with BOP (12 mg, 28 μ mol) and DIPEA (7 μ l, 42 μ mol). After incubating the mixture for 5 min at RT, it was added to the resin and mechanical shaking was maintained for 16h at RT. The resin was washed with DCM and the remaining resin-bound peptide free amine groups were capped with 1:1 mixture of acetic anhydride in DCM (2 ml).

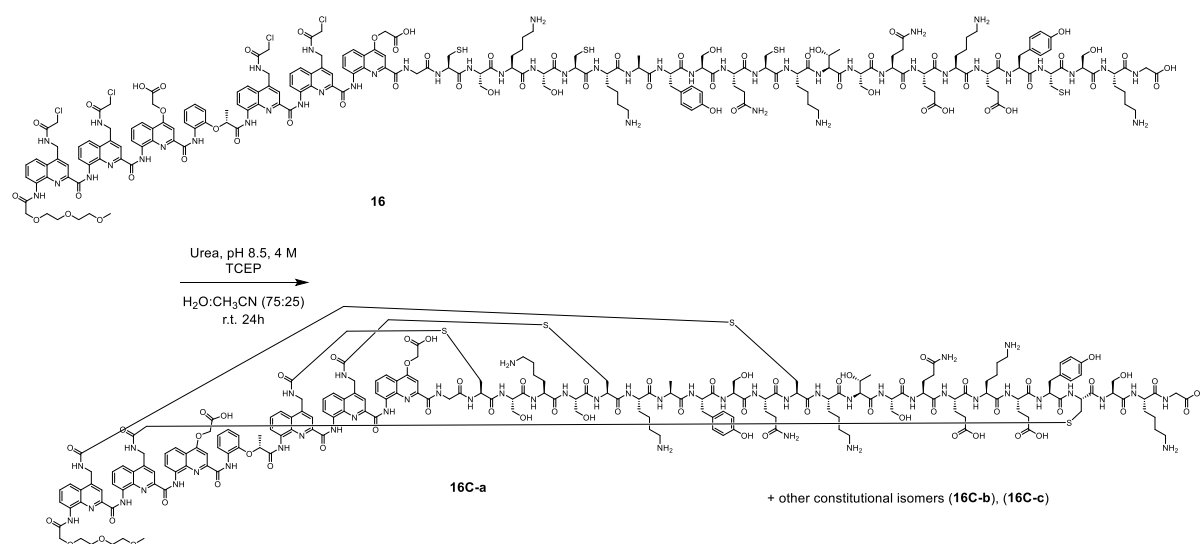
Alloc protecting groups were removed, directly followed by chloroacetylation. The resin was cleaved with TFA/TIS/H₂O/EDT (92.5:2.5:2.5:5 v:v:v:v) and the crude product (89 mg, 90%; Figure S20a) was purified by semi-preparative RP-HPLC (gradient: from 25% to 35% solvent B over 10 minutes at 25°C) to afford 14 mg of pure compound (Figure S20b). HRMS (ESI⁺) *m/z* calcd (most abundant mass peak) for C₁₉₈H₂₅₃Cl₄N₄₈O₆₁S₄ [M+3H]³⁺ 1516.8609 found 1516.8608.

Compound 15C: After lyophilization, compound **15** (7 mg) was dissolved in mixture of acetonitrile (8ml) in water (24 ml) to reach a 0.05 mM concentration and TCEP stock solution (60 μ l, 10 mM, 0.1 equiv.) was added. The solvent mixture was freed from oxygen by Freeze-Pump-Thaw. Independently, a solution of NH₄HCO₃ (24 ml, 60 mM, pH 8.5) in acetonitrile (8 ml) was prepared, oxygen removed, by Freeze-Pump-Thaw and the Foldamer solution added via syringe under inert gas atmosphere. The mixture was quickly stirred and left without stirring for 24h at RT. The progression of the macrocyclization was monitored by RP-HPLC and used in the next reaction step without further purification (Figure S20c). Benzyl mercaptan (1.5 ml) was added to block unreacted

chloroacetamide groups and the reaction mixture was stirred at RT for 5 h. After neutralizing the reaction with HCl (0.1 M), the solution was diluted with water (25ml) and the excess of benzyl mercaptan was removed by separation in an extraction funnel. Solvents were removed, by lyophilization. The obtained crude product was purified by semi-preparative RP-HPLC (hold 100% solvent A for 5 min then gradient from 10% to 35% solvent B over 15 minutes at 25°C) to afford 1 mg (**15C-a**), 1 mg (**15C-b**) and 0.3 mg (**15C-c**) as pure compounds (Figure S20e, S20f and S20g). ¹H NMR (500 MHz, CD₃CN) for **15C-a**: δ 11.85 (s, 1H), 11.14 (s, 1H), 10.64 (d, *J* = 5.6 Hz, 2H), 9.82 (s, 1H), 9.61 (s, 1H), 9.45 (s, 1H), 9.32 (s, 1H), 9.14 (d, *J* = 10.8 Hz, 1H), 8.74 (d, *J* = 8.6 Hz, 1H), 8.54 (d, *J* = 8.9 Hz, 3H), 8.34 (s, 1H), 8.22 – 7.19 (m, 53H), 7.17 – 7.01 (m, 4H), 6.90 (dd, *J* = 21.2, 8.7 Hz, 4H), 6.72 (dd, *J* = 31.9, 7.9 Hz, 7H), 6.51 (d, *J* = 10.3 Hz, 3H), 6.29 (t, *J* = 7.9 Hz, 1H), 6.07 (d, *J* = 8.6 Hz, 1H), 5.91 – 5.84 (m, 1H), 5.5-4.0 (water suppression region), 3.84 – 3.19 (m, 100H), 3.19 – 2.81 (m, 54H), 2.63 – 2.44 (m, 13H), 1.77 – 1.25 (m, 68H), 1.20 – 0.79 (m, 23H), -0.49 (d, *J* = 6.8 Hz, 3H).

¹H NMR (500 MHz, CD₃CN) for **15C-b**: ¹H NMR (500 MHz, Acetonitrile-*d*₃) δ 11.79 (s, 1H), 11.11 (s, 1H), 10.53 (s, 2H), 9.79 (s, 1H), 9.56 (s, 1H), 9.39 (s, 1H), 9.30 (s, 1H), 8.87 – 8.77 (m, 2H), 8.65 – 6.69 (m, 100H), 6.51 (d, *J* = 22.7 Hz, 2H), 6.36 (d, *J* = 8.5 Hz, 1H), 6.22 (d, *J* = 8.3 Hz, 1H), 5.86 (t, *J* = 8.4 Hz, 1H), 5.57 (s, 13H), 5.35 (s, 1H), 5.21 – 4.88 (m, 3H), 4.8-4.0 (water suppression region), 3.92 – 3.53 (m, 10H), 3.53 – 2.66 (m, 67H), 2.65 – 2.14 (m, 25H), 1.84 (s, 12H), 1.76 – 1.57 (m, 21H), 1.44 (dd, *J* = 20.6, 7.4 Hz, 22H), 1.28 (d, *J* = 7.3 Hz, 12H), 1.13 (t, *J* = 6.5 Hz, 9H), -0.44 (d, *J* = 6.8 Hz, 3H).

HRMS (ESI⁺) *m/z* calcd (most abundant peak) for C₁₉₈H₂₄₉N₄₈O₆₁S₄ [M+3H]³⁺ 1468.2258 found 1468.2256 (**15C-a**), 1468.2227 (**15C-b**) and 1468.2196 (**15C-c**).

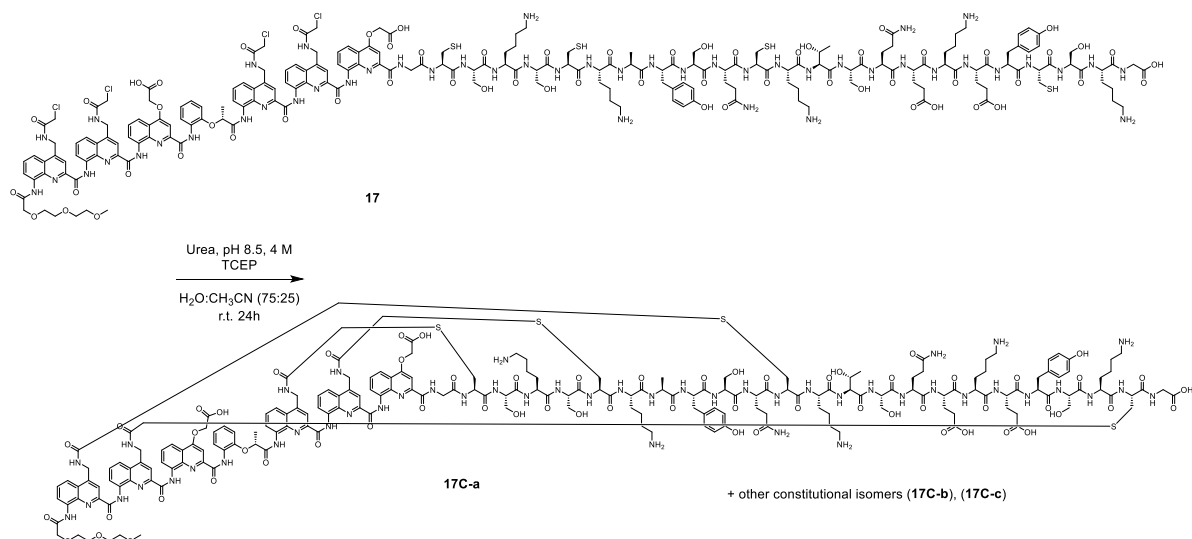


Compound 16: Foldamer-peptide **16** was built by relying on the CEM Liberty Blue microwave peptide synthesizer for the peptide segment Fmoc-Cys(Trt)-Ser(*t*Bu)-Lys(Boc)-Ser(*t*Bu)-Cys(Trt)-Lys(Boc)-Ala-

Tyr(*t*Bu)-Ser(*t*Bu)-Gln(Trt)-Cys(Trt)-Lys(Boc)-Thr(*t*Bu)-Ser(*t*Bu)-Gln(Trt)-Glu(*t*Bu)-Lys(Boc)-Glu(*t*Bu)-Tyr(*t*Bu)-Cys(Trt)-Ser(*t*Bu)-Lys(Boc)-Gly- on a 100 μ mol scale using a low loading Fmoc-Gly-preloaded Wang resin (0.27 mmol/g). Fragment condensation with foldamer fragment **F15** was next carried out in the same way as for the synthesis of foldamer-peptide **15** (see above).

Alloc protecting groups were removed, directly followed by chloroacetylation. The resin was cleaved with TFA/TIS/H₂O/EDT (92.5:2.5:2.5:5, v/v/v/v) and the crude product (120 mg, 71%, Figure S22a) was purified by semi-preparative RP-HPLC (gradient: from 25% to 35% solvent B over 10 minutes at 25°C) to afford 30 mg of pure compound (Figure S22b). HRMS (ESI⁺) *m/z* calcd (most abundant mass peak) for C₁₉₈H₂₅₃Cl₄N₄₈O₆₁S₄ [M+3H]³⁺ 1516.8609 found 1516.8180.

Compound 16C: After lyophilization, compound **16** (5 mg) was dissolved in mixture of acetonitrile (6 ml) in water (16 ml) to reach a 0.05 mM concentration and TCEP stock solution (40 μ l, 10 mM, 0.1 equiv.). The solvent mixture was freed from oxygen by Freeze-Pump-Thaw. Independently, a solution mixture of urea-buffer (16 ml, 8M, pH 8.5 with 0.1 M NaH₂PO₄) in acetonitrile (6 ml) was prepared, oxygen removed, by Freeze-Pump-Thaw and the Foldamer solution added via syringe under inert gas atmosphere. The mixture was quickly stirred and left without stirring for 24h at RT. The progression of the macrocyclization was monitored by RP-HPLC and used in the next reaction step without further purification (Figure 22c). Benzyl mercaptan (1 ml) was added to block unreacted chloroacetamide groups and the reaction mixture and was stirred at RT for 5 h. After neutralizing the reaction with HCl (0.1 M), the solution was diluted with water (30ml) and excess benzyl mercaptan was removed by separation in an extraction funnel. Solvents were removed, by lyophilisation (Figure S22d). The obtained crude product was purified by semi-preparative RP-HPLC (hold 100% solvent A for 5 min than gradient from 10% to 35% solvent B over 15 minutes at 25°C) to afford 1 mg of pure compound (**16C-a**), 2 mg of pure compound (**16C-b**), and 1mg of pure compound (**16C-c**) (Figure S22d, S22e, S22f). HRMS (ESI⁺) *m/z* calcd (most abundant mass peak) for C₁₉₈H₂₄₉N₄₈O₆₁S₄ [M+3H]³⁺ 1468.2258 found 1468.1650 (**16C-a**), 1468.1661 (**16C-b**) and 1468.1640 (**16C-c**).

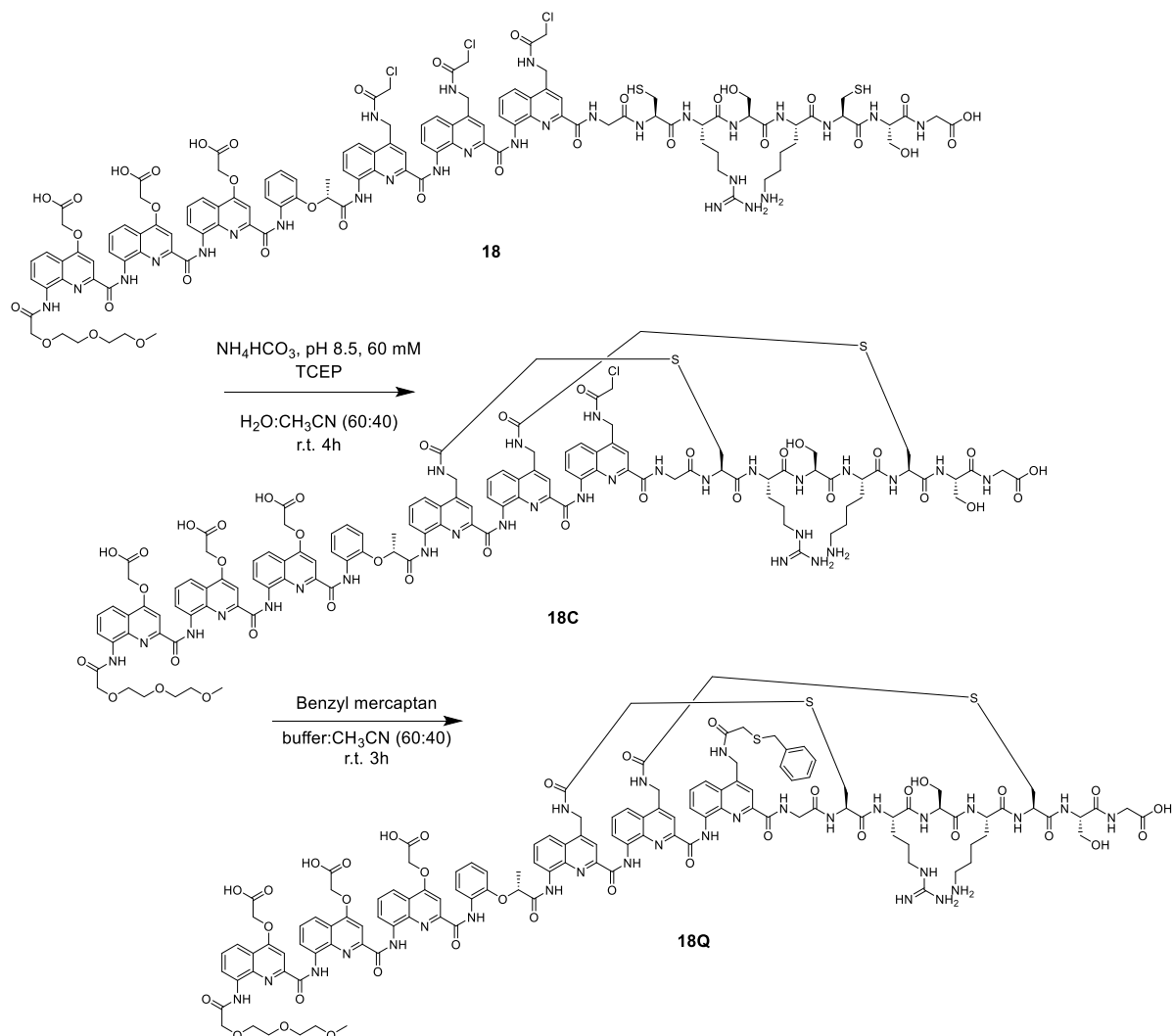


Compound 17: Foldamer-peptide **17** was built by relying on the CEM Liberty Blue microwave peptide synthesizer for the peptide segment Cys(Trt)-Ser(tBu)-Lys(Boc)-Ser(tBu)-Cys(Trt)-Lys(Boc)-Ala-Tyr(tBu)-Ser(tBu)-Gln(Trt)-Cys(Trt)-Lys(Boc)-Thr(tBu)-Ser(tBu)-Gln(Trt)-Glu(tBu)-Lys(Boc)-Glu(tBu)-Tyr(tBu)-Ser(tBu)-Lys(Boc)-Cys(Trt)-Gly- on a 100 μ mol scale using a low loading Fmoc-Gly-preloaded Wang resin (0.27 mmol/g). Fragment condensation with foldamer fragment **F15** was next carried out in the same way as for the synthesis of foldamer-peptide **15** (see above).

Alloc protecting groups were removed, directly followed by chloroacetylation. The resin was cleaved with TFA/TIS/H₂O/EDT (92.5:2.5:2.5:5, v/v/v/v) and the crude product (56 mg, Figure S24a) was purified by semi-preparative RP-HPLC (gradient: from 25% to 35% solvent B over 10 minutes at 25°C) to afford 1 mg of pure compound (Figure S24b). HRMS (ESI⁺) *m/z* calcd (most abundant mass peak) for C₁₉₈H₂₅₃Cl₄N₄₈O₆₁S₄ [M+3H]³⁺ 1516.8609 found 1516.8877.

Compound 17C: After lyophilization, compound **17** (0.5 mg) was dissolved in a mixture of acetonitrile (0.6 ml) in water (1.6 ml) to reach a 0.05 mM concentration and TCEP stock solution (4 μ l, 10 mM, 0.1 equiv.) was added. The solvent mixture was freed from oxygen by Freeze-Pump-Thaw. Independently, a solution mixture of urea-buffer (1.6 ml, 8M, pH 8.5 with 0.1 M NaH₂PO₄) in acetonitrile (0.6 ml) was prepared, oxygen removed, by Freeze-Pump-Thaw and the Foldamer solution added via syringe under inert gas atmosphere. The mixture was quickly stirred and left without stirring for 24h at RT. The progression of the macrocyclization was monitored by RP-HPLC. Benzyl mercaptan (12 μ l) was added to block unreacted chloroacetamide groups and the reaction mixture and was stirred at RT for 5 h. After neutralizing the reaction with HCl (0.1 M) solvents were

removed, by lyophilisation (Figure S24c). HRMS (ESI⁺) *m/z* calcd (most abundant mass peak) for C₁₉₈H₂₄₉N₄₈O₆₁S₄ [M+3H]³⁺ 1468.2258 found 1468.2336. No final purification was performed.

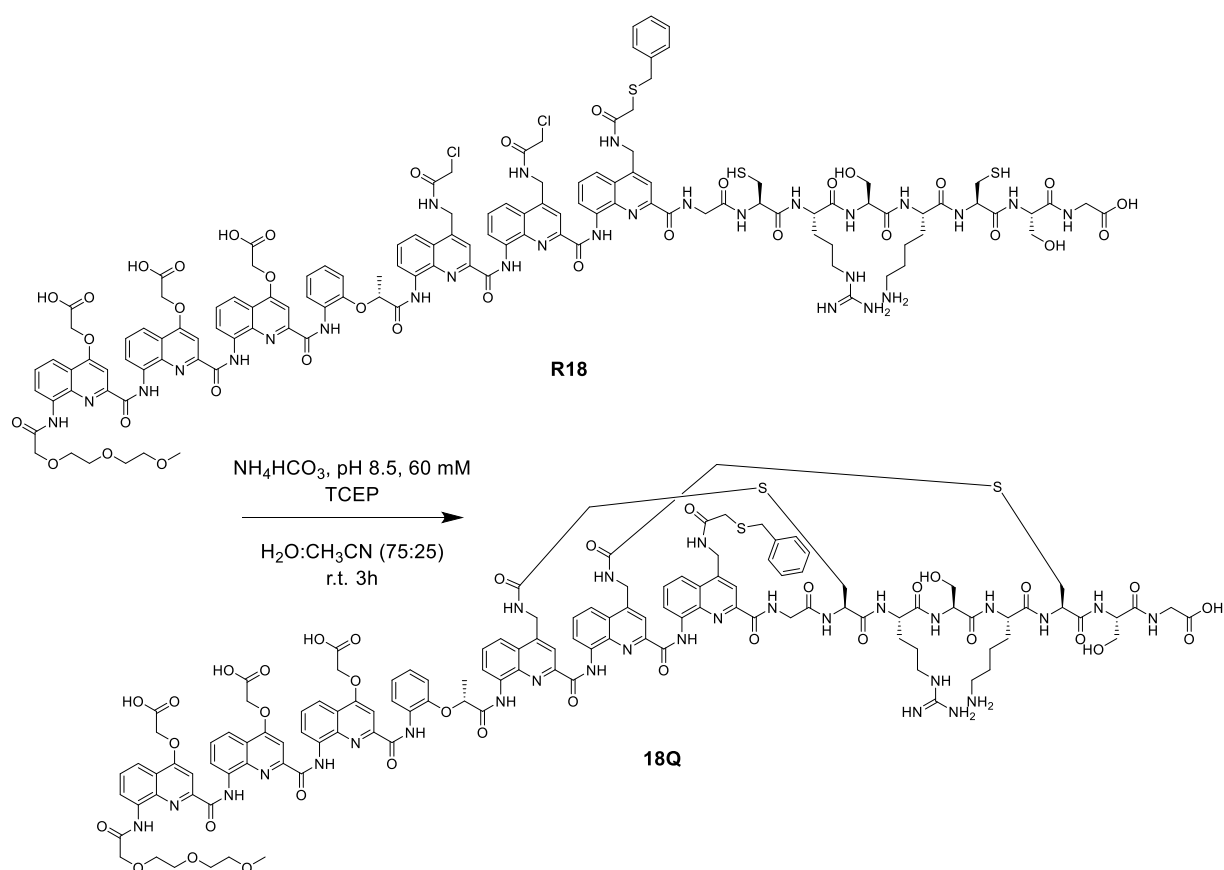


Compound 18: Foldamer-peptide **18** was built on a 25 μmol scale using a Low loading Fmoc-Gly-preloaded Wang resin (0.33 mmol/g). After terminal DEG installation, the Alloc protecting groups were removed, directly followed by chloroacetylation. The resin was cleaved with TFA/TIS/ H_2O /DODT (92.5:2.5:2.5:2.5, v/v/v/v) and the crude product (57 mg, 85%, Figure S26a) was purified by semi-preparative RP-HPLC (gradient: from 25% to 45% solvent B over 8 minutes at 25°C) to afford 8 mg of pure compound (Figure 26b). HRMS (ESI⁺) m/z calcd (most abundant mass peak) for $\text{C}_{119}\text{H}_{127}\text{Cl}_3\text{N}_{28}\text{O}_{35}\text{S}_2$ $[\text{M}+\text{H}]^+$ 2679.7612 found 2679.8652

Compound 18C: After lyophilization, compound **18** (7 mg) was dissolved in a mixture of acetonitrile (6 ml) in water (19 ml) to reach a 0.1 mM concentration and TCEP stock solution (25 μl , 10 mM, 0.1 equiv.). The solvent mixture was freed from oxygen by Freeze-Pump-Thaw. Independently, a solution of NH_4HCO_3 (37 ml, 60 mM, pH 8.5) in acetonitrile (13 ml) was prepared, oxygen removed, by Freeze-Pump-Thaw and the Foldamer solution added via syringe under inert gas atmosphere. The mixture was quickly stirred and left without stirring for 3 h at RT. The progression of the macrocyclization was monitored by RP-HPLC. After 3 h, the reaction mixture was quenched with TFA

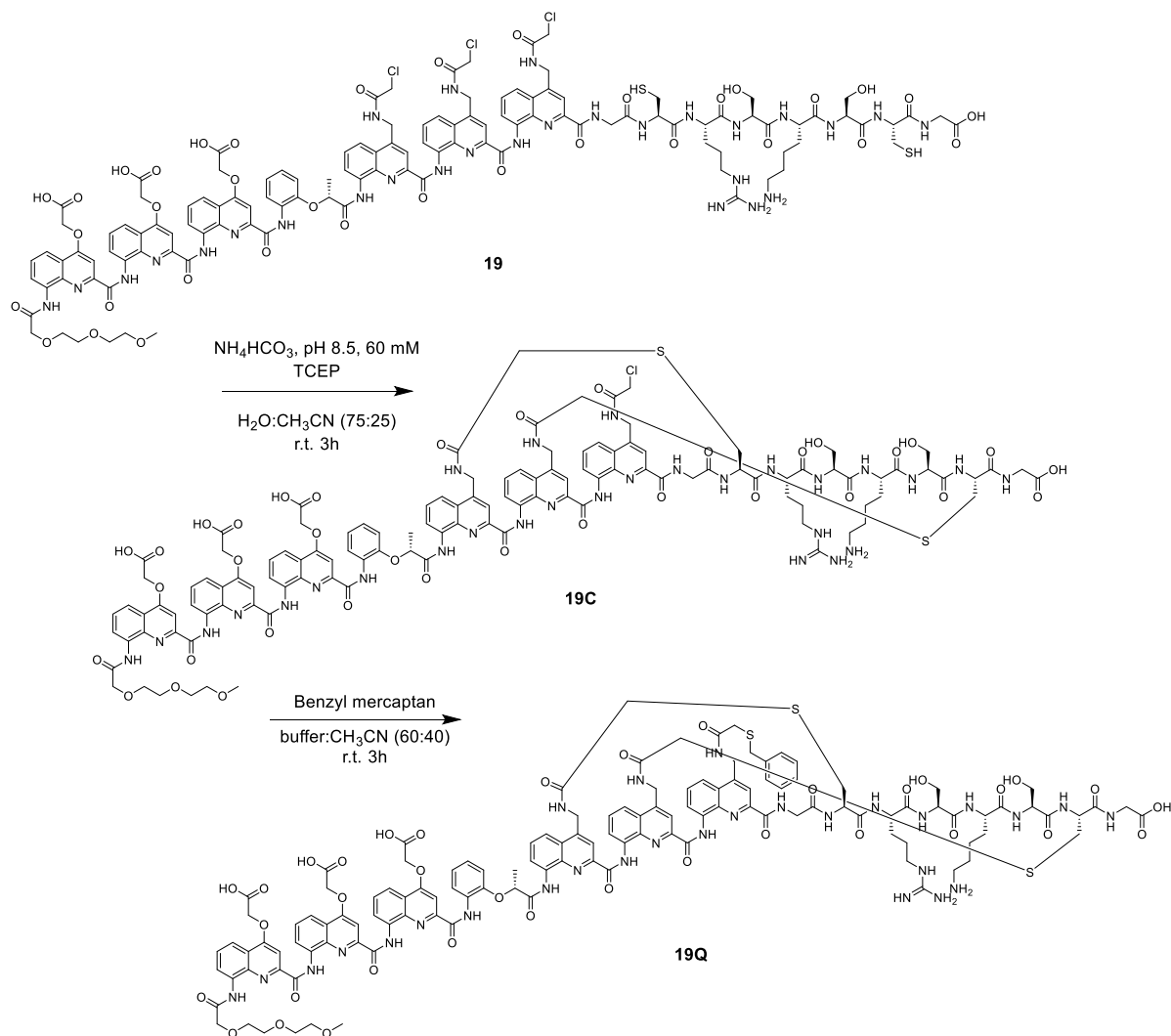
and the remaining solvent lyophilized. The obtained crude product was used in the subsequent reaction without further purification (Figure S26c). HRMS (ESI⁺) *m/z* calcd (most abundant mass peak) for C₁₁₉H₁₂₅ClN₂₈O₃₅S₂ [M+2H]²⁺ 1304.4085 found 1304.4665.

Compound 18Q: Compound **18Q** (6.8 mg) was dissolved in 1:1 mixture of NH₄HCO₃ buffer (60 mM, pH 8.5) in acetonitrile (0.4 ml total), benzyl mercaptan (4 μl) was added and the reaction mixture was stirred at RT for 16 h. Solvents were removed, by lyophilization. Pure compound was isolated after semi-preparative RP-HPLC purification with a gradient from 25% to 45% solvent B over 10 min at RT (Figure S26e). HRMS (ESI⁺) *m/z* calcd (most abundant mass peak) for C₁₂₆H₁₃₂N₂₈O₃₅S₃ [M+2H]²⁺ 1347.9373 found 1348.0021.



Compound R18: Foldamer-peptide **R18** was built on a 25 μmol scale using a Low loading Fmoc-Gly-preloaded Wang resin (0.33 mmol/g). After terminal DEG installation, the Alloc protecting groups were removed, directly followed by chloroacetylation. The resin was cleaved with TFA/TIS/H₂O/DODT (92.5:2.5:2.5:2.5, v/v/v/v) and the crude product (50 mg, 72%, Figure S27a) was purified by semi-preparative RP-HPLC (gradient: from 30% to 50% solvent B over 10 minutes at 25°C) to afford 5 mg of pure compound (Figure S27b). HRMS (ESI⁺) *m/z* calcd (most abundant mass peak) for C₁₂₆H₁₃₆Cl₂N₂₈O₃₅S₂ [M+2H]²⁺ 1384.4136 found 1384.4135.

Compound 18Q: After lyophilization, compound **R18** (5 mg) was dissolved in a mixture of acetonitrile (6 ml) in water (12 ml) to reach a 0.1 mM concentration and TCEP stock solution (18 μ l, 10 mM, 0.1 equiv.) was added. The solvent mixture was freed from oxygen by Freeze-Pump-Thaw. Independently, a solution of NH_4HCO_3 (24 ml, 60 mM, pH 8.5) in acetonitrile (12 ml) was prepared, oxygen removed, by Freeze-Pump-Thaw and the Foldamer solution added via syringe under inert gas atmosphere. The mixture was quickly stirred and left without stirring for 2 h at RT. The progression of the macrocyclization was monitored by RP-HPLC. After 2 h, the reaction mixture was quenched with TFA and the remaining solvent lyophilized (Figure S27c). The obtained crude product was purified by semi-preparative RP-HPLC with a gradient from 25% to 45% solvent B over 10 min at RT (Figure S27d). ^1H NMR (500 MHz, CD_3CN) δ 11.69 (s, 1H), 11.12 (s, 1H), 10.63 (s, 1H), 10.54 (s, 1H), 9.63 (d, $J = 17.9$ Hz, 2H), 9.41 (s, 1H), 9.32 (s, 1H), 8.94 (d, $J = 9.3$ Hz, 1H), 8.71 (d, $J = 8.8$ Hz, 2H), 8.46 (d, $J = 9.3$ Hz, 1H), 8.28 (s, 2H), 8.21 – 7.47 (m, 27H), 7.52 – 7.24 (m, 16H), 7.24 – 6.77 (m, 13H), 6.70 (s, 1H), 6.60 – 6.31 (m, 3H), 6.25 (d, $J = 9.5$ Hz, 1H), 6.01 (t, $J = 9.1$ Hz, 1H), 5.50 – 5.25 (m, 1H), 5.02 (d, $J = 23.3$ Hz, 2H), 4.8-3.9 (water suppression region) 3.58 (d, $J = 17.0$ Hz, 2H), 3.47 – 2.88 (m, 19H), 2.88 – 2.65 (m, 9H), 2.65 – 2.33 (m, 5H), 1.55 (d, $J = 69.2$ Hz, 5H), 1.45 – 1.10 (m, 5H), 1.10 – 0.69 (m, 2H), -0.32 (d, $J = 7.0$ Hz, 3H). HRMS (ESI⁺) m/z calcd (most abundant mass peak) for $\text{C}_{126}\text{H}_{134}\text{N}_{28}\text{O}_{35}\text{S}_3$ $[\text{M}+2\text{H}]^{2+}$ 1347.9376 found 1347.9450.

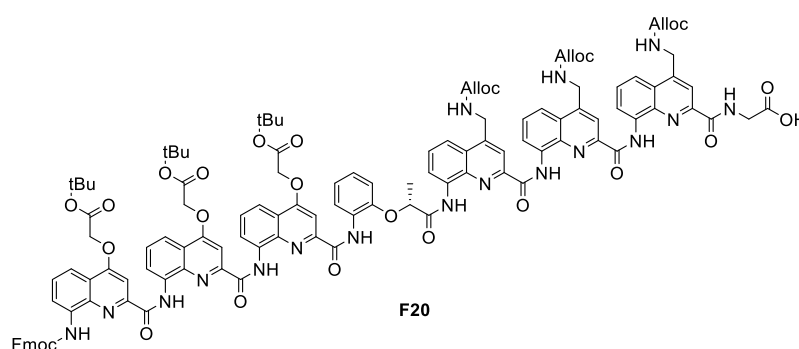


Compound 19: Foldamer-peptide **19** was built on a 25 μmol scale using a low loading Fmoc-Gly-preloaded Wang resin (0.33 mmol/g). After terminal DEG installation, the Alloc protecting groups were removed, directly followed by chloroacetylation. The resin was cleaved with TFA/TIS/ H_2O /DODT (92.5:2.5:2.5:2.5, v/v/v/v) and the crude product (50 mg, 75%, Figure S29a) was purified by semi-preparative RP-HPLC (gradient: from 25% to 45% solvent B over 8 minutes at 25°C) to afford 5 mg of pure compound (Figure S29b). HRMS (ESI⁺) m/z calcd (most abundant mass peak) for $\text{C}_{119}\text{H}_{127}\text{Cl}_3\text{N}_{28}\text{O}_{35}\text{S}_2$ [M+H]⁺ 2679.7612 found 2679.8642.

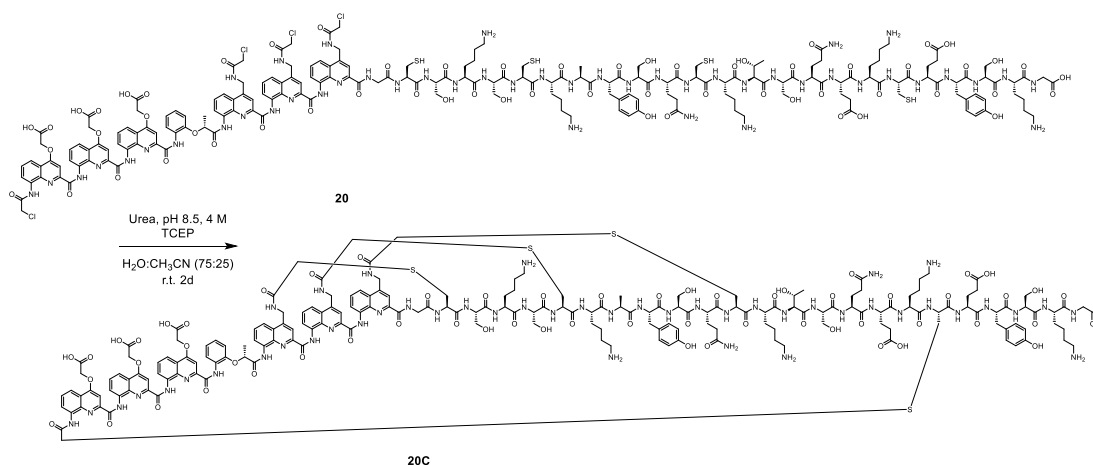
Compound 19C: After lyophilization, compound **19** (2.7 mg) was dissolved in a mixture of acetonitrile (2.5 ml) in water (7.5 ml) to reach a 0.1 mM concentration and TCEP stock solution (10 μl , 10 mM, 0.1 equiv.) was added. The solvent mixture was freed from oxygen by Freeze-Pump-Thaw. Independently, a solution of NH_4HCO_3 (15 ml, 60 mM, pH 8.5) in acetonitrile (5 ml) was prepared, oxygen removed, by Freeze-Pump-Thaw and the Foldamer solution added via syringe under inert gas atmosphere. The mixture was quickly stirred and left without stirring for 3 h at RT. The progression of the macrocyclization was monitored by RP-HPLC. After 3 h, the reaction mixture

was neutralized with formic acid and the remaining solvent lyophilized. The obtained crude product was used in the subsequent reaction without further purification (Figure S29c). HRMS (ESI⁺) *m/z* calcd (most abundant mass peak) for C₁₁₉H₁₂₅ClN₂₈O₃₅S₂ [M+2H]²⁺ 1304.4085 found 1304.4509.

Compound 19Q: Compound **19C** (2.0 mg) was dissolved in 1:1 mixture of NH₄HCO₃ buffer (60 mM, pH 8.5) in acetonitrile (0.4 ml total), benzyl mercaptan (4 μl) was added and the reaction mixture was stirred at RT for 8 h. Solvents were removed, by lyophilization. Pure compound was isolated after semi-preparative RP-HPLC purification with a gradient from 25% to 45% solvent B over 10 min at RT (Figure S29e). HRMS (ESI⁺) *m/z* calcd (most abundant mass peak) for C₁₂₆H₁₃₄N₂₈O₃₅S₃ [M+2H]²⁺ 1347.9878 found 1347.9450.



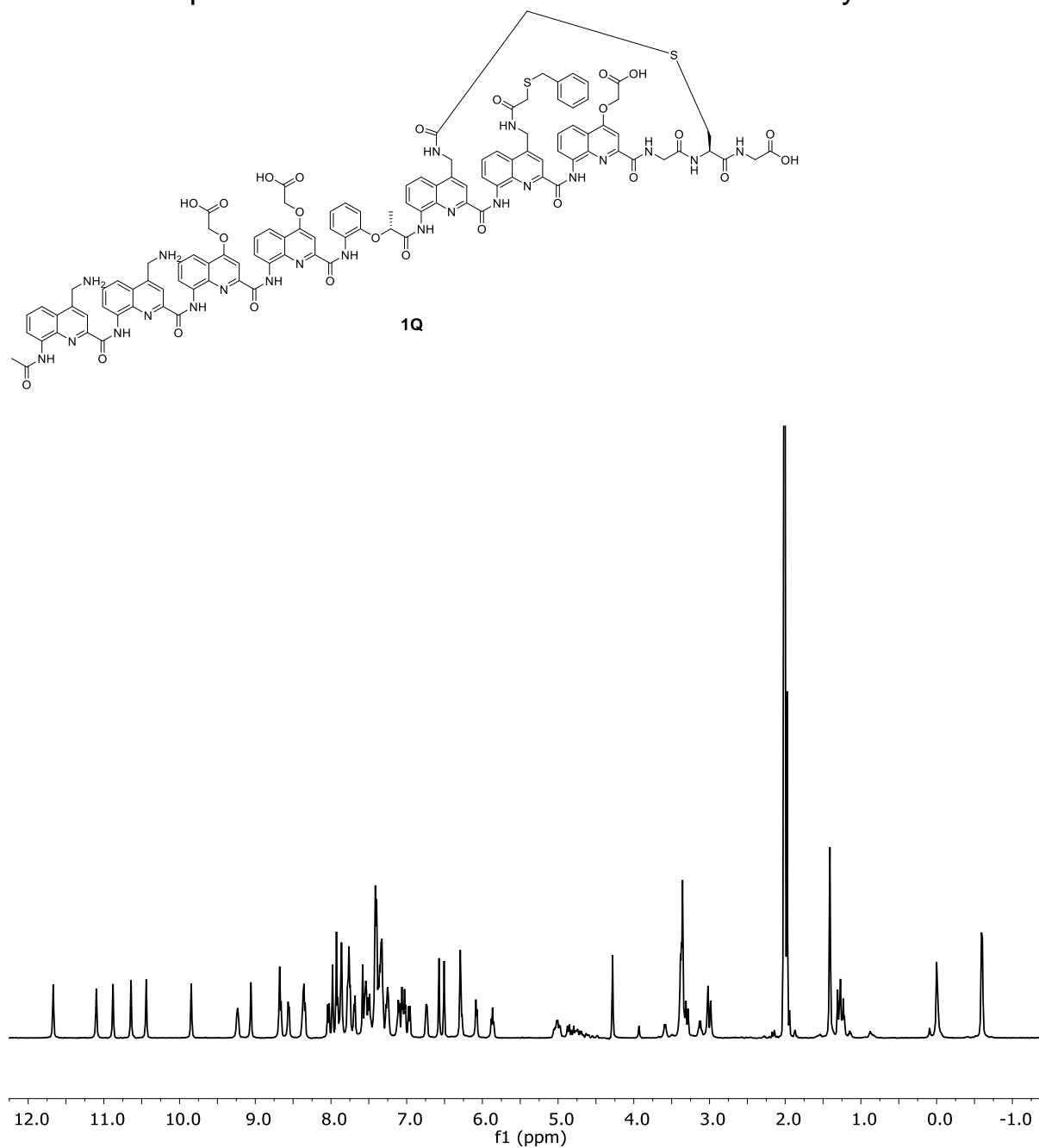
Foldamer fragment F20: **F20** was synthesized on a preloaded Fmoc-Gly-SASRIN resin (0.72 mmol/g) using general SPFS procedure on a 50 μmol scale. Crude **F20** was recovered in 83% yield (90 mg) after cleavage using a mixture of HFIP in DCM (6 ml, 80:20, v/v) 2 × 30 min at r.t. The obtained crude product was purified by semi-preparative HPLC (gradient: from 90% to 100% solvent B over 10 minutes at 25°C) to achieve 51 mg purified compound. HRMS (ESI⁻) *m/z* calcd for C₁₁₁H₁₁₁N₁₇O₂₇ [M+2H]²⁺ 1106.4007 found 1106.4142.



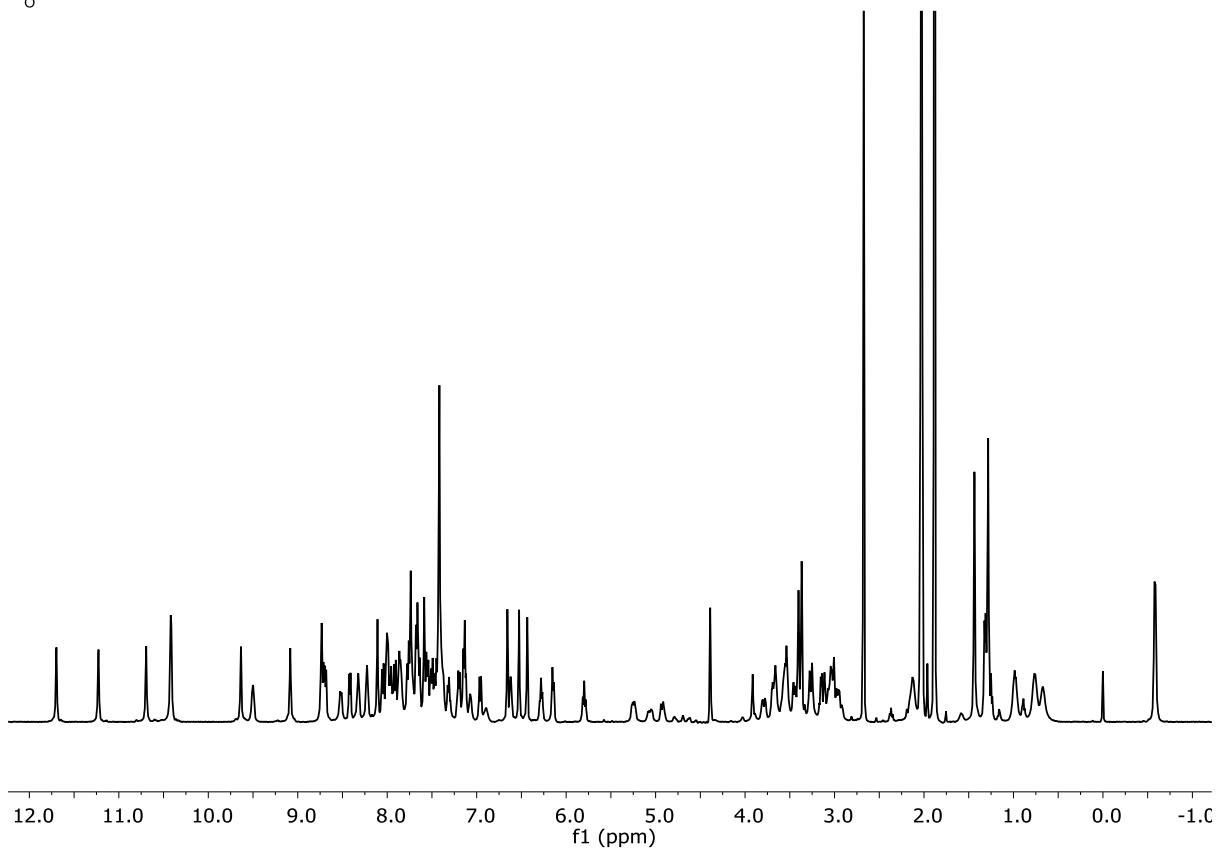
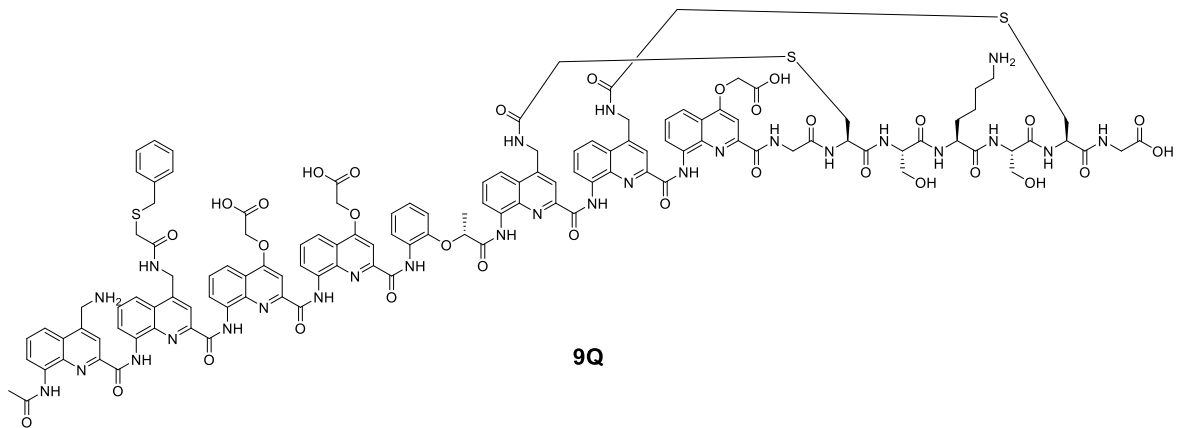
Compound 20: Foldamer-peptide **20** was built by relying on the CEM Liberty Blue microwave peptide synthesizer for the protected resin-bound Fmoc-Cys(Trt)-Ser(tBu)-Lys(Boc)-Ser(tBu)-Cys(Trt)-Lys(Boc)-Ala-Tyr(tBu)-Ser(tBu)-Gln(Trt)-Cys(Trt)-Lys(Boc)-Thr(tBu)-Ser(tBu)-Gln(Trt)-Glu(tBu)-Lys(Boc)-Cys(Trt)-Glu(tBu)-Tyr(tBu)-Ser(tBu)-Lys(Boc)-Gly- peptide on a 100 μ mol scale using a low loading Fmoc-Gly-preloaded Wang resin (0.27 mmol/g). Fragment condensation with foldamer fragment **F20** was next performed on a 25 μ mol scale of resin-bound free amine peptide. Fragment condensation with foldamer fragment **F20** was next carried out in the same way as for the synthesis of foldamer-peptide **20** (see above). Fmoc was deprotected followed by the removal of Alloc protecting groups, directly followed by chloroacetylation. The resin was cleaved with TFA/TIS/H₂O/EDT (92.5:2.5:2.5:2.5, v/v/v/v) and the crude product (50 mg, Figure S30a) was purified by semi-preparative RP-HPLC (gradient: from 25% to 35% solvent B over 10 minutes at 25°C) to afford 3 mg of pure compound (Figure S30b). HRMS (ESI⁺) *m/z* calcd (most abundant mass peak) for C₁₉₂H₂₃₇Cl₄N₄₇O₆₀S₄ [M+3H]³⁺ 1478.4944 found 1478.5140.

Compound 20C: After lyophilization, compound **20** (1.5 mg) was dissolved in a mixture of acetonitrile (1 ml) in water (3 ml) to reach a 0.05 mM concentration and TCEP stock solution (10 μ l, 10 mM, 0.1 equiv.). The solvent mixture was freed from oxygen by Freeze-Pump-Thaw. Independently, a solution mixture of urea-buffer (3 ml, 8M, pH 8.5 with 0.1 M NaH₂PO₄) in acetonitrile (1 ml) was prepared, oxygen removed, by Freeze-Pump-Thaw and the foldamer solution added via syringe under inert gas atmosphere. The mixture was quickly stirred and left without stirring for 2d at RT. The progression of the macrocyclization was monitored by RP-HPLC. After neutralizing the reaction with HCl (0.1 M), the solvents were removed, by lyophilization. The obtained crude product was purified by semi-preparative RP-HPLC (hold 100% solvent A for 5 min then gradient from 10% to 35% solvent B over 15 minutes at 25°C) to afford 0.2 mg (Figure S30d). ¹H NMR (500 MHz, CD₃CN) δ 11.76 (s, 1H), 11.32 (s, 1H), 10.61 (s, 1H), 10.55 (s, 1H), 9.70 (s, 1H), 9.61 (s, 1H), 9.42 (s, 1H), 9.31 (s, 1H), 8.79 (d, *J* = 8.4 Hz, 1H), 8.50 (d, *J* = 7.6 Hz, 4H), 8.39 (d, *J* = 8.0 Hz, 2H), 8.28 (d, *J* = 20.8 Hz, 4H), 8.15 (d, *J* = 8.9 Hz, 4H), 8.08 (d, *J* = 8.2 Hz, 2H), 8.01 (d, *J* = 13.8 Hz, 3H), 7.94 (d, *J* = 7.4 Hz, 4H), 7.90 – 7.79 (m, 4H), 7.72 (s, 2H), 7.69 – 7.51 (m, 11H), 7.51 – 7.21 (m, 28H), 7.17 (d, *J* = 36.0 Hz, 4H), 7.09 – 6.91 (m, 5H), 6.73 – 6.30 (m, 11H), 6.30 – 6.05 (m, 5H), 5.94 (t, *J* = 8.2 Hz, 1H), 5.54 (d, *J* = 49.4 Hz, 10H), 5.05 (d, *J* = 30.5 Hz, 8H), 3.89 – 3.37 (m, 36H), 3.37 – 3.09 (m, 19H), 3.09 – 2.46 (m, 41H), 1.64 (d, *J* = 99.7 Hz, 31H), 1.39 – 1.23 (m, 34H), 1.23 – 0.78 (m, 21H), -0.34 (d, *J* = 6.6 Hz, 3H). HRMS (ESI⁺) *m/z* calcd (most abundant mass peak) for C₁₉₂H₂₃₃N₄₇O₆₀S₄ [M+2H]²⁺ 2144.2816 found 2144.2216.

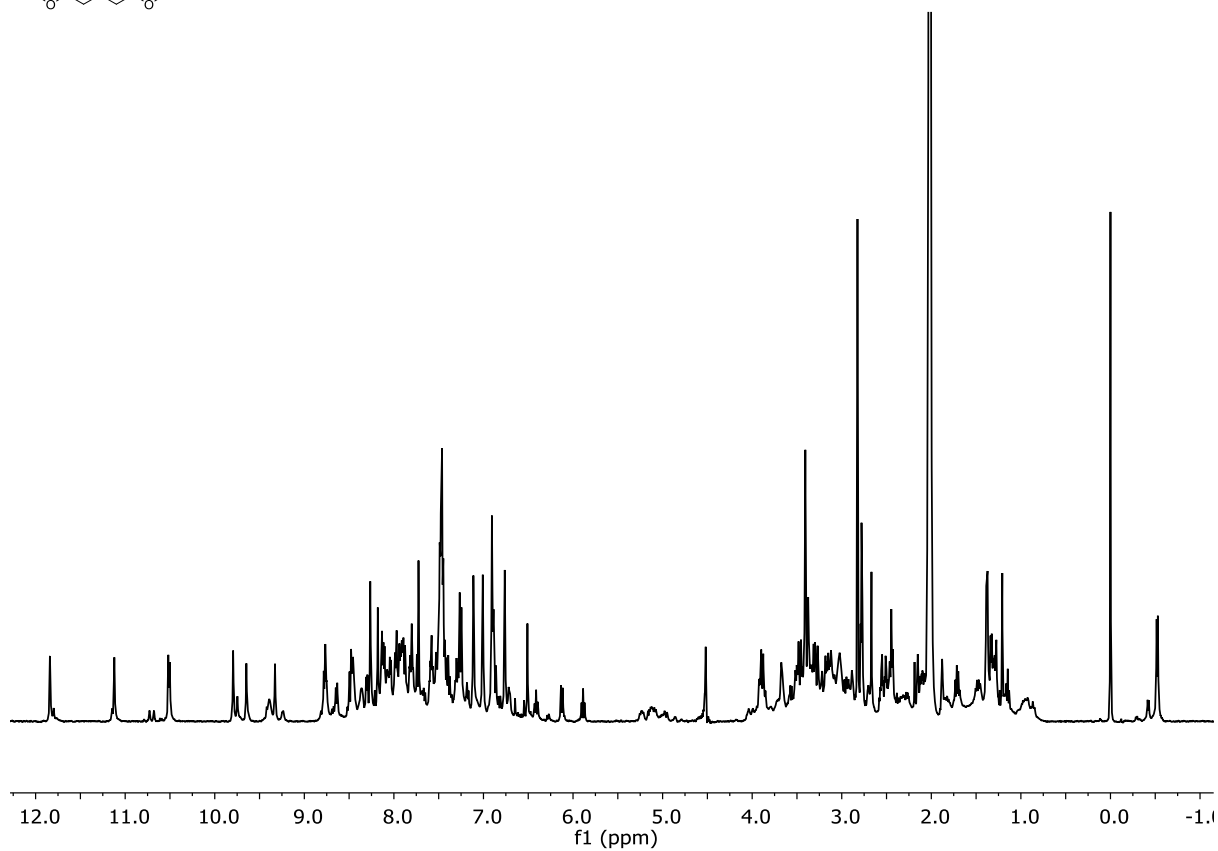
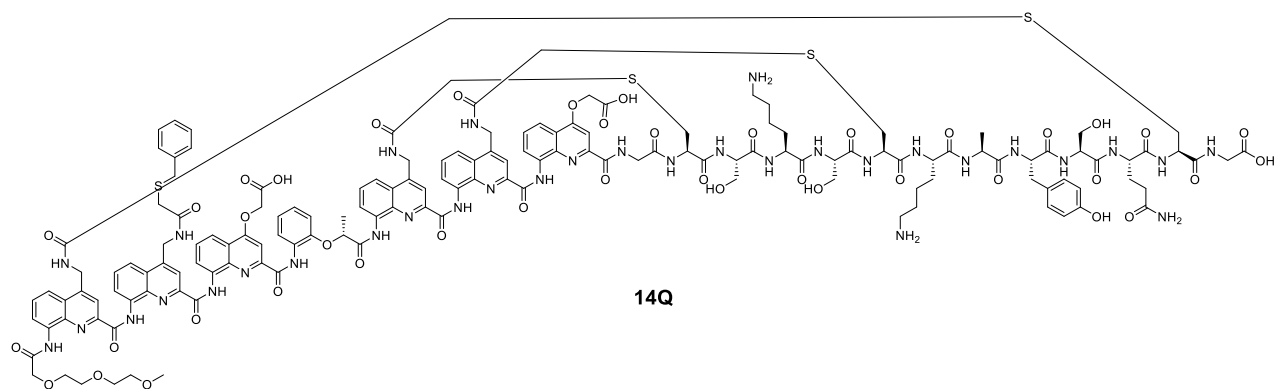
11.3. NMR spectra of new monomers and isolated macrocycles



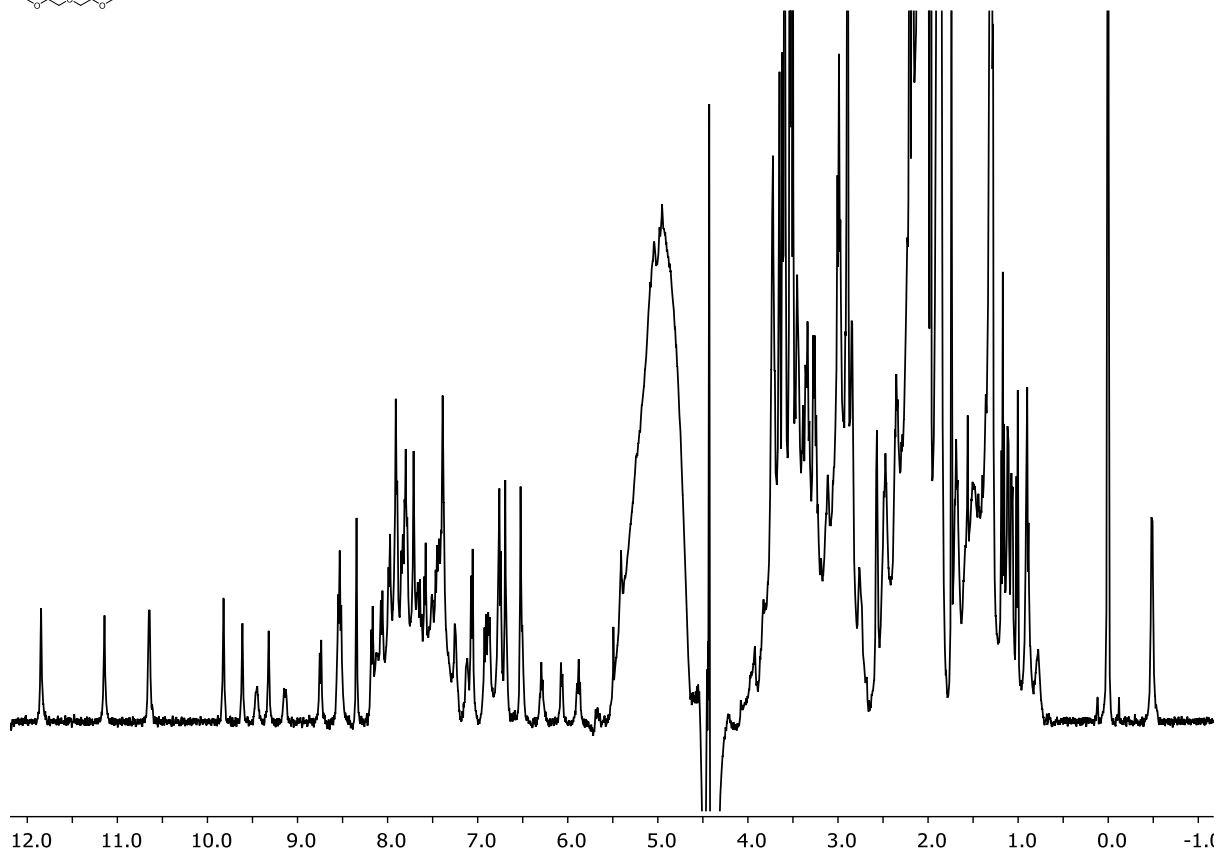
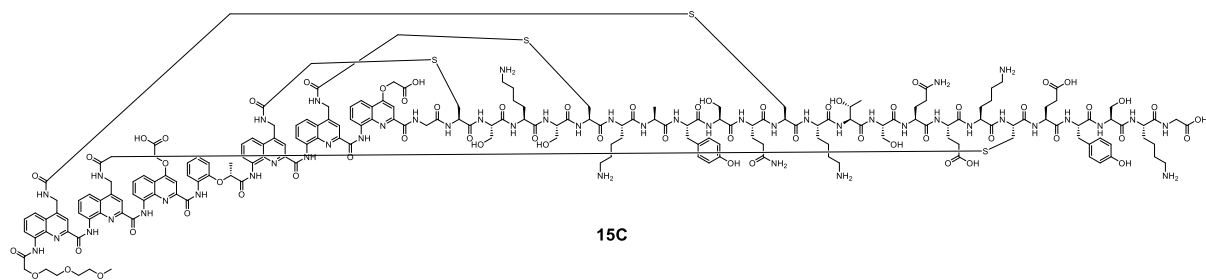
¹H NMR Spectrum of **1Q** recorded in a mixture of NH₄OAc (3mM, pH 8.5) in CD₃CN (50:50, v/v) with the addition of TMS (500 MHz, 25°C).



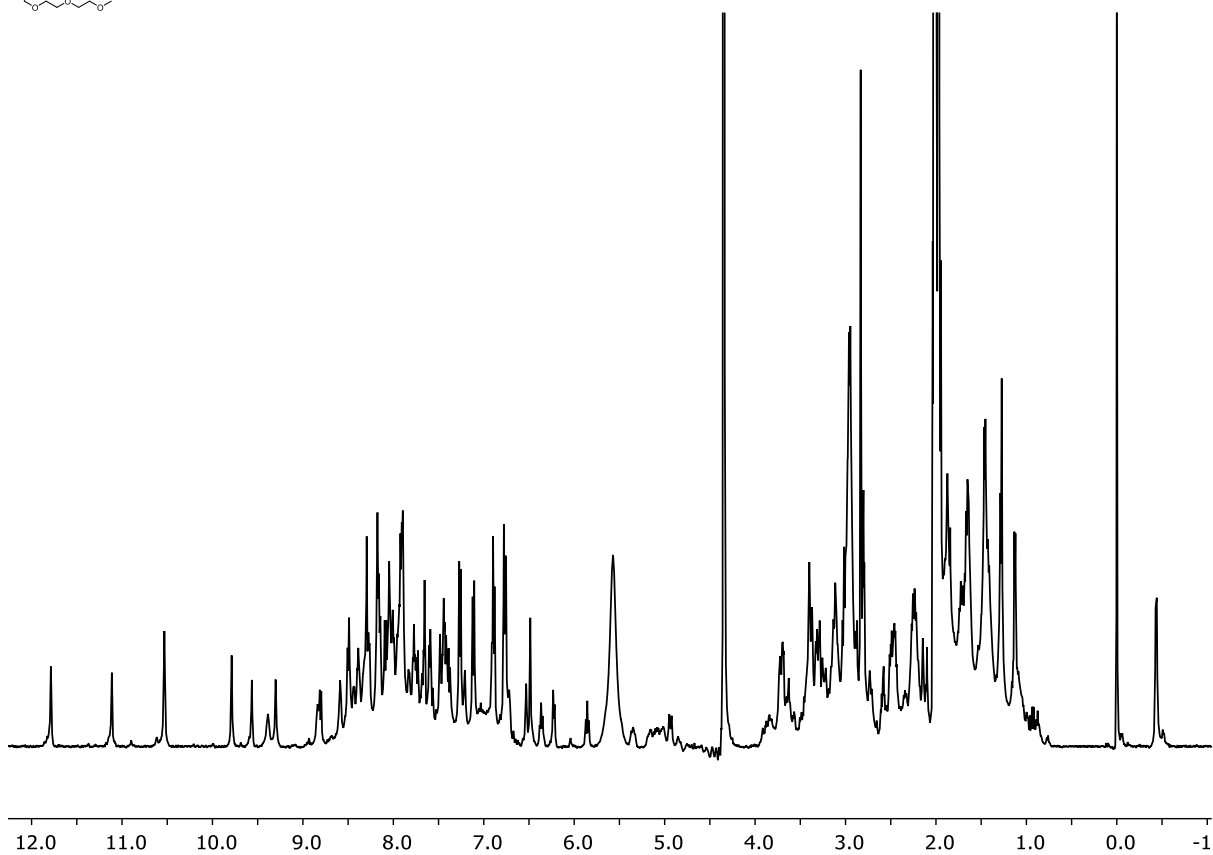
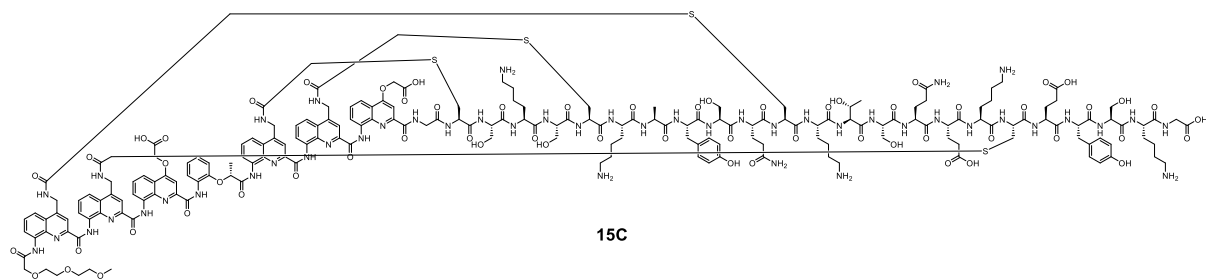
1H NMR Spectrum of 9Q recorded in a mixture of NH₄OAc (3mM pH 8.5) in CD₃CN (50:50, v/v) with the addition of TMSP (500 MHz, 25°C).



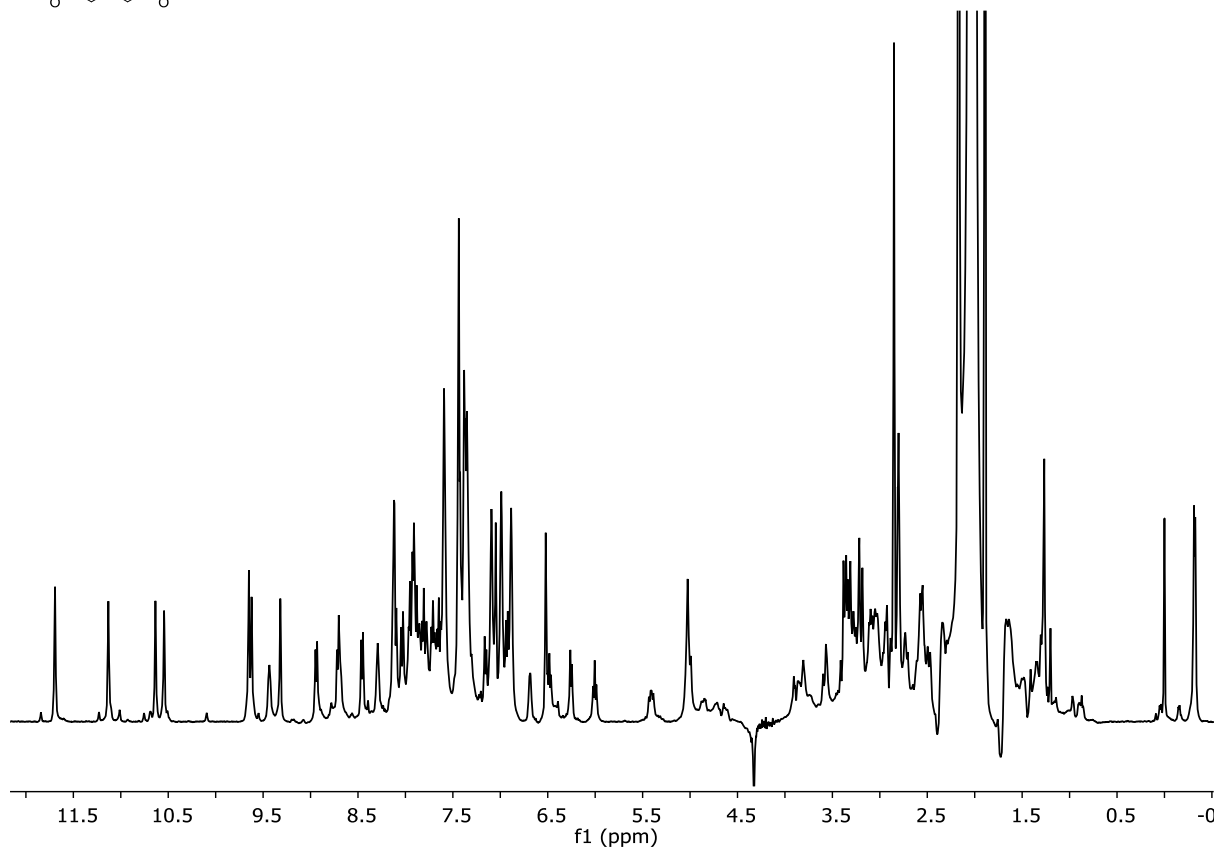
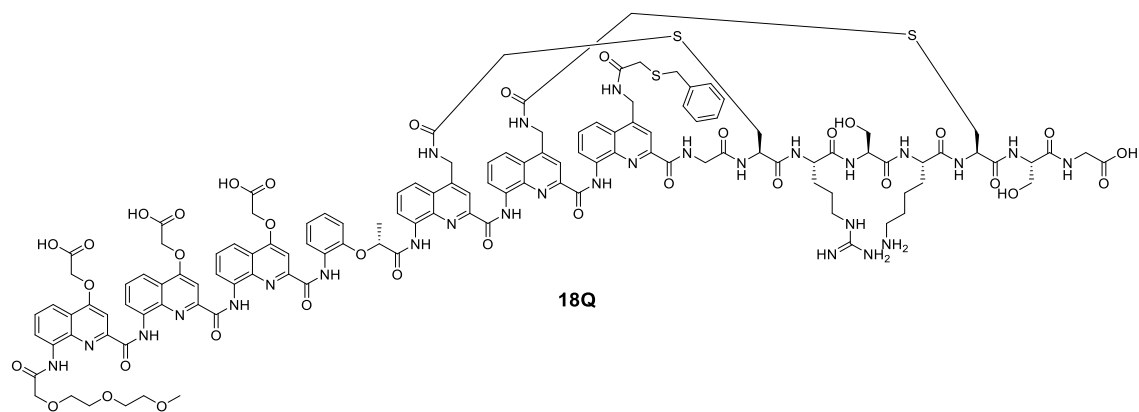
1H NMR Spectrum of 14Q recorded in a mixture of NH_4OAc (3mM pH 8.5) in CD_3CN (50:50, v/v) with the addition of TMSP (500 MHz, 25°C).



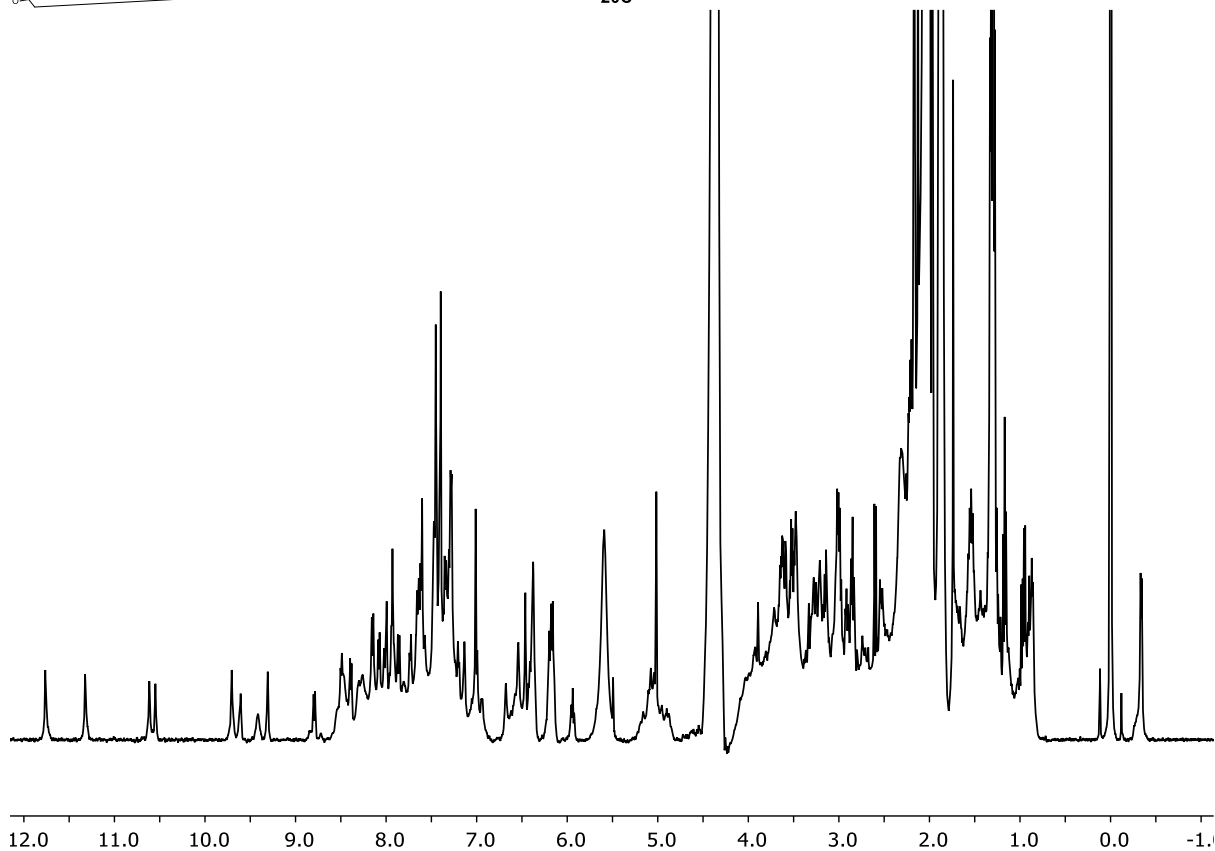
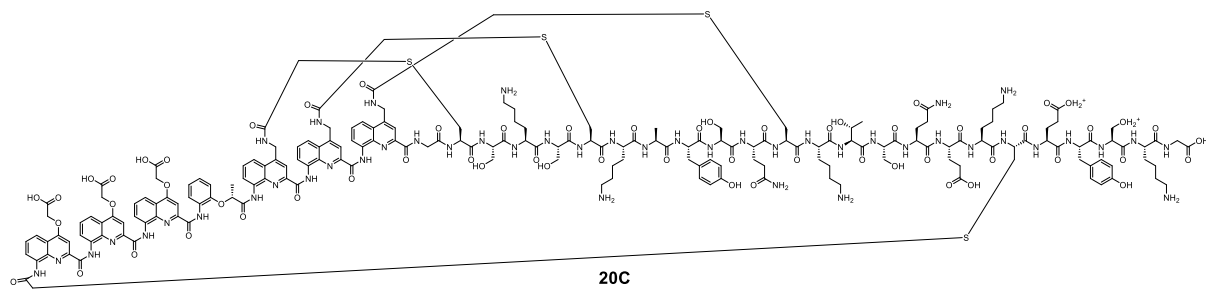
¹H NMR Spectrum of 15C-a recorded in a mixture of NH₄OAc (3mM, pH 8.5) in CD₃CN (50:50, v/v) with the addition of TMS (500 MHz, 25°C). Similar NMR signal patterns of 15C-a and 15C-b indicate that helices are similarly folded.



1H NMR Spectrum of 15C-b recorded in a mixture of NH_4OAc (3mM pH 8.5) in CD_3CN (50:50, v/v) with the addition of TMS (500 MHz, 25°C). Similar NMR signal patterns of 15C-a and 15C-b indicate that helices are similarly folded.

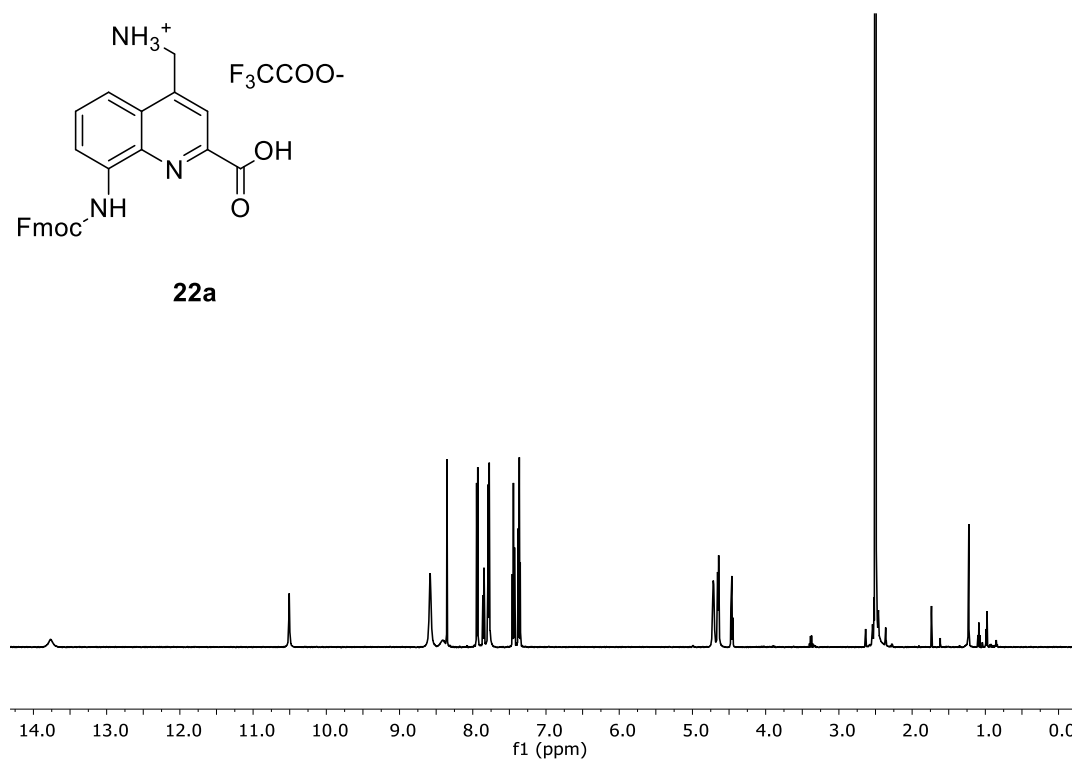
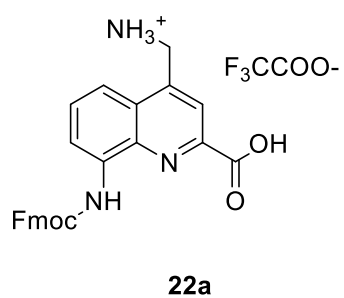


1H NMR Spectrum of 18Q recorded in a mixture of NH_4OAc (3mM pH 8.5) in CD_3CN (50:50, v/v) with the addition of TMSP (500 MHz, 25°C).

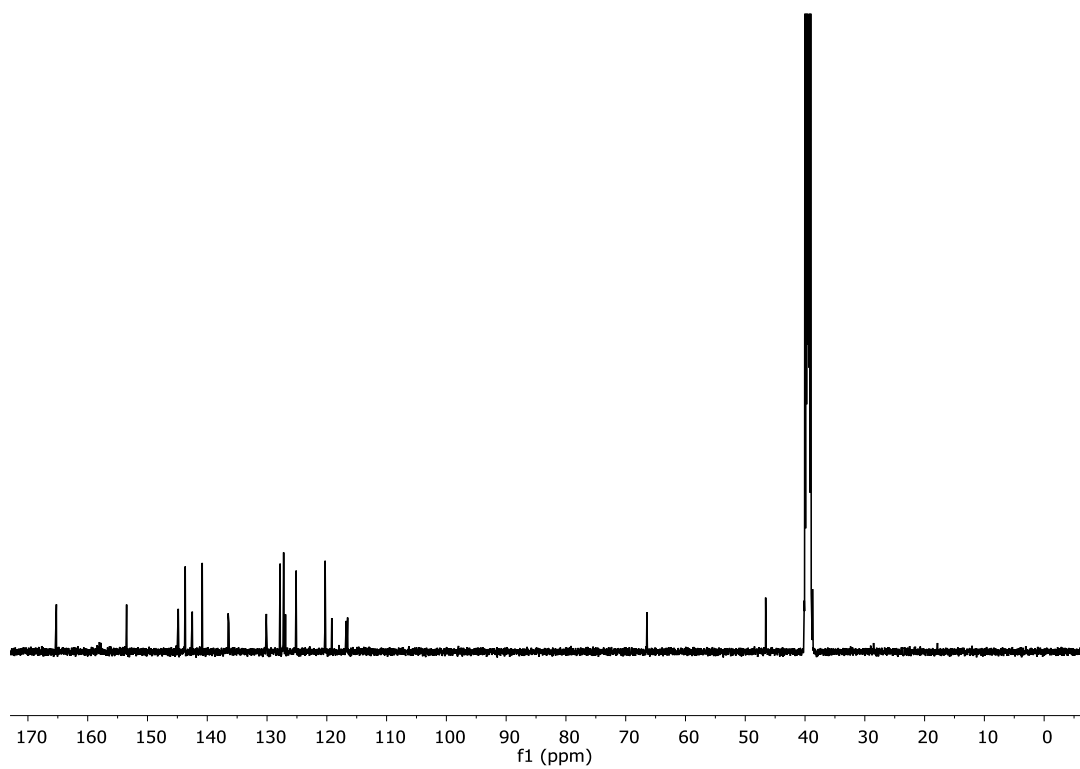


1H NMR Spectrum of 20C recorded in a mixture of NH₄OAc (3mM pH 8.5) in CD₃CN (50:50, v/v) with the addition of TMSIP (500 MHz, 25°C).

Compound **22a**

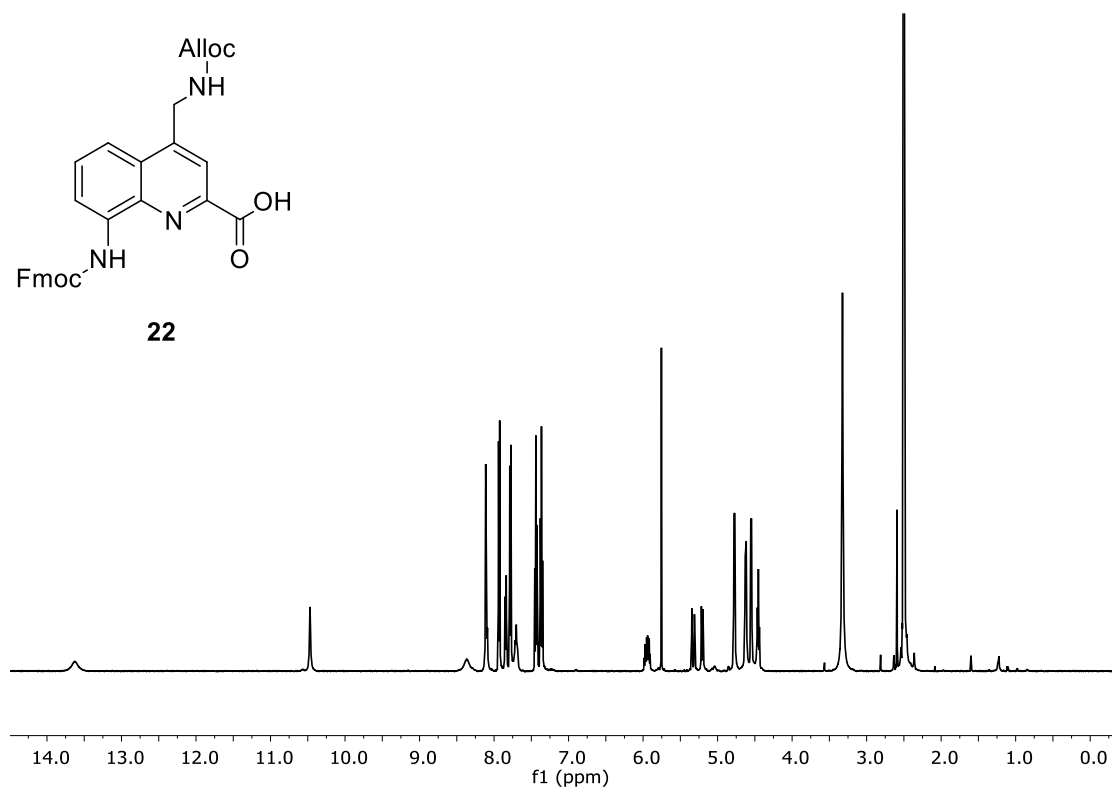
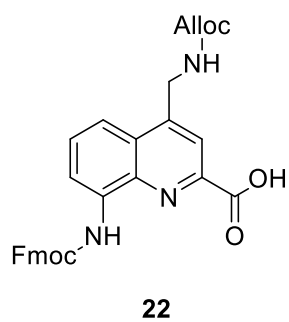


^1H NMR Spectrum of **22a** recorded in $\text{DMSO-}d_6$ (500 MHz, 25 °C)

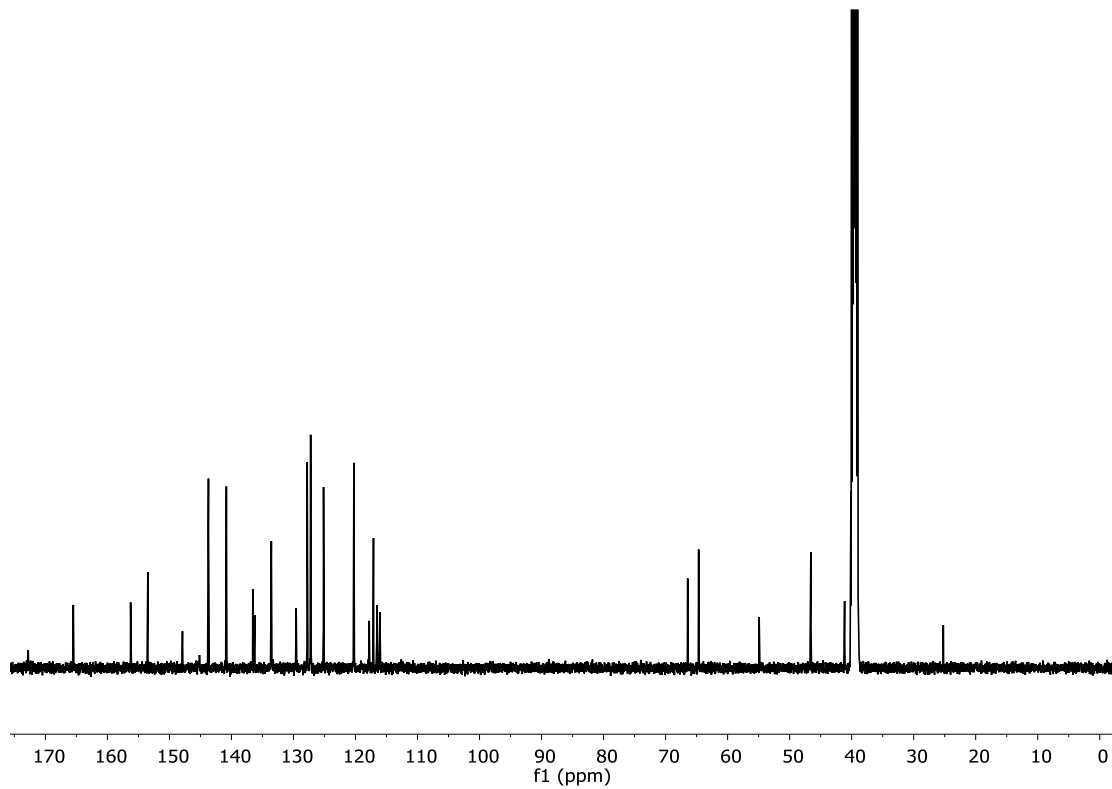


^{13}C NMR Spectrum of **22a** recorded in $\text{DMSO-}d_6$ (126 MHz, 25 °C).

Compound **22**

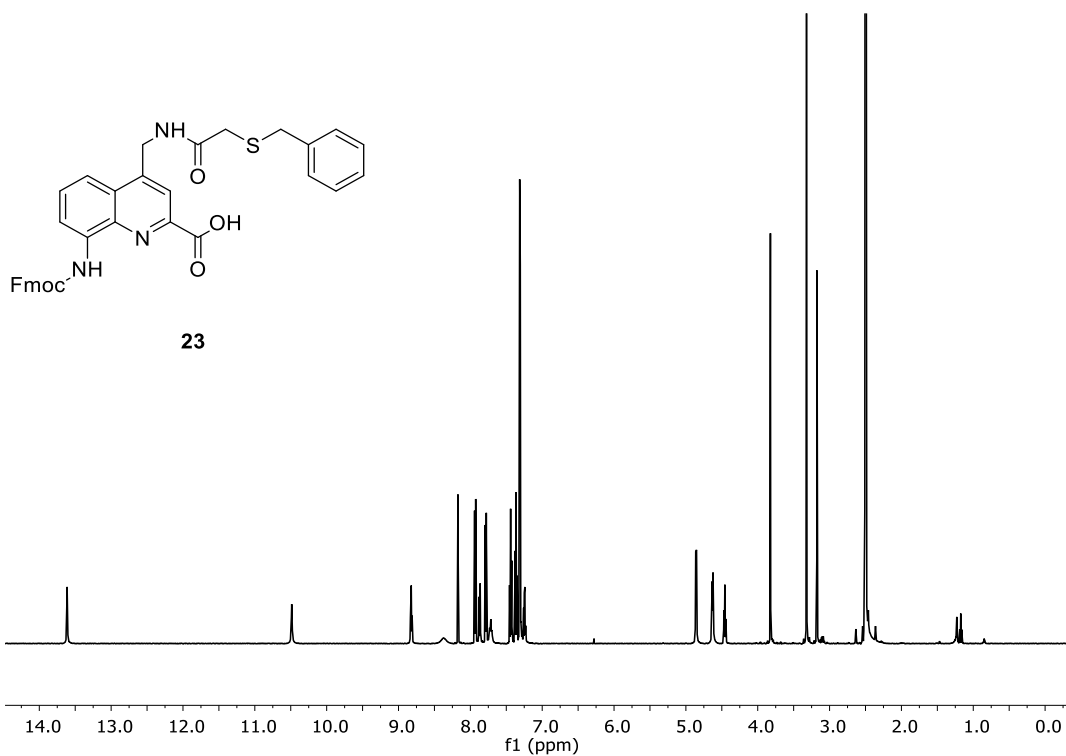


¹H NMR Spectrum of **22** recorded in DMSO-*d*₆ (500 MHz, 25 °C).

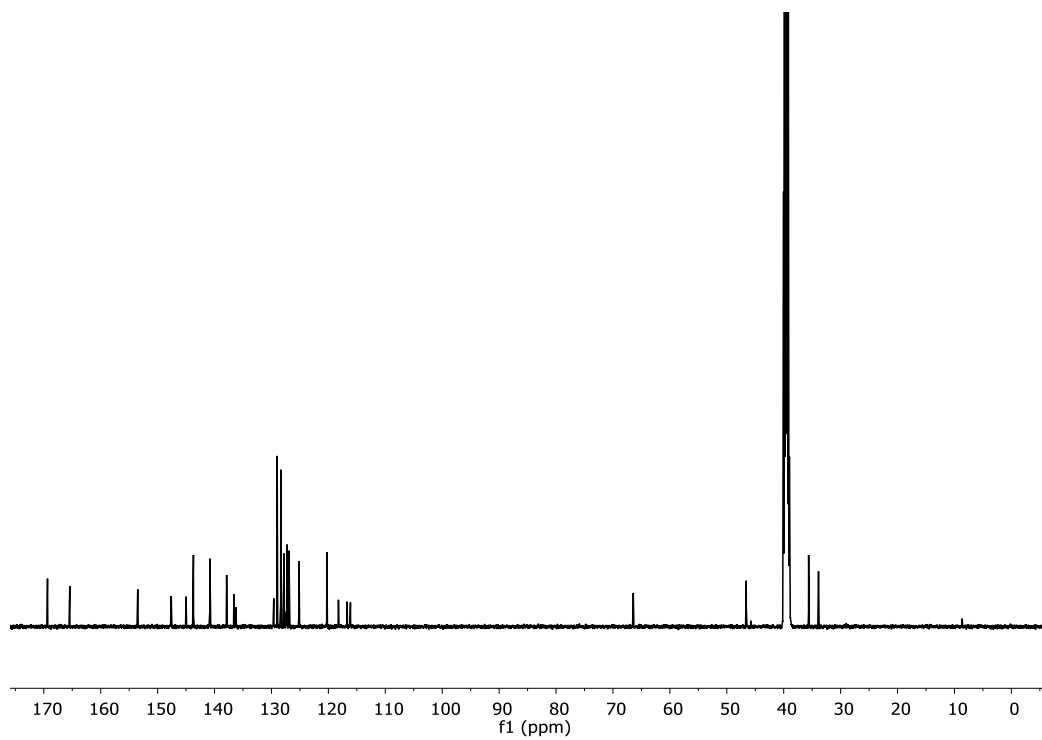


¹³C NMR Spectrum of **22** recorded in DMSO-*d*₆ (126 MHz, 25 °C).

Compound **23**



^1H NMR Spectrum of **23** recorded in $\text{DMSO-}d_6$ (500 MHz, 25 °C).



^{13}C NMR Spectrum of **23** recorded in $\text{DMSO-}d_6$ (126 MHz, 25 °C).

References

1. a) M. Vallade, P. Sai Reddy, L. Fischer, I. Huc, *Eur. J. Org. Chem.*, **2018**, 2018, 5489-5498. b) X. Hu, S. J. Dawson, P. K. Mandal, X. de Hatten, B. Baptiste, I. Huc, *Chem. Sci.*, **2017**, 8, 3741-3749. c) D. Bindl, E. Heinemann, P. K. Mandal, I. Huc, *Chem. Commun.*, **2021**, 57, 5662-5665.
2. S. Dengler, P. K. Mandal, L. Allmendinger, C. Douat, I. Huc. *Chem. Sci.*, **2021**, 12, 11004-11012.

12. Summary and Perspective

The purpose of this PhD thesis was first to investigate the interplay of peptide and aromatic foldamer conformation in hybrid macrocycles of various lengths and compositions. We could show that independent of its length (3–6 α -amino acid residues) or charge state (from -5 to +1 at neutral pH), the peptide strongly biases the helix handedness of aromatic foldamer segments composed of quinoline (**Q**)- and aminomethylpyridine (**P**)-type monomers. Results show that when α -amino acid residues in the peptide have L-configuration, the foldamers were biased towards a *P*-helix via remote communication between the two segments. In addition, the peptide stabilizes the helical folding of the foldamer, which was further proven with achiral Gly-based peptide-foldamer hybrid macrocycles. Reciprocally, the foldamer acts as some sort of staple, which (i) stretches short peptide segments and (ii) preserves the overall peptide conformation. Additionally, a hybrid macrocycle composed of nine aromatic units and five α -amino acid residues was synthesized. The foldamer segment contained multiple **P** units, which promote the unfolding of the foldamer in organic solvent so much that interconversion between the (*P*) and (*M*) equilibrium is expected to be fast. This folding disruption of the linear sequence made cyclization possible (the helically folded nonamer and the peptide loop did not cyclize in aqueous environment) through partially unfolded states. In water, the macrocycle showed complete (*P*)-helical folding which could be disrupted upon DMF addition. After successful macrocyclization in organic solvent, when shifting to aqueous medium the foldamer segment folded back to its canonical (*P*)-helix and forced the peptide to adopt a stretched conformation. Macrocycles with non-dynamic aromatic nonamers and composed of relatively long peptide loops (up to 13 amino acids) were also produced. The conformational analyses showed that these specific sequences resulted in diastereoisomers (no preference for the aromatic helix handedness) with different physico-chemical properties so as such allowing separation via RP-HPLC analysis. Additionally, in biodegradability studies, exemplarily picked macrocyclic hybrids showed higher resistance towards proteolytic degradation during protease exposure compared to their linear versions. These results could have a positive impact on potential *in vivo* applications. To pave the way in this direction, we wanted to demonstrate that we were able to identify peptide-foldamer macrocycles as good binders of defined protein targets *in vitro* by relying on mRNA display.

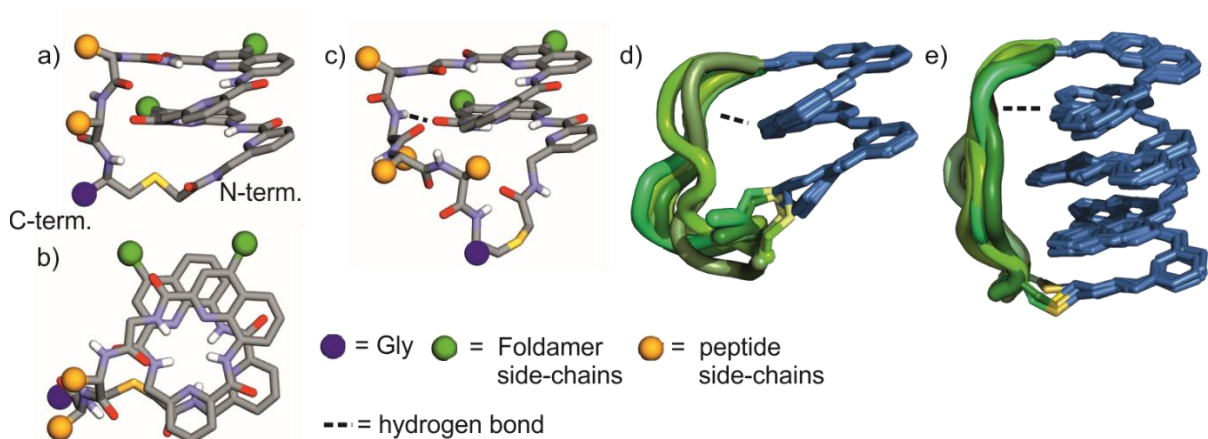


Figure 13 – Solid-state structures of a peptide-foldamer hybrid macrocycle. 1 (a, b), 3 c), 7 d) and 9 e). d) Overlay of eight different conformers obtained from the crystal structure of **7**. e) Overlay of six different conformers obtained from the crystal structure of **9**. Inter segment hydrogen bond indicated by dashed lines. Compounds numbers refer to chapter 6.

As was proven in earlier studies, short foldamers are accommodated by the ribosome and incorporated at the N-terminus of translated peptides or proteins. These sequences spontaneously cyclize after translation as the first Cys-thiol reacts with the N-terminal chloroacetamide moiety to form a thioether. In this study, we demonstrated that this system is compatible with RaPID screening platform that allows the screening of up to 10^{12} cyclic peptide candidates with non-canonical modifications and identifies binders with high target affinity. In a first step, we made slight variations on short foldamers so much so that high tRNA acylation yields and high ribosomal peptide initiation could be achieved. In this way, we were able to create a library of macrocyclic peptide-foldamer hybrids and then screen them in iterative rounds against an immobilized protein target (C-lobe domain of the E6AP HECT domain). Two libraries, each containing a tetramer foldamer in the macrocycle, with either 4-9 amino acid residues or 10–15 amino acid residues in the loop were screened, of which the library with the shorter peptide loops showed high sequence convergence. One of the identified top candidates was chemically resynthesized and successfully co-crystallized with the C-lobe domain, leading to a high-resolution X-ray crystal structure of the complex. The structure revealed that both segments of the macrocycle – the foldamer and the peptide – are helical folded. The α -helical peptide interacts with the protein surface, an area of approx. 400 \AA^2 , by hydrophobic contacts, salt bridges, and hydrogen bonds. In addition, molecular dynamics simulations could show that the Tyr11 of the macrocycle, which does not show interactions with the protein surface in the crystal but has a high convergence in the selection experiment, is stacked tight and persistent on the foldamer. The Tyr11 might act as some sort of folding stabilizer, which seemed to be crucial during selection.

To obtain data on the binding in solution between the macrocycle and the C-lobe domain, surface plasmon resonance (SPR) studies were performed, with the C-lobe (ligand) immobilized on an SPR chip and the macrocycle (analyte) in solution. The binding study revealed a K_D value of ~ 1 μM , which is a moderate affinity for the protein target with respect to most of the RaPID selection reported so far.

In another approach, the foldamer peptide macrocycles were subsequently chemically modified after the selection of a binder. Once a binder is discovered through a RaPID campaign, it is hoped that the selected macrocycle can be further modified to improve its physiochemical properties with more bulky appendages on the foldamer segment than allowed during the ribosomal synthesis. Screening of the quinoline side chains, post-selection, could indeed improve the solubility of the macrocycles and their cell-penetration capacity without affecting the overall binding affinity. Investigation of the potential of this class of compounds to penetrate biological membranes and the contribution of the foldamer patch, in general, will be explored in the future.

To further apply the concept of RaPID selection with foldamer peptide macrocycles, new protein targets are currently being investigated: Sirtuin-2 (SIRT2), a NAD-dependent deacetylase that is associated with tumorigenesis, and heterochromatin protein 1 (HP1), a conserved chromatin-binding protein that acts as a transcriptional repressor are among the proteins recently expressed and for which RaPID campaigns have been scheduled. With such biological targets, high-affinity ligands are expected to be found that might also have an inhibitory effect on the protein. To achieve this, "warheads" (*i.e.* reactive non-natural amino acid residues known to well-interact in the protein-binding site) are introduced during the selection and are aimed to guide the selection specifically to the active site of the protein.

Another project currently investigated is to exploit the α -helical conformation of the intracyclic peptide promoted by the foldamer staple in the hybrid macrocycle obtained from the C-lobe selection and apply this hybrid architecture on other relevant and well-studied α -helical peptide sequences found in protein-protein interactions. Initial experiments target the tumor suppressor P53, which interacts with the human double minute (HDM2). This interaction between P53 and the protein HDM2 is frequently corrupted in cancer cells, and inhibition of HDM2 has attracted attention in cancer therapy because it leads to tumor suppression.¹⁶ The N-terminal domain of P53 binds to the hydrophobic groove of HDM2 via three key residues (F19, W23, and L26). The corresponding P53 sequence (ETFSDLWKLLPEN) adopts a α -helix secondary structure in the P53 protein. This peptide has been extensively used as a model of study to develop among other stapled peptides with enhanced folding capacity and protease resistances. The resulting hybrid

¹⁶ P. Chène, *Nat. Rev. Cancer*, **2003**, 3, 102-109

macrocyclic architecture is expected to reproduce well the P53 secondary structure, and optimally orient the three hot-spot residues for optimal binding to the HDM2 surface. Proof of efficient design will be gathered by structural studies performed at the solid state with a successful crystallization of the hybrid macrocycle/HDM2 complex. Working with this well-established PPI system will also allow us to implement cell-penetration studies of the resulting macrocycles where the quinoline side-chain will be further modified by organic moieties known to facilitate cell-penetration (*i.e.* guanidinium groups, *cf.* previous section).

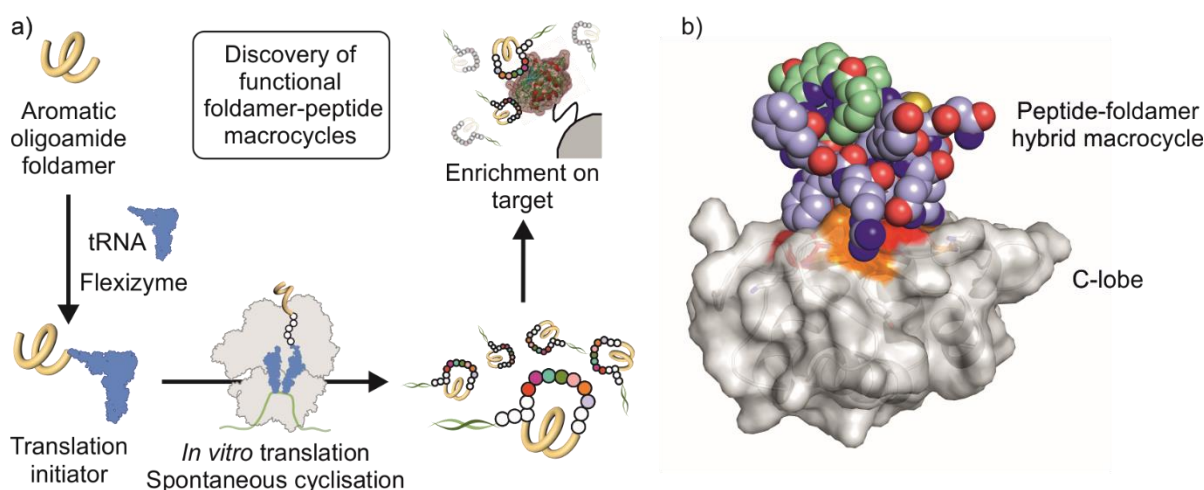


Figure 14 – Display selection of a hybrid peptide-foldamer macrocycle: a) Schematic incorporation of aromatic oligoamide foldamers by the flexible in vitro translation (FIT) system into macrocyclic peptide-foldamer hybrids that can undergo selection against a molecular target by mRNA display. b) Crystal structure of the complex between the C-lobe domain of E6AP-HECT domain and a peptide-foldamer hybrid macrocycle (PDB #7QPB).

Concurrently to the mRNA display, we sought to develop aromatic foldamers compatible with other selection tools. In particular, we focused our attention on phage display technology to screen for foldamer-peptide macrocycles. The advantage of the phage display technology over the RaPID one is that the foldamers used are less constrained by their size and flexibility. Larger constructs, such as 9mers having an architecture similar to the one depicted in Figure 13 e) can indeed be incorporated and screened against a specific target. In this context, peptides expressed and presented on the surface of bacteriophages can be further functionalized post-translationally with foldamers to form hybrid macrocycles linked to the peptide-encoding phage. This strategy can be achieved by the insertion of two distinct functional groups with orthogonal reactivity on each terminus of the foldamer that can further selectively react with the peptide.¹⁷ First, the

¹⁷ T. R. Oppewal, I. D. Jansen, J. Hekelaar, C. Mayer, *J. Am. Chem. Soc.* **2022**, 144, 3644-3652

expressed cysteine thiol reacts readily in an SN2 reaction with a bromoacetamide at the N-terminus of the foldamer to form a thioether. Second, an aldehyde at the C-terminus of the foldamer reacts with the N-terminal primary amine of the peptide by reductive amination to form a secondary amine and thus the macrocycle. The validation of this strategy from a chemical point of view is still in progress in the laboratory. Once the robustness of the macrocyclization and its versatility would have been confirmed, it would be applied to an entire bacteriophage library and screened against a protein target of interest that still have to be identified.

Next, by taking advantage of the judicious thioether linkage formation, we showed that in a series of peptide-foldamer hybrid structures, different consecutive occurring macrocyclization reactions can occur selectively on the surface of a rigid foldamer helix. A structurally well-defined foldamer helix can indeed carry several reactive chloroacetamide functions, which imparts the placing of these reactive centers out of reach of others. The cysteine thiols, embedded at specific positions of the peptide chain, react with the closer chloroacetamide in space and, at the difference of foldamer, the peptide backbone can adjust its conformation to satisfy the macrocyclization. The resulting macrocyclizations are predictable, selective, and guided by ring size with the smallest macrocycle forming first. As a result, a reaction trail along the surface of the foldamer is generated. This allowed us to introduce this concept of reaction trail and resulted in the conception of up to tetracyclic structures via two different reaction trails with good efficiency. With this, new synthetic hybrid architectures composed of a hydrophobic core surrounded by peptide loops, with a size comparable to small proteins, could be designed and next synthesized and characterized. They are reminiscent of protein structures and might thus find use as multivalent protein binders.

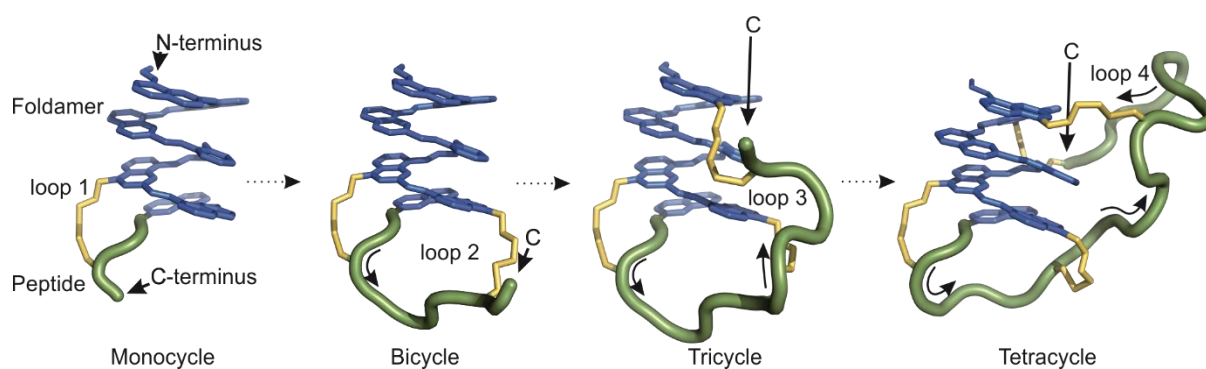


Figure 15 – Differential peptide multimacrocylation on the surface of a helical template. Molecular models which illustrate the cyclization trail of the mono-, di-, tri-, and tetracycle.